

Smart Molecular Probes for Selective Sensing of Nitric Oxide and Nitroxyl with Cell Imaging Applications

**THESIS SUBMITTED FOR THE
DEGREE OF DOCTOR OF PHILOSOPHY (SCIENCE)**

OF

JADAVPUR UNIVERSITY

APRIL, 2023



By

ANANYA DUTTA

DEPARTMENT OF CHEMISTRY

JADAVPUR UNIVERSITY

JADAVPUR

KOLKATA-700032

INDIA

2023

যাদবপুর বিশ্ববিদ্যালয়
কলকাতা-৭০০০৩২, ভারত



*JADAVPUR UNIVERSITY
KOLKATA-700 032, INDIA

FACULTY OF SCIENCE: DEPARTMENT OF CHEMISTRY: INORGANIC CHEMISTRY SECTION

CERTIFICATE FROM THE SUPERVISOR

This is to certify that the thesis entitled “Smart Molecular Probes for Selective Sensing of Nitric Oxide and Nitroxyl with Cell Imaging Applications” submitted by Miss Ananya Dutta who got her name registered on 2nd February, 2018 (Index No. 15/18/Chem./25) for the award of Ph.D. (Science) degree of Jadavpur University, is absolutely based upon her own work under my direct supervision and that neither this thesis nor any part of it has been submitted for either any degree / diploma or any other academic award anywhere before.

Date: 06/04/2023

Mahammad Ali
(Prof. Mahammad Ali)

Signature of the Supervisor & date with seal

Department of Chemistry
Jadavpur University
Kolkata 700 032


Dr. Mahammad Ali
Professor
Department of Chemistry
Jadavpur University
Kolkata-700 032

* Established on and from 24th December, 1955 vide Notification No.10986-Edn/IU-42/55 dated 6th December, 1955 under Jadavpur University Act, 1955 (West Bengal Act XXXIII of 1955) followed by Jadavpur University Act, 1981 (West Bengal Act XXIV of 1981)

দূরভাষ: ২৪১৪-৬৬৬৬/৬১৯৪/৬৬৪০/৬৪৯০/৬৪৪০ প্রসারণ: ২৪৬৯
দূরবার্তা: (৯১)-০৩০-২৪১৪-৬৪১৪/৬২১০/২৪১০-৭১২১

Website: www.jadavpur.edu
E-mail : hod@chemistry.jdvu.ac.in

Phone: 2414-6666/6194/6643/6495/6443 Extn.2469
Fax: (91)-033-2414-6414/6210/2413-7121



To
My Beloved Parents
(Baba & Ma)
and
Supportive Siblings
(Amrita & Mohit)

*This journey is totally incomplete
without their endless love, support and
faith in me.*

When the going gets tough, the tough get going.

Joseph P. Kennedy.

Acknowledgements

Now that I am finishing this PhD, I understand better why people often refer to it as a journey. It is not only about the vast amount of knowledge you acquire about your topic, but also about how acquiring this knowledge impacts you. These past years have made me learn more about myself, my strengths, and my limitations, but I cannot take all the credit for making this PhD possible. Without the help and support of all the incredible people around me, this work would not have been possible in the same way. I don't think there are enough words to express my gratitude, but I'll give it my best shot.

First and foremost, I wish to thank my advisor, Prof. Mahammad Ali for his guidance and the opportunity to perform a very challenging project, "Nitric Oxide Sensing". I am grateful for his irreplaceable advice, invaluable time and confidence about not only my present research work but future endeavors also.

I also want to convey my sincere gratitude to the Inorganic Chemistry faculty members at Jadavpur University, especially the present Dean of Science, Prof. Subenoy Chakraborty, Head, Department of Chemistry, Prof. Subratanath Koner, and Sectional In-Charge, Inorganic Chemistry, Prof. Saurabh Das, for their kind cooperation and encouragement. I am also thankful to Prof. J. P. Naskar, Prof. C. R. Sinha, Prof. S. Mukhopadhyaya, Prof. S. Baitalik, Dr. B. B. Show, Prof. P. Roy and Prof. T. K. Mandol, Department of Chemistry, Jadavpur University, for providing me their laboratory facilities as needed. I truly acknowledge all the faculty members and non-teaching staff, especially Mr. Baidyanath Paul, Mr. Atikur Rahaman, Raju Biswas (NMR operator) for their helpful gestures whenever required. I am also thankful to the authorities of the Jadavpur University for allowing me to utilize the necessary infrastructure.

Secondly, this journey will be incomplete without my labmates: Dr. Malay Dolai, Dr. Luna Paul, Dr. Rabiul Alam, Dr. Rahul Bhowmick, Dr. Arindam Giri, Dr. Abu Saleh Musha Islam, Dr. Animesh Mondal, Dr. Rittwik Modak, Dr. Kajari Ghosh, Mr. Habib Ali Molla, Dr. Dipankar Das, Mr. Hasan Mohammad, Mrs. Kaberi Pal, Miss. Debjani Maiti, Mr. Mihir Sasmal, Mrs. Rousunara Khatun and Miss Dolan Moni. In every hard and tough situation, they were with me to provide their important suggestions, and I will never forget the beautiful memories that we shared together. A special thanks goes to Miss. Debjani Maiti for her constant support and continuous help to solve various problems that I have faced during this journey.

I am greatly gratified to my Collaborators Mr. Chandrodaya Prodhan and Dr. Atul Katarakar, (former research scholar at CSIR-Indian Institute of Chemical Biology, Kolkata-700032, India) for their cooperation in my research work.

I do not have enough words for the fantastic supporting network that I have around me. I would like to thank Sourav Ghosh for keeping in touch and for the constant encouragement throughout my journey. I would like to extend my gratitude to my friends, seniors who have helped in this journey (Aindrila, Mouparna, Shreya, Ismatara, Sunanda, Hasina, Tanusree, Argyadip, Arnab, Avick, Robi, Milon, Ayan, Rakesh, Naba, Sourav, Animesh da, Gurupada da). Without their support this journey would not be easy and pleasurable. I should also mention the name of my PG-mates Soumi, Sudipa, Rituparna, Farahana, Srija, Sarbari for their cooperative behaviors and I am really very blessed to have them. I would especially like to thank Mrs. Soumi Das for all the chats, walks and endless laughs we shared together during this journey.

Last but not the least, no word is enough to express my gratitude to Ma and Baba for having faith in me and giving me the liberty to choose what I wanted. Without you I might not be the person I am today. You have both been my guide and philosopher in this journey. I should also mention the efforts of my beloved sister (Amrita), brother (Mohit) and niece (Diya) for making me smile at the difficult hours. Also a special thank goes to my brother in law Debdeep Bhandari.

Finally, I would like to thank everyone directly or indirectly involved to the successful insight of the thesis, as well as I apologize for not addressing them personally one by one.

*Department of Chemistry
Jadavpur University
Kolkata- 700032*

Ananya Dutta

Preface

The work presented in this thesis entitled “**Smart Molecular Probes for Selective Sensing of Nitric Oxide and Nitroxyl with Cell Imaging Applications**” was commenced in February, 2018 and have been carried out in the Department of Chemistry, Jadavpur University.

The thesis consists of six chapters which are summarized below.

Chapter 1 deals with a brief introduction of small bio-molecule NO (Nitric Oxide) and its kin HNO (Nitroxyl) along with a literature survey on selective detection of NO/HNO by fluorimetric technique.

Chapter 2 illustrates the synthesis and characterization of a new N-nitrosation based fluorescent sensor (NDAQ) utilizing 8-aminoquinoline and Nitrobenzoxadiazole as fluorophoric units. The probe exhibits high selectivity towards NO by eliminating the interference of reactive species (RCS/ ROS/RNS) with ~27 fold fluorescence enhancement at $\lambda_{em} = 542$ nm. The high sensitivity (LOD=7 nM) and shorter response time makes it a potential candidate to sense both endogenous and exogenous NO in living organisms. The kinetic assay illustrates the second-order dependency w.r.to [NO] and first order with [NDAQ]. The biological studies of the probe also supports its successful application to track both endogenous and exogenous NO in living organisms.

Chapter 3 introduce a simple, least-cytotoxic NO sensitive probe HqEN₄₈₀ to recognize NO in 100% aqueous solution by employing (quinolin-8-yloxy)-acetic acid ethyl ester (L¹) and N,N-dimethyl ethylene diamine. Its marked selectivity and sensitivity towards NO, makes it a highly suitable probe for NO under in vitro conditions with the possibility of in vivo monitoring of NO. Upon addition of 3.5 equivalents of NO, there is ~7 fold enhancement in fluorescence intensity in aqueous solution with a corresponding K_f value of $(1.75 \pm 0.07) \times 10^4 \text{ M}^{-1}$. In terms of the $3\sigma/\text{slope}$ method, the LOD for nitric oxide was found to be 53 nM thus, making the probe highly suitable to track NO in biological systems.

Chapter 4 describes a new dihydropyridine based NO sensitive probe (CQME) with benzochromene as the fluorophore unit. The probe exhibits ~30 fold enhancement in the

emission intensity at 615 nm on excitation at 470 nm. Investigation of the cause of this enhancement reveals that the cleavage of C-C bond between benzochromene and 1,4-dihydropyridine (DIPY) units occurs due to nitration on the 2H-pyran ring of benzochromene moiety leading to the formation of 2-nitro-3H-benzo[f]chromene (PYNO₂) and dimethyl 2,6-dimethylpyridine-3,5-dicarboxylate (PYMAA) as major products. While the simple chromene-DIPY based probe (SALDPY) gives dimethyl 4-(2H-chromen-3-yl)-2,6-dimethylpyridine-3,5-dicarboxylate (SALPY) as the major product with a very small amount of C-nitrosated product (SALNO₂). Now, the biocompatibility, high selectivity and sensitivity (~42 nM) along with pH independency of CQME makes it a premier candidate to be utilized to trace both endogenous and exogenous nitric oxide (NO) in biological systems.

Chapter 5 deals with a simple Cu(II) based sensor (1) for highly sensitive and selective recognition of HNO and S²⁻ over other biologically abundant anions with prominent enhancement in absorption and emission intensities. The Cu(II) based sensor (1) was synthesized by complexation between (quinolin-8-ylamino)-acetic acid hydrazide (L²) and Cu²⁺ ions. The sensor (1) exhibits weak fluorescence due to ET (electron transfer) but upon addition of HNO and S²⁻, a large enhancement in fluorescence intensity (F.I.) was observed over other possible competitive anions on the basis of reduction of Cu(II) to Cu(I) and formation of CuS, respectively. The HRMS studies, Job's plot strongly supports the 1:1 complexation between (quinolin-8-ylamino)-acetic acid hydrazide (L²) and Cu²⁺ ions. The corresponding K_f value for complex formation with Cu²⁺ from Uv-Vis absorption titration was determined as $(4.934 \pm 0.05) \times 10^4 \text{ M}^{-1}$. DFT studies also supports the sensing mechanism of Cu(II) based sensor (1) towards HNO and S²⁻.

Chapter 6 represents the highlights of the thesis.

List of Abbreviations

EDRF	Endothelium-derived Relaxation Factor
SMC	Smooth Muscle Cells
NOS	Nitric Oxide Synthase
FAD	Flavin Adenine Dinucleotide
FMN	Flavin Mononucleotide
NADPH	Nicotinamide Adenine Dinucleotide Phosphate
τ	Fluorescence Lifetime
$\Delta\bar{\nu}$	Stokes shift
Φ	Quantum yield
CHEQ	Chelation Enhancement of Quenching
CHEF	Chelation Enhancement of Fluorescence
MLCT	Metal–Ligand Charge Transfer
ILCT	Intra–Ligand Charge Transfer
PET	Photo-induced Electron Transfer
ICT	Intramolecular Charge Transfer
FRET	Fluorescence Resonance Energy Transfer
ESIPT	Excited-State Intramolecular Proton Transfer
HOMO	Highest Occupied Molecular Orbital
LUMO	Lowest Unoccupied Molecular Orbital
AA	Ascorbic Acid
DHA	Dehydroascorbic Acid
MGO	Methylglyoxal
HEPES	4-(2-Hydroxyethyl)piperazine-1-ethanesulfonic acid
DFT	Density functional theory
TDDFT	Time-dependent density functional theory
CPCM	Conductor-like Polarizable Continuum Model
MeCN	Acetonitrile
MeOH	Methanol
NaOH	Sodium hydroxide
NaCl	Sodium chloride
DCM	Dichloromethane
DMF/dmf	Dimethyl formamide
H ₂ O	Water
DMSO/dmsO	Di-methyl sulfoxide
mL	Milliliter
μ M	Micro molar
μ L	Micro liter

nM	Nano molar
mM	Mili Molar
K_a	Binding constant/Association constant
K_{ass}	Association constant
K_d	Dissociation constant
K_f	Formations constant
ex	Excitation
em	Emission
λ	Wavelength
HeLa	Human epithelial carcinoma cell
HepG2	Human hepatocellular liver carcinoma cells
PBS	Phosphate-buffered saline
DMEM	Dulbecco's Modified Eagle's Medium
MTT	3-(4,5-di methylthiazol-2-yl)-2,5 diphenyltetrazolium bromide
%T	Percentage of Transmittance
FBS	Fetal Bovine Serum
LOD	Limit of detection
MS	Mass spectroscopy
NMR	Nuclear magnetic resonance
FT-IR	<u>Fourier transform Infrared</u>
Fig.	Figure
AIE	<u>Aggregation-induced emission</u>
SMMC-7721	Hepatocellular carcinoma cell
FI /F.I	Fluorescence Intensity
GSH	Glutathione
Cys	Cysteine
Raw 264.7	Abelson leukemia virus transformed <i>cell</i>
hMSCs	Human mesenchymal stem cells
BINOL	<u>1,1'-Bi-2-naphthol</u>
NIR	<u>Near-infrared</u>
MCF7	Acronym of Michigan Cancer Foundation-7 cell
FE	Fluorescence Enhancement
EJ	Lung cancer cell
Tris-HCl	Tris (hydroxymethyl) aminomethane hydrochloride
UV	Ultraviolet
Vis	Visible
h	Hours
HPLC	<u>High-performance liquid chromatography</u>
TMS	Tetramethylsilane

KBr	Potassium bromide
K ₂ CO ₃	Potassium carbonate
ESI-MS ⁺	Electrospray ionization mass spectrometry
HRMS	<u>High-resolution mass spectrometry</u>
CH ₂ Cl ₂	dichloromethane
SOCl ₂	<u>Thionyl chloride</u>
CDCl ₃	<u>Chloroform-d</u>
DMSO- <i>d</i> ₆	<u>Deuterated Dimethyl sulfoxide</u>
LiCl	<u>Lithium chloride</u>
ATP	Adenosine triphosphate
Pi	<u>Phosphate - Wikipedia</u>
PPi	<u>Pyrophosphate</u>
CD ₃ OD	<u>Methanol-d4</u>
Et ₃ N	<u>Triethylamine</u>
MHz	Megahertz
<i>f</i>	Oscillator strength
°	degree
Å	<u>Angstrom</u>
eV	Electron volt

Contents

	Page No.
Acknowledgements	I-II
Preface	III-IV
List of Abbreviations	V-VII

Chapter 1

Fluorescent Molecular Probes for Nitric Oxide and Nitroxyl Sensing

1	Introduction	2
1.1	Nitric Oxide (NO) and its kin Nitroxyl (HNO)	3
1.2	Endogenous synthesis of NO and its biological influence	3
1.3	Popular Methods for monitoring the unprecedented role of Nitric Oxide	5
1.3.1	Griess Analysis	5
1.3.2	Chemiluminescence	6
1.3.3	Electrochemical detection	7
1.3.4	Fluorometric detection	7
1.4	Outline of Reported Strategies for the Recognition of NO by Fluorescent Molecular probes	8
1.4.1	NO sensing probes based on purely organic molecules	8
1.4.1.1	<i>o</i> -phenylenediamine leading to triazole formation through cyclization reaction	8
1.4.1.2	N-nitrosation based sensing approach	17
1.4.1.2.(a)	N-nitrosation of aromatic secondary amines	18
1.4.1.2.(b)	Deamination of aromatic primary amines in presence of NO	22
1.4.1.2.(c)	Cyclization of <i>o</i> -amino-3'-dimethylaminophenyl aromatics	24
1.4.1.3	DIPY (dihydropyridine) based sensing strategy	25
1.4.1.4	Unusual sensing strategies	28
1.4.2	NO recognition strategy by utilizing metal-complex probe	31
1.4.2.1	Reported Metal-based fluorescent sensors for NO detection	32
1.5	Nitroxyl	38
1.5.1	Why HNO, among all other nitrogen oxides?	39
1.5.2	Source of HNO	40
1.5.2.1	Angeli's salt	40
1.5.2.2	Piloty's acid and derivatives	40
1.5.2.3	Diazeniumdiolates	40
1.5.2.4	Nitrosocarbonyls	41
1.5.2.5	Hydroxylamine	41
1.5.2.6	Cyanamide	41

	Page No.
1.5.2.7. Acyloxy nitroso compounds	42
1.5.3. HNO detection	42
1.5.3.1. Cu(II) complex based HNO Probes	43
1.5.3.2. Triphenylphosphine-based (Staudinger ligation) HNO probes	46
1.5.3.3. Nitroxide-based prefluorescent probes:	52
1.5.3.4. Mercapto-2-methylpropionic acid-based fluorescent probes:	53
1.6. Objective and aim of the thesis	54
1.7. Physical measurements	55
References	57-77

Chapter 2

A Novel N-nitrosation based Highly Sensitive and Selective Turn-On Fluorescent Sensor for NO: Kinetic appraisal, DFT studies and Biological application

2.1	Introduction	79
2.2	Experimental Section	81
	2.2.1 Materials and Apparatus	81
	2.2.2 Preparation of Stock Solution of Analytes	82
	2.2.3 Kinetic Studies	82
	2.2.4 Calculation of LOD	83
	2.2.5 Quantum Yield	83
	2.2.6 Computational method	83
	2.2.7 Cell Imaging Experiments	84
	2.2.7.1 Cell viability assay	84
	2.2.7.2 In-Vitro Cell incubation and imaging	84
	2.2.8 Synthesis	84
	2.2.8.1 Synthesis and characterization of AmQNH	84
	2.2.8.2 Synthesis and characterization of NDAQ	87
	2.2.8.3 Synthesis and characterization of NDAQ—NO	89
2.3	Results and Discussion	91
	2.3.1 Uv-Vis study	92
	2.3.2 Emission study	93
	2.3.3 Kinetic Study	94
	2.3.4 Selectivity study	98
	2.3.5 Limit of detection	102
	2.3.6 TCSPC studies	102
	2.3.7 pH Study	103
	2.3.8 Confirmation of Nitric Oxide Sensing Mechanism	104
	2.3.9 DFT studies	105

	Page No.
2.3.10 Cell viability assay	109
2.3.11 Cell Imaging studies of NO (Exogenous and Endogenous)	110
2.4 Conclusion	111
References	113-117

Chapter 3

A smart molecular probe for selective recognition of nitric oxide in 100% aqueous solution with cell imaging application and DFT studies

3.1 Introduction	119
3.2 Experimental Section	121
3.2.1 Physical measurements	121
3.2.2 Materials and methods	122
3.2.3 Synthesis	122
3.2.3.1 Preparation of (quinolin-8-yloxy)-acetic acid ethyl ester (L ¹)	122
3.2.3.2 Preparation of N-(2-dimethylamino-ethyl)-2-(quinolin-8-yloxy)- acetamide (HqEN ₄₈₀)	122
3.2.3.3 Preparation of N-propyl-2-(quinolin-8-yloxy) acetamide (HqPA)	125
3.2.4 Solution preparation for UV–Vis absorption and fluorescence studies	126
3.2.5 Calculation of LOD	127
3.2.6 Calculation of the quantum yield	127
3.2.7 Computational details	127
3.2.8 Cell culture	128
3.2.9 Cell imaging study	128
3.2.10 Cell cytotoxicity assay	128
3.3 Results and discussion	129
3.3.1 Spectral response of HqEN ₄₈₀ to NO	130
3.3.1.1 Uv-Vis absorption studies	130
3.3.1.2 Fluorescence studies	131
3.3.2 Sensing mechanism	133
3.3.3 Confirmation of the sensing mechanism	133
3.3.4 TCSPC studies	137
3.3.5 Selectivity study	138
3.3.6 pH study	140
3.3.7 Geometry optimization and electronic structure	141
3.3.8 NO detection in living cells	145
3.4 Conclusion	147
References	148-153

Chapter 4

A Subtle Structural Change in the Fluorophore alters Nitric Oxide Mediated Reactivity of the Dihydropyridine based Probe Resulting Aromatic Nitration assisted C-C bond breaking

4.1	Introduction	155
4.2	Experimental Section	160
4.2.1	Reagents and Equipments	160
4.2.2	Preparation of Stock Solutions	160
4.2.3	Calculation of LOD	161
4.2.4	Cell Imaging Experiments	161
4.2.4.1	Cell viability assay	161
4.2.4.2	In-Vitro Cell incubation and imaging	161
4.2.5	Synthesis and characterization	162
4.2.5.1	Synthesis of BZALD	162
4.2.5.2	Synthesis of CQME	164
4.2.5.3	Synthesis of CQET	165
4.2.5.4	Synthesis of SALD	168
4.2.5.5	Synthesis of SALDPY	169
4.2.5.6	Synthesis of PYNO ₂ and PYMAA from CQME	172
4.2.5.7	Synthesis of PYNO ₂ and PYEAA from CQET	175
4.2.5.8	Synthesis of SALPY	177
4.3	Results and Discussion	180
4.3.1	Crystal structure of CQME and PYNO ₂	180
4.3.2	Absorption and emission spectra	181
4.3.3	Comparison of reactivity of CQME, CQET and SALDPY towards NO	184
4.3.4	Mechanistic Insights describing the difference in reactivity of NO towards CQME, CQET, and SALDPY	185
4.3.5	Selectivity studies	187
4.3.6	Reaction Kinetics	189
4.3.7	pH study	190
4.3.8	Cell imaging studies (Exogenous and Endogenous) in Live Cells	191
4.3.9	Comparison Table	193
4.4	Conclusion	195
	References	196-199

Chapter 5

A dual response fluorescent sensor for HNO and S²⁻ ions using a Cu(II) complex based probe assisted by detailed DFT studies

5.1	Introduction	201
5.2	Experimental section	203
5.2.1	Materials and methods	203
5.2.2	Synthesis	203
5.2.2.1	Preparation of (quinolin-8-ylamino)-acetic acid ethyl ester (L ¹)	203
5.2.2.2	Preparation of (quinolin-8-ylamino)-acetic acid hydrazide (L ²)	204
5.2.2.3	Solution preparation for UV-Vis and fluorescence studies	207
5.2.2.4	Preparation of sensor (1)	207
5.2.3	Job's plot	207
5.2.4	Computational details	208
5.3	Results and discussion	208
5.3.1	Uv-Vis absorption studies	209
5.3.2	Fluorescence quenching studies	210
5.3.3	HNO-induced reduction of Cu ²⁺ and HNO sensing	212
5.3.4	S ²⁻ Induced displacement of Cu ²⁺ and S ²⁻ sensing	215
5.3.5	Geometry optimization and electronic structure	218
5.4	Conclusion	225
	References	226-230

Chapter 6

	Highlights of the Thesis	231-233
--	---------------------------------	---------

Appendix

	List of Publication	234-235
--	----------------------------	---------

CHAPTER 1

*Fluorescent Molecular Probes
for Nitric Oxide and Nitroxyl
Sensing*

1. Introduction

Although Nitric Oxide (NO) is recognized as a critical signaling messenger molecule and participates in various physiological processes, however, it was assessed as an industrial and automotive pollutant with environmentally damaging and toxic effects initially after its discovery by Joseph Priestly in the year 1772. Nitroglycerin was invented in the year 1847 and was exploited as a drug molecule for innumerable medical purposes, but at that time researchers were totally unaware of its working strategy and NO releasing property. About a decade later, Nitric oxide releasing property of sodium nitroprusside and nitroglycerin were discovered by Murad and co-workers and they proposed that this NO releasing property may be responsible for the relaxation of smooth muscle cells.¹ After revealing the role of an endothelial-derived relaxation factor (EDRF) towards relaxation of smooth muscle cells by Furchgott and co-workers,² the whole vasodilation related researches became a puzzle for researchers which was solved by Ignarro *et al.*³ Subsequently, Robert F. Furchgott, Louis J. Ignarro, and Ferid Murad shared the Nobel Prize in Physiology in 1998 for their remarkable discoveries concerning "*nitric oxide as a signaling molecule in the cardiovascular system*". The subsequent researches unveil that the presence of nitric oxide in lower concentration (nanomolar or picomolar range) is beneficial, whereas aberrantly high amounts (micromolar level) of nitric oxide causes the generation of cytotoxic reactive nitrogen species causing DNA damage.⁴ Therefore, Nitric oxide is acquainted as a striking player to the researchers for this dichotomous role. NO coins an integral role in the regulation of growth, vascular smooth muscle relaxation and also in the defense signaling against microbial pathogens. It led researchers to further explore the mechanism of action of this gaseous molecule in the living organisms. Meanwhile, the one-electron reduced and protonated cousin of NO such as nitroxyl (HNO), has become the spotlight in this area of research, as physiological and pathological effects of HNO have not yet been fully elucidated. The subsequent investigation discloses the pharmacological potential of HNO for the treatment of cardiovascular diseases and also in the regulation of cellular function.⁵ Consequently, these versatile contributions of NO/HNO to physiological systems demand modern scientists to enrich the field of research on sensitive, selective detection and quantification of NO/HNO levels in biological systems by synthesizing some convenient strategies to clearly elucidate their biological roles.

1.1. Nitric Oxide (NO) and its kin Nitroxyl (HNO)

Nitric oxide (NO), one of the smallest and simplest biologically active gasotransmitter, has acquired an immense attention because of its unique and engrossing chemistry. NO is a colorless, highly reactive and heteronuclear diatomic gaseous molecular radical with paramagnetic behavior. High reactivity of NO due to its transient half-life (in the order of milliseconds to seconds depending upon the local oxygen and reactive biomolecules concentration)⁶ poses a significant challenge to the investigators in eliciting the mechanism of its action in physiological systems. In biological milieu, L-arginine acts as a primary precursor of this intracellular signaling molecule, however, in case of HNO although it could be produced from various metabolites, the question of its biosynthesis remains unresolved till date.⁷ In spite of their close structural resemblance, HNO exhibits distinct biological and chemical properties from that of NO.⁸⁻¹² Even though the biological targets (for example thiols, metalloproteins and radicals) are identical, the mechanism of their interactions are different. Depending on the reaction conditions, HNO provide either sulfinamides or disulfides by interacting with thiols, whereas, NO provide S-nitrosothiol as an initial product through oxidation to an 'NO⁺' (nitrosonium) equivalent species.¹³ Another major discrimination between NO and HNO is that NO[•] scavengers such as 2-(4-carboxyphenyl)-4,4,5,5-tetramethyl-imidazoline-1-oxy-3-oxide(carboxy-PTIO) and hydroxocobalamin are capable of scavenging NO[•] but not HNO.¹⁴⁻¹⁷ Furthermore, HNO is regarded as the sibling of Nitric oxide because of its some similarities with NO, yet recent researches have enlightened that HNO and NO serves as potent vasorelaxants and both are utilized in the treatment of cardiovascular diseases.^{18,19}

1.2. Endogenous synthesis of NO and its biological influence

Concisely, conversion of L-arginine into L-citrulline is the pivotal resource for NO production. This transformation proceeds under the influence of molecular oxygen, nicotinamide adenine dinucleotide phosphate (NADPH), and other biological factors such as tetrahydrobiopterin (BH₄), flavin adenine dinucleotide (FAD), flavin mononucleotide (FMN).²⁰ In this whole metabolization, the major constituent is the Nitric oxide synthases, a class of heme proteins which regulate the production of NO from L-arginine as depicted in **Figure 1.1a**.²¹⁻²³ Generally, nitric oxide synthases emerge in three isomeric forms in mammalian organisms and these are:

CHAPTER 1

neuronal NOS (nNOS), inducible NOS (iNOS), and endothelial NOS (eNOS). (the most abundant isomeric form in body). All these NOS isoenzymes are comprise of an oxygenase domain and a reductase domain which are linked through a Ca^{2+} /calmodulin binding region.^{24, 25}

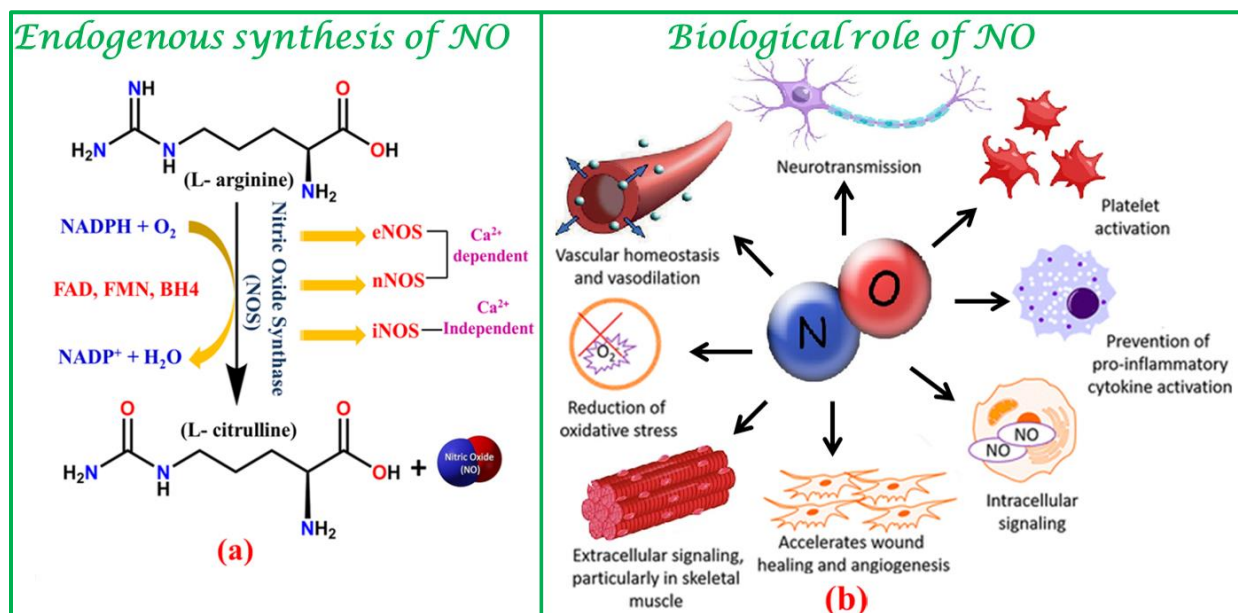


Figure 1.1.a. The most common endogenous synthetic pathway of NO. **b.** The pivotal role of NO in physiological systems.

In the process of generating NO from L-arginine, all these enzymes must cycle twice resulting in the formation of N^{G} -hydroxy-L-arginine as an intermediate.²⁶ The first step of reaction pathway involves the generation of N^{G} -hydroxy-L-arginine from L-arginine whereas the second step is associated with metabolization of N^{G} -hydroxy-L-arginine to L-citrulline and NO. Although there is a global consensus regarding the mechanism of conversion of L-arginine to N^{G} -hydroxy-L-arginine, yet again there is a lot of controversy concerning the pathway by which NOS isoenzymes metabolize N^{G} -hydroxy-L-arginine to L-citrulline and NO.²⁶

On the basis of biological perspective, the most significant job that nitric oxide play in the physiological system is the activation of soluble guanylate cyclase (sGC) in vascular smooth muscle. As a result, intracellular levels of cyclic guanosine 3',5'-monophosphate increase, and this causes smooth muscle cell relaxation and vasodilation.²⁷⁻²⁹ In the nervous system, NO acts as a neurotransmitter because NO has a major contribution in synaptic signaling and also in the regulation of memory and neurogenesis.³⁰ Further emerging researches unveil that NO influence

CHAPTER 1

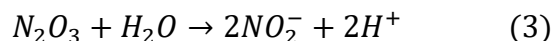
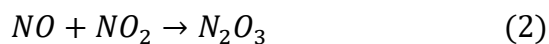
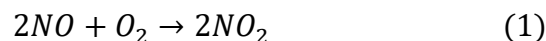
the immune functions³¹, apoptosis³², wound healing and angiogenesis³³, anticancer activities³⁴, inhibition in platelet aggregation, adhesion³⁵ and so on. Thus, the diverse biological roles of NO (Figure 1.1b) encouraged various scientists to develop numerous NO detection techniques to understand NO chemical biology *in vitro* and *in vivo*. Moreover, some biological activities of NO still remain elusive towards researchers.

1.3. Popular Methods for monitoring the unprecedented role of Nitric Oxide

Numerous techniques have been developed to detect as well as to analyze the activities of nitric oxide, in the living organisms till date. The most widely adopted techniques for the detection of NO are (a) *Griess analysis* (b) *Chemiluminescence* (c) *Electrochemical detection* (d) *Fluorometric detection*. Among all these reported techniques, some are available for direct analysis of NO, some are capable to measure the concentration of NO, and others methods are effective for unveiling the activities of NO adequately. The utilization of all these existing methods varies with what researchers want to explore in the field of nitric oxide chemical biology.

1.3.1. Griess Analysis

After the discovery of this method for nitrite (NO_2^-) detection in the year 1879 by Johann Peter Griess³⁶, according to the name of this German chemist, it is termed as **Griess Analysis**. This is an example of indirect approach of NO detection because by estimating the amount of NO_2^- with the help of griess assay, the amount of NO can be quantified as NO directly converts to NO_2^- under aerobic condition (given below).³⁷



Primitively, sulfanilic acid and α -naphthylamine were utilized for recognition of NO_2^- but later slightly modified so that it can be marketed as NO detection kits. In modified case, sulfanilamide (SA) and N-(1-naphthyl)ethylenediamine (NED) are used, in which after interaction with nitrite,

CHAPTER 1

an azo dye with high molar absorptivity (ϵ) via azo coupling reaction is formed as delineated in **Figure 1.2.**³⁸

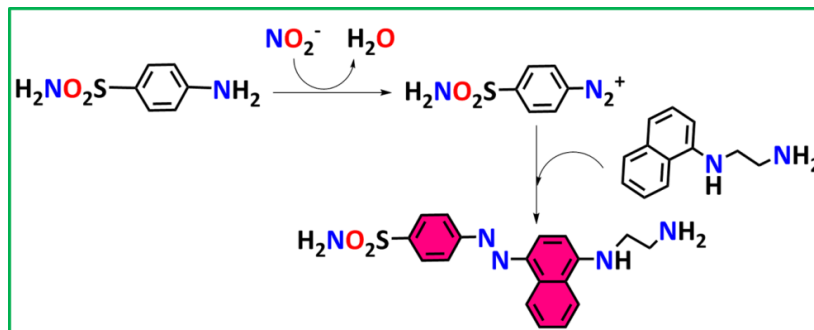
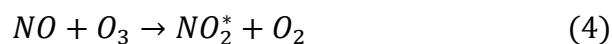


Figure 1.2. Modified form of Griess Analysis.

From which nitric oxide is estimated approximately. This method is not widely used as there are some major drawbacks reported. Firstly, this not a direct approach for NO detection, secondly, highly acidic medium needed for this to happen and lastly, during formation of NO from nitrite (NO_2^-), nitrate (NO_3^-) is generated as a byproduct.³⁷

1.3.2. Chemiluminescence

Chemiluminescence (luminescence that is produced by a chemical reaction to induce the transition of an electron from its ground state to an excited electronic state) analyses are found to be the most sensitive NO detection tool. Till now, two types of Chemiluminescence approaches have been reported³⁹, among which the ozone gas involvement technique is one of the most common approach for NO detection. The following reaction justifies that if during the analysis other conditions remain constant, the signal intensity of emitted photon is directly proportional to the concentration of nitric oxide from NO donor samples.⁴⁰



In addition, for sensitive detection of NO another Chemiluminescence analysis was initiated by Kikuchi et al.⁴¹ Though, this method is widely utilized in research, it also has some shortcomings for the detection of NO.

1.3.3. Electrochemical detection

Electrochemical sensors deal with the electro oxidation or electroreduction of NO. The major advantage of synthesizing these sensors are, their capability for real-time detection of NO.⁴² The selective recognition of nitric oxide by these electrochemical sensors are quite challenging task, as NO has great reactivity and structural resemblance with CO. Nonetheless, in NO chemical biology various investigations are explored by utilizing these electrochemical sensors.

1.3.4. Fluorometric detection

Among all the above mentioned techniques involved in the selective and sensitive detection of nitric oxide, fluorometric detection have acquired an immense attention of scientists, because of its experimental simplicity and high sensitivity towards target analyte.⁴³ The direct or indirect detection of Nitric oxide in biological systems are accomplished by fluorometric analysis depending upon the nature of fluorescent probes. So far, numerous fluorescent probes have been constructed for monitoring NO, its role as well as its production in cellular systems through *in vitro* and *in vivo* analysis. Therefore, for an efficient, selective and sensitive nitric oxide fluorescent sensor, the probes should be synthesized by considering the below facts:

- a. High specificity and sensitivity towards NO even in the presence of other biologically reactive species.
- b. The probe should have excitation wavelength (λ_{ex}) more than 400 nm to interrupt the cell damage by UV rays and emission wavelength (λ_{em}) \geq 500 nm is required to avoid interference from auto-fluorescence..
- c. The quantum yield should be high enough.
- d. Sensors should have sufficient cell permeability.

Till today, so many fruitful fluorescent NO sensors have been enlisted with their various positive and negative traits. Now, in brief, the recent growth in NO chemical biology related to fluorescent probes (by our and other research groups) has been delineated with all possible reaction mechanisms.

1.4. Outline of Reported Strategies for the Recognition of NO by Fluorescent Molecular probes

From the perspective of the most effective nitric oxide sensing mechanisms reported so far, two approaches are found out to be the most impressive ones as outlined below.

1. NO sensing probes based on purely organic molecules and
2. NO sensing probes based on transition metal complexes of fluorescent molecules.

1.4.1. NO sensing probes based on purely organic molecules

The backbone of this approach is the synthesis of various attractive fluorophoric entities with different NO recognition sites as given below.

- (1) *O*-phenylenediamine (OPD) leading to triazole formation through cyclization reaction.
- (2) Aromatic amines like
 - (a) N-nitrosation of aromatic secondary amines,
 - (b) Oxidative deamination of aromatic primary amines,
 - (c) Cyclization of *o*-amino-3'-dimethylaminophenyl aromatics
- (3) Dihydropyridine and
- (4) Others.

The widespread application of nitric oxide in living organisms has encouraged researchers to synthesize numerous nitric oxide sensing probes capable of revealing the activities of this messenger molecule precisely by targeting specific organelles (mitochondria, lysosomes and so on). This type of structural modification in fluorophoric entity to target specific organelle is mainly accomplished by utilizing the above mentioned organic entity based approach.

1.4.1.1. *O*-phenylenediamine leading to triazole formation through cyclization reaction

- **General reaction mechanism**

Upon exposure to NO, the *o*-phenylenediamine attached fluorophores become highly fluorescent in most of the cases. Generally, a photoinduced electron transfer (PET) mechanism is operative.

CHAPTER 1

Briefly, in the absence of nitric oxide, the electron density is transferred from the highly electron rich region (*o*-phenylenediamine moiety) to the fluorophore causing negligible or no fluorescence response — a phenomenon called **PET-ON, fluorescence OFF**. However, in the presence of NO under aerobic conditions leads to the formation of an electron deficient triazole moiety which disfavors the PET process resulting fluorescence ON which is also called **PET Blocked, Fluorescence ON**. This causes the generation of an intense fluorescence.

Nagano group⁴⁴ was pioneer to disclose the involvement of this mechanism for the sensing of NO by numerous fluorophores containing *o*-phenylenediamine moiety as the NO receptor. Thus, various derivatives of fluorescein (**1-8**) (Figure 1.3) appended with *o*-phenylenediamine showed negligible fluorescence due to the prevalence of spiro-lactum ring in the fluorescein moiety. However, on treatment with NO, an electron deficient triazole ring is formed which favors the opening of spiro-lactum ring. As a result an intense fluorescence was observed. The LOD value lies ~5 nM. In case of probes⁴⁵ **7** and **8** there are N-substituted *o*-phenylenediamine moiety which might be responsible for the dependence of fluorescence intensity on the pH of the medium and needs some alterations to make them biocompatible.

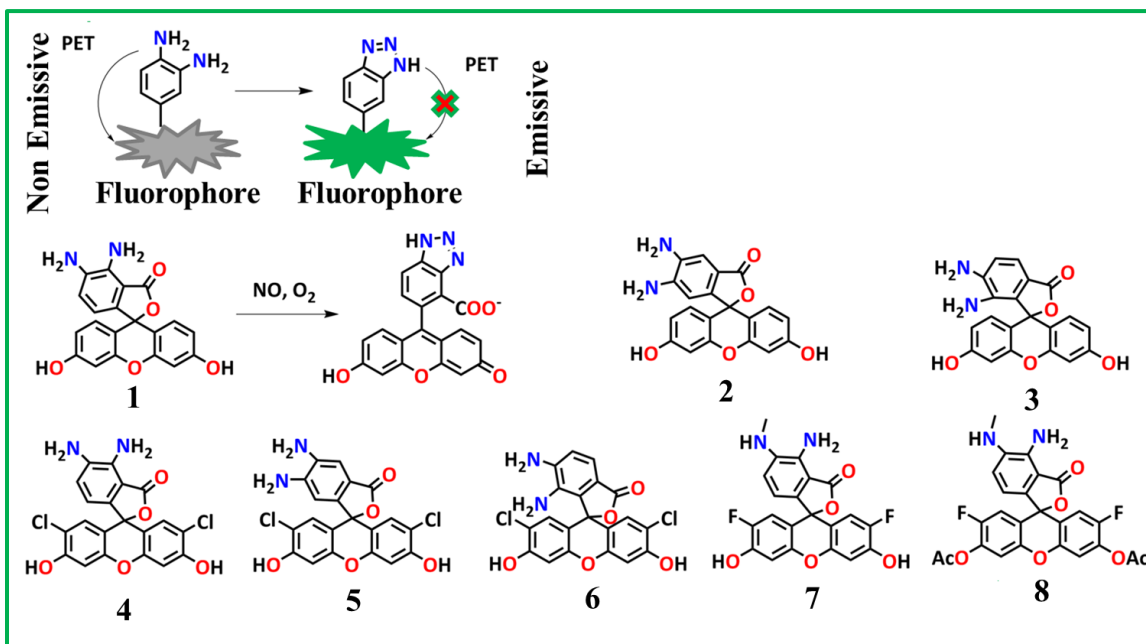


Figure 1.3. Under aerobic condition Fluorescein based NO probes.

CHAPTER 1

The aforementioned sensing strategy has been exploited to explore the activities of this messenger molecule to understand the NO chemical biology. Some interesting reported OPD based fluorophoric systems are discussed in below.

In the year 2012, Jin et al.⁴⁶ reported a new two-photon lysosome targeted highly sensitive and selective nitric oxide fluorescent sensor **9** (Figure 1.4) in which *o*-phenylenediamine embedded naphthalimide moiety was anchored as NO recognition site. The sensor **9** exhibits a dramatic enhancement (16 times) in fluorescence intensity at 530 nm upon excitation at 440 nm on addition of 5 equivalents NO. The two-photon fluoresce behaviour of **9** with detection limit in the nanomolar range (5 nM) makes it suitable to recognize NO in lysosome. Cho et al.⁴⁷ also reported a new OPD connected 2-acetyl-6-dialkylaminonaphthalene (acedan) based highly efficacious two photon probe **10** (Figure 1.4). On excitation at 370 nm, Probe **10** displayed a 68 fold increase in fluorescence intensity in response to NO at 502 nm. The one and two photon excitation ability of the probe makes it highly suitable to analyze the activities of NO in living cells.

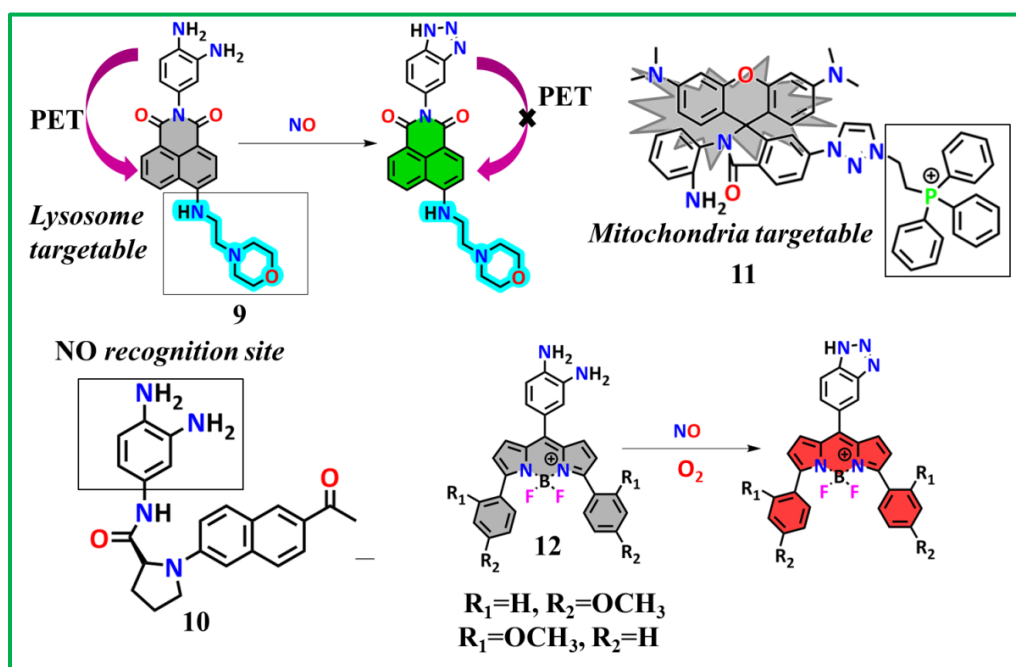


Figure 1.4. Some NO probes with OPD unit as NO recognition site.

Since, in case of mammalian cells, Mitochondrion is the main organelle to produce NO by inducible NOS enzymes, therefore, it encourages the scientists to further track NO in

CHAPTER 1

mitochondria. In 2013, first mitochondria targeted nitric oxide sensitive fluorescent probe was introduced by Jin and his coworkers.⁴⁸ Probe **11** (Figure 1.4) upon exposure to NO displays a 60 fold enhancement in fluorescence intensity at 585 nm without any biological interference. The most striking feature of this probe is that it is capable to exhibit real time monitoring of mitochondrial NO in living organism. In the same year, Zhang and his team⁴⁹ developed two bis-methoxyphenyl-boron dipyrromethene (BODIPY) embedded fluorophoric systems **12** (Figure 1.4), which were identified as potential candidates for cellular studies of NO due to their large Stoke shift (38 nm).

In 2016 Wang team⁵⁰ introduced a new NO sensitive BODIPY based fluorescent probe **13** (Figure 1.5). The amphiphilic behavior of the probe makes it suitable for monitoring the diffusion of nitric oxide across the cell membrane. Along with the low LOD value (0.83 nM), the dramatic enhancement and quick response of the probe towards NO at 529 nm, has attracted immense attention in the research area of NO sensing.

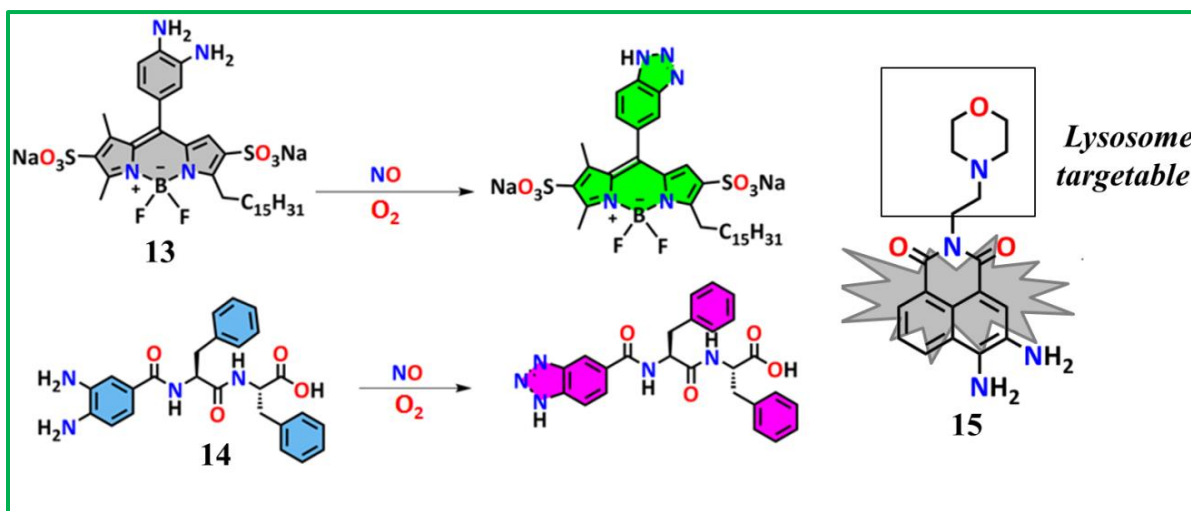


Figure 1.5. Examples of some OPD based Nitric Oxide sensors.

Meanwhile, considering the fact that for nitric oxide related intracellular studies the solubility of the probes in aqueous medium is the main factor, Liang and his research team⁵¹ synthesized a sensor **14** (Figure 1.5) in which 3,4-diaminobenzoic acid is attached to two amino acids to improve its water solubility. Here, **14**, on treatment with NO, displays about 73 nm blue shift from 440 nm due to involvement of ICT mechanism. Inspired by Jin et al.⁴⁶, Xu and his

CHAPTER 1

colleagues⁵² in 2016 developed another lysosome targeted probe **15** (Figure 1.5) with high pH (4-12) stability and LOD (4.57 μM). An overlap between the images of the probe and lysosome specific dye (Neutral Red), obtained by fluorescence localization assay, evidences the efficacy of the probe to target lysosomes.

Ding and his research group⁵³ revealed a more advance way to sense more accurately the lysosomal nitric oxide relevant to pathological processes, where a NO specific donor-acceptor-donor (D-A-D) entity **16** (Figure 1.6) was framed by exploiting benzothiadiazole-diamine as an acceptor system and two alkyloxy moieties as an electron donor. On reaction with NO a benzotriazole ring is formed which induces a strong ICT process, as evidenced from a red shift λ_{em} from 565 nm to 625 nm. The real time monitoring of variation in lysosomal NO concentration was executed in an acute liver injury mouse model, which clearly demonstrates the potentiality of the probe for therapeutic treatment of liver injury.

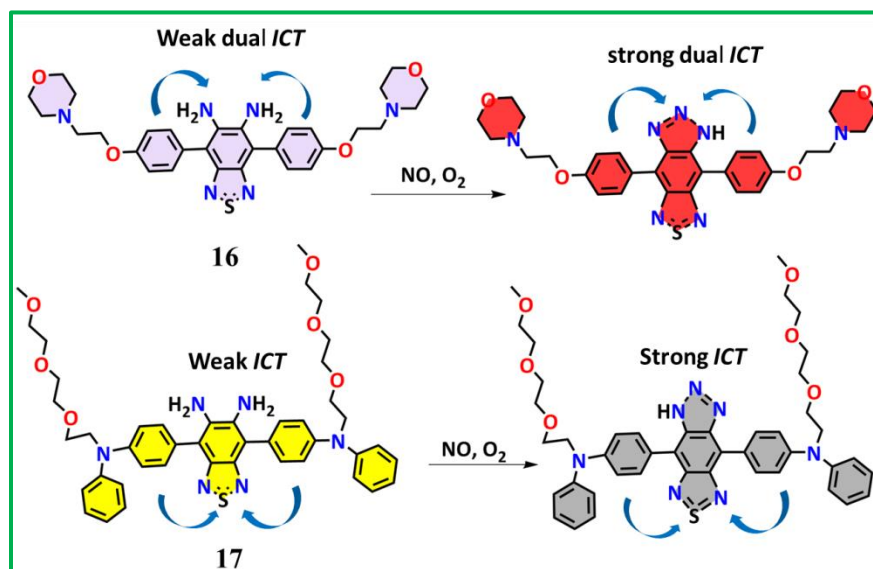


Figure 1.6. D-A-D sensing strategy followed NO sensors.

A similar D-A-D strategy was employed by Zheng and his group⁵⁴ to fabricate a novel photoacoustic NO probe **17** (Figure 1.6) in which benzothiadiazole-diamine entity acts as a bridge between two oligoether embedded diphenylamine. Here, the role of oligoether is to enhance its amphipathic and cell-penetrating properties. Here, also ICT mechanism was found to

CHAPTER 1

being operated. The excellent photoacoustic imaging capabilities of the probe was verified by performing an experiment to recognize nitric oxide in infected mouse tissue.

In 2022, Ji et.al.⁵⁵ synthesized a new hemicyanine-based fluorescent probe **18** (Figure 1.7) that quenches the fluorescence signal in presence of NO rather than enhancement due to the involvement of ICT process instead of normal PET mechanism. The consecutive addition of NO results in decreasing the fluorescence intensity at 490 nm on excitation at 420 nm giving a detection limit of 20 nM.

Hypoxia is a well-known term in tumor therapeutic studies. Now, under hypoxic conditions NO is overproduced in tumor cells causing tumor cell proliferation and metastasis. Consequently, to better understand the interplay between hypoxia and NO precisely, in 2018, the Singh group⁵⁶ open up a new ground in tumor physiology by reporting a dual-analyte fluorescent probe **19** (Figure 1.7) to detect both hypoxia condition and NO concentration in live cells. Probe **19** was designed by linking anticancer drug Chlorambucil with nitrocoumarin through an ester bond which in hypoxic atmosphere generates NO trapping unit (diaminocoumarin) through the reduction of $-\text{NO}_2$ to NH_2 resulting green fluorescence. Now, this anticancer drug embedded diaminocoumarin based probe reacts with NO to give fluorescence in the blue region and the resulted triazole entity can also be photoirradiated leading to release of the drug.

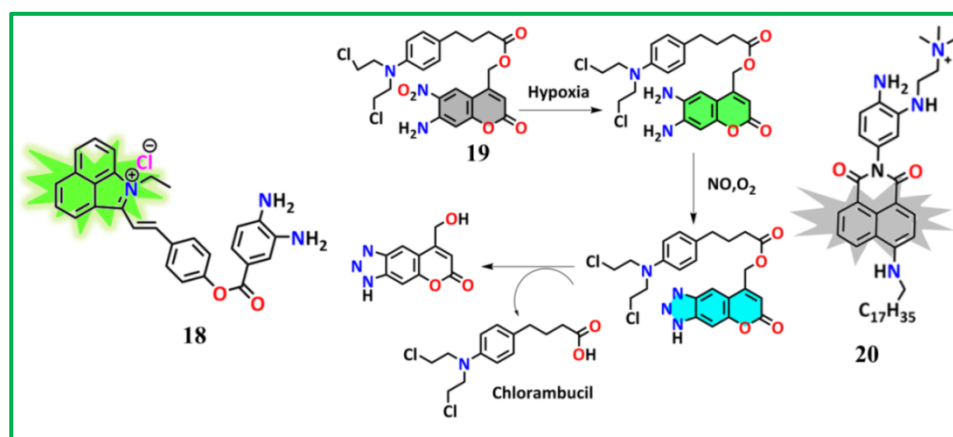


Figure 1.7. Some simple OPD based Probes 18, 20 and probe 19 is drug linked NO sensor.

Although *o*-phenylenediamine acts as a NO recognition site, there are some limitations exhibiting false positive fluorescent signals by other interfering species such as dehydroascorbic

CHAPTER 1

acid (DHA), ascorbic acid (AA), and methylglyoxal (MGO) which are present in the biological systems. One way to overcome this hurdle is to reduce the reactivity of OPD by protecting one of the amino groups. Based on this concept, Wang and his research team⁵⁷ introduced a modified OPD based amphiphilic sensor **20** (Figure 1.7), where the quaternary ammonium unit attached to OPD enhances the hydrophilicity, whereas the N-alkyl side chain attached to naphthalimide fluorophoric unit increases the hydrophobicity. The treatment with NO leads to 16.7 fold enhancement in fluorescent intensity. The visualization of the brain slice image clearly displays the location of this concerned two photon probe on cell membrane and imaged nitric oxide discharged from cells. Now, the direct linking of one of the amino groups of OPD with fluorophore also provides aromatic secondary amine. So, keeping this strategy in mind, Guo et al.⁵⁸ reported a silicon-substituted xanthenes embedded near-infrared (NIR) probe **21** (Figure 1.8) which emits at 710 nm after reaction with NO and favors the monitoring of mitochondrial NO in real time. The interrelation between Endoplasmic reticulum (ER) and NO has encouraged scientists to develop ER targeting NO probe, as the significant role played by ER is perturbed by NO causing ER stress and cell apoptosis.

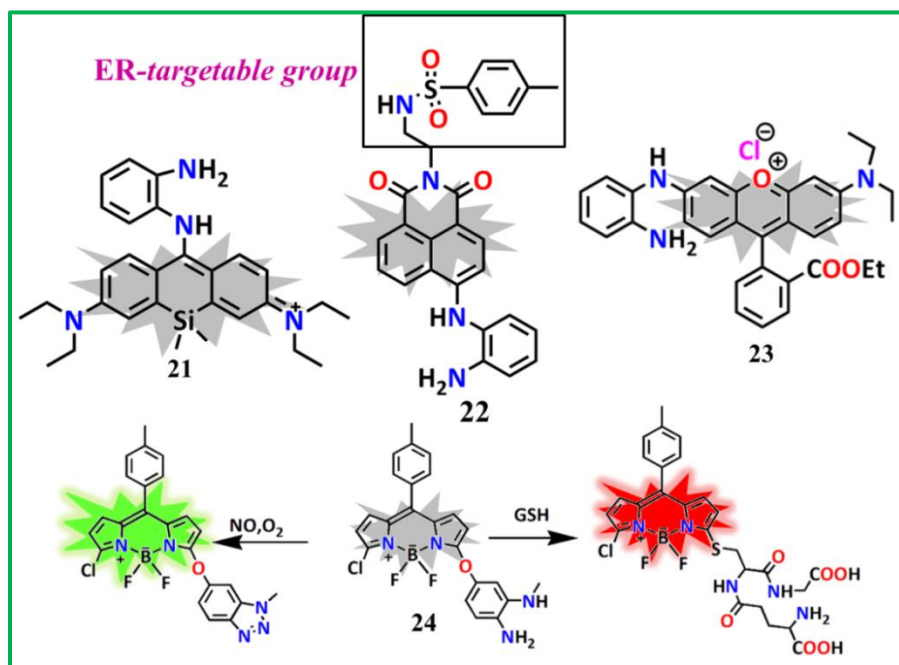


Figure 1.8. NO sensors based on modified form of OPD.

CHAPTER 1

In 2018, by adapting similar sensing approach, Li and co-workers⁵⁹ designed a two-photon probe **22** (Figure 1.8) in which naphthalimide is linked between an OPD unit and Endoplasmic reticulum (ER) targeting methyl sulfonamide group (emission 538 nm). Investigation in mice model treated with Tunicamycin (TM, a drug that promotes ER-stress) clearly demonstrates that it can detect the ER stress in animal by recognizing NO. Probe **23** (Figure 1.8) has also been synthesized by Zeng research group⁶⁰ utilizing a similar modified OPD strategy. In probe **23** rhodamine was used as fluorophoric entity and the presence of cationic charge enhances its water solubility and cell-membrane penetrating power. In 2019, a novel BODIPY based dual-channel analyzing probe **24** (Figure 1.8) was reported by Niu et al.⁶¹ for monitoring NO and GSH. Here, treatment of probe **24** with NO displays an enhancement in fluorescence signal at 528 nm (green region) and reaction with GSH shows changes in spectral intensity at 558 nm (red region). Therefore, biological investigation was applied to delineate the precise recognition of both NO and GSH in inflamed RAW 264.7 cells. This enlighten a new path in NO research area regarding physiological correlation between NO and GSH.

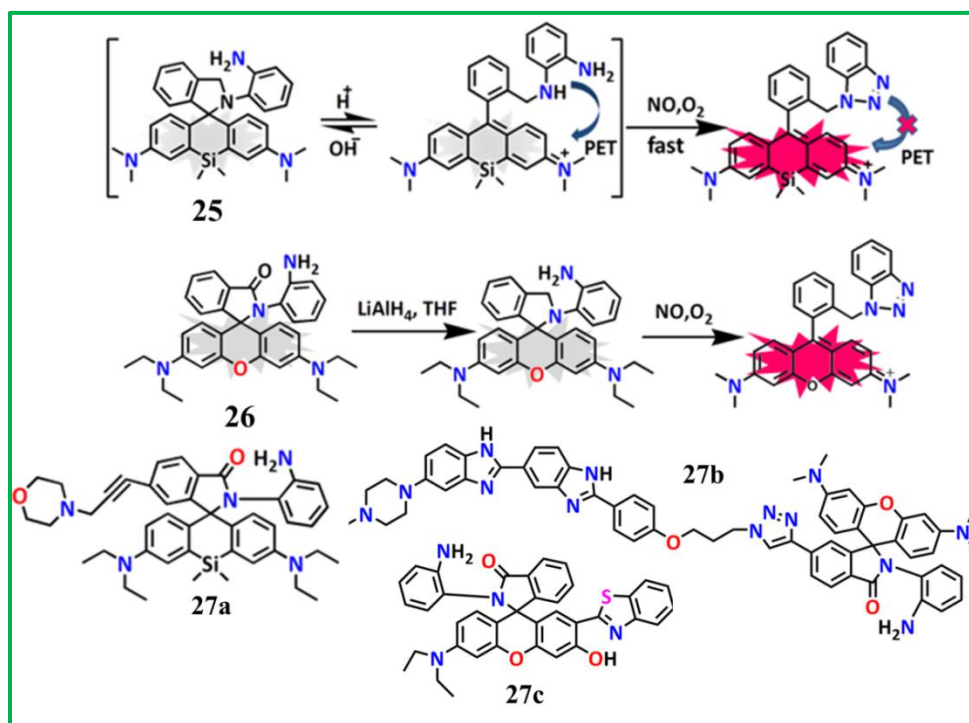


Figure 1.9. Rhodamine based NO sensing probes.

CHAPTER 1

Attachment of OPD with rhodamine fluorophoric moiety generates a spirolactam ring which under acidic condition provides aromatic secondary amine as a NO trapping unit. Both the probes **25** (Figure 1.9) and **26** (Figure 1.9) reported by different research groups,^{62, 63} follows the same reaction mechanism. Here, Si-rhodamine was exploited as a fluorophoric entity for the former (**25**) whereas rhodamine-B is utilized for the later (**26**). In both cases under acidic condition reaction with NO provides enhancement in fluorescence signal.

By following the similar sensing strategy Wang group⁶³ reported a lysosome targeting Si-rhodamine system **27a** (Figure 1.9) attached with OPD. In lysosome under acidic condition in the presence of NO, the spirolactam ring opens up, resulting an increase in the fluorescence intensity at 680 nm. The suitability of the probe for analyzing the lysosomal NO activities was illustrated by conducting biological assays with RAW 264.7 macrophages induced by interferon- γ and LPS. Recently, Zhang et al.⁶⁴ has introduced a nucleus targeted ratiometric nitric oxide sensing probe **27b** (Figure 1.9) by conjugating the Hoechst part to the rhodamine spirolactam. The spectral changes upon addition of NO are indicated by an increase in the fluorescence intensity at 603 nm and a decrease at 463 nm. Biological investigations further confirm that the probe has the capability to sense NO in the nucleus and also recognize NO in inflamed living organisms due to its high sensitivity (58 nM), selectivity and low cytotoxic effect. Now, based on OPD related sensing strategy, Song et al.⁶⁵ developed a rhodol system **27c** (Figure 1.9) (difference in emission wavelength before and after NO addition by 154 nm) by conjugating OPD as a NO recognition entity to monitor the fluctuations of NO in live cells and also studied the detection of NO in Inflamed mice model. Now, the pivotal role of NO in physiological system is widespread. As chronic liver inflammation causes excess generation of endogenous NO leading to liver cancer, it is obvious to design hepatocyte targeting probes for better understanding the role of NO in liver cells. In 2018, Zhang group⁶⁶ has introduced a rhodamine-B based probe **28** (Figure 1.10) interlinked with galactose and OPD units which on treatment with NO displays emission at 580 nm. High water solubility as well as high sensitivity (LOD = 1.62 nM) and specificity towards NO facilitate its application for visualizing hepatocellular NO in HepG2 cells and zebrafish.

CHAPTER 1

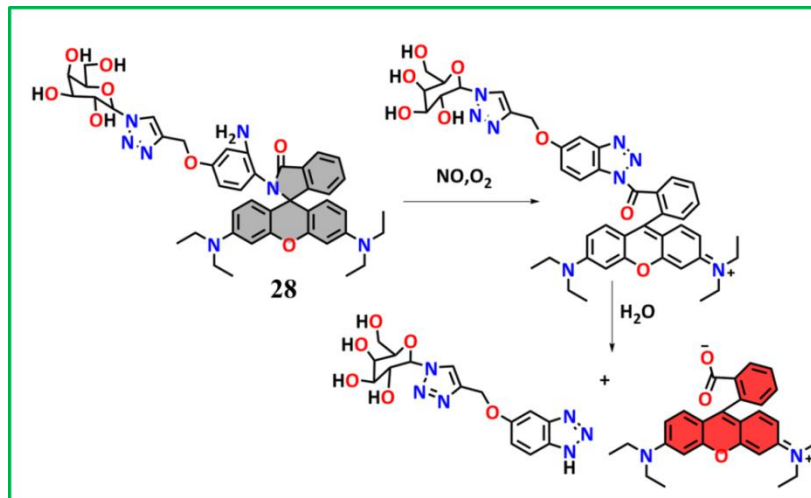


Figure 1.10. Galactose conjoined rhodamine based NO sensing probe.

1.4.1.2. N-nitrosation based sensing approach

Sensing mechanisms related to (a) N-nitrosation of aromatic secondary amines, (b) oxidative deamination of aromatic primary amines and also (c) cyclization of o-amino-3'-dimethylaminophenyl aromatics are considered to be more appealing approaches as in these cases the biological interference by the reactive species (RNS, ROS and RCS) can be safely excluded.

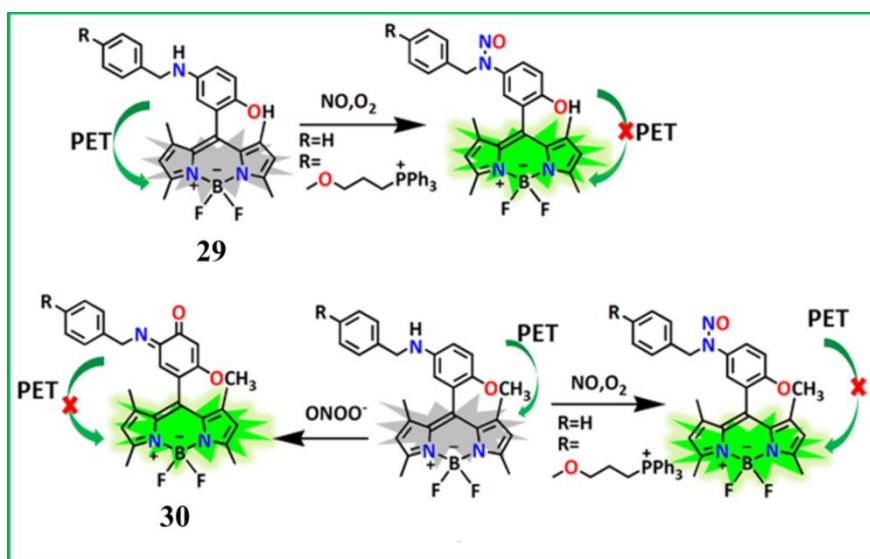


Figure 1.11. BODIPY based NO sensors with aromatic secondary amine.

CHAPTER 1

1.4.1.2 (a) N-nitrosation of aromatic secondary amines

In 2015, Guo group⁶⁷ designed a N-nitrosation based fluorescent probe **29** (Figure 1.11) in which BODIPY is attached to a N-benzyl-4-hydroxylaniline group which acts as a NO trapping unit. 92-fold enhancement in fluorescence signal at ~ 518 nm ($\lambda_{\text{ex}} = 490$ nm) with 4.8 nM detection limit makes it a potential candidate to recognize NO in mitochondria. Later, the same research group⁶⁸ in 2019 reported the same fluorescent probe **30** (Figure 1.11) with slight modification converting phenolic OH to corresponding methoxido group that exhibits a change in fluorescence property. The probe now can detect both NO and ONOO⁻ in living cells with higher selectivity and lower LOD (0.4 nM).

Inspired by the previously reported BODIPY based NO sensor, Chen and coworkers⁶⁹ introduced a series of BODIPY based probes **31** (Figure 1.12) that are capable of targeting both mitochondria and lysosomes by appropriate tuning of 5-amino-2-methoxy-phenyl system. All these probes on reaction with NO display increase in fluorescence intensity at 515 nm, leading to its beneficial role for analyzing the localized nitric oxide in specific organelles. Now, by utilizing 4-methoxy-N-methylaniline entity (which was first introduced by Guo group as NO trapping unit), Liu group⁷⁰ has developed two photon Si-rhodamine based NIR sensor **32** (Figure 1.12) in 2017. Both excitation (633 nm) and emission (672 nm) of the probe in NIR region with quick response towards NO (90 s) and low detection limit (14 nM) enable it for *in vivo* nitric oxide recognition in xenograft tumor mouse model. The investigation has revealed the generation of NO during tumor progression.

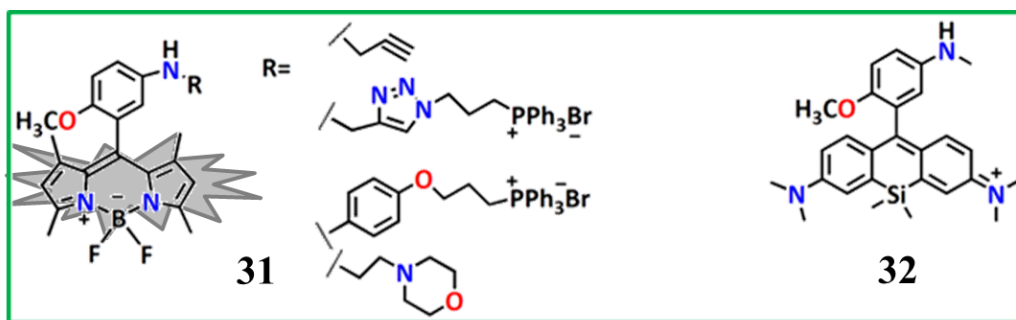


Figure 1.12. NO probes that follows N-nitrosation sensing strategy

CHAPTER 1

In the same year the same research group⁷¹ developed a novel two photon benzocoumarin based NIR probe **33a** (Figure 1.13) by attaching modified *p*-phenylenediamine through amide bond. This probe is also enlisted as a good NO sensor due to its high selectivity and sensitivity with low detection limit (37 nM). The unique capability of the probe to detect NO generation during ischemia reperfusion injury (IRI) process in mice kidneys was successfully revealed for the first time through an experiment. The success in this experiment introduces a new role of NO in physiological systems. They also reported an OPD based probe **33b** (Figure 1.13) for NO by exploiting Nile red as a fluorophoric unit.⁷² The two photon excitation ability of the probe with high selectivity and sensitivity towards NO enhances its application in mouse model.

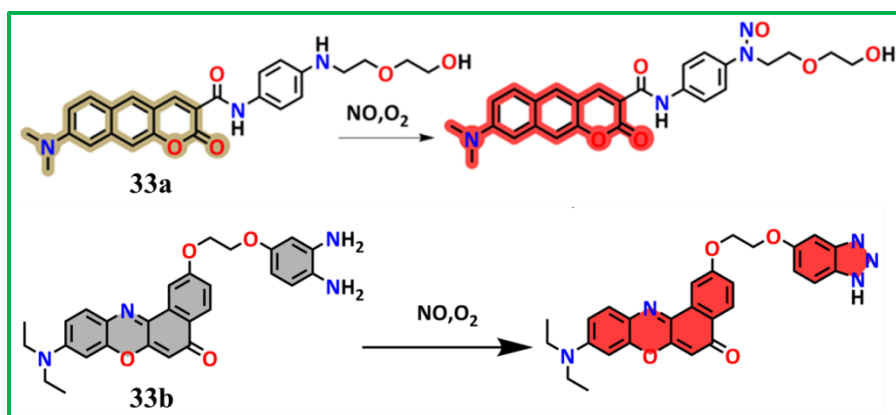


Figure 1.13. Two different NO sensing strategies reported by same research group.

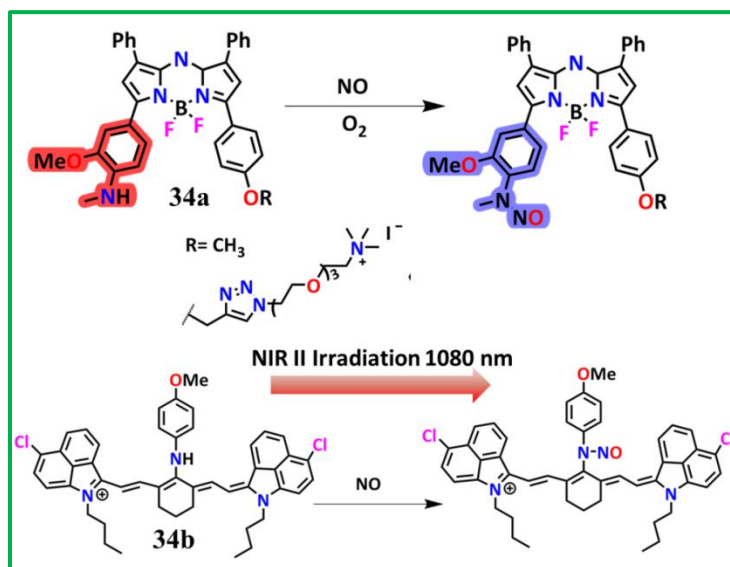


Figure 1.14. NO sensing probes based on Photoacoustic N-nitrosation sensing mechanism.

CHAPTER 1

Photoacoustic imaging is now gaining a lot of attention due to its ability to acquire high resolution images at centimeter depth. In 2018, the Chan research group⁷³ developed a series of new N-nitrosated photoacoustic probes based on *o*-methoxy methyl aniline embedded BODIPY dye. A PEGylated tetraalkylammonium entity has been linked to the concerned probe **34a** (Figure 1.14) to enhance its water solubility, resulting better cellular investigations. Among all the series of PA probes reported, probe **34a** stands out to be the best one because of its high specificity towards NO and rapid conversion to the N-nitrosated product with a hypsochromic shift in λ_{\max} by 91 nm. The detection of NO by the probe **34a** in LPS (lipopolysaccharide) induced inflamed murine model without the sacrifice of animal reveals that PA imaging are always superior compare to other imaging techniques. Now, recently, due to its diverse biomedical applications, the same research team⁷⁴ first successfully designed a novel NIR-II acoustogenic probe **34b** (Figure 1.14) for detection of endogenous, cancer-derived NO in deep-tissue. Herein, aromatic secondary amine, the NO recognition unit acts as a bridge between *p*-anisidine and IR-1048. The most important feature of this probe is that the interaction with nitric oxide has an absorption maximum at 1080 nm without any spectral overlap with the probe. As a result, the breakthrough approach of this probe in NO chemical biology was displayed by executing the endogenous detection of nitric oxide in cancer murine models.

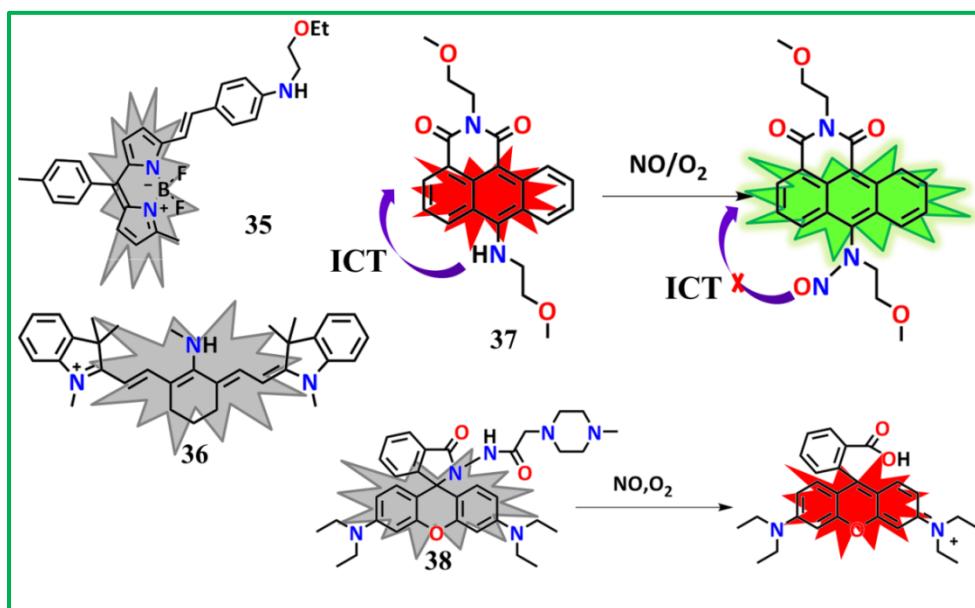


Figure 1.15. Some simple N-nitrosated based NO sensors.

CHAPTER 1

Another N-nitrosation based sensor **35** (Figure 1.15) was developed by Song et.al.⁷⁵ in which BODIPY was linked with an active secondary amine unit as NO receptor. This probe (LOD=10 nM) displays enhancement in fluorescence signal at 585 nm on reaction with NO. However, quenching of fluorescence intensity that is developed after NO treatment was found to be suppressed significantly on further treatment with GSH. Deep tissue penetrations as well as biocompatibility arising out of emission light in the NIR region are the important aspects of NIR probes. However very few reports on the NO sensing by NIR probes are available in the literature. NIR probe **36** (Figure 1.15) has been designed by employing cyanine as a fluorophore⁷⁶ in which the halide atom is replaced by methyl amine to form a secondary amine unit. Now, it reacts with nitric oxide (within a 5 min) by following ICT mechanism to form N-nitrosated product giving emission at $\lambda_{em} = 800$ nm. Excitation at 760 nm reveals its successful application to determine the NO level *in vitro* by cell imaging studies. In 2020, by following the similar ICT reaction mechanism, Wang research group⁷⁷ synthesized an anthracene carboximide based moiety **37** (Figure 1.15) in which the presence of secondary amine at the 6th position of the fluorophoric entity served as a NO recognition unit. The unique feature of this probe is that on interaction with NO, there is a change in fluorescence emission wavelength from red ($\lambda_{em} = 625$ nm) to green ($\lambda_{em} = 525$ nm) which makes it a good NO probe (LOD= 4.05 nM) and useful for its application in analyzing the endogenous NO in Raw 264.7 macrophage cells as well as in zebrafish in ratiometric pattern.

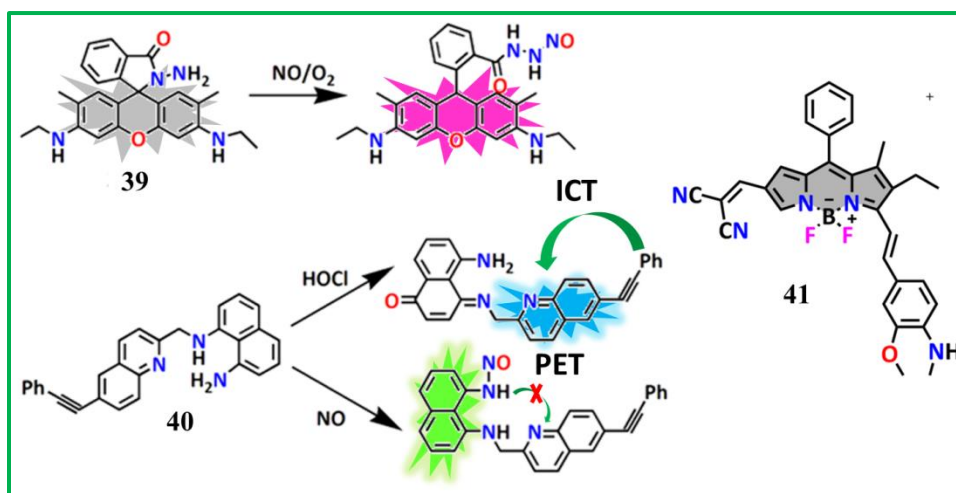


Figure 1.16. N-nitrosation of the probes in primary (39 and 40) and secondary amine (41).

CHAPTER 1

N-nitrosated probes **38** (Figure 1.15) and **39** (Figure 1.16) were designed by different research groups using rhodamine⁷⁸ as the fluorophore for the former and rhodamine 6G⁷⁹ for the latter. In both the cases, fluorescence intensity was increased due to their spirolactum ring opening reaction followed by N-nitrosation. Moreover, the biological studies by the probe **39** in inflamed zebrafish model manifest its potentiality to diagnose various NO related diseases. In 2021, Zheng et al.⁸⁰ designed a dual analyte (HOCl and NO both) recognizing fluorescent probe **40** (Figure 1.16) in which 1,8-naphthalene diamine act as a reactive unit. Inhibition of PET process operating within this moiety causes enhancement in fluorescence signal ($\lambda_{em} = 512$ nm) upon treatment with NO within 20s. This probe is capable of detecting both HOCl and NO for *in vitro* and *in vivo* studies. The Guo research group⁸¹ has recently synthesized a BODIPY embedded N-nitrosated probe **41** (Figure 1.16) that on reaction with NO enhances its signal intensity at ~600 nm like any other good nitric oxide probe. Now, encapsulation of the probe into the core of the copolymer *m*-PEG-DSPE 2000 (amphiphilic in nature) increases its water solubility, so that the modified probe is able to detect NO through the enzymatic pathway (eNOS) in living cells.

1.4.1.2 (b) Deamination of aromatic primary amines in presence of NO

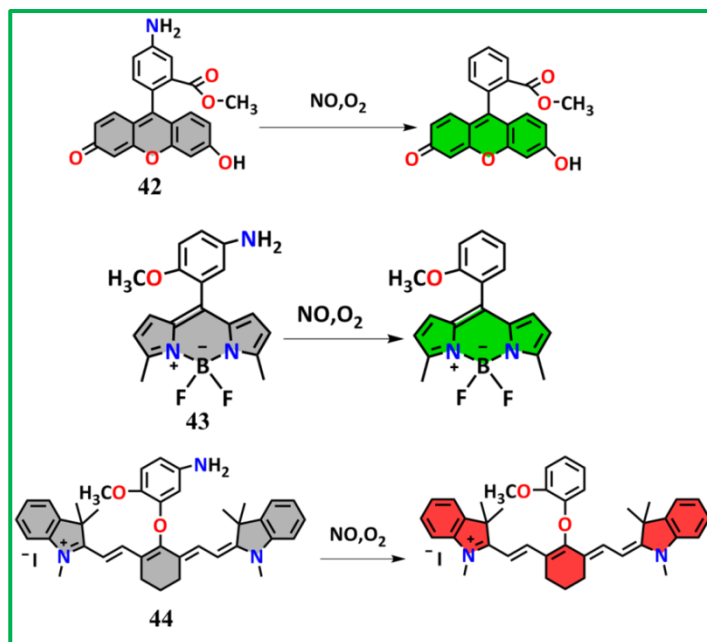


Figure 1.17. NO sensors involving sensing strategy of deamination of aromatic primary amines.

CHAPTER 1

Another NO sensing mechanism involving oxidative deamination of aromatic primary amines has gained much attention because false positive response by AA (ascorbic acid), DHA (dehydroascorbic acid), MGO (methylglyoxal), etc can be safely avoided. Wang et al.⁸² first reported this sensing mechanism by considering fluorescein-based aromatic amino ester as a probe (**42**) (Figure 1.17) in which the interaction with NO causes an increase in fluorescence intensity ($\lambda_{em}=524$ nm) by blocking the PET process. The high specificity, sensitivity and also the biological applications make it an impressive NO probe. Both the probes **43** and **44** (Figure 1.17) were synthesized by the same research group⁸³ (Guo et al.). For probe **43** BODIPY ($\lambda_{ex} = 475$ nm, $\lambda_{em} = 519$ nm) and probe **44** cyanine, ($\lambda_{ex} = 750$ nm and $\lambda_{em} = 794$ nm) have been used as a fluorophoric platform. In both the cases *p*-methoxyaniline unit acts as a NO recognition site. The sensing strategies of both the probes are very similar but for probe **44** the fluorescence emissions in the NIR region makes it superior compare to **43** due to its tissue penetration ability. So, probe **44** was applied for further biological studies in an inflammatory mouse model.

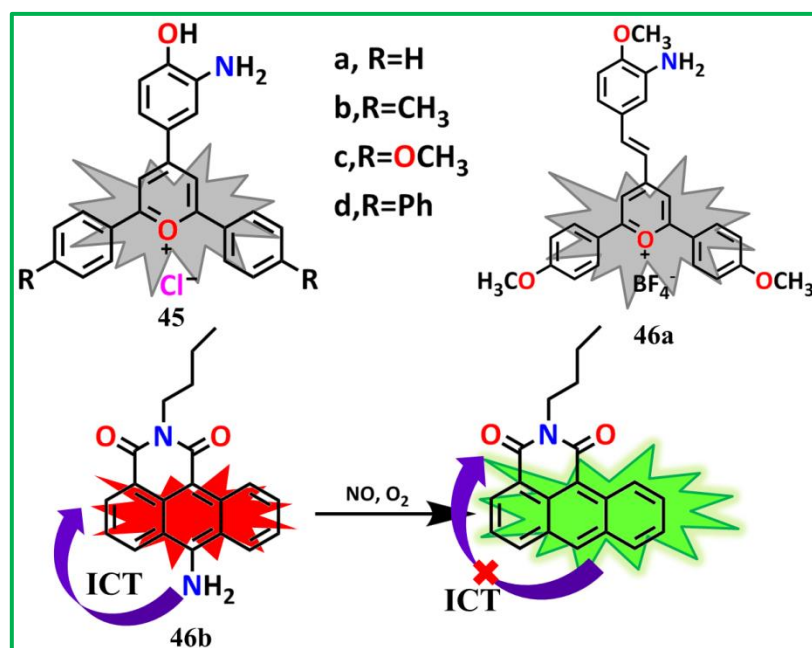


Figure 1.18. Reported various NO sensors based on deamination of aromatic primary amines.

Luis, Galindo and their research groups⁸⁴ introduced a series of NO sensitive fluorescent probes (**45-a**, **45-b**, **45-c**, **45-d**) (Figure 1.18) among which **45-c** ($\lambda_{em} = 550$ nm, $\lambda_{ex} = 470$ nm) is found to be the best with higher sensitivity (83 fold) as well as selectivity towards NO with LOD 2.1 μ M.

CHAPTER 1

X-ray crystallographic studies revealed that the sensing mechanism of the probe with nitric oxide occurs through oxidative de-amination. Now, in 2021, the same research group⁸⁵ developed a new mitochondria targeting pyrylium based sensor **46a** (Figure 1.18) without linking any mitochondria targeted unit. The probe exhibits enhancement in fluorescence intensity at 585 nm with high selectivity and sensitivity (LOD = 88 nM). The superiority of this probe was established by executing various biological experiments related with endogenous and exogenous detection of NO. An interesting dual channel NO sensor **46b** (Figure 1.18) was designed by Liu and coworkers⁸⁶ by utilizing oxidative deamination sensing mechanism on dicarboximide anthracene moiety. Due to ICT, on treatment with NO the probe changes its emission from red to green and this enhances its better applicability for analyzing endogenous NO in live cells.

1.4.1.2 (c) Cyclization of *o*-amino-3'-dimethylaminophenyl aromatics:

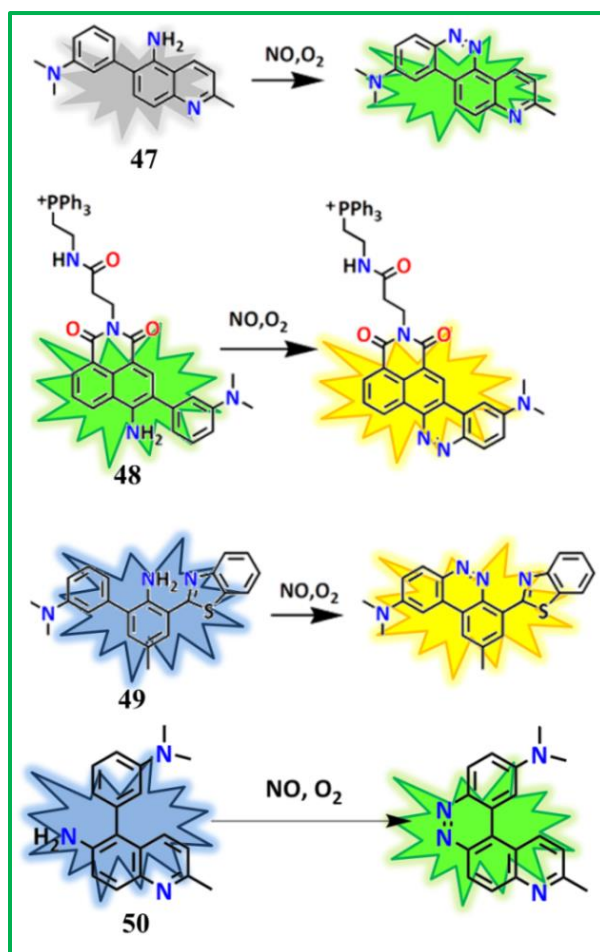


Figure 1.19. Sensing of NO through cyclization of *o*-amino-3'-dimethylaminophenyl aromatics.

CHAPTER 1

Another approach involving N-nitrosation of aromatic amine in *o*-amino-3'-dimethylaminophenyl aromatics plays a crucial role of NO trapping leading to the formation of highly fluorescent *ortho*- or *para*- azoic isomers.⁸⁷ In 2017, Zhou, Song and their research team⁸⁸ fabricated a novel NO sensitive probe **47** (Figure 1.19) in which 6-position of 5-aminoquinoline is directly linked with 3-dimethylaminophenyl moiety through C-C bond formation by exploiting Suzuki coupling reaction. Now, the reaction with NO generates two azoic regioisomers through the formation of diazonium ion as an intermediate. Among these two azoic regioisomers, one *p*-form is capable of enhancing fluorescence intensity through intramolecular charge transfer (ICT) mechanism. This *p*- form of azoic regioisomer is capable of detecting both endogenous and exogenous NO during biological studies under one and two photon environment. In the same year Zhang and coworkers⁸⁹ reported naphthalimide embedded mitochondria specific two-photon ratiometric NO probe **48** (Figure 1.19) using the same sensing strategy. The unique feature of this probe is that it changes its fluorescence region at 595 nm, a yellow region, to 540 nm, a green region, after addition of NO. This enhances its potentiality for recognizing NO in living cells and also in mice model. Another ratiometric probe **49** (Figure 1.19) was synthesized by Yoon et al.⁹⁰ in 2017. Upon exposure with NO the fluorescence region of this probe is also changed from blue to yellow (470 nm to 560 nm) by following the ESIPT sensing mechanism. The probe is also able to detect NO in living cells. The same research group⁹¹ in 2021 has developed a new ratiometric NO sensitive probe **50** (Figure 1.19) which is actually the positional isomer of reported NO sensitive probe **47**. Quick response of the probe towards NO enhances its capability to detect both exogenous and endogenous NO. The azoic product that produced upon addition of NO interacts with natural DNA. As in presence of natural DNA, fluorescence intensity of the probe **47** increases, indicating higher sensitivity towards NO (mainly in nucleus).

1.4.1.3. DIPY (dihydropyridine) based sensing strategy:

Literature survey reveals that for designing various nitric oxide sensitive fluorescent probes dihydropyridine entity can be employed as NO trapping unit.⁹² On interaction with NO, dihydropyridine undergoes aromatization reaction to generate pyridine which may result in fluorescence either increase or decrease through PET mechanism. In 2014, this dihydropyridine based sensing strategy is exploited by He et. al.⁹³ to design a new probe **51a** (Figure 1.20). Now,

CHAPTER 1

by considering this probe another nitric oxide sensitive probe **51b** (Figure 1.20) was subsequently synthesized by the same research group⁹⁴ and this probe (**51b**) is actually a positional isomer of **51a**. Both these NO probes are highly sensitive, selective and superior to other probes particularly for biological applications. The same research group⁹⁵ has synthesized a probe **52** (Figure 1.20) by creating a distance by two carbon atoms through an alkyl chain between the fluorophore (7-methoxy coumarin) and the dihydropyridine unit to analyze the long range interaction towards fluorescence sensing of NO via *PET-Off* mechanism. Probe **52** exhibits an enhancement in fluorescence signal (~80 fold) at 392 nm with high sensitivity (LOD=17nM) and is also capable of successful recognition of endogenous NO. Again, the introduction of a quaternary ammonium unit (hydrophilic part) into the probe **52**⁹⁶ leads to the development of the new probe **53** (Figure 1.20) with emission at 450 nm. The low LOD value of this probe makes its application successful for endogenous NO recognition.

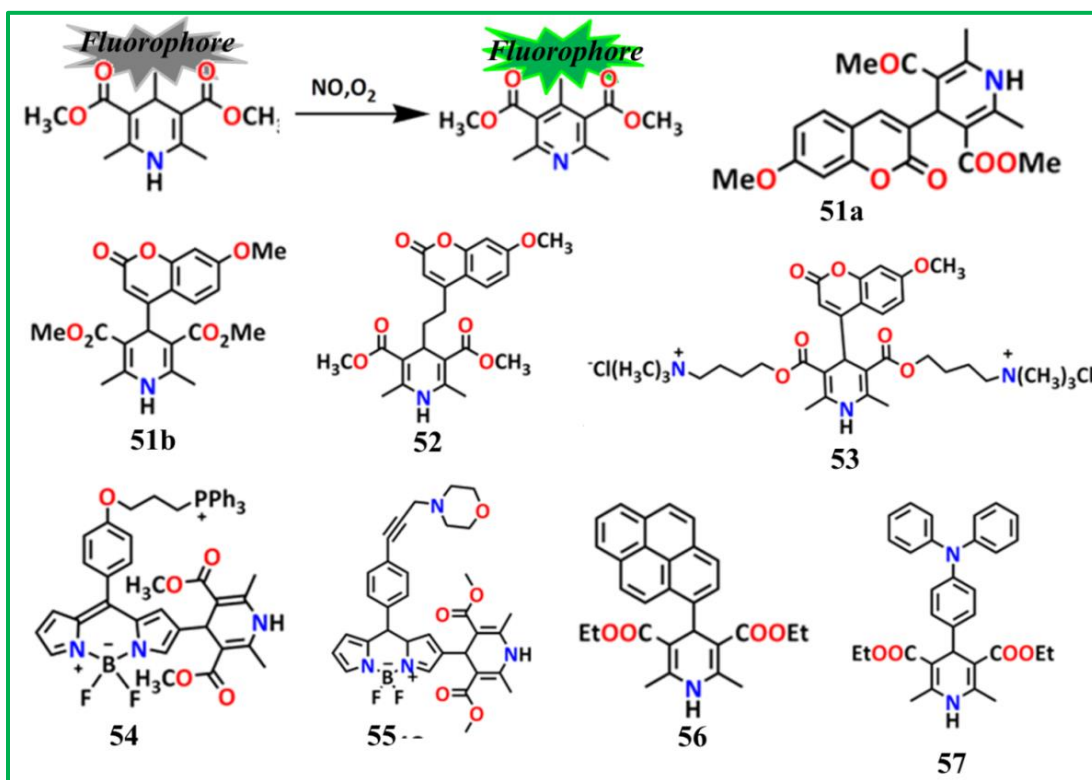


Figure 1.20. Reported dihydropyridine based NO sensor.

Lu, He and their research group^{97, 98} has developed two new dihydropyridine embedded BODIPY based mitochondria targeting **54** (Figure 1.20) and lysosome specific **55** (Figure 1.20)

CHAPTER 1

nitric oxide sensors. The 63 fold enhancement of fluorescence intensity in greener region ($\lambda_{\text{ex}}=470$ nm and $\lambda_{\text{em}}=525$ nm) for probe **54**, and 140 fold for probe **55**, ($\lambda_{\text{ex}}=475$ nm and $\lambda_{\text{em}}=535$ nm) were achieved on interaction with NO supporting the fact that both the probes are stand out to be a good NO sensitive sensors. Both the probes are applicable for endogenous and exogenous imaging of NO. Mahapatra *et. al.*,⁹⁹ has introduced two DHP based NO sensitive probes **56** (Figure 1.20) and **57** (Figure 1.20) that employ pyrene and triphenylamine units as fluorophoric units. Cellular applications were executed by utilizing probe **57** in thin epithelium Vero cells as it shows increase in fluorescence signal ($\lambda_{\text{ex}}=308$ nm and $\lambda_{\text{em}}=502$ nm) on addition of NO. However, pyrene based NO sensor **56** displays fluorescence quenching with high LOD value (2.6 μM).

Now, Zhang, Li and their research team¹⁰⁰ have designed an unique probe **58** (Figure 1.21) that cleaves the C-C bond following the FRET process instead of following the normal aromatization reaction pathway in NO sensing. Since this ratiometric NO sensitive probe ($\lambda_{\text{em}}=525$ nm, $\lambda_{\text{ex}}=490$ nm) demonstrates an approximately 8-fold difference between Freund's adjuvant-stimulated paws and normal rat paws after intravenous injection during biological investigations, it is the first successful example of fluorescence imaging of endogenous NO in mammals for cell imaging studies.

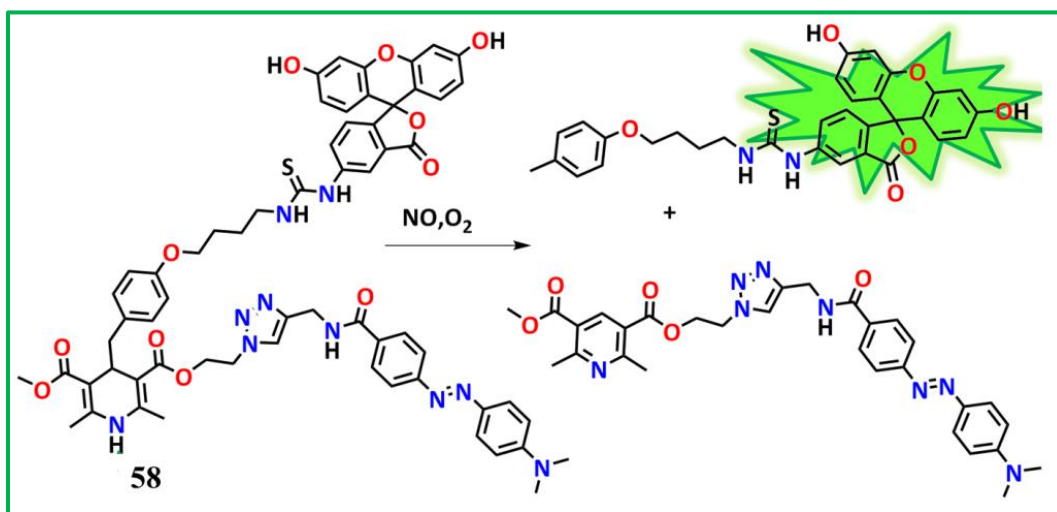


Figure 1.21. Unique mechanism of dihydropyridine based NO sensor.

CHAPTER 1

1.4.1.4. Unusual sensing strategies:

Recently, various fluorescent probes have been reported where unusual/ unprecedented NO sensing mechanisms were operative showing high selectivity and sensitivity for exogenous and endogenous detection of NO in living organisms. Inspired by Ohsawa et al.¹⁰¹, Song et al.¹⁰² designed a BODIPY based probe **59** (Figure 1.22) in which hydrazine was attached at its 8th position. Now, addition of NO generates a mixture of products where the major component is BODIPY and the minor component is 8-azido BODIPY. Enhancement (50 fold) in fluorescence intensity in greener region ($\lambda_{ex} = 480$ nm and $\lambda_{em} = 512$ nm) is due to generation of BODIPY, as 8-azido BODIPY is non-fluorescent in nature. The probe is capable of detecting endogenous NO in RAW 264.7 cells.

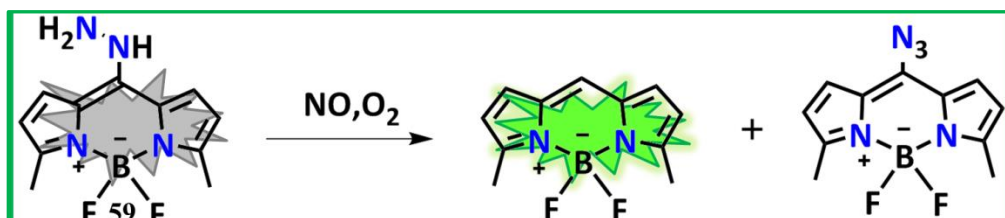


Figure 1.22. BODIPY based NO Sensor.

Inspired by the work of Hrabie's group¹⁰³, Li and Co-workers¹⁰⁴ also designed a two-photon Schiff base-based NO probes **60a** and **60b** (Figure 1.23). Here, treatment with NO causes enhancement in fluorescence due to formation of the fluorophoric aldehyde by the cleavage of azomethine bond of the Schiff base. The faster response time, lysosome targeting property and higher enhancement of fluorescence intensity (7.5-fold *visa-vis* 2.8 fold) for probe **60a** towards NO over **60b** makes **60a** more potent for biological applications.

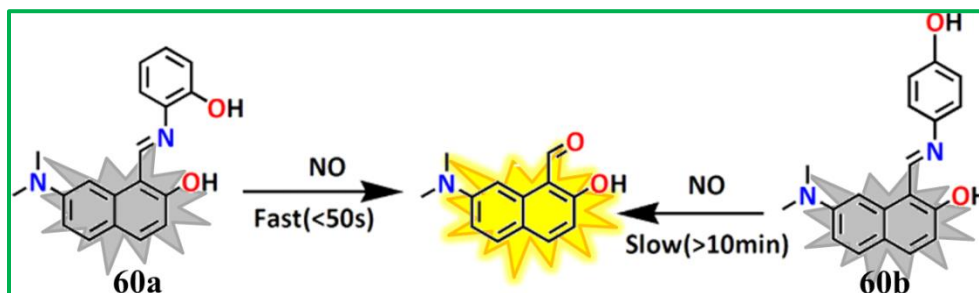


Figure 1.23. Schiff based related NO sensor.

CHAPTER 1

Ali and co-workers^{105, 106} has introduced a new sensing strategy for NO detection by synthesizing quinoline embedded thiosemicarbazide linked NO probe **61a** (Figure 1.24) which on reaction with NO generates 1,3,4-oxadiazole through elimination of thionitrous acid (HSNO) in quantitative yield. This gives an idea about the interconnection between NO and H₂S in biological systems. The probe **61a** has good sensitivity, high selectivity as well as a great biological application. Now, again the same research group has reported another new NO sensing strategy by considering the same fluorophoric entity with slight modification. The sensing pathway displays the formation of 1,2,3,4-oxatriazole in presence of NO upon excitation at 380 nm. The probe **61b** (Figure 1.24) is capable of detecting NO endogenously similar to probe **61a**. Kinetics assessment of both the probes indicates the first-order and 2nd-order dependencies on probe and NO concentrations, respectively.

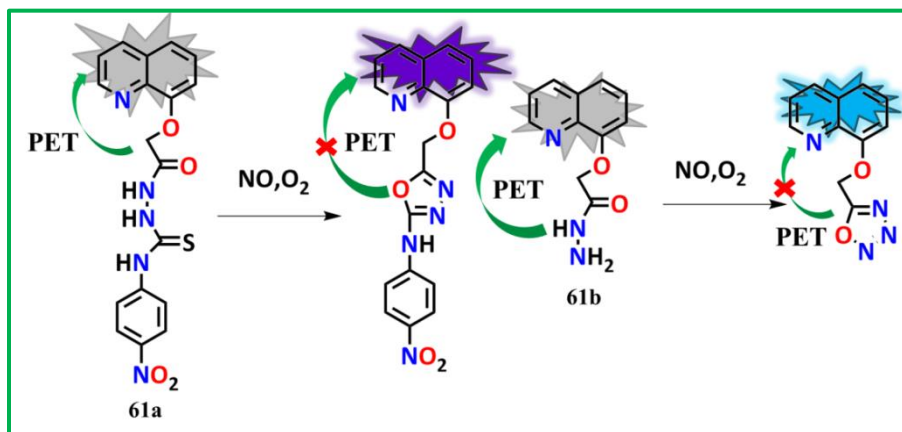


Figure 1.24. NO sensing strategy by forming oxadiazole and oxatriazole.

Influenced by Ali et al.¹⁰², Zhang group¹⁰⁷ reported a new NO sensor **62** (Figure 1.25) in which instead of quinoline, coumarin was used as fluorophore and thiosemicarbazide as NO receptor.

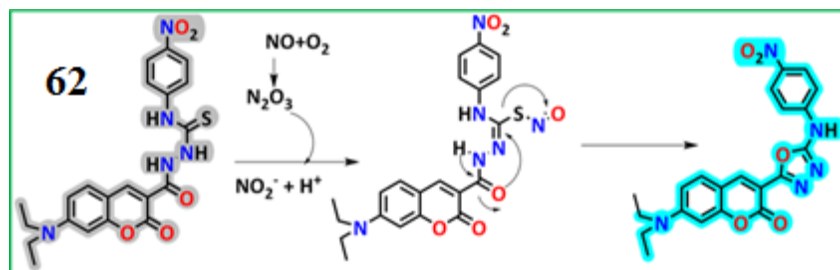


Figure 1.25. Coumarin embedded NO sensor.

CHAPTER 1

This probe **62** follows the similar sensing mechanism to that was exhibited by probe **61a** and there is an increase in fluorescence due to restriction of N-N bond rotation by forming oxadiazole. Biological investigations regarding endogenous and exogenous NO detection were executed in zebrafish model.

Another thiosemicarbazide linked naphthalimide based probe **63** (Figure 1.26) was reported by Kang, Lee and their research team.¹⁰⁸ The probe is capable of detecting cellular viscosity and NO simultaneously. The probe is non-fluorescent in nature but with increase in viscosity of the medium the rotation around the NH—NH bond in the Ph-NH-C(=S)-NH-NH-C(=O)- fragment is somehow restricted leading to an enhancement (λ_{em} = 470 nm, λ_{ex} = 405 nm) in fluorescence intensity. However, in case of NO detection, the sensing pathway is different. NO reacts with N-(4-nitrophenyl) thiosemicarbazide moiety followed by the cleavage of the Naphthalimide—N—C(=O) bond to generate Naphthalimide—NH₂ that is responsible for turn-ON response at 550 nm.

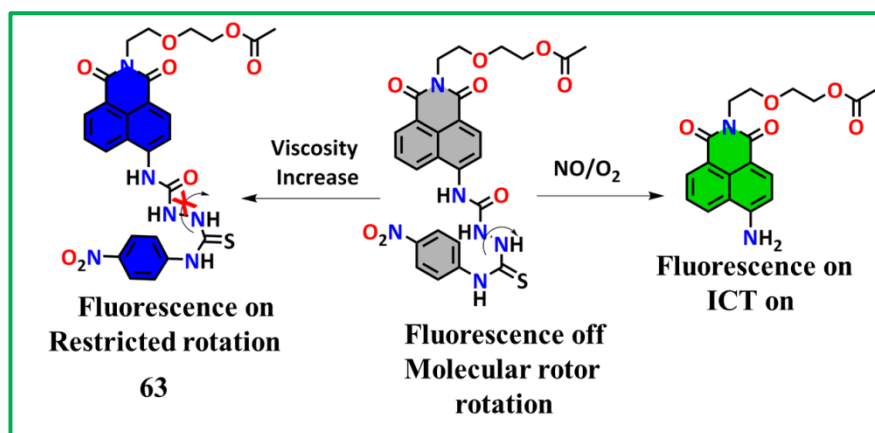


Figure 1.26. Naphthalimide based NO probe.

Recently, Lin et al.¹⁰⁹ designed a new cyanine-7 based mitochondria-targeted NO probe **64** (Figure 1.27) which instead of fluorescence enhancement (λ_{em} = 460 nm and 581 nm, λ_{ex} = 400 nm) becomes non-fluorescent on treatment with NO due to the formation of electron deficient 4H-pyrazole ring which inhibits the ICT process occurring between two indolium units. The biological applications of this mitochondria targeted probe were checked in HeLa cells and zebrafish model.

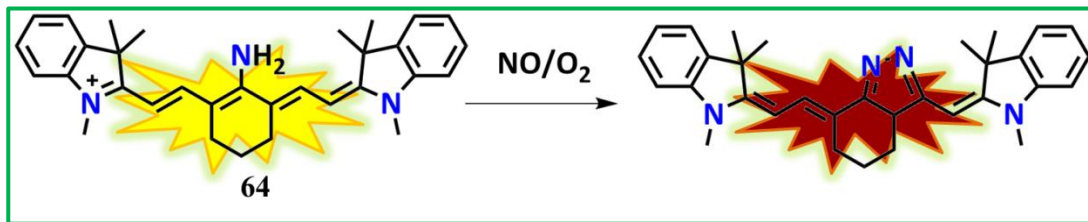


Figure 1.27. Unique sensing of cyanine7 based probe towards NO.

1.4.2. NO recognition strategy by utilizing metal-complex probe

Usually, fluorescent sensors based on organic molecules employed amines as NO recognition units where fluorescence enhancement occurs either due to (i) cyclization or (ii) N-nitrosation as the major reaction pathways. In many cases, these sensing approaches towards NO are interfered in biological environment. To overcome these limitations, researchers have been immensely interested in synthesizing various metal complex based fluorescent NO sensors.

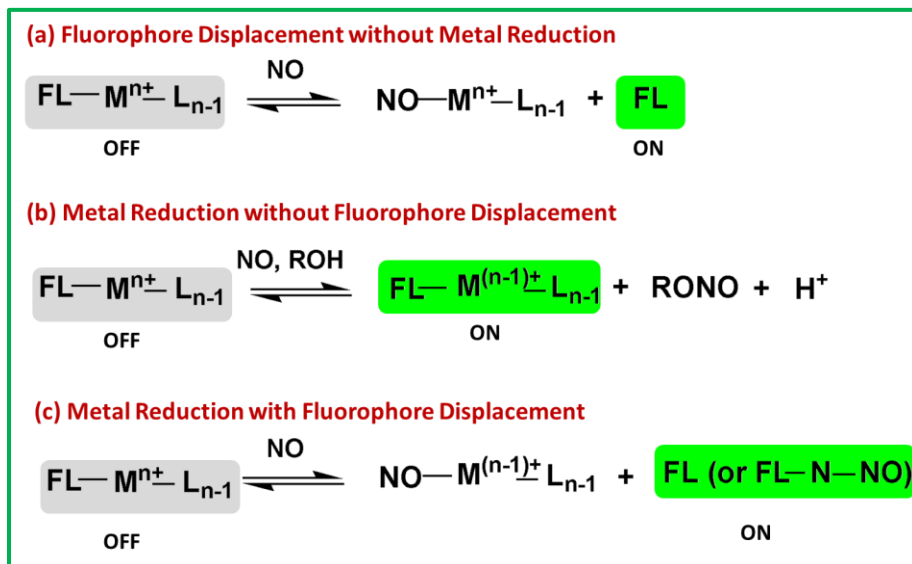


Figure 1.28. NO sensing pathways for metal bound probes.

The idea of utilizing transition metal complexes as NO sensing probes was advanced by Lippard and coworkers,¹¹⁰⁻¹¹⁷ which fall under three categories as outlined in Figure 1.28 and described below.

- **Fluorophore Displacement without Metal Reduction**

This type sensing strategy involves fluorescent quenching of the probe on coordination with the metal ion, which must be paramagnetic in nature. Now, the treatment of NO causes the restoration of fluorescence intensity by forming metal nitrosyl adduct with simultaneous release of fluorophore from the metal center (**Figure 1.28a**).¹¹⁸⁻¹²⁰

- **Metal Reduction without Fluorophore Displacement**

In this sensing strategy the presence of NO resulted in the restoration of fluorescence signal by reducing the paramagnetic metal ion to the diamagnetic one. The main requirement for this sensing strategy is the presence of protic solvent (ROH) which on interaction with NO form an alkyl nitrite (RONO) (**Figure 1.28b**).¹²¹

- **Metal Reduction with Fluorophore Displacement**

The last one is the most widely used sensing mechanism for NO. Copper based nitric oxide probes are included in this sensing approach. Here, reduction of metal ion from paramagnetic to diamagnetic state causes regeneration of fluorescence signal either by releasing the free probe or by coordinating nitric oxide with metal center/ bonding with free probe to form N-nitrosated adduct (**Figure 1.28c**).¹²²⁻¹²⁷

1.4.2.1. Reported Metal-based fluorescent sensors for NO detection

Chao et al.¹²⁸ designed a new iridium(III) complex **65** (**Figure 1.29**) for mitochondrial NO sensing which contains two monodentate 2-phenylquinoline and one 5,6-Diamino-1,10-phenanthroline ligands. The latter being used as a receptor of NO causing a 48 fold phosphorescence enhancement and also suitable for NO detection in living cells, 3D multicellular spheroids and also in Zebra fish. Inspired by this strategy, Ma and coworkers¹²⁹ introduced a similar iridium(III) complex **66** (**Figure 1.29**) that displays a 15 fold enhancement in fluorescence intensity at 580 nm through blocking of PET process by forming electron deficient 1,2,3-triazole. The biological studies by using this probe have yielded positive results.

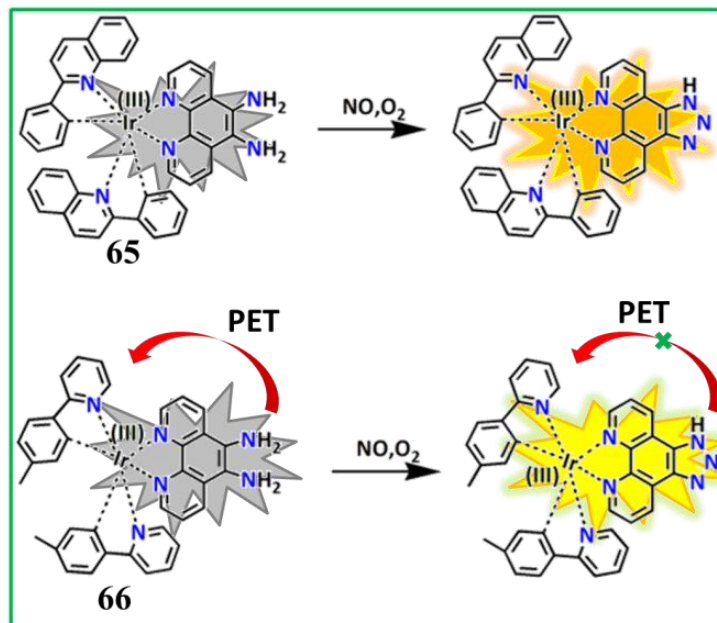


Figure 1.29. Iridium(III) complex based NO sensor.

Organelle specific fluorescent sensors are always interesting and more demanding for researchers due to their potentiality to *in vivo* applications. Various organelles specific NO sensors have been reported till now, but most of them suffer from some limitations like photo bleaching and accumulation of the probes in the organelles thereby increasing their local concentration which are highly essential to be overcome. Song, Yuan and their research groups¹³⁰ reported a lanthanide complex **67** (**Figure 1.30**) as luminophore to detect NO. Here, piperazine acts as a bridge between luminescent terbium (Tb^{3+}) complex (LTC) as an energy donor and 5-carboxy-N,N,N',N'-tetramethyl rhodamine (CTMR) as an energy acceptor.

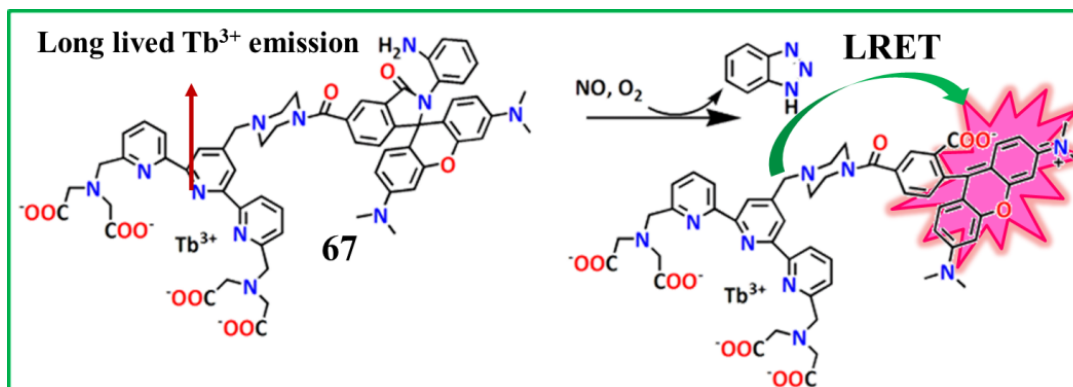


Figure 1.30. An example of lanthanide complex based ratiometric NO sensor.

CHAPTER 1

Now, the probe **67** itself delineates the luminescence due to inhibition of LRET (luminescence resonance energy transfer) mechanism which is not because of CTMR unit rather LTC, whereas the presence of NO favored the LRET process occurring from Tb^{3+} complex to rhodamine results in the generation of remarkable fluorescence emission (I_{565}/I_{540} , 28.8 fold) due to removal of triazole unit followed by spiro lactum ring opening. The probe can detect NO in *Daphnia magna*, an important species in ecosystem without any interference and Dye co-localization analysis also supports its ability to detect NO in lysosome precisely.

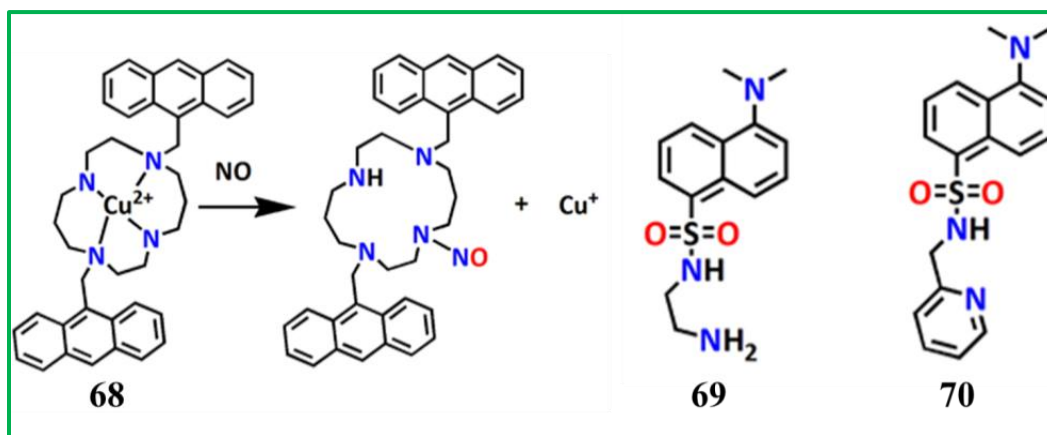


Figure 1.31. Some reported metal bound NO sensor.

In most of the transition metal complex based NO probes, Cu(II) is the most frequently used due to its efficient complexation with the fluorescent receptor molecules to give non-fluorescent species and easy reduction to the corresponding diamagnetic Cu(I) ion by NO to restore its fluorescence. In most of the cases, the mechanism involves the reduction of the metal by fluorophore displacement with or without N-nitrosation. Ford and his research group¹²⁷ designed an anthracene-tetraamine cyclam based Cu(II) complex **68** (Figure 1.31) which follows the same sensing pathway by forming N-nitrosated product of the anthracene-tetraamine cyclam. Lippard et al.¹¹⁶ also introduced two water soluble probes **69** and **70** (Figure 1.31) which exhibit 6 and 8 fold enhancement in fluorescence signal, respectively. In addition to that, the same research group¹³¹ reported a series of seminaphtho-fluorescein based probe **71** (Figure 1.32) which also follows the same NO sensing strategy. Biological experiments for endogenous nitric oxide recognition were performed in RAW264.7 cells without any interference.

CHAPTER 1

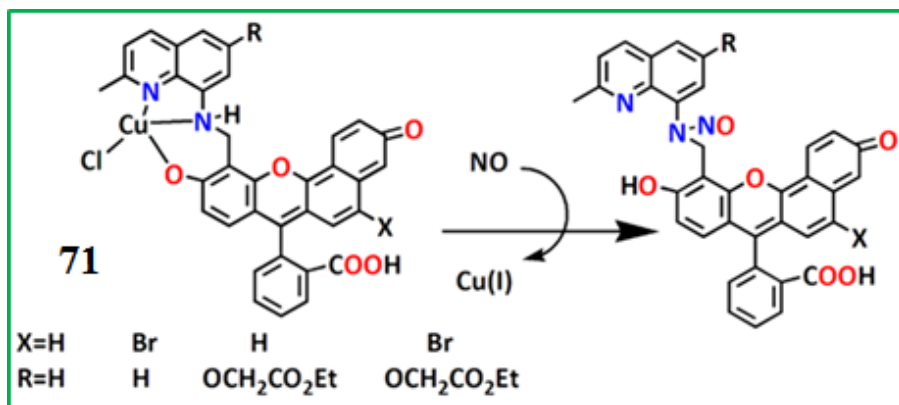


Figure 1.32. Series of seminaphtho-fluorescein based NO sensor.

James and his colleague¹³² reported a good NO probe **72** (Figure 1.33) by employing 1,8-naphthalimide as a fluorophore and 8-aminoquinoline as a Cu(II) binding site. The unique feature of this probe is that it has the potential to detect both NO and HNO simultaneously in living organisms where N-nitrosation of the free probe is responsible for fluorescence enhancement (for NO ~18 fold and for HNO ~32 fold).

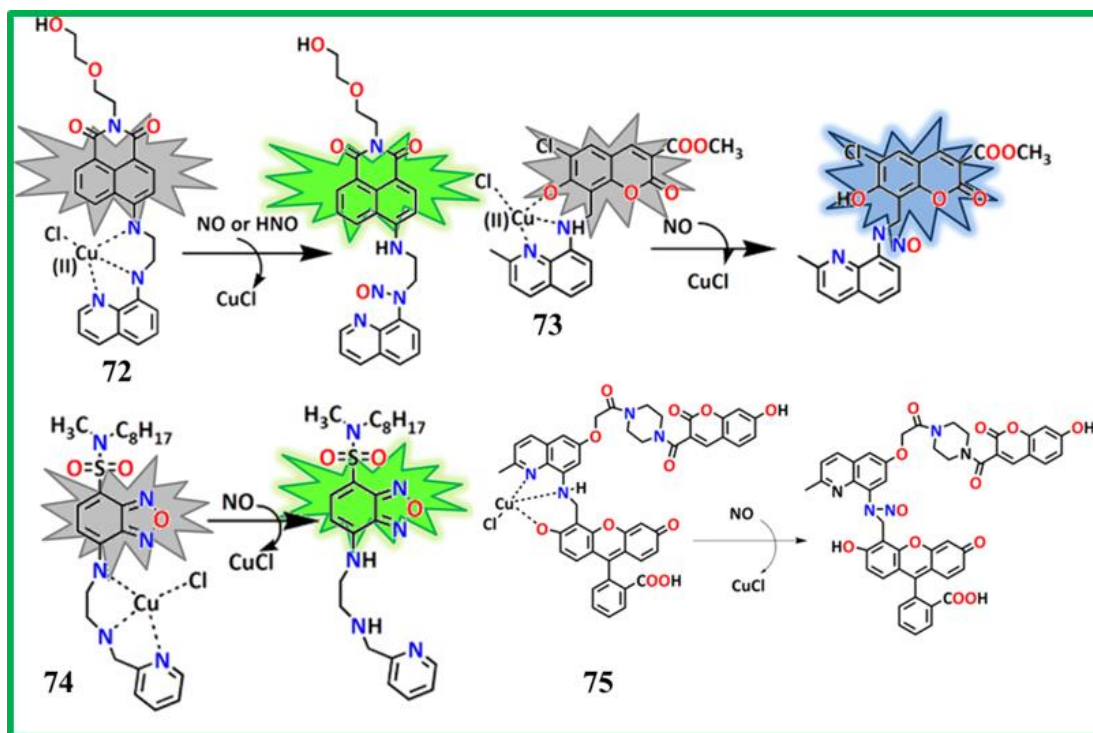


Figure 1.33. Reported metal bound NO probes with different fluorophoric entities.

CHAPTER 1

Norton et al.¹³³ reported a good NO sensing probe **73** (Figure 1.33) where coumarin serves the role of fluorophore ($\lambda_{em} = 445$ nm, $\lambda_{ex} = 405$ nm) and is able to detect mitochondrial NO. Vilar and coworkers¹³⁴ designed a copper complex based NO probe **74** (Figure 1.33) by attaching a linker between pyridyl unit and a 4-N-octyl-N-methylaminosulfonyl-7-chloro-2,1,3-benzoxadiazole which on treatment with NO enhances the fluorescence intensity ($\lambda_{em} = 580$ nm) by releasing the free probe. Lippard and his coworkers¹³⁵ has reported first ratiometric copper(II) complex based probe **75** (Figure 1.33) by using piperazine as a spacer between the derivatives of hydroxycoumarin and fluorescein for the detection of nitric oxide. Enhancement in fluorescent intensity ($F_{fluorescein}/F_{coumarin} = \sim 11$ fold) arises due to formation of N-nitrosated derivative of the probe by following the Förster resonance energy transfer (FRET) process.

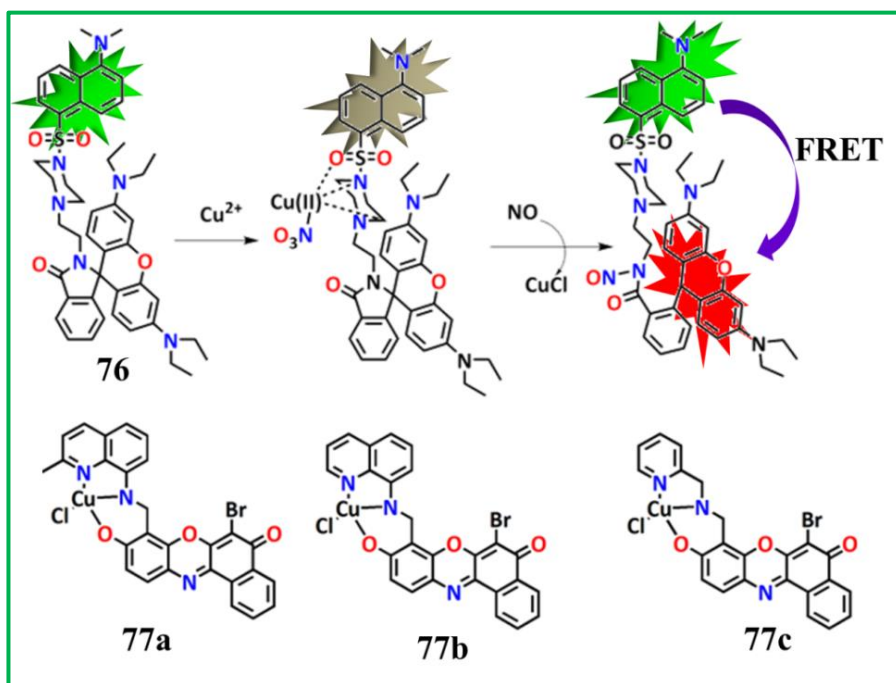


Figure 1.34. Rhodamine and benzoresorufin based NO sensor.

Another ratiometric Cu(II) complex based NO sensor **76** (Figure 1.34) was reported by Patra et al.¹³⁶ by using the same piperazine unit as a spacer between rhodamine B and dansyl entity. The intensity of green fluorescence arising out of dansyl groups is quenched upon treatment with Cu(II) ions but the presence of NO reduces Cu(II) to Cu(I) facilitating the rhodamine emission (at 580 nm, ~ 750 fold with LOD value 1nM) through FRET process. Lippard and his

CHAPTER 1

coworkers¹³⁷ has synthesized a series of benzoessorufin-based Cu(II) bound probes **77a**, **77b**, **77c** (**Figure 1.34**) which exhibit enhancement in fluorescence intensity at 625 nm on treatment with NO/HNO. For NO, the enhancement is due to formation of N-nitrosated derivative of the metal free probe whereas for HNO, no N-nitrosation reaction occurs. Both NO and HNO detections have successfully done in biological samples indicating the potentiality of the probe to recognize biological NO/HNO.

Duan and his research team¹³⁸ reported a rhodamine embedded triethylene tetraamine (tren) based copper(II) bound probe **78** (**Figure 1.35**). In the presence of NO the probe forms N-nitrosated spiro-lactum ring opened rhodamine derivative which is responsible for the increase in fluorescence signal.

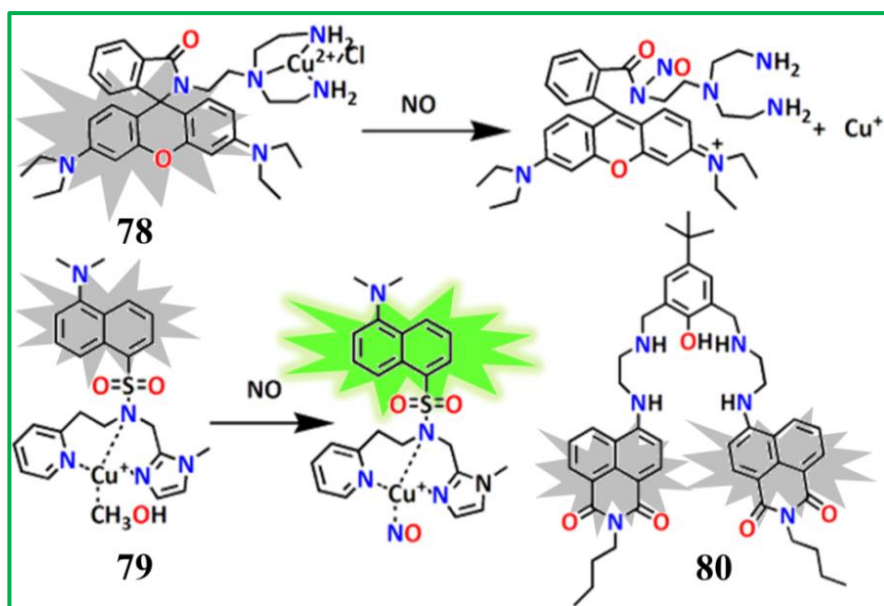


Figure 1.35. Example of metal complex based NO sensor.

The unique feature of probe **78** is the 700 fold fluorescence enhancement in pure aqueous medium (LOD= 1nM) making it suitable for endogenous NO recognition in living organisms. Mondal *et. al.*,¹³⁹ also reported a new Cu(II) complex based probe **79** (**Figure 1.35**) in which dansyl fluorophore is attached to a tridentate N-donor ligand. The non-fluorescent Cu(II) probe exhibits an increase in fluorescence intensity (8.3 fold, $\lambda_{em} \approx 555$ nm) in the presence of NO where the paramagnetic Cu(II) is reduced to diamagnetic Cu(I). Duan *et. al.*,¹⁴⁰ designed a new NO sensor **80** (**Figure 1.35**) containing naphthalimide as a fluorophore unit and N₄O donor unit

CHAPTER 1

as receptor. Here, formation of N-nitrosated probe in metal free state results in fluorescence enhancement ($\lambda_{em}=530$ nm, $\lambda_{ex}=466$ nm, ~ 8-fold). Cellular studies were also executed for testing its *in vitro* application.

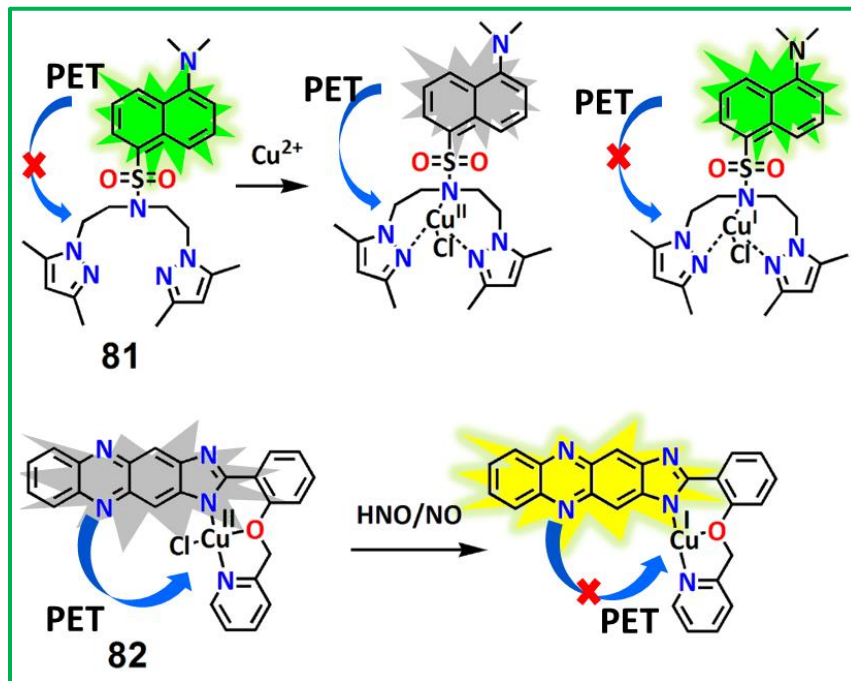


Figure 1.36. Example of metal complex based NO sensor

Ali *et. al.*^{141, 142} synthesized two new fluorescent probes **81** (Figure 1.36) and **82** (Figure 1.36) with dansyl as fluorophore moiety for the former and phenazine for the latter. Both follow a similar sensing mechanism where complexation with Cu(II) ion causes quenching of fluorescence. However, on further treatment with NO reduction of Cu(II) to Cu(I) occurs as evidenced by EPR studies, leading to restoration of fluorescence properties (for **81** $\lambda_{em}=532$ nm, $\lambda_{ex}=345$ nm, ~15 fold and for **82** $\lambda_{em}=560$ nm, $\lambda_{ex}=400$ nm ~5 fold). Biological investigations indicate the superiority of these probes to recognize nitric oxide.

1.5. Nitroxyl

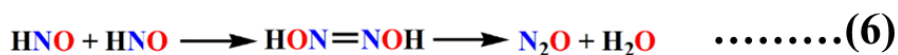
Recent advances in nitric oxide chemistry reveal that both nitric oxide and other nitrogen oxides play a key role in various physiological and pathophysiological processes. Moreover, among all other nitrogen oxides, "azanone", an electron-reduced and protonated derivative of NO, has acquired

CHAPTER 1

an immense attention from researchers.⁹ The existence of HNO during the photolysis of methyl nitrite in an argon matrix was established spectroscopically by Brown and Pimentel in 1958.¹⁴³

1.5.1. Why HNO, among all other nitrogen oxides?

- Among various simple nitrogen oxides, HNO is found to be relatively stranger in comparison to others. Now, because of its shorter life time, (rapid dimerization followed by its dehydration to nitrous oxide (N₂O)) the endogenous detection of HNO is still a challenging task for chemists.



Researchers are not fully familiar with the physiological mechanisms for endogenous generation of HNO yet.¹⁴⁴

- There are some specific thiol proteins (mostly related to heart failure response) that are used as biological targets for HNO. This is because interaction with HNO causes slight modification in cysteine residues, but why this specification towards this kind of thiol proteins are still remain undiscovered.¹⁴⁵

The physiological and pathological roles of HNO in biological systems are still a matter of debate.

- **Essential key role of HNO (nitroxyl) in biological milieu**

HNO acts as a potent vasorelaxant as exhibited by NO. Recent studies revealed the potentiality of HNO as a pharmacological agent to treat heart failure, alcoholism and so on.¹⁴⁶ These observations motivated the researchers to develop drugs which can be a source of HNO for treating heart diseases. It has been evidenced that HNO interacts with thiol proteins and peptides that are present in our living systems, such as myocardial thiol proteins, to recover from heart failure through opening of voltage-gated Ca²⁺ channels facilitating the release of CGRP (Calcitonin gene-related peptide).¹⁴⁷ HNO is also considered as an EDHF (endothelium-derived hyperpolarizing factor) similar to EDRF (Endothelium-derived relaxing factor) exhibited by NO in vascular system.¹⁴⁵ So, chemists and biologists are actively engaged in exploring the contribution of HNO in biological systems.

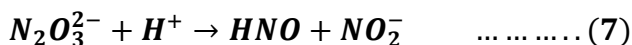
CHAPTER 1

1.5.2. Source of HNO

Now the usage of HNO donors is essential as HNO undergoes rapid dimerization followed by its dehydration to nitrous oxide (N₂O). Various stable HNO donors for example *1. Angeli's salt 2. Piloty's acid and derivatives 3. Diazeniumdiolates 4. Nitrosocarbonyls 5. Hydroxylamine 6. Cyanamide 7. Acyloxy nitroso compounds* are synthesized and discussed below briefly.

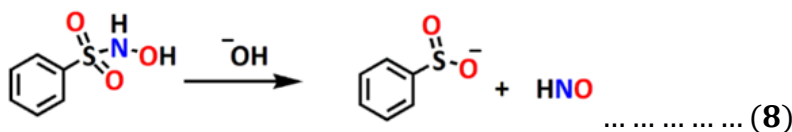
1.5.2.1. Angeli's salt

Most of the research related to pharmacological as well as physiological role of HNO have been performed by considering Angeli's salt (AS), sodium trioxodinitrate (Na₂N₂O₃), as the source of HNO.^{148, 149} It is easy to synthesize and undergoes decomposition to produce HNO and NO₂⁻ in neutral aqueous solution. Now this conversion from Na₂N₂O₃ to HNO and NO₂⁻ is pH dependent. Though AS is stable at higher pH, but generates NO at acidic pH.¹⁴⁸ So, precautions have to be taken while executing experiments in acidic conditions.



1.5.2.2. Piloty's acid and derivatives

To avoid the pH limitation of AS, Piloty's acid (N-hydroxysulfenamides) and its derivatives are used as HNO source at lower pH¹⁵⁰ where rate of release of HNO is enhanced with increase in pH. The major drawback of Piloty's acid is that it liberates NO, instead of HNO at biological pH.¹⁵¹

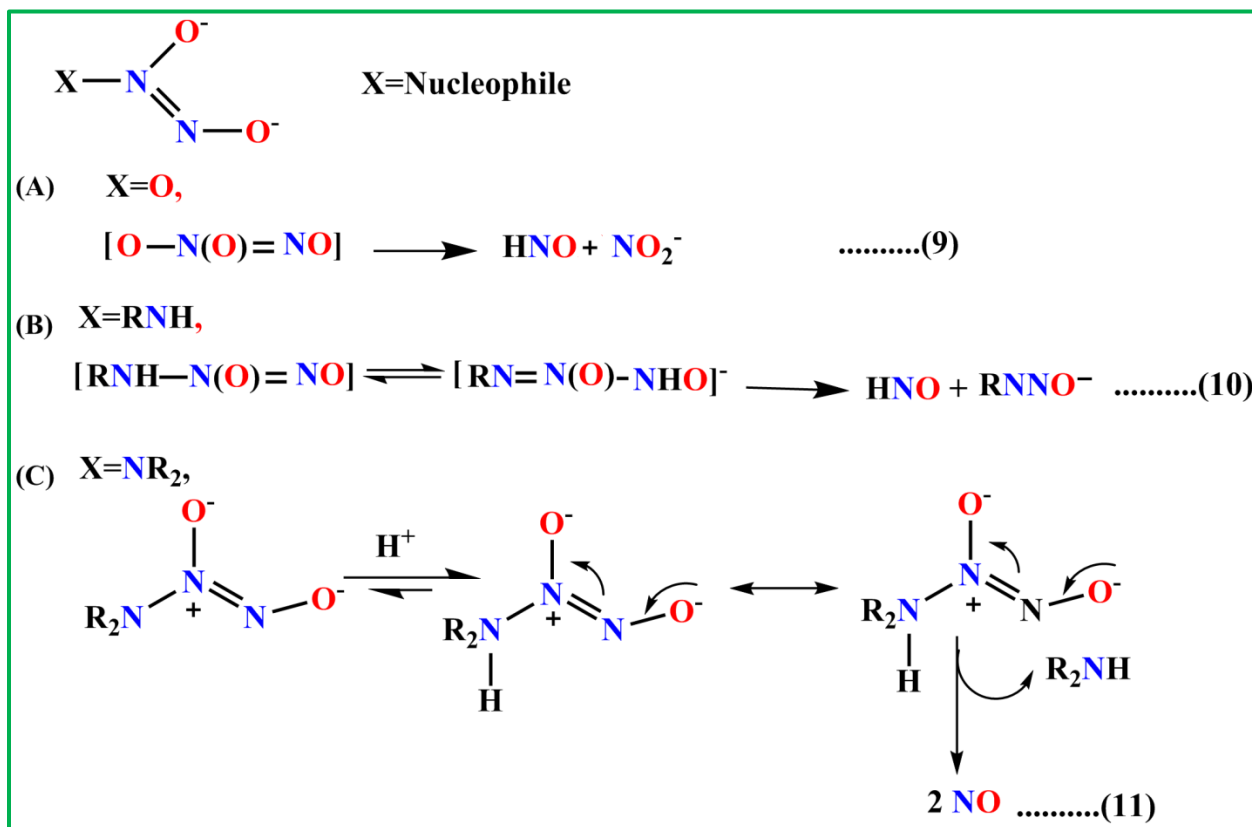


1.5.2.3. Diazeniumdiolates

Diazeniumdiolates ((⁻X—N(O)=NO⁻)) mostly referred as “NONOates”) generates both NO or HNO depending upon the nature of the nucleophile (X)¹⁵² used as given below:

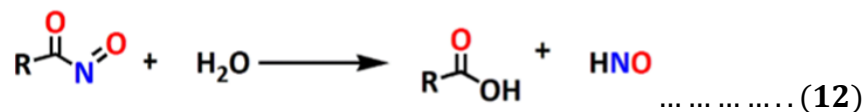
- (a) X = O diazeniumdiolate is nothing but AS, a source of HNO,
- (b) X=RNH, acts as an exclusive source of HNO
- (c) X=R₂N, acts as an exclusive source of NO

CHAPTER 1



1.5.2.4. Nitrosocarbonyls

Nitrosocarbonyls [RC(O)(NO)], unstable species, produce HNO and the corresponding carboxylic acid (RCOOH) in aqueous solution.

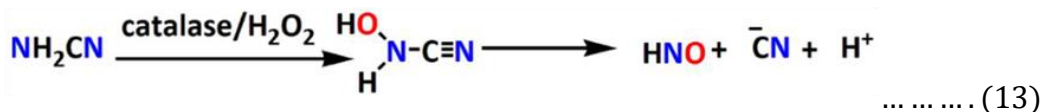


1.5.2.5. Hydroxylamine

It is experimentally found that successive reduction of NO produces NH₂OH by forming HNO, N₂ (as well as ·NHOH) as an intermediate. ¹⁵²

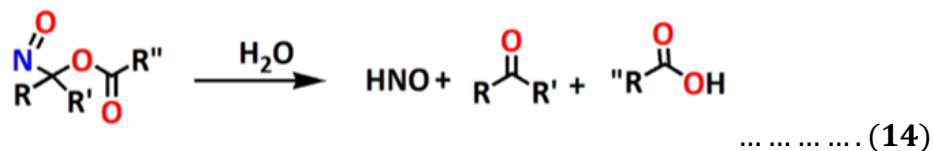
1.5.2.6. Cyanamide

Cyanamide is an anti-alcoholism drug and also serves as HNO donors (Eqn. 13) in cardiovascular related diseases. ¹⁵³



1.5.2.7. Acyloxy nitroso compounds

King et al.¹⁵⁴ has developed a new α -acyloxy-C-nitroso based compounds that act as a source of HNO and can be prepared by the oxidation of oximes (Eqn. 14). Under biological conditions these compounds are able to release HNO either through ester hydrolysis or via esterase activity but the HNO release rate depends upon the nature of organic groups. Because of this structural adjustability, this type of HNO donors plays a significant role in drug related researches.



1.5.3. HNO detection

Now, HNO detection is more challenging compare to NO because HNO undergoes self-dimerization to produce nitrous oxide (N₂O) and water (Eqn. 6). As N₂O or other side products are being produced quantitatively during decomposition of HNO, this may be quantified indirectly through headspace gas chromatography for N₂O, high-performance liquid chromatography, mass spectroscopy (HPLC-MS), and electron paramagnetic resonance (EPR) spectroscopy for other side products.¹⁵⁵⁻¹⁵⁸ Fluorescence imaging is thought to be the most promising approach in comparison to others for analyzing endogenous HNO and its biological role. Various fluorescence strategies that are involved in recognition of HNO (Figure 1.37) in physiological systems are:

- (A) Non-fluorescent copper-bound probes (Figure 1.37A).
- (B) Triphenylphosphine-based probes (Staudinger ligation) (Figure 1.37B).
- (C) N-nitroxide-based probes (Figure 1.37C).
- (D) 2-mercapto-2-methylpropionic acid with the fluorophore (Figure 1.37D).

Fluorescence based HNO probes are best suited to locate and estimate the level of HNO in biological systems.

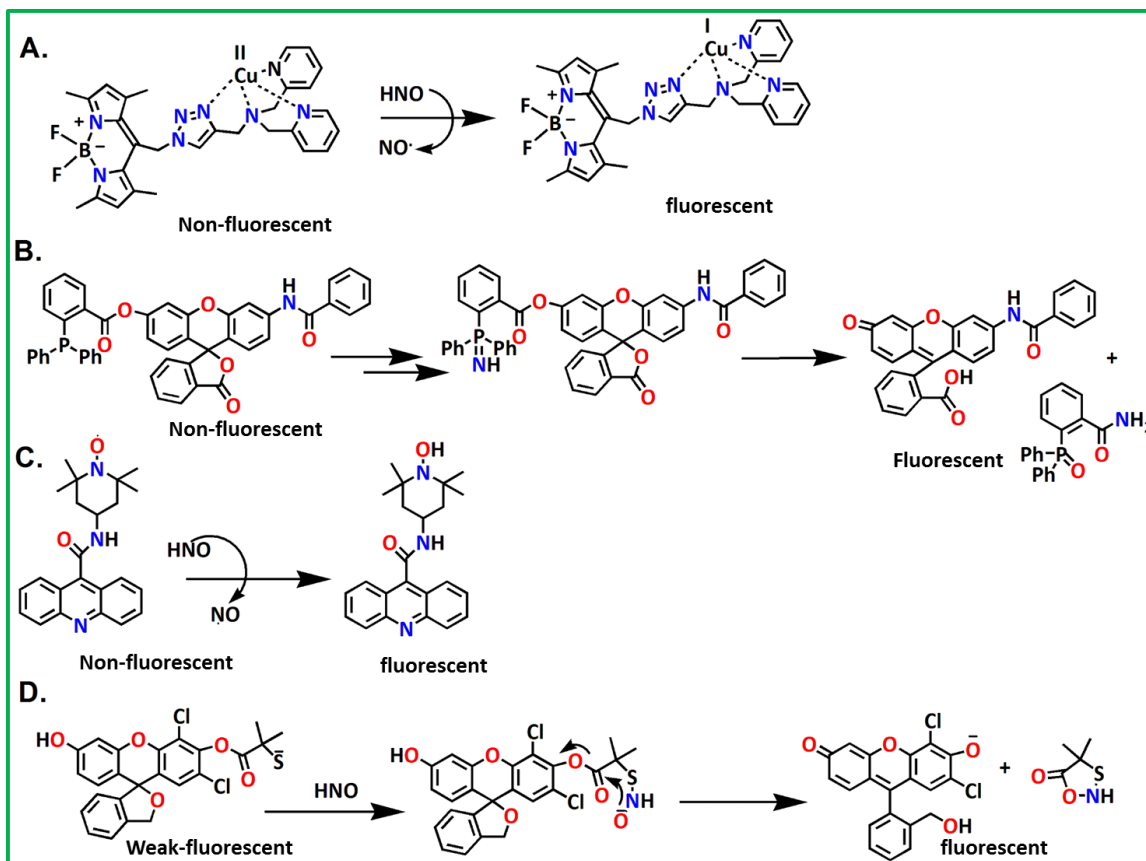


Figure 1.37. The reported recognition strategies of HNO like A. reduction of Cu(II) r complex, B. Staudinger ligation of triphenylphosphine, C. proton abstraction by nitroxide radical, D. fluorophore regeneration from 2-mercapto-2-methylpropionic acid.

1.5.3.1. Cu(II) complex based HNO Probes

Doctorovich and team¹⁵⁶ has proposed the discrimination between HNO and NO by synthesizing Mn(III) porphyrins **83** (Figure 1.38) that are insensitive towards NO. Upon treatment with HNO donors (AS and TSHA), Mn^{III} porphyrins generates {MnNO}⁷ which is responsible for quick and specific interaction of the probe with HNO.

CHAPTER 1

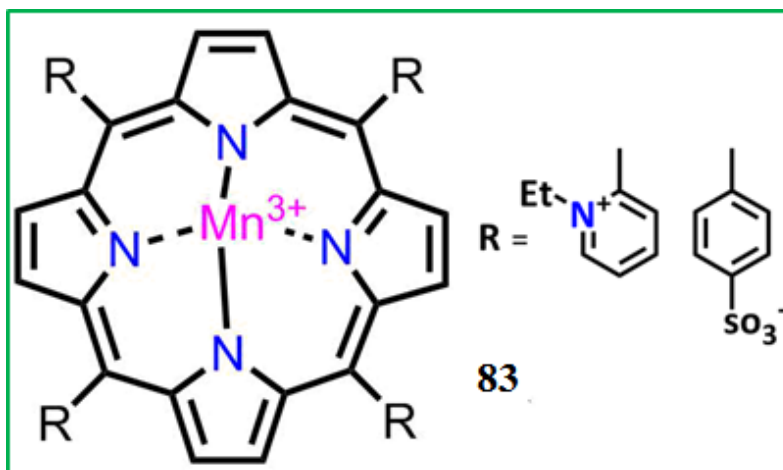


Figure 1.38. Probe that discriminate NO and HNO.

Now, the interaction of HNO with metal complexes was further extended by Lippard et al.¹⁵⁹

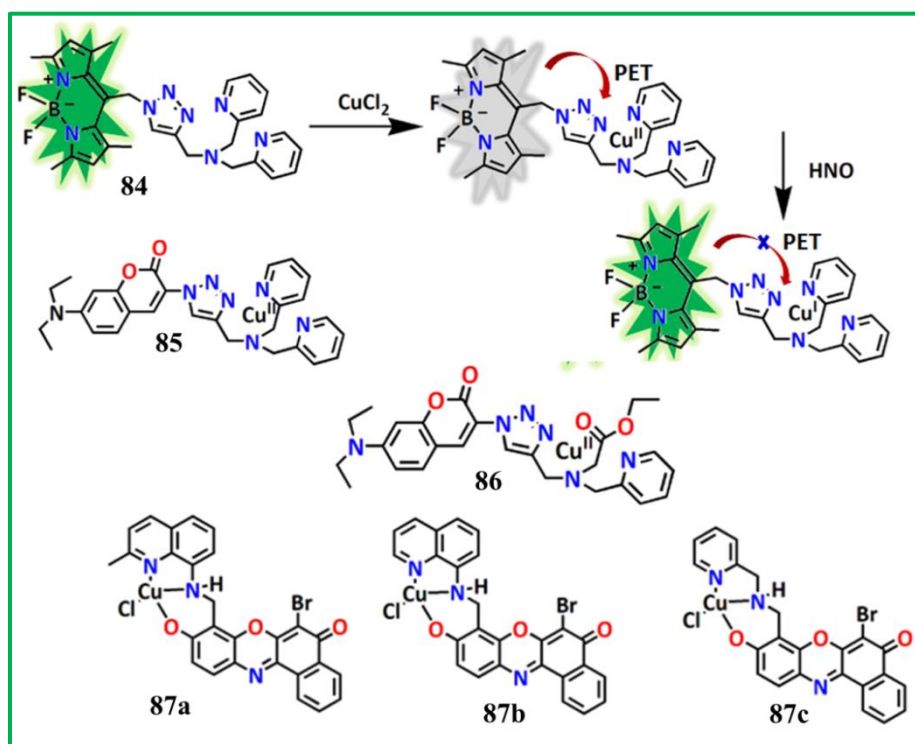


Figure 1.39. Copper complex based HNO sensor.

A Cu(II) bound BODIPY-based probe **84** (Figure 1.39) was used, for the first time, to detect HNO in biological systems having both excitation and emission wavelengths in the visible region. In this case, a triazole unit acts as a bridge between a tripodal dipicolylamine based

CHAPTER 1

receptor and BODIPY fluorophore. Treatment with Angeli's salt reduces Cu(II) to Cu(I) with 4.3 fold ($\lambda_{\text{ex}} = 450 \text{ nm}$) enhancement in fluorescence intensity at 526 nm. Inspired by this sensing strategy, Yao and group¹⁶⁰ developed a probe **85** (Figure 1.39), similar to **84** having coumarin fluorophore instead of BODIPY. In this case, HNO induced Cu(II) \rightarrow Cu(I) reduction was supported by fluorescence enhancement and EPR spectroscopy. The Cu(II) \rightarrow Cu(I) reduction leading to 17.3 fold enhancement in fluorescence intensity at 499 nm making it suitable for HNO detection in biological systems. The same group¹⁶¹ also reported another HNO probe **86** (Figure 1.39) keeping fluorophoric unit intact but replacing one of the pyridine unit by an ester group for better cellular applications (*in vivo*). The probe **86** suffers from some limitations like high energy absorption (in UV or near UV region) and a relatively short Stokes shift. To overcome this problem, Lippard's group¹³⁷ developed a series of benzoessorufin appended NIR-based Cu bound probes **87a**, **87b** and **87c** (Figure 1.39) with slight modifications. Here the sensing strategy is different from the probes cited above on the fact that here Cu(II) \rightarrow Cu(I), makes the complex unstable facilitating the release of free Cu(I) resulting an enhancement in fluorescence intensity. In 2014, the same research group introduced a NIR based fluorescent sensor¹⁶² capable of detecting HNO selectively over other biological interfering species. The Cu bound probe **88** (Figure 1.40) is also designed by employing dihydroxanthene (DHX) as a fluorophore and a cyclam derivative as a Cu(II) binding site to detect HNO in physiological systems. Another breakthrough approach regarding HNO recognition was proposed by the same research group¹⁶³ by fabricating a HNO probe **89** (Figure 1.40) with a linker between tetramethyl-rhodamine unit and the copper chelating scaffold cyclam. The ability to discriminate nitroxyl with thiols ($\lambda_{\text{em}} = 580 \text{ nm}$) makes this probe suitable for analyzing the biological HNO.

James *et al.*¹³² reported new water soluble Cu bound probe **90** (Figure 1.40) where ethylenediamine acts as a bridge between two fluorophoric units like naphthalimide and 8-aminoquinoline. This probe is capable of detecting both NO and HNO employing a new sensing strategy for HNO where it forms N-nitrosated product of the metal free probe resulting an increase in fluorescence intensity. Wang *et al.*¹⁶⁴ developed a new benzothiazole based copper bound probe **91** (Figure 1.40) where reduction of Cu(II) to Cu(I) is responsible for the enhancement in fluorescence signal ($\lambda_{\text{em}} = 450 \text{ nm}$, $\lambda_{\text{ex}} = 358 \text{ nm}$, LOD = 9.05 μM). Biological applications were checked by using zebrafish model and living organisms. Xing and coworkers¹⁶⁵ reported a dual sensor **92** (Figure 1.40) for H₂S and HNO by employing hemicyanine attached

CHAPTER 1

carbazole as a fluorophoric unit and bipyridine-triazole-Cu(II) complex as a receptor. On treatment with HNO, there is an increment ($\lambda_{em} = 595 \text{ nm}$) in fluorescence emission and was found to be successful in biological applications.

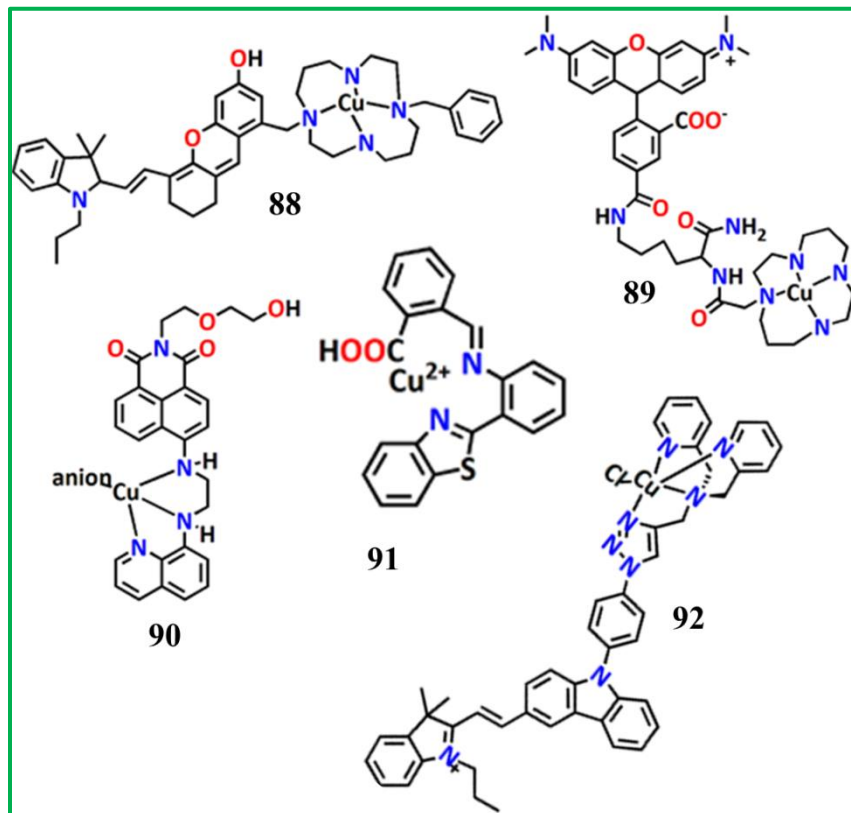


Figure 1.40. Reported various HNO sensors with copper bound fluorogenic unit.

1.5.3.2. Triphenylphosphine-based (Staudinger ligation) HNO probes

Triphenylphosphine (Staudinger ligation) based HNO probes immensely useful due to its abiotic behavior and unreactive nature towards various biomolecules in living systems.^{166, 167} Compared to metal based HNO probes, metal-free triphenylphosphine-based HNO probes are mostly reductant-resistant and display high positive fluorescence response. This sensing strategy involves the generation of transient five membered cyclic intermediate by an intramolecular attack of ylide amine to the carbonyl center of the ester unit. Now, it acquires stabilization by the release of an alcohol and the resulting species undergoes hydrolyzation to produce benzamide phosphine oxide, the HNO recognition unit. (Figure 1.41)

CHAPTER 1

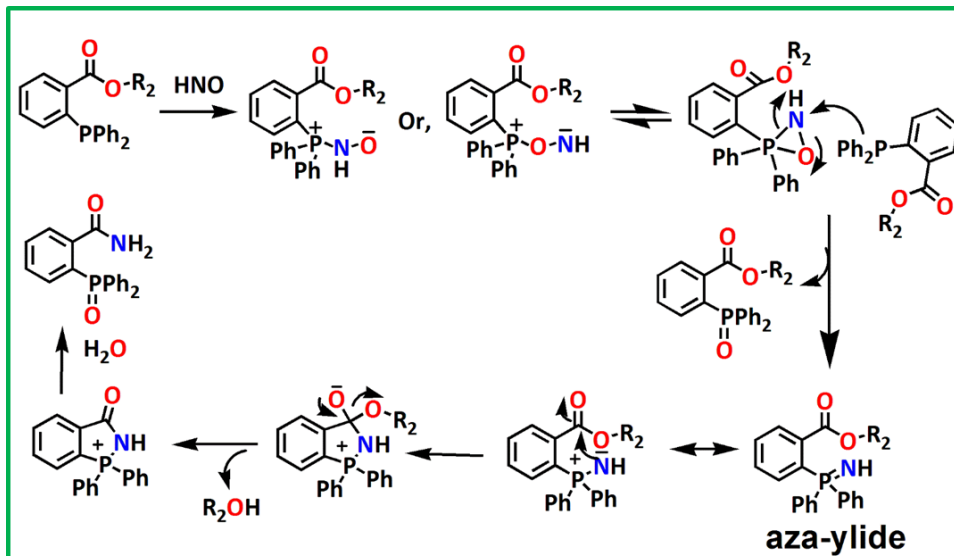


Figure 1.41. Mechanistic pathway for Staudinger ligation based HNO sensor.

Following this sensing strategy, Nakagawa *et al.*¹⁶⁸ first reported a metal free and reductant resistant HNO probe **93** (Figure 1.42) which was derived by employing acylated derivative of amino rhodol as a fluorophoric unit. Huge increment in fluorescence intensity makes this probe highly preferential for recognition of HNO as supported by cellular studies in A549 cells. The probe has attracted an immense attention of the researchers to study the role of HNO in biological systems.

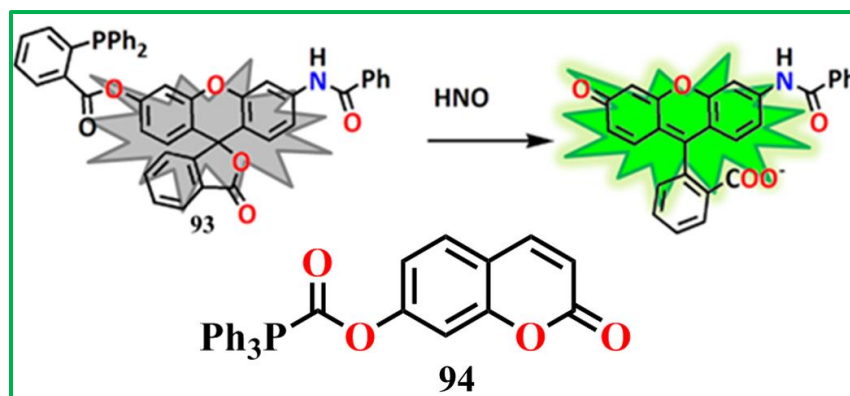


Figure 1.42. First Staudinger-ligation based HNO sensor reported by Nakagawa.

Zhang and co-workers¹⁶⁹ have designed a coumarin based HNO sensor **94** (Figure 1.42) which displays an increment in fluorescence signal at 450 nm in aqueous solution. The same

CHAPTER 1

experiment when repeated with bovine serum, the reactivity is somewhat less due to interaction of HNO with thiols but the probe is able to detect HNO in the presence of BSA.

Various Staudinger-ligation based HNO sensors **95-105** are mentioned here with their salient characteristics and biological applications (Figure 1.43).¹⁷⁰⁻¹⁸²

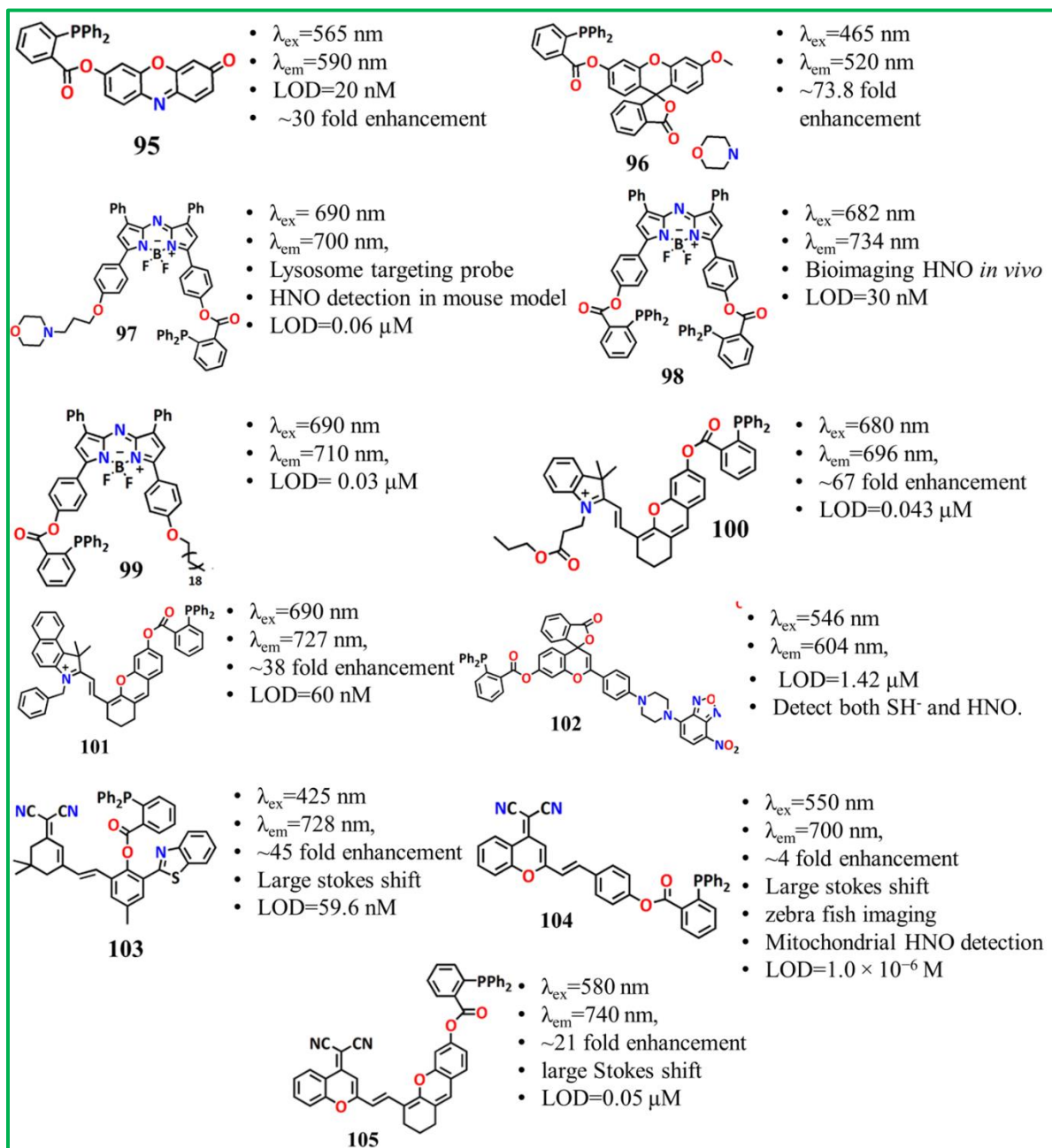


Figure 1.43. Triphenylphosphine linked intensity based HNO sensors.

CHAPTER 1

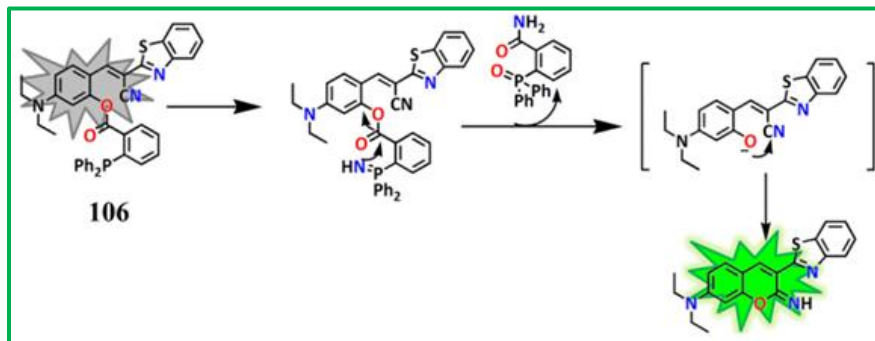


Figure 1.44. Probe **106** follows Staudinger based cascade reaction.

In 2021 as reported by Zhang et al.¹⁸³ another HNO sensitive probe **106** exhibits a slightly different sensing mechanism which is associated with HNO-induced cascade reaction to produce imino-coumarin (**Figure 1.44**). The high selectivity and quick response ($\lambda_{em} = 520$ nm, LOD = 9 nM) of the probe towards HNO makes its application successful in live HeLa cells and zebrafish larvae.

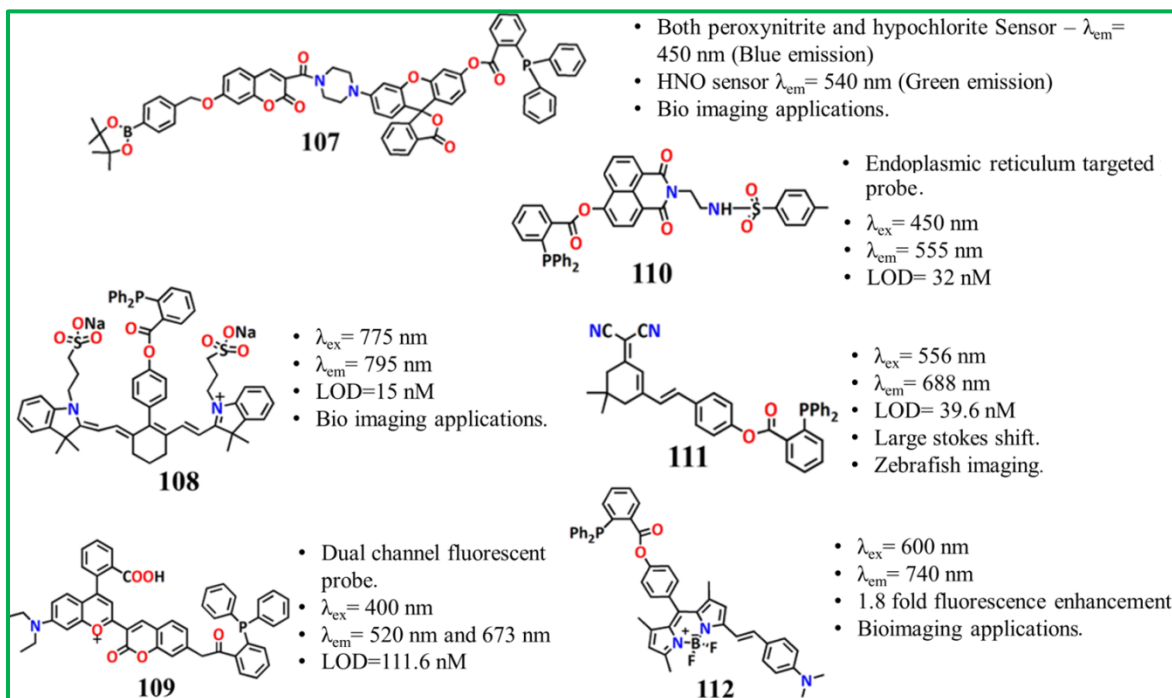


Figure 1.45. Probe **107-112** follows Staudinger ligation based sensing strategy.

Zhang et al.¹⁸⁴ first synthesized a multichannel probe **107** (**Figure 1.45**) to detect peroxyxynitrite, hypochlorite ($\lambda_{em} = 450$ nm, blue emission) and HNO ($\lambda_{em} = 540$ nm, green emission).

CHAPTER 1

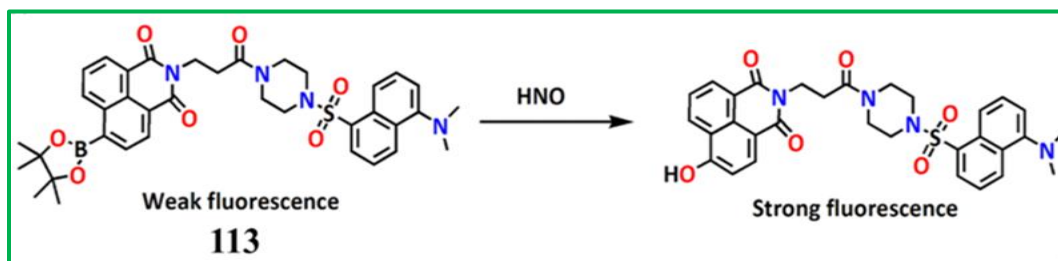


Figure 1.46. Probe **113** involves different sensing mechanism for HNO.

The probe **107** holds the capability of recognizing peroxynitrite together with nitroxyl in HeLa cells in real time. Now, here also various triphenylphosphine linked intensity based HNO sensors **108-112** (Figure 1.45) are reported by different research groups.¹⁸⁵⁻¹⁸⁹

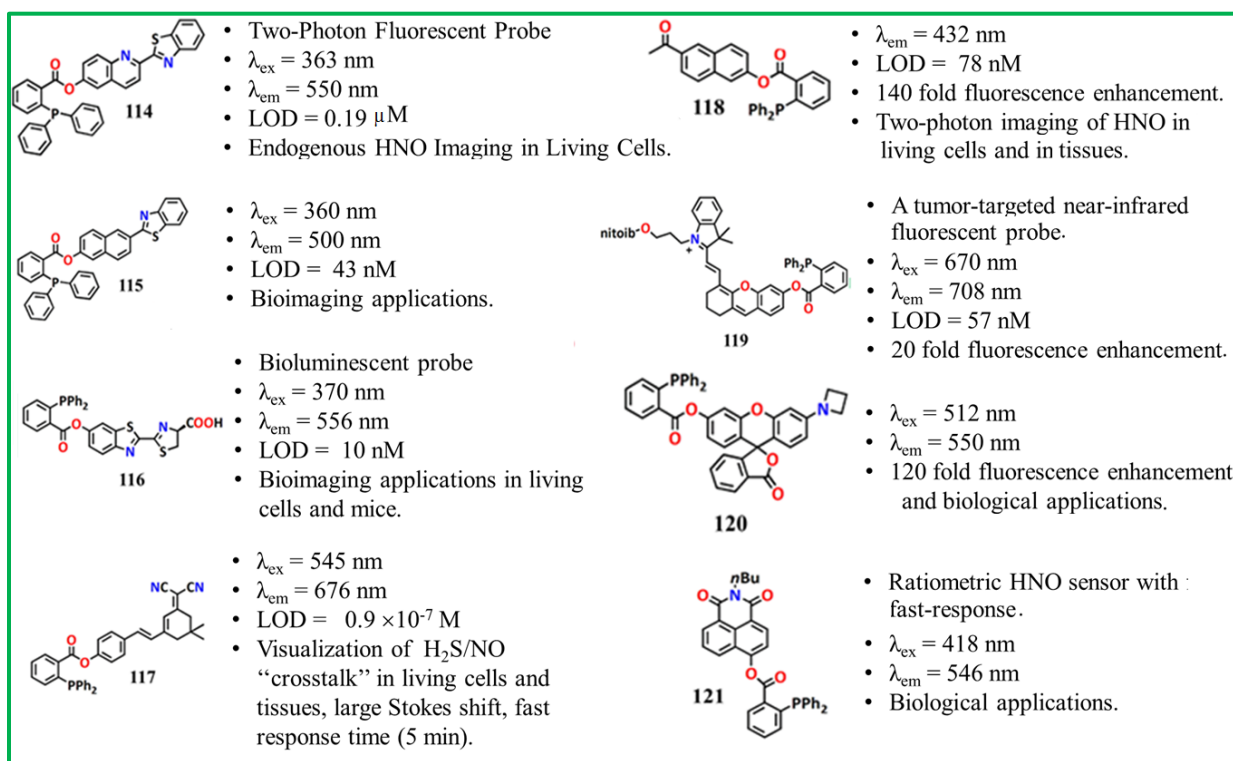


Figure 1.47. An example of various kind of intensity based HNO sensor.

Gao, Gui, Qin and their coworkers¹⁹⁰ has designed a HNO probe **113** (Figure 1.46) in which benzeneboronic acid pinacol ester was employed as a HNO recognition site instead of triphenylphosphine. The generation of aromatic alcohol through hydrolysis in presence of HNO, is responsible for the increment in fluorescence signal at 555 nm. Successful biological

CHAPTER 1

experiments on mouse model and live cells to detect HNO demonstrated that the probe is a good HNO sensor.

For monitoring the fluctuations in HNO concentration in living cells and tissues, some another fluorescent HNO sensors¹⁹¹⁻¹⁹⁷ **114-120** (Figure 1.47) has been synthesized by exploiting triphenylphosphine based HNO sensing mechanism. Among all these reported HNO sensors, first bioluminescent HNO sensor **116** (Figure 1.47) was suggested by Li et al.¹⁹⁴. This probe **116** is highly sensitive (LOD = 10 nM) and selective towards HNO. The biological applications were done in mouse model. All the above discussed HNO probes are intensity based.

Now, first ratiometric probe **121** (Figure 1.47) was reported by Zhang et al.¹⁹⁸ by exploiting naphthalimide as a fluorophoric unit. The presence of HNO shifted the emission region from blue (at 418 nm) to green (at 546 nm) without any interference by other biological species. Moreover, a promising approach for HNO recognition in living cells and tissues is the synthesis of various ratiometric HNO probes **122-127**, **128-132** (Figure 1.48 and Figure 1.49).¹⁹⁹⁻²⁰⁹ Among all these reported HNO sensors, some are discussed in detail due to their attractive applications in living organisms.

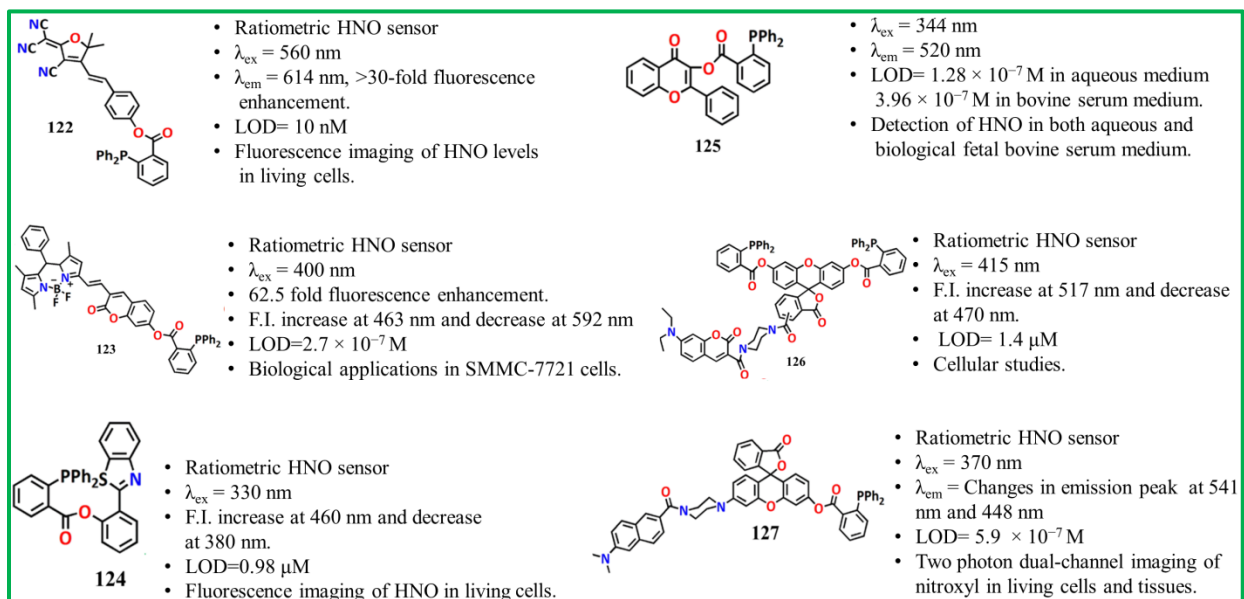


Figure 1.48. Triphenylphosphine based ratiometric HNO sensor.

Sun, Zaho and their research team²⁰⁶ have revealed for the first time a new ratiometric BODIPY embedded nanoprobes **129** (Figure 1.49) for determination of HNO precisely both *in vivo* and *in*

CHAPTER 1

vitro. Interaction with HNO causes the changes in fluorescence intensity in ratiometric manner ($\lambda_{\text{ex}} = 480 \text{ nm}$, $\lambda_{\text{em}} = 601 \text{ nm}$ (increase) and $\lambda_{\text{em}} = 568 \text{ nm}$ (decrease)). By utilizing this probe endogenous HNO determination were performed in zebrafish larvae. In 2021, Li and his research team²⁰⁹ has fabricated for the first time an aggregation induced ratiometric HNO probe **132** (Figure 1.49). The sensitive (LOD = 157.6 nM) and selective enhancement (~10 fold) in fluorescence signal in presence of HNO makes its biological investigations successful in living organisms.

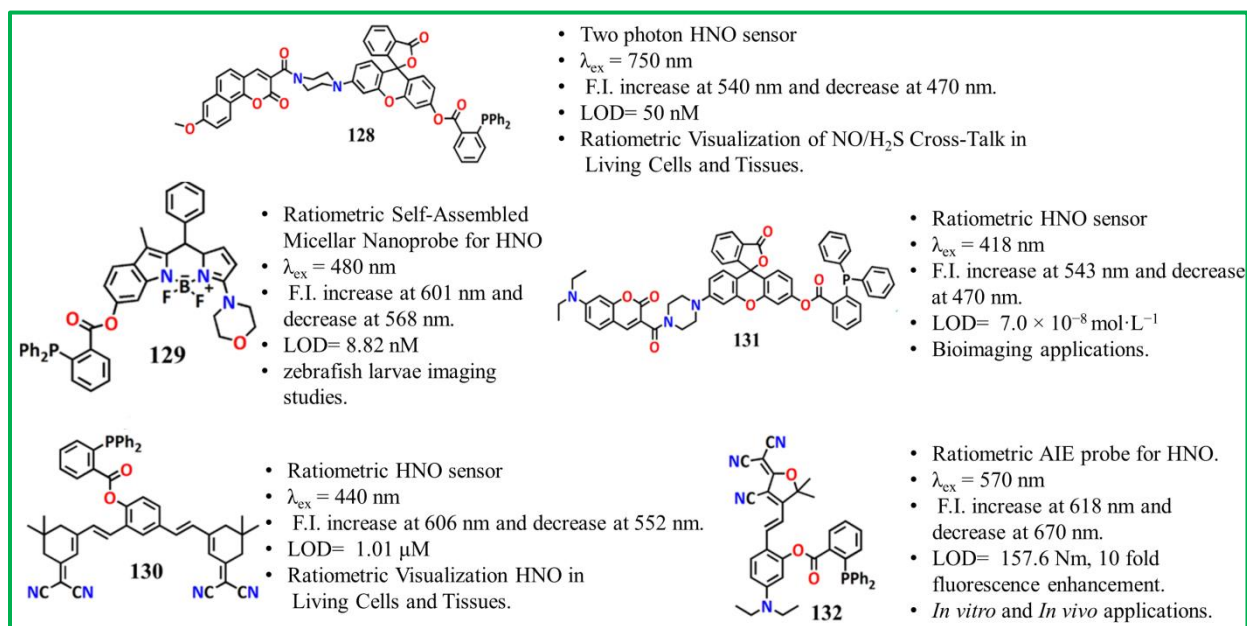


Figure 1.49. Some reported ratiometric HNO sensors.

1.5.3.3. Nitroxide-based prefluorescent probes:

The interaction of HNO with 4-Hydroxy-TEMPO (TEMPOL) through abstraction of the hydrogen atom from HNO by the nitroxide radical inspired Toscano et al.²¹⁰ to synthesis a nitroxide based probe **133** (Figure 1.50) by bridging an amide unit between TEMPO and acridine. The weak fluorescent nature of the probe becomes highly fluorescent ($\lambda_{\text{em}} = 430 \text{ nm}$) on treatment with HNO with great selectivity.

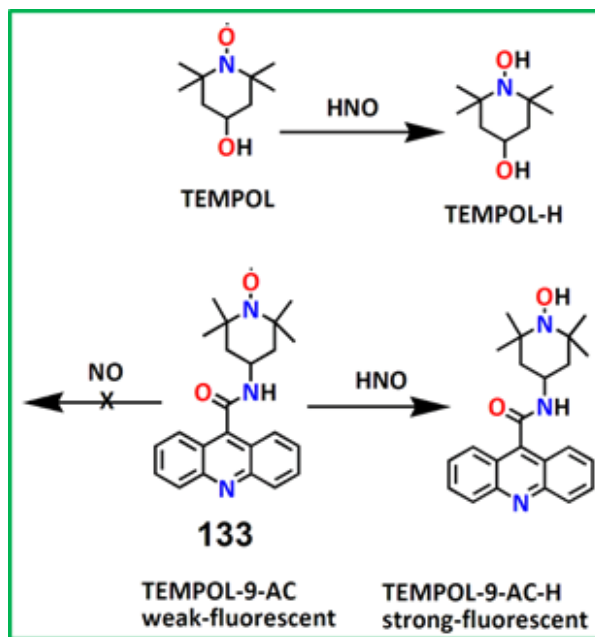


Figure 1.50. Nitroxide-based prefluorescent probes.

1.5.3.4. Mercapto-2-methylpropionic acid-based fluorescent probes:

A new sensing strategy was introduced by Chan et al.²¹¹ in which HNO recognition unit 2-mercapto-2-methylpropionic acid is attached with two fluorescent dyes one is coumarin **134** (Figure 1.51) and the other is fluorescein **135** (Figure 1.51). In both the cases on treatment with HNO the fluorescent intensity increases by following the same sensing mechanism.

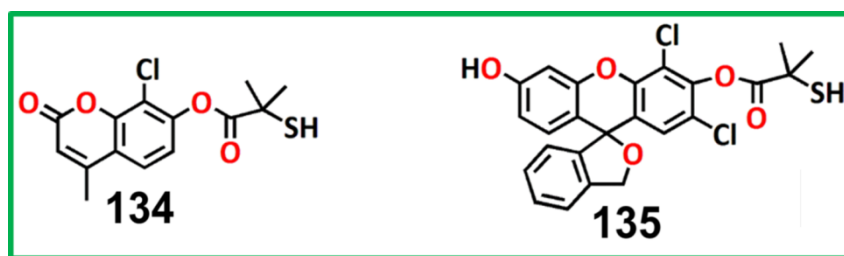


Figure 1.51. 2-Mercapto-2-methylpropionic acid linked HNO probes.

The sensing strategy involves the generation of an intermediate (i.e. an analogous N-hydroxysulfenamide species) which in the next step releases the fluorophore followed by cyclization. This causes enhancement in fluorescence intensity. Now, the fluorescein based probe

is highly specific towards HNO over other biological species indicating its better potentiality to study the role of HNO in living cells.

1.6. Objective and aim of the thesis

Most of the reactive oxygen (ROS) and nitrogen (RNS) species are either neutral or anionic small molecules being commonly present in our physiological systems playing vital roles in many biological processes. Literature study reveals that the concentrations of ROS/RNS to certain levels are beneficial and physiological as it regulates various biological functions, whereas higher ROS/RNS concentration relates with pathological processes.⁴ As for example Alzheimer's disease (AD), cardiovascular disease cancerous tumor, diabetes mellitus and aging are the result of pathological processes. For some time, the physiological role of reactive nitrogen species (RNS) has attracted an immense attention of researchers due to their intriguing behavior. Now, among the various reactive nitrogen species, nitric oxide (NO) and its kin nitroxyl (HNO) are being studied more extensively because of their interesting and unexplored roles in physiological systems. The endogenous production of NO in living cells by the nitric oxide synthase (NOS), a class of enzymes, and its rapid diffusion across the cell membrane, influences a variety of physiological processes. However, the misregulation of NO production turns the physiological role of NO into a pathological one, resulting cancer, cardiovascular disease, damaging of biomolecules (DNA, nucleic acids, lipids, proteins etc) and so on. Therefore, the diverse role of NO in mammalian cells encourages researchers to unveil its physiological role more precisely by developing suitable NO detection tools. But its engrossing physicochemical properties like short life span (in the order of milliseconds to seconds) and ready diffusion across lipid membranes make its detection quite challenging.

Similarly, Nitroxyl (HNO), the one electron reduced and protonated derivative of NO, have an unique and interesting physicochemical properties in comparison to other reactive nitrogen species. Though for both NO and HNO biological targets are same but their mechanism of interactions are different.⁸⁻¹² NO interact with thiols to form S-nitrosothiol whereas HNO gives disulfide or sulfinamide. The efficacy of HNO as a pharmacological agent in heart failure, alcoholism, IR (ischemia reperfusion) injury prevention, etc. further motivate chemists and biologists to investigate the biological roles of HNO. There is still a debate on the issues like

CHAPTER 1

endogenous synthesis of HNO and some physiological roles of both HNO and NO. As a result, in the current Ph.D. research endeavor attempts have been taken to design of various sensing strategies for the recognition of NO and HNO to enlighten the unexplored area of NO and HNO. Now, considering all these challenging aspects and the important characteristics of these two biomolecules (NO and HNO), we have designed some NO and HNO fluorescent sensors that are capable to interact with NO/HNO through a novel mechanism to avoid the limitation encountered in the previously reported NO/HNO probes. We have synthesized some smart molecular probes (136-139) (Figure 1.52) for selective and sensitive sensing of NO and HNO. The water fair solubility, least cytotoxicity, reasonable bio-compatibility enhances their efficacy for biological applications. Now, my research works are related with synthesizing of NO and HNO probes that are depicted elaborately in this thesis.

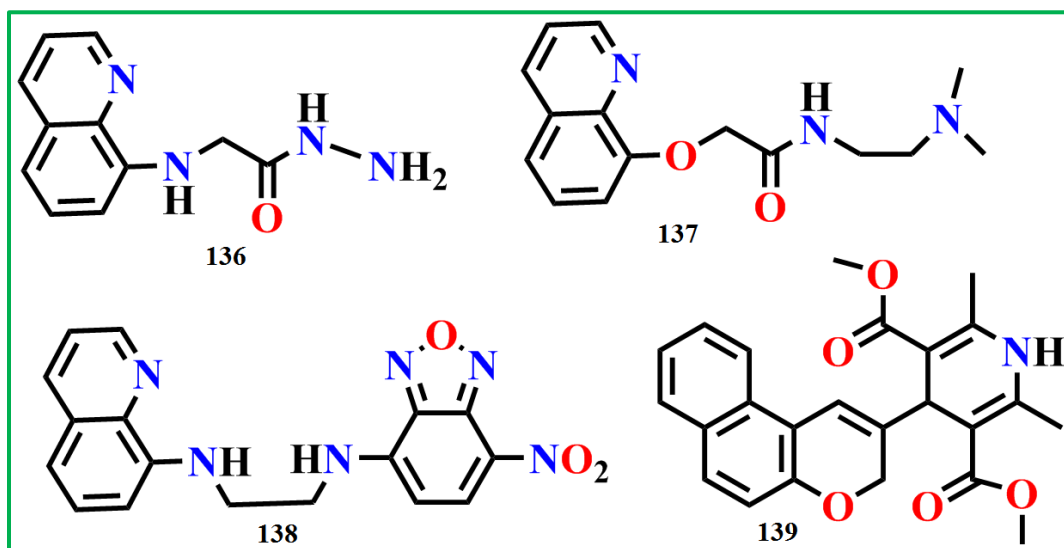


Figure 1.52. Structures of the targeted probes for NO and HNO sensing.

1.7. Physical measurements

- (i) **FTIR spectra:** Infrared spectra ($400\text{--}4000\text{ cm}^{-1}$) were recorded on a Nicolet Magna IR 750 series-II FTIR spectrometer on solid KBr discs.
- (ii) **NMR spectra:** ^1H -NMR spectra were recorded in DMSO- d_6 , CDCl_3 , CD_3CN on a Bruker 300 MHz and 400 MHz NMR spectrometer using tetramethylsilane ($\delta = 0$) as an internal standard.

CHAPTER 1

- (iii) **UV-vis spectra:** UV-vis spectra were collected on an Agilent diode-array spectrophotometer (Model, Agilent 8453).
- (iv) **Mass spectra:** ESI-MS⁺ (m/z) of the ligand and complexes were found from Waters' HRMS spectrometer (Model: QTOF Micro YA263).
- (v) **Fluorescence spectra:** All the fluorescence studies were performed with a PTI (Model QM-40) spectrofluorometer.
- (vi) **Life time measurements:** Lifetimes were calculated in Horiba-Jobin-Yvon on a Hamamatsu MCP photomultiplier (R3809) and surveyed using IBH DAS6 software.
- (vii) **DFT calculations:** Ground state electronic structure of the ligand and complexes have been calculated using Gaussian 09W software package, correlated with the conductor-like polarizable continuum model (CPCM).
- (viii) **Cell imaging:** Cell imaging experiments have been carried out using fluorescence microscope. Bright field and fluorescence images of the HepG2 cells, A375cells, Raw 264.7 murine macrophages cells, were obtained utilizing a fluorescence microscope (Leica DM3000, Germany) having the objective lens of 40x, 63x magnification.
- (ix) **pH study:** The pH of the solutions was recorded in a Systronics digital pH meter (Model 335, India) in 2–12 pH range.

References

1. Katsuki, S.; Arnold, W.; Mittal, C.; Murad, F., Stimulation of guanylate cyclase by sodium nitroprusside, nitroglycerin and nitric oxide in various tissue preparations and comparison to the effects of sodium azide and hydroxylamine. *J Cyclic Nucleotide Res* **1977**, *3* (1), 23-35.
2. Furchgott, R. F.; Zawadzki, J. V., The obligatory role of endothelial cells in the relaxation of arterial smooth muscle by acetylcholine. *Nature* **1980**, *288* (5789), 373-376.
3. Ignarro, L. J.; Byrns, R. E.; Buga, G. M.; Wood, K. S., Endothelium-derived relaxing factor from pulmonary artery and vein possesses pharmacologic and chemical properties identical to those of nitric oxide radical. *Circ. Res.* **1987**, *61* (6), 866-879.
4. Pacher, P.; Beckman, J. S.; Liaudet, L., Nitric Oxide and Peroxynitrite in Health and Disease. *Physiol. Rev.* **2007**, *87* (1), 315-424.
5. Kemp-Harper, B. K., Nitroxyl (HNO): A Novel Redox Signaling Molecule. *Antioxid. Redox Signal.* **2011**, *14* (9), 1609-1613.
6. Thomas, D. D.; Liu, X.; Kantrow, S. P.; Lancaster, J. R., The biological lifetime of nitric oxide: Implications for the perivascular dynamics of NO and O₂. *Proc. Natl. Acad. Sci. U.S.A.* **2001**, *98* (1), 355-360.
7. Gallego, C. M.; Mazzeo, A.; Vargas, P.; Suárez, S.; Pellegrino, J.; Doctorovich, F., Azanone (HNO): generation, stabilization and detection. *Chem. Sci.* **2021**, *12* (31), 10410-10425.
8. Donzelli, S.; Espey, M. G.; Flores-Santana, W.; Switzer, C. H.; Yeh, G. C.; Huang, J.; Stuehr, D. J.; King, S. B.; Miranda, K. M.; Wink, D. A., Generation of nitroxyl by heme protein-mediated peroxidation of hydroxylamine but not N-hydroxy-L-arginine. *Free Radic. Biol. Med.* **2008**, *45* (5), 578-584.
9. Irvine, J. C.; Ritchie, R. H.; Favaloro, J. L.; Andrews, K. L.; Widdop, R. E.; Kemp-Harper, B. K., Nitroxyl (HNO): the Cinderella of the nitric oxide story. *Trends Pharmacol. Sci.* **2008**, *29* (12), 601-608.
10. Ma, X. L.; Gao, F.; Liu, G.-L.; Lopez, B. L.; Christopher, T. A.; Fukuto, J. M.; Wink, D. A.; Feelisch, M., Opposite effects of nitric oxide and nitroxyl on postischemic myocardial injury. *Proc. Natl. Acad. Sci. U.S.A.* **1999**, *96* (25), 14617-14622.

CHAPTER 1

11. Miranda, K. M.; Paolocci, N.; Katori, T.; Thomas, D. D.; Ford, E.; Bartberger, M. D.; Espey, M. G.; Kass, D. A.; Feelisch, M.; Fukuto, J. M.; Wink, D. A., A biochemical rationale for the discrete behavior of nitroxyl and nitric oxide in the cardiovascular system. *Proc. Natl. Acad. Sci. U.S.A.* **2003**, *100* (16), 9196-9201.
12. Paolocci, N.; Saavedra, W. F.; Miranda, K. M.; Martignani, C.; Isoda, T.; Hare, J. M.; Espey, M. G.; Fukuto, J. M.; Feelisch, M.; Wink, D. A.; Kass, D. A., Nitroxyl anion exerts redox-sensitive positive cardiac inotropy in vivo by calcitonin gene-related peptide signaling. *Proc. Natl. Acad. Sci. U.S.A.* **2001**, *98* (18), 10463-10468.
13. Fukuto, J. M.; Cisneros, C. J.; Kinkade, R. L., A comparison of the chemistry associated with the biological signaling and actions of nitroxyl (HNO) and nitric oxide (NO). *J. Inorg. Biochem.* **2013**, *118*, 201-208.
14. Irvine, J. C.; Favalaro, J. L.; Kemp-Harper, B. K., NO⁻ Activates Soluble Guanylate Cyclase and Kv Channels to Vasodilate Resistance Arteries. *Hypertension* **2003**, *41* (6), 1301-1307.
15. Irvine, J. C.; Favalaro, J. L.; Widdop, R. E.; Kemp-Harper, B. K., Nitroxyl Anion Donor, Angeli's Salt, Does Not Develop Tolerance in Rat Isolated Aortae. *Hypertension* **2007**, *49* (4), 885-892.
16. Wanstall, J. C.; Jeffery, T. K.; Gambino, A.; Lovren, F.; Triggle, C. R., Vascular smooth muscle relaxation mediated by nitric oxide donors: a comparison with acetylcholine, nitric oxide and nitroxyl ion. *Br. J. Pharmacol.* **2001**, *134* (3), 463-472.
17. Ellis, A.; Lu, H.; Li, C. G.; Rand, M. J., Effects of agents that inactivate free radical NO (NO•) on nitroxyl anion-mediated relaxations, and on the detection of NO• released from the nitroxyl anion donor Angeli's salt. *Br. J. Pharmacol.* **2001**, *134* (3), 521-528.
18. Dai, T.; Tian, Y.; Tocchetti, C. G.; Katori, T.; Murphy, A. M.; Kass, D. A.; Paolocci, N.; Gao, W. D., Nitroxyl increases force development in rat cardiac muscle. *J. Physiol. (Lond.)* **2007**, *580* (3), 951-960.
19. Tocchetti, C. G.; Wang, W.; Froehlich, J. P.; Huke, S.; Aon, M. A.; Wilson, G. M.; Di Benedetto, G.; O'Rourke, B.; Gao, W. D.; Wink, D. A.; Toscano, J. P.; Zaccolo, M.; Bers, D. M.; Valdivia, H. H.; Cheng, H.; Kass, D. A.; Paolocci, N., Nitroxyl Improves Cellular Heart Function by Directly Enhancing Cardiac Sarcoplasmic Reticulum Ca²⁺ Cycling. *Circ. Res.* **2007**, *100* (1), 96-104.

CHAPTER 1

20. Luiking, Y. C.; Engelen, M. P.; Deutz, N. E., Regulation of nitric oxide production in health and disease. *Curr. Opin. Clin. Nutr. Metab. Care* **2010**, *13* (1), 97-104.
21. Bredt, D. S.; Snyder, S. H., Isolation of nitric oxide synthetase, a calmodulin-requiring enzyme. *Proc. Natl. Acad. Sci. U.S.A.* **1990**, *87* (2), 682-685.
22. Moncada, S.; Palmer, R. M. J.; Higgs, E. A., Biosynthesis of nitric oxide from l-arginine: A pathway for the regulation of cell function and communication. *Biochem. Pharmacol.* **1989**, *38* (11), 1709-1715.
23. Stuehr, D. J.; Nathan, C. F., Nitric oxide. A macrophage product responsible for cytostasis and respiratory inhibition in tumor target cells. *J. Exp. Med.* **1989**, *169* (5), 1543-1555.
24. Marletta, M. A., Nitric oxide synthase structure and mechanism. *J. Biol. Chem.* **1993**, *268* (17), 12231-12234.
25. Abu-Soud, H. M.; Yoho, L. L.; Stuehr, D. J., Calmodulin controls neuronal nitric-oxide synthase by a dual mechanism. Activation of intra- and interdomain electron transfer. *J. Biol. Chem.* **1994**, *269* (51), 32047-32050.
26. Stuehr, D. J.; Kwon, N. S.; Nathan, C. F.; Griffith, O. W.; Feldman, P. L.; Wiseman, J., N omega-hydroxy-L-arginine is an intermediate in the biosynthesis of nitric oxide from L-arginine. *J. Biol. Chem.* **1991**, *266* (10), 6259-6263.
27. Joyner, M. J.; Dietz, N. M., Nitric oxide and vasodilation in human limbs. *J. Appl. Physiol.* **1997**, *83* (6), 1785-1796.
28. Moncada, S.; Higgs, A., The L-Arginine-Nitric Oxide Pathway. *N. Engl. J. Med.* **1993**, *329* (27), 2002-2012.
29. Roberts, C. K.; Barnard, R. J.; Jasman, A.; Balon, T. W., Acute exercise increases nitric oxide synthase activity in skeletal muscle. *Am. J. Physiol. - Endocrinol. Metab.* **1999**, *277* (2), E390-E394.
30. Vincent, S. R., Nitric oxide neurons and neurotransmission. *Prog. Neurobiol.* **2010**, *90* (2), 246-255.
31. Bogdan, C. J. N. i., Nitric oxide and the immune response. **2001**, *2* (10), 907-916.
32. Kim, P. K. M.; Zamora, R.; Petrosko, P.; Billiar, T. R., The regulatory role of nitric oxide in apoptosis. *Int. Immunopharmacol.* **2001**, *1* (8), 1421-1441.

CHAPTER 1

33. Luo, J.-d.; Chen, A. F. J. A. P. S., Nitric oxide: a newly discovered function on wound healing. **2005**, *26* (3), 259-264.
34. Kumar, V.; Hong, S. Y.; Maciag, A. E.; Saavedra, J. E.; Adamson, D. H.; Prud'homme, R. K.; Keefer, L. K.; Chakrapani, H., Stabilization of the Nitric Oxide (NO) Prodrugs and Anticancer Leads, PABA/NO and Double JS-K, through Incorporation into PEG-Protected Nanoparticles. *Mol. Pharm.* **2010**, *7* (1), 291-298.
35. Seabra, A. B.; Da Silva, R.; De Souza, G. F. P.; De Oliveira, M. G., Antithrombogenic Polynitrosated Polyester/Poly(methyl methacrylate) Blend for the Coating of Blood-Contacting Surfaces. *Artificial Organs* **2008**, *32* (4), 262-267.
36. Griess, J. P.; Hofmann, A. W. V., XVIII. On a new series of bodies in which nitrogen is substituted for hydrogen. *Philos. Trans. R. Soc.* **1864**, *154*, 667-731.
37. Williams, D. L. H., A chemist's view of the nitric oxide story. *Org. Biomol. Chem.* **2003**, *1* (3), 441-449.
38. Tsikas, D., Analysis of nitrite and nitrate in biological fluids by assays based on the Griess reaction: Appraisal of the Griess reaction in the l-arginine/nitric oxide area of research. *J. Chromatogr. B* **2007**, *851* (1), 51-70.
39. Hetrick, E. M.; Schoenfisch, M. H., Analytical Chemistry of Nitric Oxide. *Annu. Rev. Anal. Chem.* **2009**, *2* (1), 409-433.
40. Bates, J. N., Nitric oxide measurement by chemiluminescence detection. *Neuroprotocols* **1992**, *1* (2), 141-149.
41. Kikuchi, K.; Nagano, T.; Hayakawa, H.; Hirata, Y.; Hirobe, M., Detection of nitric oxide production from a perfused organ by a luminol-hydrogen peroxide system. *Anal. Chem.* **1993**, *65* (13), 1794-1799.
42. Yamasaki, H.; Watanabe, N. S.; Sakihama, Y.; Cohen, M. F., An Overview of Methods in Plant Nitric Oxide (NO) Research: Why Do We Always Need to Use Multiple Methods? In *Plant Nitric Oxide: Methods and Protocols*, Gupta, K. J., Ed. Springer New York: New York, NY, 2016; pp 1-14.
43. Ulissi, Z. W.; Sen, F.; Gong, X.; Sen, S.; Iverson, N.; Boghossian, A. A.; Godoy, L. C.; Wogan, G. N.; Mukhopadhyay, D.; Strano, M. S., Spatiotemporal Intracellular Nitric Oxide Signaling Captured Using Internalized, Near-Infrared Fluorescent Carbon Nanotube Nanosensors. *Nano Lett.* **2014**, *14* (8), 4887-4894.

CHAPTER 1

44. Kojima, H.; Nakatsubo, N.; Kikuchi, K.; Kawahara, S.; Kirino, Y.; Nagoshi, H.; Hirata, Y.; Nagano, T., Detection and Imaging of Nitric Oxide with Novel Fluorescent Indicators: Diaminofluoresceins. *Anal. Chem.* **1998**, *70* (13), 2446-2453.
45. Kojima, H.; Urano, Y.; Kikuchi, K.; Higuchi, T.; Hirata, Y.; Nagano, T., Fluorescent Indicators for Imaging Nitric Oxide Production. *Angew. Chem. Int. Ed.* **1999**, *38* (21), 3209-3212.
46. Yu, H.; Xiao, Y.; Jin, L., A Lysosome-Targetable and Two-Photon Fluorescent Probe for Monitoring Endogenous and Exogenous Nitric Oxide in Living Cells. *J. Am. Chem. Soc.* **2012**, *134* (42), 17486-17489.
47. Seo, E. W.; Han, J. H.; Heo, C. H.; Shin, J. H.; Kim, H. M.; Cho, B. R., A Small-Molecule Two-Photon Probe for Nitric Oxide in Living Tissues. *Chem. Eur. J.* **2012**, *18* (39), 12388-12394.
48. Yu, H.; Zhang, X.; Xiao, Y.; Zou, W.; Wang, L.; Jin, L., Targetable Fluorescent Probe for Monitoring Exogenous and Endogenous NO in Mitochondria of Living Cells. *Anal. Chem.* **2013**, *85* (15), 7076-7084.
49. Chen, J.-B.; Zhang, H.-X.; Guo, X.-F.; Wang, H.; Zhang, H.-S., "Off-on" red-emitting fluorescent probes with large Stokes shifts for nitric oxide imaging in living cells. *Anal. Bioanal. Chem.* **2013**, *405* (23), 7447-7456.
50. Yao, H.-W.; Zhu, X.-Y.; Guo, X.-F.; Wang, H., An Amphiphilic Fluorescent Probe Designed for Extracellular Visualization of Nitric Oxide Released from Living Cells. *Anal. Chem.* **2016**, *88* (18), 9014-9021.
51. Liu, X.; Liu, S.; Liang, G., Fluorescence turn-on for the highly selective detection of nitric oxide in vitro and in living cells. *Analyst* **2016**, *141* (8), 2600-2605.
52. Feng, W.; Qiao, Q.-L.; Leng, S.; Miao, L.; Yin, W.-T.; Wang, L.-Q.; Xu, Z.-C., A 1,8-naphthalimide-derived turn-on fluorescent probe for imaging lysosomal nitric oxide in living cells. *Chin. Chem. Lett.* **2016**, *27* (9), 1554-1558.
53. Wang, F.; Yu, S.; Xu, Z.; Li, L.; Dang, Y.; Xu, X.; Luo, Y.; Cheng, Z.; Yu, H.; Zhang, W.; Zhang, A.; Ding, C., Acid-Promoted D-A-D Type Far-Red Fluorescent Probe with High Photostability for Lysosomal Nitric Oxide Imaging. *Anal. Chem.* **2018**, *90* (13), 7953-7962.

CHAPTER 1

54. Wang, S.; Li, Z.; Liu, Y.; Feng, G.; Zheng, J.; Yuan, Z.; Zhang, X., Activatable photoacoustic and fluorescent probe of nitric oxide for cellular and in vivo imaging. *Sens. Actuators B Chem.* **2018**, *267*, 403-411.
55. Zhang, Y.; Jia, C.; Wang, Y.; Yu, H.; Ji, M., Hemicyanine-based turn-off fluorescent probe for monitoring of nitric oxide in living cells. *Dyes Pigm.* **2022**, *197*, 109871.
56. Biswas, S.; Rajesh, Y.; Barman, S.; Bera, M.; Paul, A.; Mandal, M.; Pradeep Singh, N. D., A dual-analyte probe: hypoxia activated nitric oxide detection with phototriggered drug release ability. *Chem. Commun.* **2018**, *54* (57), 7940-7943.
57. Zhang, X.; Wang, B.; Xiao, Y.; Wang, C.; He, L., Targetable, two-photon fluorescent probes for local nitric oxide capture in the plasma membranes of live cells and brain tissues. *Analyst* **2018**, *143* (17), 4180-4188.
58. Tang, J.; Guo, Z.; Zhang, Y.; Bai, B.; Zhu, W.-H., Rational design of a fast and selective near-infrared fluorescent probe for targeted monitoring of endogenous nitric oxide. *Chem. Commun.* **2017**, *53* (76), 10520-10523.
59. Li, S.-J.; Zhou, D.-Y.; Li, Y.; Liu, H.-W.; Wu, P.; Ou-Yang, J.; Jiang, W.-L.; Li, C.-Y., Efficient Two-Photon Fluorescent Probe for Imaging of Nitric Oxide during Endoplasmic Reticulum Stress. *ACS Sens.* **2018**, *3* (11), 2311-2319.
60. Wang, Q.; Jiao, X.; Liu, C.; He, S.; Zhao, L.; Zeng, X., A rhodamine-based fast and selective fluorescent probe for monitoring exogenous and endogenous nitric oxide in live cells. *J. Mater. Chem. B* **2018**, *6* (24), 4096-4103.
61. Chen, X.-X.; Niu, L.-Y.; Shao, N.; Yang, Q.-Z., BODIPY-Based Fluorescent Probe for Dual-Channel Detection of Nitric Oxide and Glutathione: Visualization of Cross-Talk in Living Cells. *Anal. Chem.* **2019**, *91* (7), 4301-4306.
62. Huo, Y.; Miao, J.; Han, L.; Li, Y.; Li, Z.; Shi, Y.; Guo, W., Selective and sensitive visualization of endogenous nitric oxide in living cells and animals by a Si-rhodamine deoxylactam-based near-infrared fluorescent probe. *Chem. Sci.* **2017**, *8* (10), 6857-6864.
63. Jiang, W.-L.; Li, Y.; Liu, H.-W.; Zhou, D.-Y.; Ou-Yang, J.; Yi, L.; Li, C.-Y., A rhodamine-deoxylactam based fluorescent probe for fast and selective detection of nitric oxide in living cells. *Talanta* **2019**, *197*, 436-443.

CHAPTER 1

64. Zhao, L.; Huang, Z.; Ma, D.; Yan, Y.; Zhang, X.; Xiao, Y., A nucleus targetable fluorescent probe for ratiometric imaging of endogenous NO in living cells and zebrafishes. *Analyst* **2021**, *146* (13), 4130-4134.
65. Wang, X.; Sun, Q.; Song, X.; Wang, Y.; Hu, W., Development of a ratiometric nitric oxide probe with baseline resolved emissions by an ESIPT and rhodol ring opened-closed integrated two-photon platform. *RSC Adv.* **2022**, *12* (5), 2721-2728.
66. Zhang, P.; Tian, Y.; Liu, H.; Ren, J.; Wang, H.; Zeng, R.; Long, Y.; Chen, J., In vivo imaging of hepatocellular nitric oxide using a hepatocyte-targeting fluorescent sensor. *Chem. Commun.* **2018**, *54* (52), 7231-7234.
67. Miao, J.; Huo, Y.; Lv, X.; Li, Z.; Cao, H.; Shi, H.; Shi, Y.; Guo, W., Fast-response and highly selective fluorescent probes for biological signaling molecule NO based on N-nitrosation of electron-rich aromatic secondary amines. *Biomaterials* **2016**, *78*, 11-19.
68. Huo, Y.; Miao, J.; Fang, J.; Shi, H.; Wang, J.; Guo, W., Aromatic secondary amine-functionalized fluorescent NO probes: improved detection sensitivity for NO and potential applications in cancer immunotherapy studies. *Chem. Sci.* **2019**, *10* (1), 145-152.
69. Yu, Z.; Zhou, J.; Dong, X.; Zhao, W.; Chen, Z., Visualizing Nitric oxide in mitochondria and lysosomes of living cells with N-Nitrosation of BODIPY-based fluorescent probes. *Anal. Chim. Acta* **2019**, *1067*, 88-97.
70. Mao, Z.; Jiang, H.; Song, X.; Hu, W.; Liu, Z., Development of a Silicon-Rhodamine Based Near-Infrared Emissive Two-Photon Fluorescent Probe for Nitric Oxide. *Anal. Chem.* **2017**, *89* (18), 9620-9624.
71. Mao, Z.; Jiang, H.; Li, Z.; Zhong, C.; Zhang, W.; Liu, Z., An N-nitrosation reactivity-based two-photon fluorescent probe for the specific in situ detection of nitric oxide. *Chem. Sci.* **2017**, *8* (6), 4533-4538.
72. Mao, Z.; Feng, W.; Li, Z.; Zeng, L.; Lv, W.; Liu, Z., NIR in, far-red out: developing a two-photon fluorescent probe for tracking nitric oxide in deep tissue. *Chem. Sci.* **2016**, *7* (8), 5230-5235.
73. Reinhardt, C. J.; Zhou, E. Y.; Jorgensen, M. D.; Partipilo, G.; Chan, J., A Ratiometric Acoustogenic Probe for in Vivo Imaging of Endogenous Nitric Oxide. *J. Am. Chem. Soc.* **2018**, *140* (3), 1011-1018.

CHAPTER 1

74. Lucero, M. Y.; East, A. K.; Reinhardt, C. J.; Sedgwick, A. C.; Su, S.; Lee, M. C.; Chan, J., Development of NIR-II Photoacoustic Probes Tailored for Deep-Tissue Sensing of Nitric Oxide. *J. Am. Chem. Soc.* **2021**, *143* (18), 7196-7202.
75. Li, H.; Hao, Y.-H.; Feng, W.; Song, Q.-H., Rapid and sensitive detection of nitric oxide by a BODIPY-based fluorescent probe in live cells: glutathione effects. *J. Mater. Chem. B* **2020**, *8* (42), 9785-9793.
76. Liu, Y.; Fan, H.; Wen, Y.; Jia, T.; Su, Q.; Li, F., ICT-based near infrared fluorescent switch-on probe for nitric oxide bioimaging in vivo. *Dyes Pigm.* **2019**, *166*, 211-216.
77. Liu, P.; Li, B.; Zheng, J.; Liang, Q.; Wu, C.; Huang, L.; Zhang, P.; Jia, Y.; Wang, S., A novel N-nitrosation-based ratiometric fluorescent probe for highly selective imaging endogenous nitric oxide in living cells and zebrafish. *Sens. Actuators B Chem.* **2021**, *329*, 129147.
78. Liu, Y.; Jiao, C.; Wei, Y.; Lu, W.; Zhang, P.; Wang, Y., A highly specific rhodamine B based turn-on fluorescent probe for nitric oxide and application in living cells. *Tetrahedron* **2020**, *76* (46), 131622.
79. Tang, Q.; Li, P.; Zhou, Z.; Lu, Q.; Gu, B.; Tang, S.; Zhang, Y., An N-nitrosation reaction-based fluorescent probe for detecting nitric oxide in living cells and inflammatory zebrafish. *Spectrochim. Acta A* **2022**, *270*, 120728.
80. Wang, L.-L.; Bai, J.-Y.; Li, X.-F.; Zheng, M.-H.; Miao, Y.; Jin, J.-Y., Simultaneous imaging of hypochlorous acid and nitric oxide in live cells based on a dual-channel fluorescent probe. *Anal. Chim. Acta* **2021**, *1183*, 338980.
81. Ouyang, Z.; Ma, M.; Yin, K.; Guo, N.; Fu, W.; Guo, W.; Gu, X., An activatable fluorescent probe for imaging endogenous nitric oxide via the eNOS enzymatic pathway. *Bioorg. Med. Chem. Lett.* **2022**, *59*, 128544.
82. Shiue, T.-W.; Chen, Y.-H.; Wu, C.-M.; Singh, G.; Chen, H.-Y.; Hung, C.-H.; Liaw, W.-F.; Wang, Y.-M., Nitric Oxide Turn-on Fluorescent Probe Based on Deamination of Aromatic Primary Monoamines. *Inorg. Chem.* **2012**, *51* (9), 5400-5408.
83. Huo, Y.; Miao, J.; Li, Y.; Shi, Y.; Shi, H.; Guo, W., Aromatic primary monoamine-based fast-response and highly specific fluorescent probes for imaging the biological signaling molecule nitric oxide in living cells and organisms. *J. Mater. Chem. B* **2017**, *5* (13), 2483-2490.

CHAPTER 1

84. Beltrán, A.; Isabel Burguete, M.; Abánades, D. R.; Pérez-Sala, D.; Luis, S. V.; Galindo, F., Turn-on fluorescent probes for nitric oxide sensing based on the ortho-hydroxyamino structure showing no interference with dehydroascorbic acid. *Chem. Commun.* **2014**, 50 (27), 3579-3581.
85. Muñoz Resta, I.; Bedrina, B.; Martínez-Planes, E.; Minguela, A.; Galindo, F., Detection of subcellular nitric oxide in mitochondria using a pyrylium probe: assays in cell cultures and peripheral blood. *J. Mater. Chem. B* **2021**, 9 (48), 9885-9892.
86. Wang, L.; Wang, Z.; Chen, Y.; Huang, Z.; Huang, X.; Xue, M.; Cheng, H.; Li, B.; Liu, P., A novel dual-channel fluorescent probe for selectively and sensitively imaging endogenous nitric oxide in living cells and zebrafish. *Spectrochim. Acta A* **2022**, 277, 121280.
87. Yang, Y.; Seidlits, S. K.; Adams, M. M.; Lynch, V. M.; Schmidt, C. E.; Anslyn, E. V.; Shear, J. B., A Highly Selective Low-Background Fluorescent Imaging Agent for Nitric Oxide. *J. Am. Chem. Soc.* **2010**, 132 (38), 13114-13116.
88. Dai, C.-G.; Wang, J.-L.; Fu, Y.-L.; Zhou, H.-P.; Song, Q.-H., Selective and Real-Time Detection of Nitric Oxide by a Two-Photon Fluorescent Probe in Live Cells and Tissue Slices. *Anal. Chem.* **2017**, 89 (19), 10511-10519.
89. Zhu, X.; Chen, J.-Q.; Ma, C.; Liu, X.; Cao, X.-P.; Zhang, H., A ratiometric mitochondria-targeting two-photon fluorescent probe for imaging of nitric oxide in vivo. *Analyst* **2017**, 142 (24), 4623-4628.
90. Chen, L.; Wu, D.; Yoon, J., An ESIPT based fluorescence probe for ratiometric monitoring of nitric oxide. *Sens. Actuators B Chem.* **2018**, 259, 347-353.
91. Li, C.; Tang, W.-J.; Feng, W.; Liu, C.; Song, Q.-H., A rapid-response and ratiometric fluorescent probe for nitric oxide: From the mitochondria to the nucleus in live cells. *Anal. Chim. Acta* **2020**, 1096, 148-158.
92. Itoh, T.; Nagata, K.; Matsuya, Y.; Miyazaki, M.; Ohsawa, A., Reaction of Nitric Oxide with Amines. *J. Org. Chem.* **1997**, 62 (11), 3582-3585.
93. Ma, S.; Fang, D.-C.; Ning, B.; Li, M.; He, L.; Gong, B., The rational design of a highly sensitive and selective fluorogenic probe for detecting nitric oxide. *Chem. Commun.* **2014**, 50 (49), 6475-6478.

CHAPTER 1

94. Ma, S.; Sun, X.; Yu, Q.; Liu, R.; Lu, Z.; He, L., Dihydropyridine-coumarin-based fluorescent probe for imaging nitric oxide in living cells. *Photochem. Photobiol. Sci.* **2020**, *19* (9), 1230-1235.
95. Ma, S.-F.; Wang, Q.-H.; Liu, F.-T.; Wang, H.-L.; Fang, D.-C.; Gong, B.; He, L.; Lu, Z.-L., Dihydropyridine-based fluorescence probe for nitric oxide. *RSC Adv.* **2016**, *6* (89), 85698-85703.
96. Wang, H.-L.; Liu, F.-T.; Ding, A.-X.; Ma, S.-F.; He, L.; Lin, L.; Lu, Z.-L., Water-soluble Hantzsch ester as switch-on fluorescent probe for efficiently detecting nitric oxide. *Spectrochim. Acta A* **2016**, *169*, 1-6.
97. Gao, C.; Lin, L.; Sun, W.; Tan, Z.-L.; Huang, J.-R.; He, L.; Lu, Z.-L., Dihydropyridine-derived BODIPY probe for detecting exogenous and endogenous nitric oxide in mitochondria. *Talanta* **2018**, *176*, 382-388.
98. Tang, F.; Gao, C.; Liu, J.-Y.; Lu, Z.-L.; He, L.; Ding, A.-X., Lysosome-targeting BODIPY-derived Hantzsch ester for nitric oxide detection and imaging in live cells. *Sens. Actuators B Chem.* **2021**, *339*, 129880.
99. Mahapatra, A. K.; Ali, S. S.; Maiti, K.; Mondal, S.; Maji, R.; Manna, S.; Manna, S. K.; Uddin, M. R.; Mandal, S., Highly sensitive ratiometric fluorescence probes for nitric oxide based on dihydropyridine and potentially useful in bioimaging. *RSC Adv.* **2016**, *6* (114), 113219-113227.
100. Li, H.; Zhang, D.; Gao, M.; Huang, L.; Tang, L.; Li, Z.; Chen, X.; Zhang, X., Highly specific C–C bond cleavage induced FRET fluorescence for in vivo biological nitric oxide imaging. *Chem. Sci.* **2017**, *8* (3), 2199-2203.
101. Itoh, T.; Matsuya, Y.; Nagata, K.; Ohsawa, A., Reaction of arylhydrazines with nitric oxide in the presence of oxygen. *Tetrahedron Lett.* **1997**, *38* (23), 4117-4120.
102. Fu, Y.-L.; Li, H.; Wei, X.-Z.; Song, Q.-H., BODIPY-based hydrazine as a fluorescent probe for sensitive and selective detection of nitric oxide: a new strategy. *J. Mater. Chem. B* **2019**, *7* (24), 3792-3795.
103. Hrabie, J. A.; Srinivasan, A.; George, C.; Keefer, L. K., Reaction of nitric oxide with the imine double bond of certain Schiff bases. *Tetrahedron Lett.* **1998**, *39* (33), 5933-5936.
104. Xu, C.; Xin, C.; Yu, C.; Wu, M.; Xu, J.; Qin, W.; Ding, Y.; Wang, X.; Li, L.; Huang, W., Fast response two-photon fluorogenic probe based on Schiff base derivatives

CHAPTER 1

- for monitoring nitric oxide levels in living cells and zebrafish. *Chem. Commun.* **2018**, 54 (96), 13491-13494.
105. Islam, A. S. M.; Bhowmick, R.; Pal, K.; Katarkar, A.; Chaudhuri, K.; Ali, M., A Smart Molecule for Selective Sensing of Nitric Oxide: Conversion of NO to HSNO; Relevance of Biological HSNO Formation. *Inorg. Chem.* **2017**, 56 (8), 4324-4331.
106. Islam, A. S. M.; Bhowmick, R.; Chandra Garain, B.; Katarkar, A.; Ali, M., Nitric Oxide Sensing through 1,2,3,4-Oxatriazole Formation from Acylhydrazide: A Kinetic Study. *J. Org. Chem.* **2018**, 83 (21), 13287-13295.
107. Han, Q.; Liu, J.; Meng, Q.; Wang, Y.-L.; Feng, H.; Zhang, Z.; Xu, Z. P.; Zhang, R., Turn-On Fluorescence Probe for Nitric Oxide Detection and Bioimaging in Live Cells and Zebrafish. *ACS Sens.* **2019**, 4 (2), 309-316.
108. Kim, S. J.; Park, S. Y.; Yoon, S. A.; Kim, C.; Kang, C.; Lee, M. H., Naphthalimide-4-(4-nitrophenyl)thiosemicarbazide: A Fluorescent Probe for Simultaneous Monitoring of Viscosity and Nitric Oxide in Living Cells. *Anal. Chem.* **2021**, 93 (10), 4391-4397.
109. Su, W.; Huang, L.; Liang, X.; Zhu, L.; Lin, W., Dual channel mitochondria-targeted fluorescent probe for detection of nitric oxide in living cells and zebrafish. *J. Photochem. Photobiol. A* **2021**, 412, 113256.
110. Franz, K. J.; Singh, N.; Lippard, S. J., Metal-Based NO Sensing by Selective Ligand Dissociation. *Angew. Chem. Int. Ed.* **2000**, 39 (12), 2120-2122.
111. Yoon, S.; Lippard, S. J., Synthesis, Characterization, and Dioxygen Reactivity of Tetracarboxylate-Bridged Diiron(II) Complexes with Coordinated Substrates. *Inorg. Chem.* **2003**, 42 (26), 8606-8608.
112. Hilderbrand, S. A.; Lippard, S. J., Cobalt Chemistry with Mixed Aminotroponimate Salicylaldimate Ligands: Synthesis, Characterization, and Nitric Oxide Reactivity. *Inorg. Chem.* **2004**, 43 (15), 4674-4682.
113. Hilderbrand, S. A.; Lippard, S. J., Nitric Oxide Reactivity of Fluorophore Coordinated Carboxylate-Bridged Diiron(II) and Dicobalt(II) Complexes. *Inorg. Chem.* **2004**, 43 (17), 5294-5301.
114. Smith, R. C.; Tennyson, A. G.; Lim, M. H.; Lippard, S. J., Conjugated Polymer-Based Fluorescence Turn-On Sensor for Nitric Oxide. *Org. Lett.* **2005**, 7 (16), 3573-3575.

CHAPTER 1

115. Hilderbrand, S. A.; Lim, M. H.; Lippard, S. J., Dirhodium Tetracarboxylate Scaffolds as Reversible Fluorescence-Based Nitric Oxide Sensors. *J. Am. Chem. Soc.* **2004**, *126* (15), 4972-4978.
116. Lim, M. H.; Lippard, S. J., Copper Complexes for Fluorescence-Based NO Detection in Aqueous Solution. *J. Am. Chem. Soc.* **2005**, *127* (35), 12170-12171.
117. Tonzetich, Z. J.; McQuade, L. E.; Lippard, S. J., Detecting and Understanding the Roles of Nitric Oxide in Biology. *Inorg. Chem.* **2010**, *49* (14), 6338-6348.
118. Soh, N.; Katayama, Y.; Maeda, M., A fluorescent probe for monitoring nitric oxide production using a novel detection concept. *Analyst* **2001**, *126* (5), 564-566.
119. Lim, M. H.; Lippard, S. J., Fluorescence-Based Nitric Oxide Detection by Ruthenium Porphyrin Fluorophore Complexes. *Inorg. Chem.* **2004**, *43* (20), 6366-6370.
120. Smith, R. C.; Tennyson, A. G.; Lippard, S. J., Polymer-Bound Dirhodium Tetracarboxylate Films for Fluorescent Detection of Nitric Oxide. *Inorg. Chem.* **2006**, *45* (16), 6222-6226.
121. Ford, P. C.; Fernandez, B. O.; Lim, M. D., Mechanisms of Reductive Nitrosylation in Iron and Copper Models Relevant to Biological Systems. *Chem. Rev.* **2005**, *105* (6), 2439-2456.
122. Franz, K. J.; Singh, N.; Spingler, B.; Lippard, S. J., Aminotroponimines as Ligands for Potential Metal-Based Nitric Oxide Sensors. *Inorg. Chem.* **2000**, *39* (18), 4081-4092.
123. Lim, M. H.; Kuang, C.; Lippard, S. J., Nitric Oxide-Induced Fluorescence Enhancement by Displacement of Dansylated Ligands from Cobalt. *ChemBioChem* **2006**, *7* (10), 1571-1576.
124. Khin, C.; Lim, M. D.; Tsuge, K.; Iretskii, A.; Wu, G.; Ford, P. C., Amine Nitrosation via NO Reduction of the Polyamine Copper(II) Complex $\text{Cu}(\text{DAC})_2^+$. *Inorg. Chem.* **2007**, *46* (22), 9323-9331.
125. Lim, M. H.; Wong, B. A.; Pitcock, W. H., Jr.; Mokshagundam, D.; Baik, M.-H.; Lippard, S. J., Direct Nitric Oxide Detection in Aqueous Solution by Copper(II) Fluorescein Complexes. *J. Am. Chem. Soc.* **2006**, *128* (44), 14364-14373.
126. Lim, M. H.; Xu, D.; Lippard, S. J., Visualization of nitric oxide in living cells by a copper-based fluorescent probe. *Nat. Chem. Biol.* **2006**, *2* (7), 375-380.

CHAPTER 1

127. Tsuge, K.; DeRosa, F.; Lim, M. D.; Ford, P. C., Intramolecular Reductive Nitrosylation: Reaction of Nitric Oxide and a Copper(II) Complex of a Cyclam Derivative with Pendant Luminescent Chromophores. *J. Am. Chem. Soc.* **2004**, *126* (21), 6564-6565.
128. Chen, X.; Sun, L.; Chen, Y.; Cheng, X.; Wu, W.; Ji, L.; Chao, H., A fast and selective two-photon phosphorescent probe for the imaging of nitric oxide in mitochondria. *Biomaterials* **2015**, *58*, 72-81.
129. Wu, C.; Wu, K.-J.; Kang, T.-S.; Wang, H.-M. D.; Leung, C.-H.; Liu, J.-B.; Ma, D.-L., Iridium-based probe for luminescent nitric oxide monitoring in live cells. *Sci. Rep.* **2018**, *8* (1), 12467.
130. Dai, Z.; Tian, L.; Song, B.; Liu, X.; Yuan, J., Development of a novel lysosome-targetable time-gated luminescence probe for ratiometric and luminescence lifetime detection of nitric oxide in vivo. *Chem. Sci.* **2017**, *8* (3), 1969-1976.
131. Pluth, M. D.; Chan, M. R.; McQuade, L. E.; Lippard, S. J., Seminaaphthofluorescein-Based Fluorescent Probes for Imaging Nitric Oxide in Live Cells. *Inorg. Chem.* **2011**, *50* (19), 9385-9392.
132. Sun, X.; Kim, G.; Xu, Y.; Yoon, J.; James, T. D., A Water-Soluble Copper(II) Complex for the Selective Fluorescence Detection of Nitric Oxide/Nitroxyl and Imaging in Living Cells. *ChemPlusChem* **2016**, *81* (1), 30-34.
133. Sadek, M. M.; Barzegar Amiri Olia, M.; Nowell, C. J.; Barlow, N.; Schiesser, C. H.; Nicholson, S. E.; Norton, R. S., Characterisation of a novel coumarin-based fluorescent probe for monitoring nitric oxide production in macrophages. *Bioorg. Med. Chem.* **2017**, *25* (20), 5743-5748.
134. Wilson, N.; Mak, L. H.; Cilibrizzi, A.; Gee, A. D.; Long, N. J.; Woscholski, R.; Vilar, R., A lipophilic copper(ii) complex as an optical probe for intracellular detection of NO. *Dalton Trans.* **2016**, *45* (45), 18177-18182.
135. Loas, A.; Lippard, S. J., Direct ratiometric detection of nitric oxide with Cu(ii)-based fluorescent probes. *J. Mater. Chem. B* **2017**, *5* (45), 8929-8933.
136. Srivastava, P.; Verma, M.; Sivakumar, S.; Patra, A. K., A smart FRET probe exhibiting a molecular keypad lock device based on rapid detection of nitric oxide mediated by Cu²⁺ ion. *Sens. Actuators B Chem.* **2019**, *291*, 478-484.

CHAPTER 1

137. Apfel, U.-P.; Buccella, D.; Wilson, J. J.; Lippard, S. J., Detection of Nitric Oxide and Nitroxyl with Benzoessorufin-Based Fluorescent Sensors. *Inorg. Chem.* **2013**, *52* (6), 3285-3294.
138. Hu, X.; Wang, J.; Zhu, X.; Dong, D.; Zhang, X.; Wu, S.; Duan, C., A copper(ii) rhodamine complex with a tripodal ligand as a highly selective fluorescence imaging agent for nitric oxide. *Chem. Commun.* **2011**, *47* (41), 11507-11509.
139. Mondal, B.; Kumar, P.; Ghosh, P.; Kalita, A., Fluorescence-based detection of nitric oxide in aqueous and methanol media using a copper(ii) complex. *Chem. Commun.* **2011**, *47* (10), 2964-2966.
140. Hu, X.; Zhang, X.; Song, H.; He, C.; Bao, Y.; Tang, Q.; Duan, C., A novel copper(II) complex-based fluorescence probe for nitric oxide detecting and imaging. *Tetrahedron* **2012**, *68* (39), 8371-8375.
141. Alam, R.; Mistri, T.; Mondal, P.; Das, D.; Mandal, S. K.; Khuda-Bukhsh, A. R.; Ali, M., A novel copper(ii) complex as a nitric oxide turn-on fluorosensor: intracellular applications and DFT calculation. *Dalton Trans.* **2014**, *43* (6), 2566-2576.
142. Islam, A. S. M.; Sasmal, M.; Maiti, D.; Dutta, A.; Ganguly, S.; Katarkar, A.; Gangopadhyay, S.; Ali, M., Phenazine-Embedded Copper(II) Complex as a Fluorescent Probe for the Detection of NO and HNO with a Bioimaging Application. *ACS Appl. Bio Mater.* **2019**, *2* (5), 1944-1955.
143. Brown, H. W.; Pimentel, G. C., Photolysis of Nitromethane and of Methyl Nitrite in an Argon Matrix; Infrared Detection of Nitroxyl, HNO. *J. Chem. Phys.* **1958**, *29* (4), 883-888.
144. Fukuto, J. M.; Dutton, A. S.; Houk, K. N., The Chemistry and Biology of Nitroxyl (HNO): A Chemically Unique Species with Novel and Important Biological Activity. *ChemBioChem* **2005**, *6* (4), 612-619.
145. Fukuto, J. M., A recent history of nitroxyl chemistry, pharmacology and therapeutic potential. *Br. J. Pharmacol.* **2019**, *176* (2), 135-146.
146. Paolocci, N.; Katori, T.; Champion, H. C.; St. John, M. E.; Miranda, K. M.; Fukuto, J. M.; Wink, D. A.; Kass, D. A., Positive inotropic and lusitropic effects of HNO/NO⁻ in failing hearts: Independence from β -adrenergic signaling. *Proc. Natl. Acad. Sci. U.S.A.* **2003**, *100* (9), 5537-5542.

CHAPTER 1

147. Arcaro, A.; Lembo, G.; Tocchetti, C. G., Nitroxyl (HNO) for Treatment of Acute Heart Failure. *Curr. Heart Fail. Rep.* **2014**, *11* (3), 227-235.
148. Bonner, F. T.; Ravid, B., Thermal decomposition of oxyhyponitrite (sodium trioxodinitrate(II)) in aqueous solution. *Inorg. Chem.* **1975**, *14* (3), 558-563.
149. Bonner, F. T.; Hughes, M. N., The Aqueous Solution Chemistry of Nitrogen in Low Positive Oxidation States. *Comments Inorg. Chem.* **1988**, *7* (4), 215-234.
150. Bonner, F. T.; Ko, Y., Kinetic, isotopic, and nitrogen-15 NMR study of N-hydroxybenzenesulfonamide decomposition: an nitrosyl hydride (HNO) source reaction. *Inorg. Chem.* **1992**, *31* (12), 2514-2519.
151. Zamora, R.; Grzesiok, A.; Weber, H.; Feelisch, M., Oxidative release of nitric oxide accounts for guanylyl cyclase stimulating, vasodilator and anti-platelet activity of Piloty's acid: a comparison with Angeli's salt. *Biochem. J.* **1995**, *312* (2), 333-339.
152. Keefer, L. K.; Nims, R. W.; Davies, K. M.; Wink, D. A., "NONOates" (1-substituted diazen-1-ium-1,2-diolates) as nitric oxide donors: Convenient nitric oxide dosage forms. In *Methods in Enzymology*, Academic Press: 1996; Vol. 268, pp 281-293.
153. DeMaster, E. G.; Redfern, B.; Nagasawa, H. T., Mechanisms of Inhibition of Aldehyde Dehydrogenase by Nitroxyl, the Active Metabolite of the Alcohol Deterrent Agent Cyanamide. *Biochem. Pharmacol.* **1998**, *55* (12), 2007-2015.
154. Sha, X.; Isbell, T. S.; Patel, R. P.; Day, C. S.; King, S. B., Hydrolysis of Acyloxy Nitroso Compounds Yields Nitroxyl (HNO). *J. Am. Chem. Soc.* **2006**, *128* (30), 9687-9692.
155. Paolucci, N.; Jackson, M. I.; Lopez, B. E.; Miranda, K.; Tocchetti, C. G.; Wink, D. A.; Hobbs, A. J.; Fukuto, J. M., The pharmacology of nitroxyl (HNO) and its therapeutic potential: Not just the janus face of NO. This review is dedicated to the career of Prof. Herbert T. Nagasawa, a pioneer in the field of HNO chemistry, biochemistry and pharmacology. *Pharmacol. Ther.* **2007**, *113* (2), 442-458.
156. Martí, M. A.; Bari, S. E.; Estrin, D. A.; Doctorovich, F., Discrimination of Nitroxyl and Nitric Oxide by Water-Soluble Mn(III) Porphyrins. *J. Am. Chem. Soc.* **2005**, *127* (13), 4680-4684.
157. Cline, M. R.; Tu, C.; Silverman, D. N.; Toscano, J. P., Detection of nitroxyl (HNO) by membrane inlet mass spectrometry. *Free Radic. Biol. Med.* **2011**, *50* (10), 1274-1279.

CHAPTER 1

158. Miao, Z.; King, S. B., Recent advances in the chemical biology of nitroxyl (HNO) detection and generation. *Nitric Oxide* **2016**, *57*, 1-14.
159. Rosenthal, J.; Lippard, S. J., Direct Detection of Nitroxyl in Aqueous Solution Using a Tripodal Copper(II) BODIPY Complex. *J. Am. Chem. Soc.* **2010**, *132* (16), 5536-5537.
160. Zhou, Y.; Liu, K.; Li, J.-Y.; Fang, Y.; Zhao, T.-C.; Yao, C., Visualization of Nitroxyl in Living Cells by a Chelated Copper(II) Coumarin Complex. *Org. Lett.* **2011**, *13* (6), 1290-1293.
161. Zhou, Y.; Yao, Y.-W.; Li, J.-Y.; Yao, C.; Lin, B.-P., Nitroxyl induced fluorescence enhancement via reduction of a copper(II) coumarin-ester complex: Its application for bioimaging in vivo. *Sens. Actuators B Chem.* **2012**, *174*, 414-420.
162. Wrobel, A. T.; Johnstone, T. C.; Deliz Liang, A.; Lippard, S. J.; Rivera-Fuentes, P., A Fast and Selective Near-Infrared Fluorescent Sensor for Multicolor Imaging of Biological Nitroxyl (HNO). *J. Am. Chem. Soc.* **2014**, *136* (12), 4697-4705.
163. Loas, A.; Radford, R. J.; Deliz Liang, A.; Lippard, S. J., Solid-phase synthesis provides a modular, lysine-based platform for fluorescent discrimination of nitroxyl and biological thiols. *Chem. Sci.* **2015**, *6* (7), 4131-4140.
164. Palanisamy, S.; Wang, Y.-L.; Chen, Y.-J.; Chen, C.-Y.; Tsai, F.-T.; Liaw, W.-F.; Wang, Y.-M. In Vitro and in Vivo Imaging of Nitroxyl with Copper Fluorescent Probe in Living Cells and Zebrafish *Molecules* [Online], 2018.
165. Lv, H.-j.; Ma, R.-f.; Zhang, X.-t.; Li, M.-h.; Wang, Y.-t.; Wang, S.; Xing, G.-w., Surfactant-modulated discriminative sensing of HNO and H₂S with a Cu²⁺-complex-based fluorescent probe. *Tetrahedron* **2016**, *72* (35), 5495-5501.
166. Reisz, J. A.; Klorig, E. B.; Wright, M. W.; King, S. B., Reductive Phosphine-Mediated Ligation of Nitroxyl (HNO). *Org. Lett.* **2009**, *11* (13), 2719-2721.
167. Reisz, J. A.; Zink, C. N.; King, S. B., Rapid and Selective Nitroxyl (HNO) Trapping by Phosphines: Kinetics and New Aqueous Ligations for HNO Detection and Quantitation. *J. Am. Chem. Soc.* **2011**, *133* (30), 11675-11685.
168. Kawai, K.; Ieda, N.; Aizawa, K.; Suzuki, T.; Miyata, N.; Nakagawa, H., A Reductant-Resistant and Metal-Free Fluorescent Probe for Nitroxyl Applicable to Living Cells. *J. Am. Chem. Soc.* **2013**, *135* (34), 12690-12696.

CHAPTER 1

169. Mao, G.-J.; Zhang, X.-B.; Shi, X.-L.; Liu, H.-W.; Wu, Y.-X.; Zhou, L.-Y.; Tan, W.; Yu, R.-Q., A highly sensitive and reductant-resistant fluorescent probe for nitroxyl in aqueous solution and serum. *Chem. Commun.* **2014**, *50* (43), 5790-5792.
170. Bobba, K. N.; Zhou, Y.; Guo, L. E.; Zang, T. N.; Zhang, J. F.; Bhuniya, S., Resorufin based fluorescence ‘turn-on’ chemodosimeter probe for nitroxyl (HNO). *RSC Adv.* **2015**, *5* (103), 84543-84546.
171. Miao, Z.; Reisz, J. A.; Mitroka, S. M.; Pan, J.; Xian, M.; King, S. B., A selective phosphine-based fluorescent probe for nitroxyl in living cells. *Bioorg. Med. Chem. Lett.* **2015**, *25* (1), 16-19.
172. Jing, X.; Yu, F.; Chen, L., Visualization of nitroxyl (HNO) in vivo via a lysosome-targetable near-infrared fluorescent probe. *Chem. Commun.* **2014**, *50* (91), 14253-14256.
173. Liu, P.; Jing, X.; Yu, F.; Lv, C.; Chen, L., A near-infrared fluorescent probe for the selective detection of HNO in living cells and in vivo. *Analyst* **2015**, *140* (13), 4576-4583.
174. Liu, P.; Han, X.-Y.; Yu, F.-B.; Chen, L.-X., A Near-Infrared Fluorescent Probe for Detection of Nitroxyl in Living Cells. *Chinese Journal of Analytical Chemistry* **2015**, *43* (12), 1829-1836.
175. Tan, Y.; Liu, R.; Zhang, H.; Peltier, R.; Lam, Y.-W.; Zhu, Q.; Hu, Y.; Sun, H., Design and Synthesis of Near-infrared Fluorescent Probes for Imaging of Biological Nitroxyl. *Sci. Rep.* **2015**, *5* (1), 16979.
176. Gong, X.; Yang, X.-F.; Zhong, Y.; Chen, Y.; Li, Z., A mitochondria-targetable near-infrared fluorescent probe for imaging nitroxyl (HNO) in living cells. *Dyes Pigm.* **2016**, *131*, 24-32.
177. Niu, H.; Mi, X.; Hua, X.; Zhang, Y.; Zhai, Y.; Qin, F.; Ye, Y.; Zhao, Y., A bifunctional fluorescent probe based on “AND logic” for the simultaneous recognition of H₂S/HNO and its bioimaging applications. *Anal. Chim. Acta* **2022**, *1192*, 339341.
178. Zhang, C.; Qian, M.; Zhang, L.; Zheng, H.; Zhang, M.; Jiao, Y.; Kafuti, Y. S.; Chen, Q.; Wang, J., A near-infrared fluorescent probe with ultra-large Stokes shift for the detection of HNO in cells and mice. *J. Lumin.* **2022**, *241*, 118496.
179. Zhang, H.; Qiao, Z.; Wei, N.; Zhang, Y.; Wang, K., A rapid-response and near-infrared fluorescent probe for imaging of nitroxyl in living cells. *Talanta* **2020**, *206*, 120196.

CHAPTER 1

180. Wang, T.; Chai, Y.; Chen, S.; Yang, G.; Lu, C.; Nie, J.; Ma, C.; Chen, Z.; Sun, Q.; Zhang, Y.; Ren, J.; Wang, F.; Zhu, W.-H., Near-infrared fluorescent probe for imaging nitroxyl in living cells and zebrafish model. *Dyes Pigm.* **2019**, *166*, 260-265.
181. Wang, J.; Zhu, W.; Li, C.; Zhang, P.; Jiang, G.; Niu, G.; Tang, B. Z., Mitochondria-targeting NIR fluorescent probe for rapid, highly sensitive and selective visualization of nitroxyl in live cells, tissues and mice. *Sci. China Chem.* **2020**, *63* (2), 282-289.
182. Zhang, C.-X.; Xiang, M.-H.; Liu, X.-J.; Wang, F.; Yu, R.-Q.; Jiang, J.-H., Development of large Stokes shift, near-infrared fluorescence probe for rapid and bioorthogonal imaging of nitroxyl (HNO) in living cells. *Talanta* **2019**, *193*, 152-160.
183. Zhang, C.; He, F.; Huang, F.; Xu, J.; Hu, Y., A fluorescent probe with low-background for visualization of nitroxyl in living cells and zebrafish. *Dyes Pigm.* **2021**, *185*, 108889.
184. Li, W.; Wang, X.; Zhang, Y.-M.; Zhang, S. X.-A., Single probe giving different signals towards reactive oxygen species and nitroxyl. *Dyes Pigm.* **2018**, *148*, 348-352.
185. Palanisamy, S.; Chen, L.-F.; Tzou, S.-C.; Wang, Y.-M., Near-infrared templated fluorescent probe for nitroxyl: Selective and sensitive turn-on detection in living cells. *Sens. Actuators B Chem.* **2020**, *310*, 127839.
186. Li, Z.; Li, J.; Zhang, D.; Zhu, X.; Ye, Y.; Zhao, Y., A novel dual-channel fluorescent probe for nitroxyl detection and its application in HepG-2 cells. *Sens. Actuators B Chem.* **2020**, *312*, 127944.
187. Peng, S.; Li, Z.; Zhang, Y.; Cao, W.; Liu, J.; Zhu, W.; Ye, Y., A two-photon fluorescent probe for HNO rapid visualization in endoplasmic reticulum. *Sens. Actuators B Chem.* **2020**, *317*, 128211.
188. Wei, C.; Wang, X.; Li, X.; Jia, X.; Hao, X.; Zhang, J.; Zhang, P.; Li, X., An isophorone-fused near-infrared fluorescent probe with a large Stokes shift for imaging endogenous nitroxyl in living cells and zebrafish. *Spectrochim. Acta A* **2020**, *227*, 117765.
189. Liu, Z.; Sun, Q., A near-infrared fluorescent probe for imaging of nitroxyl in living cells. *Spectrochim. Acta A* **2020**, *241*, 118680.
190. Kong, Y.; Wan, X.; Liu, Z.; Chen, F.; Wu, F.; Qin, G.; Cao, D.; Cui, Y., A novel dansyl-naphthalimide fluorescent probe for visualizing nitroxyl (HNO) in biological systems. *Sens. Actuators B Chem.* **2022**, *350*, 130852.

CHAPTER 1

191. Li, H.; Yao, Q.; Xu, F.; Xu, N.; Ma, X.; Fan, J.; Long, S.; Du, J.; Wang, J.; Peng, X., Recognition of Exogenous and Endogenous Nitroxyl in Living Cells via a Two-Photon Fluorescent Probe. *Anal. Chem.* **2018**, *90* (7), 4641-4648.
192. Ma, Q.; Xu, J.; Mao, G.; Guo, X.; Liang, B.; Bai, Y.; Wang, C., A highly sensitive and selective fluorescent probe for nitroxyl based on a naphthalene derivative. *Anal. Methods* **2019**, *11* (6), 832-843.
193. Zhang, P.; Lian, P.; Wang, X.; Li, X.; Wei, C.; Li, X., A 6-acetyl-2-naphthol based two-photon fluorescent probe for the selective detection of nitroxyl and imaging in living cells. *Anal. Methods* **2019**, *11* (10), 1299-1303.
194. Li, J.-B.; Wang, Q.; Liu, H.-W.; Yin, X.; Hu, X.-X.; Yuan, L.; Zhang, X.-B., Engineering of a bioluminescent probe for imaging nitroxyl in live cells and mice. *Chem. Commun.* **2019**, *55* (12), 1758-1761.
195. Yang, M.; Fan, J.; Sun, W.; Du, J.; Long, S.; Shao, K.; Peng, X., A nitroxyl-responsive near-infrared fluorescent chemosensor for visualizing H₂S/NO crosstalk in biological systems. *Chem. Commun.* **2019**, *55* (59), 8583-8586.
196. Chai, Z.; Liu, D.; Li, X.; Zhao, Y.; Shi, W.; Li, X.; Ma, H., A tumor-targeted near-infrared fluorescent probe for HNO and its application to the real-time monitoring of HNO release in vivo. *Chem. Commun.* **2021**, *57* (41), 5063-5066.
197. Staikopoulos, V.; Zhang, X.; Pullen, B. P.; Reineck, P.; Vidanapathirana, A. K.; Lee, S. M.; Liu, J.; Bursill, C.; Hutchinson, M. R.; Abell, A. D., Multi-coloured fluorescent sensing toolbox for selective detection of nitroxyl in vitro and ex vivo. *Sens. Diagn.* **2022**, *1* (2), 280-293.
198. Liu, C.; Wu, H.; Wang, Z.; Shao, C.; Zhu, B.; Zhang, X., A fast-response, highly sensitive and selective fluorescent probe for the ratiometric imaging of nitroxyl in living cells. *Chem. Commun.* **2014**, *50* (45), 6013-6016.
199. Liu, C.; Wang, Y.; Tang, C.; Liu, F.; Ma, Z.; Zhao, Q.; Wang, Z.; Zhu, B.; Zhang, X., A reductant-resistant ratiometric, colorimetric and far-red fluorescent probe for rapid and ultrasensitive detection of nitroxyl. *J. Mater. Chem. B* **2017**, *5* (19), 3557-3564.
200. Zheng, K.; Chen, H.; Fang, S.; Wang, Y., A ratiometric fluorescent probe based on a Bodipy-Coumarin conjugate for sensing of nitroxyl in living cells. *Sens. Actuators B Chem.* **2016**, *233*, 193-198.

CHAPTER 1

201. Lv, H.-M.; Yi, C.; Lei, J.; Au, C.-T.; Yin, S.-F., An ESIPT-based ratiometric fluorescent probe for the imaging of nitroxyl in living cells. *Anal. Methods* **2015**, *7* (9), 3883-3887.
202. Jin, X.; Sun, X.; Di, X.; Zhang, X.; Huang, H.; Liu, J.; Ji, P.; Zhu, H., Novel fluorescent ESIPT probe based on flavone for nitroxyl in aqueous solution and serum. *Sens. Actuators B Chem.* **2016**, *224*, 209-216.
203. Zhang, H.; Liu, R.; Tan, Y.; Xie, W. H.; Lei, H.; Cheung, H.-Y.; Sun, H., A FRET-based Ratiometric Fluorescent Probe for Nitroxyl Detection in Living Cells. *ACS Appl. Mater. Interfaces* **2015**, *7* (9), 5438-5443.
204. Zhu, X.; Xiong, M.; Liu, H.-w.; Mao, G.-j.; Zhou, L.; Zhang, J.; Hu, X.; Zhang, X.-B.; Tan, W., A FRET-based ratiometric two-photon fluorescent probe for dual-channel imaging of nitroxyl in living cells and tissues. *Chem. Commun.* **2016**, *52* (4), 733-736.
205. Zhou, Y.; Zhang, X.; Yang, S.; Li, Y.; Qing, Z.; Zheng, J.; Li, J.; Yang, R., Ratiometric Visualization of NO/H₂S Cross-Talk in Living Cells and Tissues Using a Nitroxyl-Responsive Two-Photon Fluorescence Probe. *Anal. Chem.* **2017**, *89* (8), 4587-4594.
206. Yuan, S.; Wang, F.; Yang, G.; Lu, C.; Nie, J.; Chen, Z.; Ren, J.; Qiu, Y.; Sun, Q.; Zhao, C.; Zhu, W.-H., Highly Sensitive Ratiometric Self-Assembled Micellar Nanoprobe for Nitroxyl and Its Application In Vivo. *Anal. Chem.* **2018**, *90* (6), 3914-3919.
207. Li, H.; Wang, C.; Cai, L.; Yu, X.; Wu, L.; Yuan, N.; Zhu, Y.; Jia, N.; James, T. D.; Huang, C., Versatile Ratiometric Fluorescent Probe Based on the Two-Isophorone Fluorophore for Sensing Nitroxyl. *Ind. Eng. Chem. Res.* **2021**, *60* (44), 15913-15920.
208. Xu, J.; Bai, Y.; Ma, Q.; Sun, J.; Tian, M.; Li, L.; Zhu, N.; Liu, S., Ratiometric Determination of Nitroxyl Utilizing a Novel Fluorescence Resonance Energy Transfer-Based Fluorescent Probe Based on a Coumarin-Rhodol Derivative. *ACS Omega* **2022**, *7* (6), 5264-5273.
209. Li, C.; Jiang, G.; Liu, X.; Lai, Q.; Kang, M.; Wang, D.; Zhang, P.; Wang, J.; Tang, B. Z., An easily available ratiometric AIE probe for nitroxyl visualization in vitro and in vivo. *Mater. Chem. Front.* **2021**, *5* (4), 1817-1823.
210. Cline, M. R.; Toscano, J. P., Detection of nitroxyl (HNO) by a prefluorescent probe. *J. Phys. Org. Chem.* **2011**, *24* (10), 993-998.

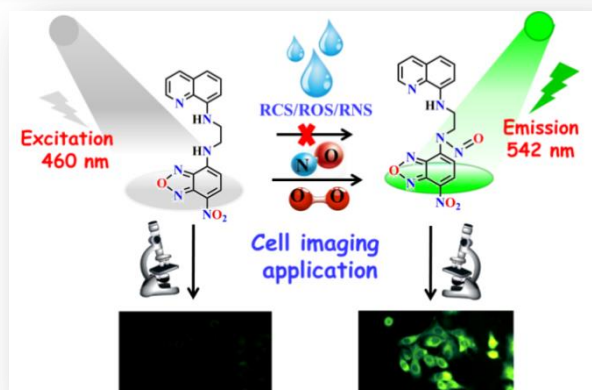
CHAPTER 1

211. Pino, N. W.; Davis, J., III; Yu, Z.; Chan, J., NitroxylFluor: A Thiol-Based Fluorescent Probe for Live-Cell Imaging of Nitroxyl. *J. Am. Chem. Soc.* **2017**, *139* (51), 18476-18479.

A Novel N-nitrosation based Highly Sensitive and Selective Turn-On Fluorescent Sensor for NO: Kinetic appraisal, DFT studies and Biological application

Abstract:

Nitric oxide (NO) is an ubiquitous messenger molecule playing a keystone role in various physiological and pathological processes. However, the selective turn-on fluorescence response of NO is a challenging task due to (a) very short half-life of NO (typically in the range of 0.1–10 s) in biological milieu; (b) false positive response to reactive carbonyl species (RCS) (e.g. dehydroascorbic acid and methylglyoxal etc.) and some other reactive oxygen/nitrogen species (ROS/RNS), especially by *o*-phenylenediamine (OPD) based fluorosensors. To avoid these limitations NO sensors should be designed in such a way that it react spontaneously with NO to give turn-on response within the time frame of $t_{1/2}$ (typically in the range of 0.1–10 s) of NO and λ_{em} in the visible wavelength along with good cell permeability to meet up with biocompatibility. With these views in mind, a new N-nitrosation based fluorescent sensor, NDAQ, has been developed which is highly selective to NO with ~ 27 fold fluorescence enhancement at $\lambda_{em} = 542$ nm with high sensitivity (LOD=7 nM) and shorter response time, eliminating the interference of reactive species (RCS/ROS/RNS). Furthermore, all the photophysical studies of NDAQ have been performed in pure aqueous medium at physiological pH, indicating its good stability under physiological condition. The kinetic assay illustrates the second-order dependency w.r.to [NO] and first order with [NDAQ]. The biological studies reveal the successful application of the probe to track both endogenous and exogenous NO in living organisms.



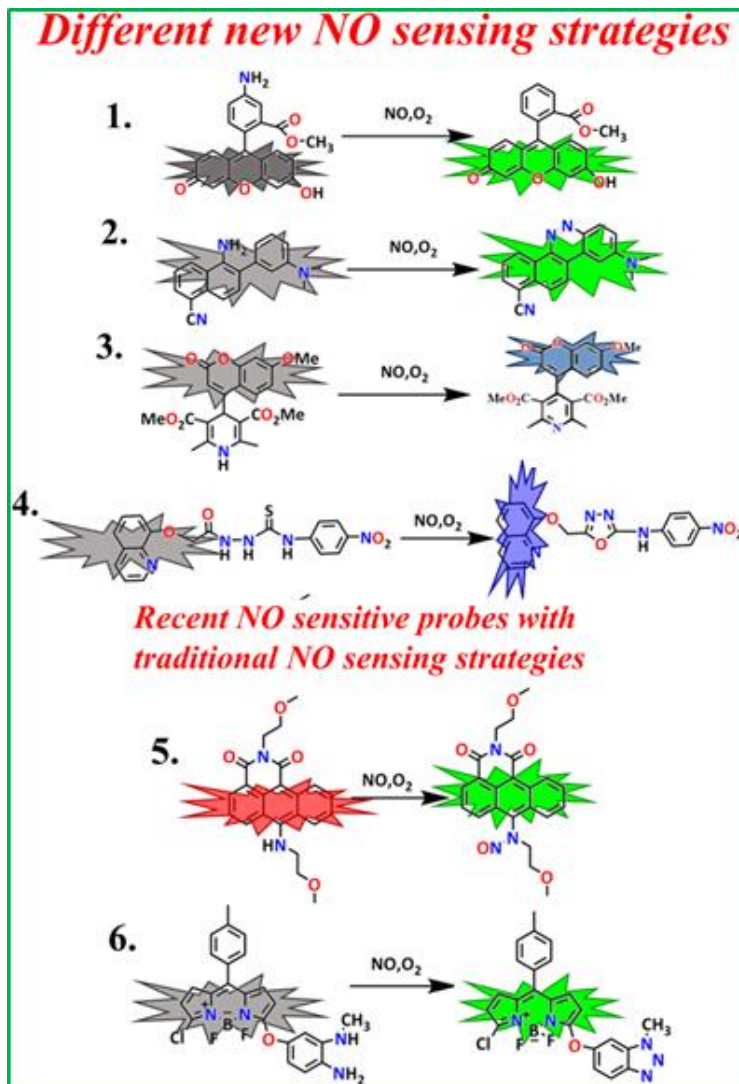
2.1 Introduction

Nitric oxide (NO) is conceded as a versatile player in the area of biochemistry, immunology and neuroscience because of its integral role in the cardiovascular system as a vasodilator, in the immune system as a protective agent and also in the nervous system as a neurotransmitter.¹⁻⁴ In the year 1992, NO was declared as the “Molecule of the Year”.⁵⁻⁶ In 1998, it was discovered that NO is a potent vasodilator identical to the role played by endothelium-derived relaxing factor (EDRF) in the vascular endothelium. Since then its selective detection in living systems has attracted much more attention of chemists and biologists.⁷ NO is synthesized during the conversion of L-arginine to L-citrulline through the enzymatic activity of nitric oxide synthases (NOS) which consist of an oxygenase domain and a reductase domain that are linked through a Ca^{2+} /calmodulin binding region.⁸⁻¹² Recent studies have revealed that at low concentration (pM-nM), NO exerts the protective and proliferative roles in living cells. However, at high concentration range ($>1 \mu\text{M}$), it promotes cell cycle arrest, senescence and apoptosis. The misregulation of NO and its biotransformation products (such as peroxynitrite (ONOO^-), dinitrogen trioxide (N_2O_3) and others (RNS)) are associated with damaging of lipids, DNA and proteins.¹¹ To treat the detrimental effects of NO, determining the exact concentration of it in the biological systems is of utmost importance.

To delineate the spatial and temporal distributions of NO in living systems, bioimaging techniques are found to be the most promising one among various NO detection tools.¹³⁻¹⁶ In comparison to other NO imaging techniques, fluorescence imaging studies have acquired an immense attention due to its noninvasive detection and high sensitivity as well as selectivity towards analytes. By considering all these facts, numerous nitric oxide fluorescent probes have been developed to date, which conventionally exploit the specific reactions of this ubiquitous signaling agent with *o*-phenylenediamine (OPD)¹⁷ and metal–ligand complexes.¹⁸ However, in most of the cases fluorescent NO probes suffer from some serious limitations like (a) very short half-life of NO in biological milieu (typically in the range of 0.1–10 s); (b) false positive response to reactive carbonyl species (RCS) (e.g. dehydroascorbic acid and methylglyoxal etc.) and some other reactive oxygen/nitrogen species (ROS/RNS), especially by *o*-phenylenediamine (OPD) based fluorosensors; and also (c) high pH sensitivity as particularly at lower pH (<4.0) the triazole moiety gets protonated causing autofluorescence. Whereas, in case of NO sensors with metal ion receptors attached to fluorophoric unit suffer from metal ion toxicity. Therefore,

CHAPTER 2

designing of fluorophoric moieties for selective and sensitive detection of NO is an extremely demanding and challenging task. Over the last few years, various novel NO sensing strategies have acquired an immense attention from the chemists and biologists.



Scheme 2.1 Various approaches for designing the fluorescent probes for NO sensing and bioimaging.

Now, to understand more precisely the role of NO in physiological systems, some modern NO sensing strategies are enlisted e.g. (1) oxidative deamination of aromatic primary monoamines¹⁹, (2) the diazo ring generation from o-amino-3'-dimethylaminophenyl aromatics²⁰ (3) aromatization of the Hantzsch ester²¹ and (4) others²²⁻²⁵. However, the conventional NO sensing strategies such as, (5) the nitrosation reaction with a secondary amine²⁶, (6) the formation of the

CHAPTER 2

triazole unit²⁷ in a modified form have also been implicated to date in determining the influential role of this messenger molecule (NO) in living organisms (as shown in **Scheme 2.1**).

In recent times, by conceiving all the previously mentioned concerns, N-nitrosation based fluorophoric entities acquired special interest due to its outstanding sensitivity, selectivity and prompt positive response towards NO. In N-nitrosation based fluorophoric probes, the presence of an aromatic secondary amines (as a NO recognition center) produce N-nitroso products on interaction with NO. This causes an obvious change in fluorescence intensity via obstructing either the intramolecular charge transfer (ICT) or PeT processes.^{26, 28-32}

In our current research endeavor, we have designed a new N-nitrosation based fluorescent probe for selective and sensitive recognition of NO in biological systems. Here, ethane-1,2-diamine act as a spacer between two fluorophoric systems — one is quinoline which functions as an electron donating group and the other is NBD (4-Chloro-7-nitro-2,1,3-benzoxadiazole) which performs as an electron-withdrawing group (**Scheme 2.2**). As a consequence, weak ICT reaction mechanism operates due to the generation of Donor-Acceptor model of the concerned probe as confirmed from DFT studies (*vide supra*). Now, the ICT process is further strengthened by the formation of N-nitrosoamine under aerobic conditions, resulting in the generation of fluorescence signal in the green region (shown in **Scheme 2.3**) (~542 nm). The high specificity and sensitivity of NDAQ towards NO in ~100% HEPES buffer at pH 7.2 makes this probe highly suitable to track both exogenous and endogenous NO without any interference from other biological species that are present in the living organisms.

2.2 EXPERIMENTAL SECTION

2.2.1 Materials and Apparatus

All the starting materials such as 8-aminoquinoline, bromoethylamine hydrobromide, 4-Chloro-7-nitrobenzofurazan and triethylamine were procured from Sigma-Aldrich and used as received. All the metal ions in the form of nitrates and chloride salts and all the anions in the form of sodium/ammonium salts and other reactive oxygen/nitrogen species were purchased from commercial sources and were utilized without further purification. Unless otherwise mentioned, all the solvents like dimethylformamide (DMF), acetonitrile (MeCN) etc were of analytical grade

CHAPTER 2

and dried before use by applying standard procedure. ^1H and ^{13}C NMR were operated on Bruker 300 MHz spectrometer in DMSO-d_6 (Trimethylsilane ($\delta = 0$) as an internal standard). The High resolution mass spectra (HRMS) of the designed probe (NDAQ) and the N-nitrosated adduct (NDAQ—NO) were executed on QT of Micro YA263 spectrometer. The UV-Vis absorption spectra, emission spectra and also the infrared spectra have been acquired by utilizing the instruments of same model described in our previous work.²²

2.2.2 Preparation of Stock Solution of Analytes

Mili-Q-Millipore water was used in every experimental study even in the preparation of stock solutions of various analytes (cations, anions and others). For the preparation of the solutions of $\cdot\text{OH}$, HNO and ONOO^- the same procedures have been adopted as described in the literature.³³ The solution of NO having concentration 1.73×10^{-3} M was prepared by following the reported method.²² The stock solution of the probe (NDAQ) with concentration 1.0×10^{-3} mL^{-1} was prepared in CH_3CN by adding minimum amount of DMSO. All the experimental studies for estimating the sensitivity of the probe towards NO were done in 10 mM HEPES buffer at pH 7.2. Probe concentration was adjusted to 20 μM by adding 50 μL (1.0×10^{-3} M) of the probe to 2.5 ml of 10.0 mM HEPES buffer taken in a cuvette, and the fluorescence spectra were then recorded after an incremental addition of NO (0-44 μM) in each case.

2.2.3 Kinetic Studies

By considering pseudo-first-order conditions, kinetic studies were accomplished with variable concentrations of NO in the range 5-30 μM keeping NDAQ as a minor component (2 μM) at 15 $^\circ\text{C}$ in 10 mM HEPES buffer (pH 7.2, $\mu = 0.10$ M NaCl). Similarly, while NO is considered as a minor component, the concentration of NDAQ was varied from 5 to 50 μM to determine the rate dependency on [NDAQ] keeping [NO] at 2 μM . The confirmation of first-order dependency w.r.t. [NDAQ] was supported from the slope $\{(1.03 \pm 0.09)$ with $R = 0.988\}$ of the plot $\log k_{\text{obs}}$ vs. $\log[\text{NDAQ}]$. Similarly the slope $\{(2.16 \pm 0.07)$ and $R = 0.998\}$ of the plot $\log k_{\text{obs}}$ vs. $\log[\text{NO}]$ demonstrates the second order dependency on [NO].

CHAPTER 2

2.2.4 Calculation of LOD

The Limit of Detection of NO is estimated by using the 3σ /slope method (eqn.1)

$$\text{LOD} = 3 \times S_d/S \quad \dots\dots\dots(1)$$

Where, the standard deviation of the blank is denoted by the term 'S_d' and the slope of the plot F.I. (a.u.) vs. [NO] in fluorescence titration data is denoted by the term 'S'.

2.2.5 Quantum Yield

Fluorescence quantum yields (Φ) of NDAQ and NDAQ—NO were calculated with the help of eqn.2.

$$\Phi_{\text{sample}} = (\text{OD}_{\text{std}} \times A_{\text{sample}})/(\text{OD}_{\text{sample}} \times A_{\text{std}}) \times \Phi_{\text{std}} \quad \dots\dots(2)$$

Where, the respective areas under the fluorescence spectral curves of the sample and the standard are symbolized as A_{sample} and A_{std} . The optical densities of the standard and the sample are represented by OD_{std} and $\text{OD}_{\text{sample}}$, respectively at $\lambda_{\text{ex}}=460$ nm. Here, aqueous acidic solution of quinine sulfate was used as the standard with $\Phi_{\text{std}} = 0.54$.

2.2.6 Computational method

For the theoretical investigations we have carried out the computational data analysis by the DFT method³⁴ coupled with the conductor-like polarizable continuum model (CPCM).³⁵⁻³⁷ In this study, the Becke's hybrid functions³⁸ with the Lee-Yang-Parr (LYP)³⁹ correlation function are also adapted. To get an idea about the fully optimized geometry of NDAQ and NDAQ—NO, we have used 6-31G (d,p) basis set and for electron density plots Gauss View 5.1 software was accepted. Absorption spectra of both the compounds were evaluated by TD-DFT method using 6-31G (d, p) basis set. All the related calculations were made applying Gaussian 09W software package⁴⁰ and for the calculation of molecular orbital contributions we have applied Gauss Sum 2.1 software.⁴¹

CHAPTER 2

2.2.7 Cell Imaging Experiments

2.2.7.1 Cell viability assay

Human lung adenocarcinoma cells (A549) and murine macrophages Raw 264.7 cells were grown in Dulbecco's modified Eagle's (DMEM) medium provided with 10% FBS and 1% antibiotic at 37 °C with 5% CO₂. Cell viability of the probe NDAQ for A549 and Raw 264.7 cells were analyzed with NDAQ for 24h by MTT assay.²³

2.2.7.2 In-Vitro Cell incubation and imaging

A549 cells were grown on glass coverslips in 35x10 mm culture dishes to detect exogenous NO. A549 cells were treated in the presence and absence of DEA-NONOate, the source of NO (5 μM and 10 μM) and then incubated with 5% CO₂ for 30 mins at 37°C and then cells were washed with media. Now, A549 cells were further treated with NDAQ (5 μM and 10 μM) for about 30 mins and then washed. The live cell imaging experiments were performed by fluorescence microscope (Leica DM3000, Germany) with an objective lens of 40X magnification. For endogenous NO detection, Raw 264.7 cells were co-stimulated with LPS (1.0 mg/mL) and IFN-γ (1000U/mL) for 4h, and then further incubated with NDAQ (5 μM) for 30 mins without co-stimulant (control). The generation of green fluorescence intracellularly was due to endogenous formation of NO which was confirmed by NO scavenger PTIO (2-Phenyl-4, 4, 5, 5-tetramethylimidazoline-1-oxyl-3-oxide) treatment. Raw 264.7 cells were co-stimulated in the absence and presence of LPS (1.0 mg/mL) and IFN-γ (1000 U/mL) for 4h, along with PTIO (200 mM) followed by treatment with the probe NDAQ (5 μM) for 30 min. Now, the live fluorescence images were performed.

2.2.8 Synthesis

2.2.8.1 Synthesis and characterization of AmQNH

AmQNH has been synthesized by utilizing the following procedure. Both 8-aminoquinoline and 2-bromoethylamine hydrobromide were mixed together in anhydrous toluene and refluxed under nitrogen atmosphere for about 1 day. After removing the solvent under reduced pressure, the residue was dissolved in 20% aqueous solution of NaOH. Now, the resulted solution was extracted with dichloromethane (50 ml in each time) three times and finally dried over anhydrous

CHAPTER 2

sodium sulphate. Now, the solvent was reduced under vacuum and the resultant crude product was subjected to silica gel chromatography for further purification (CH_2Cl_2 : CH_3OH : Et_3N , 100: 0.5: 0.25, v/v/v). The solvent of the effluent was removed under reduced pressure to get yellow oil which was washed with pet ether to obtain the desired whitish yellow product in pure form. Yield: 52%. $\text{C}_{11}\text{H}_{13}\text{N}_3$. Molecular Weight: 187.1109. ^1H -NMR (300 MHz, DMSO-d_6)(δ , ppm): 8.75 (dd, 1H, -NH), 8.23 (dd, 1H, ArH), 7.96 (s, 1H, - NH_2), 7.50-7.54 (m, 1H, -ArH), 7.39 (t, 1H, -ArH), 7.12 (d, 1H, -ArH), 6.83-6.77 (m, 2H, -ArH), 3.50-3.60 (m, 2H, - CH_2), 3.10 (t, 2H, - CH_2)(**Figure 2.1**). ^{13}C NMR (75 MHz, DMSO-d_6): 147.00, 144.06, 137.65, 136.04, 128.40, 127.75, 121.84, 113.98, 104.50, 40.25, 37.74 (**Figure 2.2**). ESI $\text{MS}^+(\text{m/z})$: ($\text{AmQNH} + \text{Na}^+$) 228.1086 (experimental);(**Figure 2.3**).

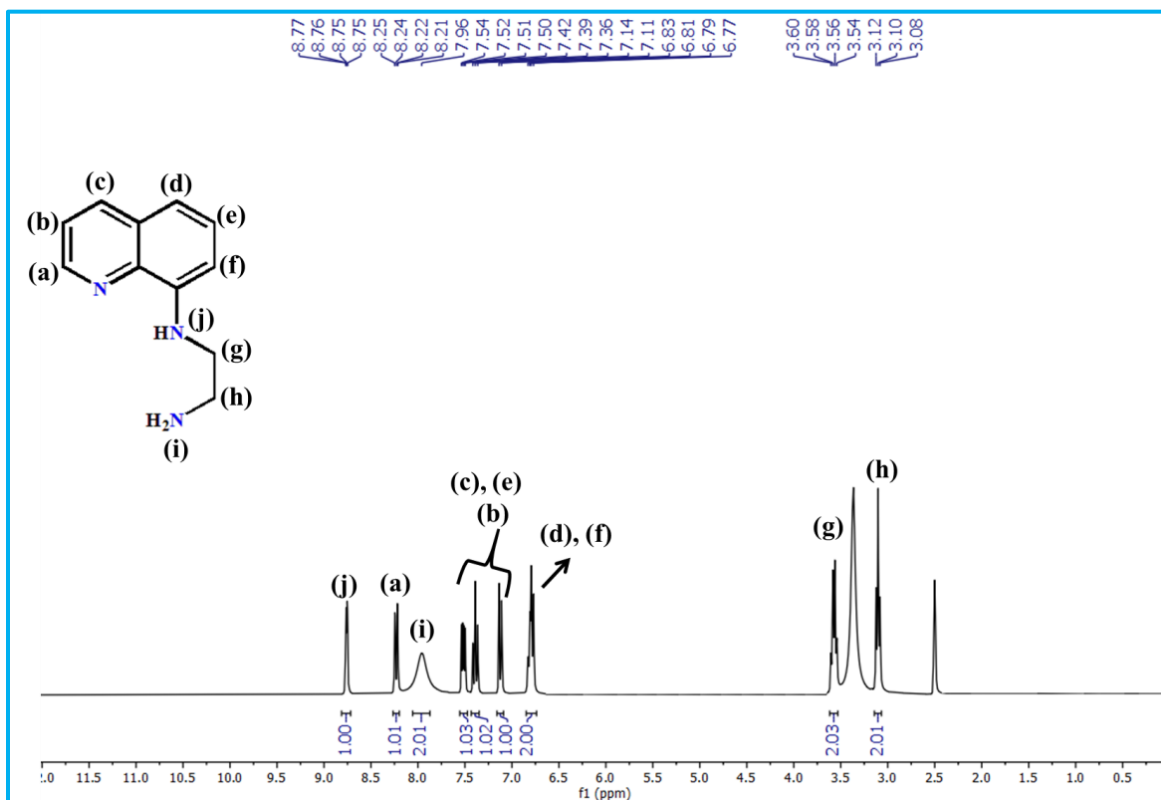


Figure 2.1. ^1H NMR spectrum of AmQNH in DMSO-d_6 .

CHAPTER 2

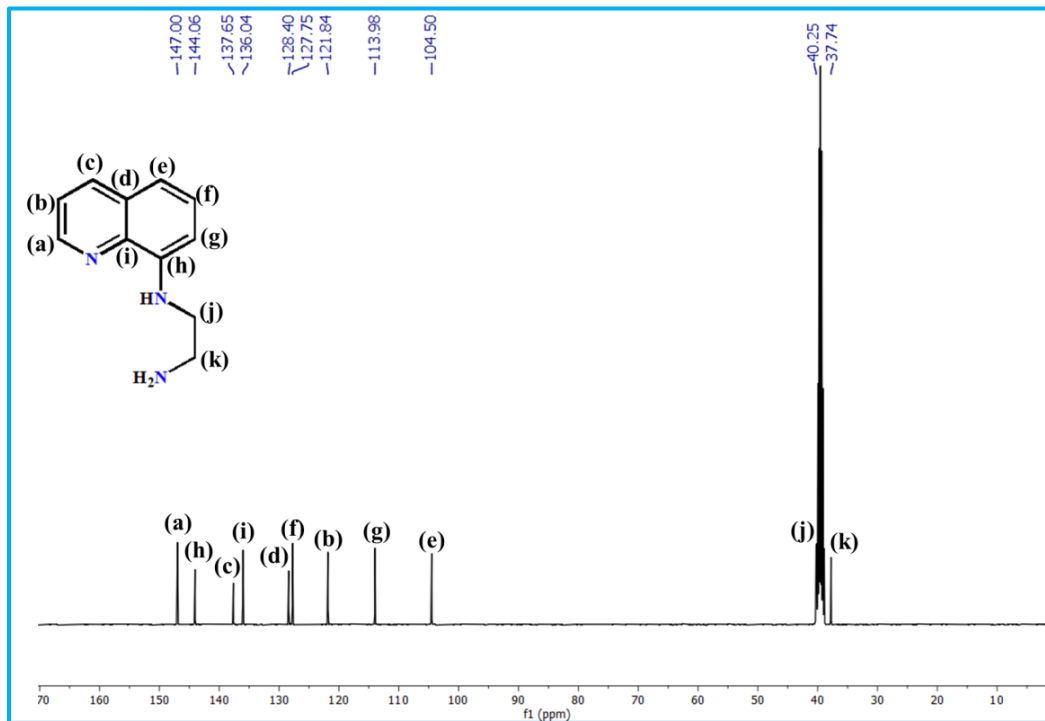


Figure 2.2. ^{13}C NMR spectrum of AmQNH in DMSO-d_6 .

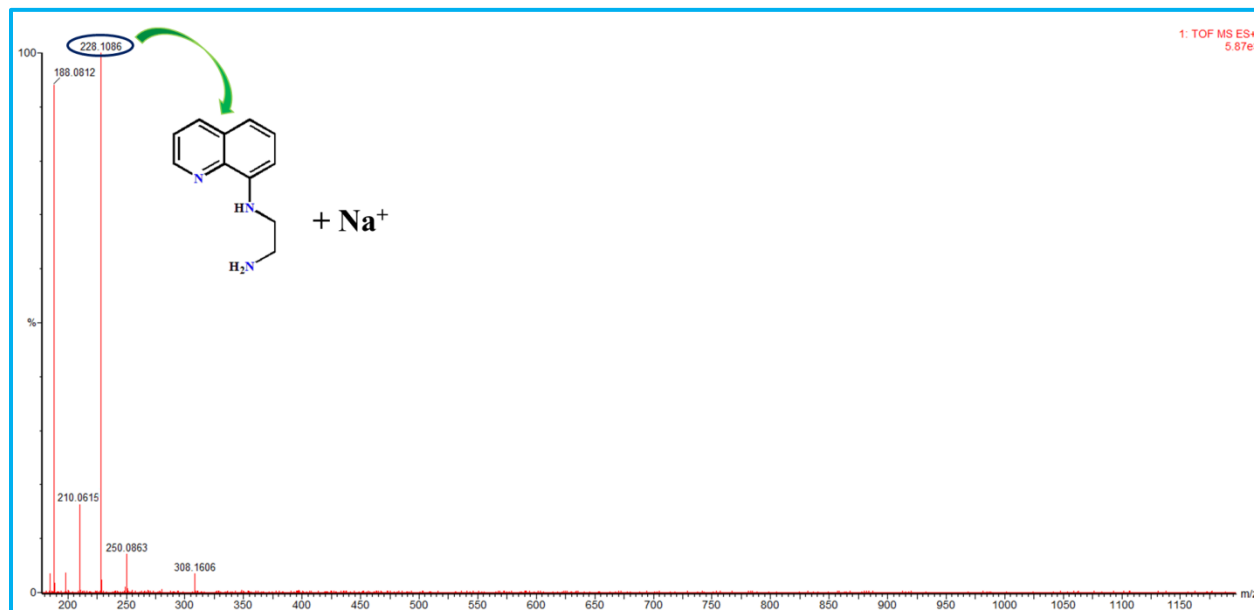


Figure 2.3. Mass spectrum of AmQNH in MeCN.

CHAPTER 2

2.2.8.2 Synthesis and characterization of NDAQ

Triethylamine (4.5 mmol, 0.4550 g) was slowly added to the stirred solution of AmQNH (1.8 mmol, 0.3370 g) in anhydrous DMF (3 ml) under inert atmosphere. After stirring at room temperature for 1 hour, a solution of 4-Chloro-7-nitrobenzofurazan (1.8 mmol, 0.3590 g) in anhydrous DMF was added drop wise to the reaction mixture and allowed to stir for overnight. Subsequently, the solvent was removed under reduced pressure and the crude product was purified by silica gel chromatography using ethyl acetate: hexane = 3.5:7.5 as an eluent to obtain the desired reddish brown product. Yield: 82%. $C_{17}H_{14}N_6O_3$. Molecular Weight: 350.3326. 1H -NMR (300 MHz, DMSO- d_6)(δ , ppm): 9.61 (s, 1H, -NH), 8.71 (d, 1H, ArH), 8.41 (d, 1H, -ArH), 8.19 (d, 1H, -ArH), 7.50-7.46 (m, 1H, -ArH), 7.36 (t, 1H, -ArH), 7.05 (d, 1H, -ArH), 6.95 (s, 1H, -NH), 6.80 (d, 1H, -ArH), 6.44 (d, 1H, -ArH), 3.76-3.69 (s, 4H, -CH₂)(**Figure 2.4**); ^{13}C NMR (75 MHz, DMSO- d_6): 147.50, 146.82, 145.31, 144.36, 144.07, 137.76, 137.52, 135.95, 128.39, 127.74, 121.70, 120.80, 113.45, 104.30, 99.37, 42.52, 40.58 (**Figure 2.5**); ESIMS⁺(m/z): (NDAQ + H⁺) 351.0535 experimental (**Figure 2.6**).

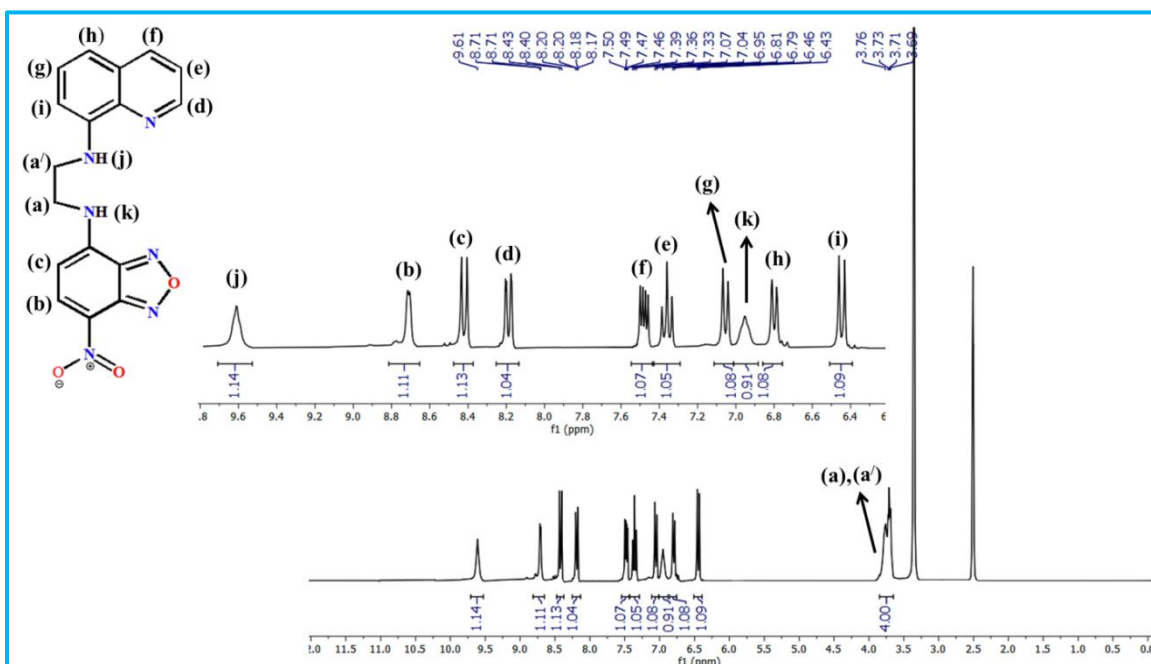


Figure 2.4. 1H NMR spectrum of NDAQ in DMSO- d_6 .

CHAPTER 2

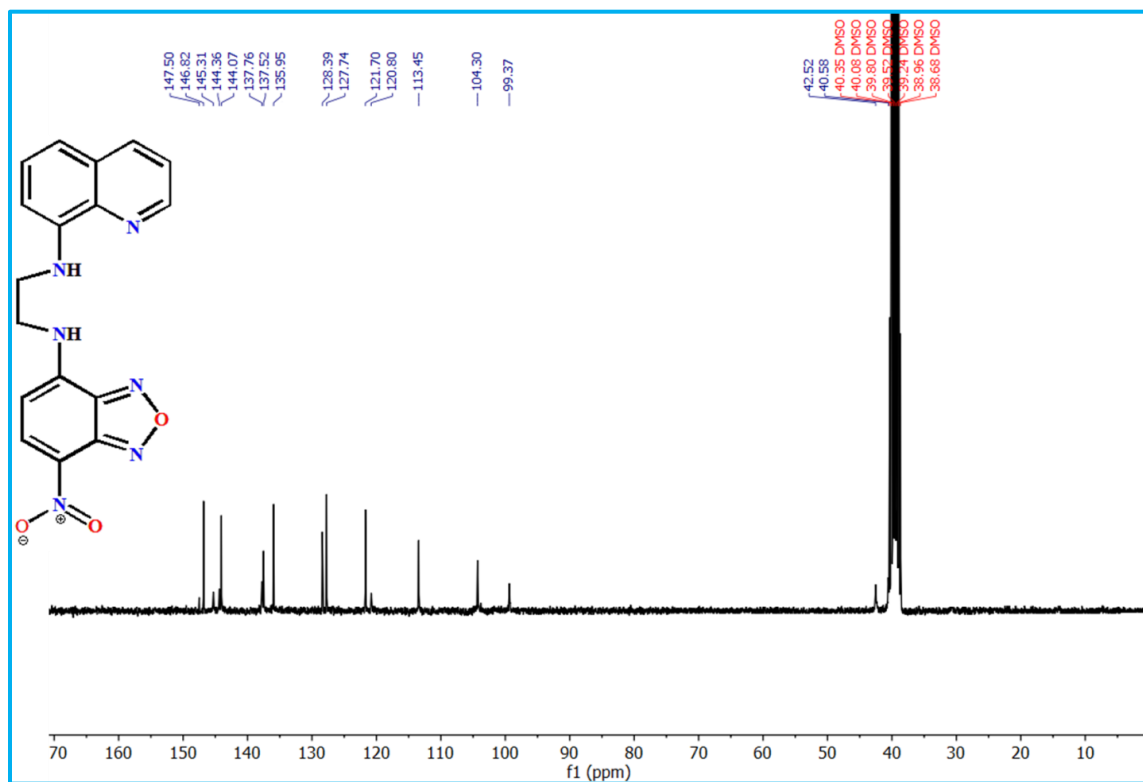


Figure 2.5. ^{13}C NMR spectrum of NDAQ in DMSO-d_6 .

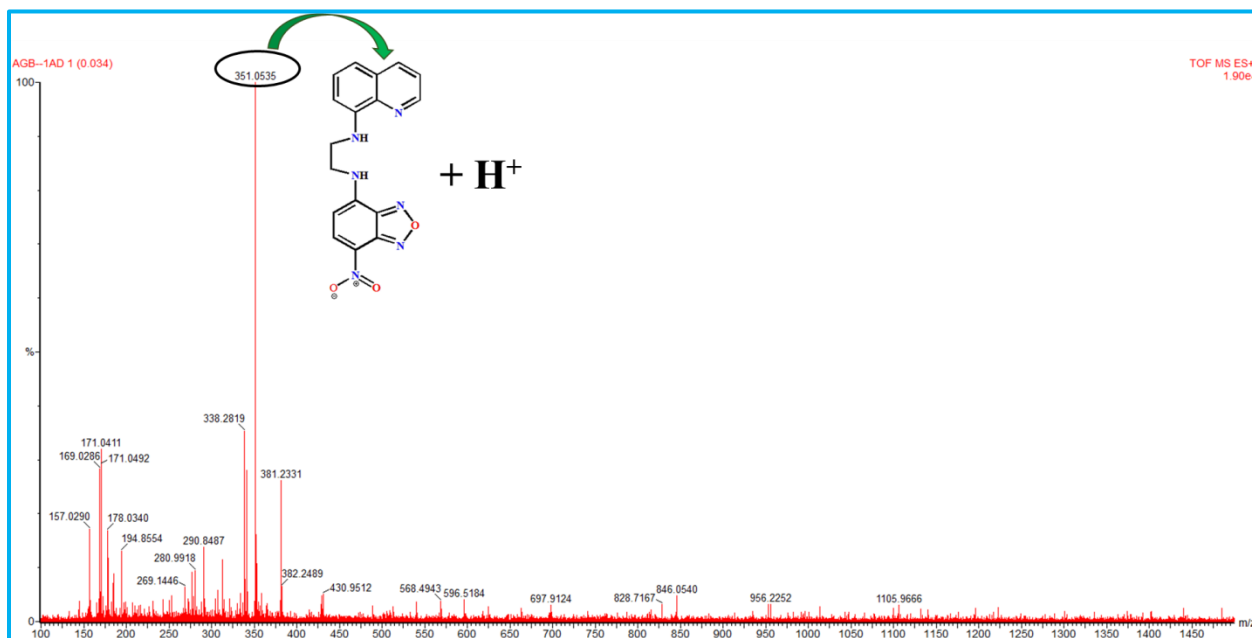


Figure 2.6. Mass spectrum of NDAQ in CH_3OH .

CHAPTER 2

2.2.8.3 Synthesis and characterization of NDAQ—NO

NDAQ (0.24 mmol, 84 mg) was dissolved in dry dichloromethane. After that NO gas was allowed to bubble through the dry DCM solution for about 15 minutes under pressure. As a result, the color of the solution changes from brown to yellow with bright green fluorescence. The resultant solution was then washed with saturated NaHCO₃ solution and then brine mixture. It was dried over anhydrous sodium sulphate. After filtration, the solvent was allowed to evaporate to get crude product which was then purified by silica gel chromatography (ethyl acetate: hexane= 3:7 as an eluent). This provided pure NDAQ—NO as Orange crystalline compound. Yield: 25 %. C₁₇H₁₃N₇O₄. Molecular Weight: 379.3360. ¹H-NMR (300 MHz, DMSO-d₆)(δ , ppm): 9.41 (s, 1H, -NH), 8.92 (d, 1H, ArH), 8.50-8.42 (m, 2H, -ArH), 8.09 (d, 1H, -ArH), 7.89 (d, 1H, -ArH), 7.72-7.62 (m, 2H, -ArH), 6.42 (dd, 1H, -ArH), 5.84 (td, 1H, -NH), 3.86 (d, 2H, -CH₂)(Figure 2.7). ¹³C NMR (75 MHz, DMSO-d₆): 151.30, 142.26, 141.87, 137.65, 136.87, 135.13, 130.23, 129.88, 129.48, 128.88, 127.60, 126.50, 126.40, 122.47, 122.38, 99.51, 45.58 (Figure 2.8). ESI MS⁺ (m/z): (NDAQ+H₂O) 397.0566 experimental (Figure 2.9).

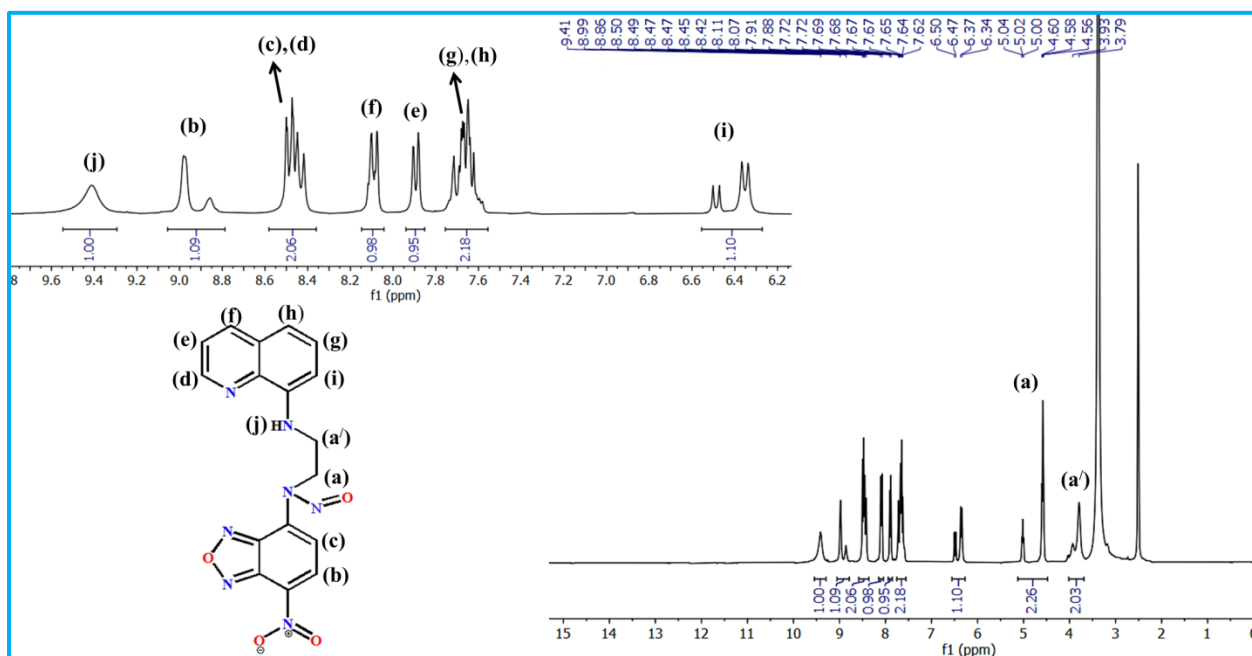


Figure 2.7. ¹H NMR spectrum of NDAQ—NO in DMSO-d₆.

CHAPTER 2

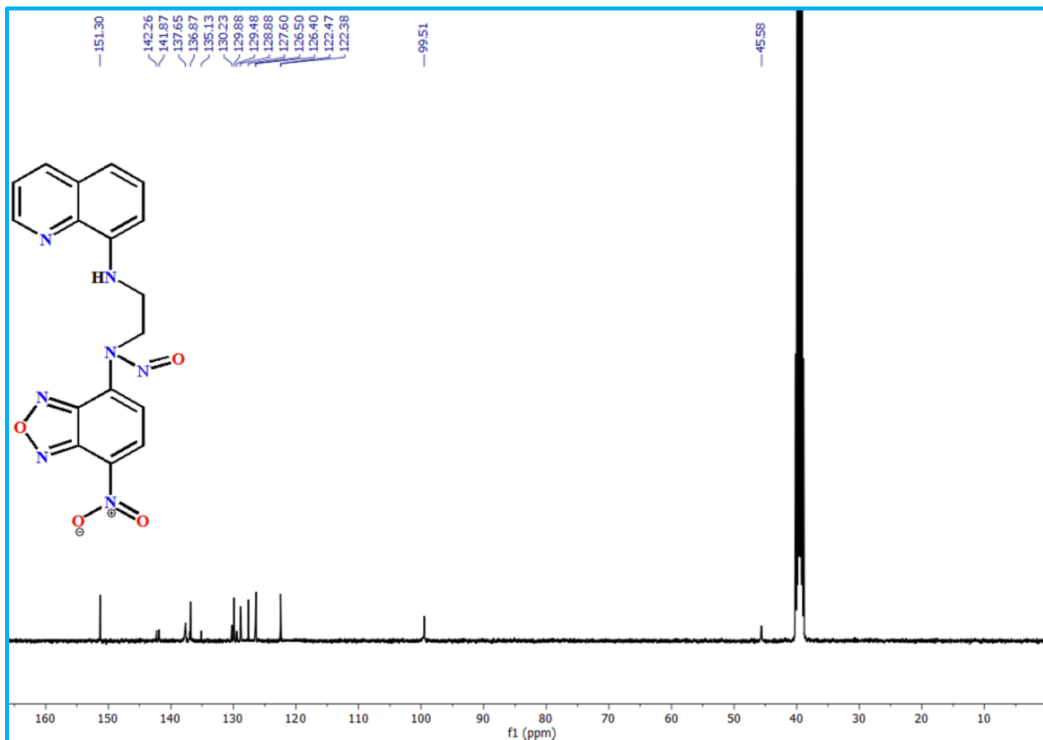


Figure 2.8. ^{13}C NMR spectrum of NDAQ-NO in DMSO-d_6 .

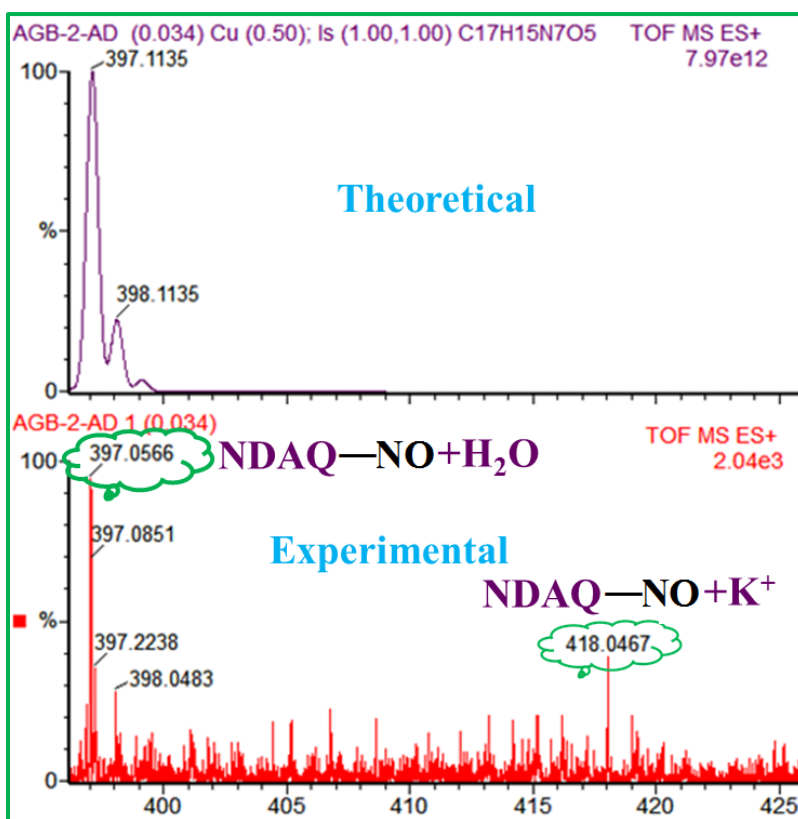
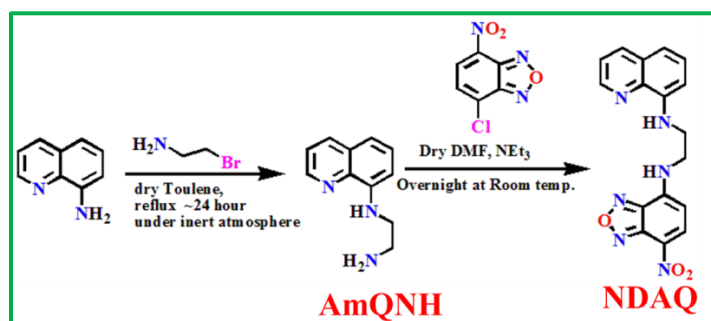


Figure 2.9. Mass spectrum of NDAQ-NO in CH_3OH .

CHAPTER 2

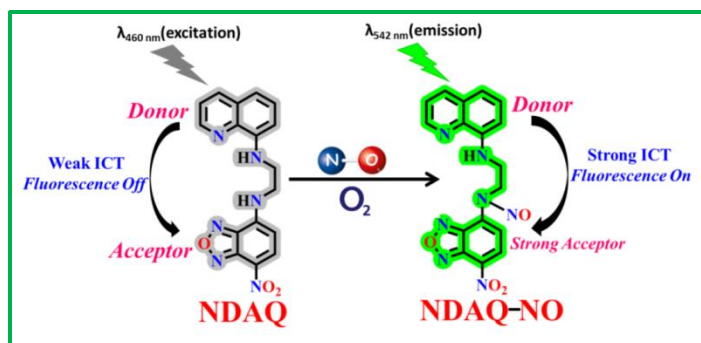
2.3 RESULTS AND DISCUSSION

Herein, to employ N-nitrosation sensing mechanism a NO sensitive probe, NDAQ, has been fabricated as portrayed in **scheme 2.2**. To derive the targeted probe, two very important fluorophores (Quinoline and NBD) are connected by ethylenediamine as a spacer. The quinoline moiety bears an excellent photostability⁴² while NBD exhibits its vast applications in the field of biology.⁴³⁻⁴⁶ As portrayed in **Scheme 2.2** the reaction between 8-amino quinoline and 2-bromoethylamine hydrobromide affords N-(2-aminoethyl)quinolin-8-amine (AmQNH), which in the next step reacted with 4-Chloro-7-nitro-2,1,3-benzoxadiazole (NBD) at room temperature to get N-(2-(7-nitrobenzo[c]-[1,2,5]oxadiazol-4-ylamino)ethyl)quinolin-8-amine (NDAQ).



Scheme 2.2. Schematic representation of synthesis of NDAQ

In the presence of NO under aerobic conditions, NDAQ is converted to its N-nitrosated product, NDAQ—NO (**Scheme 2.3**). All the compounds have been well characterized by various spectroscopic techniques.



Scheme 2.3. Schematic representation of Nitric Oxide sensing by NDAQ.

2.3.1 Uv-Vis study

Photophysical studies (UV-Vis and fluorescence) are carried out to analyze the response of NDAQ (20 μM) towards NO in 10 mM HEPES buffer (pH 7.20, μ = 0.10 M NaCl at 25 °C). NDAQ displays two absorption bands with peaks centered at about 349 nm (minor) and 485 nm (major). Upon consecutive addition of variable concentration of NO (0-42 μM ~2.1 equivalent), the absorbance of the probe slightly increased at 485 nm (major band) with ~ 8 nm blue shift and there is also a slight increase in absorbance at 349 nm (minor band) with ~ 6 nm blue shift in the wavelength (Figure 2.10(a)). The linear part was easily solved by utilizing eqn (3) under the condition $1 \gg cx^n$ and $n = 1$.

$$y = \frac{(a + b \times c \times x^n)}{1 + c \times x^n} \dots \dots \dots (3)$$

Where parameters a and b denote the absorbance of the probe in the absence and presence of excess NO, respectively and c is the formation constant designated as K_f . The slope ($b \times c$) obtained from the curve (using $b =$ absorbance in the presence of a large excess of NO) gives $c = K_f$. Here $K_f = (2.22 \pm 0.016) \times 10^4 \text{ M}^{-1}$ for Uv-vis studies. Based on absorption titration data the formation constant was evaluated to be $(2.22 \pm 0.016) \times 10^4 \text{ M}^{-1}$ by applying previously reported equation (Figure 2.10(b)).²² Upon addition of NO, the color of the solution also changes from lightish brown to yellow, indicating a possibility of NDAQ to detect NO colorimetrically.

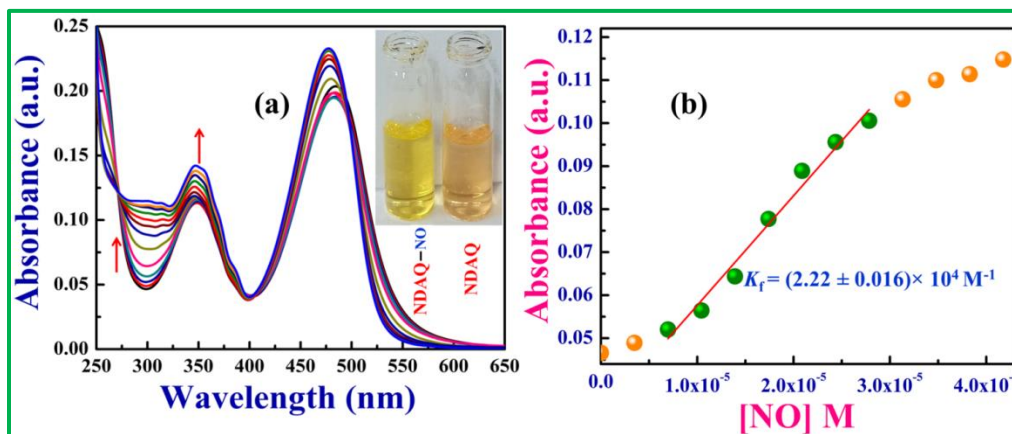


Figure 2.10. (a) UV/Vis absorption changes of NDAQ (20 μM) with incremental addition of NO (0-42 μM) in 10 mM HEPES buffer (pH 7.20, μ = 0.10 M NaCl at 25 °C). Inset: Images of visual changes in color of NDAQ and NDAQ—NO; and (b) The plot of absorbance vs. [NO].

2.3.2 Emission study

The fluorimetric studies showed a significant change in fluorescence spectra upon addition of NO to a 10 mM HEPES buffer solution of NDAQ (pH 7.20, $\mu = 0.10$ M NaCl at 25 °C). As expected, on excitation at 460 nm (3 X 3 slits) this probe exhibits very weak fluorescence but upon continuous addition of variable concentration (0-44 μ M) of NO, a drastic increase in fluorescence intensity (~ 27 fold) was observed (Figure 2.11(a)). The appearance of a vivid green fluorescence at 542 nm arises due to the formation of N-nitrosated compound NDAQ—NO. The probe displays a good linear relationship between fluorescence intensity and NO concentration ranging from 6.96 μ M to 17.4 μ M which helps to extract the binding constant value [$K_f = (8.29 \pm 0.23) \times 10^4$ M⁻¹] with the help of the reported method (Figure 2.11(b)).²² The excellent compatibility between two K_f values derived from absorption and fluorescence titrations justifies the logical consistency of our results. Quantum yields were determined for both NDAQ and NDAQ—NO which were found to be 0.0135 and 0.276 respectively.

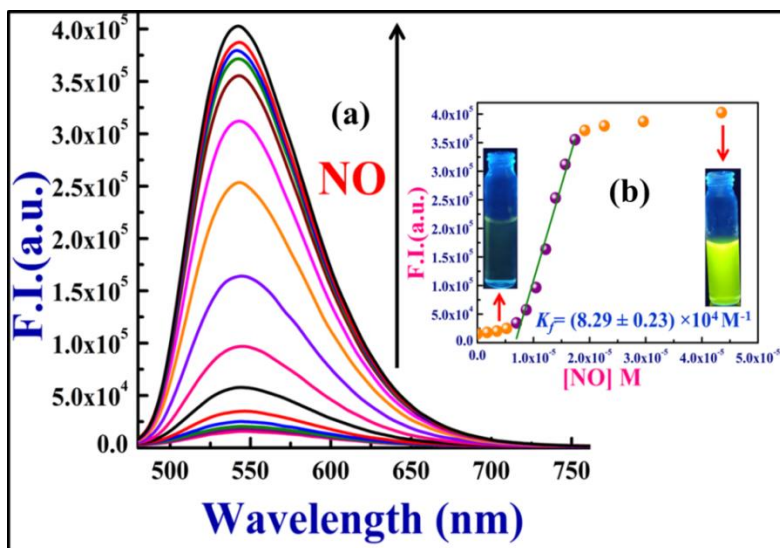


Figure 2.11. (a) Spectral changes in fluorescence ($\lambda_{\text{ex}} = 460$ nm, $\lambda_{\text{em}} = 542$ nm) of NDAQ (20 μ M) to NO (0-44 μ M) in 10 mM HEPES buffer (pH 7.20, $\mu = 0.10$ M NaCl at 25 °C); and (b) The plot of fluorescence intensity vs. the concentration of NO at 542 nm and the images of changes in fluorescence of NDAQ and NDAQ—NO.

CHAPTER 2

The fluorescence emission spectra of NDAQ and NDAQ in presence of 2.2 equivalent NO were also investigated in various organic solvents of different polarity (**Figure 2.12(a) & Figure 2.12(b)**). It is noteworthy that in the solvents with lower polarity like dioxane and THF the probe displays emission maxima at 523 nm and 525 nm respectively for *in situ* generated NDAQ—NO. On the contrary, in highly polar solvents like DMSO or aqueous HEPES buffer, the emission maxima appear at 539 nm and 542 nm respectively ascertaining a red shift (~ 20 nm) with respect to that in dioxane solvent (**Figure 2.12(a)**). Based on these observations it may be concluded that the NDAQ displays fluorescence enhancement via ICT mechanism on N- nitrosation. It is to be mentioned here that among all the solvents tested for fluorescence studies for the reaction between NDAQ and NO, aqueous medium was found to be the best one as it displays the highest enhancement (~ 27 fold) of fluorescence intensity upon reaction with NO (**Figure 2.12(b)**). Thus the emission wavelength (~ 542 nm) and the sensing medium (aqueous) clearly validate the suitability of the probe NDAQ in recognizing NO in living organisms.

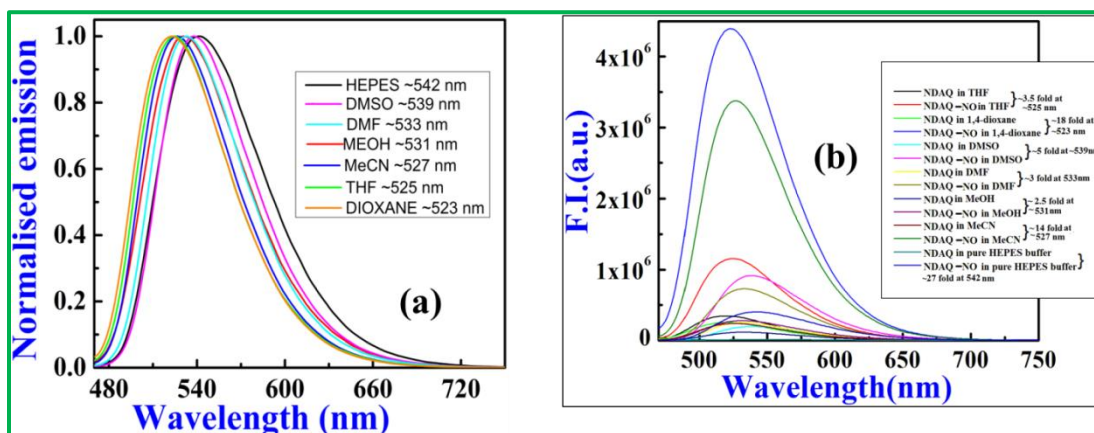


Figure 2.12. (a) Normalized spectra of the *in situ* generated N-nitrosated product (NDAQ—NO) in various solvents; and (b) Spectral changes of the probe (NDAQ) (20 μ M) and *in situ* generated N-nitrosated product (NDAQ—NO) in various solvents.

2.3.3 Kinetic Study

To get a thorough perception about the rate of the reaction operating in between NDAQ and NO at pH 7.2 (10 mM HEPES buffer, $\mu = 0.10$ M NaCl at 15°C), kinetic studies are executed fluorimetrically at 460 nm under pseudo-first-order conditions keeping one of the reactants as minor component. During this study, the concentration of NDAQ (2 μ M) has been kept constant

CHAPTER 2

and the concentration of NO is altered in the range between 5 to 30 μM . The plot of k_{obs} (Pseudo-first-order rate constant) vs. $[\text{NO}]$ delineates a nonlinear curve with upward curvature (**Figure 2.13**), while, the plot of k_{obs} vs. $[\text{NO}]^2$ displays the linearity, elucidating the second order dependency on $[\text{NO}]$. This statement has been further validated when the plot $\log(k_{\text{obs}})$ vs. $\log[\text{NO}]$ gives a straight line with a slope $(=2.16 \pm 0.07)$ with $R=0.998$ (**Figure 2.14(a)**). Now, to determine the rate dependency w.r.to $[\text{NDAQ}]$, the second experiment has been performed keeping $[\text{NO}] = 2 \mu\text{M}$ at different concentration of NDAQ (5-50 μM). Again, a plot of $\log(k_{\text{obs}})$ vs. $\log[\text{NDAQ}]$ gives straight line with slope $=1.03 \pm 0.09$ ($R=0.988$) indicating a first-order dependence of rate on $[\text{NDAQ}]$ (**Figure 2.14(b)**). Thus the reaction of NDAQ and NO was found to be overall third-order, second-order on NO and first-order on NDAQ. The most conceivable reaction sequences are outlined as:

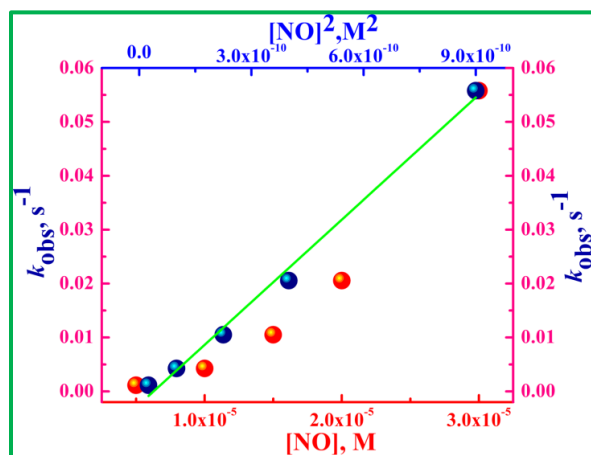
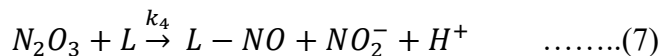
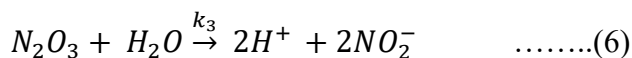


Figure 2.13. The k_{obs} vs. $[\text{NO}]$ plot depicts an upward curvature (red circles), while a plot of k_{obs} vs. $[\text{NO}]^2$ depicts a straight line (blue circles). Experimental conditions are: $[\text{NDAQ}] = 2 \mu\text{M}$ and $[\text{NO}] = (5\text{--}30) \mu\text{M}$, temperature = $15 \text{ }^\circ\text{C}$ in 10 mM HEPES buffer (pH = 7.2, NaCl = 0.10M). All the analyzation was done using the fluorescence technique.

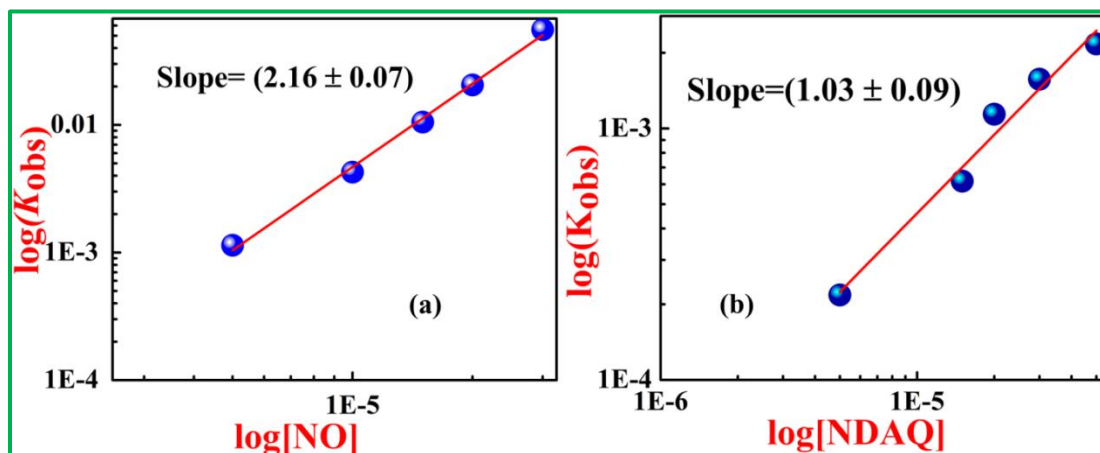


Figure 2.14. (a) Plot of $\log(k_{\text{obs}})$ vs. $\log [\text{NO}]$ and (b) Plot of $\log(k_{\text{obs}})$ vs. $\log [\text{NDAQ}]$.

Eq.7 depicts the interaction of NDAQ (here represented as L) with N_2O_3 thereby generating N-nitrosated product (here L—NO signifies NDAQ—NO). The literature survey reveals the magnitude of these above mentioned rate constants. So, here, $k_1 = 6.33 \times 10^6 \text{ M}^{-2} \text{ s}^{-1}$,⁴⁷ $k_2 = 1.1 \times 10^9 \text{ M}^{-1} \text{ s}^{-1}$ ⁴⁸ and $k_3[\text{H}_2\text{O}] = 1.6 \times 10^3 \text{ s}^{-1}$.⁴⁹ Now, considering all these parameters, we may illuminate that as both NO_2 and N_2O_3 are contributing negligibly, they must behave like a reactive intermediates. As a consequence, **Eq.8** has been constructed by considering the steady state approximation on the $[\text{NO}_2]$ and $[\text{N}_2\text{O}_3]$ for the formation of L-NO.

$$\frac{d[\text{L} - \text{NO}]}{dt} = \frac{k_1 k_4 [\text{L}]}{2(k_3[\text{H}_2\text{O}] + k_4[\text{L}])} [\text{NO}]_t^2 [\text{O}_2]_t \quad \dots (8)$$

As we have mentioned previously that the rate of the reaction pursues the second order and first order kinetics with respect to NO and NDAQ respectively, therefore we may assume that $k_3[\text{H}_2\text{O}] \gg k_4[\text{L}]$. So now **Eq.8** modifies to **Eq. 9**

$$\frac{d[\text{L} - \text{NO}]}{dt} = \frac{k_1 k_4 [\text{L}]}{2k_3[\text{H}_2\text{O}]} [\text{NO}]_t^2 [\text{O}_2]_t \quad \dots (9)$$

Eq.9 now modified to **eq.10** where $k_{\text{obs}} = \{d[\text{L-NO}]/dt\}/[\text{L}]$, while studying the kinetics of the reaction under pseudo-first- order conditions with L as a minor component, in aerated environment (the dissolved $[\text{O}_2]_t = 2.5 \text{ mM}$ at 25°C).

CHAPTER 2

$$k_{obs} = k' [NO]_t^2 \quad \dots \dots (10)$$

Where,

$$k' = \frac{k_1 k_4}{2k_3 [H_2O]} [O_2]_t \quad \dots \dots (11)$$

Here, k' represents the slope of the plot k_{obs} vs. $[NO]_t^2$ with a value of $(6.33 \pm 0.29) \times 10^7 \text{ M}^{-2} \text{ s}^{-1}$ at 15°C . Now, by employing the previously recorded values of k_1 , $k_3[H_2O]$ and k' in **eq.11**, the magnitude of k_4 is evaluated which is of the same order of 10^7 as referred in the literature.⁵⁰

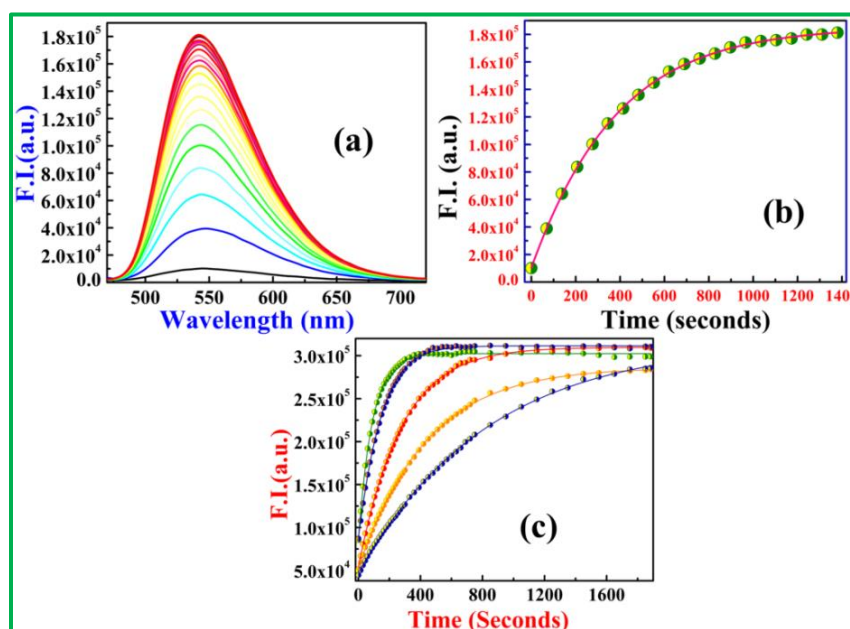


Figure 2.15. (a) Spectral variation in fluorescence intensity of NDAQ (5 μM) over time (0-24 mins) on addition of NO (11 μM) in HEPES buffer (10 mM, pH 7.2) at 15°C ; (b) The corresponding kinetic growth plot; and (c) Kinetic traces of NDAQ (10 μM) in HEPES buffer (10 mM, pH 7.2) at 15°C after addition of NO (10, 12, 15, 19, 22 μM).

Now, the time dependent fluorescence experiment was further carried out to investigate the spectral signature of the probe NDAQ in presence of NO. It is obvious that the treatment of 2.2 equivalent of NO (11 μM) in 10 mM HEPES buffer solution (pH 7.2) of NDAQ (5 μM) at 15°C causes enhancement in fluorescence intensity at 542 nm (**Figure 2.15(a)**). The steeper nature of the curve commences to attain plateau within ~ 7 mins (**Figure 2.15(b)**). The kinetic traces of the

CHAPTER 2

probe (NDAQ) were also recorded by altering the concentration of NO with a fixed 10 μM [NDAQ] at 15°C. Here, with an increase in the concentration of NO, the nature of the curve becomes more and more steeper, implying an increase in the rate of the reaction (**Figure 2.15(c)**). The kinetic traces of the probe also illustrates that once the plateau nature of the curve is attained, the fluorescence intensity of the probe remains unaffected, indicating higher photo stability of the N-nitrosated product (NDAQ—NO).

2.3.4 Selectivity study

Selectivity studies have been carried out to judge the potential application of a NO sensitive probe in complicated biological systems. Here, selectivity studies of NDAQ were conducted by interacting with various interfering biological species such as $\cdot\text{OH}$, O_2^- , ClO^- , NO, ascorbic acid (AA), H_2O_2 , TEMPO radical, NO_2^- etc. in 10 mM HEPES buffer (pH 7.2, $\mu = 0.10$ M NaCl at 25°C). The result displays no significant change in fluorescent intensity at 542 nm even if they are taken in excess amount (~ 10 equivalents) (**Figure 2.16**). To evaluate the specific response of NDAQ towards NO, the similar selectivity analysis was also performed in Uv-Vis spectrophotometer which delineates no characteristic change in spectral signature of the probe except NO (**Figure 2.17**). Now, the specificity of probe NDAQ towards NO was further ensured by performing reactivity studies with various cations and anions fluorimetrically (**Figure 2.18(a)**, **Figure 2.18(b)**). Here, in this analysis, the addition of these analytes (~ 200 μM) to the solution of NDAQ (20 μM) failed to trigger the enhancement in fluorescence intensity at 542 nm except Cu(II) (~ 44 μM) which exhibits a small enhancement in fluorescence intensity (~ 2.4 fold) compare to NO (~ 27 fold) manifesting the very high selectivity of NDAQ towards NO over all the metal ions tested (**Figure 2.19(a)**). For further strengthening the selectivity of NDAQ towards NO in the presence of 44 μM Cu(II), ~ 44 μM NO was added to a 10 mM HEPES buffer solution of NDAQ (20 μM) which displays a negligible drop in fluorescence intensity as was found in the absence of Cu(II) demonstrating practically no influence towards the NO detection (**Figure 2.19(b)**).

CHAPTER 2

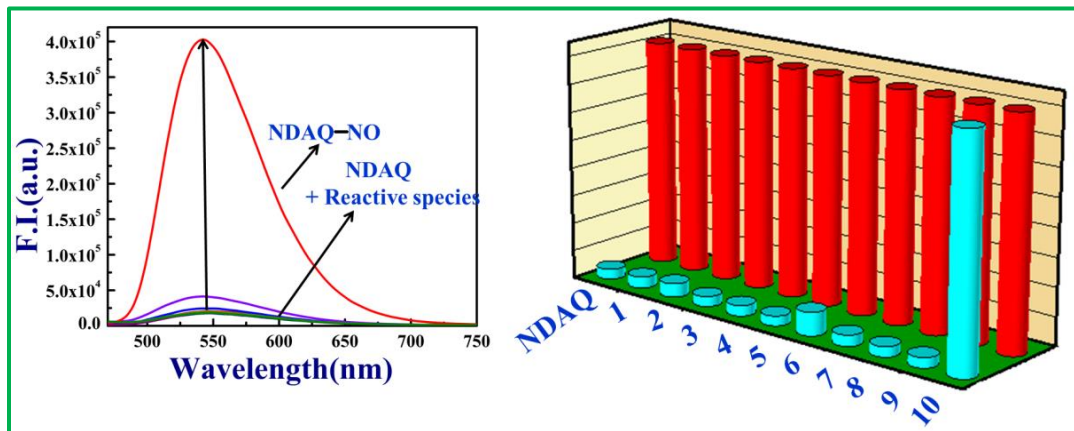


Figure 2.16. Changes in fluorescence Spectra for the probe NDAQ towards several reactive species that are recorded in HEPES buffer (10 mM, pH 7.2) NDAQ= 20 μ M, X = 200 μ M (1=TEMPO, 2=OCl⁻, 3=AA, 4=KO₂, 5=H₂O₂, 6=OH⁻, 7=ONOO⁻, 8=NO₂⁻, 9=HNO, 10=NO, λ_{ex} = 460 nm at 25^oc and the bar plot at 542 nm.

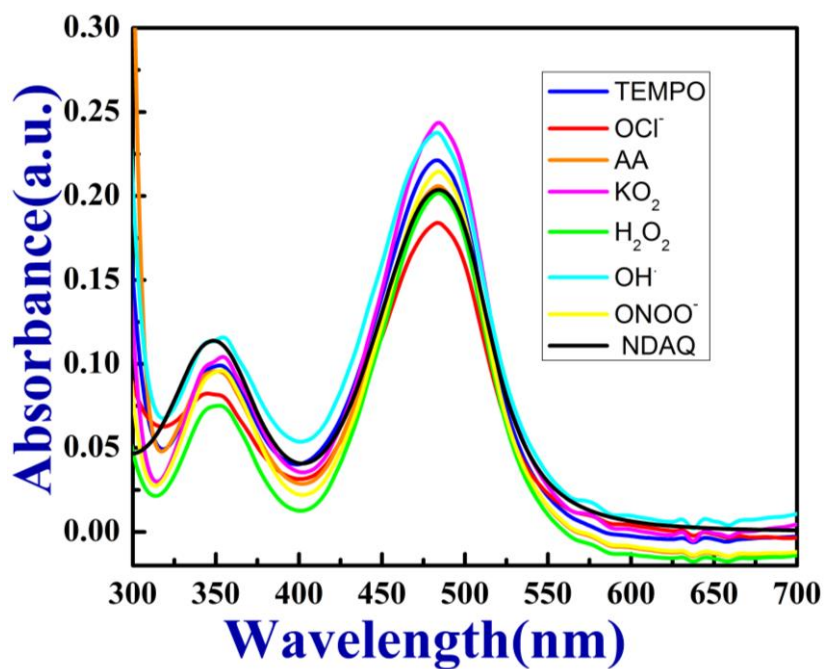


Figure 2.17. Selectivity study of the probe NDAQ in 10 mM HEPES buffer (pH 7.20, μ = 0.10 M NaCl at 25 ^oC) with 10 equivalent various reactive species such as TEMPO, OCl⁻, AA, KO₂, H₂O₂, OH⁻, ONOO⁻, NO₂⁻ in Uv-vis.

CHAPTER 2

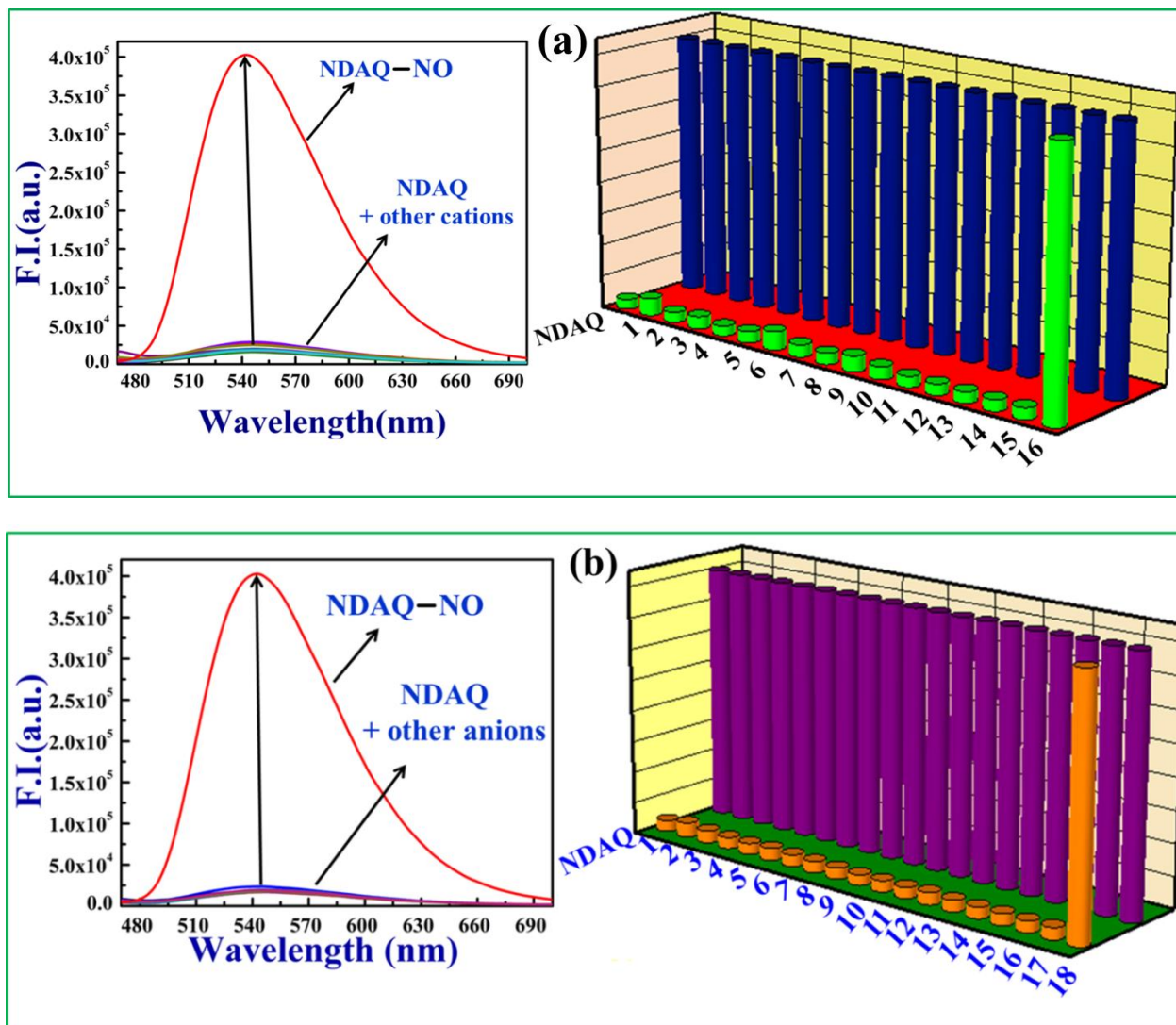


Figure 2.18. Selectivity studies of NDAQ (20 μM) with various (a) Cations ($\sim 200 \mu\text{M}$) (1= Mn^{2+} , 2= Co^{2+} , 3= Al^{3+} , 4= Cr^{3+} , 5= Fe^{3+} , 6= Fe^{2+} , 7= Zn^{2+} , 8= Hg^{2+} , 9= Ni^{2+} , 10= Mg^{2+} , 11= Na^+ , 12= K^+ , 13= Pb^{2+} , 14= Cd^{2+} , 15= NH_4^+ , 16= NO) and (b) Anions ($\sim 200 \mu\text{M}$) (1= HSO_4^- , 2= NO_2^- , 3= NO_3^- , 4= H_2PO_4^- , 5= N_3^- , 6= F^- , 7= SCN^- , 8= PPI , 9= CH_3COO^- , 10= S_2O_3^- , 11= ClO_4^- , 12= SH^- , 13= BrO_3^- , 14= CNS^- , 15= I^- , 16= Br^- , 17= Cl^- , 18= NO) in 10 mM HEPES buffer (pH 7.20, $\mu = 0.10 \text{ M NaCl}$ at 25 $^\circ\text{C}$).

This slight drop in fluorescence intensity for the reaction between NDAQ and NO in the presence of Cu(II) might be the consequence of a reaction between NO and Cu(II) to give Cu(I), thereby reducing the effective concentration of NO. In the same way, the over-selectivity of NDAQ—NO reaction was performed in the presence of 10 equivalents of various cations (Mn^{2+} ,

CHAPTER 2

Co²⁺, Zn²⁺, Fe³⁺, Cr³⁺, Mg²⁺, Cu²⁺, Ca²⁺) and anions (Br⁻, F⁻, N₃⁻, CH₃COO⁻, CNS⁻, SCN⁻) that are being present in our physiological systems. The reactivity profile diagram of NDAQ displays no significant change in fluorescence intensity at 542 nm, indicating its excellent sensitivity and specificity towards NO (**Figure 2.19(b)** and **Figure 2.19(c)**). Based on the above observations one might conclude that NDAQ is highly efficient in every aspect to detect NO precisely in a complicated biological systems.

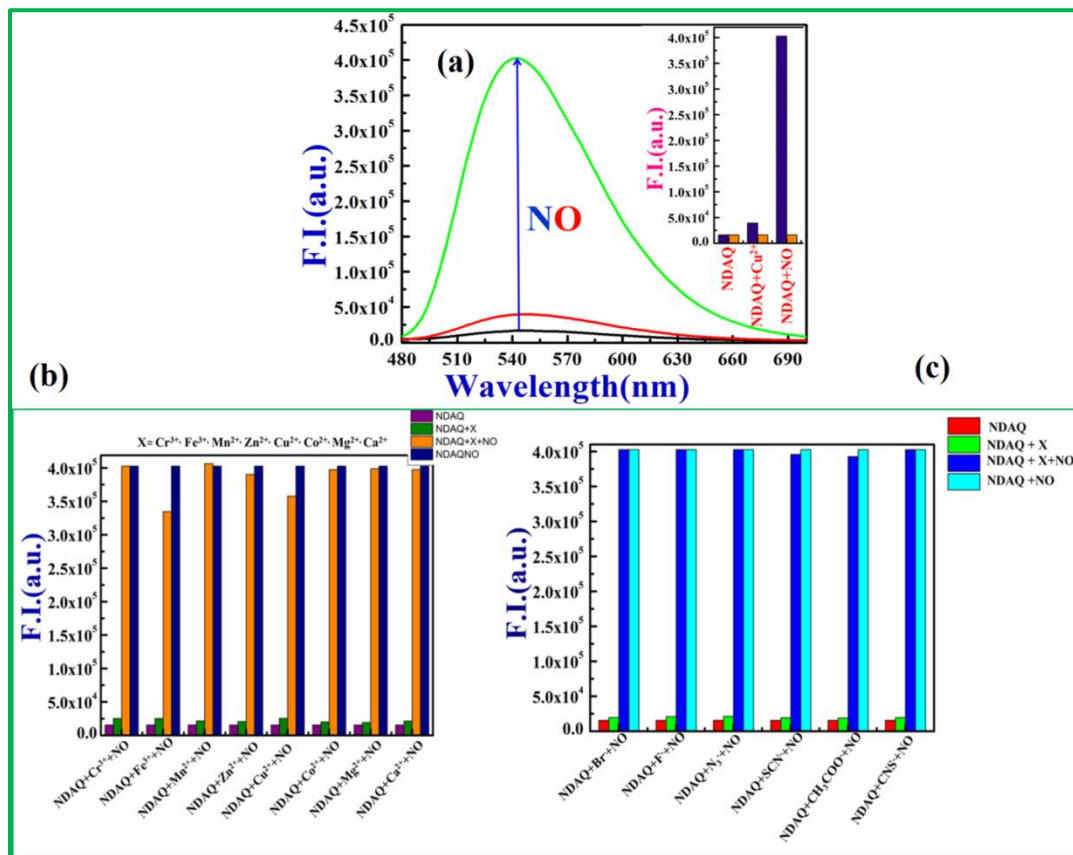


Figure 2.19. (a) Selectivity comparison study of NDAQ (20 μ M) with Cu²⁺ (~44 μ M) and NO (~44 μ M) in 10 mM HEPES buffer (pH 7.20, μ = 0.10 M NaCl at 25 °C); (b) Sensitivity of the probe towards NO (~44 μ M) in presence of various cations (~200 μ M) Mn²⁺, Co²⁺, Zn²⁺, Fe³⁺, Cr³⁺, Mg²⁺, , Ca²⁺ except Cu²⁺ (~44 μ M) in 10 mM HEPES buffer (pH 7.20, μ = 0.10 M NaCl at 25 °C); and (c) Sensitivity of the probe towards NO in presence of various anions (~200 μ M) in 10 mM HEPES buffer (pH 7.20, μ = 0.10 M NaCl at 25 °C).

2.3.5 Limit of detection

In order to get an idea about the sensitivity of the probe NDAQ towards NO in physiological systems, the LOD value which is ~ 7 nM was evaluated by $3\sigma/\text{slope}$ method (Figure 2.20(a)), thereby, justifying its capability to detect NO in cellular systems where NO concentration was found to be in the micro to nanomolar range.⁵¹

2.3.6 TCSPC studies

TCSPC (Time-correlated Single Photon Counting) studies were also performed by treating 10 mM HEPES buffer (pH 7.2, $\mu = 0.10$ M NaCl at 25°C) solution of NDAQ (20 μM) in the absence and presence of 44 μM NO solution. Here, on excitation at 482 nm, both displays single exponential decay profile which give $\tau_0 = 1.05$ ns for NDAQ and $\tau_0 = 1.46$ ns for NDAQ—NO. The increase in lifetime for N-nitrosated product over NDAQ itself indicates the higher stability of the N-nitrosated product in the excited state (Figure 2.20(b)).

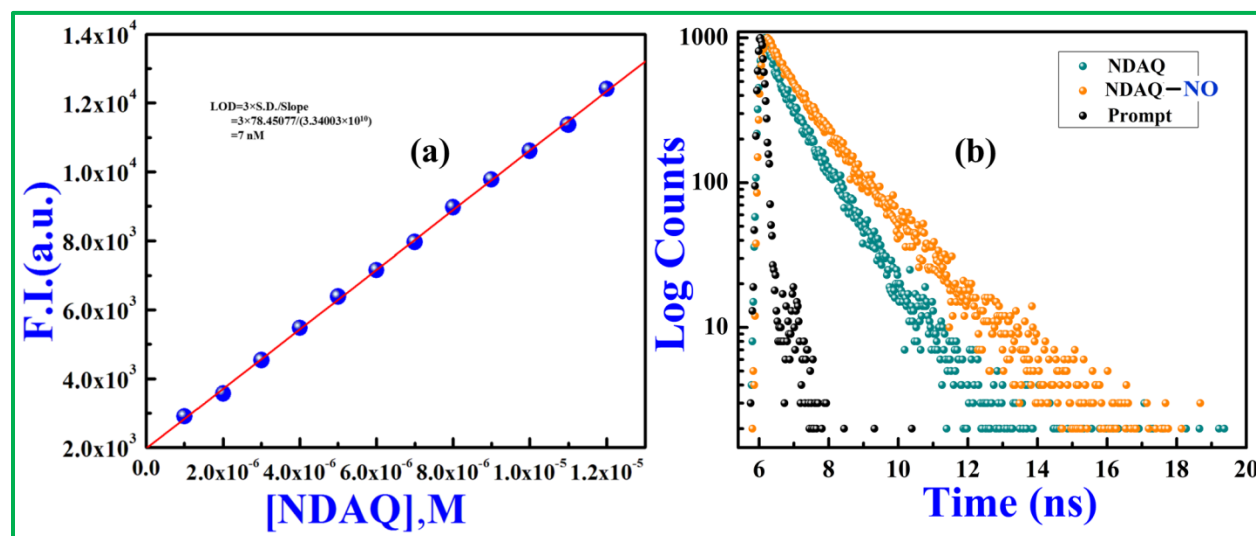


Figure 2.20. (a) LOD (Limit of detection) of NDAQ and (b) Life time calculation plot for NDAQ (20 μM) and NDAQ—NO (44 μM) in 10 mM HEPES buffer (pH = 7.2, NaCl = 0.10 M at 25°C).

2.3.7 pH Study

The excellency of a fluorescence probe for biological applications in living organisms depends on its pH tolerance over a wide physiological pH range. Therefore, interaction between the probe and NO was monitored at different pH levels (2-12). As displayed in **Figure 2.21**, the probe is most suitable to detect NO over a wide range of pH (2-8). In the low pH range, the electron push pull framework becomes highly dominating as the $-NH$ proton adjacent to the quinoline moiety is protonated and upon further treatment with NO, the electron acceptance property of the benzofurazan moiety is increased due to N-nitrosation of the $-NH$ proton attached with NBD. Furthermore, in basic medium the probe exhibits moderate sensitivity towards NO (**Figure 2.21**) because under this condition N_2O_3 , produced during the reaction between NO_2 and NO (**eq.5**), undergoes rapid decomposition (**eq.6**). Consequently, there is a lower availability of N_2O_3 to interact with NDAQ. All these outcomes lead to the interpretation that the probe has the capability to track NO in physiological systems from all perspectives.

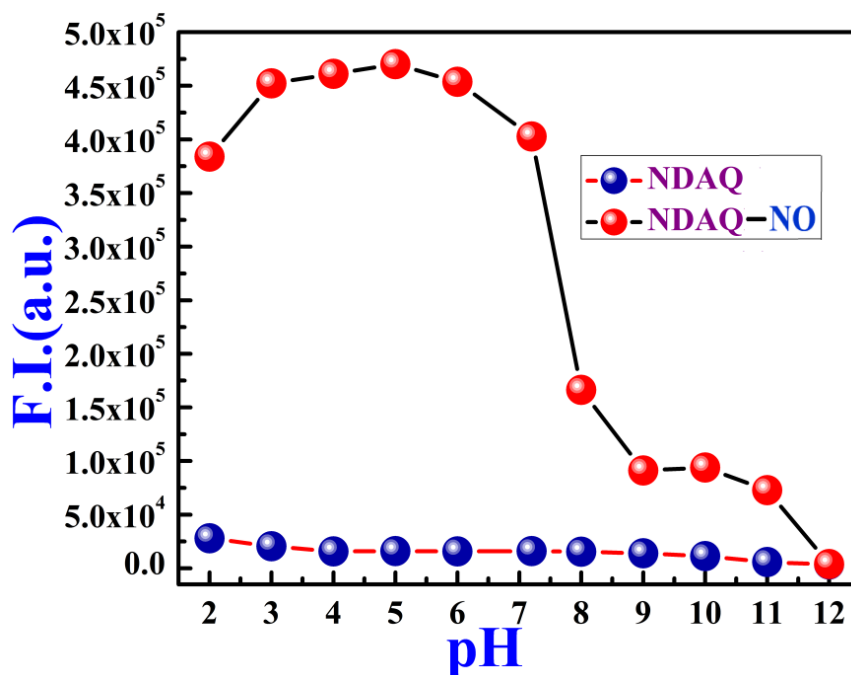


Figure 2.21. pH (2-12) tolerance of NDAQ and its N-nitrosated product after adding 2.2 equivalent NO at 25°C.

2.3.8 Confirmation of Nitric Oxide Sensing Mechanism

The designed fluorescent sensor NDAQ was synthesized from AmQNH. Both the compounds were characterized thoroughly by conventional spectroscopic studies. (For AmQNH, ^1H NMR (Figure 2.1), ^{13}C NMR (Figure 2.2), HRMS (Figure 2.3) whereas for NDAQ, ^1H NMR (Figure 2.4), ^{13}C NMR (Figure 2.5), HRMS (Figure 2.6)). Now, in order to verify the sensing mechanism of NDAQ towards NO, the dry DCM solution of the probe was bubbled for about 15 minutes by NO gas. Within 5 minutes, the color of the solution changes to yellow with the generation of vivid green fluorescence. The yellow color solution was now washed with brine followed by saturated solution of NaHCO_3 to neutralize the acidity generated through the reactions (1 to 4). After removing the solvent in vacuum, the reaction mixture was subjected for column chromatography (ethyl acetate: hexane= 3:7) to get the orange crystalline product (NDAQ—NO) in pure form. ^1H NMR (Figure 2.7), ^{13}C NMR (Figure 2.8), HRMS (Figure 2.9) and IR (Figure 2.22(a)) studies of NDAQ—NO reveal the sensing mechanism of NDAQ towards NO. The ^1H -NMR spectra of probe NDAQ and NDAQ—NO delineates that the N-nitrosation reaction mechanism being operative with the concerned probe. The peak corresponds to —NH proton attached with the NBD moiety at 6.95 ppm vanishes in the spectra of NDAQ—NO. This strongly elucidates that NO is attached to —NH proton of the NBD moiety. This is quite logical based on the fact that the NH group attached to the highly electron withdrawing NBD moiety becomes more acidic and easily replaceable by NO. A comparison of the IR spectra between NDAQ and NDAQ—NO convincingly favors the N-nitrosation at —NH group adjacent to NBD. Here, IR spectra of NDAQ—NO clearly depicts the appearance of a new peak at 1490 cm^{-1} corresponds to -N=N=O unit.⁵² The stretching frequency for both the NH protons (the quinoline —NH and the NBD —NH) appears at $\sim 3305\text{ cm}^{-1}$. Upon addition of NO, there is a decrease in -N-H stretching intensity with simultaneous shifting in frequency from $\sim 3305\text{ cm}^{-1}$ to 3343 cm^{-1} , due to replacement of one of the —NH proton with NO (Figure 2.22(a)). HRMS studies also support the N-nitrosation sensing mechanism giving a molecular ion peak (ESI-MS⁺) at 397.0566 corresponding to (NDAQ—NO + H₂O). The Uv-Vis absorption spectra of in situ generated NDAQ—NO (incremental addition of 0-42 μM of NO in 20 μM NDAQ solution) and isolated pure NDAQ—NO ($\sim 200\text{ }\mu\text{M}$) in 10 mM HEPES buffer (pH 7.2, $\mu = 0.10\text{ M NaCl}$ at 25°C) matches well to each other as in both cases there is $\sim 8\text{ nm}$ blue shift (Figure 2.22(b)). All these observations lead to the conclusion that the addition of NO causes a

change in spectral pattern of the probe due to formation $-N=N=O$ product. The presence of Donor-Acceptor framework within the concerned probe NDAQ facilitates the slight transfer of charge density from the donor site (quinoline unit) to the acceptor site (NBD unit). This results in a very weak fluorescence of the probe (weak ICT). Now, the NBD site of the NDAQ—NO becomes somehow stronger acceptor unit in compare to that in NDAQ itself due to the presence of electron withdrawing $-N=N=O$ functionality. As a result, there is a significant drifting of electron density from the quinoline (donor) site to the NBD site (acceptor) leading to an enhancement in fluorescent intensity owing to the effective intramolecular charge transfer (ICT) process (**scheme 2.3**). The above NO sensing strategy by following ICT mechanism is also supported by photo-physical studies of the concerned probe in various solvent (**Figure 2.12(a)**) and also through DFT studies.

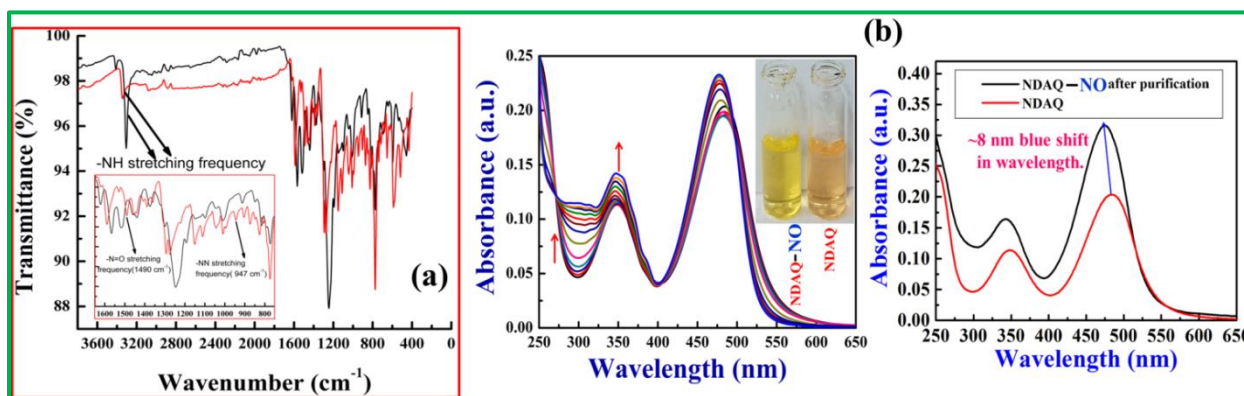


Figure 2.22. (a) IR spectrum of NDAQ and NDAQ—NO; and (b) Comparison of Uv-Vis absorption spectra of in-situ generated NDAQNO (where NDAQ is $\sim 20 \mu\text{M}$) and isolated pure NDAQNO ($\sim 200 \mu\text{M}$) in 10 mM HEPES buffer (pH = 7.2, NaCl = 0.10M) at 25°C .

2.3.9 DFT studies

The feeble Donor-Acceptor model of the concerned probe NDAQ results in a weak ICT. However, it is envisioned that, on exposure to NO, there is amplification of ICT due to a stronger D-A infrastructure in NDAQ—NO through the incorporation of NO- a strong electron-withdrawing group adjacent to NBD moiety. The preceding section favors this sensing mechanism through DFT calculations. To validate the sensing mechanism as depicted in **scheme 2.3**, the DFT and TDDFT analysis of the probe (NDAQ) and its NO treated product

CHAPTER 2

(NDAQ—NO) have been accomplished. The optimized structures of both these compounds belong to C_1 point group. Mass spectroscopy also clearly demonstrates the formation of N-nitrosation adduct of the concerned probe upon exposure to NO. All these information are utilized to elucidate the skeletal composition of these compounds (**Figure 2.23**).

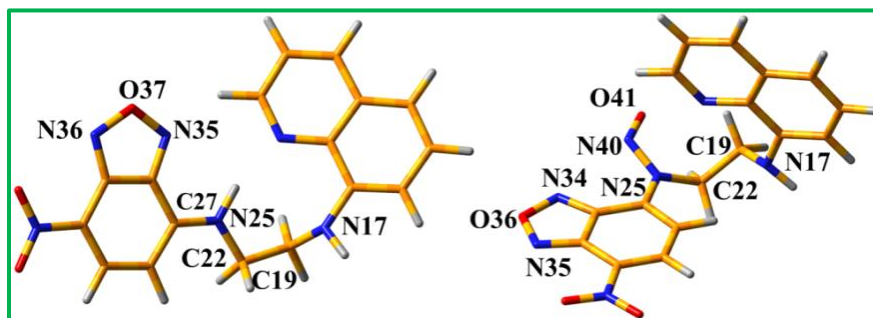


Figure 2.23. Optimized geometries of NDAQ and NDAQ—NO.

The geometrical parameters of the optimized geometries of NDAQ and NDAQ—NO are listed in tabular form (**Table 2.1 and Table 2.2**). For the NDAQ—NO the N—O bond distance is 1.21 Å, whereas the N—N bond distances is 1.37 Å.

Table 2.1. Some selected geometrical parameters (bond lengths and bond angles) of NDAQ in ground state calculated at B3LYP/6-31G (d,p) Levels.

Bond Lengths (Å)		Bond Angles (°)	
C22-N25	1.45064	C2N17C19	121.669
C19-N17	1.46740	C27N25C22	123.301
C22-C19	1.52881	C22C19N17	111.981
C2-N17	1.40135	N25C22C19	110.337
N25-H26	1.02813	C28C27C29	114.972

Table 2.2. Some selected geometrical parameters (bond lengths and bond angles) of NDAQ—NO in ground state calculated at B3LYP/6-31G (d,p) Levels.

Bond Lengths (Å)		Bond Angles (°)	
N25-N40	1.37369	N25N40O41	113.840
C22-N25	1.47033	C2N17C19	122.531

CHAPTER 2

C19-N17	1.46931	C26N25N40	116.134
C22-C19	1.53693	C22C19N17	113.158
C2-N17	1.40515	N25C22C19	115.271
N40-O41	1.21632	C28C26C27	116.589

The HOMOs of these two compounds were localized over entire molecular backbone of 8-aminoquinoline entity whereas the LOMOs were mainly residing on benzofurazan unit, the electron withdrawing moiety. The HOMO-LUMO band gap in NDAQ—NO is 2.15 eV which is somehow lower than that found in NDAQ (2.84 eV) supporting the relative stability of NDAQ—NO over NDAQ. DFT studies also support the N-nitrosation at N atom of –NH group adjacent to NBD moiety instead of N atom adjacent to quinoline entity. The N-nitrosation on –NH proton near the quinoline entity resulted in a substantially high HOMO –LUMO energy gap (3.28 eV) which disfavors its thermodynamic stability. This strongly ensure that NDAQ upon exposure to NO provides the N-nitrosated adduct NDAQ—NO in which NO is attached in the secondary amine, adjacent to the NBD moiety (**Figure 2.24**).

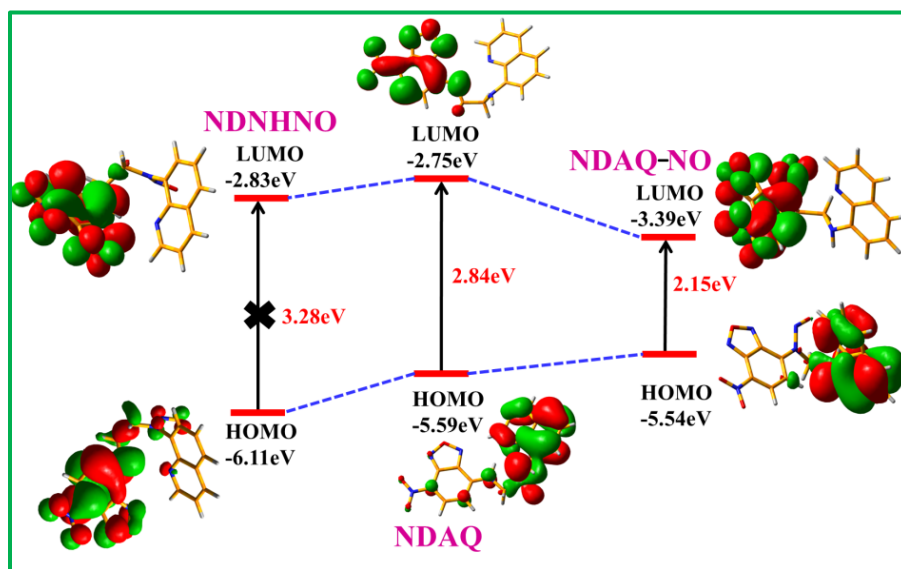


Figure 2.24. Frontier molecular orbitals of probe NDNHNO, NDAQ and NDAQ—NO.

The UV-Vis absorption spectral pattern of NDAQ was inspected at room temperature exhibiting an absorption band at 334 nm. This practical approach is consistent with theoretical TDDFT

CHAPTER 2

studies where peak appeared at ~321 nm due to $S_0 \rightarrow S_7$ electronic transitions with considerable oscillator strength ($f=0.2712$) (Figure 2.25 (a) & Table 2.3). Similarly, in case of NDAQ—NO, the theoretical absorption peaks at 346 nm ($S_0 \rightarrow S_9$) and 470 nm ($S_0 \rightarrow S_2$) matched well with the experimental peaks at 341 nm and 476 nm respectively (Figure 2.25 (b) & Table 2.4). So, all these information strongly support that there is a good correlation between the theoretical and experimental data.

Table 2.3. Vertical excitation energy and oscillator strength (f_{cal}) of low-lying excited singlet states obtained from TDDFT// B3LYP/6-31G(d,p) calculations of NDAQ which is matched with the experimental one

Electronic transition	Composition	Excitation energy	Oscillator strength (f_{cal})	CI	λ_{exp} (nm)
$S_0 \rightarrow S_7$	HOMO-1 \rightarrow LUMO+1 (90 \rightarrow 93)	3.86 eV (320.95 nm)	$f=0.2712$	0.68283	334 nm

Table 2.4. Vertical excitation energy and oscillator strength (f_{cal}) of low-lying excited singlet states obtained from TDDFT// B3LYP/6-31G(d,p) calculations of NDAQ—NO which is matched with the experimental one.

Electronic transition	Composition	Excitation energy	Oscillator strength (f_{cal})	CI	λ_{exp} (nm)
$S_0 \rightarrow S_2$	HOMO-1 \rightarrow LUMO (97 \rightarrow 99)	2.6356 eV (470.42 nm)	$f=0.0288$	0.45114	477 nm
	HOMO-4 \rightarrow LUMO+2 (94 \rightarrow 101)			0.18623	
	HOMO-3 \rightarrow LUMO+2 (95 \rightarrow 101)			0.10432	
$S_0 \rightarrow S_9$	HOMO \rightarrow LUMO+3 (98 \rightarrow 102)	3.5802 eV (346.31 nm)	$f=0.0955$	0.67106	344 nm

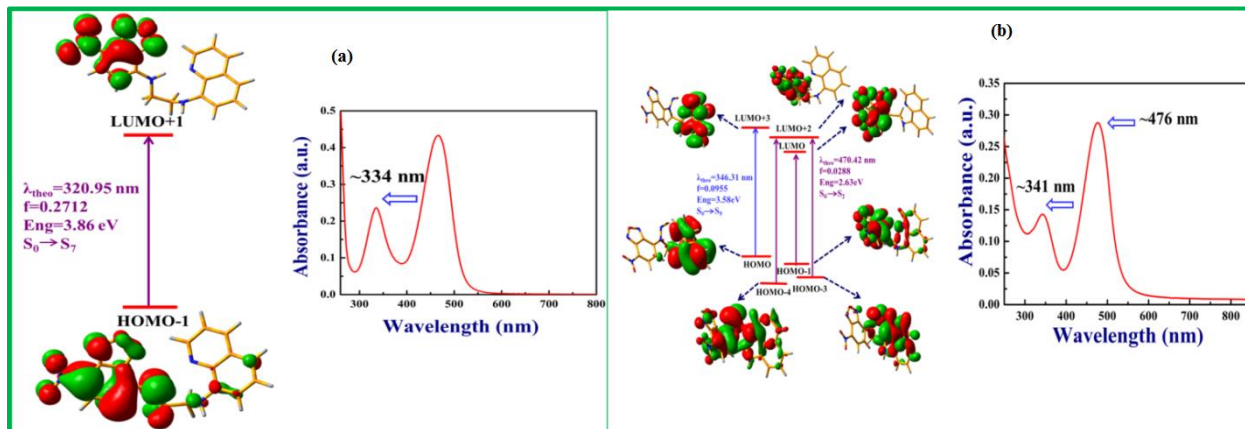


Figure 2.25. (a) Frontier molecular orbitals of NDAQ in UV-vis absorption and Uv-vis absorption spectra of NDAQ in pure MeCN; and (b) Frontier molecular orbitals of NDAQ—NO in Uv-Vis absorption and Uv-Vis absorption spectra of isolated pure NDAQ—NO in pure MeCN.

2.3.10 Cell viability assay

By utilizing A549 and Raw 264.7 cells the cytotoxicity of the probe NDAQ was evaluated. Herein, it is observed that an administration of substantially high concentration (i.e. 100 μ M) of NDAQ resulted in an existence of more than 70% living cells indicating a well-toleration (**Figure 2.26**) of NDAQ and manifesting its biocompatibility as NO sensor in living cells.

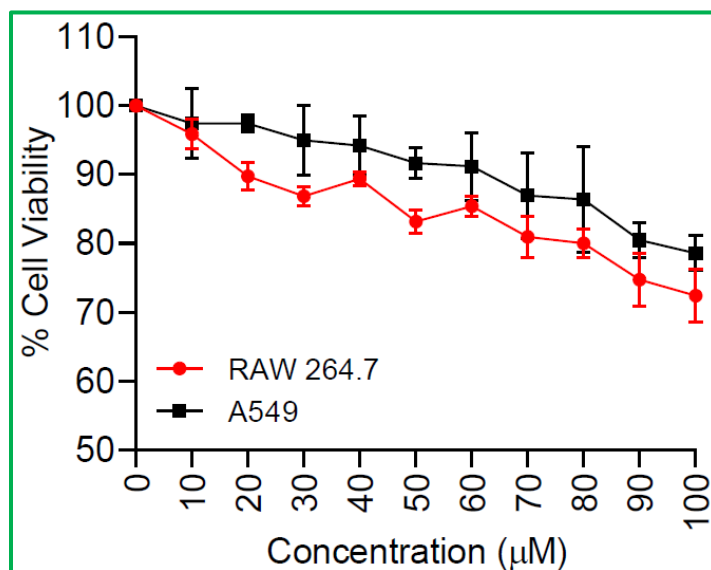


Figure 2.26. Cell Viability Assay of the probe NDAQ.

CHAPTER 2

2.3.11 Cell Imaging studies of NO (Exogenous and Endogenous)

In Raw 264.7 cells, tracking of endogenously generated NO by NDAQ was examined. Lipopolysaccharide (LPS) (1.0 mg/mL) and Interferon-gamma (IFN- γ) (1000 U/mL) were co-stimulated in the cells for 4 hours and then treated with NDAQ (5 μ M). Obviously, the stimulated cells exhibit an intense green fluorescence than an unstimulated one (Figure 2.27). Raw 264.7 cells were further incubated with the NO scavenger PTIO (2-Phenyl-4, 4, 5, 5-tetramethylimidazoline-1-oxyl-3-oxide) (200 mM) for 4 hours in the presence or absence of LPS + IFN- γ co-stimulus and then treated with NDAQ (5 μ M) for 30 minutes. The green fluorescence was shed off, this clearly manifests that endogenous NO generation is responsible for the turn on green fluorescence intracellularly (Figure 2.27 (A),(B)). We have also performed the exogenous NO detection using DEANONOate as a source of NO in the A549 cells. It is obvious that in this case also an intense green fluorescence was detected intracellularly (Figure 2.28 (A),(B)). This leads to the conclusion that NDAQ acts as a potential candidate to track both endogenous and exogenous NO.

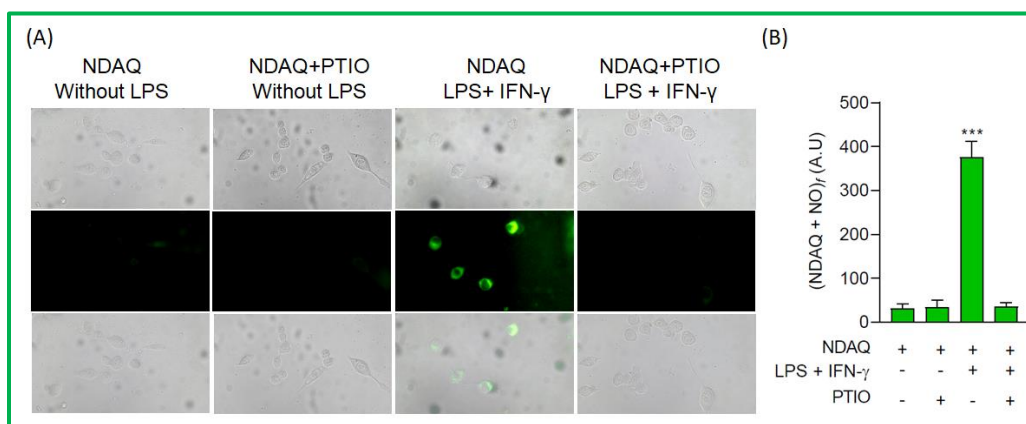


Figure 2.27. (A) Fluorescence image of Raw 264.7 cells stimulated with LPS (1.0 mg/mL) + IFN- γ (1000 U/mL) in presence and absence of iNOS inhibitor PTIO (200 mM) for 4h followed by stimulation with NDAQ (5 μ M) for 30 min. Intracellular green fluorescence was observed in response to interaction of NO with NDAQ and all the Images were obtained at 40X objective. (B) Quantified fluorescence (Mean \pm SD) turn-on in Raw 264.7 cells after stimulation with LPS (1.0 mg/mL) and IFN- γ (1000 U/mL) for 4h in the presence of NDAQ (5 μ M) with or without iNOS inhibitor PTIO compared to control. (a.u.) = arbitrary unit.

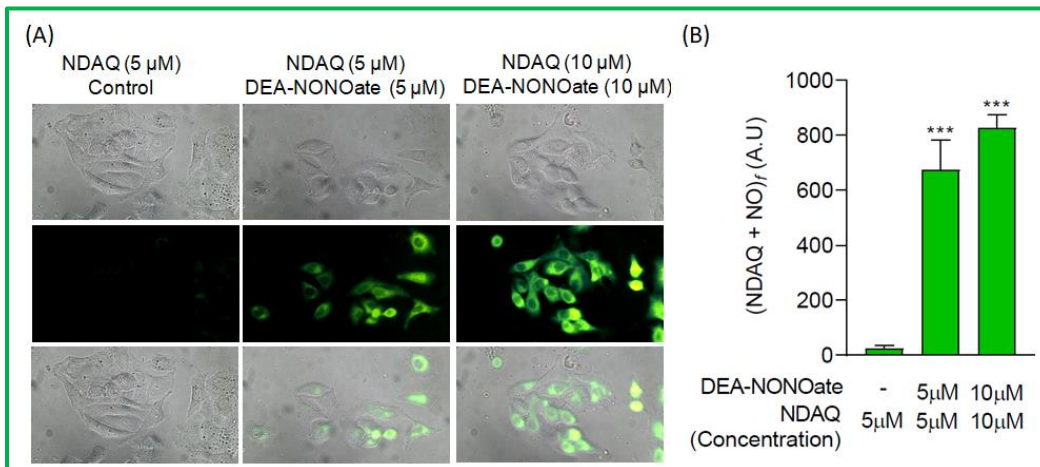


Figure 2.28. (A) Fluorescence imaging of A549 cells incubated with NDAQ (5 μM) only, NDAQ (5 μM) + DEANONOate (5 μM), and NDAQ (10 μM) + DEA-NONOate (10 μM). Increase in green fluorescence was observed with the increase in concentration of NO donor. All the images were taken at 40 \times objective. (B) Quantified fluorescence (Mean \pm SD) turn-on in A549 cells after treatment with NO donor DEA-NONOate in the presence of NDAQ. (a.u.) = arbitrary unit.

2.4 CONCLUSION

In a concise manner, we are reporting here a smart fluorogenic sensor NDAQ for tracking endogenous and exogenous NO selectively in living organisms. The formation of N-nitrosated product (NDAQ—NO) by interaction between NDAQ and NO, results in the generation of vivid green fluorescence at ~ 542 nm through ICT mechanism confirmed by the solvent dependency of emission spectra in solvents of varied polarity. The spectroscopic techniques and computational studies firmly support the formation of N-nitrosated product (NDAQ—NO). The novelty of the probe lies on the simple and easy synthetic procedure with cheap starting materials, fast positive response, high sensitivity (LOD ~ 7 nM) and specificity towards NO. The probe NDAQ has good stability at physiological pH as all the photophysical studies were performed in pure 10 mM HEPES buffer at pH = 7.2. This enhances its applicability to monitor the role of this ubiquitous messenger molecule (NO) in living cells and tissues. On the other hand, the 1st order dependency w.r.t. NDAQ and 2nd order w.r.t. NO clearly manifests the N-nitrosation sensing strategy being operative. Beside all of these, the probe NDAQ exhibits its effectiveness to track NO in

CHAPTER 2

biological milieu because of its least cytotoxicity, bio-compatibility and also no interference by other biological species that are present in complicated biological systems. However, the pH studies display prompt positive response of the probe towards NO even at low pH indicating the successful application of the probe in physiological systems. Now, all the photophysical studies and biological investigations strongly validate the wide usage of this probe to recognize *in vivo* NO.

References

1. Snyder, S. H., Nitric Oxide: First in a New Class of Neurotransmitters. *Science* **1992**, 257 (5069), 494-496.
2. Jasid, S. n.; Simontacchi, M.; Bartoli, C. G.; Puntarulo, S., Chloroplasts as a Nitric Oxide Cellular Source. Effect of Reactive Nitrogen Species on Chloroplastic Lipids and Proteins. *Plant Physiol.* **2006**, 142 (3), 1246-1255.
3. Fukumura, D.; Kashiwagi, S.; Jain, R. K., The role of nitric oxide in tumour progression. *Nat. Rev. Cancer.* **2006**, 6 (7), 521-534.
4. Coletta, C.; Papapetropoulos, A.; Erdelyi, K.; Olah, G.; Módis, K.; Panopoulos, P.; Asimakopoulou, A.; Gerö, D.; Sharina, I.; Martin, E.; Szabo, C., Hydrogen sulfide and nitric oxide are mutually dependent in the regulation of angiogenesis and endothelium-dependent vasorelaxation. *Proc. Natl. Acad. Sci. U.S.A.* **2012**, 109 (23), 9161-9166.
5. Tuteja, N.; Chandra, M.; Tuteja, R.; Misra, M. K., Nitric oxide as a unique bioactive signaling messenger in physiology and pathophysiology. *J. biotechnol. biomed.* **2004**, 2004 (4), 227-237.
6. Zhao, Y.; Vanhoutte, P. M.; Leung, S. W. S., Vascular nitric oxide: Beyond eNOS. *J. Pharmacol. Sci.* **2015**, 129 (2), 83-94.
7. Ignarro, L. J.; Buga, G. M.; Wood, K. S.; Byrns, R. E.; Chaudhuri, G., Endothelium-derived relaxing factor produced and released from artery and vein is nitric oxide. *Proc. Natl. Acad. Sci. U.S.A.* **1987**, 84 (24), 9265-9269.
8. Mayer, B., Nitric oxide. **2012**.
9. Ignarro, L. J., *Nitric oxide: biology and pathobiology*. Academic press: 2000.
10. Wink, D. A.; Mitchell, J. B., Chemical biology of nitric oxide: insights into regulatory, cytotoxic, and cytoprotective mechanisms of nitric oxide. *Free Radic. Biol. Med.* **1998**, 25 (4), 434-456.
11. Pacher, P.; Beckman, J. S.; Liaudet, L., Nitric Oxide and Peroxynitrite in Health and Disease. *Physiol. Rev.* **2007**, 87 (1), 315-424.
12. de Mel, A.; Murad, F.; Seifalian, A. M., Nitric Oxide: A Guardian for Vascular Grafts? *Chem. Rev.* **2011**, 111 (9), 5742-5767.

CHAPTER 2

13. Brown, F. O.; Finnerty, N. J.; Bolger, F. B.; Millar, J.; Lowry, J. P., Calibration of NO sensors for in-vivo voltammetry: laboratory synthesis of NO and the use of UV-visible spectroscopy for determining stock concentrations. *Anal. Bioanal. Chem.* **2005**, *381* (4), 964-971.
14. Bedioui, F.; Villeneuve, N., Electrochemical Nitric Oxide Sensors for Biological Samples – Principle, Selected Examples and Applications. *Electroanalysis* **2003**, *15* (1), 5-18.
15. Izumi, S.; Urano, Y.; Hanaoka, K.; Terai, T.; Nagano, T., A Simple and Effective Strategy To Increase the Sensitivity of Fluorescence Probes in Living Cells. *J. Am. Chem. Soc.* **2009**, *131* (29), 10189-10200.
16. Katayama, Y.; Soh, N.; Maeda, M., A New Strategy for the Design of Molecular Probes for Investigating Endogenous Nitric Oxide Using an EPR or Fluorescent Technique. *ChemPhysChem* **2001**, *2* (11), 655-661.
17. Kojima, H.; Urano, Y.; Kikuchi, K.; Higuchi, T.; Hirata, Y.; Nagano, T., Fluorescent Indicators for Imaging Nitric Oxide Production. *Angew. Chem. Int. Ed.* **1999**, *38* (21), 3209-3212.
18. Lim, M. H.; Lippard, S. J., Copper Complexes for Fluorescence-Based NO Detection in Aqueous Solution. *J. Am. Chem. Soc.* **2005**, *127* (35), 12170-12171.
19. Shiue, T.-W.; Chen, Y.-H.; Wu, C.-M.; Singh, G.; Chen, H.-Y.; Hung, C.-H.; Liaw, W.-F.; Wang, Y.-M., Nitric Oxide Turn-on Fluorescent Probe Based on Deamination of Aromatic Primary Monoamines. *Inorg. Chem.* **2012**, *51* (9), 5400-5408.
20. Yang, Y.; Seidlits, S. K.; Adams, M. M.; Lynch, V. M.; Schmidt, C. E.; Anslyn, E. V.; Shear, J. B., A Highly Selective Low-Background Fluorescent Imaging Agent for Nitric Oxide. *J. Am. Chem. Soc.* **2010**, *132* (38), 13114-13116.
21. Ma, S.; Fang, D.-C.; Ning, B.; Li, M.; He, L.; Gong, B., The rational design of a highly sensitive and selective fluorogenic probe for detecting nitric oxide. *Chem. Commun.* **2014**, *50* (49), 6475-6478.
22. Islam, A. S. M.; Bhowmick, R.; Pal, K.; Katarkar, A.; Chaudhuri, K.; Ali, M., A Smart Molecule for Selective Sensing of Nitric Oxide: Conversion of NO to HSNO; Relevance of Biological HSNO Formation. *Inorg. Chem.* **2017**, *56* (8), 4324-4331.

CHAPTER 2

23. Islam, A. S. M.; Bhowmick, R.; Chandra Garain, B.; Katarkar, A.; Ali, M., Nitric Oxide Sensing through 1,2,3,4-Oxatriazole Formation from Acylhydrazide: A Kinetic Study. *J. Org. Chem.* **2018**, *83* (21), 13287-13295.
24. Xu, C.; Xin, C.; Yu, C.; Wu, M.; Xu, J.; Qin, W.; Ding, Y.; Wang, X.; Li, L.; Huang, W., Fast response two-photon fluorogenic probe based on Schiff base derivatives for monitoring nitric oxide levels in living cells and zebrafish. *Chem. Commun.* **2018**, *54* (96), 13491-13494.
25. Fu, Y.-L.; Li, H.; Wei, X.-Z.; Song, Q.-H., BODIPY-based hydrazine as a fluorescent probe for sensitive and selective detection of nitric oxide: a new strategy. *J. Mater. Chem. B* **2019**, *7* (24), 3792-3795.
26. Liu, P.; Li, B.; Zheng, J.; Liang, Q.; Wu, C.; Huang, L.; Zhang, P.; Jia, Y.; Wang, S., A novel N-nitrosation-based ratiometric fluorescent probe for highly selective imaging endogenous nitric oxide in living cells and zebrafish. *Sens. Actuators B Chem.* **2021**, *329*, 129147.
27. Chen, X.-X.; Niu, L.-Y.; Shao, N.; Yang, Q.-Z., BODIPY-Based Fluorescent Probe for Dual-Channel Detection of Nitric Oxide and Glutathione: Visualization of Cross-Talk in Living Cells. *Anal. Chem.* **2019**, *91* (7), 4301-4306.
28. Mao, Z.; Ye, M.; Hu, W.; Ye, X.; Wang, Y.; Zhang, H.; Li, C.; Liu, Z., Design of a ratiometric two-photon probe for imaging of hypochlorous acid (HClO) in wounded tissues. *Chem. Sci.* **2018**, *9* (28), 6035-6040.
29. Mao, Z.; Jiang, H.; Song, X.; Hu, W.; Liu, Z., Development of a Silicon-Rhodamine Based Near-Infrared Emissive Two-Photon Fluorescent Probe for Nitric Oxide. *Anal. Chem.* **2017**, *89* (18), 9620-9624.
30. Reinhardt, C. J.; Zhou, E. Y.; Jorgensen, M. D.; Partipilo, G.; Chan, J., A Ratiometric Acoustogenic Probe for in Vivo Imaging of Endogenous Nitric Oxide. *J. Am. Chem. Soc.* **2018**, *140* (3), 1011-1018.
31. Huo, Y.; Miao, J.; Fang, J.; Shi, H.; Wang, J.; Guo, W., Aromatic secondary amine-functionalized fluorescent NO probes: improved detection sensitivity for NO and potential applications in cancer immunotherapy studies. *Chem. Sci.* **2019**, *10* (1), 145-152.

CHAPTER 2

32. Zuo, Y.; Wang, X.; Gou, Z.; Lin, W., Step-wise functionalization of polysiloxane towards a versatile dual-response fluorescent probe and elastomer for the detection of H₂S in two-photon and NO in near-infrared modes. *Chem. Commun.* **2020**, 56 (7), 1121-1124.
33. Dutta, A.; Islam, A. S. M.; Maiti, D.; Sasmal, M.; Pradhan, C.; Ali, M., A smart molecular probe for selective recognition of nitric oxide in 100% aqueous solution with cell imaging application and DFT studies. *Org. Biomol. Chem.* **2019**, 17 (9), 2492-2501.
34. Parr, R.; Yang, W., Density Functional Theory of Atoms and Molecules. Oxford, New York: Oxford University Press. **1989**.
35. Barone, V.; Cossi, M., Quantum Calculation of Molecular Energies and Energy Gradients in Solution by a Conductor Solvent Model. *J. Phys. Chem. A* **1998**, 102 (11), 1995-2001.
36. Cossi, M.; Barone, V., Time-dependent density functional theory for molecules in liquid solutions. *J. Chem. Phys.* **2001**, 115 (10), 4708-4717.
37. Cossi, M.; Rega, N.; Scalmani, G.; Barone, V., Energies, structures, and electronic properties of molecules in solution with the C-PCM solvation model. *J. Comput. Chem.* **2003**, 24 (6), 669-681.
38. Becke, A., Density-Functional Thermochemistry. III. The Role of Exact Exchange. *J. Chem. Phys.*, 98: 5648-5652. 1993.
39. Lee, C.; Yang, W.; Parr, R., Phys. Rev. B: Condens. Matter Mater. Phys. **1988**.
40. Frisch, M.; Trucks, G.; Schlegel, H.; Scuseria, G.; Robb, M.; Cheeseman, J.; Scalmani, G.; Barone, V.; Mennucci, B.; Petersson, G. J. G. S. T. i. n. c. r. f. t. r., Gaussian 09, Revision A. 1; Gaussian, Inc: Wallingford, CT, 2009. **1993**.
41. O'Boyle, N. M.; Tenderholt, A. L.; Langner, K. M., cclib: A library for package-independent computational chemistry algorithms. *J. Comput. Chem.* **2008**, 29 (5), 839-845.
42. Rocha, I. O.; Kappenberg, Y. G.; Rosa, W. C.; Frizzo, C. P.; Zanatta, N.; Martins, M. A.; Tisoco, I.; Iglesias, B. A.; Bonacorso, H. G., Photophysical, photostability, and ROS generation properties of new trifluoromethylated quinoline-phenol Schiff bases. *Beilstein J. Org. Chem.* **2021**, 17 (1), 2799-2811.
43. Imai, K.; Uzu, S.; Toyooka, T., Fluorogenic reagents, having benzofurazan structure, in liquid chromatography. *J. Pharm. Biomed. Anal.* **1989**, 7 (12), 1395-1403.

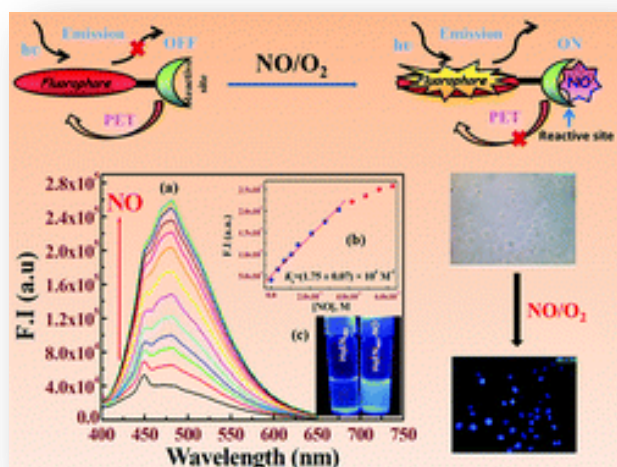
CHAPTER 2

44. Imai, K.; Uzu, S.; Kanda, S.; Baeyens, W. R. G., Availability of fluorogenic reagents having a benzofurazan structure in the biosciences. *Anal. Chim. Acta* **1994**, *290* (1), 3-20.
45. Uchiyama, S.; Santa, T.; Okiyama, N.; Fukushima, T.; Imai, K., Fluorogenic and fluorescent labeling reagents with a benzofurazan skeleton. *Biomed. Chromatogr.* **2001**, *15* (5), 295-318.
46. Santa, T.; Fukushima, T.; Ichibangase, T.; Imai, K., Recent progress in the development of derivatization reagents having a benzofurazan structure. *Biomed. Chromatogr.* **2008**, *22* (4), 343-353.
47. Kharitonov, V. G.; Sundquist, A. R.; Sharma, V. S., Kinetics of nitric oxide autoxidation in aqueous solution. *J. Biol. Chem.* **1994**, *269* (8), 5881-5883.
48. Grätzel, M.; Taniguchi, S.; Henglein, A., Pulsradiolytische Untersuchung der NO-Oxydation und des Gleichgewichts $\text{N}_2\text{O}_3 \rightleftharpoons \text{NO} + \text{NO}_2$ in wäßriger Lösung. *Ber. Bunsen-Ges. Phys. Chem* **1970**, *74* (5), 488-492.
49. Licht, W. R.; Tannenbaum, S. R.; Deen, W. M., Use of ascorbic acid to inhibit nitrosation: kinetic and mass transfer considerations for an in vitro system. *Carcinogenesis* **1988**, *9* (3), 365-372.
50. Lewis, R. S.; Tannenbaum, S. R.; Deen, W. M., Kinetics of N-Nitrosation in Oxygenated Nitric Oxide Solutions at Physiological pH: Role of Nitrous Anhydride and Effects of Phosphate and Chloride. *J. Am. Chem. Soc.* **1995**, *117* (14), 3933-3939.
51. Chen, T.; Zamora, R.; Zuckerbraun, B.; Billiar, T.R., Role of nitric oxide in liver injury. *Curr. Mol. Med.* **2003**, *3*(6) 519-526.
52. Lee, J.; Chen, L.; West, A. H.; Richter-Addo, G. B., Interactions of Organic Nitroso Compounds with Metals. *Chem. Rev.* **2002**, *102* (4), 1019-1066.

A smart molecular probe for selective recognition of nitric oxide in 100% aqueous solution with cell imaging application and DFT studies

Abstract:

Herein, a simple, least-cytotoxic as well as an efficient fluorescent sensor HqEN₄₈₀ was prepared from (quinolin-8-yloxy)-acetic acid ethyl ester (L¹) and N,N-dimethyl ethylene diamine to recognize NO in 100% aqueous solution. Its marked selectivity and sensitivity towards NO, makes it a highly suitable probe for nitric oxide under in vitro conditions with the possibility of in vivo monitoring of NO. Upon addition of 3.5 equivalents of NO, there is an approximately 7 fold enhancement in fluorescence intensity in aqueous solution with a corresponding K_f value of $(1.75 \pm 0.07) \times 10^4 \text{ M}^{-1}$. Quantum yields of HqEN₄₈₀ and [HqEN₄₈₀-NO] compounds are evaluated to be 0.04 and 0.22, respectively, using acidic quinine sulphate as a standard. In terms of the 3σ/slope method, the LOD for nitric oxide was found to be 53 nM thus, making the probe highly suitable to track NO in biological systems.

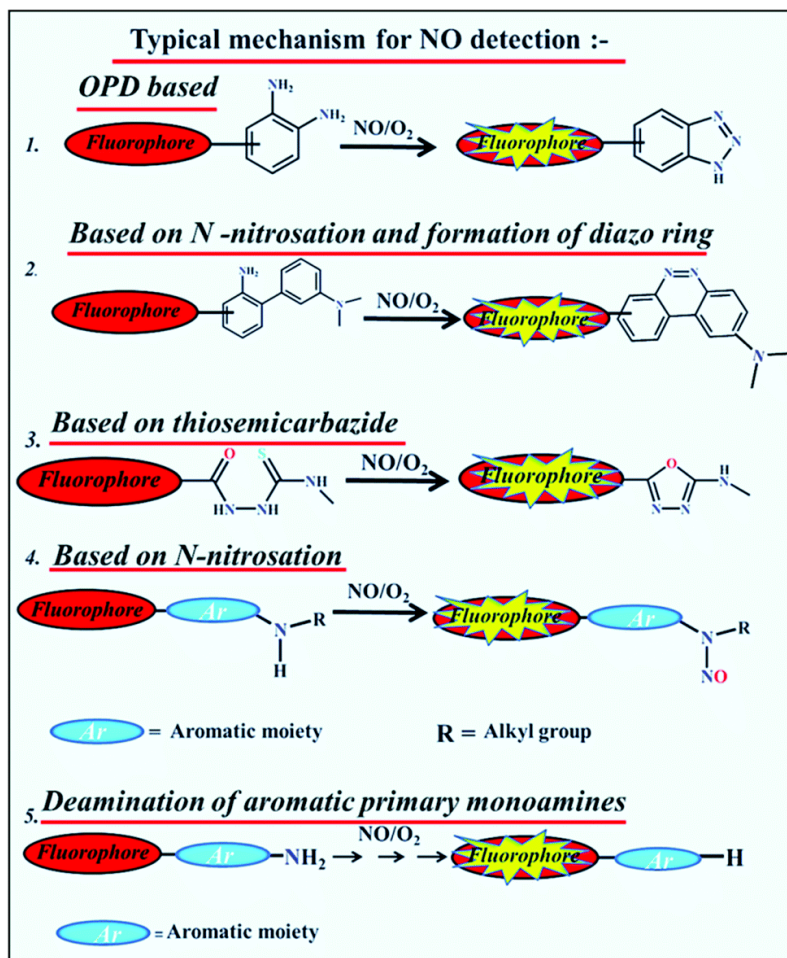


3.1 Introduction:

Nitric oxide (NO), originating from L-arginine by the action of nitric oxide synthases¹ (NOS), has not only been identified as a highly reactive gaseous free radical but also as a signaling agent for its various functions in the cardiovascular, immune, and central nervous systems.² Nitric oxide modulates gene transcription^{3,4} and m-RNA translation through binding with iron-responsive elements.^{5,6} It also regulates the production of post-translational modifications of proteins by adenosine 5'- diphosphate ribosylation^{7,8} indicating its pivotal role in the human body. However, in high concentration NO exhibits a toxic effect on all cells, including the cells that are able to produce it. Misregulation of NO production may cause diseases like stroke, cancer, hypertension, neurodegeneration and endothelial dysfunction.⁹⁻¹² Nitric oxide with a half-life less than 10 seconds makes its detection quite challenging in biological systems.¹³ To date, various techniques such as electrochemical, fluorescence, electron spin resonance etc. have been utilized widely to monitor NO generation and its biological activities in living cells.¹⁴ Compared to all other approaches, the fluorescence technique is the most favorable one due to its high sensitivity and experimental feasibility. Most of the fluorescent probes are mainly of two types: one is based on the o-phenylenediamine (OPD) moiety¹⁵⁻²¹ and the other is based on metal ligand complexes.²²⁻²⁷ Now, between these two, the former one produces triazole derivatives upon treatment with NO under aerated condition with concomitant generation of fluorescence intensity. Some limitations still exist with the OPD based probes. Firstly, they may undergo self-oxidation due to the existence of an electron rich diamino-benzene fragment. Secondly they may exhibit a false positive response towards dehydroascorbic acid (DHA) and ascorbic acid (AA) resulting in a wrong interpretation of the data. Another important drawback of this strategy is pH dependency of fluorescence intensity of the product as the formed triazole contains a secondary amine which can be protonated. The metal-complex based nitric oxide sensors also possess various disadvantages like biological incompatibility,^{22,28} easy leakage from the cells²⁹ or side effects from the metal ions.³⁰ Considering these aforementioned limitations for the detection of NO, recently a few novel strategies have been developed which include (1) the nitrosation reaction,^{31,32} (2) the reaction with thiosemicarbazide³³ leading to the formation of oxadiazole, (3) the reaction with acylhydrazide leading to the formation of 1,2,3,4-oxatriazole,³⁴ (4) the generation of the Se-NO bond³⁵ and so on (**Scheme 3.1**). Usually, most of the organic

CHAPTER 3

fluorescent probes are associated with poor water solubility which is contrary to the real physiological conditions.

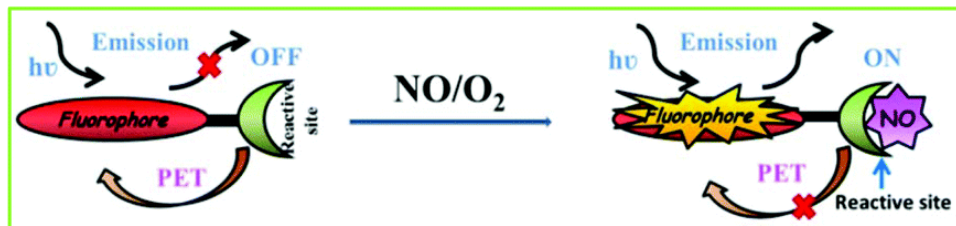


Scheme 3.1. Different strategies for the detection of NO.

All the above discussions lead to the conclusion that a fluorescent nitric oxide probe should satisfy some basic requirements like low cytotoxicity and good water solubility along with high NO selectivity and specificity. Taking all these parameters in mind, we have been interested to design an N-nitrosation based probe on the quinoline platform which could display a positive response towards nitric oxide selectively in purely aqueous medium (**Scheme 3.2**). Quinoline has an excellent photostability and the presence of the pyridine moiety magnifies its fluorescence properties by acting as an electron acceptor.³⁶ The present probe HqEN₄₈₀ shows good response to NO and is inert towards various reactive oxygen, nitrogen and sulphur species present in a biological milieu. Here in HqEN₄₈₀, NO directly reacts with the secondary nitrogen atom of the

CHAPTER 3

amide group to generate the N–N=O moiety leading to an enhancement in fluorescence intensity through blocking of the PET process. The fluorescence based bio-imaging experiment has also been executed in HepG2 cells by using HqEN₄₈₀.



Scheme 3.2. General mechanism for NO sensing using a N-nitrosation based probe.

3.2 EXPERIMENTAL SECTION

3.2.1 Physical measurements

An IR 750 series-II FTIR (Nicolet Magna) spectrophotometer was used to record IR spectra in the solid state for both pure ligand (HqEN₄₈₀) and its NO product (HqEN₄₈₀-NO) in the range of 400–4000 cm⁻¹ on KBr pellets. Electronic spectra of the probe as well as the product of its reaction with NO were recorded on an Agilent 8453 Diode-array Uv-Vis spectrophotometer using HPLC grade H₂O as a solvent with a 1 cm quartz cuvette in the range of 200–900 nm. Fluorescence studies were performed on a PTI (model QM-40) spectrofluorimeter. ¹H NMR spectra were recorded in DMSO-d₆ as well as in CDCl₃ on a Bruker 300 MHz instrument while ¹³C NMR spectra were recorded on a Bruker 75 MHz instrument using trimethylsilane ($\delta = 0$) as an internal standard. ESI-MS⁺(m/z) spectra were recorded using a high resolution mass spectrometer (model: QTOF Micro YA263). Time correlated single photon counting (TCSPC) measurements using a picosecond diode laser (IBH nanoled-07) in an IBH fluorocube apparatus were performed to determine fluorescence lifetimes. A Hamamatsu MCP photomultiplier (R3809) was used to collect the fluorescence decay data which were further examined by using the IBH DAS6 software. To obtain cell images, a fluorescence microscope (Leica DM3000, Germany) was used. The pH values of the reaction solutions were measured with a digital pH meter (model: Systronics 335, India) in the pH range of 2–12 which was prior calibrated using buffers of pH 4, 7 and 10.

3.2.2 Materials and methods

8-Hydroxyquinoline, ethyl-bromoacetate, N,N-dimethylethylenediamine (Sigma-Aldrich) and propylamine (Sigma Aldrich) were used to synthesize the ligands. Salts of Cd^{2+} , Sm^{3+} , Co^{2+} , Mg^{2+} , Mn^{2+} , Na^+ , K^+ , Zn^{2+} , Dy^{3+} , Eu^{2+} , Ni^{2+} , Cu^{2+} , Cr^{3+} , Hg^{2+} , Fe^{3+} , Pb^{2+} , Al^{3+} , F^- , PPI , N_3^- , CO_3^{2-} , Cl^- , CH_3COO^- , ClO_4^- , SO_4^{2-} , NO_3^- , $\text{S}_2\text{O}_4^{2-}$, H_2PO_4^- , NO_2^- , S^{2-} , other biological anions like H_2O_2 , O_2^- , TEMPO radical, ClO^- , ascorbic acid, ONOO^- , DHA, NO^+ , HNO etc. as well as all the amino acids were purchased either from Sigma-Aldrich or from other commercial suppliers and used without further purification. Solvents like EtOH (ethanol), MeCN (acetonitrile), etc. (Merck, India) were of reagent grade and dried before use.

3.2.3 Synthesis

3.2.3.1 Preparation of (quinolin-8-yloxy)-acetic acid ethyl ester (L^1)

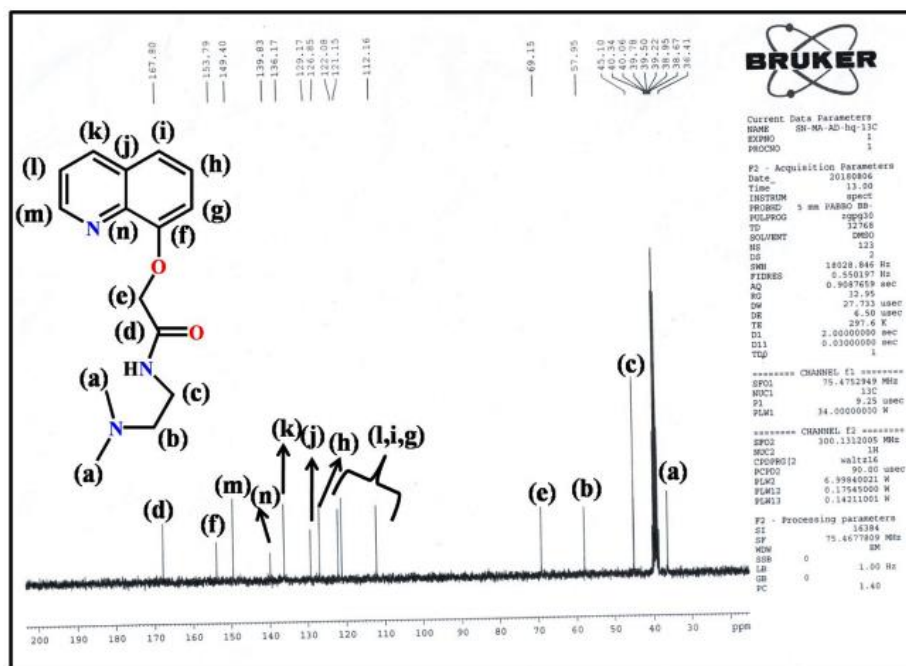
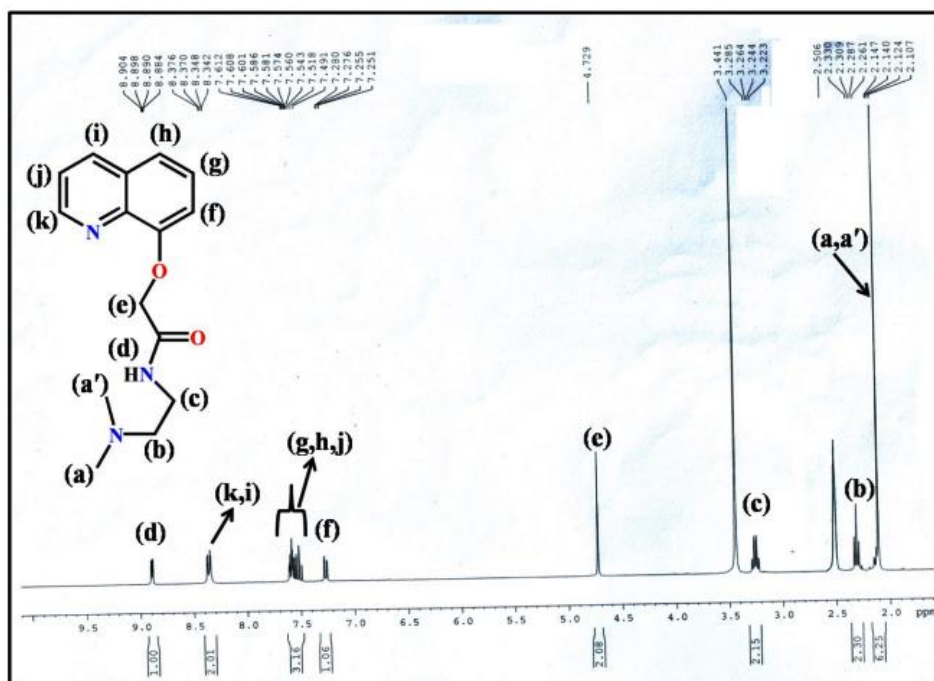
A mixture of 8-hydroxyquinoline (5 mmol, 0.73 g), ethyl bromoacetate (7.5 mmol, 1.25 g) and anhydrous K_2CO_3 (12.5 mmol, 1.73 g) in acetonitrile was refluxed on a water bath for 8 h. After cooling, the reaction mixture was filtered and then the solvent was removed under reduced pressure. The resulting oily product was further purified by column chromatography on silica gel, using ethyl acetate: pet ether (3: 2) as the eluent to afford L^1 (85% yield).

3.2.3.2 Preparation of N-(2-dimethylamino-ethyl)-2-(quinolin-8-yloxy)-acetamide (HqEN_{480})

The resulting (quinolin-8-yloxy)-acetic acid ethyl ester (L^1) (1.0 mmol) and N,N-dimethylethylenediamine (10 mmol) in ethanol were refluxed on a water bath for 6 h. After cooling, the reaction mixture was concentrated under vacuum and the resulting oily product was subjected to column chromatography on silica gel (60–120 mesh) by using DCM as the eluent to obtain HqEN_{480} in pure form. Yield: 85%. ^1H NMR (300 MHz, DMSO-d_6) δ_{ppm} : 2.14 (m, 6H, $-\text{CH}_3$, $-\text{CH}_3$), 2.33 (m, 2H, $-\text{CH}_2$), 3.28 (m, 2H, $-\text{CH}_2$), 4.72 (s, 2H, $-\text{CH}_2$), 7.28 (d, 1H, $-\text{ArH}$), 7.61–7.49 (m, 3H, $-\text{ArH}$), 8.34 (d, 1H, $-\text{ArH}$), 8.37 (d, 1H, $-\text{ArH}$) and 8.90 (m, 1H, $-\text{NH}$) (**Figure 3.1**). ^{13}C -NMR: (75 MHz, DMSO-d_6) δ_{ppm} : 36.41, 45.10, 57.95, 69.15, 112.16, 121.15, 122.08, 126.85, 129.17, 136.17, 139.83, 149.40, 153.79, 167.80 (**Figure 3.2**). ESI- MS^+ (m/z):

CHAPTER 3

296.22 (HqEN₄₈₀ + Na⁺) (**Figure 3.3**). IR spectrum: –NH (3411 cm⁻¹), –C=O (1668 cm⁻¹) (**Figure 3.4**).



CHAPTER 3

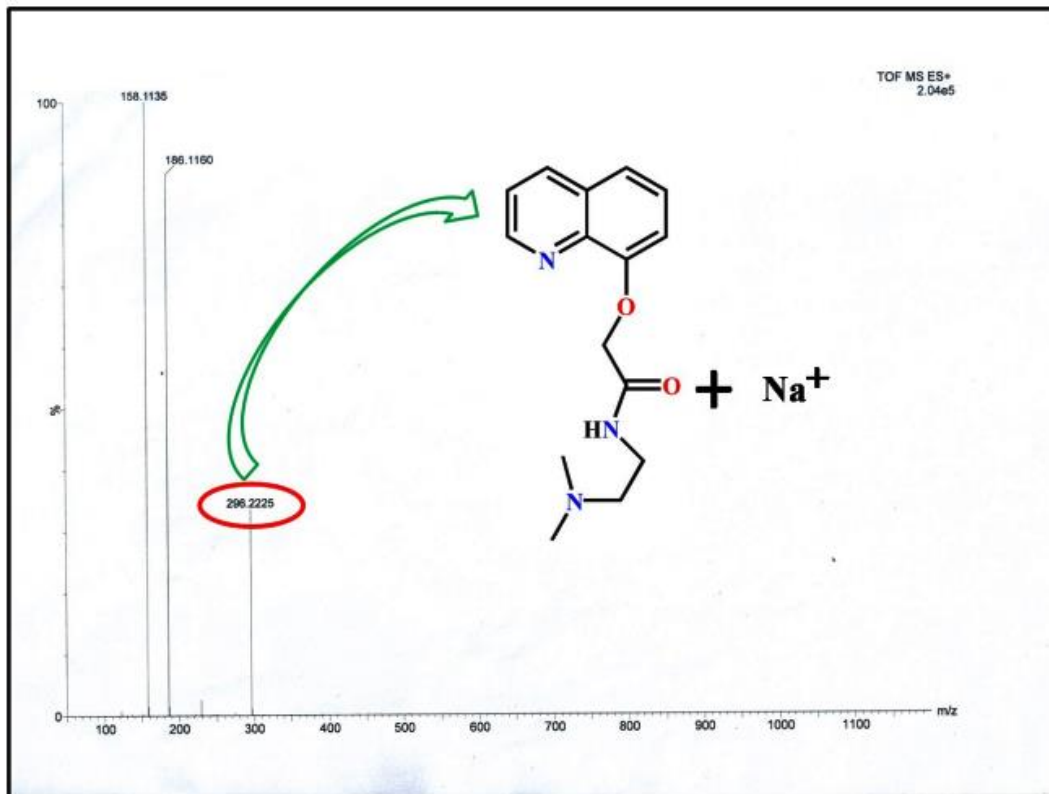


Figure 3.3. Mass spectrum of HqEN₄₈₀ in MeCN.

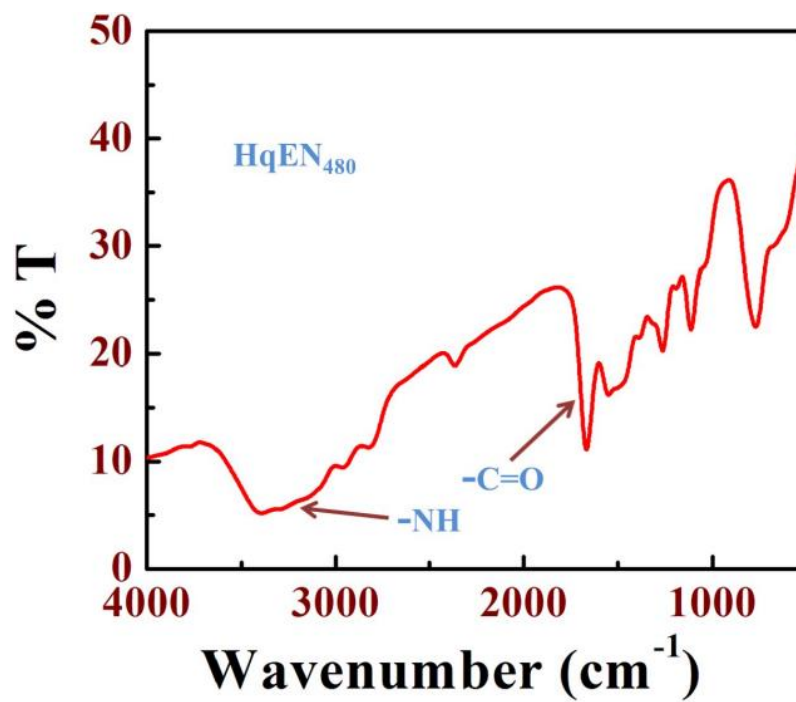


Figure 3.4. IR spectrum of HqEN₄₈₀ in solid state.

CHAPTER 3

3.2.3.3 Preparation of N-propyl-2-(quinolin-8-yloxy) acetamide (HqPA)

L¹ (1 mmol) was dissolved in 25 mL of EtOH. To this ethanolic solution propylamine (10 mmol) was added dropwise and refluxed for 5 h. The reaction mixture was then cooled to room temperature and the formed precipitate was filtered, washed with cold ethanol, and dried in an air affording a white solid. Now HqPA was further purified by recrystallization from ethanol. Yield: 80%. ESI-MS⁺ (m/z): 269.01 (HqPA + H₂O + Li⁺) (Figure 3.5). ¹H NMR (300 MHz, CDCl₃) δ_{ppm}: 0.86 (d, 3H, -CH₃), 3.59 (m, 2H, -CH₂), 3.91 (m, 2H, -CH₂), 4.67 (s, 2H, -CH₂), 7.05 (m, 1H, -ArH), 7.43–7.49 (m, 3H, -ArH), 8.18 (d, 1H, -ArH), 8.85 (d, 1H, -ArH) and 9.11 (s, 1H, -NH) (Figure 3.6).

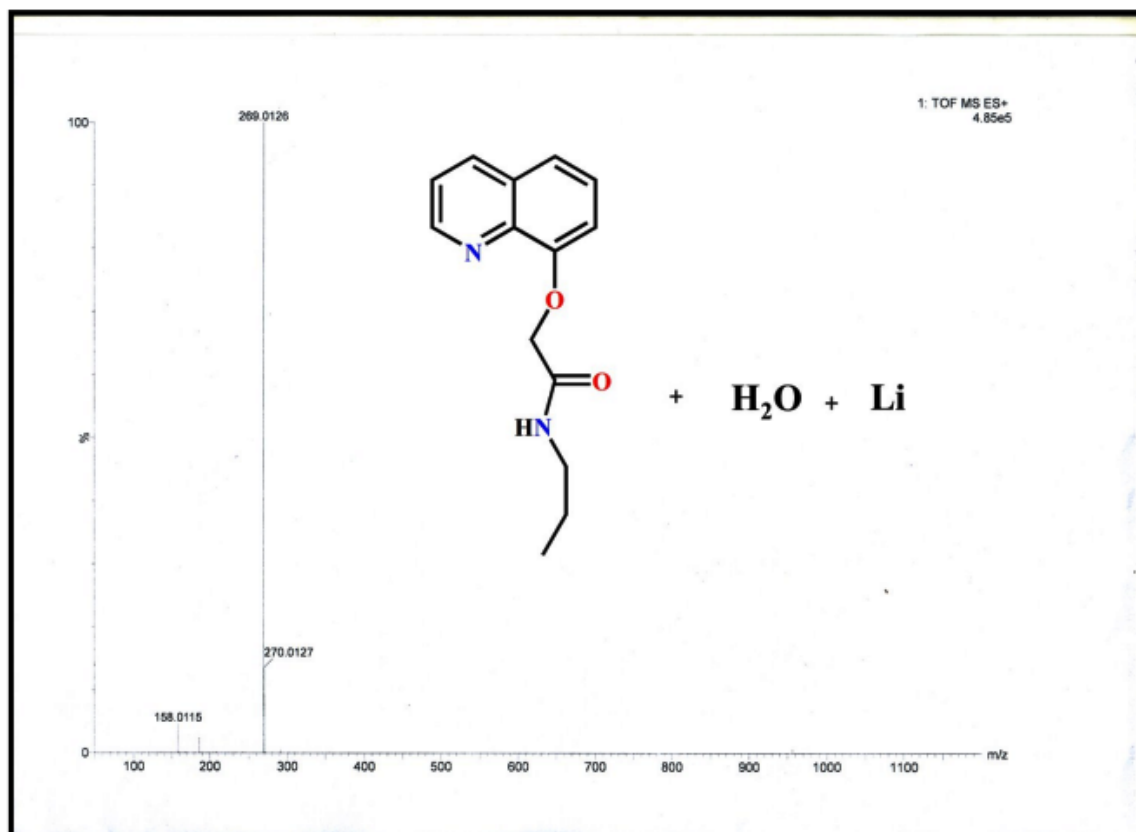


Figure 3.5. Mass spectrum of HqPA in MeOH.

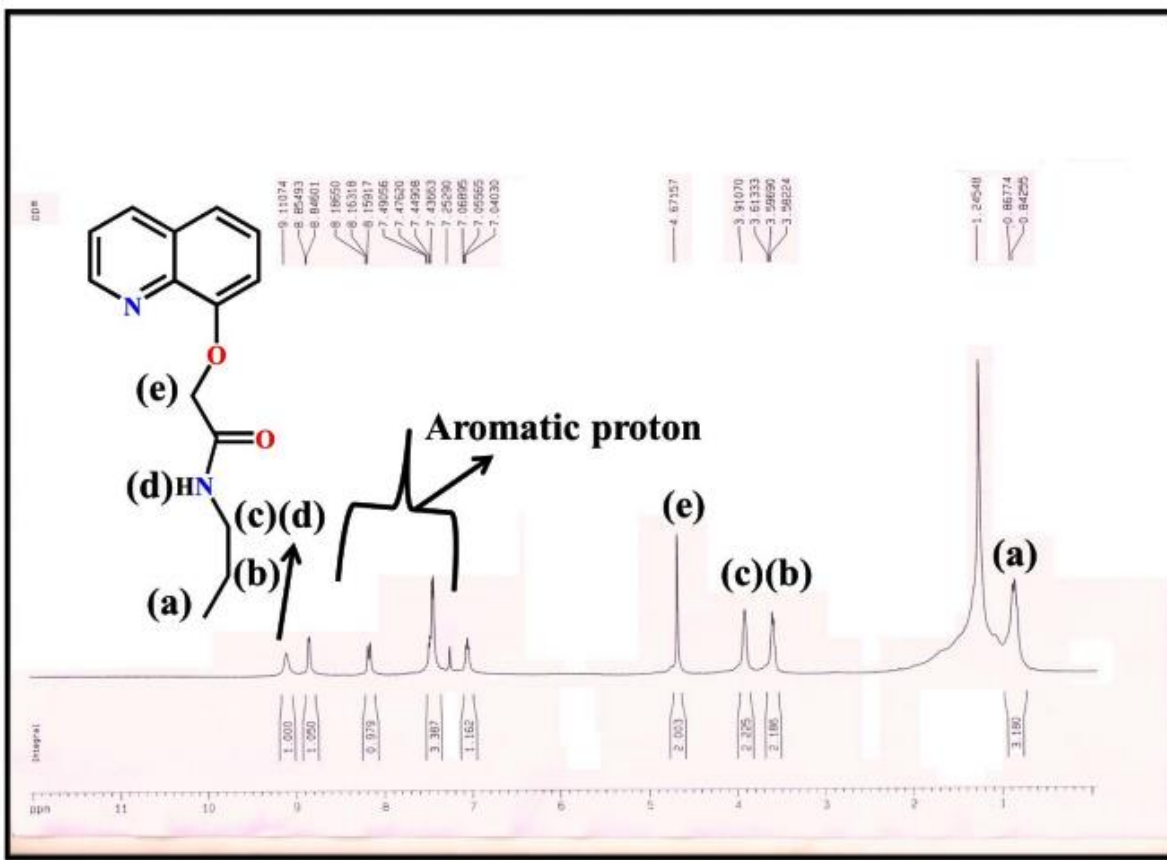


Figure 3.6. ^1H NMR spectrum of HqPA in CDCl_3 .

3.2.4 Solution preparation for UV–Vis absorption and fluorescence studies

To study the UV-Vis and fluorescence response of HqEN₄₈₀ and HqPA towards NO, stock solutions of 1.0×10^{-3} M of the probes were prepared in Milli-Q Millipore water. The stock solution of nitric oxide (1.74×10^{-3} M in deoxygenated deionized water) was prepared by bubbling nitric oxide gas for 15 min in a sealed vial with the help of a syringe. The nitric oxide gas was purified by passing through a drying tube containing solid NaOH pellets.³⁷ The OH^\bullet and ONOO^- solutions were prepared by the reported methods.³⁸ HNO was synthesized from Angeli's salt.³⁹ The solutions of other metal ions as well as anions were prepared either in H_2O or in alcohol. An aqueous solution of 10.0 mM 4-(2-hydroxyethyl)piperazine-1-ethanesulfonic acid (HEPES) buffer was prepared and the pH was adjusted to 7.20 by using HCl and NaOH. The ionic strength of the buffer solution was maintained at 0.10 M (NaCl) throughout the measurements. Then 2.5 mL of this buffer solution was pipetted out into a cuvette to which 20 μM of the probe HqEN₄₈₀ or HqPA was added and then NO was added incrementally in a regular

interval of volume and fluorescence spectra were recorded for each solution using 5 nm × 3 nm slit width

3.2.5 Calculation of LOD

The analytical detection limit was obtained by performing fluorescence titration of HqEN₄₈₀ with NO by adding aliquots in a micromolar concentration of NO to 20 μM HqEN₄₈₀ in 2.5 mL buffer and the LOD was calculated by the 3σ/slope method.

$$LOD = 3 \times \frac{S_d}{S} \dots \dots (1)$$

Where S_d is the standard deviation of the intercept of the blank (HqEN₄₈₀ only) obtained from a plot of fluorescence intensity (FI) versus [HqEN₄₈₀], and S is the slope obtained from the linear part of the plot of FI versus [NO].

3.2.6 Calculation of the quantum yield

Fluorescence quantum yields (Φ) were determined by using the equation:

$$\varphi_{sample} = (OD_{std} \times A_{sample}) / (OD_{sample} \times A_{std}) \times \varphi_{std} \dots (2)$$

Here, A_{sample} and A_{std} represent the areas under the fluorescence spectral curves. The optical densities of the sample and standard are designated as OD_{sample} and OD_{std} , respectively, at the excitation wavelength. Here, acidic quinine sulphate was taken as the standard ($\Phi_{std} = 0.54$) for the quantum yield calculation of HqEN₄₈₀ and HqEN₄₈₀-NO.

3.2.7 Computational details

The optimization of ground state electronic structures of both the ligand and NO adduct was performed by using the DFT method⁴⁰ associated with the conductor-like polarizable continuum model (CPCM).⁴¹ Becke's hybrid function⁴² with the Lee–Yang–Parr (LYP) correlation function⁴³ were applied throughout the study. The geometries of the ligand and the NO product were fully optimized without any symmetry constraints. On the basis of the optimized ground state geometry, the absorption spectral properties of HqEN₄₈₀ and [HqEN₄₈₀-NO] in water were calculated by time-dependent density functional theory (TDDFT)⁴⁴ associated with the

CHAPTER 3

conductor-like polarizable continuum model (CPCM).⁴¹ We have computed the lowest 40 singlet–singlet transitions and the presence of electronic correlation in the TDDFT (B3LYP) method⁴⁵ enables to obtain accurate electronic excitation energies. For H, C, N and O atoms, we employed 6-31+G basis sets for the optimization of the ground state. The calculated electron density plots for frontier molecular orbitals were constructed by using Gauss View 5.1 software. All the calculations were done with the Gaussian 09 W software package.⁴⁶ The Gauss Sum 2.1 program⁴⁷ was utilized to calculate the molecular orbital contributions from groups or atoms.

3.2.8 Cell culture

Human hepatocellular liver carcinoma (HepG2) cell lines (NCCS, Pune, India) were grown in DMEM supplemented with 10% FBS and antibiotics (penicillin-100 $\mu\text{g ml}^{-1}$; streptomycin-50 $\mu\text{g ml}^{-1}$). The cells were cultured at 37 °C in 95% air, 5% CO₂ incubator.

3.2.9 Cell imaging study

HepG2 cells were cultured in a 35 × 10 mm culture dish on a cover-slip for 24 h at 37 °C. The cells were treated with 10 μM solutions of HqEN₄₈₀, prepared by dissolving HqEN₄₈₀ in the mixed solvent DMSO: water = 1 : 9 (v/v) and incubated for 1 hour at 37 °C. To study the adduct formation of HqEN₄₈₀ with intracellular NO, HepG2 cells were pre-incubated separately with 10, 20 and 40 μM of sodium nitroprusside (SNP) for 60 min at 37 °C, followed by washing them thrice with 1× PBS and subsequent incubation with 10 μM HqEN₄₈₀ for 60 min at 37 °C. Fluorescence images of HepG2 cells were obtained using a fluorescence microscope (Leica DM3000, Germany) with an objective lens of 40× magnification.

3.2.10 Cell cytotoxicity assay

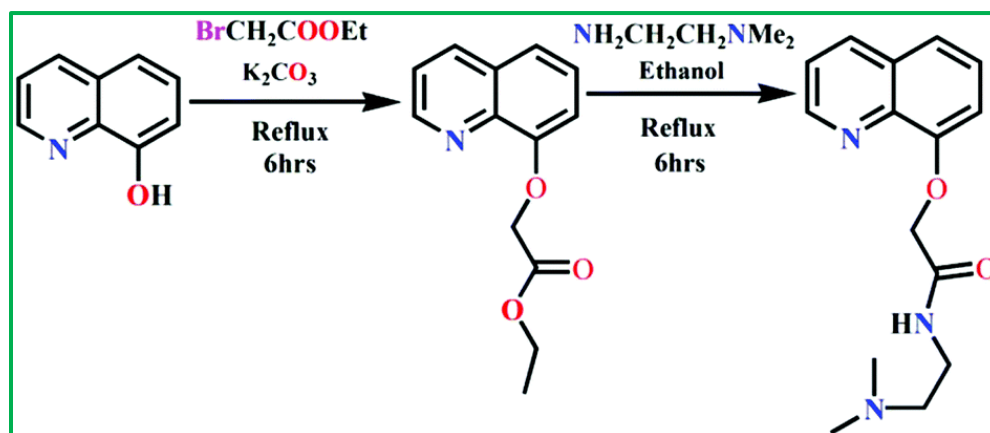
In order to evaluate the cytotoxic effect of the ligand HqEN₄₈₀, a cell viability assay was done by using 3-(4,5-dimethylthiazol-2-yl)-2,5-diphenyltetrazolium bromide (MTT).⁴⁸ HepG2 cells (1 × 10⁵ cells per well) were cultured in 96-well plates and incubated at 37°C with variable concentrations of HqEN₄₈₀ (starting from 5, 10, 20, 40, 60, 80 and 100 μM) for 24 hours. After incubation, 10 μl of MTT solution [5 mg ml^{-1} , dissolved in 1× phosphate-buffered saline (PBS)] were added to each well of a 96-well culture plate and incubated at 37 °C for 4 hours. Media were decanted from wells followed by incorporation of 100 μL of 0.04N acidic isopropyl alcohol

CHAPTER 3

into each well so that intracellular formazan crystals (blue-violet) thereby formed become easily soluble. The absorbance of each solution was measured at 595 nm (EMax Precision MicroPlate Reader, Molecular Devices, USA). Values were calculated as mean \pm standard errors of three independent experiments. The cell viability was represented as the optical density ratio of treatment to control.

3.3 RESULTS AND DISCUSSION

As delineated in **Scheme 3.3**, the receptor HqEN₄₈₀ was designed in order to achieve the selective detection of NO over other commonly interfering species (such as ascorbic acid, ROS, RNS and so on) by the reaction between (quinolin-8-yloxy)- acetic acid ethyl ester (L¹) and N,N-dimethylethylene diamine in alcoholic medium. The receptor, designated as HqEN₄₈₀, was well-characterized by ¹H NMR (**Figure 3.1**), ¹³C NMR (**Figure 3.2**), HRMS (**Figure 3.3**) and IR (**Figure 3.4**).



Scheme 3.3. Synthetic route for the probe HqEN₄₈₀.

In aqueous buffer the receptor exhibits sensitive and selective fluorogenic response towards NO. The negligible or no reactivity of this probe to other ROS and RNS arises due to the controlled electron density by the introduction of a carbonyl group such as CONH.⁴⁹ Here hydroxyquinoline is suitable as a fluorophoric moiety because of its many biological activities such as fungicides, antibacterial properties, etc.

3.3.1 Spectral response of HqEN₄₈₀ to NO

3.3.1.1 Uv-Vis absorption studies

HqEN₄₈₀ exhibits high selectivity as well as high sensitivity towards NO. By keeping the concentration fixed for the probe HqEN₄₈₀ (20 μM) in 10.0 mM HEPES buffer (pH = 7.20), the addition of NO generates a new absorption peak at 355 nm which increases gradually with the gradual addition of NO (**Figure 3.7a**). The linear dependence of absorbance as a function of [NO] was analyzed with the help of eqn (3)³³ which under the conditions $1 \gg c \times x$ with $n = 1$ becomes eqn (4)

$$y = \frac{(a+b \times c \times x^n)}{(1+c \times x^n)} \quad \dots \dots (3)$$

$$y = a + (b \times c)x \quad \dots \dots (4)$$

Where a = absorbance of the free probe, b = absorbance of the probe in the presence of excess of NO, and c = formation constant, K_f . It is interesting to note that linear least-squares analysis of Uv-Vis titration data gives $K_f = (3.35 \pm 0.06) \times 10^4 \text{ M}^{-1}$ (**Figure 3.7b**).

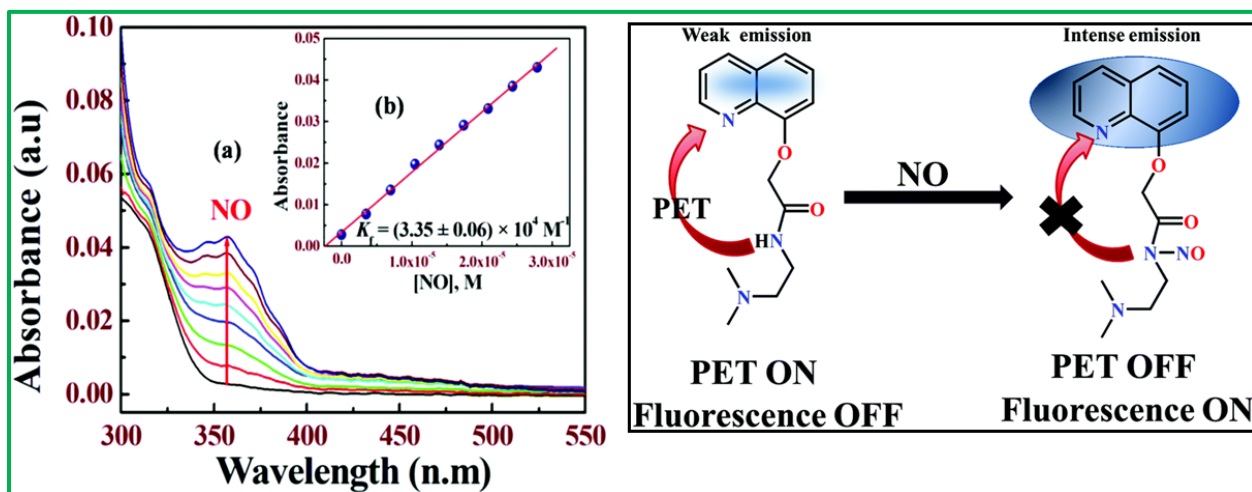


Figure 3.7. (a) Changes in Uv-Vis absorption spectra of HqEN₄₈₀ (20 μM) in aqueous HEPES buffer (10 mM) at pH 7.20 and $\mu = 0.10 \text{ M NaCl}$ with various amounts of NO (0–0.8 equivalents); (b) plot of absorbance vs. [NO]. **Scheme 3.4.** Schematic representation of N-nitrosation based fluorescent probe HqEN₄₈₀ for NO.

3.3.1.2 Fluorescence studies

To analyse the emission spectral behaviour of the probe HqEN₄₈₀, we have performed the fluorescence studies in purely aqueous medium (10.0 mM HEPES buffer, pH = 7.20) at $\lambda_{\text{ex}} = 390$ nm. The probe HqEN₄₈₀ in aqueous solution is weakly fluorescent because of PET from the amide nitrogen atom to the quinoline fluorophoric moiety. However, on reaction with NO the PET is blocked, leading to the formation of an electron deficient N=N=O moiety (Scheme 3.4). The apparent formation constant (K_f) of HqEN₄₈₀-NO, formed by the reaction between HqEN₄₈₀ and NO, was determined by performing the fluorescence titration of HqEN₄₈₀ (20 μM) in aqueous solution (2.5 ml) with NO (0–70 μM) at 25 °C. The fluorescence spectra displays a gradually increased emission band at 480 nm (Figure 3.8(a)) resulting in an approximately 7-fold enhancement in fluorescence intensity which is adequate to detect nitric oxide intracellularly.

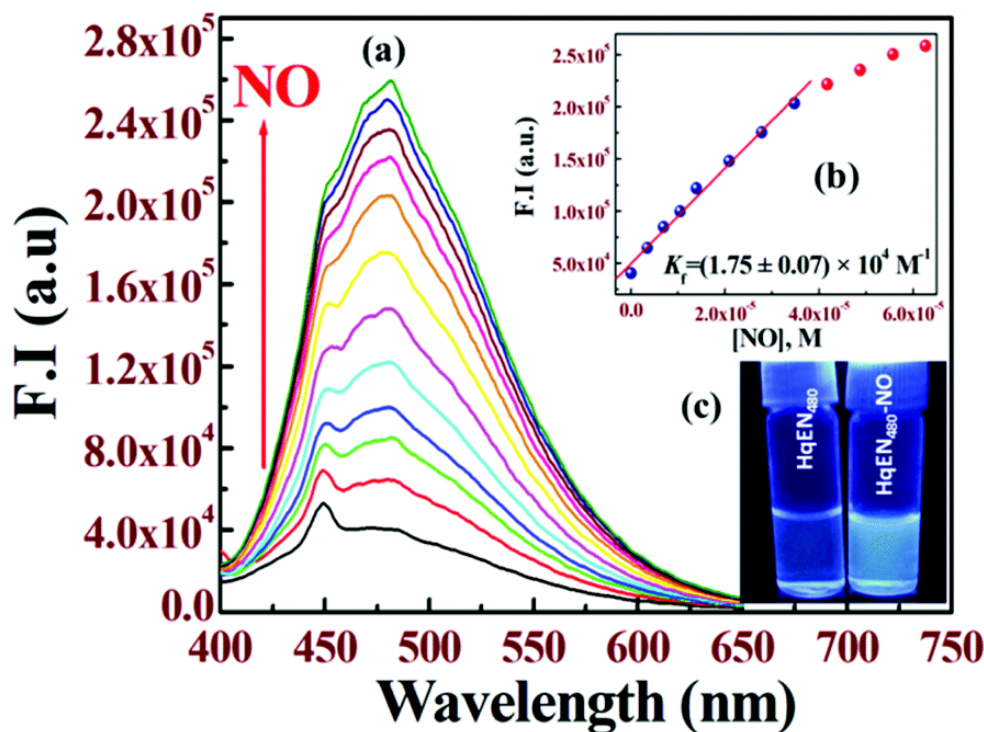


Figure 3.8. (a) Fluorescence titration of HqEN₄₈₀ (20 μM) with variable concentrations of NO (0–70 μM) at 25 °C in aqueous HEPES buffer (10 mM) at pH 7.20 and $\mu = 0.10$ M NaCl. (b) Plot of FI vs. [NO]. (c) UV exposed emission image of HqEN₄₈₀ and HqEN₄₈₀-NO.

CHAPTER 3

By adopting eqn (3)³³ under the conditions $1 \gg c \times x$ with $n = 1$ (where a, b and c represent the same denotation as mentioned for UV-Vis studies previously but in terms of fluorescence intensity), the slope of the curve gives $b \times c$, which ultimately provides $c = K_f =$ formation constant $= (1.75 \pm 0.07) \times 10^4 \text{ M}^{-1}$ (taking $b = 2.60 \times 10^5$) (**Figure 3.8(b)**). The excellent agreement between two K_f values obtained from absorption and fluorescence titrations definitely proves the self-consistent nature of our results. Again, at $\lambda_{\text{ex}} = 350 \text{ nm}$, a plot of F.I. vs. [NO] also shows enhancement in fluorescence intensity approximately about ~ 8 fold but it is not suitable for biological applications (**Figure 3.9a**). So, the entire fluorescence studies were performed at $\lambda_{\text{ex}} = 390 \text{ nm}$.

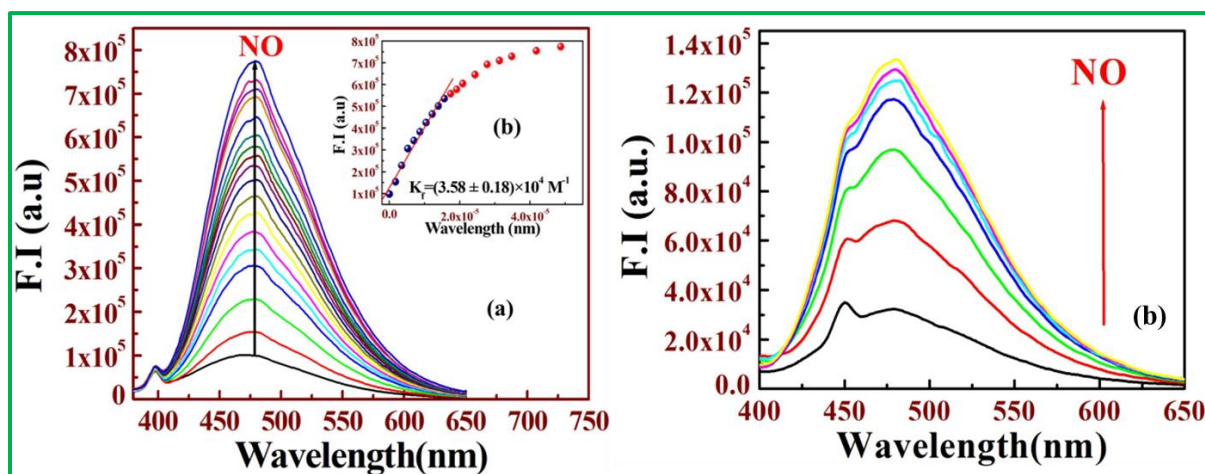


Figure 3.9. (a) Fluorescence titration of HqEN₄₈₀ with NO in aqueous HEPES buffer at $\lambda_{\text{ex}}=350\text{nm}$. (b) Fluorescence titration of (HqPA) with NO in aqueous solution at $\lambda_{\text{ex}}=390\text{nm}$.

To compare the fluorescence behaviour of HqEN₄₈₀ towards NO we have synthesized a N-nitrosation based fluorescent analogue, HqPA, following the same synthetic procedure. The fluorescence titration of HqPA with NO under identical reaction conditions displays a ~ 4 fold enhancement in fluorescence intensity at the same excitation and emission wavelengths ($\lambda_{\text{ex}} = 390 \text{ nm}$, $\lambda_{\text{em}} = 480 \text{ nm}$) while HqEN₄₈₀ displays ~ 7 fold fluorescence enhancement (**Figure 3.9(b)**). The slightly improved fluorescence response of HqEN₄₈₀ towards NO compared to HqPA may arise due to the presence of a terminal $-\text{CH}_2\text{CH}_2\text{NMe}_2$ group whose electron donating capability is higher than the $-\text{CH}_2\text{CH}_2\text{CH}_3$ group making the probe HqEN₄₈₀ more sensitive towards NO. For HqPA, we have also performed the selectivity studies by various ions (**Figure 3.10**).

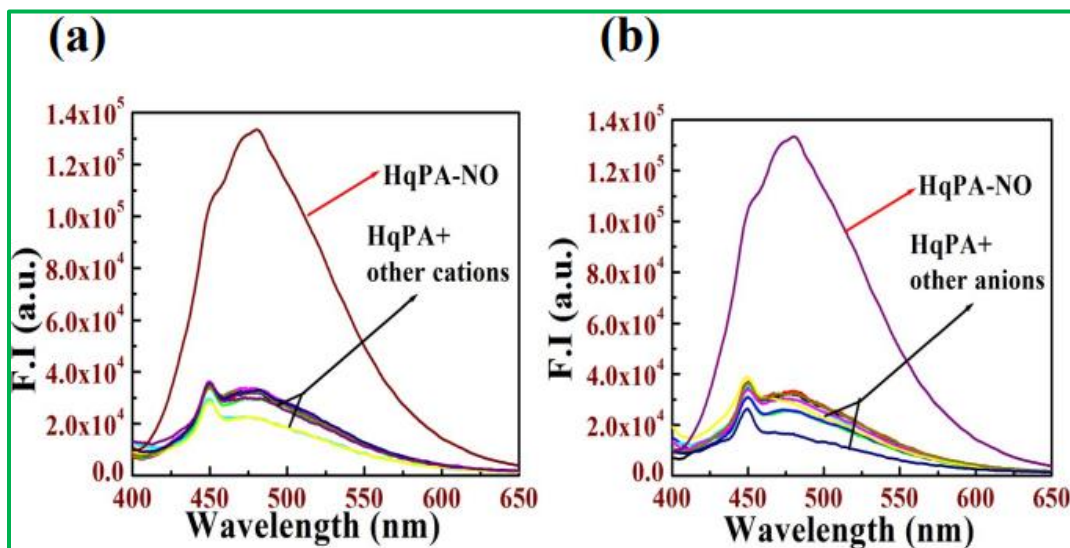


Figure 3.10. Selectivity of HqPA towards NO over various ions (a) Cd^{2+} , Sm^{3+} , Na^+ , Zn^{2+} , Al^{3+} , Fe^{3+} , Pb^{2+} , K^+ , Eu^{2+} . (b) CH_3COO^- , NO_2^- , Cl^- , N_3^- , SCN^- , NO_3^- , PPI , S^{2-} .

3.3.2 Sensing mechanism

Usually, the N-nitrosation based probes display a “turn-on” fluorescence response specifically towards NO without interference from the other commonly known reactive species. Herein, we designed a probe HqEN₄₈₀ based on quinoline as a fluorophoric moiety along with N,N-dimethylethylenediamine. The role of a side chain having terminal $-\text{NMe}_2$ is quite attractive. Here the $-\text{NMe}_2$ group functioning as an electron rich centre facilitates the amide ($-\text{CONHR}$) nitrogen atom to be more reactive towards NO. As expected, the newly designed HqEN₄₈₀ probe is weakly fluorescent because of the considerable fluorescence quenching through a photoinduced electron transfer (PET) process from the amide nitrogen atom to the quinoline moiety but HqEN₄₈₀ is capable of exhibiting large fluorescence magnification in response to NO through blocking of the PET process with concomitant formation of the electron deficient N–N=O moiety (Scheme 3.4).

3.3.3 Confirmation of the sensing mechanism

To investigate the mechanism responsible for the gradual increment of fluorescence intensity of the probe HqEN₄₈₀ in response to NO, the water soluble probe was allowed to react with excess NO in aerated MeCN medium. After evaporating, the desired product HqEN₄₈₀-NO was isolated

CHAPTER 3

and the detailed analyses were performed by using ^1H NMR (Figure 3.11), ^{13}C NMR (Figure 3.12), ESI-MS⁺ (Figure 3.13) and FT-IR (Figure 3.14) spectrometers.

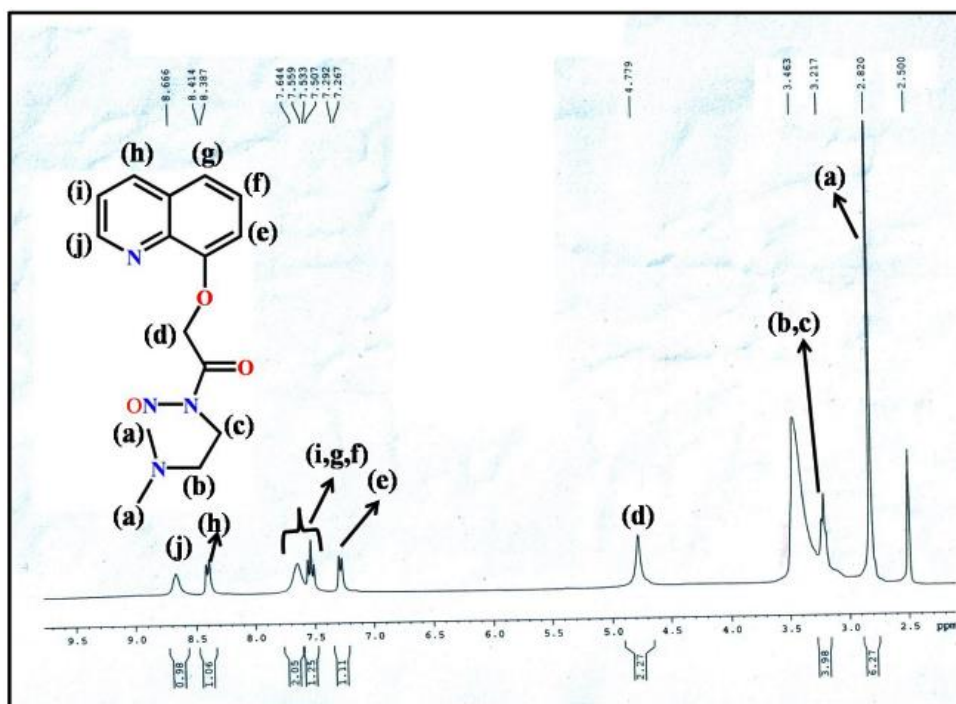


Figure 3.11. ^1H NMR spectrum of HqEN₄₈₀-NO in DMSO-*d*₆.

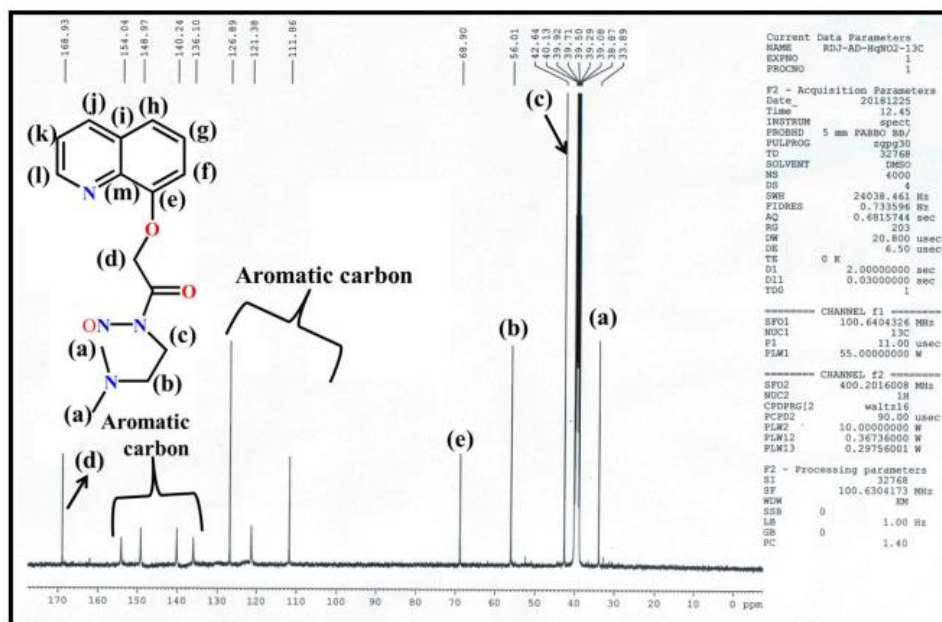


Figure 3.12. ^{13}C NMR spectrum of HqEN₄₈₀-NO in DMSO-*d*₆.

CHAPTER 3

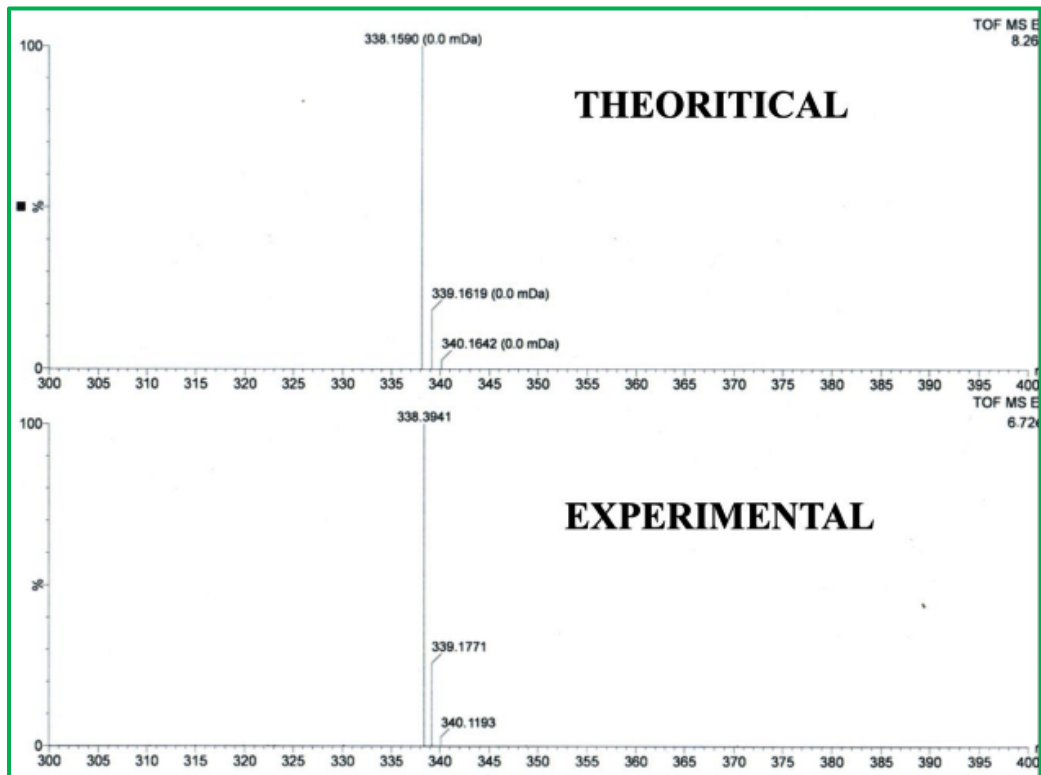


Figure 3.13. Mass spectrum of HqEN₄₈₀-NO in MeCN.

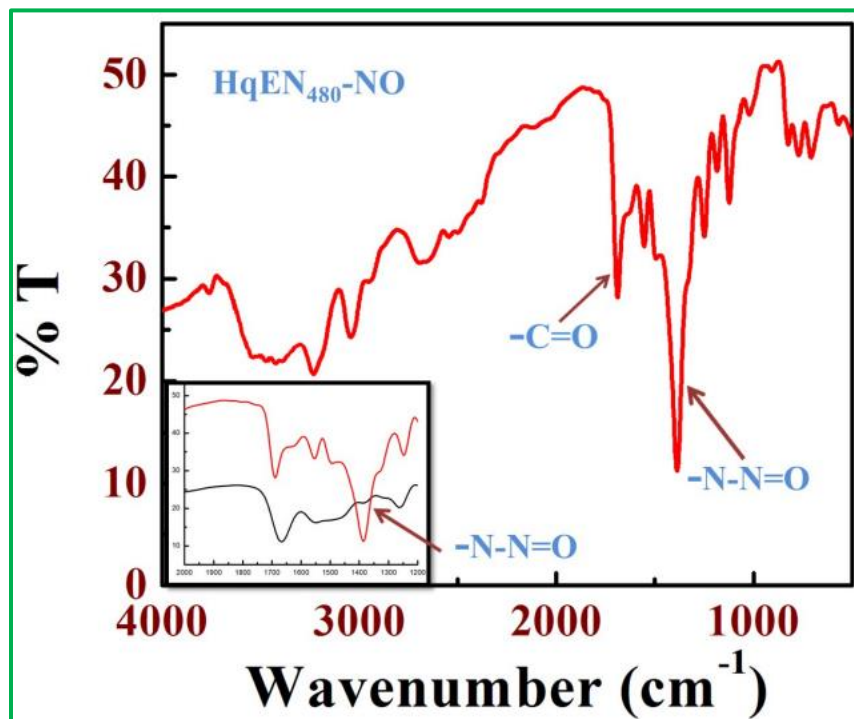


Figure 3.14. IR spectrum of (HqEN₄₈₀-NO) in solid state.

CHAPTER 3

The investigation reveals that the peak at 338.3941 (HqEN₄₈₀-NO + 2H₂O) arises due to the reaction of HqEN₄₈₀ with NO resulting in the formation of the N–N=O moiety. The ¹H-NMR spectra also reveal that the single peak responsible for the amide –NH proton of HqEN₄₈₀ at 8.90 ppm vanishes on treatment with NO leading to a conclusion that the NO is attached to the amide –N atom. There is also evidence in favor of this sensing mechanism through IR studies which clearly demonstrate that upon reaction with NO, the product HqEN₄₈₀-NO shows a new peak at 1382 cm⁻¹ corresponding to N–N=O⁵⁰ with concomitant suppression of N–H stretching frequency at 3411 cm⁻¹. So we easily conclude that nitric oxide is attached with the amide –N atom. The N-nitrosation based fluorescent analogue, HqPA, also goes through a similar sensing mechanism that is also characterized by ¹H NMR (Figure 3.15).

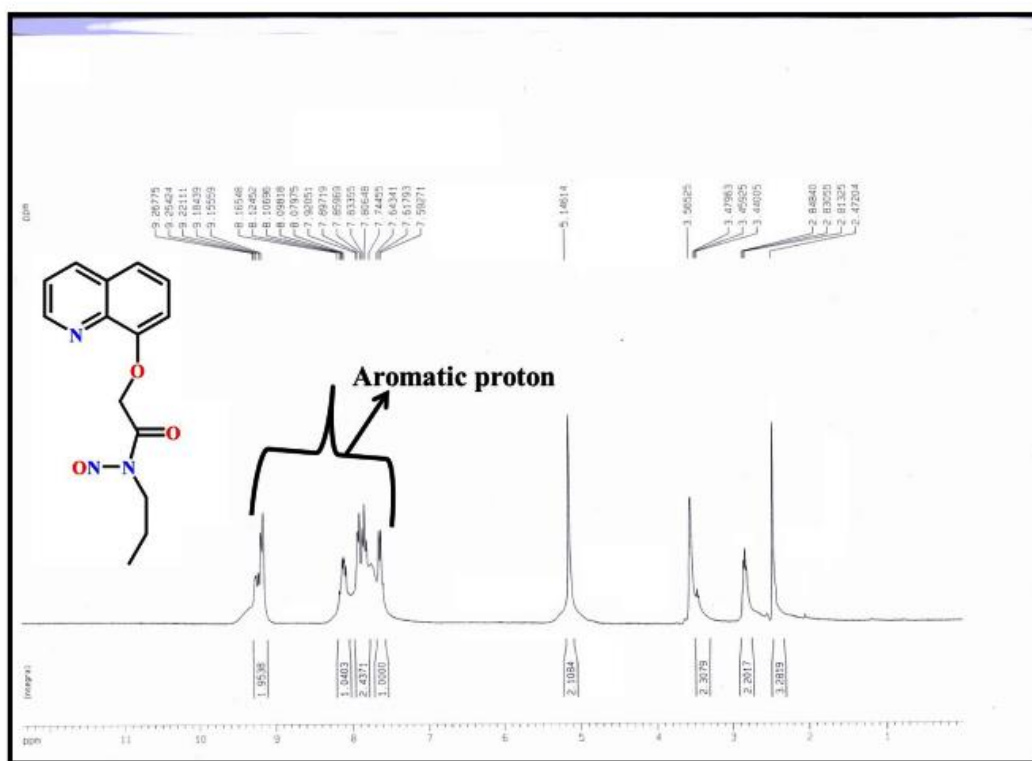


Figure 3.15. ¹H NMR spectrum of HqPA-NO in DMSO-d₆.

The magnitude of quantum yield for the compound HqEN₄₈₀-NO was $\Phi = 0.22$ and that for the ligand (HqEN₄₈₀) was 0.04 (using acidic quinine sulfate as the standard). In terms of the 3 σ /slope method the magnitude of limit of detection (LOD) for nitric oxide was found to be 53 nM (Figure 3.16 (a) and 3.16 (b)) indicating that the probe HqEN₄₈₀ is highly suitable for tracking

CHAPTER 3

NO in biological systems. From the absorption data the detection limit (LOD) of NO was determined (using $3\sigma/\text{slope}$ method) to obtain a value of $1\ \mu\text{M}$ (Figure 3.16(c)). So, based on all the above experiments, results and discussions it is apparent that the probe HqEN₄₈₀ is an efficient nitric oxide sensor.

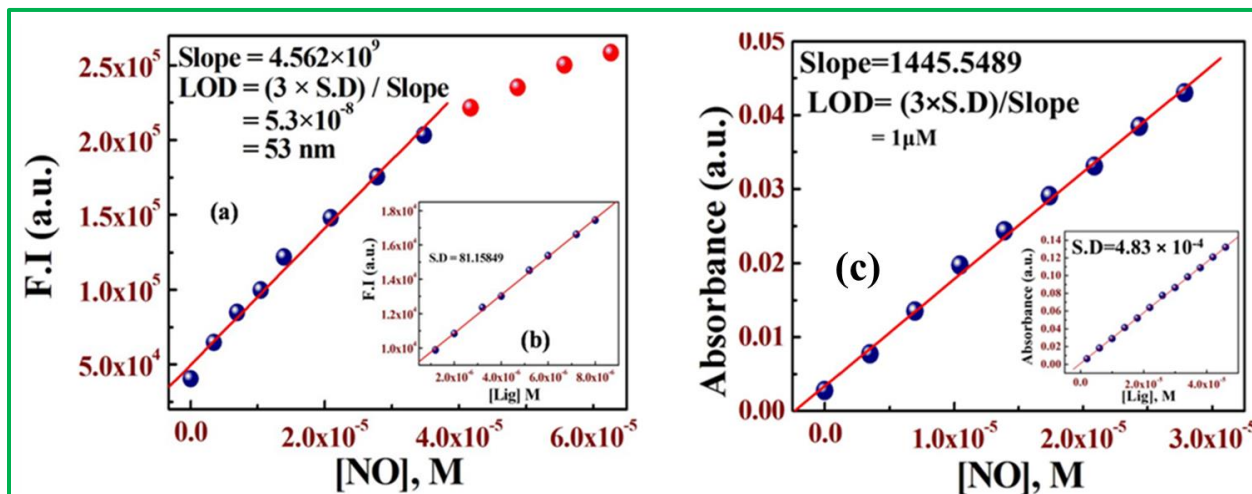


Figure 3.16. (a) LOD of (HqEN₄₈₀-NO) from fluorescence study (c) LOD of (HqEN₄₈₀-NO) from UV-vis study.

3.3.4 TCSPC studies

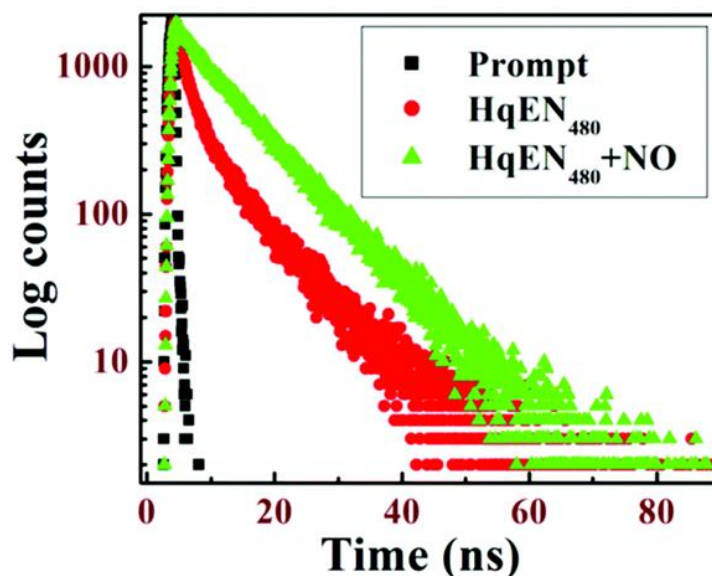


Figure 3.17. Lifetime plot of HqEN₄₈₀ and (HqEN₄₈₀ + NO) at 25 °C in aqueous HEPES buffer (10 mM) at pH 7.20 and $\mu = 0.10\ \text{M}$ NaCl.

CHAPTER 3

The average life-time of the probe HqEN₄₈₀ ($\tau_{\text{avg}} = 4.03$ ns) increases upon treatment with ~ 70 μM NO (HqEN₄₈₀-NO, $\tau_0 = 8.89$ ns) and the nature of the decay curve also changes from the bi-exponential to mono-exponential one (Figure 3.17). This study reveals that the addition of NO results in greater stability of the product HqEN₄₈₀-NO in the excited state.

3.3.5 Selectivity study

The specificity of the probe HqEN₄₈₀ was verified by recording the fluorescence spectra of HqEN₄₈₀ in the presence of various metal ions (Na^+ , Cu^{2+} , Mg^{2+} , K^+ , Dy^{3+} , Eu^{2+} , Zn^{2+} , Sm^{3+} , Co^{2+} , Ni^{2+} , Pb^{2+} , Cr^{3+} , Cd^{2+} , Mn^{2+} , Fe^{3+} , Al^{3+} , Hg^{2+}) (Figure 3.18(a)), anions (S^{2-} , SO_4^{2-} , NO_3^- , NO_2^- , H_2PO_4^- , $\text{S}_2\text{O}_4^{2-}$, ClO_4^- , OAc^- , HCO_3^- , Cl^- , CO_3^{2-} , PPi , N_3^- , F^-) (Figure 3.18(b)), amino acids (alanine, arginine, cysteine, homocysteine and so on) (Figure 3.19(a)) including biological interfering species (OCl^- , ascorbic acid, OH^\cdot , O_2^- , tempo, ONOO^- , HNO, H_2O_2 , DHA, NO^+ , NO) (Figure 3.19(b)). However, in aqueous solution for the above cases, there is no remarkable change in fluorescence intensity except for NO, where the probe HqEN₄₈₀ exhibits ~ 7 fold increment in fluorescence intensity. As a result, the fluorescence emission spectra clearly shows that HqEN₄₈₀ is highly selective and specific towards NO in aqueous solution at pH = 7.2.

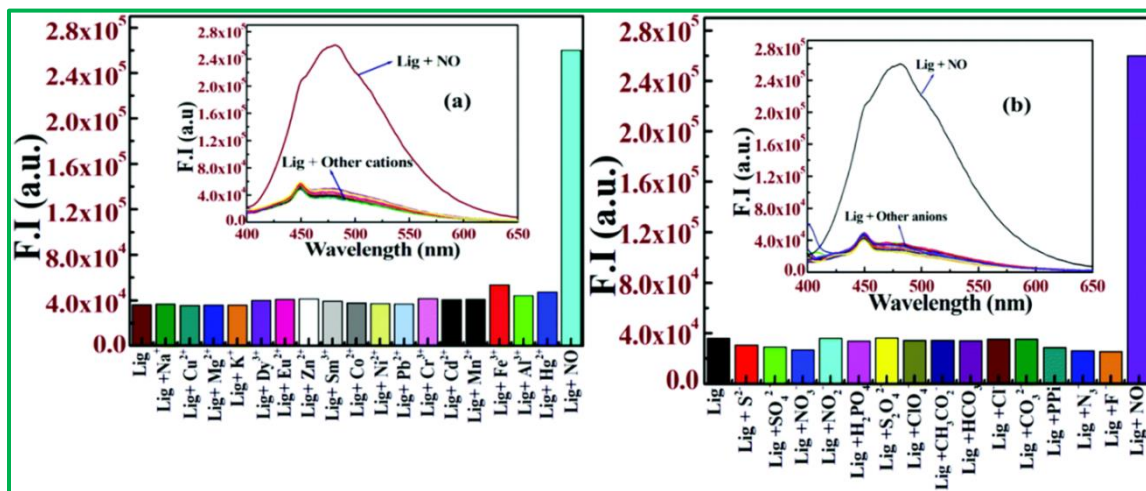


Figure 3.18(a). (i) Fluorescence response of HqEN₄₈₀ in the presence of various cations (Na^+ , Cu^{2+} , Mg^{2+} , K^+ , Dy^{3+} , Eu^{2+} , Zn^{2+} , Sm^{3+} , Co^{2+} , Ni^{2+} , Pb^{2+} , Cr^{3+} , Cd^{2+} , Mn^{2+} , Fe^{3+} , Al^{3+} , Hg^{2+}) (100 μM) in the aqueous solution of HqEN₄₈₀ (20 μM) ($\lambda_{\text{ex}} = 390$ nm); (ii) the corresponding bar plot. **Figure 3.18(b).** (i) Fluorescence response of HqEN₄₈₀ towards NO over various anions (ii) the corresponding bar plot.

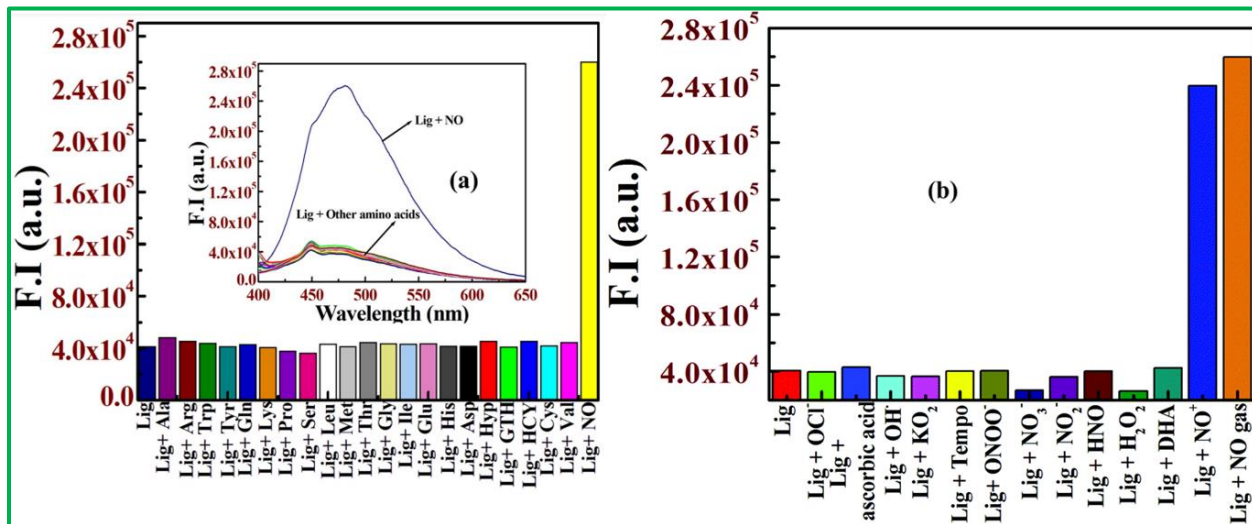


Figure 3.19. (a) Fluorescence response of HqEN₄₈₀ towards various amino acids in aqueous HEPES buffer at λ_{ex} =390 nm. (b) The corresponding bar plot **c**. Bar plot illustrating fluorescence responses of HqEN480 towards NO over other reactive species. (OCI^- , ascorbic acid, OH^\bullet , O_2^- , tempo, $ONOO^-$, NO_3^- , NO_2^- , HNO, H_2O_2 , DHA, NO^+ and NO gas).

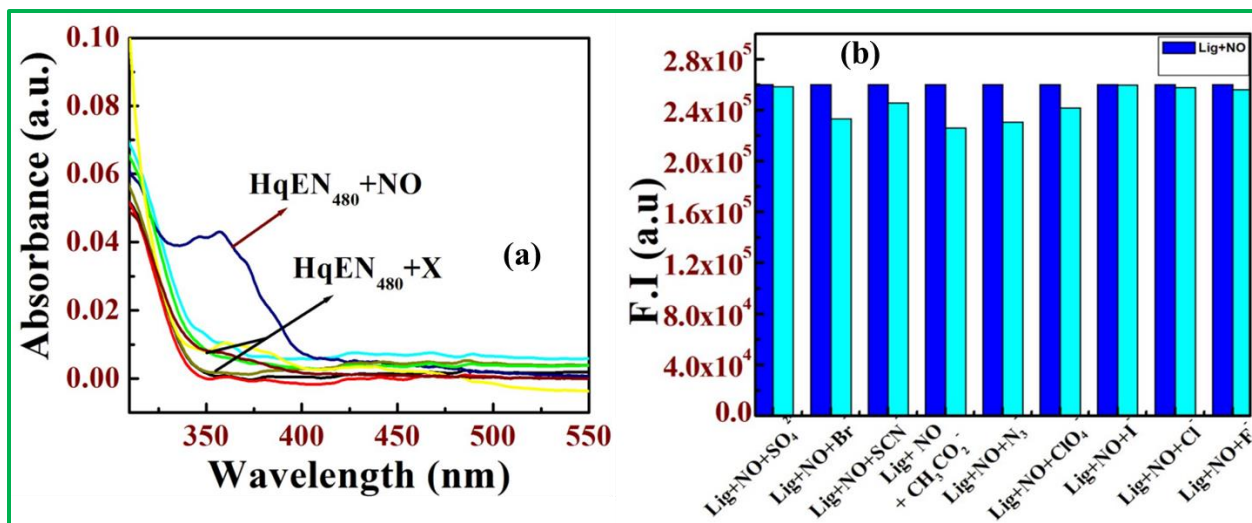


Figure 3.20. (a) Uv-Vis absorption spectra of HqEN₄₈₀ towards various reactive species (X= H_2O_2 , DHA, TEMPO, KO_2 , $ONOO^-$, AA and NO); and (b) Bar plot of Competitive study of ions over NO at λ_{ex} =390nm.

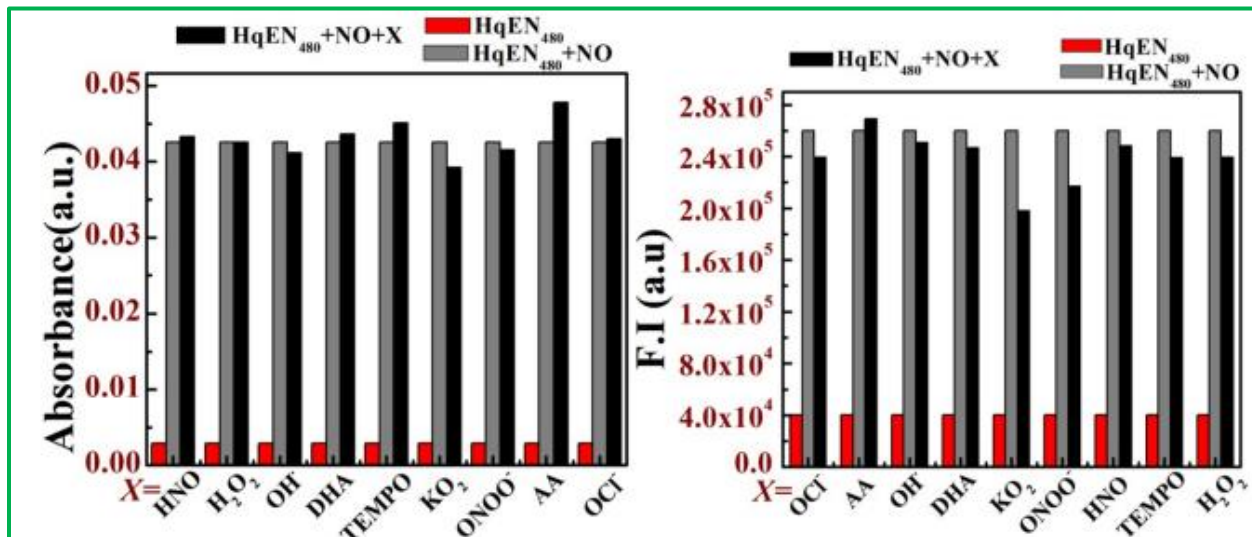


Figure 3.21. Bar plot of Competitive study of reactive species over NO from fluorescence at $\lambda_{\text{ex}}=390\text{nm}$ and Uv-Vis absorption method.

The selective behaviour of HqEN₄₈₀ towards NO over other ROS/RNS was further deliberated by using the Uv-Vis absorption method as illustrated in **Figure 3.20(a)**, whereas the over selectivity study was also performed to further strengthen the selectivity of the probe towards NO (as shown in **Figure 3.20(b)**). Interestingly, both the fluorescence and absorbance spectra of the probe HqEN₄₈₀ reveal selectivity towards NO even in the presence of various competing ions (such as hydrogen peroxide, peroxyxynitrite, ascorbic acid, dehydroascorbic acid and so on) (**Figure 3.21**).

3.3.6 pH study

To analyse the pH effects on the ability of the probe HqEN₄₈₀ to sense nitric oxide, we recorded the fluorescence spectra by taking 20 μM HqEN₄₈₀ with 3.5 equivalents (70 μM) of NO at various pH values in HEPES buffer. As displayed in (**Figure 3.22**) the probe HqEN₄₈₀ is weakly fluorescent as well as stable and shows good detectable response towards NO over a wide range of pH = 4–10. However, the probe displays the best response towards NO in the pH range of 5–7 leading to the conclusion that the probe is suitable for monitoring NO in living systems.

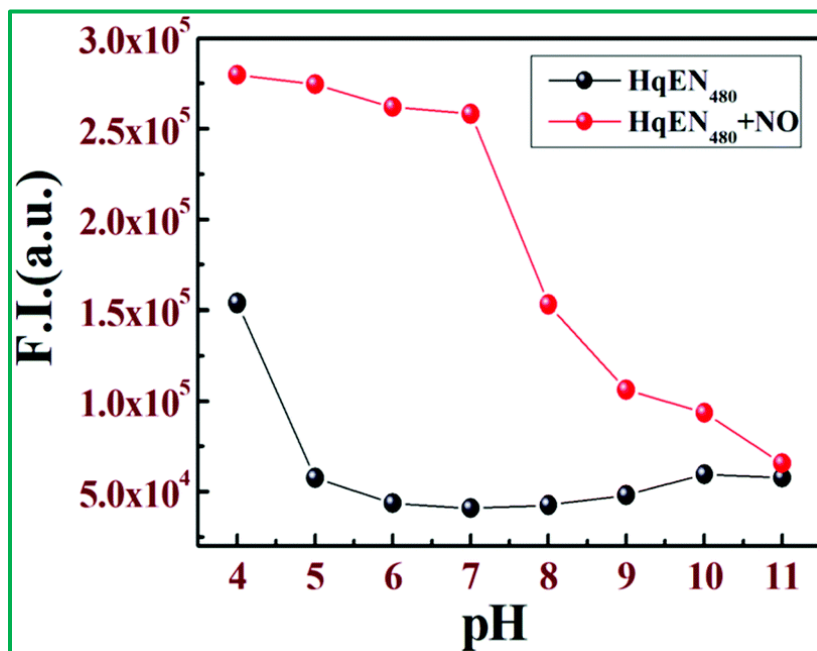


Figure 3.22. pH dependent fluorescence responses of HqEN₄₈₀ and HqEN₄₈₀-NO at 25 °C in aqueous HEPES buffer (10 mM) at pH 7.20 and $\mu = 0.10$ M NaCl.

3.3.7 Geometry optimization and electronic structure

Herein, the receptor, HqEN₄₈₀, is able to show selective positive response towards NO resulting in the formation of the N-nitrosated product, [HqEN₄₈₀-NO], which leads to electronic as well as structural changes in their geometries.

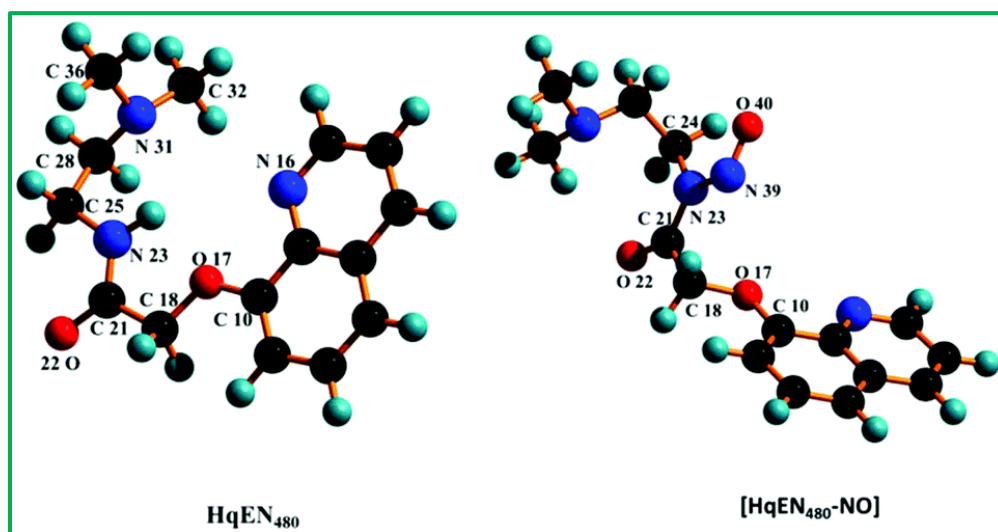


Figure 3.23. Optimized geometry of ligand HqEN₄₈₀ and the NO product [HqEN₄₈₀-NO].

CHAPTER 3

In order to have a detailed idea about the photophysical properties of the probe HqEN₄₈₀ and its N-nitrosated product, we have carried out DFT and TDDFT calculations at the B3LYP/6-31G level of the Gaussian 09 program. The optimized geometries of HqEN₄₈₀ and its NO bound form, [HqEN₄₈₀-NO], are shown in **Figure 3.23 (Table 3.1 and 3.2)**.

Table 3.1. List of some selected bond lengths of HqEN₄₈₀ in the ground state calculated at B3LYP Levels.

Bond lengths (Å ^o)			
O17-C18	1.450	C21-N23	1.351
C18-C21	1.522	N23-C25	1.459
C21-O22	1.255	C25-C28	1.532
Bondangle (°)			
O17-C18-C21	108.92	O22-C21-N23	124.97
C18-C21-O22	118.72	C21-N23-C25	122.24
C18-C21-N23	116.30	N23-C25-C28	109.87

Table 3.2. Some selected geometrical parameters for [HqEN₄₈₀-NO] in the ground state calculated at B3LYP Levels

Bond lengths(A ^o)			
C10-O17	1.385	C21-O22	1.238
O17-C18	1.453	N23-N39	1.385
C18-C21	1.517	N39-O40	1.246
C21-N23	1.404	N23-C24	1.473
Bondangle (o)			
C10-O17-C18	118.56	C21-N23-C24	121.78
O17-C18-C21	105.62	N23-N39-O40	114.22
C18-C21-N23	116.94	C21-N23-N39	116.47
C18-C21-O22	122.09		

CHAPTER 3

HqEN₄₈₀ and [HqEN₄₈₀-NO] both belong to the C_1 point group. The nature of all stationary points for both free ligand and its NO product were identified by performing normal mode analysis and all the frequencies turned out to be positive indicating their global minima. In the ground state for HqEN₄₈₀, HOMO-1 molecular orbitals carry the electron density mainly over the 8-methoxyquinoline ring moiety and the LUMO molecular orbitals resides on quinolin-8-ol portion of the ligand. On the other hand, for HOMO molecular orbitals, the electron density resides mainly on the ethyl-dimethyl-amine fragment of the ligand HqEN₄₈₀. For the free ligand, the energy gap between HOMO and LUMO is 4.17 eV (Figure 3.24). In the case of [HqEN₄₈₀-NO], the HOMO and HOMO-1 molecular orbitals carry most of the electron density in the ethyl-dimethyl-amine fragment and 8-methoxyquinoline moiety of the N-nitrosated ligand, whereas for the LUMO orbital, the electron clouds are mainly distributed over the N-nitrosoformamide fragment. For LUMO+1, the electron cloud localized on the quinolin-8-ol moiety and the contribution of electron density for LUMO+2 orbitals originate from the N-nitroso-2-hydroxyacetamide portion respectively.

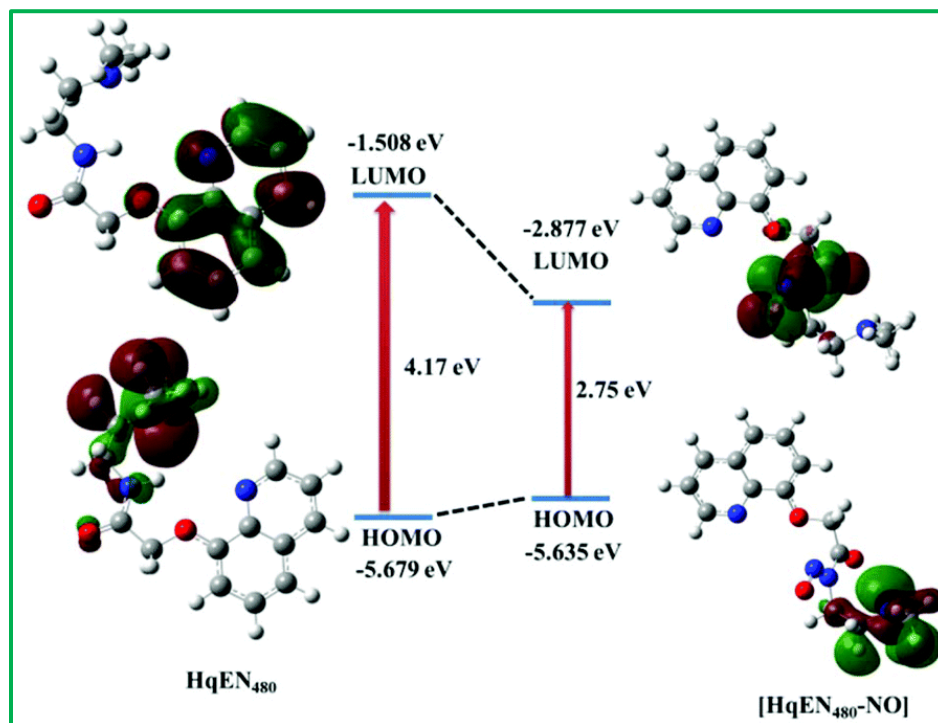


Figure 3.24. Frontier molecular orbital of ligands HqEN₄₈₀ and [HqEN₄₈₀-NO].

CHAPTER 3

Figure 3.24 shows that for the NO product, the HOMO–LUMO energy gap is 2.75 eV which is less than that of HqEN₄₈₀ (4.17 eV). Enhancement in fluorescence intensity for the NO product arises mainly due to the electron withdrawing nature of the –N–N=O moiety blocking the PET process. The ligand HqEN₄₈₀ shows absorption bands at 314.00 nm at room temperature and the corresponding calculated absorption band is found at 307.10 nm which indicates an excellent agreement with our experimental results. This band arises due to $S_0 \rightarrow S_2$ electronic transitions (**Figure 3.25a**). The absorption energies as well as their oscillator strengths are described in **Table 3.3**. The complex [HqEN₄₈₀-NO] shows an absorption bands at 304.47 nm at room temperature. These absorption bands can be assigned to the $S_0 \rightarrow S_4$ transitions (**Figure 3.25b**). For [HqEN₄₈₀-NO], the absorption energies and their oscillator strengths are also given in **Table 3.4**.

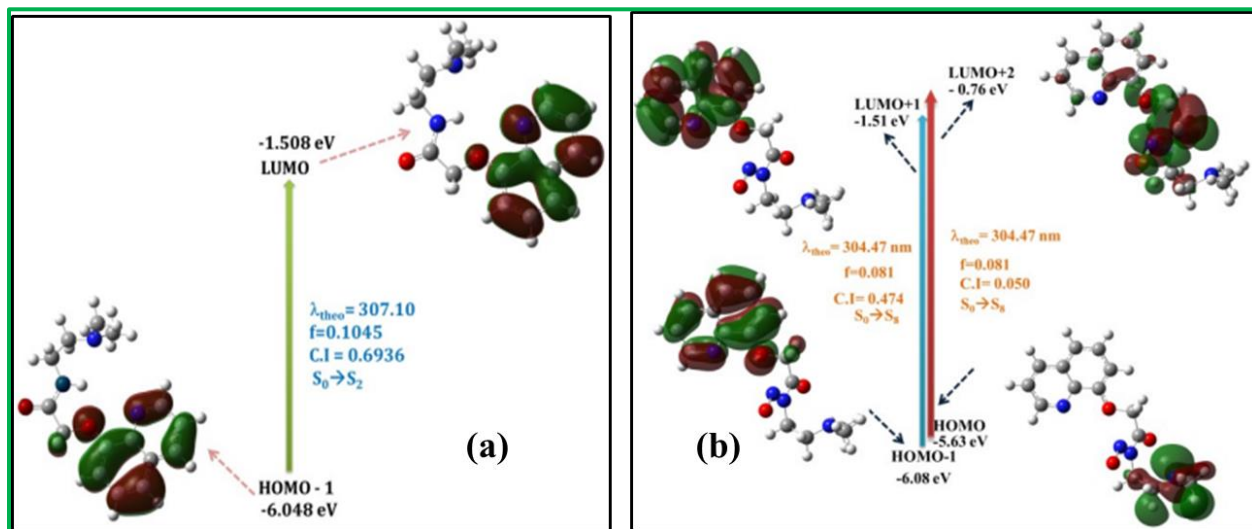


Figure 3.25a. Frontier molecular orbitals involved in the UV-Vis absorption of HqEN₄₈₀. **b.** Frontier molecular orbitals involved in the UV-Vis absorption of [HqEN₄₈₀-NO].

CHAPTER 3

Table 3.3. Vertical excitation energies and oscillator strengths (f_{cal}) of some low-lying excited singlet states obtained from TDDFT// B3LYP/6-31G calculations of HqEN₄₈₀.

Electronic transition	Composition	Excitation Energy	Oscillator strength (f)	CI	λ_{exp} (nm)
$S_0 \rightarrow S_2$	HOMO -1 \rightarrow LUMO	4.0372 eV (307.10 nm)	0.1045	0.69360	314

Table 3.4. Vertical excitation energies and oscillator strengths (f_{cal}) of some low-lying excited singlets obtained from TDDFT// B3LYP/6-31G calculations of [HqEN₄₈₀-NO].

Electronic transition	Composition	Excitation Energy	Oscillator strength (f)	CI	λ_{exp} (nm)
$S_0 \rightarrow S_8$	HOMO \rightarrow LUMO + 2	4.0721 eV (304.47 nm)	0.0814	0.50961	355
	HOMO - 1 \rightarrow LUMO + 1			0.47473	

3.3.8 NO detection in living cells

As HqEN₄₈₀ showed extensively selective reaction with nitric oxide (NO), it had been further checked for its NO sensing ability in living cells. A cell viability assay using MTT was performed to check the cytotoxic effects of HqEN₄₈₀, by calculating the % cell viability of HepG2 cells (Figure 3.26). More than 80% cell viability is reflected by no significant decrease in formazan production up to 20 μM concentration of HqEN₄₈₀. Hence, further cell imaging experiments were carried out with 10 μM of HqEN₄₈₀ at which cell viability is more than 85% and much more effective for in vitro monitoring of NO molecules. The incubation of 10 μM HqEN₄₈₀ for 1 hour exhibited no intracellular fluorescence on HepG2 cells (Figure 3.27). However, upon incubation of HepG2 cells with 10 μM of SNP, which is provided as an exogenous source for NO, followed by incubation with 10 μM HqEN₄₈₀, a distinct blue fluorescence was observed inside the cells due to the reaction between the exogenously produced NO molecules and the ligand. Fluorescence emission was mostly localized in the cytoplasmic region of the cell, indicating the formation of HqEN₄₈₀-NO outside the nucleus. Keeping the HqEN₄₈₀ concentration constant (10 μM) and increasing the concentration of SNP from 10 μM , 20 μM , to 40 μM a concentration-dependent increase in the intracellular blue fluorescence is quite apparent. These results suggest that the ligand HqEN₄₈₀ with low cytotoxicity and

CHAPTER 3

biocompatibility has a high potential for in vitro application as a sensor of intracellular NO molecules, as well as for their detection in biological samples.

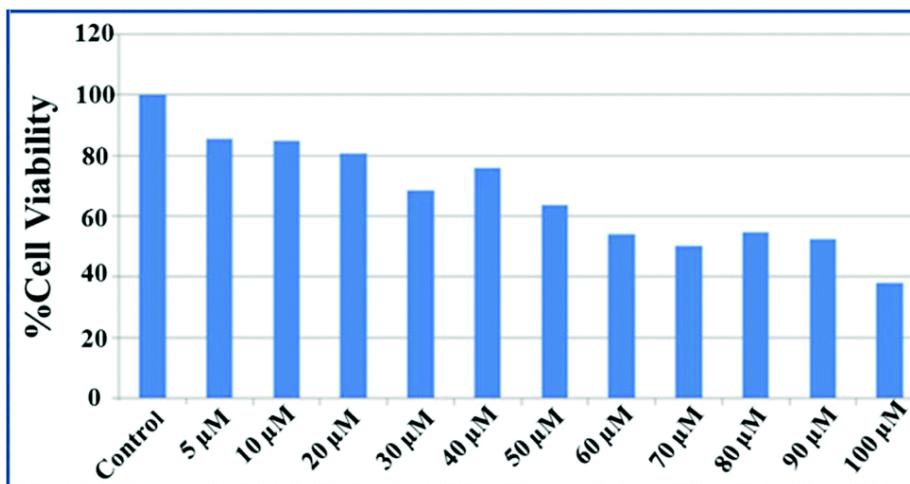


Figure 3.26. Percent (%) cell viability of HepG2 cells treated with different concentrations (5–100 μM) of HqEN₄₈₀ for 24 hours determined by the MTT assay.

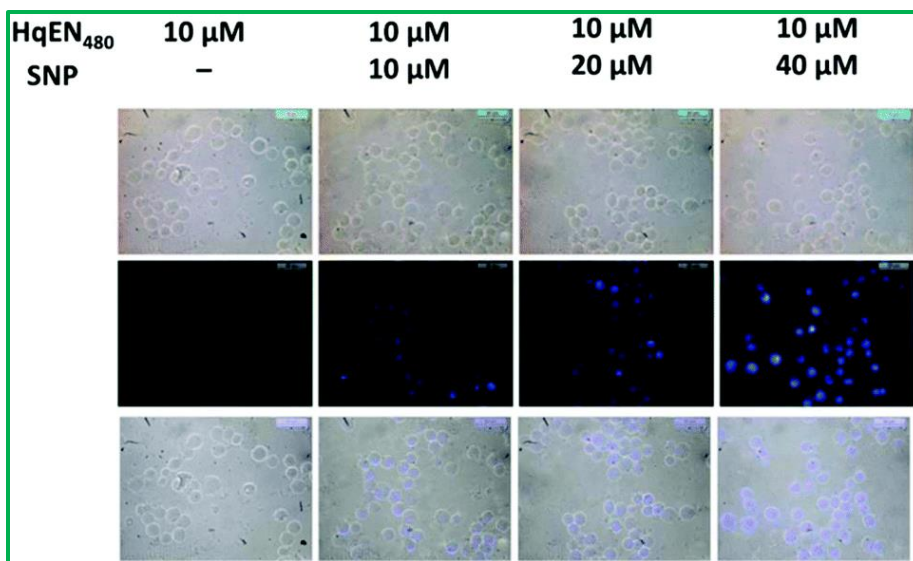


Figure 3.27. The fluorescence images of HepG2 cells were captured (40×) after incubation with 10 μM, 20 μM and 40 μM of sodium nitroprusside (SNP) for 60 min at 37 °C, followed by washing thrice with 1× PBS and incubation with 10 μM of HqEN₄₈₀ for 60 min at 37 °C. The fluorescence images show the absence of signal by the fluorophore HqEN₄₈₀ (10 μM) in the absence of NO molecule induced from SNP, while the fluorescence gradually increases, highly at 40 μM of SNP concentration.

3.4 CONCLUSION

In summary, herein we present a new fluorescent probe HqEN₄₈₀ which exhibits a dramatic turn on fluorescence response towards NO in 100% aqueous solution by utilizing the N-nitrosation based reaction, with cell imaging applications. Its pronounced selectivity towards NO over other interfering species makes it a suitable fluorescent probe for tracking NO in biological systems. Moreover, the N-nitrosated product was analyzed and well characterized by ESI-MS⁺, NMR and IR studies. The presence of a highly electron withdrawing group –N=N=O within the fluorophoric moiety pulls the electron density from the amide nitrogen atom leading to blocking of the PET process with concomitant enhancement in fluorescence intensity. The sensing reaction of HqEN₄₈₀ towards NO shows high sensitivity as evidenced from the very low detection limit of 53 nM. Thus it clearly indicates the suitability of the probe for monitoring NO in macrophage cultures⁵¹ due to the presence of NO in micromolar concentrations in these types of cells. Fluorescence titration gives a high formation constant, $(1.75 \pm 0.07) \times 10^4 \text{ M}^{-1}$, for the reaction between HqEN₄₈₀ and NO at pH 7.2. Thus, low cytotoxicity towards biological systems, water solubility, and cell-permeability along with very low LOD (53 nM) demonstrates that HqEN₄₈₀ is a highly desirable probe for tracking NO in living cells.

References

1. Chen, L.; Wu, D.; Yoon, J., An ESIPT based fluorescence probe for ratiometric monitoring of nitric oxide. *Sens. Actuators B Chem.* **2018**, *259*, 347-353.
2. (a) Calabrese, V.; Mancuso, C.; Calvani, M.; Rizzarelli, E.; Butterfield, D. A.; Giuffrida Stella, A. M., Nitric oxide in the central nervous system: neuroprotection versus neurotoxicity. *Nat. Rev. Neurosci.* **2007**, *8* (10), 766-775. (b) Szabo, C., Gasotransmitters in cancer: from pathophysiology to experimental therapy. *Nat. Rev. Drug Discov.* **2016**, *15* (3), 185-203.
3. Khan, B. V.; Harrison, D. G.; Olbrych, M. T.; Alexander, R. W.; Medford, R. M., Nitric oxide regulates vascular cell adhesion molecule 1 gene expression and redox-sensitive transcriptional events in human vascular endothelial cells. *Proc. Natl. Acad. Sci. U.S.A.* **1996**, *93* (17), 9114-9119.
4. Gudi, T.; Hong, G. K. P.; Vaandrager, A. B.; Lohmann, S. M.; Pilz, R. B., Nitric oxide and cGMP regulate gene expression in neuronal and glial cells by activating type II cGMP-dependent protein kinase. *FASEB J.* **1999**, *13* (15), 2143-2152. (15), 2143-2152.
5. Pantopoulos, K.; Hentze, M. W., Nitric oxide signaling to iron-regulatory protein: direct control of ferritin mRNA translation and transferrin receptor mRNA stability in transfected fibroblasts. *Proc. Natl. Acad. Sci. U.S.A.* **1995**, *92* (5), 1267-1271.
6. Liu, X.-b.; Hill, P.; Haile, D. J., Role of the Ferroportin Iron-Responsive Element in Iron and Nitric Oxide Dependent Gene Regulation. *Blood Cells Mol. Dis.* **2002**, *29* (3), 315-326.
7. Pozdnyakov, N.; Lloyd, A.; Reddy, V. N.; Sitaramayya, A., Nitric Oxide-Regulated Endogenous ADP-Ribosylation of Rod Outer Segment Proteins. *Biochem. Biophys. Res. Commun.* **1993**, *192* (2), 610-615.
8. Brüne, B.; Dimmeler, S.; y Vedia, L. M.; Lapetina, E. G., Nitric oxide: A signal for ADP-ribosylation of proteins. *Life Sci.* **1994**, *54* (2), 61-70.
9. Taysi, S.; Uslu, C.; Akcay, F.; Sutbeyaz, M. Y., Malondialdehyde and Nitric Oxide Levels in the Plasma of Patients with Advanced Laryngeal Cancer. *Surg. Today* **2003**, *33* (9), 651-654.

CHAPTER 3

10. P Biro, G, Adverse HBOC-endothelial dysfunction synergism: a possible contributor to adverse clinical outcomes?. *Curr. Drug Discov. Technol.* **2012**, 9 (3), 194-203.
11. Choi, D.-Y.; Lee, Y.-J.; Hong, J. T.; Lee, H.-J., Antioxidant properties of natural polyphenols and their therapeutic potentials for Alzheimer's disease. *Brain Res. Bull.* **2012**, 87 (2), 144-153.
12. Yuan, S.; Patel, R. P.; Kevil, C. G., Working with nitric oxide and hydrogen sulfide in biological systems. *Am. J. Physiol. Lung Cell. Mol.* **2014**, 308 (5), L403-L415.
13. Thomas, D. D.; Ridnour, L. A.; Isenberg, J. S.; Flores-Santana, W.; Switzer, C. H.; Donzelli, S.; Hussain, P.; Vecoli, C.; Paolocci, N.; Ambs, S.; Colton, C. A.; Harris, C. C.; Roberts, D. D.; Wink, D. A., The chemical biology of nitric oxide: Implications in cellular signaling. *Free Radic. Biol. Med.* **2008**, 45 (1), 18-31.
14. Hu, W.; Boateng, D.; Kong, J.; Zhang, X., Advancement of fluorescent methods for detection of Nitric Oxide. *Austin J. Biosens. Bioelectron.* **2015**, 1, 1-9.
15. Kojima, H.; Urano, Y.; Kikuchi, K.; Higuchi, T.; Hirata, Y.; Nagano, T., Fluorescent Indicators for Imaging Nitric Oxide Production. *Angew. Chem.* **1999**, 38 (21), 3209-3212.
16. Sasaki, E.; Kojima, H.; Nishimatsu, H.; Urano, Y.; Kikuchi, K.; Hirata, Y.; Nagano, T., Highly Sensitive Near-Infrared Fluorescent Probes for Nitric Oxide and Their Application to Isolated Organs. *J. Am. Chem. Soc.* **2005**, 127 (11), 3684-3685.
17. Yu, H.; Zhang, X.; Xiao, Y.; Zou, W.; Wang, L.; Jin, L., Targetable Fluorescent Probe for Monitoring Exogenous and Endogenous NO in Mitochondria of Living Cells. *Anal. Chem.* **2013**, 85 (15), 7076-7084.
18. Zhang, H.-X.; Chen, J.-B.; Guo, X.-F.; Wang, H.; Zhang, H.-S., Highly Sensitive Low-Background Fluorescent Probes for Imaging of Nitric Oxide in Cells and Tissues. *Anal. Chem.* **2014**, 86 (6), 3115-3123.
19. Huang, C.-B.; Huang, J.; Xu, L., A highly selective fluorescent probe for fast detection of nitric oxide in aqueous solution. *RSC Adv.* **2015**, 5 (18), 13307-13310.
20. Liu, X.; Liu, S.; Liang, G., Fluorescence turn-on for the highly selective detection of nitric oxide in vitro and in living cells. *Analyst* **2016**, 141 (8), 2600-2605.
21. Zhou, J.; Wang, C.; Zhao, Y.; Song, Q., Detection of latent fingerprints based on gas phase adsorption of NO and subsequent application of an ultrasonically nebulized fluorescent probe. *Anal. Methods* **2017**, 9 (10), 1611-1616.

CHAPTER 3

22. Lim, M. H.; Lippard, S. J., Copper Complexes for Fluorescence-Based NO Detection in Aqueous Solution. *J. Am. Chem. Soc.* **2005**, *127* (35), 12170-12171.
23. Lim, M. H.; Xu, D.; Lippard, S. J., Visualization of nitric oxide in living cells by a copper-based fluorescent probe. *Nat. Chem. Biol* **2006**, *2* (7), 375-380.
24. Lim, M. H.; Wong, B. A.; Pitcock, W. H., Jr.; Mokshagundam, D.; Baik, M.-H.; Lippard, S. J., Direct Nitric Oxide Detection in Aqueous Solution by Copper(II) Fluorescein Complexes. *J. Am. Chem. Soc.* **2006**, *128* (44), 14364-14373.
25. Pluth, M. D.; McQuade, L. E.; Lippard, S. J., Cell-Trappable Fluorescent Probes for Nitric Oxide Visualization in Living Cells. *Org. Lett.* **2010**, *12* (10), 2318-2321.
26. McQuade, L. E.; Ma, J.; Lowe, G.; Ghatpande, A.; Gelperin, A.; Lippard, S. J., Visualization of nitric oxide production in the mouse main olfactory bulb by a cell-trappable copper(II) fluorescent probe. *Proc. Natl. Acad. Sci. U.S.A.* **2010**, *107* (19), 8525-8530.
27. Chen, X.; Sun, L.; Chen, Y.; Cheng, X.; Wu, W.; Ji, L.; Chao, H., A fast and selective two-photon phosphorescent probe for the imaging of nitric oxide in mitochondria. *Biomaterials* **2015**, *58*, 72-81.
28. Franz, K. J.; Singh, N.; Spingler, B.; Lippard, S. J., Aminotroponimines as Ligands for Potential Metal-Based Nitric Oxide Sensors. *Inorg. Chem.* **2000**, *39* (18), 4081-4092.
29. McQuade, L. E.; Lippard, S. J., Fluorescent probes to investigate nitric oxide and other reactive nitrogen species in biology (truncated form: fluorescent probes of reactive nitrogen species). *Curr. Opin. Chem. Biol.* **2010**, *14* (1), 43-49.
30. Wardman, P., Fluorescent and luminescent probes for measurement of oxidative and nitrosative species in cells and tissues: Progress, pitfalls, and prospects. *Free Radic. Biol. Med.* **2007**, *43* (7), 995-1022.
31. (a) Miao, J.; Huo, Y.; Lv, X.; Li, Z.; Cao, H.; Shi, H.; Shi, Y.; Guo, W., Fast-response and highly selective fluorescent probes for biological signaling molecule NO based on N-nitrosation of electron-rich aromatic secondary amines. *Biomaterials* **2016**, *78*, 11-19. (b) Islam, A. S. M.; Sasmal, M.; Maiti, D.; Dutta, A.; Show, B.; Ali, M., Design of a Pyrene Scaffold Multifunctional Material: Real-Time Turn-On Chemosensor for Nitric Oxide, AIEE Behavior, and Detection of TNP Explosive. *ACS Omega* **2018**, *3* (8), 10306-10316.

CHAPTER 3

32. Maiti, D.; Islam, A. S. M.; Sasmal, M.; Prodhan, C.; Ali, M., Selective sensing of nitric oxide by a 9,10-phenanthroquinone–pyridoxal based fluorophore. *Photochem. Photobiol. Sci.* **2018**, *17* (9), 1213-1221.
33. Islam, A. S. M.; Bhowmick, R.; Pal, K.; Katarkar, A.; Chaudhuri, K.; Ali, M., A Smart Molecule for Selective Sensing of Nitric Oxide: Conversion of NO to HSNO; Relevance of Biological HSNO Formation. *Inorg. Chem.* **2017**, *56* (8), 4324-4331.
34. Islam, A. S. M.; Bhowmick, R.; Chandra Garain, B.; Katarkar, A.; Ali, M., Nitric Oxide Sensing through 1,2,3,4-Oxatriazole Formation from Acylhydrazide: A Kinetic Study. *J. Org. Chem.* **2018**, *83* (21), 13287-13295.
35. Sun, C.; Shi, W.; Song, Y.; Chen, W.; Ma, H., An unprecedented strategy for selective and sensitive fluorescence detection of nitric oxide based on its reaction with a selenide. *Chem. Commun.* **2011**, *47* (30), 8638-8640.
36. Dai, C.-G.; Liu, X.-L.; Du, X.-J.; Zhang, Y.; Song, Q.-H., Two-Input Fluorescent Probe for Thiols and Hydrogen Sulfide Chemosensing and Live Cell Imaging. *ACS Sens.* **2016**, *1* (7), 888-895.
37. Mesáros, Š.; Grunfeld, S.; Mesárosová, A.; Bustin, D.; Malinski, T., Determination of nitric oxide saturated (stock) solution by chronoamperometry on a porphyrine microelectrode. *Anal. Chim. Acta* **1997**, *339* (3), 265-270.
38. Miyamoto, S.; Martinez, G. R.; Martins, A. P. B.; Medeiros, M. H. G.; Di Mascio, P., Direct Evidence of Singlet Molecular Oxygen [O₂ (1Δg)] Production in the Reaction of Linoleic Acid Hydroperoxide with Peroxynitrite. *J. Am. Chem. Soc.* **2003**, *125* (15), 4510-4517.
39. Dutta, A.; Alam, R.; Islam, A. S. M.; Dutta, A.; Ali, M., A dual response fluorescent sensor for HNO and S²⁻ ions using a Cu(ii) complex based probe assisted by detailed DFT studies. *Dalton Trans.* **2018**, *47* (33), 11563-11571.
40. Parr, R.G., Density functional theory of atoms and molecules. In *Horizons of Quantum Chemistry: Proceedings of the Third International Congress of Quantum Chemistry Held at Kyoto, Japan, October 29-November 3, 1979*, 5-15. Springer Netherlands, 1980.
41. (a) Barone, V.; Cossi, M., Quantum Calculation of Molecular Energies and Energy Gradients in Solution by a Conductor Solvent Model. *J. Phys. Chem. A* **1998**, *102* (11), 1995-2001. (b) Cossi, M.; Barone, V., Time-dependent density functional theory for

CHAPTER 3

- molecules in liquid solutions. *J. Chem. Phys.* **2001**, *115* (10), 4708-4717. (c) Cossi, M.; Rega, N.; Scalmani, G.; Barone, V., Energies, structures, and electronic properties of molecules in solution with the C-PCM solvation model. *J. Comput. Chem.* **2003**, *24* (6), 669-681.
42. Becke, A.D.; Becke's three parameter hybrid method using the LYP correlation functional. *J. Chem. Phys.* **1993**, *98*(492), 5648-5652.
43. Lee, C.; Yang, W.; Parr, R.G., Effective homogeneity of the exchange-correlation energy functional. *Phys. Rev. B*, **1998**, *37*, 785.
44. (a) Casida, M. E.; Jamorski, C.; Casida, K. C.; Salahub, D. R., Molecular excitation energies to high-lying bound states from time-dependent density-functional response theory: Characterization and correction of the time-dependent local density approximation ionization threshold. *J. Chem. Phys.* **1998**, *108* (11), 4439-4449. (b) Stratmann, R. E.; Scuseria, G. E.; Frisch, M. J., An efficient implementation of time-dependent density-functional theory for the calculation of excitation energies of large molecules. *J. Chem. Phys.* **1998**, *109* (19), 8218-8224. (c) Bauernschmitt, R.; Ahlrichs, R., Treatment of electronic excitations within the adiabatic approximation of time dependent density functional theory. *Chem. Phys. Lett.* **1996**, *256* (4), 454-464.
45. (a) Liu, T.; Zhang, H.-X.; Xia, B.-H., Theoretical Studies on Structures and Spectroscopic Properties of a Series of Novel Cationic [trans-(CAN)2Ir(PH3)2]⁺ (CAN = ppy, bzq, ppz, dfppy). *J. Phys. Chem. A* **2007**, *111* (35), 8724-8730. (b) Zhou, X.; Zhang, H.-X.; Pan, Q.-J.; Xia, B.-H.; Tang, A.-c., Theoretical Studies of the Spectroscopic Properties of [Pt(trpy)C:CR]⁺ (trpy = 2,2',6',2''-Terpyridine; R = H, CH₂OH, and C₆H₅). *J. Phys. Chem. A* **2005**, *109* (39), 8809-8818. (c) Zhou, X.; Ren, A.-M.; Feng, J.-K., Theoretical studies on the ground states in M(terpyridine)₂²⁺ and M(n-butylphenylterpyridine)₂²⁺ (M=Fe, Ru, Os) and excited states in Ru(terpyridine)₂²⁺ using density functional theory. *J. Organomet. Chem.* **2005**, *690* (2), 338-347. (d) Albertino, A.; Garino, C.; Ghiani, S.; Gobetto, R.; Nervi, C.; Salassa, L.; Rosenberg, E.; Sharmin, A.; Viscardi, G.; Buscaino, R.; Croce, G.; Milanese, M., Photophysical properties and computational investigations of tricarbonylrhenium(I)[2-(4-methylpyridin-2-yl)benzo[d]-X-azole]L and tricarbonylrhenium(I)[2-(benzo[d]-X-azol-2-yl)-4-methylquinoline]L

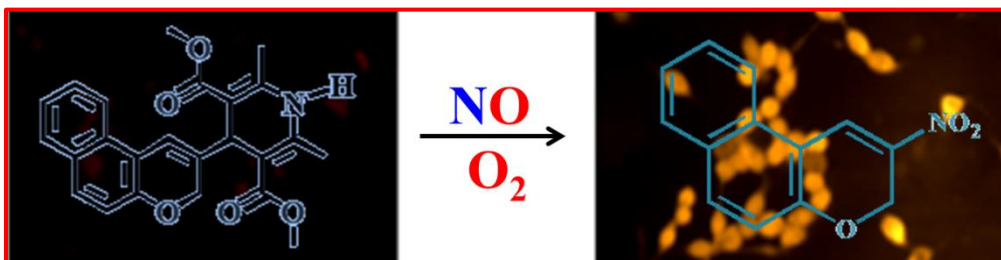
CHAPTER 3

- derivatives (X=N-CH₃, O, or S; L=Cl⁻, pyridine). *J. Organomet. Chem* **2007**, 692 (6), 1377-1391.
46. Frisch, M.; Trucks, G.; Schlegel, H.; Scuseria, G.; Robb, M.; Cheeseman, J.; Scalmani, G.; Barone, V.; Mennucci, B.; Petersson, G. J. A., U. Haeussermann, M. Dolg, H. Stoll, H. Preuss, Theor. Chem. Acta, Gaussian 09, Revision A. 1, Gaussian Inc, Wallingford, CT, 2009;(c) D. **1990**, 77, 123-141.
47. O'Boyle, N. M.; Tenderholt, A. L.; Langner, K. M., cclib: A library for package-independent computational chemistry algorithms. *J. Comput. Chem.* **2008**, 29 (5), 839-845.
48. Twentyman, P. R.; Luscombe, M., A study of some variables in a tetrazolium dye (MTT) based assay for cell growth and chemosensitivity. *Br. J. Cancer* **1987**, 56 (3), 279-285.
49. (a) Peng, T.; Chen, X.; Gao, L.; Zhang, T.; Wang, W.; Shen, J.; Yang, D., A rationally designed rhodamine-based fluorescent probe for molecular imaging of peroxynitrite in live cells and tissues. *Chem. Sci.* **2016**, 7 (8), 5407-5413. (b) Wu, X.; Li, L.; Shi, W.; Gong, Q.; Ma, H., Near-Infrared Fluorescent Probe with New Recognition Moiety for Specific Detection of Tyrosinase Activity: Design, Synthesis, and Application in Living Cells and Zebrafish. *Angew. Chem.* **2016**, 55 (47), 14728-14732. (c) Xu, K.; Qiang, M.; Gao, W.; Su, R.; Li, N.; Gao, Y.; Xie, Y.; Kong, F.; Tang, B., A near-infrared reversible fluorescent probe for real-time imaging of redox status changes in vivo. *Chem. Sci.* **2013**, 4 (3), 1079-1086.
50. Hu, X.; Wang, J.; Zhu, X.; Dong, D.; Zhang, X.; Wu, S.; Duan, C., A copper(ii) rhodamine complex with a tripodal ligand as a highly selective fluorescence imaging agent for nitric oxide. *Chem. Commun.* **2011**, 47 (41), 11507-11509.
51. Chen, T.; Zamora, R.; Zuckerbraun, B.; Billiar, T.R., Role of nitric oxide in liver injury. *Curr. Mol. Med.*, **2003**, 3(6), 519-526.

A Subtle Structural Change in the Fluorophore alters Nitric Oxide Mediated Reactivity of the Dihydropyridine based Probe Resulting Aromatic Nitration assisted C-C bond breaking

ABSTRACT:

A dihydropyridine based nitric oxide sensitive probe (CQME) with benzochromene as the fluorophoric unit was synthesized. The probe exhibits ~30 fold enhancement in the emission intensity at 615 nm on excitation at 470 nm resulting a huge stoke-shifts of 145 nm assuring a minimum interference from the excitation light for *in vivo* applications. Investigation of the cause of this enhancement reveals that the cleavage of the C-C bond between the benzochromene and 1,4-dihydropyridine (DIPY) units occurs due to the nitration on the 2H-pyran ring of the benzochromene moiety leading to the formation of 2-nitro-3H-benzo[f]chromene (PYNO₂) and dimethyl 2,6-dimethylpyridine-3,5-dicarboxylate (PYMAA) as the major products. The probe (CQME) and the product (PYNO₂) were structurally characterized by single crystal X-ray diffraction method while PYMAA only by spectroscopic (NMR, HRMS and IR) techniques. However, previous studies on NO sensing by various fluorophores containing DIPY unit as NO receptor indicated the canonical aromatization reaction. While the simple chromene-DIPY based probe gives dimethyl 4-(2H-chromen-3-yl)-2,6-dimethylpyridine-3,5-dicarboxylate (SALPY) as the major product with a very small amount of C-nitrosated product (SALNO₂). Now, the biocompatibility, high selectivity and sensitivity (~42 nM) along with pH independency of CQME makes it a premier candidate to be utilized to trace both endogenous and exogenous nitric oxide (NO) in biological systems.



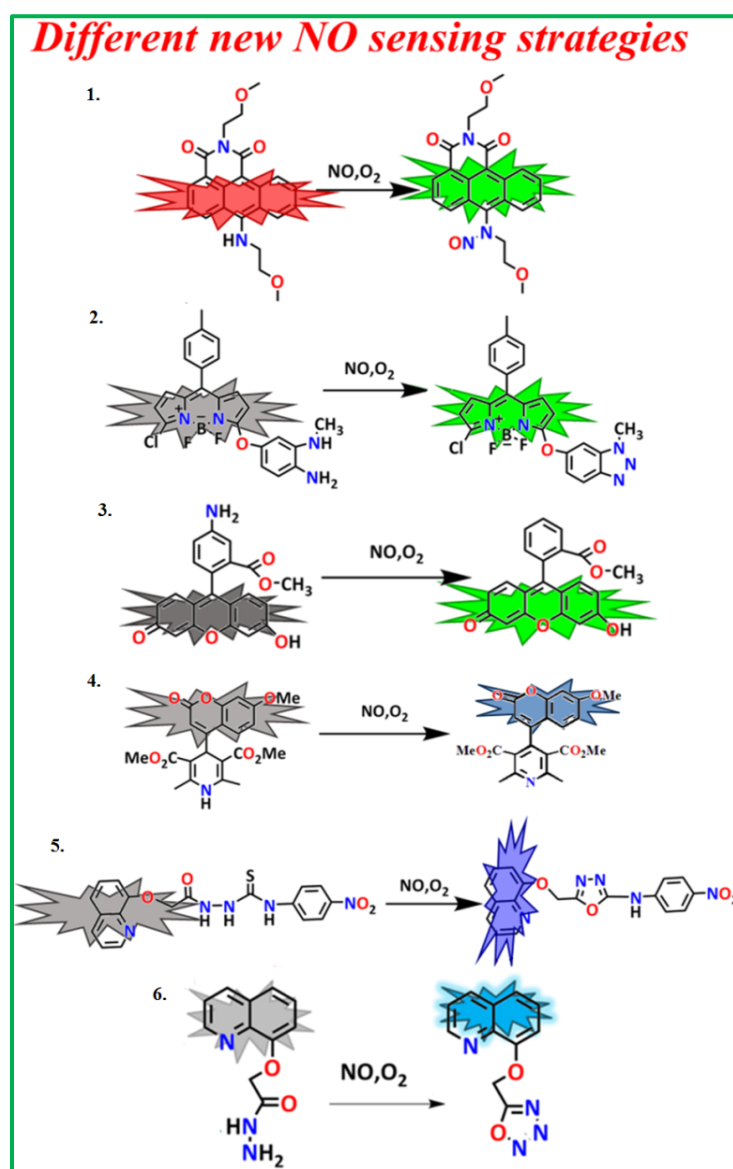
4.1 Introduction

Nitric oxide (NO), an essential and ubiquitous signaling molecule, is induced via oxidation of L-arginine to L-citrulline by nitric oxide synthase (NOS) enzymes under normoxic conditions.¹ On the other way, under acidic or hypoxic environment nitrite turns into a source of NO.² However, the detailed mechanism of functioning of endogenous NO still remained elusive. The dichotomous role of NO in biological systems is endorsed by the regulation or impairment of various physiological processes, depending upon the certain concentration of NO. Five basic distinct concentration levels of NO activity have been proposed as: (a) $[\text{NO}] < (1\text{--}30) \text{ nM}$ promotes cGMP mediated processes; (b) $[\text{NO}] = (30\text{--}100 \text{ nM})$ promotes Akt phosphorylation; (c) $[\text{NO}] = (100\text{--}300 \text{ nM})$ stabilizes HIF-1 α ; (d) $[\text{NO}] > 400 \text{ nM}$ promotes phosphorylation of p53 and (e) $[\text{NO}] \geq 1 \text{ }\mu\text{M}$ exerts nitrosative stress. This leads to the conclusion that the standard range of NO (pM-nM) can control the process of vasodilation, immune response, neurotransmission, apoptosis, gene expression³⁻⁵ etc., whereas the elevated levels of NO ($\geq 1 \text{ }\mu\text{M}$) may cause some life-threatening diseases like endothelial dysfunction, stroke, septic shock syndrome, Parkinson's and Alzheimer's disease⁶⁻⁹ etc. Excessive NO production induces the generation of highly reactive and toxic nitrification species such as NO_2^- , N_2O_3 , ONOO^- (peroxynitrite) etc., resulting in a damage of DNA, proteins, enzymes and other bio-receptors as well as cellular death.¹⁰ As a result, the tracking of NO generation, distribution and activities biological systems becomes a highly demanding as well as a challenging task to the chemists and biologists. To unveil its contribution in live organisms, various conventional methods have been developed which often employed are: Electronparamagnetic resonance (EPR) spectroscopy,¹¹ amperometry,¹² spectrophotometry,¹³ Chemiluminescence¹⁴ and fluorescence spectrophotometry¹⁵⁻¹⁷ etc. Among all these reported techniques, the fluorimetric approach has acquired an immense attention because of its tremendous sensitivity, good selectivity and non-invasive visualization. The generation as well as transportation of NO in cellular entity is entirely a challenging task. This is due to its transient life time (half-life $< 10 \text{ s}$) in blood and high reactivity towards endogenous biomolecules (mainly thiols).¹⁸

So far, an extensive variety of fluorescent probes have been designed to investigate the role of NO in living cells. Initially, most of the fluorescent probes fall into two categories: the first one was innovated by Nagano's group¹⁹ through attachment of *o*-phenylenediamino (OPD) entity as

CHAPTER 4

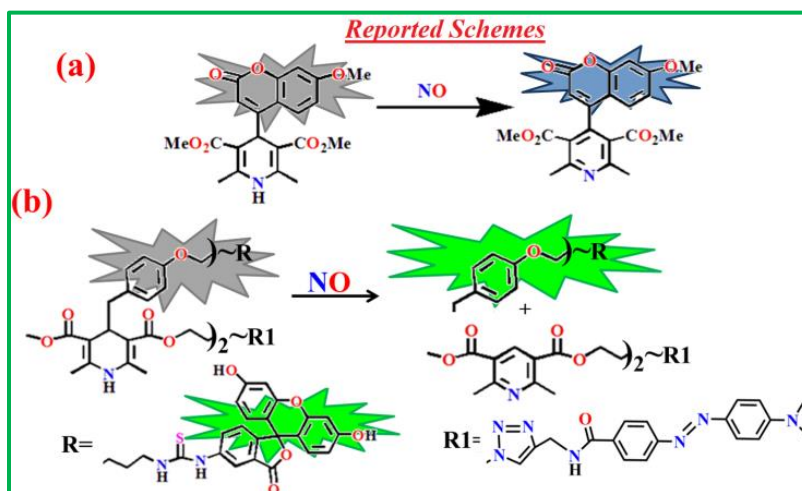
the NO-capturing unit with the probe, whereas the second one was related with metal–ligand complexes, initiated by Lippard’s group.²⁰ Despite being promising, both these two conventional NO sensing mechanisms have some limitations. The major drawback for OPD based probes involve the false positive response by RCS (Reactive carbonyl species) e.g. dehydroascorbic acid (DHA), ascorbic acid (AA) and methylglyoxal (MGO) etc. and also the high sensitivity of the triazole unit towards acidic pH. On the other hand, the metal-ligand complexes involve the leakage of heavy metals from the probe, inducing toxicity towards cells, and also influence the reaction between the probe and NO.



Scheme 4.1. Various NO sensing strategies.

CHAPTER 4

In recent years, various NO sensing strategies have been developed to overcome these limitations. These include (1) nitrosation reaction,²¹ (2) the formation of a diazo ring by protecting one of the amines in *o*-phenylenediamine,²² (3) oxidative deamination of aromatic primary monoamines,²³ (4) aromatization of the Hantzsch ester,²⁴ (5) the formation of oxadiazole from thiosemicarbazide,²⁵ (6) generation of 1,2,3,4-oxatriazole from acylhydrazide²⁶ and so forth (Scheme 4.1). Among all these NO sensing strategies, Hantzsch ester, a dihydropyridine derivative, has added advantages on selectivity towards NO, as it can react with NO without any dependence on oxygen and is silent towards RCS. Actually, as reported to date^{24,27-30}, upon exposure to NO, the dihydropyridine based fluorescent probes produce the corresponding pyridine through oxidative aromatization as demonstrated in Scheme 4.2(a).



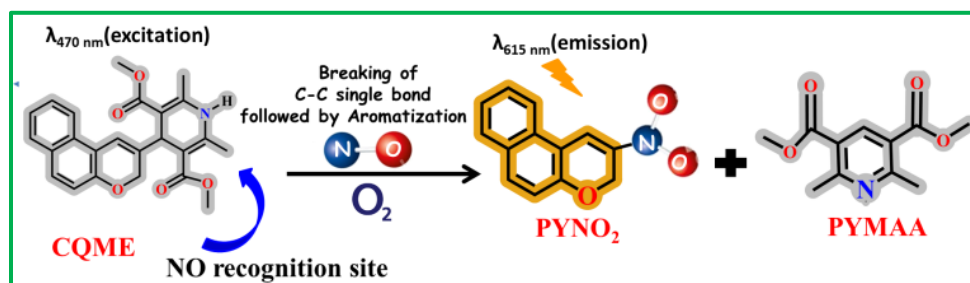
Scheme 4.2. (a) Normal aromatization reaction from dihydropyridine to pyridine; and (b) Breakage of C-C bond followed by aromatization of dihydropyridine to pyridine.

To the best of our knowledge, however, there is only one exception regarding the dihydropyridine based NO sensing mechanism reported by Zang and workers³¹ (Scheme 4.2(b)). Here the authors claimed that on stimulation with NO, the 1,4-dihydropyridine attached fluorescent probe causes the cleavage of the C–C bond between the 1,4-dihydropyridine unit and the benzyl group attached to the C₄ position of the dihydropyridine entity, though no detail characterization of the products have been carried out except LC-MS studies.

In our current research endeavour, a new benzochromene based fluorescence probe has been introduced for selective and sensitive sensing of NO in living organisms. This structurally simple

CHAPTER 4

fluorescent probe is designed by exploiting benzochromene moiety as the signaling unit and the dihydropyridine unit as the NO recognition site. We prefer benzochromene as a fluorophoric entity because of its excellent photochemical and photophysical properties as well as its interesting role in pharmacology.³² Now, the presence of NO under aerobic condition causes the cleavage of the C-C bond between the benzochromene moiety and the 1,4-dihydropyridine unit, resulting in the generation of C-nitrated product (PYNO₂) which is responsible for turn-on fluorescence response in the amber region (~ 615 nm) (Scheme 4.3). Here the C-C bond breaking is assisted by the nitration on the 2H-pyran ring of the benzochromene moiety as well as the steric crowding generated across the carbon atoms connecting the benzochromene and the DIPY units.

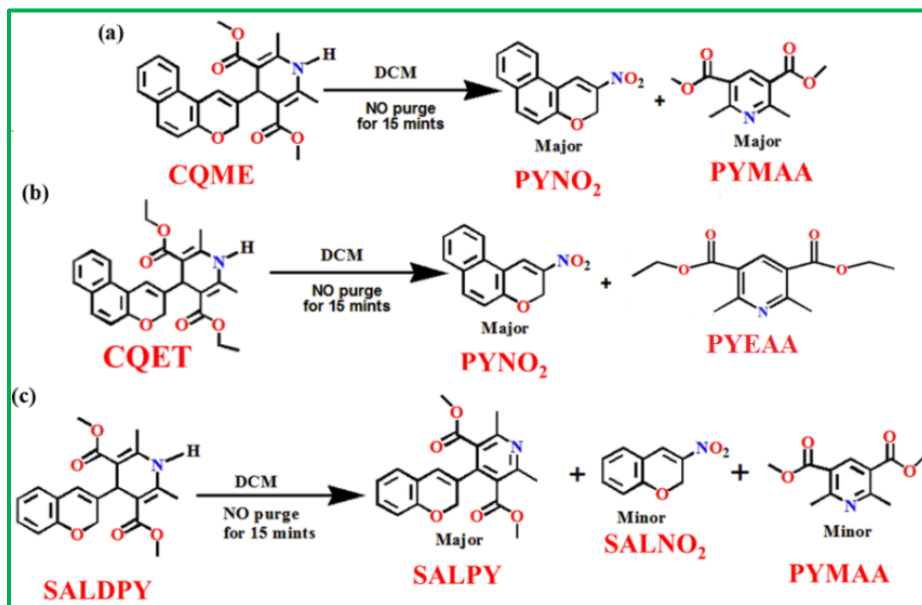


Scheme 4.3: Schematic illustration of reaction of CQME with NO.

To the best of our knowledge, a NO turn-on fluorescent probe through the cleavage of the C-C bond followed by the formation of the C-nitrated product (PYNO₂) has never been reported. However, it is reported that under disease conditions, tyrosine nitration occurs by the reactive nitrogen species such as peroxynitrite anion (ONOO⁻) and nitrogen dioxide ($\bullet\text{NO}_2$) which are formed as the secondary products of NO metabolism in the presence of oxidants.³³ In that sense this is the first example, where a subtle structural change in the fluorophore alters nitric oxide mediated reactivity of the dihydropyridine based probe to result an aromatic nitration assisted C-C bond breaking that occurs exogenously under mild conditions. The reaction between the benzochromene based probe (CQME) and NO is highly sensitive and specific, as on excitation at 470 nm it exhibits a negligible change in fluorescence intensity at 615 nm over other biological interfering species present in the biological milieu. We further synthesized another benzochromene based probe (CQET), analogous to CQME and also a chromene based probe SALDPY. Herein, under identical reaction conditions, CQET also generates the same C-nitrated

CHAPTER 4

product (PYNO₂), indicating that both the probes (CQME and CQET) followed the same mechanistic pathway on reaction with NO (Scheme 4.4). However, while dealing with the simple chromene-based probe (SALDPY), surprisingly, the normal aromatization reaction mechanism emerged as the major pathway (Scheme 4.4).



Scheme 4.4. Reaction products of (a) CQME (b) CQET and (c) SALDPY on treatment with NO at room temperature.

The structure of the concerned probe (CQME) and the product (PYNO₂) were validated utilizing spectroscopic studies (HRMS, ¹H-NMR, ¹³C-NMR etc.) and X-ray crystallography studies. The biological applications of CQME clearly demonstrate its ability to track both endogenous and exogenous NO over other biomolecules present in living organisms. This work mainly highlights a new NO sensing strategy where exposure to NO triggers the cleavage of the C-C bond to generate the C-nitrated product (PYNO₂) via a turn-on response in fluorescence intensity at 615 nm. Most interestingly, the stokes shift was found to be 145 nm which is quite large thereby ensuring the bypass of minimum interference from the excitation light for *in vivo* applications.

4.2 EXPERIMENTAL PROCEDURES

4.2.1 Reagents and Equipments

All the synthetic reagents such as 2-Hydroxy-1 naphthaldehyde, Salicylaldehyde, Methylacetoacetate, Ethylacetoacetate, Ammonium acetate, Acrolein, 4-Dimethylaminopyridine (DMAP) were purchased from Sigma Aldrich and utilized as received without further purification. Unless otherwise stated, the chemical analytes for example salts of K^+ , Na^+ , Ca^{2+} , Mg^{2+} , Cr^{3+} , Al^{3+} , Fe^{2+} , Mn^{2+} , Fe^{3+} , Cu^{2+} , Co^{2+} , Ni^{2+} , Hg^{2+} , Zn^{2+} , Pb^{2+} , Cd^{2+} etc., sodium salts of anions suchlike SCN^- , NO_3^- , NO_2^- , N_3^- , I^- , Br^- , F^- , BrO_3^- , HPO_4^- , OAc^- , $S_2O_3^{2-}$, $S_2O_4^{2-}$, SH^- , NCS^- etc. and other reactive species for example H_2O_2 , $\cdot OH$, O_2^- , TEMPO, NO_3^- , NO_2^- , $ONOO^-$, ascorbic acid (AA), and DEA-NONOate (sodium salt) were obtained from commercial channels and used without further purification. Infrared spectra of ligands (CQME, CQET, and SALDPY) and the generated products upon reaction with nitric oxide (NO) were recorded on a Perkin-Elmer RX I FTIR spectrophotometer on solid KBr discs. 1H and ^{13}C NMR spectra were measured utilizing Bruker 300 MHz spectrometer in $CDCl_3$ and DMSO- d_6 (Trimethylsilane ($\delta = 0$) as an internal standard). High resolution mass spectra (HRMS) of the probe and its NO reaction products were performed on QT of Micro YA263 spectrometer. Emission spectra and UV-Vis absorption spectra were recorded on a PTI (Model QM-40) spectrofluorimeter and an Agilent 8453 Diode-array spectrophotometer, respectively. Single crystal X-ray diffraction data were collected using Bruker APEX III D8 Venture, PHOTON II detector ($MoK\alpha$ ($\lambda = 0.7107 \text{ \AA}^0$)) and Bruker Kappa Apex-2, CCD Area Detector.

4.2.2 Preparation of Stock Solutions

For the preparation of NO solution at first the purification of NO was performed by passing the NO gas through solid NaOH pellets and then the purified NO gas was bubbled through deoxygenated deionized water for 15 min in a sealed vial. As a result, NO concentration in the solution becomes 1.74×10^{-3} M. The solutions of Hydroxyl radical ($\cdot OH$) and Peroxynitrite ($ONOO^-$) were prepared according to the reported procedure.²⁶ Each stock solution (1.0×10^{-3} M) of inorganic cations, anions and several reactive species were prepared in Mili-Q-Millipore water. The stock solution of the probe (CQME) was prepared at the concentration of $1.0 \times 10^{-3} \text{ mL}^{-1}$ in 10 mL of CH_3CN . All the analytic studies were accomplished in 10 mM HEPES buffer at pH 7.2. An equal amount of 10.0 mM HEPES buffer and MeCN were pipetted in a cuvette so

CHAPTER 4

that the volume of the solution become 2.5 ml and 50 μL of the probe (1.0×10^{-3} M) (CQME) was added, which gives the probe concentration 20 μM , and then (0 - 73 μM) NO was added incrementally and the fluorescence spectra were recorded for each solution after 3 mints.

4.2.3 Calculation of LOD

3σ /slope criteria was accepted for the Limit of Detection of NO (eqn. 1)

$$\text{LOD} = 3 \times S_d/S \quad \dots\dots (1)$$

Where, S_d represents the standard deviation of the blank and S denotes the slope generated from the linear plot of F.I. vs. [NO] in the fluorescence titration data.

4.2.4 Cell Imaging Experiments

4.2.4.1 Cell viability assay

Human lung adenocarcinoma A549 cells and Raw 264.7 murine macrophages were cultured in Dulbecco's modified Eagle's (DMEM) medium provided with 10% FBS and 1% antibiotic at 37 °C with 5% CO_2 . Cell viability of the probe CQME for A549 and Raw 264.7 cells were analyzed with CQME for 24h by MTT assay.²⁶

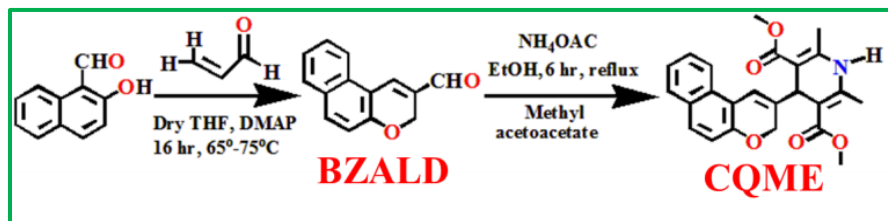
4.2.4.2 In-Vitro Cell incubation and imaging

Raw 264.7 murine macrophages and A549 cells were exploited for endogenous and exogenous NO detection, respectively. On glass coverslips, A549 cells were cultured for the detection of exogenous NO utilizing 35x10 mm culture dishes. A549 cells were treated with in presence and absence of DEA-NONOate (NO Donor, 5 μM and 10 μM) and incubated at 37°C with 5% CO_2 for 30 min and then the cells were washed with media, followed by further incubation with CQME (5 μM and 10 μM) for 30 min, washed, and then live cell imaging studies was executed with fluorescence microscope (Leica DM3000, Germany) with an objective lens of 40X magnification. For Endogenous NO detection, Raw 264.7 cells were co-stimulated with LPS (1.0 mg/mL) and IFN- γ (1000U/mL) for 4h, and without co-stimulant (control) and further incubated with CQME (5 μM) for 30 min. The treatment with NO scavenger PTIO (2-Phenyl-4, 4, 5, 5-tetramethylimidazoline-1-oxyl-3-oxide) also supports the spontaneous generation of cellular fluorescence with NO production. Raw 264.7 cells were co-stimulated in the presence and absence of LPS (1.0 mg/mL) and IFN- γ (1000 U/mL) for 4h, along with PTIO (200 mM) followed by incubation with CQME (5 μM) for 30 min to perform live fluorescence images.

CHAPTER 4

4.2.5 SYNTHESIS AND CHARACTERIZATION

CQME was conveniently synthesized according to the synthetic route portrayed in **Scheme 4.5**. The products of each step were well characterized by ^1H NMR, ^{13}C NMR, HRMS and IR spectra.



Scheme 4.5. Synthetic scheme for CQME.

4.2.5.1 Synthesis of BZALD

A solution of 2-hydroxynaphthalene-1-carbaldehyde (1.03 g, 6 mmol), DMAP (0.733 g, 6 mmol) and acrylaldehyde (~0.8 ml, 12 mmol) in anhydrous THF was refluxed under inert atmosphere for 16 hour. After cooling to room temperature, the solvent was removed under reduced pressure and the residue was purified by silica gel column chromatography ((60-120 mesh), DCM : Hexane = 9:1 as an eluent) to provide yellow crystalline compound. **Yield:** 60%. $\text{C}_{14}\text{H}_{10}\text{O}_2$ Molecular Weight: 210.2320.

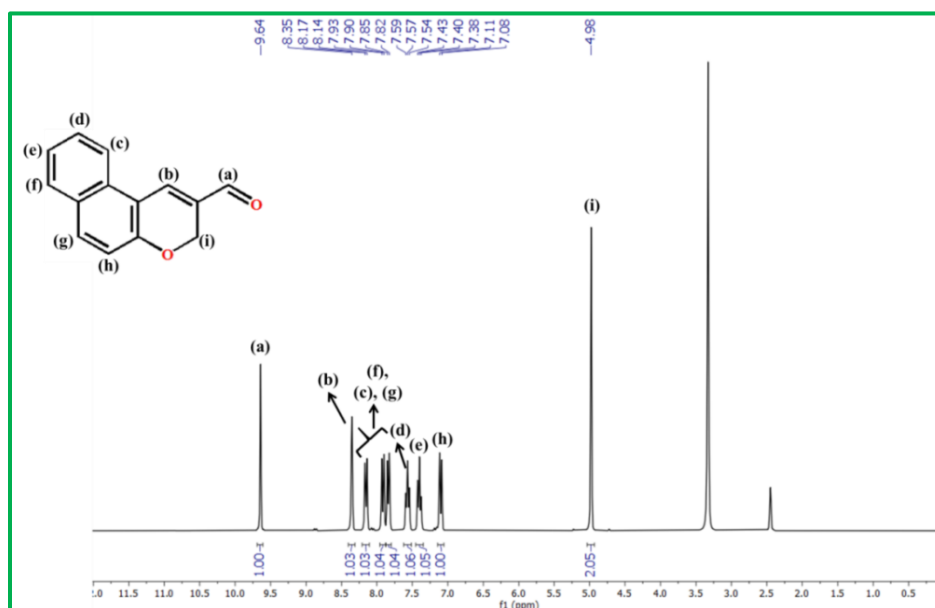


Figure 4.1. ^1H -NMR spectra of BZALD in DMSO-d_6 .

CHAPTER 4

$^1\text{H-NMR}$ (300 MHz, DMSO-d_6) (δ , ppm): 9.64 (s, 1H, -CHO), 8.35 (s, 1H, =CH), 8.15 (d, -ArH), 7.91 (d, 1H, -ArH), 7.83 (d, 1H, -ArH), 7.57 (m, 1H, -ArH), 7.40 (m, 1H, -ArH), 7.09 (d, 1H, -ArH) (**Figure 4.1**). $^{13}\text{C NMR}$ (75 MHz, DMSO-d_6): 190.88, 155.39, 138.31, 134.48, 130.84, 129.87, 129.47, 129.23, 128.54, 125.09, 122.07, 117.94, 114.32, 63.07 (**Figure 4.2**). ESIMS⁺ (m/z): (BZALD+ H^+) 211.0480 (**Figure 4.3**).

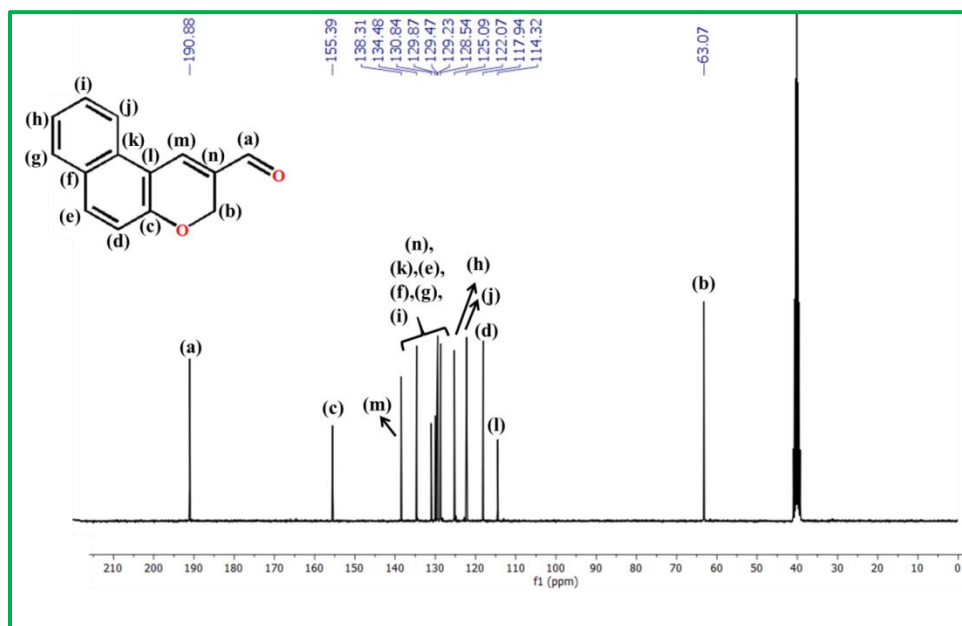


Figure 4.2. $^{13}\text{C-NMR}$ spectra of BZALD in DMSO-d_6 .

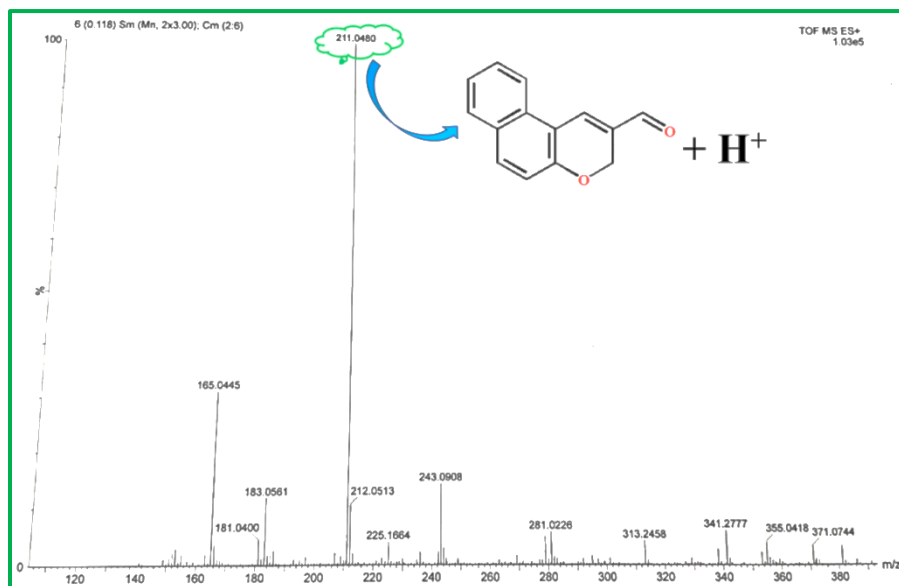


Figure 4.3. HRMS Spectra of BZALD in MeOH.

CHAPTER 4

4.2.5.2 Synthesis of CQME

A mixture of BZALD (0.440 g, 2.09 mmol), methyl acetoacetate (0.728 g, 6.27 mmol) and ammonium acetate (0.4833 g, 6.27 mmol) in ethanol was refluxed for 6 hour. After attaining room temperature, the reaction mixture was concentrated in vacuum and subjected for column chromatography using ethyl acetate : petroleum ether = 1: 9 as eluent. Yellowish white crystalline product was collected as a desired compound. Yield: 75%. $C_{24}H_{23}NO_5$. Molecular Weight: 405.4500. 1H -NMR (300 MHz, $CDCl_3$)(δ , ppm): 7.87 (d, 1H, -ArH), 7.71 (d, 1H, ArH), 7.57 (d, 1H, -ArH), 7.44 (t, 1H, -ArH), 7.30 (t, 1H, -ArH), 7.02 (d, 1H, -ArH), 6.81 (s, 1H, -ArH), 5.84 (s, 1H, -NH), 4.83 (s, 1H, -ArH), 4.67 (s, 1H, -CH), 3.73 (s, 6H, - CH_3), 2.37 (s, 6H, - CH_3) (**Figure 4.4**). ^{13}C NMR (75 MHz, $CDCl_3$): 167.82, 151.13, 145.26, 137.70, 129.79, 129.43, 128.52, 128.48, 126.28, 123.44, 121.37, 117.32, 116.12, 115.29, 101.10, 67.43, 51.23, 37.83, 19.60 (**Figure 4.5**). ESIMS⁺ (m/z): 405.1034 (**Figure 4.6(a)**). IR stretching frequencies: 3350 cm^{-1} (-N-H stretching), 1683 cm^{-1} (-C=O stretching) (**Figure 4.6(b)**).

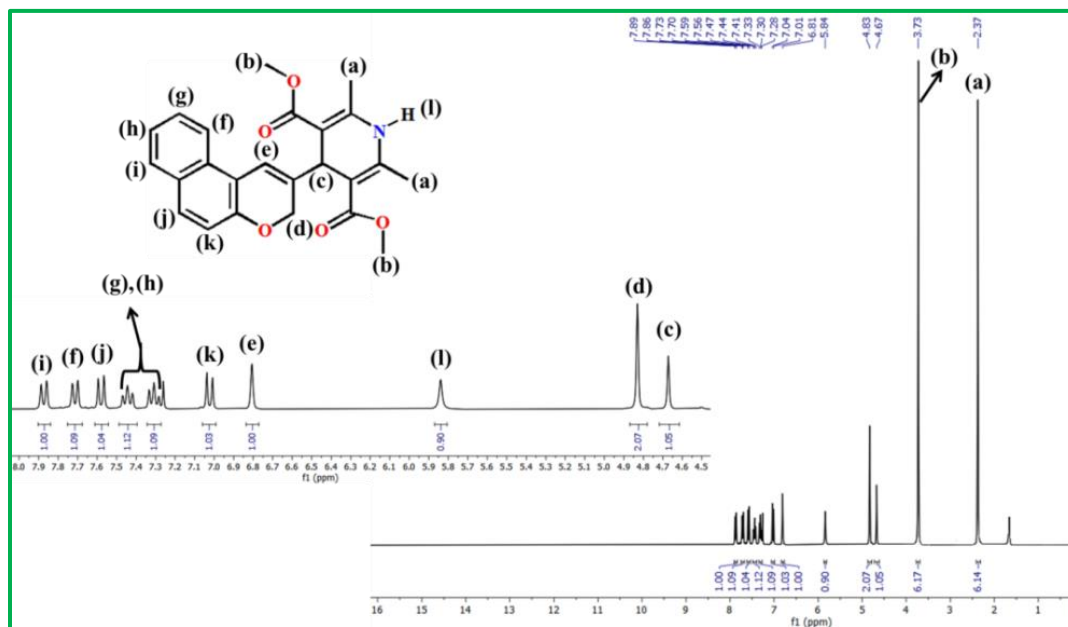


Figure 4.4. 1H -NMR spectra of CQME in $CDCl_3$.

CHAPTER 4

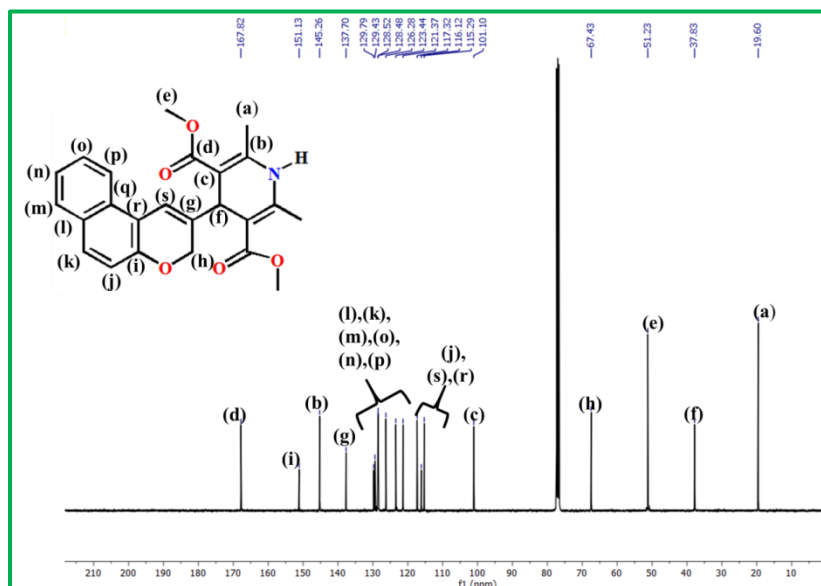


Figure 4.5. ^{13}C -NMR spectra of CQME in CDCl_3 .

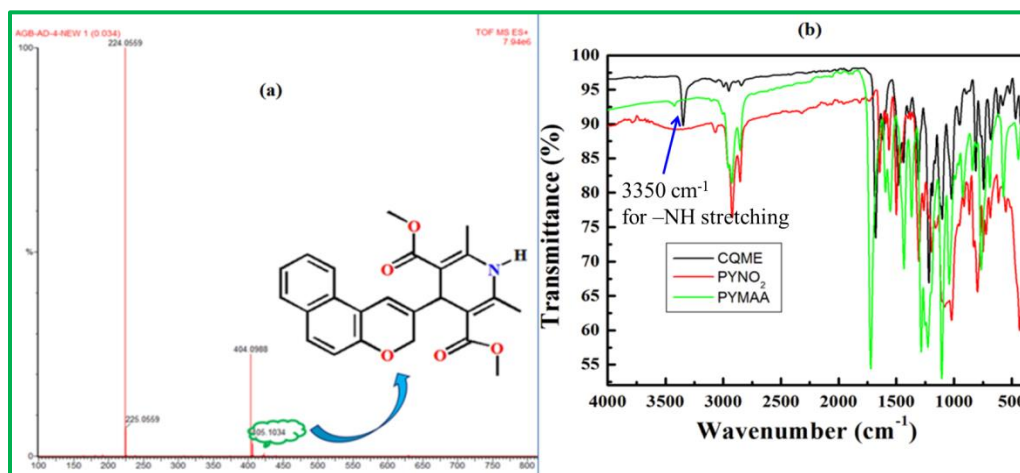
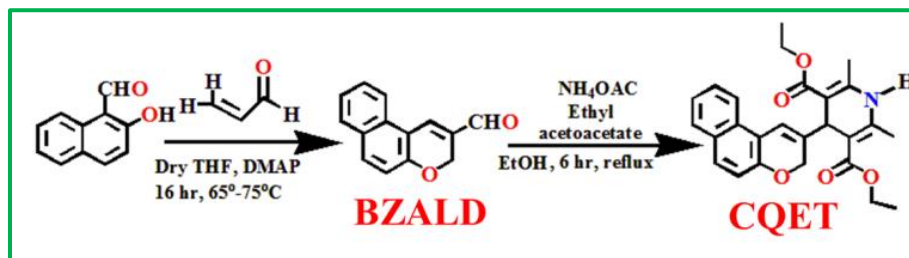


Figure 4.6. (a) HRMS spectra of CQME in MeOH; (b) IR spectra of CQME, PYNO_2 and PYMAA in solid state.

4.2.5.3 Synthesis of CQET



Scheme 4.6. Synthetic scheme for CQET.

CHAPTER 4

CQET was synthesized by following the same synthetic route as delineated for CQME (Scheme 4.6). Herein, Ethylacetoacetate was used as one of the reagent instead of methylacetoacetate. Yield: 72%. $C_{26}H_{27}NO_5$. Molecular Weight: 433.4963.

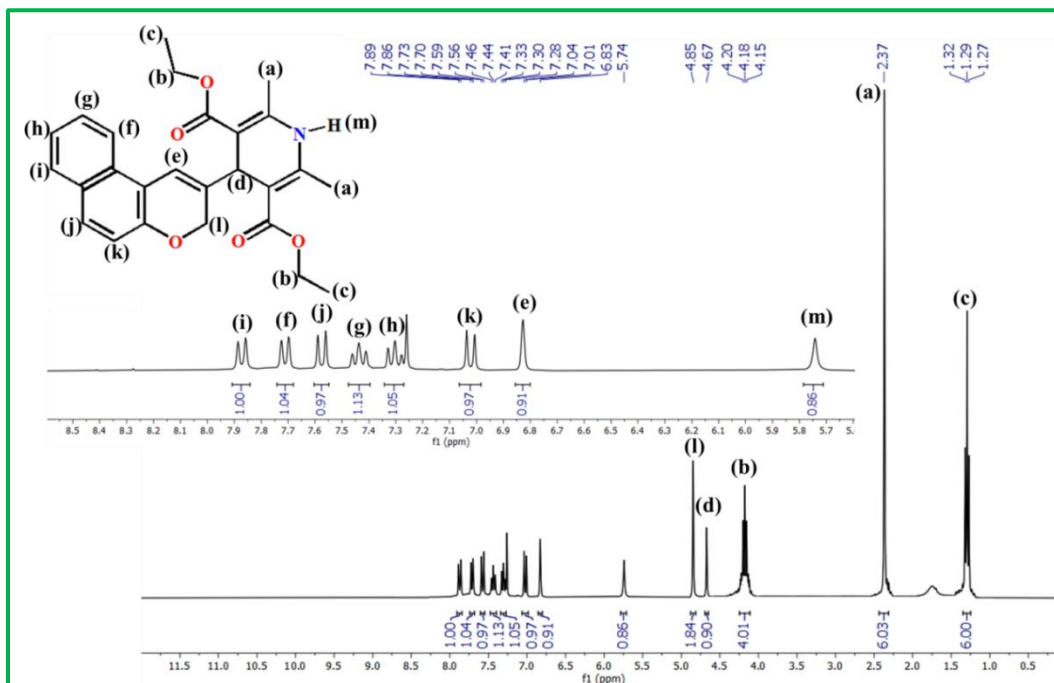


Figure 4.7(a). ^1H -NMR spectra of CQET in CDCl_3 .

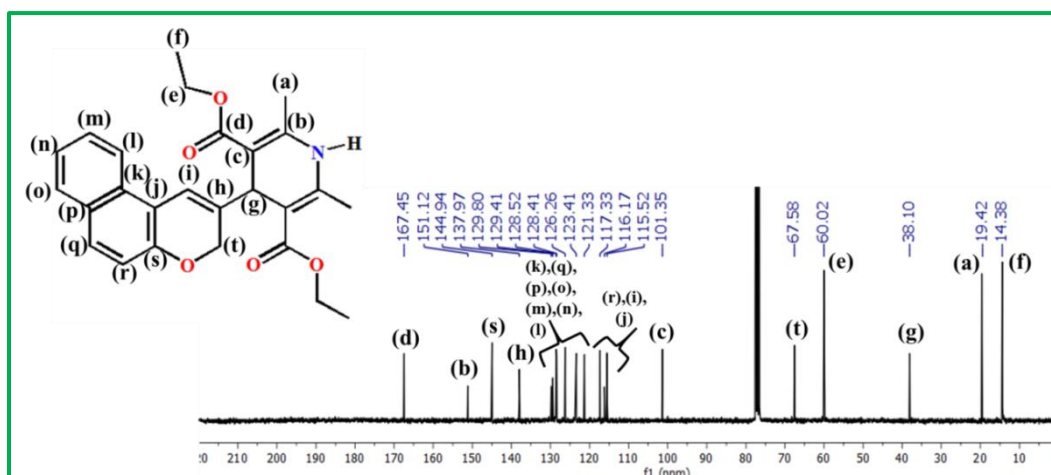


Figure 4.7(b). ^{13}C -NMR spectra of CQET in CDCl_3 .

^1H -NMR (300 MHz, CDCl_3)(δ , ppm): 7.87 (d, 1H, -ArH), 7.71 (s, 1H, -ArH), 7.57 (d, 1H, -ArH), 7.44 (t, 1H, -ArH), 7.30 (t, 1H, -ArH), 7.02 (m, 1H, -ArH), 6.83 (m, 1H, -ArH), 5.74 (d, 1H, -

CHAPTER 4

NH) 4.85 (s, 2H, -ArCH₂), 4.67 (s, 1H, -CH), 4.18(m, 4H, -CH₂), 2.37 (s, 6H, -CH₃), 1.29 (t, 6H, -CH₃) (**Figure 4.7(a)**). ¹³C NMR (75 MHz, CDCl₃): 167.45, 151.12, 144.94, 137.97, 129.80, 129.41, 128.52, 128.41, 126.26, 123.41, 121.33, 117.33, 116.17, 115.32, 101.35, 67.58, 60.02, 38.10, 19.42, 14.38 (**Figure 4.7(b)**). ESIMS⁺ (m/z): (CQET + Na⁺): 456.1664 (**Figure 4.7(c)**). IR stretching frequencies: 3314 cm⁻¹ (-N-H stretching), 1644 cm⁻¹ (-C=O stretching) (**Figure 4.7(d)**).

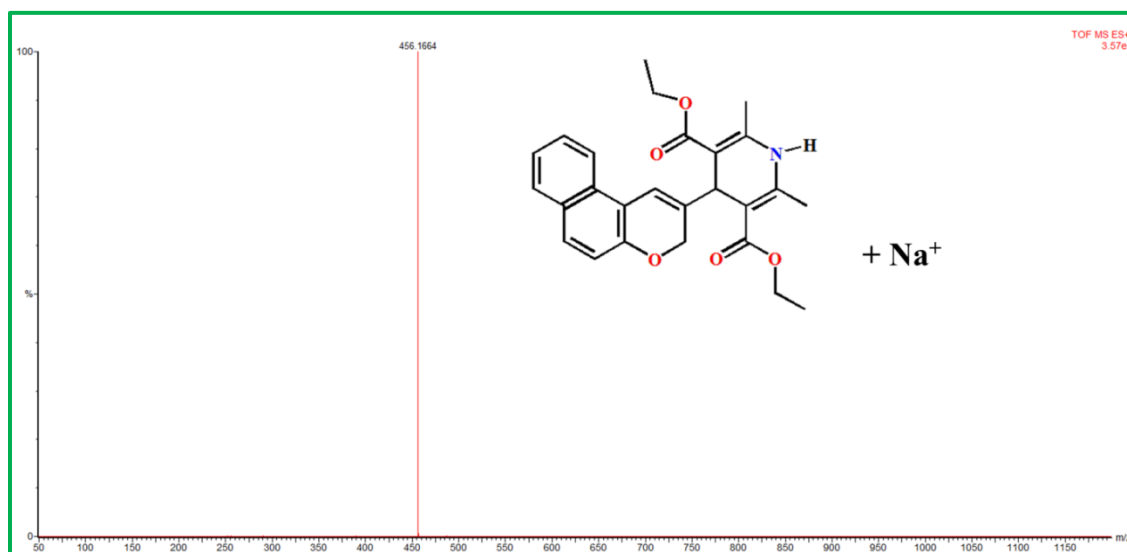


Figure 4.7(c). HRMS spectra of CQET in MeOH.

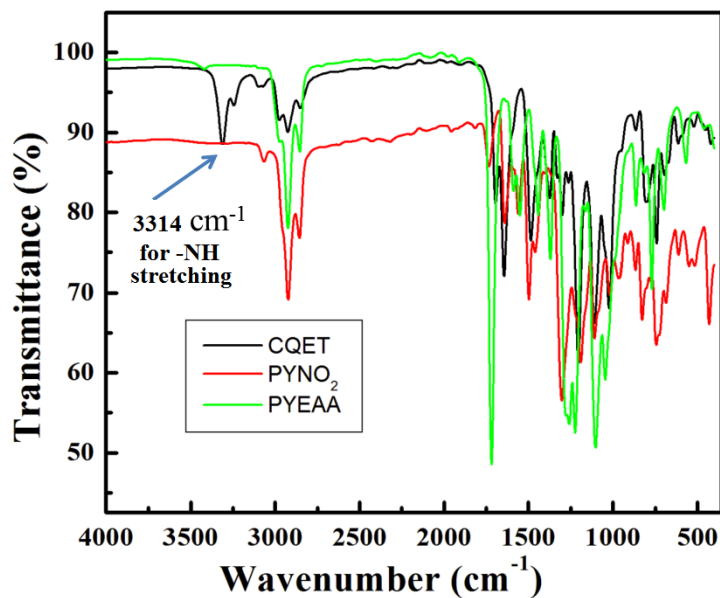


Figure 4.7(d). IR spectra of CQET, PYNO₂ and PYEAA in solid state.

CHAPTER 4

4.2.5.4 Synthesis of SALD

A solution of 2-hydroxybenzaldehyde (0.5 g, 4.09 mmol) and DMAP (0.499 g, 4.09 mmol) in dry THF was stirred at room temperature for 5 mins. Then acrylaldehyde (~0.6 ml, 8.18 mmol) was added drop-wise to the solution under N₂ atmosphere and was heated under refluxing environment for 16 hour. After achieving the room temperature, the solvent was allowed to evaporate off and the residue was allotted for further purification using silica gel column chromatography (where Hexane : DCM = 9.8 : 0.2 was utilized as an eluent). The pure product thus obtained was used in the next steps. Yield: 50%. C₁₀H₈O₂. Molecular Weight: 160.1693. ¹H-NMR (300 MHz, CDCl₃)(δ , ppm): 9.60 (s, 1H, -CHO), 7.34-7.22 (m, 3H, -ArH), 6.98 (t, 1H, -ArH), 6.88 (d, 1H, -ArH), 5.05 (s, 2H, -ArCH₂)(**Figure 4.8(a)**). ¹³C NMR (75 MHz, CDCl₃): 189.85, 156.12, 141.39, 133.31, 131.76, 129.12, 121.83, 120.55, 116.59, 63.29 (**Figure 4.8(b)**)

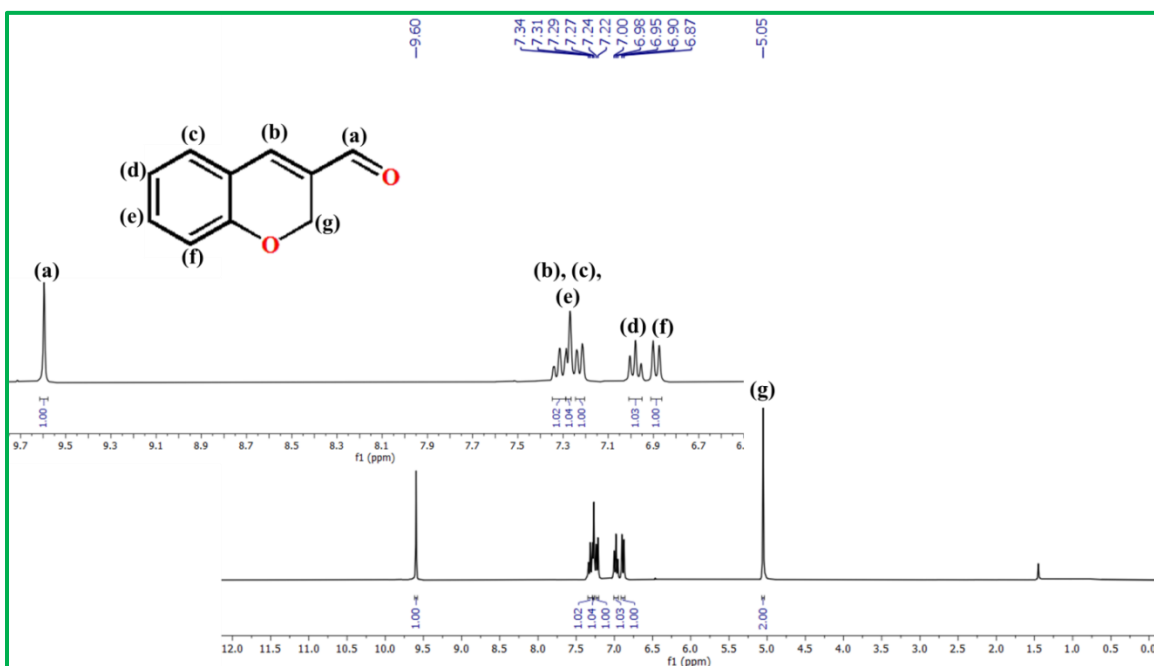


Figure 4.8(a). ¹H-NMR spectra of SALD in CDCl₃

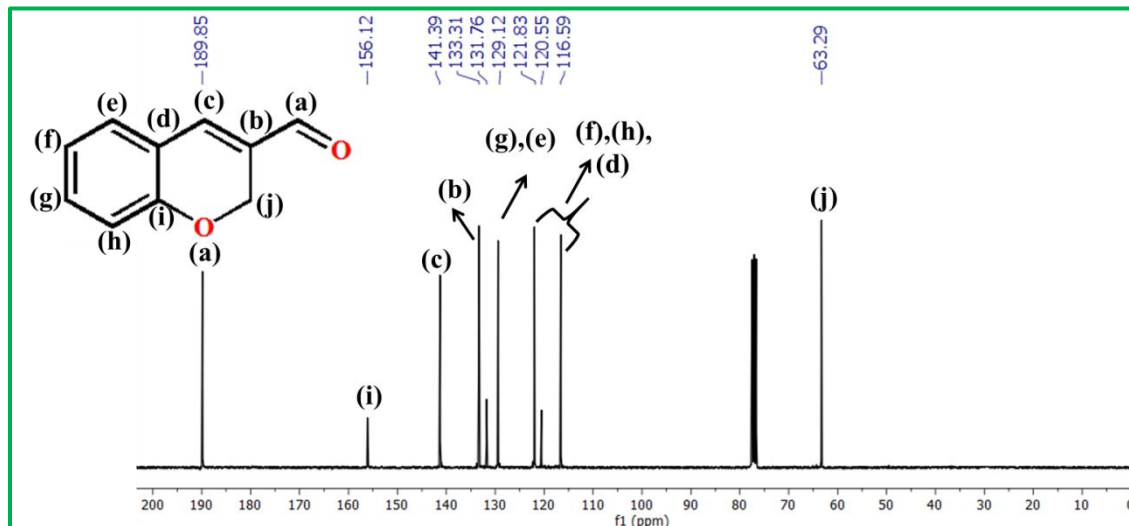
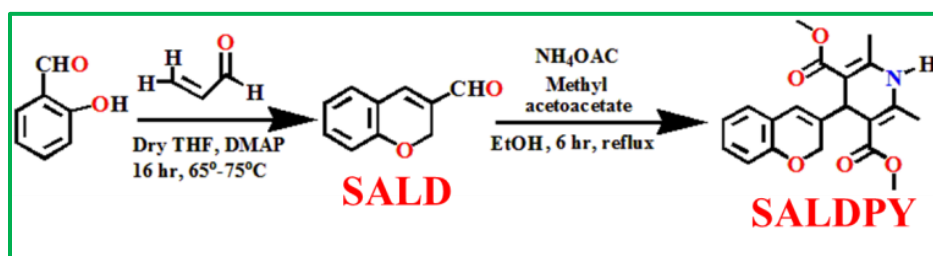


Figure 4.8(b). ^{13}C -NMR spectra of SALD in CDCl_3

4.2.5.5 Synthesis of SALDPY

An ethanolic solution of SALD (0.4 g, 2.49 mmol), methyl acetoacetate (0.867 g, 7.47 mmol) and ammonium acetate (0.575 g, 7.47 mmol) was heated under reflux condition for 6 hour. After cooling to room temperature, the solvent was removed in vacuum and the obtained crude product was further purified using silica gel column chromatography (ethyl acetate: petroleum ether = 1.5: 8.5 as an eluent). The afforded probe SALDPY is yellow in color. Yield: 75%. $\text{C}_{22}\text{H}_{25}\text{NO}_5$.

(Scheme 4.7)



Scheme 4.7. Synthetic scheme for SALDPY.

Molecular Weight: 383.4376. ^1H -NMR (300 MHz, CDCl_3) (δ , ppm): 7.02 (dt, 1H, -ArH), 6.89 (dd, 1H, -ArH), 6.80 (t, 1H, -ArH), 6.71 (d, 1H, -ArH), 6.08 (s, 1H, -ArH), 5.82 (s, 1H, -NH), 4.77 (s, 2H, -ArCH₂), 4.51 (s, 1H, -CH), 3.72 (s, 6H, -OCH₃), 2.34 (s, 6H, -CH₃) (Figure 4.9(a)). ^{13}C NMR (75 MHz, CDCl_3): 167.80, 153.10, 145.34, 139.09, 128.57, 126.36, 123.29,

CHAPTER 4

121.14, 119.14, 115.19, 100.88, 67.51, 51.22, 37.15, 19.57 (Figure 4.9(b)). ESIMS⁺ (m/z): (SALDPY + Na⁺): 378.1818 (Figure 4.9(c)). IR stretching frequencies: 3335 cm⁻¹ (-N-H stretching), 1650 cm⁻¹ (-C=O stretching) (Figure 4.9(d)).

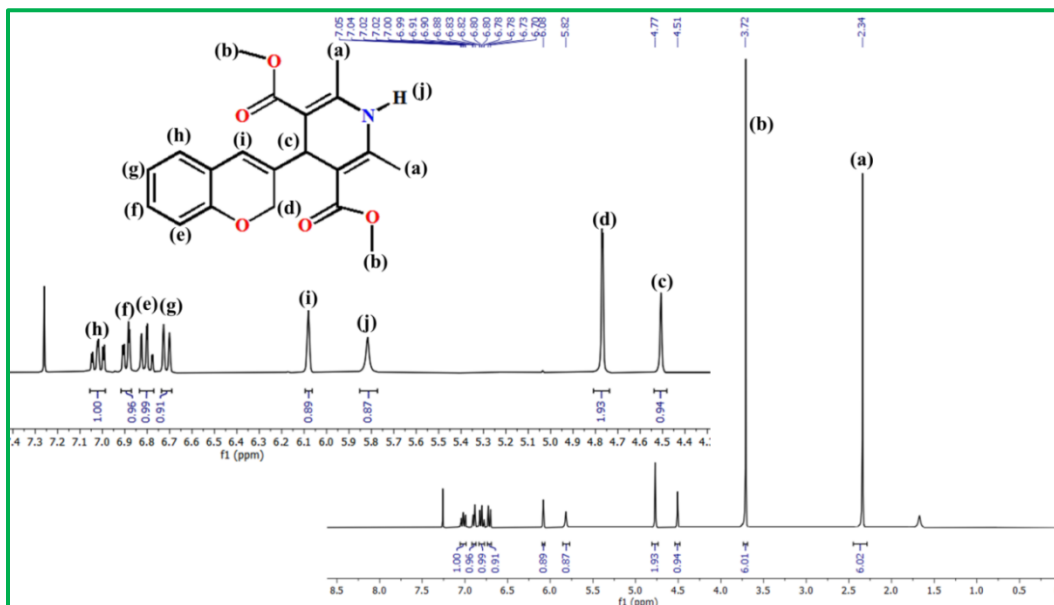


Figure 4.9(a). ¹H-NMR spectra of SALDPY in CDCl₃.

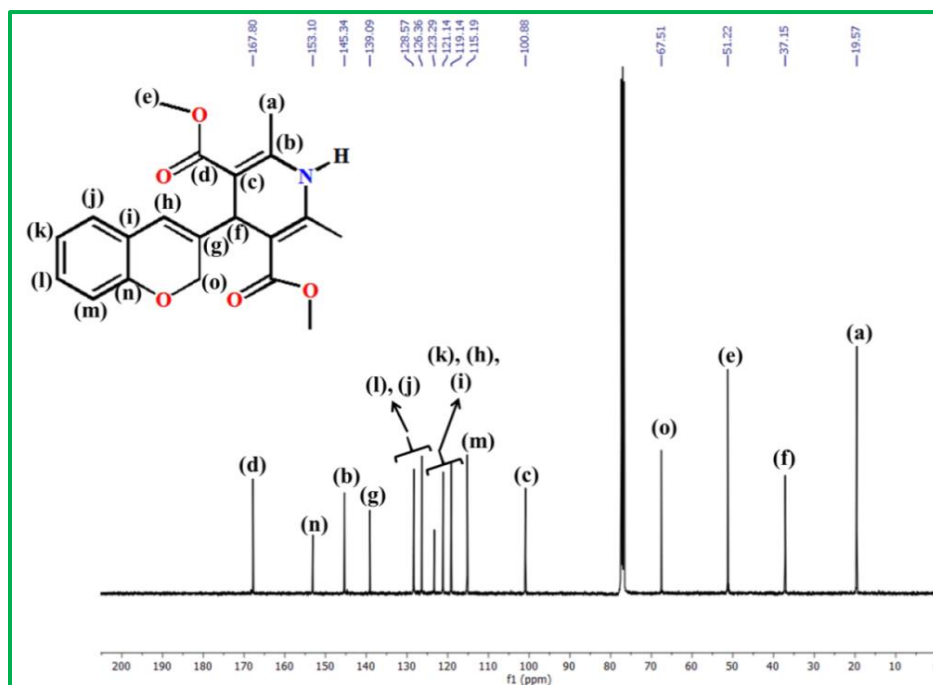


Figure 4.9(b). ¹³C-NMR spectra of SALDPY in CDCl₃.

CHAPTER 4

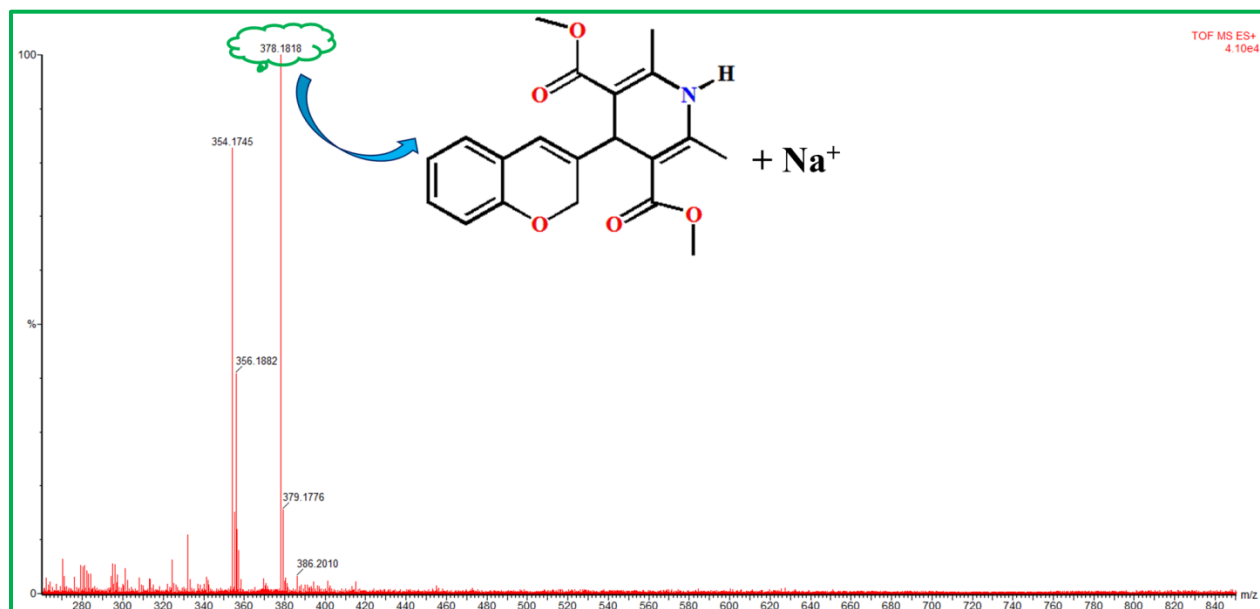


Figure 4.9(c). HRMS Spectra of SALDPY in MeOH.

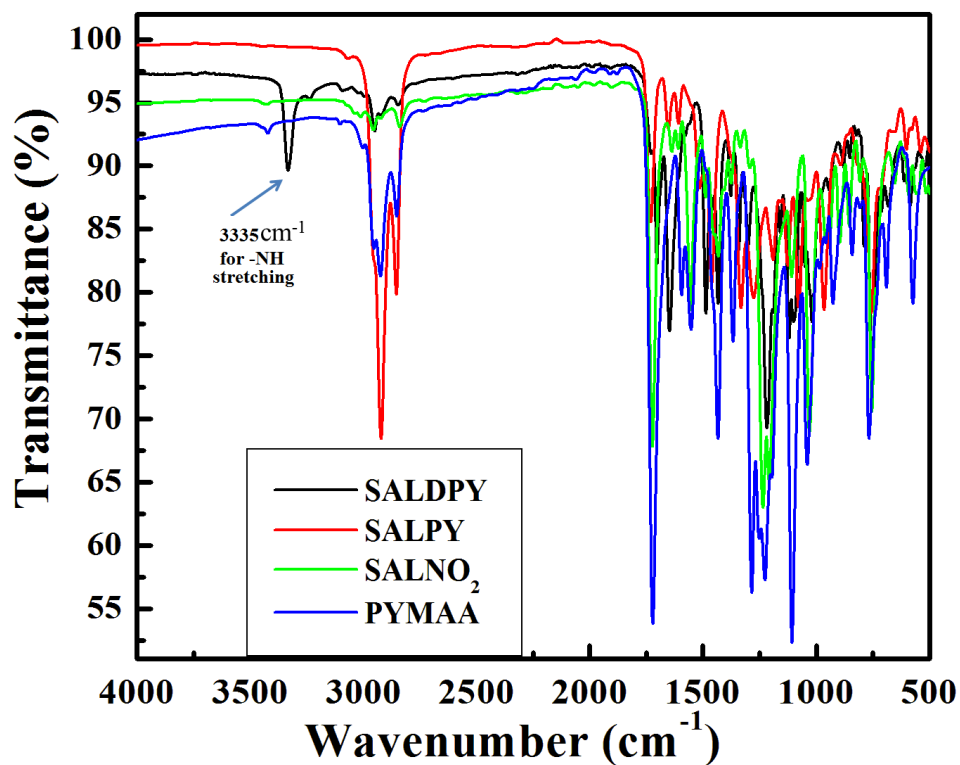


Figure 4.9(d). IR spectra of SALDPY, SALPY, SALNO₂ and PYMAA in solid state.

CHAPTER 4

4.2.5.6 Synthesis of PYNO₂ and PYMAA from CQME

CQME was first dissolved in 5 ml of dry DCM and then NO gas was bubbled through the CH₂Cl₂ solution for about 15-20 minutes at room temperature which exhibited the change in color of the solution from yellow to orange with high fluorescence. The reaction mixture was consecutively washed with saturated sodium bicarbonate and brine solution, and dried over anhydrous Na₂SO₄. Hereafter, the solution was removed under reduced pressure and subjected for purification using silica gel to give the desired products.

When the crude product was purified by column chromatography using ethyl acetate: petroleum ether = 0.2: 9.8 as an eluent, then PYNO₂, an orange crystalline compound was purified first which is responsible for generation of yellowish orange fluorescence in the solution. Yield: ~20%. C₁₃H₉NO₃. Molecular Weight: 227.2155. ¹H-NMR (300 MHz, CDCl₃)(δ, ppm): 8.54 (s, 1H, -ArH), 8.00 (d, 1H, -ArH), 7.87 (d, 1H, -ArH), 7.81 (d, 1H, -ArH), 7.62 (t, 1H, -ArH) 7.46 (t, 1H, -ArH) 7.13 (d, 1H, -ArH) 5.38 (s, 2H, -ArCH₂) (Figure 4.10(a)). ¹³C NMR (75 MHz, CDCl₃): 155.29, 136.75, 135.22, 131.17, 129.74, 129.19, 128.72, 126.12, 125.25, 121.31, 117.43, 111.88, 63.08 (Figure 4.10(b)). ESIMS⁺ (m/z): (PYNO₂ + K⁺) 266.1945 (Figure 4.10(c)). IR stretching frequencies: 1502 cm⁻¹ and 1303 cm⁻¹ (-NO₂ stretching) (Figure 4.6(b)).

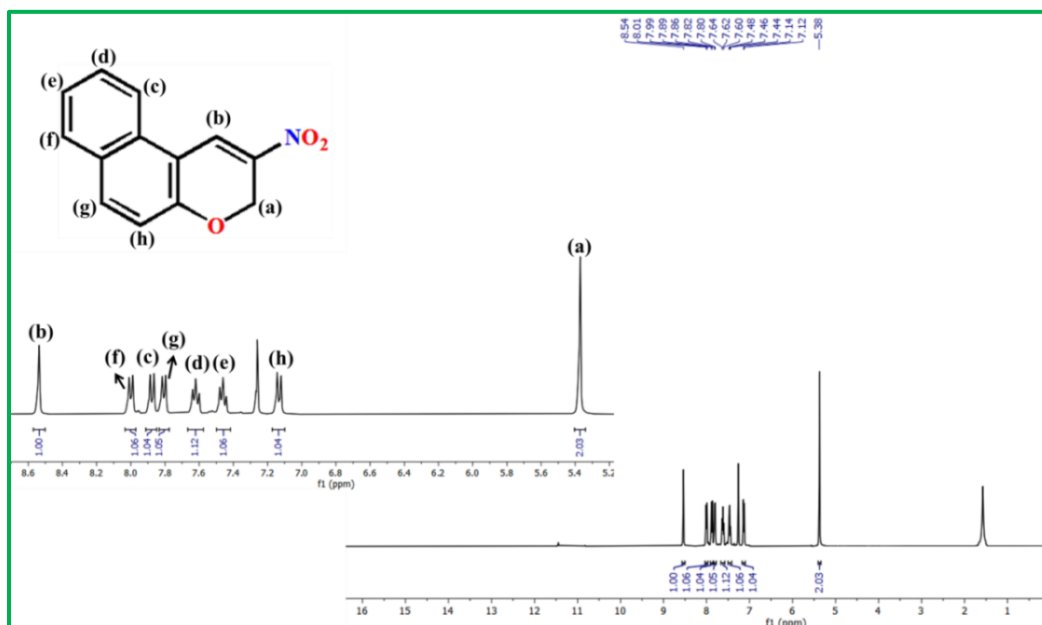


Figure 4.10(a). ¹H-NMR spectra of PYNO₂ in CDCl₃.

CHAPTER 4

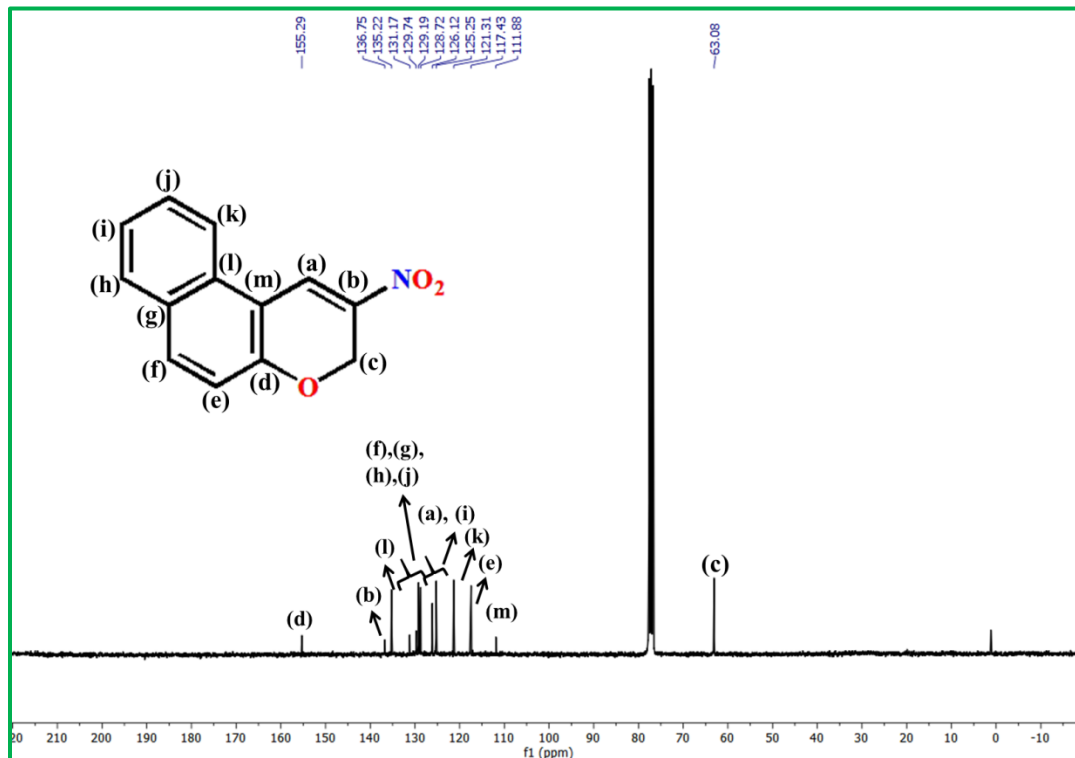


Figure 4.10(b). ¹³C-NMR spectra of PYNO₂ in CDCl₃.

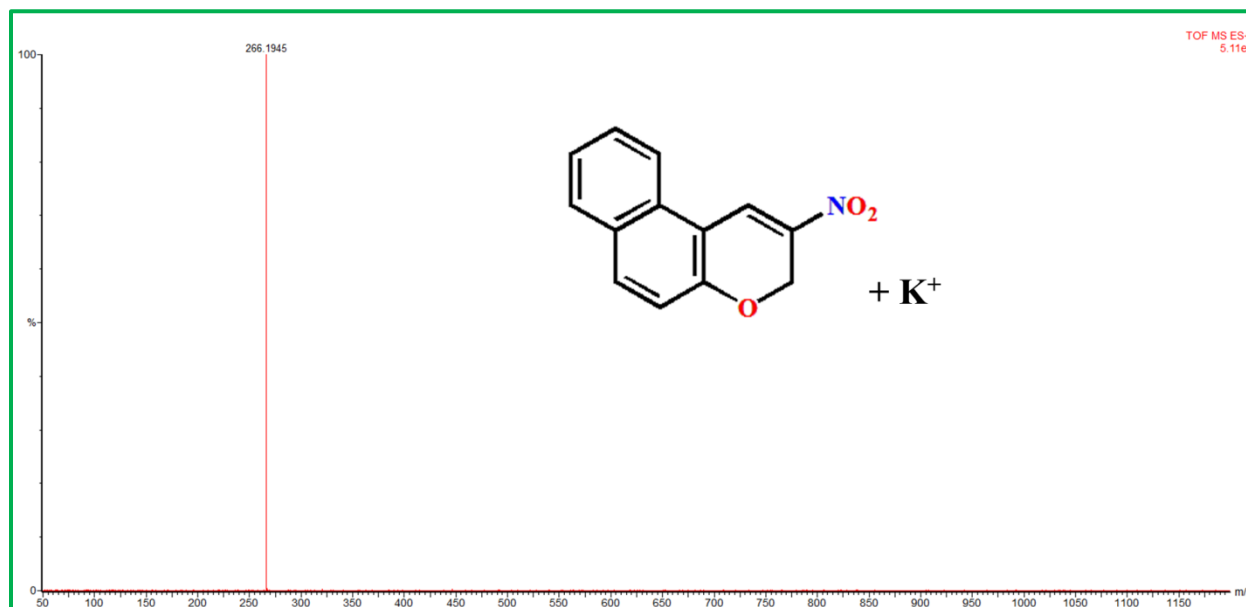


Figure 4.10(c). HRMS spectra of PYNO₂ in MeOH.

After complete separation of PYNO₂ in purified form, the polarity of the eluent was changed to 95% petroleum ether (petroleum ether: ethyl acetate = 95:5). As a result the next desired product

CHAPTER 4

PYMAA comes out in a purified form as a whitish yellow crystalline compound. Yield: ~19%. $C_{11}H_{13}NO_4$. Molecular Weight: 223.2252. 1H -NMR (300 MHz, $CDCl_3$) (δ , ppm): 8.70 (s, 1H, –ArH), 3.92 (s, 6H, – OCH_3), 2.85 (s, 6H, – CH_3) (**Figure 4.11(a)**). ^{13}C NMR (75 MHz, $CDCl_3$): 166.21, 162.63, 141.38, 122.62, 52.32, 24.93 (**Figure 4.11(b)**). ESIMS⁺ (m/z): (PYMAA+H⁺) 224.0988 (**Figure 4.11(c)**). IR stretching frequencies: 1720 cm^{-1} (–C=O stretching) (**Figure 4.6(b)**).

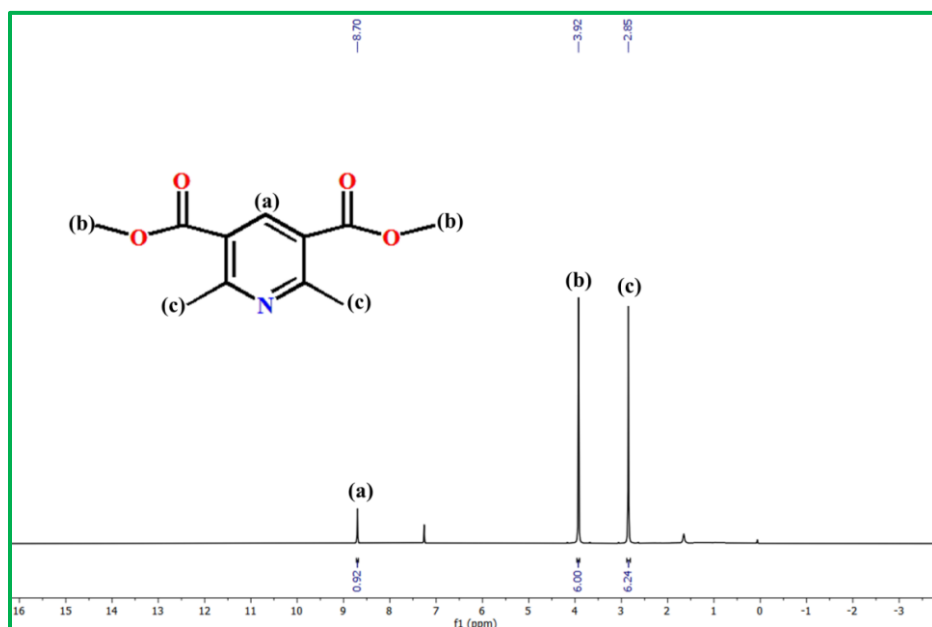


Figure 4.11(a). 1H -NMR spectra of PYMAA in $CDCl_3$.

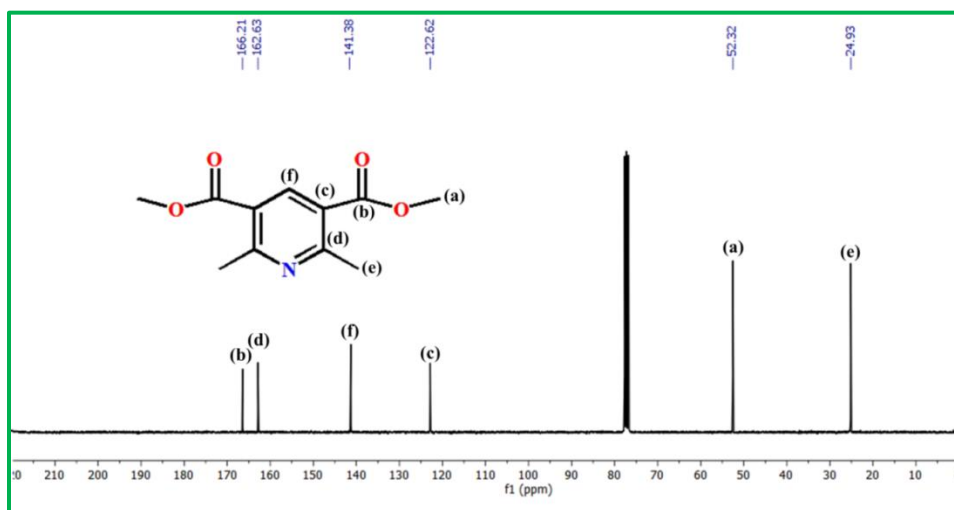


Figure 4.11(b). ^{13}C -NMR spectra of PYMAA in $CDCl_3$.

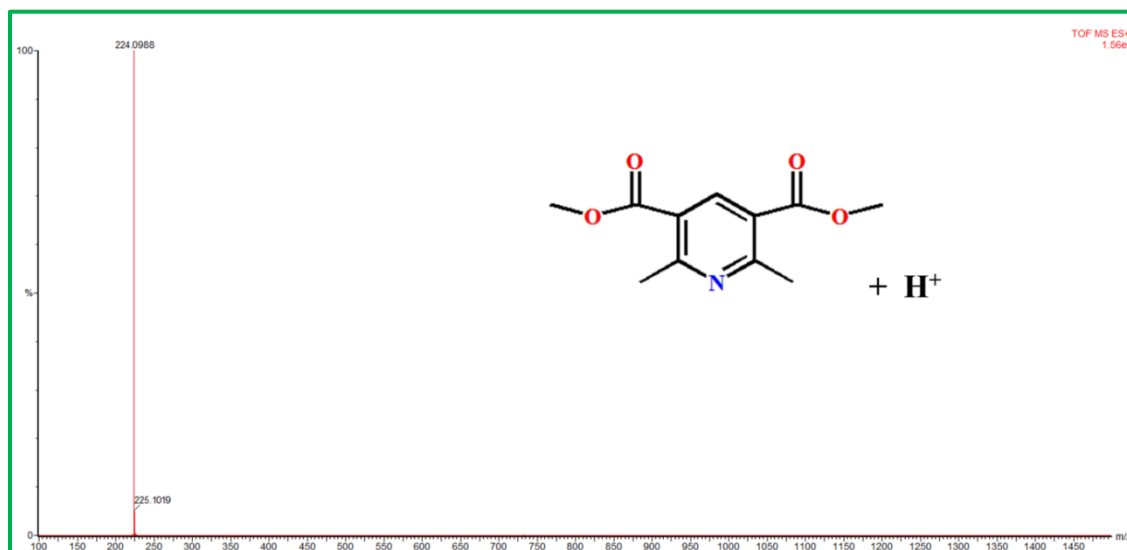


Figure 4.11(c). HRMS spectra of PYMAA in MeOH.

4.2.5.7 Synthesis of PYNO₂ and PYEAA from CQET

The same procedure as described for CQME has been followed for CQET. In case of CQET same type of products has been isolated one is PYNO₂ and the other is PYEAA.

PYNO₂ was obtained as an orange crystalline compound. Yield: ~19 %. C₁₃H₉NO₃. Molecular Weight: 227.2155. ¹H-NMR (300MHz, CDCl₃)(δ, ppm): 8.54 (s, 1H, -ArH), 8.00 (d, 1H, -ArH), 7.87 (d, 1H, -ArH), 7.81 (d, 1H, -ArH), 7.62 (t, 1H, -ArH), 7.46 (t, 1H, -ArH), 7.13 (d, 1H, -ArH), 5.38 (s, 2H, -ArCH₂) (Figure 4.10(a)). ¹³C NMR (75 MHz, CDCl₃): 155.29, 136.75, 135.22, 131.17, 129.74, 129.19, 128.72, 126.12, 125.25, 121.31, 117.43, 111.88, 63.08 (Figure 4.10(b)). ESIMS⁺ (m/z): (PYNO₂ + K⁺): 266.1945 (Figure 4.10(c)). IR stretching frequencies: 1502 cm⁻¹ and 1303 cm⁻¹ (-NO₂ stretching) (Figure 4.7(d)).

After column, PYEAA was obtained in pure form which is yellow crystalline in color. Yield: ~19 %. C₁₃H₁₇NO₄. Molecular Weight: 251.2784. ¹H-NMR (300 MHz, CDCl₃)(δ, ppm): 8.67 (s, 1H, -ArH), 4.42-4.35 (m, 4H, -CH₂), 2.86 (s, 6H, -CH₃), 1.41 (t, 6H, -CH₃) (Figure 4.12(a)). ¹³C NMR (75 MHz, CDCl₃): 165.98, 162.23, 140.93, 123.09, 61.42, 24.95, 14.28 (Figure 4.12(b)). ESIMS⁺ (m/z): (PYEAA + H⁺): 252.1801 (Figure 4.12(c)). IR stretching frequencies: 1716 cm⁻¹ (-C=O stretching) (Figure 4.7(d)).

CHAPTER 4

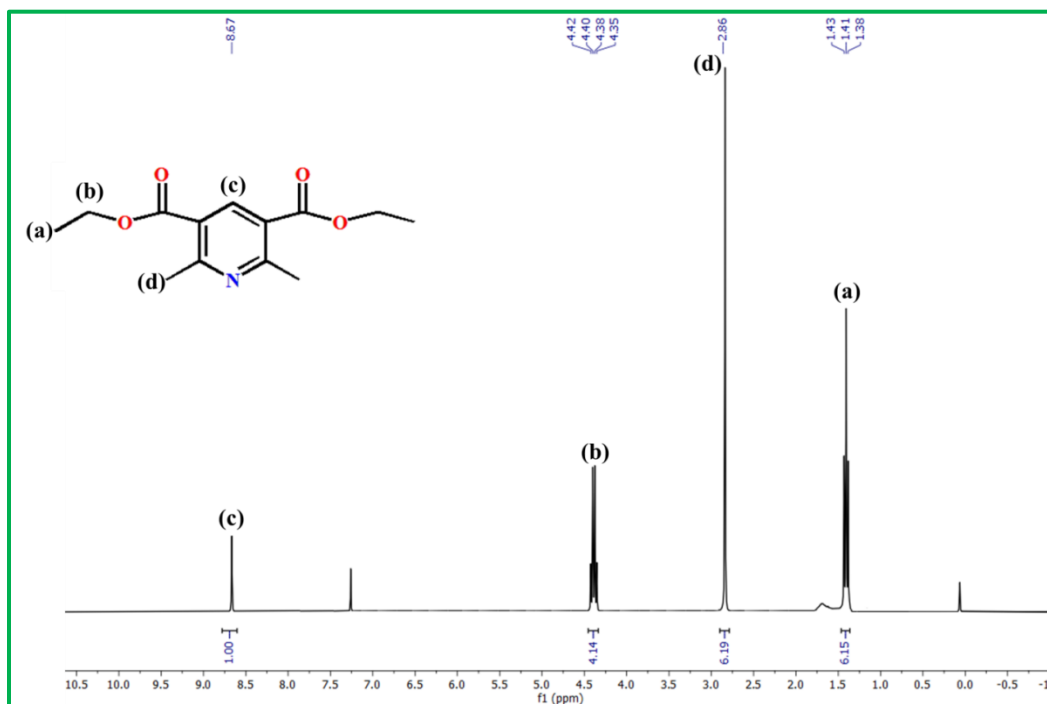


Figure 4.12(a). ¹H-NMR spectra of PYEAA in CDCl₃

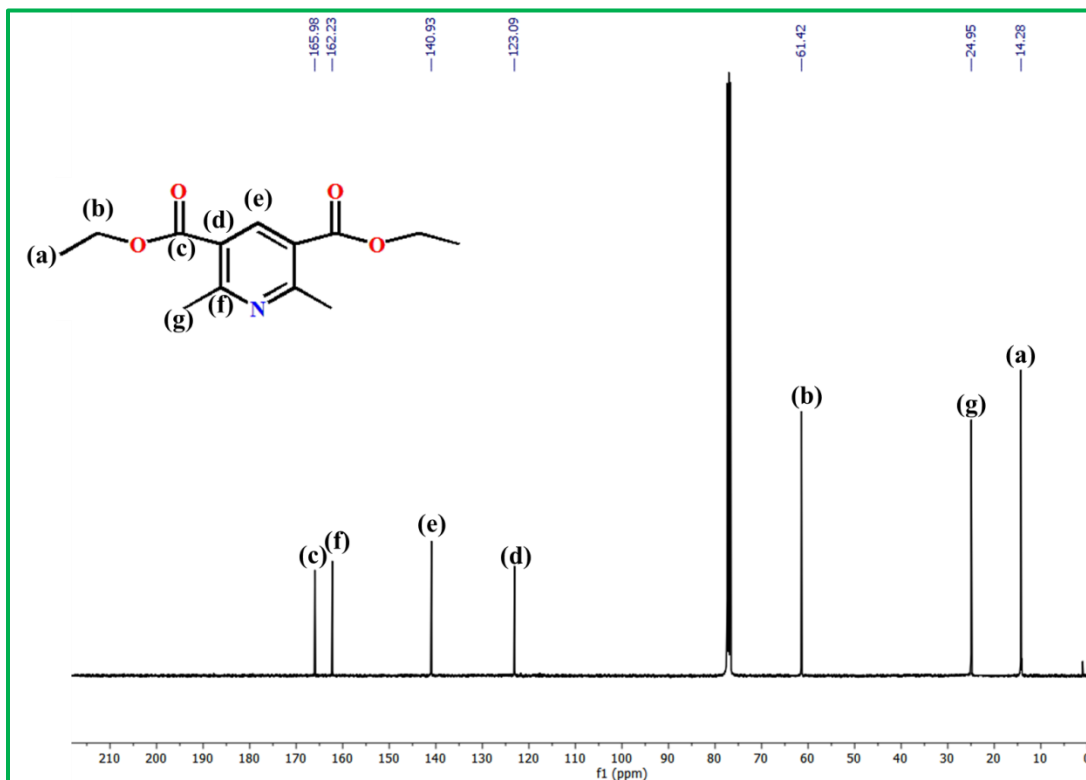


Figure 4.12(b). ¹³C-NMR spectra of PYEAA in CDCl₃

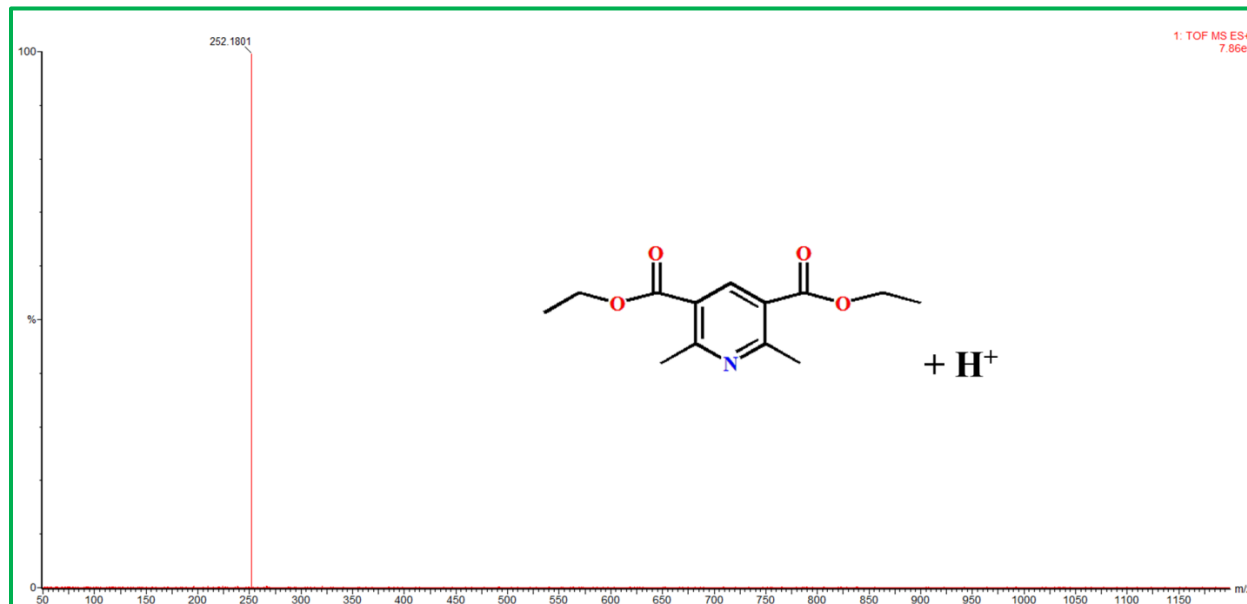


Figure 4.12(c). HRMS spectra PYEAA in MeOH.

4.2.5.8 Synthesis of SALPY

The same approach as delineated for CQET and CQME has been performed for SALDPY but the outcome of the reaction between NO and SALDPY contrast with both CQME and CQET. For SALDPY the major product is SALPY which is generated by following the normal aromatized reaction although there is at least a little bit cleaved products SALNO₂ and PYMAA are formed. SALPY, a whitish green compound is produced as the major product. Yield: ~50%. C₂₀H₁₉NO₅. Molecular Weight: 353.3686. ¹H-NMR (300 MHz, CDCl₃)(δ, ppm): 7.16 (dt, 1H, –ArH), 7.02 (dd, 1H, ArH), 6.91 (dd, 1H, –ArH), 6.87 (d, 1H, –ArH), 6.32 (s, 1H, –ArH), 4.79 (s, 2H, –ArCH₂), 3.82 (s, 6H, –OCH₃), 2.59 (s, 6H, –CH₃) (Figure 4.13(a)). ¹³C NMR (75 MHz, CDCl₃): 168.11, 156.66, 153.68, 143.83, 130.12, 129.92, 127.27, 126.11, 124.39, 122.14, 121.72, 115.65, 67.93, 52.70, 23.23 (Figure 4.13(b)). ESIMS⁺ (m/z): (SALPY + H⁺) 354.0667 (Figure 4.13(c)). IR stretching frequencies: 1730 cm⁻¹ (–C=O stretching) (Figure 4.9(d)). SALNO₂ and PYMAA have been formed by following the pathway that CQME and CQET follows. SALNO₂ is yellow in colour and it is generated as a minor product. Yield: 3%. C₉H₇NO₃. Molecular Weight: 177.1568. ¹H-NMR (300 MHz, CDCl₃)(δ, ppm): 7.79 (s, 1H, –ArH), 7.34 (t, 1H, ArH), 7.25 (t, 1H, –ArH), 7.01 (t, 1H, –ArH), 6.91 (d, 1H, –ArH), 5.26 (s, 2H, –ArCH₂) (Figure 4.14). IR stretching frequencies: (Figure 4.9(d)) A Spectroscopic detail of PYMAA is narrated in previous section. Yield: ~3%. IR stretching frequencies: (Figure 4.9(d))

CHAPTER 4

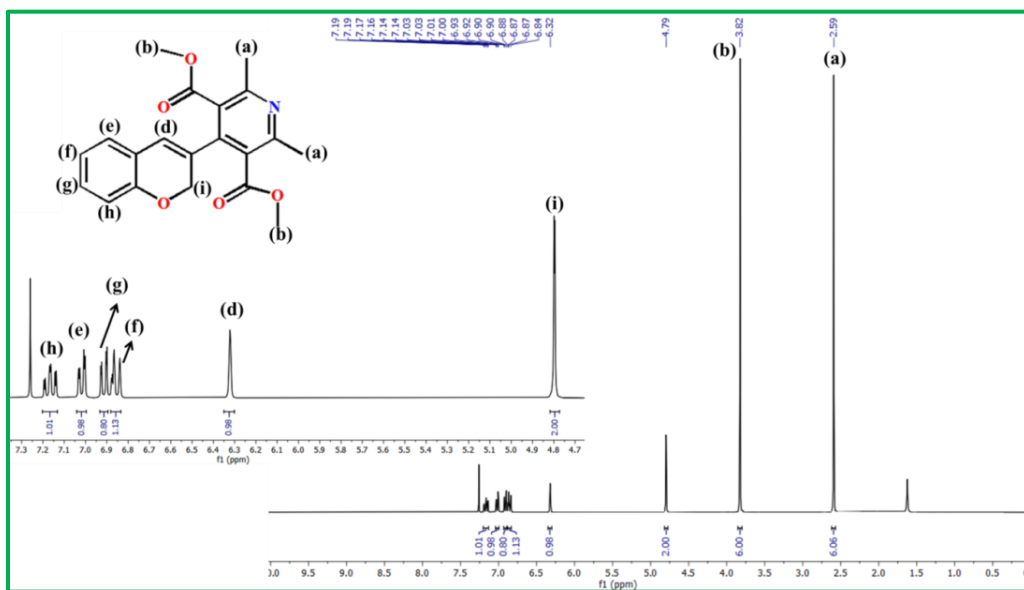


Figure 4.13(a). $^1\text{H-NMR}$ spectra of SALPY in CDCl_3 .

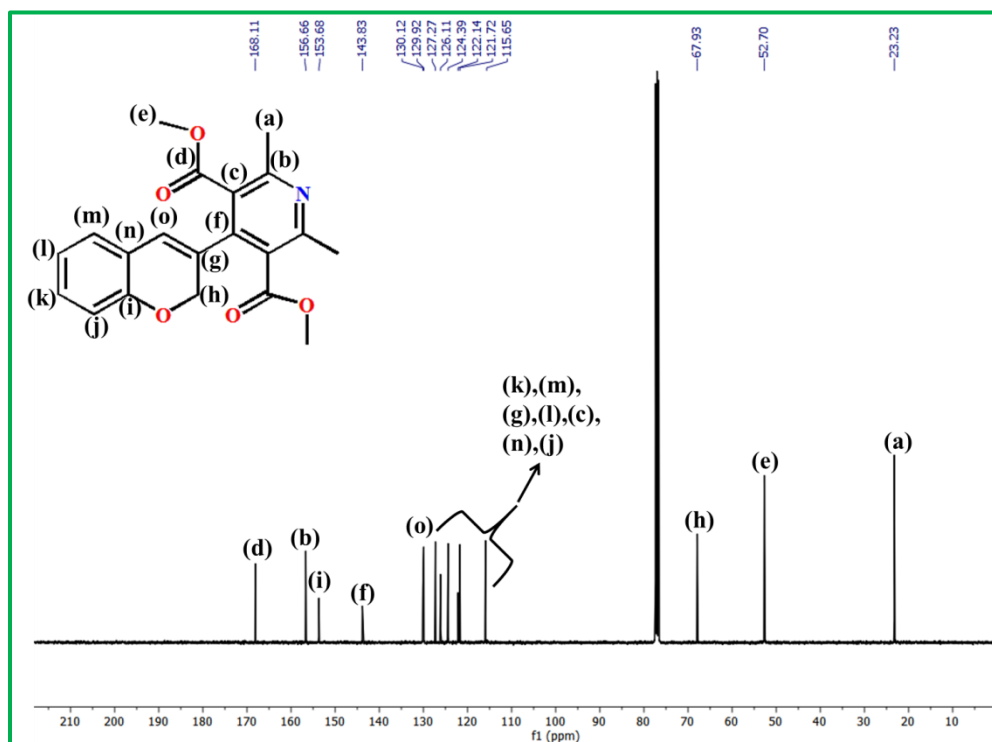


Figure 4.13(b). $^{13}\text{C-NMR}$ spectra of SALPY in CDCl_3 .

CHAPTER 4

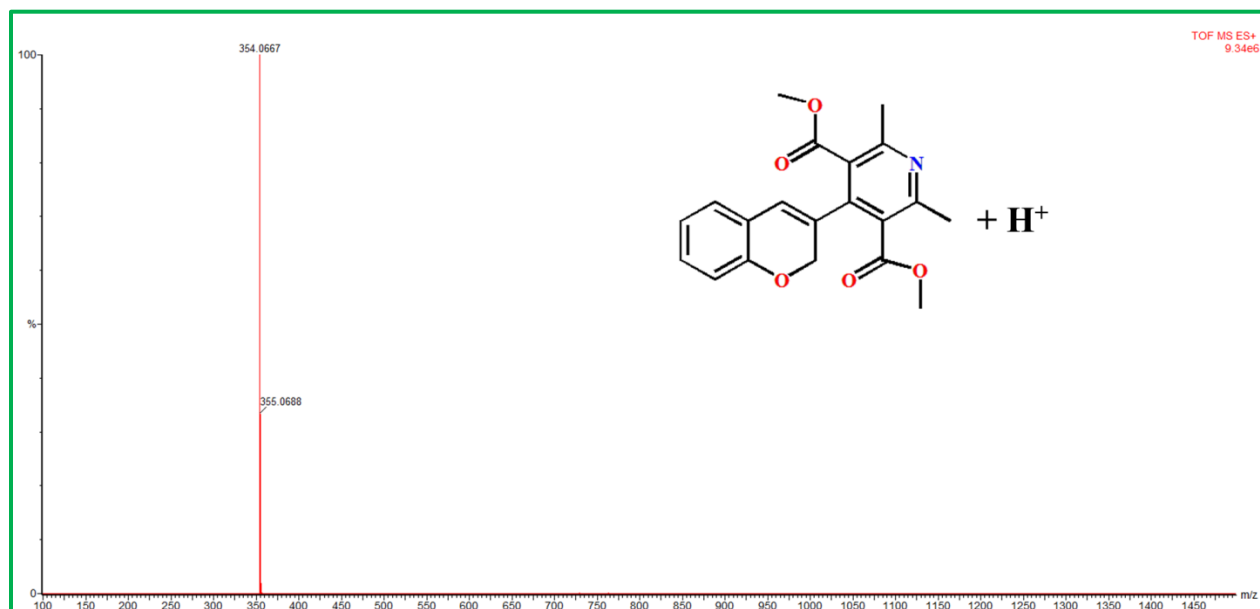


Figure 4.13(c). HRMS Spectra of SALPY in MeOH.

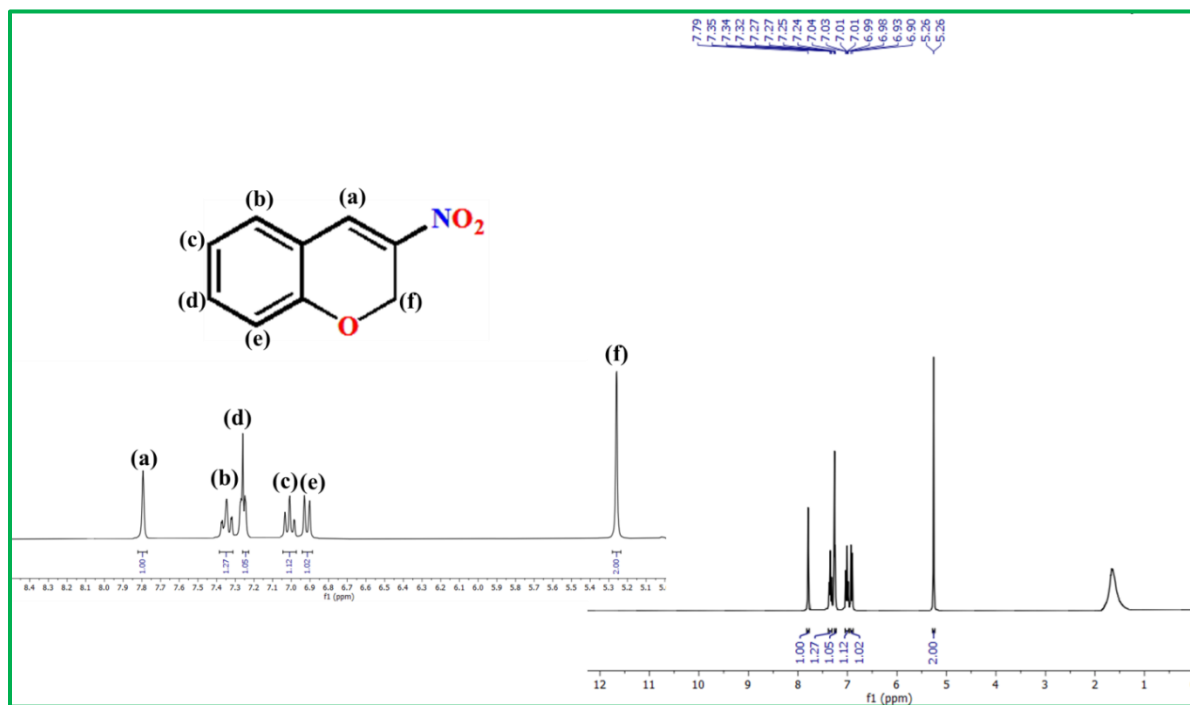


Figure 4.14. ¹H-NMR spectra of SALNO₂ in CDCl₃.

4.3 RESULTS AND DISCUSSION

Our synthetic strategy involves the formation of 3H-benzo [f] chromin-2-carbaldehyde (BZALD) from 2-hydroxy-1-naphthaldehyde in the presence of acrolein, followed by its condensation with methylacetoacetate in an ethanolic medium to produce CQME (**Scheme 4.5**). Both CQET and SALDPY were synthesized following the same synthetic procedure with the initial substrates benzochromene—ethylacetoacetate and chromene—methylacetoacetate, respectively. The formation of CQME is validated by $^1\text{H-NMR}$ (**Figure 4.4**), $^{13}\text{C-NMR}$ (**Figure 4.5**), HRMS (**Figure 4.6(a)**), FTIR (**Figure 4.6(b)**) and X-ray crystallographic analysis (**Figure 4.15(a)**).

4.3.1 Crystal structure of CQME and PYNO₂

The pure compounds were dissolved in dichloromethane and allowed a slow evaporation that led to the formation of needle shaped single crystals for CQME and flake shaped single crystals for PYNO₂. The crystal data were collected in X-ray spectroscopy and the data was analyzed utilizing OLEX2 software.

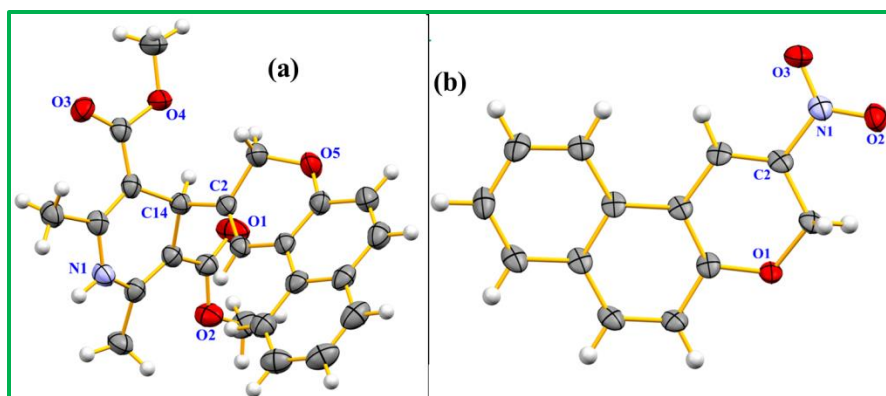


Figure 4.15. X-ray crystallographic structure of (a) CQME; and (b) PYNO₂.

Table 4.1. Crystallographic data and details of the structure determination for CQME and PYNO₂

Identification code	CQME	PYNO ₂
Empirical formula	C ₂₄ H ₂₃ NO ₅	C ₁₃ H ₉ NO ₃
Formula weight	405.43	227.21
Temperature/K	145.0	100.0

CHAPTER 4

Crystal system	monoclinic	monoclinic
Space group	P 21/c	P21/n
a/Å	15.933(3)	8.1352(2)
b/Å	10.902(2)	6.3468(2)
c/Å	11.833(2)	19.8559(6)
α /°	90	90
β /°	79.85(3)	96.6300(10)
γ /°	90	90
Volume/Å ³	2023.3(7)	1018.35(5)
Z	4	4
$\rho_{\text{calc}}/\text{g}/\text{cm}^3$	1.331	1.482
μ/mm^{-1}	0.093	0.888
F(000)	856.0	472.0
Crystal size/mm ³	-	-
Radiation	MoK α ($\lambda = 0.71073$)	CuK α ($\lambda = 1.54178$)
2 θ range for data collection/°	2.274 to 24.999	6.153 to 68.199
Index ranges	-18 \leq h \leq 18, -12 \leq k \leq 12, -14 \leq l \leq 14	-9 \leq h \leq 9, -7 \leq k \leq 7, -23 \leq l \leq 23
Reflections collected	20093	16287
Independent reflections	3561 [R _{int} = 0.1002, R _{sigma} = 0.0516]	1856 [R _{int} = 0.0816, R _{sigma} = 0.0803]
Data/restraints/parameters	3561/0/279	1856/0/154
Goodness-of-fit on F ²	1.002	1.38

4.3.2 Absorption and emission spectra

The photophysical properties of CQME (20 μM) and PYNO₂ (60 μM) were investigated to assess the response of the probe (CQME) towards NO in 10 mM HEPES buffer (pH 7.20, $\mu = 0.10$ M NaCl, containing 50% MeCN at 25°C), utilizing UV/Vis and fluorescence spectroscopies. CQME exhibits the maximum absorption band at 355 nm, whereas the UV/Vis absorption peak for the isolated pure PYNO₂ appears at 440 nm with 85 nm red shift compare to CQME (**Figure 4.16(a)**). The NO-mediated cleavage of the C-C bond of CQME, followed by aromatization, generates PYNO₂ and also the corresponding pyridine unit (PYMAA). Therefore, as shown in **Figure 4.16(b)**, the UV/Vis absorption humps for isolated PYMAA (60 μM) are centered at 200 nm, 276 nm and 384 nm, indicating the presence of an aromatized unit.³⁴

CHAPTER 4

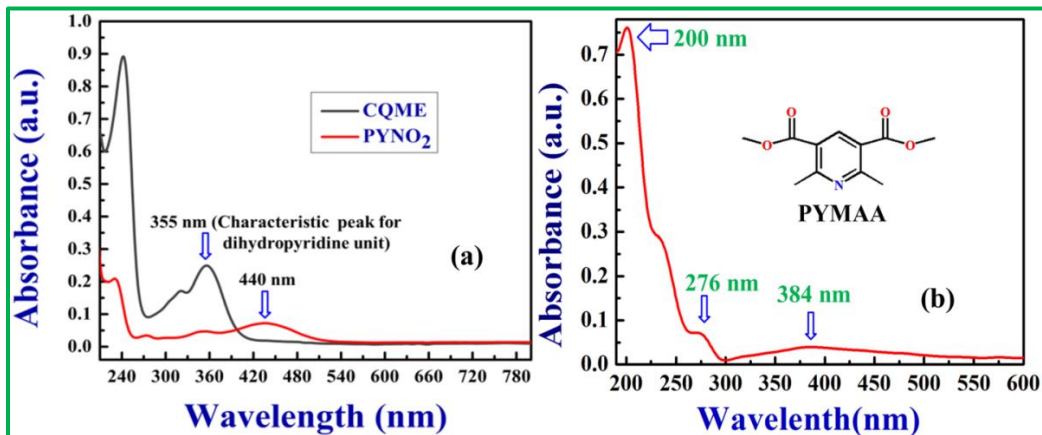


Figure 4.16. (a) UV-vis absorption spectra of CQME (20 μM), PYNO₂ (60 μM) and (b) PYMAA (60 μM) in 10 mM HEPES buffer (pH 7.20, $\mu = 0.10$ M NaCl, containing 50% MeCN at 25°C). All the adsorption studies were carried out by preparing 10^{-3} M solutions of CQME, PYNO₂ and PYMAA in pure form.

The UV-Vis titration for the reaction between CQME and NO could not be performed due to the interference by N_2O_3 formed by the reaction: $\text{NO} + \text{O}_2 \rightarrow \text{N}_2\text{O}_3$. However, the fluorescence titration of CQME with NO was performed without any interference from N_2O_3 produced in the reaction medium in the presence of dissolved oxygen. Thus the variation in the spectral signature of the probe (CQME) with consecutive additions of NO was investigated fluorimetrically upon excitation at 470 nm (3 X 3 slits). As anticipated, the probe (20 μM) itself displays very weak fluorescence. However, the incremental addition of NO (0-73 μM) leads to the NO-mediated cleavage of the C-C bond of CQME, resulting ~ 30 fold enhancement in the emission intensity at 615 nm (**Figure 4.17(a)**). Now, the fluorescence intensity (F.I.) was plotted against [NO] to evaluate the magnitude of K_f (the apparent formation constant) for the reaction between CQME and NO (**Figure 4.17(b)**). It was observed that in the concentration range 3.48 μM to 31.32 μM , the fluorescence intensity of the probe maintained a good linearity ($R^2 = 0.9937$) with respect to [NO] at 615 nm. The linear form of **eqn. 2** where $1 \gg c \cdot x$ with $n = 1$ provides $c = K_f$ (**eqn. 3**) by considering a and b as Fluorescence intensities of CQME and the fluorescent product (PYNO₂) generated on its reaction with NO ($\geq 73 \mu\text{M}$), and the evaluated value is $K_f = (2.85 \pm 0.03) \times 10^4 \text{ M}^{-1}$.

CHAPTER 4

$$Y = \frac{a + b \times c \times x^n}{1 + c \times x^n} \dots\dots\dots(2)$$

$$Y = a + b \cdot c \cdot x. \quad (3)$$

As anticipated, the emission peak of an isolated pure PYNO₂ matches well with that of *in situ* generated PYNO₂, indicating the fact that the formation of PYNO₂ is responsible for initiating the turn-on fluorescence response at 615 nm (**Figure 4.18(a)**). Now, to determine the sensitivity of CQME towards NO, the *limit of detection* (LOD) was determined by employing 3σ/slope method which was evaluated to be ~42 nM, manifesting its high sensitivity to track both endogenous and exogenous NO in living organisms (**Figure 4.18(b)**).

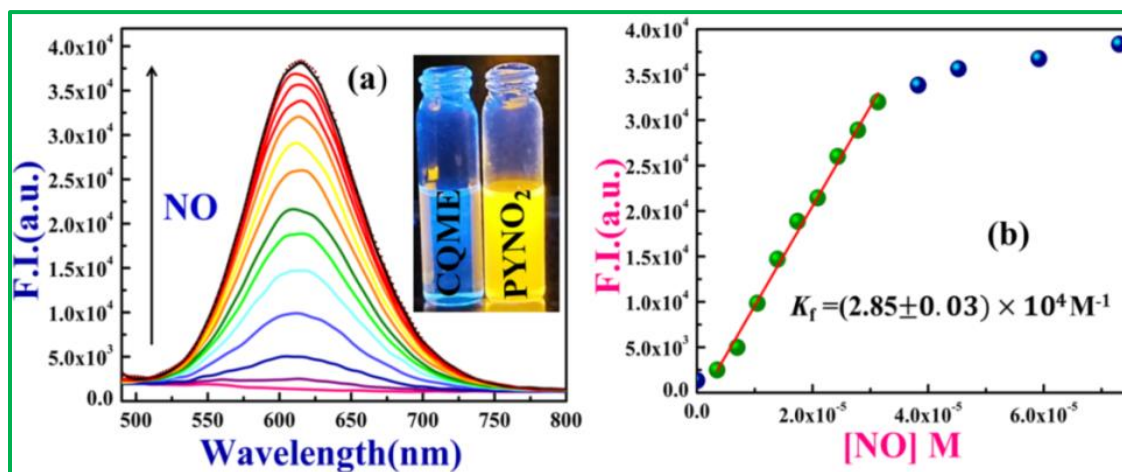


Figure 4.17. (a) Fluorescence titration ($\lambda_{\text{ex}} = 470 \text{ nm}$, $\lambda_{\text{em}} = 615 \text{ nm}$) of $20 \mu\text{M}$ CQME upon addition of increasing concentration of NO ($0 - 73 \mu\text{M}$) in 10 mM HEPES buffer ($\text{pH } 7.20$, $\mu = 0.10 \text{ M}$ NaCl containing 50% MeCN at 25°C); and (b) The plot of fluorescence intensity vs. [NO] at 615 nm .

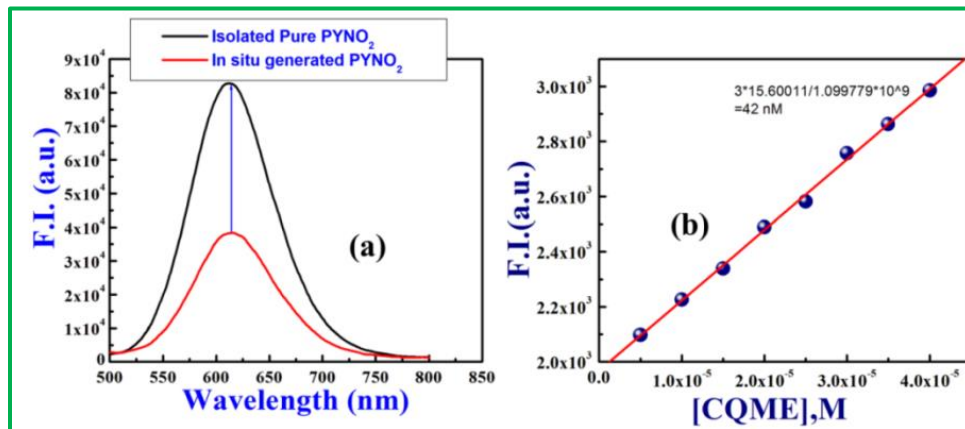


Figure 4.18. (a) Fluorescence spectra of in-situ generated PYNO₂ and isolated pure PYNO₂; (b) Limit of detection of CQME.

4.3.3 Comparison of reactivity of CQME, CQET and SALDPY towards NO

The fluorimetric analysis of CQME by incremental additions of NO in a 10 mM HEPES buffer (pH 7.20, $\mu = 0.10$ M NaCl containing 50% MeCN) clearly manifests a strong interaction between CQME and NO that leads to a generation of a new emission peak at 615 nm. To ascertain the mode of interaction the detail product analysis was performed for CQME, CQET and SALDPY (**Scheme 4.4**). For this purpose, NO gas was allowed to flow through a dry DCM solution of CQME for more than 15 minutes under aerobic conditions, resulting in an intense fluorescence in the amber region. Consequently, this yellowish orange colored solution was washed with a saturated solution of NaHCO₃ and brine mixture and then dried over anhydrous Na₂SO₄. After filtration, it was subjected to evaporation followed by purification using column chromatography to yield the desired product responsible for the enhancement in emission intensity at 615 nm. The formation of PYNO₂ and PYMAA is confirmed by ¹H-NMR (**Figure 4.10(a) and 4.11(a)**), ¹³C-NMR (**Figure 4.10(b) and 4.11(b)**), HRMS (**Figure 4.10(c) and 4.11(c)**) and IR spectroscopy (**Figure 4.6(b)**). The structural framework of CQME and PYNO₂ were further confirmed by X-ray crystallographic studies (**Figure 4.15**). The ¹H-NMR spectra of both PYNO₂ and CQME display the allylic proton of CQME shifts to 8.54 ppm from 6.81 ppm, indicating the presence of a highly electron withdrawing nitro group (-NO₂) in the benzochromene entity. Moreover, the absence of all the protons of dimethyl 2,6-dimethyl-1,4-dihydropyridine-3,5-dicarboxylate entity strongly justifies the unprecedented NO-mediated cleavage of the C-C bond of CQME. The ¹³C-NMR spectra of PYNO₂ even more clearly delineates the absence of pyridine entity, whereas the ¹H-NMR and ¹³C-NMR spectra of

PYMAA reveal the origin of the pyridine constituent from the C-C bond cleavage of CQME and subsequent aromatization pathway. Again, this structural transformation of CQME on treatment with NO was further confirmed by HRMS studies. The peaks at m/z 266.1945 [PYNO₂+K⁺] and 224.0988 [PYMAA+H⁺] are consistent with PYNO₂ and PYMAA, respectively. In the case of CQME, the -NH stretching frequency appears at 3350 cm⁻¹ but upon exposure to NO, the -NH stretching band disappears for both PYNO₂ and PYMAA, respectively, validating the above-mentioned sensing mechanism of CQME. Now, these entire spectroscopic observations manifest that the probe CQME undergoes aromatic nitration assisted C-C single bond cleavage, followed by the aromatization pathway to produce PYMAA and PYNO₂ as the major components instead of a simple aromatization. The similar results were also obtained for CQET—NO reaction indicating the NO-mediated C-C bond cleavage as the major pathway. When the same reaction was performed with SALDPY the normal aromatized product (SALPY) was formed as the major one with SALNO₂ and PYMAA as the minor products. Herein, to obtain SALPY, SALNO₂, and PYMAA in pure form, the identical synthetic procedure was followed as in case of CQME. The ¹H-NMR spectra of SALPY reveals a slight shifting of the allylic proton peak from 6.08 ppm to 6.32 ppm, validating the formation of a normal aromatized product (**Figure 4.9(a) and 4.13(a)**). The ¹³C-NMR spectra of SALPY (**Figure 4.9(b) and 4.13 (b)**) and also the generation of a new peak at m/z 354.0667 [SALPY+H⁺] (**Figure 4.13(c)**) in HRMS analysis, indicate the formation of a normal aromatized product. The origin of SALPY from SALDPY is also supported by IR spectroscopic technique (**Figure 4.9(d)**). However, for SALNO₂ (**Figure 4.14**), the allylic proton shifts its position from 6.08 ppm to 7.79 ppm, similar to PYNO₂. This clearly manifests that the nitro group (-NO₂) is conjoined within the chromene moiety. The ¹³C-NMR spectra are not possible for SALNO₂ as it is formed in extremely low amount. All the spectroscopic studies lead to the conclusion that CQME favors the aromatic nitration assisted C-C single bond cleavage, followed by the aromatization pathway to produce PYMAA and PYNO₂ as the major components, whereas SALDPY prefers the canonical aromatization reaction as the major one.

4.3.4 Mechanistic Insights describing the difference in reactivity of NO towards CQME, CQET, and SALDPY

For both CQME and SALDPY, the reaction is initiated either by a simple electron transfer from the probe (**1 and 8**) towards NO to produce an ammoniumyl radical (**2 and 9**), or through the

CHAPTER 4

abstraction of -NH proton from the dihydropyridine entity. Both the pathways (**Figure 4.19**) support the formation of an aminyl radical (**3a and 10**). This aminyl radical is capable to delocalize upto the oxygen end of the methylester (**3a \leftrightarrow 3b \leftrightarrow 3c**) through resonance. Now, in case of CQME due to the presence of benzochromene unit, the rotation about the pivotal bond between the benzochromene and dimethyl 2,6-dimethyl-1,4-dihydropyridine-3,5-dicarboxylate moieties is somehow restricted. As a consequence, the $\bullet\text{O}$ radical on the methyl ester group (**3c**) comes closer to the allylic double bond of benzochromene moiety leading to the formation of intermediate **4** which is conjoined with the nitro radical in the next step. The excessive steric crowding between the nitro group and the methylester moiety, originated in the intermediate (**5**) facilitates the cleavage of the C-C bond leading to the formation of PYNO_2 (**6**) and PYMAA (**7**) as the major products in 1:1 ratio (yield 20%).

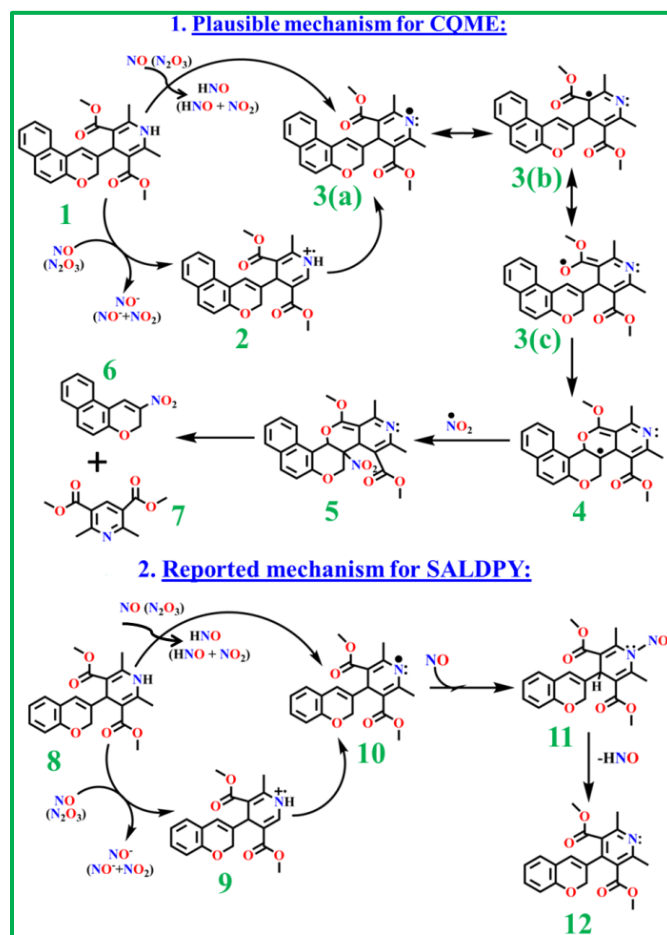


Figure 4.19. Probable reaction mechanism of CQME and SALDPY on treatment with NO at room temperature.

Meanwhile, for SALDPY, coupling of aminyl radical (10) with NO leads to the formation of N-nitroso derivative (11), which in the subsequent step undergoes aromatization to generate SALPY (50%) as the major product (12) through the elimination of HNO. However, SALDPY also follows the abnormal pathway to yield SALNO₂ and PYMAA as the minor components in extremely low yield (3%) (Scheme 4.4(c)).

4.3.5 Selectivity studies

The selectivity response of CQME towards NO was investigated to check the interferences imposed by the various interfering species present in the complicated biological systems. These interfering species are categorized as (a) Reactive carbon/oxygen/nitrogen species like ascorbic acid (AA), TEMPO, OCl⁻, KO₂, H₂O₂, •OH, ONOO⁻, NO₂⁻, NO₃⁻ etc, (b) cations, or (c) anions. Now, the variation in the spectral signature of CQME (20 μM) was analyzed utilizing these species in excess (200 μM) in 10 mM HEPES buffer (pH 7.2, containing 50% CH₃CN, at 25°C). As expected, the presence of these biologically reactive species does not exhibit any remarkable spectral changes in emission intensity of the probe at 615 nm (Figure 4.20(a)). The spectral response of CQME towards various reactive species has also been checked by UV/Vis analysis under identical reaction conditions (Figure 4.20(b)). Likewise, to ensure whether various cations and anions have any possible interference towards the spectral signature of CQME, the selectivity analysis of CQME were carried out with various cations and anions under identical conditions (Figure 4.21(a), (b)). There were no characteristic changes in fluorescence intensity as observed in case of NO. To further strengthen the specificity of the probe towards NO, the over-selectivity analysis of CQME was performed utilizing various biological reactive species in presence of NO which reveals that the extent of enhancement in fluorescence intensity is very close to that observed in the sole presence of excess of NO except TEMPO (2,2,6,6-Tetramethylpiperidine 1-oxyl). The inability of CQME to detect NO in the presence of TEMPO strongly favors a free radical reaction mechanism operating between the probe (CQME) and NO (Figure 4.21(c)). All of these analyses enlightened the superiority of the probe (CQME) for tracking both endogenous and exogenous NO selectively in living organisms.

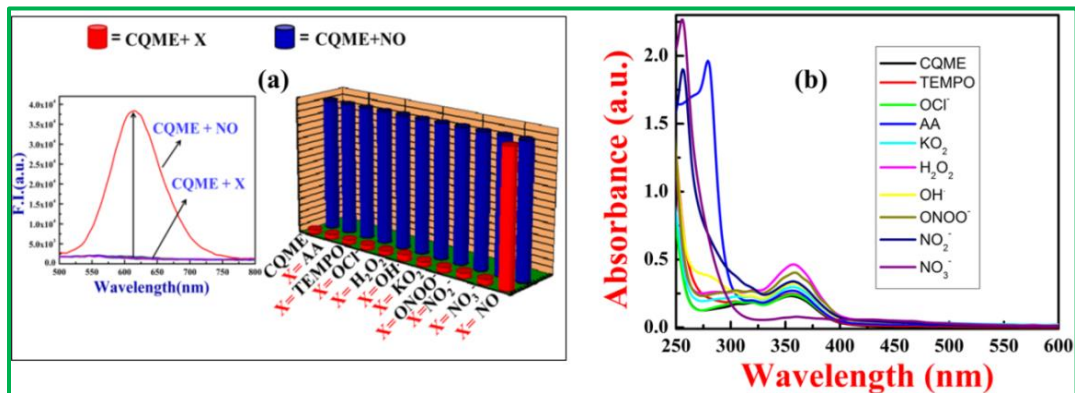


Figure 4.20. (a) Fluorescence ($\lambda_{\text{ex}} = 470 \text{ nm}$ and Bar plot at 615 nm); (b) UV-vis absorption spectra for the probe CQME toward various reactive species recorded in HEPES buffer (10 mM, pH 7.2, containing 50% CH₃CN at 25°C) CQME = 20 μM , X = 200 μM .

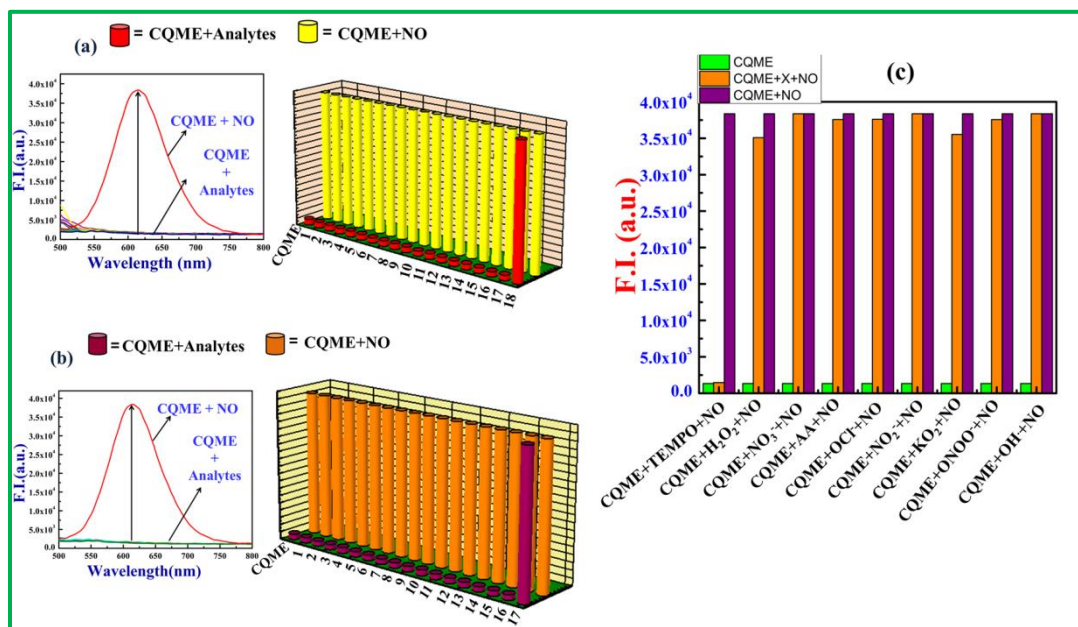


Figure 4.21. (a) Fluorescence response of the probe CQME towards various cations (1:Cu²⁺; 2:Co²⁺; 3:Zn²⁺, 4:Hg²⁺, 5:Fe²⁺, 6:Fe³⁺, 7:Cr³⁺, 8:Mn²⁺, 9:Al³⁺, 10:Mg²⁺, 11:NH₄⁺, 12:Ca²⁺, 13:Ni²⁺, 14:Pb²⁺, 15:Ca²⁺, 16:Na⁺, 17:K⁺, 18:NO); (b) anions (1:ClO₄⁻, 2:N₃⁻, 3:HSO₄⁻, 4:Γ⁻, 5:S₂O₄²⁻, 6:F⁻, 7:CH₃COO⁻, 8:SCN⁻, 9:H₂PO₄⁻, 10:PO₄³⁻, 11:BrO₃⁻, 12:Cl⁻, 13:Br⁻, 14:S₂O₃⁻, 15:CNS⁻, 16:SH⁻, 17:NO) where CQME = 20 μM , X = 100 μM , $\lambda_{\text{ex}} = 470 \text{ nm}$ and the Bar plot at 615 nm; and (c) The over selectivity of CQME (20 μM) towards NO in 10 mM HEPES buffer (pH 7.20, $\mu = 0.10 \text{ M NaCl}$, containing 50% MeCN at 25°C) in presence of various reactive species.

4.3.6 Reaction Kinetics

In addition, we have analyzed the Time-dependent fluorescence response of CQME at 25°C, where, upon treatment with NO (3.6 equivalent), the fluorescence intensity of the probe increased immediately and the corresponding growth curve at 615 nm achieved a plateau nature within 40 min (**Figure 4.22(a), (b)**). The time dependent fluorescence response of CQME is also influenced with the concentration of NO. With increasing the concentration of NO, the fluorescence intensity versus time profile analysis reveal the steeper nature of the curve indicating an increase in the rate of the reaction. This curve also illustrates that once a plateau is achieved the fluorescence intensity of the probe remains unaffected indicating the higher photo stability of PYNO₂ for more than 1 hour (**Figure 4.22(c)**).

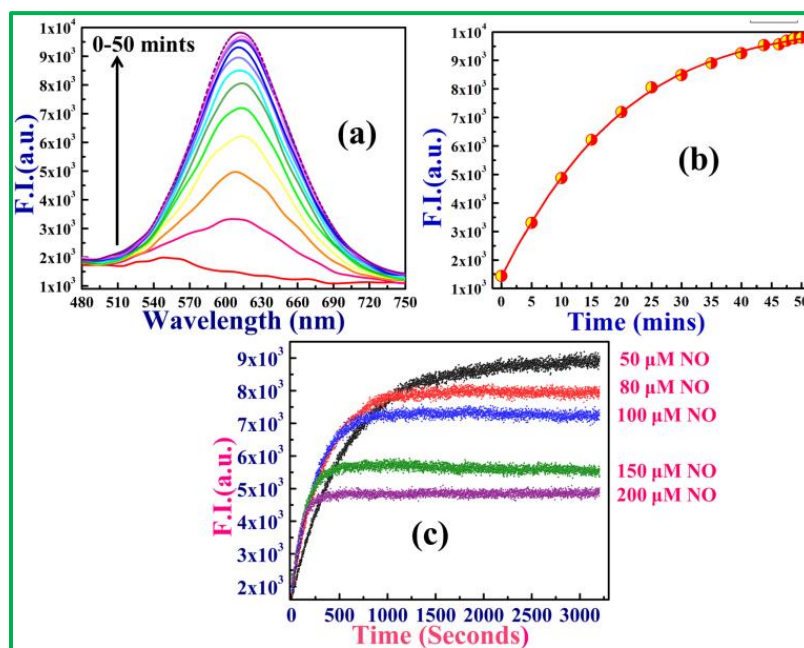


Figure 4.22. (a) Spectral changes of CQME in fluorescence over time (0-50 mins) upon addition of NO (3.6 equivalent) in 10 mM HEPES buffer (pH 7.2, containing 50% CH₃CN) at 25°C; (b) The corresponding kinetic growth plot at 615 nm; (c) The Kinetic traces of CQME (5 μM) in 10 mM HEPES buffer (pH 7.2, containing 50% CH₃CN) at 25°C after addition of NO (50, 80, 100, 150, 200 μM).

4.3.7 pH study

Next, we analyzed the fluorescence response of CQME towards NO over a wide range of pH (2-12). The biocompatibility of a good NO sensitive probe relies on its pH tolerance over a wide range. The practical application of this newly designed NO sensitive probe (CQME) was evaluated by performing the effect of pH on its fluorescence intensity both in presence and absence of NO. As shown in **Figure 4.23**, the FI steeply increases with the increase in pH in the range 2-4 and then attains plateau and remains almost constant in the range pH 5-7. On further increase in pH the FI decreases rapidly with increase in pH and becomes almost constant in the range pH 10-12. Initial increase in FI with the increase in pH may be due to the involvement of proton equilibrium $\text{DIPY-NH} + \text{H}^+ \rightarrow \text{DIPY-NH}_2^+$ ($1/K_a^1$) while in the pH range 8-12, the protic equilibrium $\text{DIPY-NH} \rightarrow \text{DIPY-N}^- + \text{H}^+$ (K_a^2) will be operative. Both DIPY-NH_2^+ and DIPY-N^- disfavors the reaction between the probe and NO, as a consequence we observe lower FI both in the lower pH range ($\text{pH} \leq 4.0$) and higher pH range ($\text{pH} \geq 8.0$) as the formation of aminyl radical is not feasible to generate the desired product (PYNO_2).

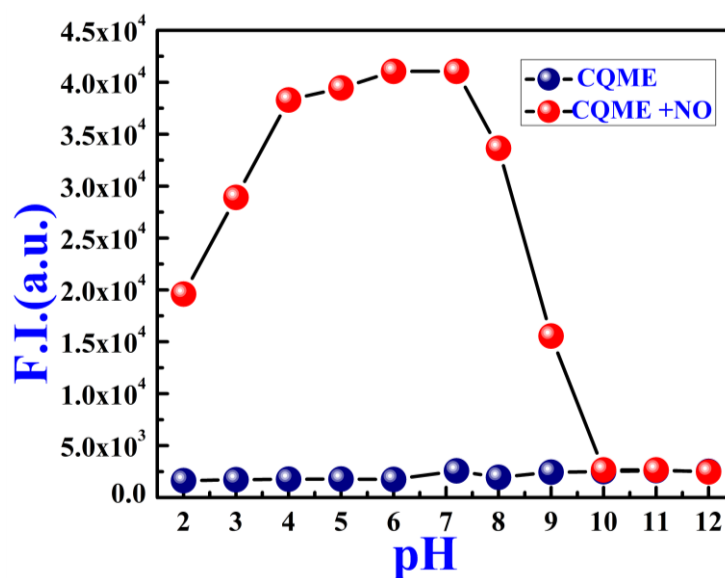


Figure 4.23. pH (2-12) tolerance of CQME and its reaction mixture on addition of 3.6 equivalent of NO at 25°C.

However, the pH experiment delineates no remarkable change in fluorescence intensity for CQME but there is an elevation in fluorescence intensity at 615 nm on addition of NO over the pH range from 2 - 9, proposing that CQME is able to sense NO in weakly acidic, neutral and

even in weakly basic medium. The unaltered fluorescence intensity of CQME over a wide pH range strongly manifests the generation of remarkable fluorescence intensity in cells is predominantly from intracellular NO (both endogenous and exogenous).

4.3.8 Cell imaging studies (Exogenous and Endogenous) in Live Cells

Prior to the application of the probe CQME to track both endogenous and exogenous NO in living organisms, the cellular toxicity of CQME was investigated in A549 and Raw 264.7 cells by executing MTT (3-(4,5-dimethylthiazol-2-yl)-2,5-diphenyltetrazolium bromide) assay. On incubation of CQME (0-70 μM) for 24 hour, more than 80% of the cells are still alive (Figure 4.24).

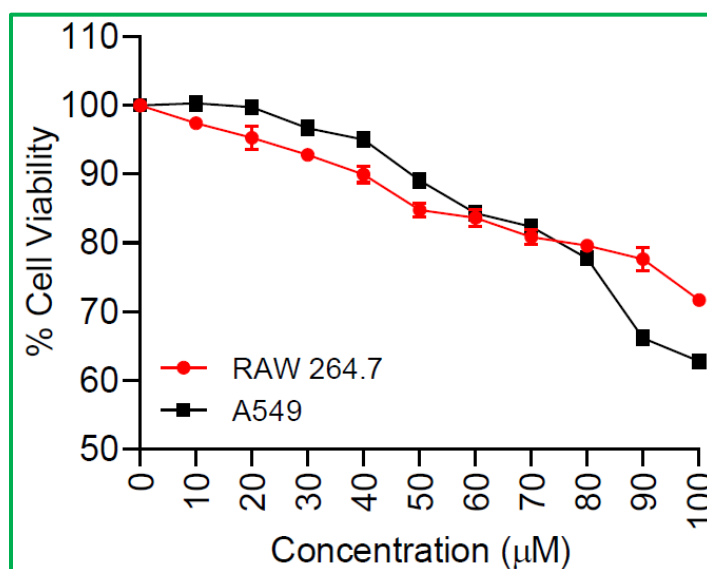


Figure 4.24. Graphical representation of Cell Viability Assay performed by using probe CQME.

The least cytotoxic effect of CQME towards cell enhances its applicability for detecting both endogenous and exogenous NO in living cells. Consequently, the well tolerance of cells towards CQME strongly supports its biocompatibility. To demonstrate whether CQME is able to detect endogenous NO, fluorescence microscopic analysis were performed utilizing Raw 264.7 cells where, LPS (1.0 mg/mL) and IFN- γ (1000 U/mL) were co-stimulated for 4 hours, since they are responsible for endogenous NO generation, and then treated with 5 μM CQME. As anticipated, the stimulated cells exhibit an intense yellowish orange fluorescence compared to the

CHAPTER 4

unstimulated one (**Figure 4.25**). The further incubation with PTIO (the NO scavenger, 200 mM) for 4 h in presence and absence of LPS + IFN- γ co-stimulus and then the administration with (5 μ M) CQME for 30 min did not show the significant generation of fluorescence in the amber region.

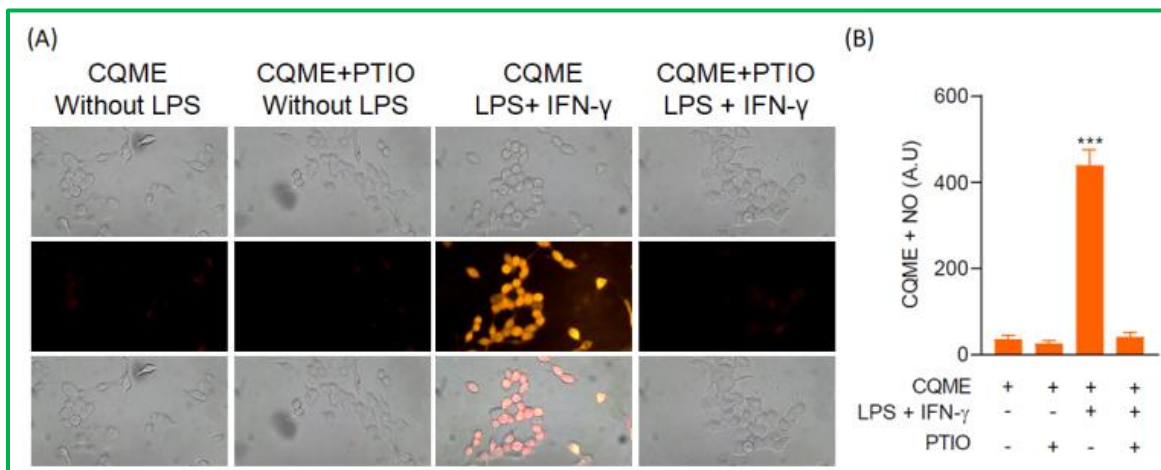


Figure 4.25. (A) Fluorescence cell image of Raw 264.7 cells stimulated with LPS (1.0 mg/mL) + IFN- γ (1000 U/mL) with or without iNOS inhibitor PTIO (200 mM) for 4h followed by CQME (5 μ M) for 30 min. Intracellular yellowish orange fluorescence was observed in response to NO interaction with CQME and all the Images were obtained at 40X objective. (B) Quantified fluorescence (Mean \pm SD) turn-on in Raw 264.7 cells after stimulation with LPS (1.0 mg/mL) and IFN- γ (1000 U/mL) for 4h in presence of CQME (5 μ M) with or without iNOS inhibitor PTIO compared to control. (a.u.) = Arbitrary unit.

This strongly manifests the generation of endogenous NO and its recognition by CQME (**Figure 4.25(A),(B)**). Now, DEA-NONOate is exploited as a NO donor for exogenous determination of NO in A549 cells. Initially, the cells were incubated with CQME followed by an incremental addition of DEA-NONOate (5 μ M and 10 μ M) resulting in a remarkably gradual increase in fluorescence intensity at amber region (**Figure 4.26**).

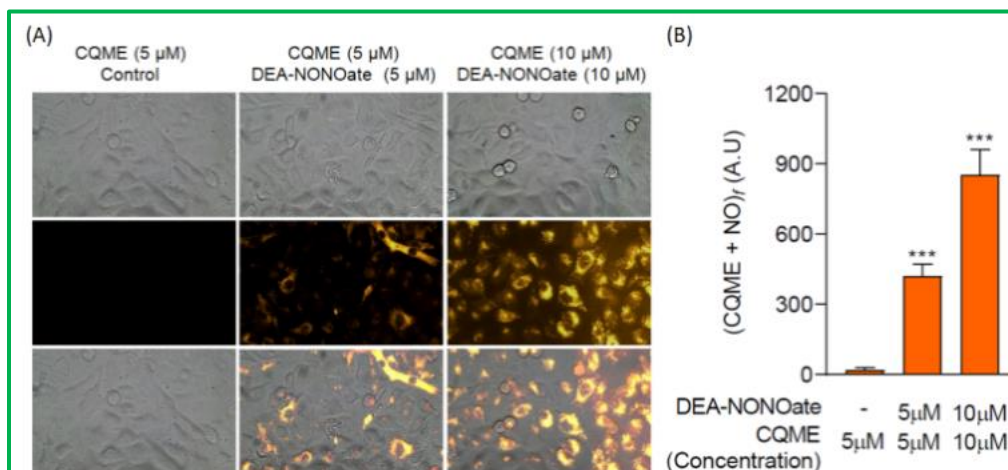
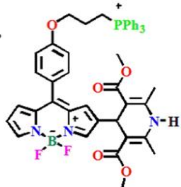


Figure 4.26. (A) Fluorescence imaging of A549 cells incubated with CQME (5 μM) only, CQME (5 μM) + DEANONOate (5 μM), and CQME (10 μM) + DEA-NONOate (10 μM), Increase in yellowish orange fluorescence was observed with the increase in concentration of NO donor. All the images were taken at 40X objective. (B) Quantified fluorescence (Mean ± SD) turn-on in A549 cells after treatment with NO donor DEA-NONOate in the presence of CQME. (a.u.) = Arbitrary unit.

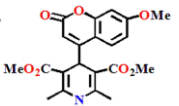
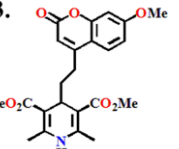
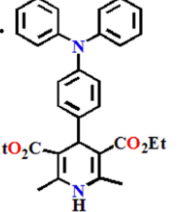
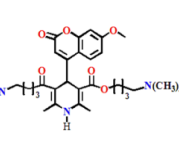
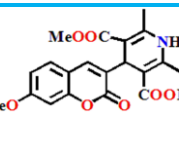
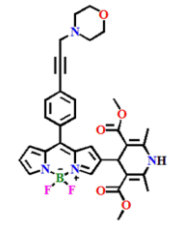
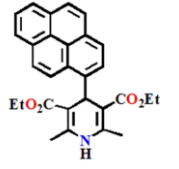
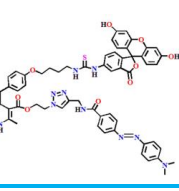
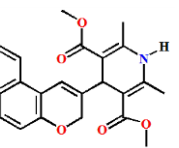
4.3.9 Comparison Table

We have analyzed the results obtained from the recognition of NO by a number of dihydropyridine based NO sensors (Table 4.2). Among all these reported dihydropyridine based NO sensitive probe, our present work on the NO sensing by benzochromene probe (CQME) seems to be superior with respect to $\lambda_{ex}/\lambda_{em}$ (470/615 nm) and stokes shift resulting its deep penetration ability and low background autofluorescence.

Table 4.2. Reported Dihydropyridine based probes

Serial No	$\lambda_{ex}/\lambda_{em}$	Stokes shift	LOD	Variety of product	Reference
1. 	470 /525	55	25 nM	Simple Aromatization of dihydropyridine to pyridine.	Talanta 2018 , 176, 382-388.

CHAPTER 4

2.		334 /450	116	13 nM	”	<i>Chem Comm.</i> 2014 , 50(49), 6475-6478
3.		323 /392	69	17 nM	”	<i>RSC Adv.</i> 2016 , 6(89), 85698-85703
4.		308/439	131	0.08μ M	”	<i>RSC Adv.</i> 2016 , 6(114),1 13219-113227
5.		324/450	126	18 nM	”	<i>Spectrochim.</i> <i>Acta - A: Mol.</i> <i>Biomol</i> 2016. , 169, 1-6.
6.		365 /423	58	–	”	<i>Photochem.</i> <i>Photobiol.</i> <i>Sci.</i> 2020 , 19, 1230-1235.
7.		475 /535	60	47 nM	”	<i>Sens.</i> <i>Actuators B</i> <i>Chem.</i> 2021 , 339, 129880
8.		346 /502	156	2.6 μM	”	<i>RSC Adv.</i> 2016 , 6(114),1 13219- 113227.
9.		490 /525	35	In nM level.	<i>Breakage of C-C bond attached with DIPY and fluorophore followed by aromatization.</i>	<i>Chem. Sci.</i> 2017 , 8 (3), 2199-2203.
10.		470/615	145	42 nM	<i>C-C bond breaking for the formation of C- nitrated product along with aromatization of DIPY.</i>	<i>Present work</i>

4.4 CONCLUSION

In summary, we have designed a new dihydropyridine based NO sensitive probe (CQME) which undergoes aromatic nitration assisted C-C single bond cleavage, followed by the aromatization pathway to produce PYMAA and PYNO₂ as the major components instead of a simple aromatization reaction. Notably, The probe exhibits ~30 fold enhancement in the emission intensity at 615 nm on excitation at 470 nm resulting a huge stoke-shifts of 145 nm assuring a minimum interference from the excitation light for *in vivo* applications. Moreover, the fluorescence emission peak at 615 nm for PYNO₂ strongly supports its excellent biological applications due to its deep penetration ability and low background autofluorescence. In addition to that, the probe CQME exhibits its effectiveness to track both endogenous and exogenous NO in biological milieu because of its least cytotoxicity, bio-compatibility and also no interference by other biological species that are present in complicated biological systems. The pH studies also display prompt positive response of the probe towards NO over a wide range of pH. Now, all the photophysical studies and biological applications strongly justifies the superiority of the probe to sense both endogenous and exogenous NO selectively over other biological interfering species present in living organisms.

References

1. Sasaki, E.; Kojima, H.; Nishimatsu, H.; Urano, Y.; Kikuchi, K.; Hirata, Y.; Nagano, T., Highly Sensitive Near-Infrared Fluorescent Probes for Nitric Oxide and Their Application to Isolated Organs. *J. Am. Chem. Soc.* **2005**, *127* (11), 3684-3685.
2. Stuehr, D.J.; Santolini, J.; Wang, Z.Q.; Wei, C.C.; Adak, S., Update on mechanism and catalytic regulation in the NO synthases. *J. Biol. Chem.* **2004**, *279*(35), 36167-36170.
3. Wink, D. A.; Mitchell, J. B., Chemical biology of nitric oxide: insights into regulatory, cytotoxic, and cytoprotective mechanisms of nitric oxide. *Free Radic. Biol. Med.* **1998**, *25* (4), 434-456.
4. de Mel, A.; Murad, F.; Seifalian, A.M., Nitric oxide: a guardian for vascular grafts?. *Chem. Rev.* **2011**, *111*(9), 5742-5767.
5. Loscalzo, J., Nitric oxide insufficiency, platelet activation, and arterial thrombosis. *Circ. Res.* **2001**, *88*(8), 756-762.
6. Fukumura, D.; Kashiwagi, S.; Jain, R. K., The role of nitric oxide in tumour progression. *Nat. Rev. Cancer* 2006, *6* (7), 521-534.
7. Calabrese, V.; Mancuso, C.; Calvani, M.; Rizzarelli, E.; Butterfield, D.A.; Giuffrida Stella, A.M., Nitric oxide in the central nervous system: neuroprotection versus neurotoxicity. *Nat. Rev. Neurosci.* **2007**, *8*(10), 766-775.
8. Pacher, P.; Beckman, J.S.; Liaudet, L., Nitric oxide and peroxynitrite in health and disease. *Physiol. Rev.* **2007**, *87*(1), 315-424.
9. Tennyson, A.G.; Lippard, S.J., Generation, translocation, and action of nitric oxide in living systems. *Chem. Biol.* **2011**, *18*(10), pp.1211-1220.
10. Pacher, P.; Beckman, J.S.; Liaudet, L., Nitric oxide and peroxynitrite in health and disease. *Physiol. Rev.* **2007**, *87*(1), 315-424.
11. Henry, Y.; Guissani, A. J. A., Contribution of spin-trapping EPR techniques for the measurement of NO production in biological systems. **2000**, *28* (6), 445-454.
12. Bedioui, F.; Villeneuve, N., Electrochemical Nitric Oxide Sensors for Biological Samples – Principle, Selected Examples and Applications. *Electroanalysis* **2003**, *15* (1), 5-18.
13. Ridnour, L. A.; Sim, J. E.; Hayward, M. A.; Wink, D. A.; Martin, S. M.; Buettner, G. R.; Spitz, D. R., A Spectrophotometric Method for the Direct Detection and Quantitation

CHAPTER 4

- of Nitric Oxide, Nitrite, and Nitrate in Cell Culture Media. *Anal. Biochem.* **2000**, *281* (2), 223-229.
14. Laver, J. R.; Stevanin, T. M.; Read, R. C., Chapter Seven - Chemiluminescence Quantification of NO and Its Derivatives in Liquid Samples. In *Methods in Enzymology*, Poole, R. K., Ed. Academic Press: 2008; Vol. 436, pp 113-127.
15. Li, Y.; Wu, W.; Yang, J.; Yuan, L.; Liu, C.; Zheng, J.; Yang, R., Engineering a nanolab for the determination of lysosomal nitric oxide by the rational design of a pH-activatable fluorescent probe. *Chem. Sci.* **2016**, *7* (3), 1920-1925.
16. Mao, Z.; Feng, W.; Li, Z.; Zeng, L.; Lv, W.; Liu, Z., NIR in, far-red out: developing a two-photon fluorescent probe for tracking nitric oxide in deep tissue. *Chem. Sci.* **2016**, *7* (8), 5230-5235.
17. Wang, B.; Yu, S.; Chai, X.; Li, T.; Wu, Q.; Wang, T., A Lysosome-Compatible Near-Infrared Fluorescent Probe for Targeted Monitoring of Nitric Oxide. *Chem. Eur. J.* **2016**, *22* (16), 5649-5656.
18. Adarsh, N.; Krishnan, M.S.; Ramaiah, D., Sensitive naked eye detection of hydrogen sulfide and nitric oxide by aza-BODIPY dyes in aqueous medium. *Anal. Chem.*, **2014**, *86*(18), 9335-9342.
19. Gabe, Y.; Urano, Y.; Kikuchi, K.; Kojima, H.; Nagano, T., Highly Sensitive Fluorescence Probes for Nitric Oxide Based on Boron Dipyrromethene Chromophore Rational Design of Potentially Useful Bioimaging Fluorescence Probe. *J. Am. Chem. Soc.* **2004**, *126* (10), 3357-3367.
20. Lim, M. H.; Lippard, S. J., Copper Complexes for Fluorescence-Based NO Detection in Aqueous Solution. *J. Am. Chem. Soc.* **2005**, *127* (35), 12170-12171.
21. Lucero, M. Y.; East, A. K.; Reinhardt, C. J.; Sedgwick, A. C.; Su, S.; Lee, M. C.; Chan, J., Development of NIR-II Photoacoustic Probes Tailored for Deep-Tissue Sensing of Nitric Oxide. *J. Am. Chem. Soc.* **2021**, *143* (18), 7196-7202.
22. Chen, X.-X.; Niu, L.-Y.; Shao, N.; Yang, Q.-Z., BODIPY-Based Fluorescent Probe for Dual-Channel Detection of Nitric Oxide and Glutathione: Visualization of Cross-Talk in Living Cells. *Anal. Chem.* **2019**, *91* (7), 4301-4306.

23. Muñoz Resta, I.; Bedrina, B.; Martínez-Planes, E.; Minguela, A.; Galindo, F., Detection of subcellular nitric oxide in mitochondria using a pyrylium probe: assays in cell cultures and peripheral blood. *J. Mater. Chem. B* **2021**, *9* (48), 9885-9892.
24. Ma, S.; Fang, D.-C.; Ning, B.; Li, M.; He, L.; Gong, B., The rational design of a highly sensitive and selective fluorogenic probe for detecting nitric oxide. *Chem. Commun.* **2014**, *50* (49), 6475-6478.
25. Islam, A. S. M.; Bhowmick, R.; Pal, K.; Katarkar, A.; Chaudhuri, K.; Ali, M., A Smart Molecule for Selective Sensing of Nitric Oxide: Conversion of NO to HSNO; Relevance of Biological HSNO Formation. *Inorg. Chem.* **2017**, *56* (8), 4324-4331.
26. Islam, A. S. M.; Bhowmick, R.; Chandra Garain, B.; Katarkar, A.; Ali, M., Nitric Oxide Sensing through 1,2,3,4-Oxatriazole Formation from Acylhydrazide: A Kinetic Study. *J. Org. Chem.* **2018**, *83* (21), 13287-13295.
27. Gao, C.; Lin, L.; Sun, W.; Tan, Z.-L.; Huang, J.-R.; He, L.; Lu, Z.-L., Dihydropyridine-derived BODIPY probe for detecting exogenous and endogenous nitric oxide in mitochondria. *Talanta* **2018**, *176*, 382-388.
28. Ma, S.-F.; Wang, Q.-H.; Liu, F.-T.; Wang, H.-L.; Fang, D.-C.; Gong, B.; He, L.; Lu, Z.-L., Dihydropyridine-based fluorescence probe for nitric oxide. *RSC Adv.* **2016**, *6* (89), 85698-85703.
29. Tang, F.; Gao, C.; Liu, J.-Y.; Lu, Z.-L.; He, L.; Ding, A.-X., Lysosome-targeting BODIPY-derived Hantzsch ester for nitric oxide detection and imaging in live cells. *Sens. Actuator B-Chem.* **2021**, *339*, 129880.
30. Wang, H.-L.; Liu, F.-T.; Ding, A.-X.; Ma, S.-F.; He, L.; Lin, L.; Lu, Z.-L., Water-soluble Hantzsch ester as switch-on fluorescent probe for efficiently detecting nitric oxide. *Spectrochim. Acta A* **2016**, *169*, 1-6.
31. Li, H.; Zhang, D.; Gao, M.; Huang, L.; Tang, L.; Li, Z.; Chen, X.; Zhang, X., Highly specific C–C bond cleavage induced FRET fluorescence for in vivo biological nitric oxide imaging. *Chem. Sci.* **2017**, *8* (3), 2199-2203.
32. Speck-Planche, A.; Kleandrova, V. V.; Luan, F.; Cordeiro, M. N. D. S., Multi-target drug discovery in anti-cancer therapy: Fragment-based approach toward the design of potent and versatile anti-prostate cancer agents. *Bioorg. Med. Chem.* **2011**, *19* (21), 6239-6244.

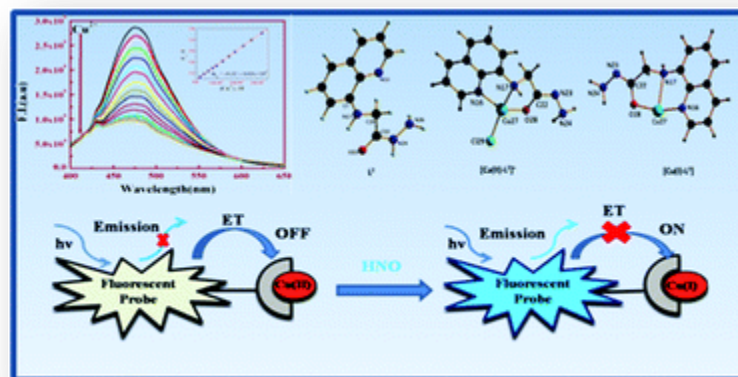
CHAPTER 4

33. Radi, R., Nitric oxide, oxidants, and protein tyrosine nitration. *Proc. Natl. Acad. Sci. U.S.A.* **2004**, 101(12), 4003-4008.
34. De Ruyck, J.; Famerée, M.; Wouters, J.; Perpète, E.A.; Preat, J.; Jacquemin, D.,. Towards the understanding of the absorption spectra of NAD (P) H/NAD (P)+ as a common indicator of dehydrogenase enzymatic activity. *Chem. Phys. Lett.*, **2007**, 450(1-3), 119-122.

A dual response fluorescent sensor for HNO and S²⁻ ions using a Cu(II) complex based probe assisted by detailed DFT studies

Abstract:

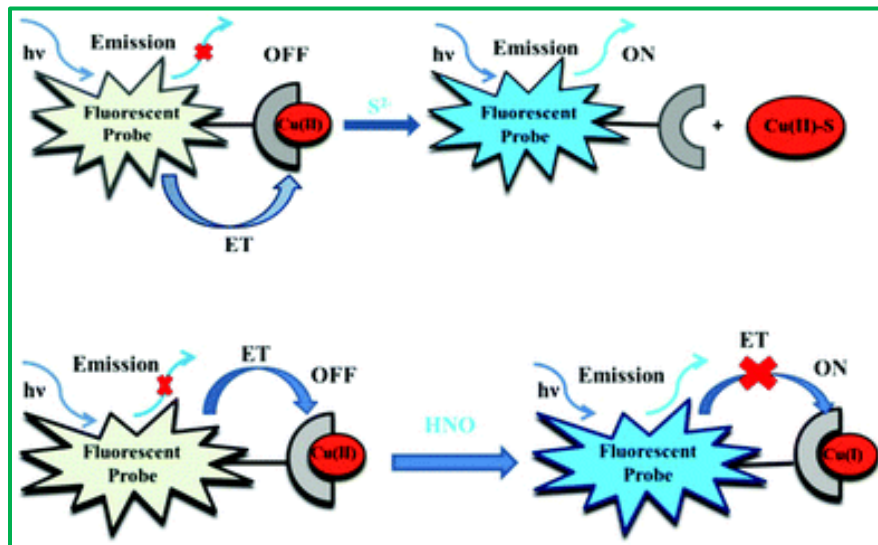
A Cu(II) based sensor (1) was developed by complexation between (quinolin-8-ylamino)-acetic acid hydrazide (L²) and Cu²⁺ ions for highly sensitive and selective recognition of HNO and S²⁻ over other biologically abundant anions with prominent enhancement in absorption and emission intensities. The sensor (1) exhibits weak fluorescence due to ET (electron transfer) but upon addition of HNO and S²⁻, a large enhancement in fluorescence intensity (F.I.) was observed over other possible competitive anions on the basis of reduction of Cu(II) to Cu(I) and formation of CuS, respectively. The 1:1 complexation was characterized by mass spectrometry (MS), elemental analysis and Job's plot. The corresponding K_f value for Cu²⁺ from Uv-Vis absorption titration was evaluated as $(4.934 \pm 0.05) \times 10^4 \text{ M}^{-1}$. Quantum yields of L² and [Cu-L² + S²⁻] and [Cu-L² + HNO] complexes in acetonitrile (CH₃CN) are found to be 0.107, 0.09 and 0.07 respectively, using quinine sulphate as the standard.



5.1 Introduction

In many areas and disciplines, fluorescent sensors are in high demand because of their selective and efficient signaling properties for the detection of various chemical and biological analytes.¹ Copper, an essential trace metal ion, plays an important role in various biological and metabolic processes, the level of which can be regulated haemostatically.² Accumulation of a large excess of copper in the brain and the liver is highly toxic and causes Alzheimer's, Parkinson's, Prion, Menkes and Wilson's diseases.³⁻⁶ Fluorescence measurement is one of the great technique to detect copper ion because of its high sensitivity and specificity towards analytes and also real-time monitoring with a fast response time.⁷ Moreover, the Cu^{2+} complexes have the ability to sense other substances (e.g. NO, HNO, S^{2-} etc.).⁸ Nitric oxide (NO) is an important signaling agent for various processes that involve the cardiovascular,⁹ immune¹⁰ and nervous systems.¹¹ HNO, the one-electron reduced and protonated derivative of NO, displays distinct chemistry and biochemistry from that of NO.¹²⁻¹⁴ Recent studies reveal that exogenous administration of HNO increases the contractility of heart cells¹⁵ leading to vasorelaxation in muscle cells¹⁶ and also decreases platelet aggregation.¹⁷ HNO also exacerbates ischemia-related injury¹⁸ and induces neurotoxicity.¹⁹ These lead to the conclusion that HNO plays a crucial role in biology. Detecting HNO in biological systems is a challenge that has caught the attention of chemists. Difficulties associated with HNO sensing include differentiation from NO and other biologically relevant analytes, rapid detection in low concentrations and compatibility of the sensing mechanism with biological environments, particularly at neutral or slightly acidic pH, high ionic strength and a temperature of 37 °C. Considering all these, it may be concluded that the most effective strategy for detecting HNO is to take advantage of its redox activity.^{20,21} Probes that are able to be reduced selectively by HNO act as a sensor if an appropriate output signal is linked to the reduction step. Although there are various chemical reactions that can be used to detect and trap HNO,²² usually, azanone (HNO, nitroxyl) reacts with copper(II) ions, resulting in the formation of NO and Cu^+ .²³ This strategy is utilized for the construction of copper based pro-fluorescent HNO probes. We discuss here on the systems that collocate a Cu(II) coordination complex with a fluorophoric moiety. The sensing mechanism of such probes depends on the unpaired electron of the Cu(II) center which quenches the fluorescence of a photo emissive ligand by either electron or energy transfer (**Scheme 5.1**). Reduction of Cu(II) to Cu(I) by HNO restores the fluorescence of the ligand.

CHAPTER 5



Scheme 5.1. General mechanism of S^{2-} sensing and HNO sensing using the copper complex.

Hydrogen sulfide (H_2S), a deadly chemical species, is naturally produced by geological and microbial activities.²⁴ Exposure to H_2S can trigger eye and respiratory tract irritation.²⁵ Inhalation of excess H_2S can result in the loss of consciousness, cardiac arrest and in extreme cases, death.²⁶ H_2S functions as an endogenous signaling molecule and also exerts a regulative function in the intracellular redox status.²⁷ It can regulate the activities of ion channels and act as a tumor suppressor and it may be the actual signaling molecule in cell signal transduction.^{28–31} Once protonated, HS^- or H_2S are even more toxic than sulfide (S^{2-}) itself. Abnormal concentration of H_2S can cause Alzheimer's disease, Down syndrome and liver cirrhosis.³² Therefore, it is essential to develop a rapid and sensitive method for the detection of sulfide anions. By utilizing the displacement approach, the ligand metal ion “ensemble” that is non-fluorescent due to metal-ion induced fluorescence quenching, however, becomes fluorescent on subsequent treatment of the ensemble with an anion which displaces the metal ion from the coordination sphere of the original organic receptor and releases the ligand into the solution with a revival of the fluorescence^{33–35} (Scheme 5.1). As sulfide is known to react with copper ions to form very stable CuS ($K_{sp} = 6.3 \times 10^{-36}$),³⁵ among various approaches for sulfide sensing, this reversible sensing exploiting copper sulfide affinity attracted our special attention.^{36–39} In this paper, we report a Cu-based sensor (1) prepared by the complexation between (quinolin-8-ylamino)-acetic acid hydrazide (L^2) and Cu^{2+} ions which has been developed for a highly sensitive and selective recognition of HNO and S^{2-} over other possible competitive anions on the basis of the reduction

of Cu(II) to Cu(I) and forming CuS. The 1:1 complexation between the probe and Cu^{2+} was characterized by mass spectrometry (MS), elemental analysis and Job's plot. The photophysical properties and recognition behaviors of the chemosensor have been investigated in detail through Uv-Vis absorption spectra, fluorescence spectra, MS and theoretical calculations.

5.2 EXPERIMENTAL SECTION

5.2.1 Materials and methods

8-Aminoquinoline, ethyl bromoacetate (Sigma Aldrich), hydrazine hydrate (Sigma Aldrich), absolute ethanol and salts of Cr^{3+} , Co^{2+} , Hg^{2+} , Mg^{2+} , Mn^{2+} , Dy^{3+} , Pb^{2+} , Zn^{2+} , Sm^{3+} , F^- , Br^- , Cl^- , I^- , SCN^- , HSO_4^- , SO_3^{2-} , SO_4^{2-} , HSO_3^- , PO_4^{3-} , CH_3COO^- , N_3^- , NO_2^- and S^{2-} were obtained from commercial suppliers and used without further purification. Angeli's salt was prepared by the reported method.⁴⁰ Solvents like MeOH (methanol), MeCN (acetonitrile) etc. (Merck, India) were of reagent grade. All other reagents were procured from commercial sources and used without further purification. Physical measurements, Elemental analyses were carried out using a CHN analyzer (PerkinElmer 240). Infrared spectra were recorded in the solid state on a Nicolet Magna IR 750 series-II FTIR spectrometer in the range $400\text{--}4000\text{ cm}^{-1}$. $^1\text{H-NMR}$ spectra were recorded in DMSO-d_6 on a Bruker 300 MHz NMR spectrometer with TMS ($\delta = 0$) acting as an internal standard. ESI- MS^+ (m/z) of the ligand and complexes were recorded on a Waters XEVO G2QT of HRMS spectrometer. An Agilent diode-array spectrophotometer (Model, Agilent 8453) was used for Uv-Vis studies. Steady-state fluorescence studies were carried out on a PTI QM-40 spectrofluorimeter. Lifetimes were measured using a Horiba Jobin-Yvon Hamamatsu MCP photomultiplier (R3809) and data were analyzed by using the IBH DAS6 software. X-band EPR spectra were recorded on an EPR-Spectrometer (Model: JEOL, JES-FA 200).

5.2.2 Synthesis

5.2.2.1 Preparation of (quinolin-8-ylamino)-acetic acid ethyl ester (L^1)

A mixture of 8-aminoquinoline (5 mmol), ethyl bromoacetate (7.5 mmol) and anhydrous K_2CO_3 (12.5 mmol) in acetonitrile was refluxed in a water bath for 8 h. The mixture was then filtered and the solvent was removed under reduced pressure. The resulting oily product was purified by column chromatography on silica gel, using DCM (dichloromethane): MeOH (methanol) (9 : 1)

as the eluent to afford L^1 (85% yield). L^1 was characterized by ^1H NMR analysis. ^1H NMR (in DMSO- d_6 , 300 MHz, ppm): δ_{ppm} : 1.20 (m, 3H, $-\text{CH}_3$), 4.17 (m, 4H, $-\text{CH}_2$, $-\text{CH}_2$), 6.57 (d, 1H, $-\text{ArH}$), 6.86 (s, 1H, $-\text{ArH}$), 7.36 (m, 1H, $-\text{ArH}$), 7.50 (m, 1H, $-\text{ArH}$), 8.21 (d, 1H, $-\text{ArH}$), 8.75 (s, 1H, $-\text{NH}$) (Figure 5.1).

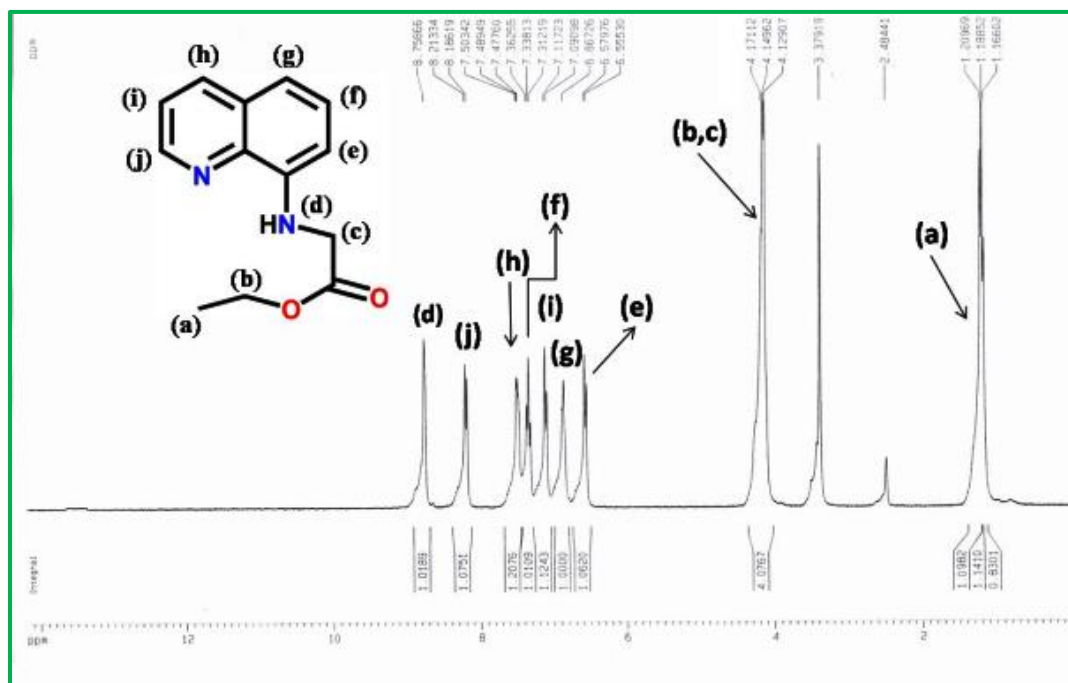


Figure 5.1. ^1H -NMR spectrum of L^1 in DMSO- d_6 .

5.2.2.2 Preparation of (quinolin-8-ylamino)-acetic acid hydrazide (L^2)

The resulting (quinolin-8-ylamino)-acetic acid ethyl ester (1.0 mmol) and hydrazine hydrate (10 mmol) in ethanol were refluxed in a water bath for 6 h. After cooling, the solid that separated out was filtered and washed with water, dried and recrystallized from ethanol. Needle shaped crystals were obtained. (Yield ~70%). CHN analysis for $\text{C}_{11}\text{H}_{12}\text{N}_4\text{O}$ Calculated (%): C, 61.10; H, 5.59; N, 25.91 found (%): C, 60.90; H, 5.58; N, 25.81. ^1H NMR (300 MHz, DMSO- d_6) δ_{ppm} : 3.85 (s, 2H, $-\text{CH}_2$), 4.27 (s, 2H, $-\text{NH}_2$), 6.53 (d, 1H, $-\text{ArH}$), 6.82 (m, 1H, $-\text{ArH}$), 7.35 (m, 1H, $-\text{ArH}$), 7.50 (m, 1H, $-\text{ArH}$), 8.22 (d, 1H, $-\text{ArH}$), 8.75 (s, 1H, $-\text{NH}$) and 9.19 (s, 1H, $-\text{NH}$) (Figure 5.2). ^{13}C -NMR: (300 MHz, DMSO- d_6) δ_{ppm} : 45.18, 105.16, 114.43, 122.25, 128.13, 128.66, 136.40, 138.01, 144.51, 147.60, 169.34 (Figure 5.3). ESI-MS+ (m/z): 239.07 ($L^2 + \text{Na}^+$)

CHAPTER 5

(Figure 5.4). IR spectrum: $-\text{NH}_2$ (3430 cm^{-1}), $-\text{NH}$ (3302 cm^{-1}), $-\text{C}=\text{O}$ (1640 cm^{-1}) (Figure 5.5).

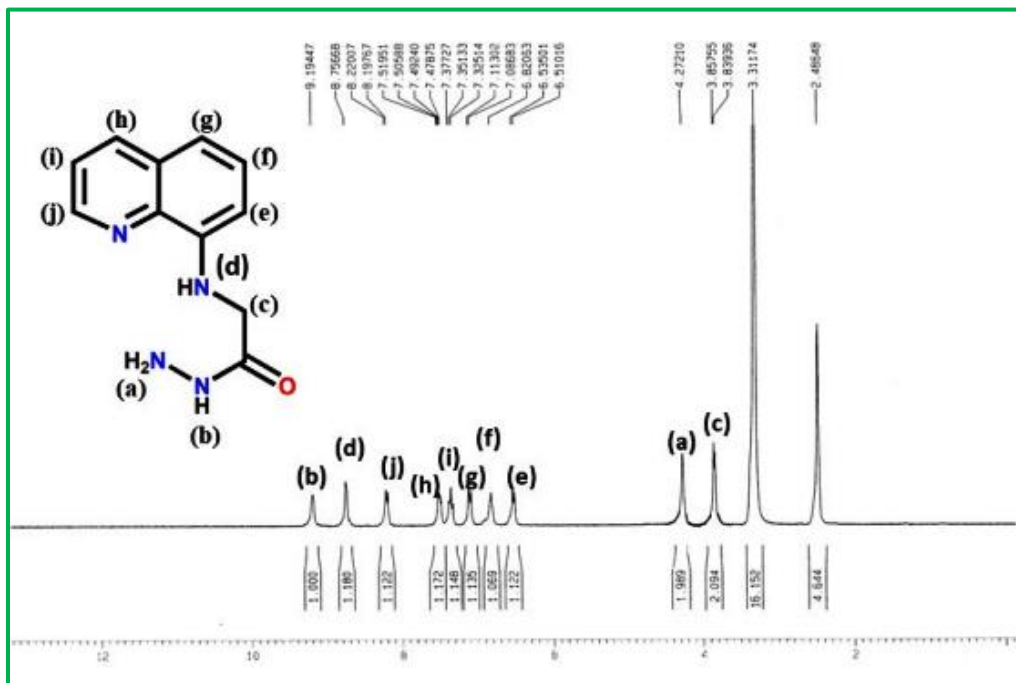


Figure 5.2. $^1\text{H-NMR}$ spectrum of L^2 in DMSO-d_6 .

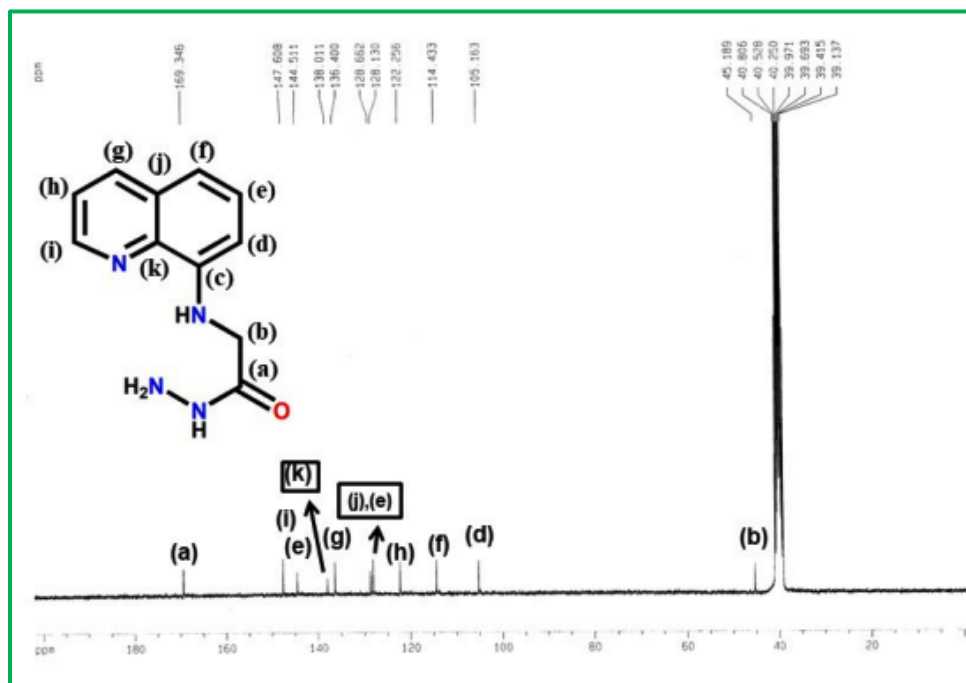


Figure 5.3. $^{13}\text{C-NMR}$ spectrum of L^2 in DMSO-d_6 .

CHAPTER 5

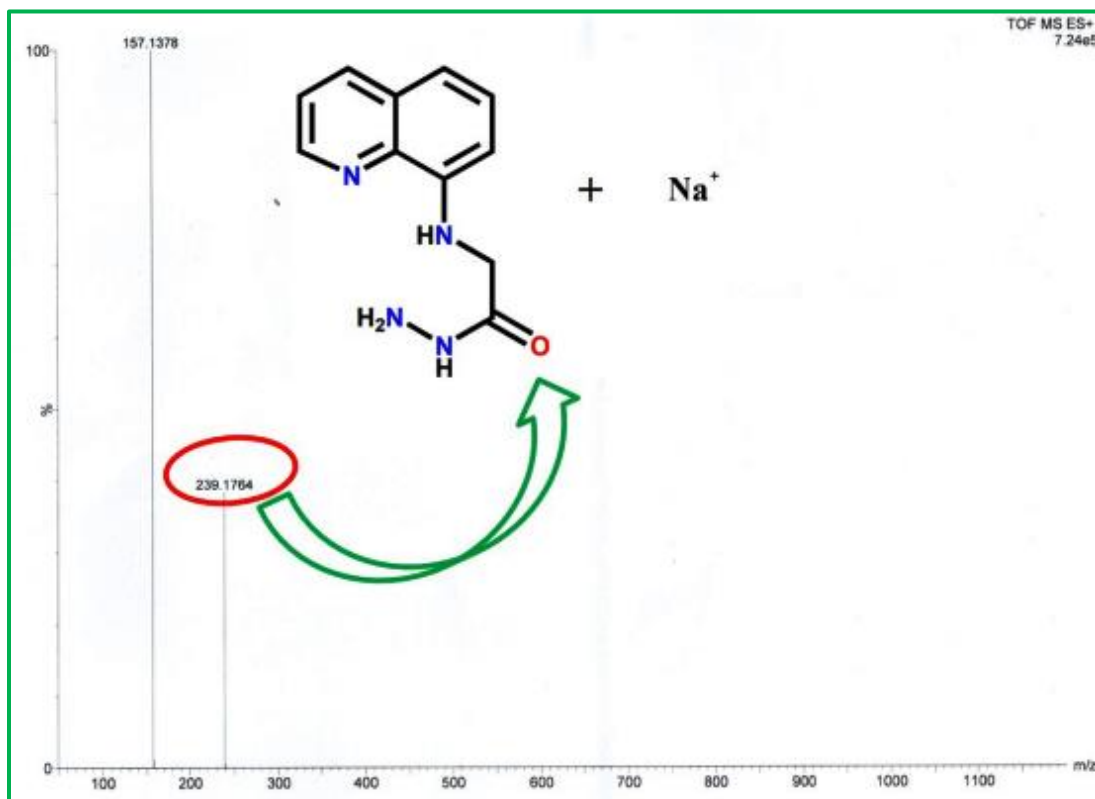


Figure 5.4. Mass spectrum of L² in MeCN

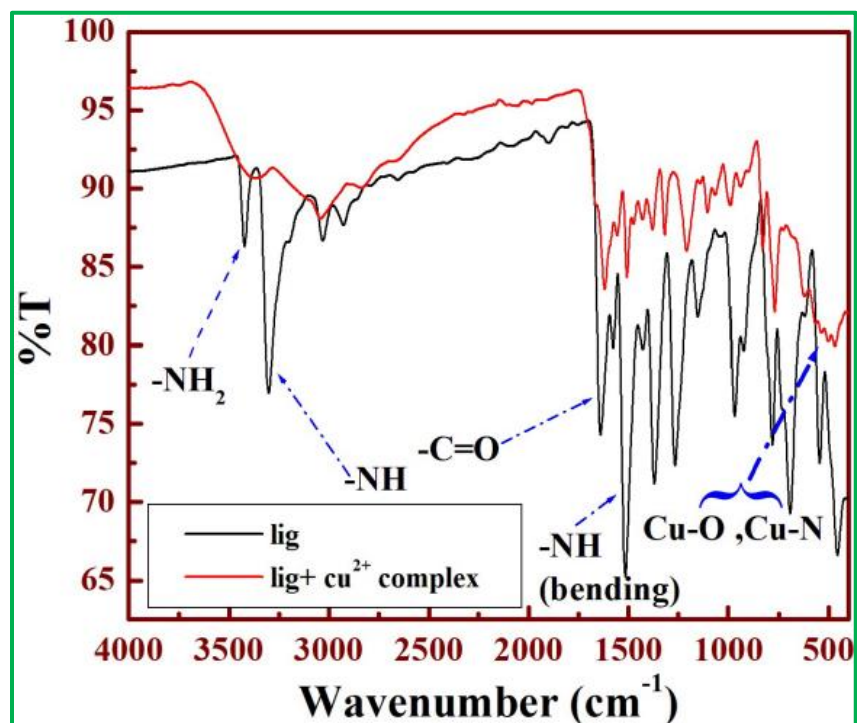


Figure 5.5. IR spectrum of for L² and [Cu(L²)Cl] in solid state.

5.2.2.3 Solution preparation for UV-Vis and fluorescence studies

For both Uv-Vis and fluorescence titrations, a stock solution of 1.0×10^{-3} M of the ligand (L^2) was prepared in degassed CH_3CN under a nitrogen atmosphere. 1.0×10^{-2} M stock solutions of $CuCl_2 \cdot 2H_2O$ and Na_2S in water were prepared separately under a N_2 atmosphere. Similarly, 1.0×10^{-3} M stock solution of Angeli's salt in water was prepared in degassed water under a nitrogen atmosphere. Stock solutions of tested metal ions as well as anions were prepared in CH_3CN-H_2O under anaerobic conditions by purging nitrogen gas in a gas tight vessel. 2.5 ml of degassed CH_3CN was pipetted out in a gas tight cuvette to which 20 μM of L^2 was added. Then metal ions (~ 5 equivalents) were added by injecting into the headspace of the gas tight cuvette before measuring fluorescence. Likewise titration of the resulting complex, $[Cu^{II}(L^2)]^+$, was carried out by the incremental addition of Angeli's salt (0–10 μM). The path lengths of the cells for absorption and emission studies were 1 cm. Fluorescence measurements were performed using a 5 nm \times 3 nm slit width.

5.2.2.4 Preparation of sensor (1)

Copper(II) chloride dihydrate, $CuCl_2 \cdot 2H_2O$ (65 mg, 0.5 mmol), was dissolved in 10 ml of freshly distilled acetonitrile and to this yellow solution, ligand L^2 (108 mg, 0.5 mmol) was added. The color of the solution changed to light green. The resulting mixture was stirred for 3 h. The volume of the solution was reduced to 5 ml under reduced pressure and diethyl ether (10 mL) was added and kept at 0 °C for 12 h to afford complex (1) as microcrystals (M.W. 314.23). Yield: 138 mg ($\sim 80\%$). CHN analyses for $C_{11}H_{11}ClCuN_4O$, calculated (%): C, 42.04; H, 3.53; N, 17.83 found (%): C, 42.03; H, 3.54; N, 17.84. ESI-MS⁺ (m/z): 320.3290 ($[(L^2)Cu^{II}(Cl)] + Li^+$) **(Figure 5.6)**.

5.2.3 Job's plot

The composition of the complex was determined by Job's method. In this method, we carried out the absorption measurements of a series of solutions keeping the sum of two reactants constant in a fixed volume but varying molar concentrations of Cu^{2+} ions and plotted against the molar fraction of the fluorophore. A minimum absorbance appeared at the molar ratio of the reactants which was found to be 1 : 1 with respect to the ligand for the Cu^{2+} complex.

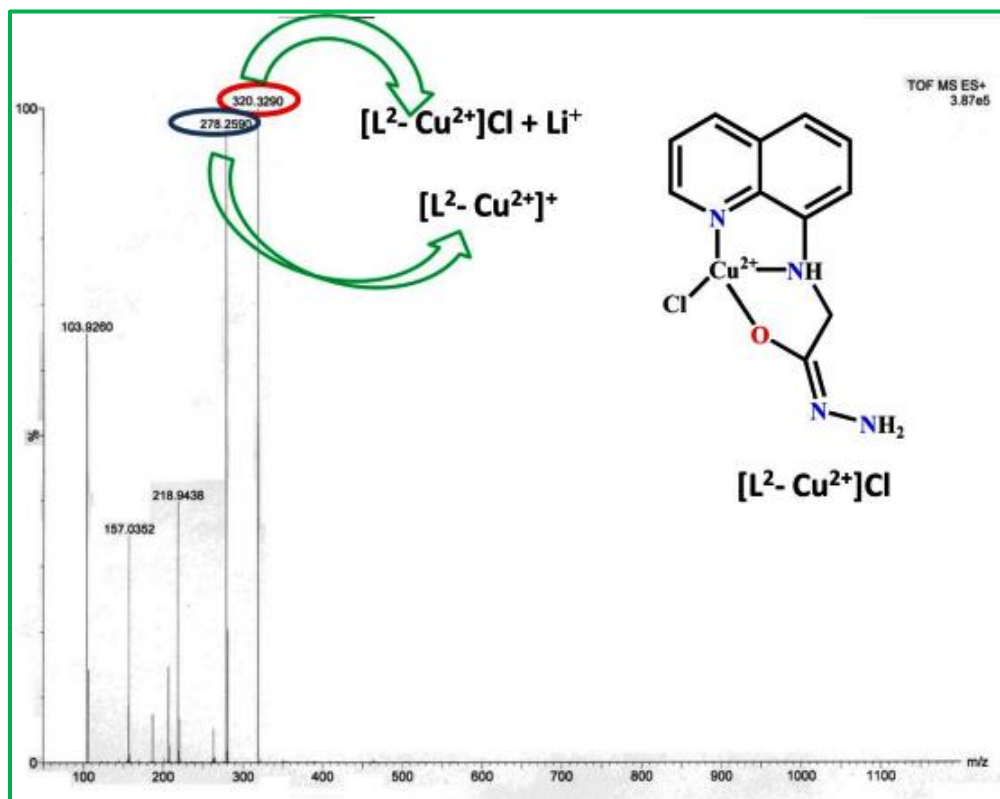


Figure 5.6. Mass spectrum of $[\text{Cu}(\text{L}^2)\text{Cl}]$ in MeOH.

5.2.4 Computational details

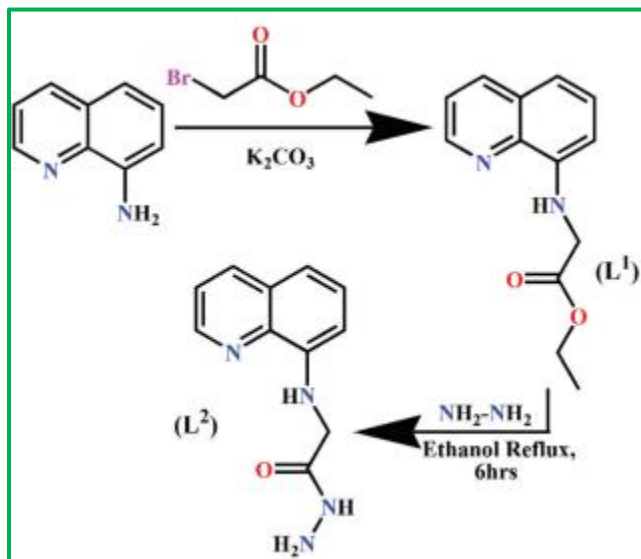
L^2 was fully optimized using a Gaussian 09 W software package.⁴¹ The B3LYP functional was adopted with 6-31G as the basis set for all the atoms (C, H, N and O) and for the Cu complex we used the B3LYP/6-31+g (d,p) basis set. The global minima of all these species were confirmed by the positive vibrational frequencies. Time dependent density functional theory (TDDFT)^{42,43} with the B3LYP density functional associated with the conductor-like polarizable continuum model (CPCM)⁴⁴⁻⁴⁶ was applied for the study of the low-lying excited states of the ligand and the complexes in CH_3CN using the optimized geometry of the ground state (S_0). The vertical excitation energies of the lowest 40 singlet states are also computed here.

5.3 RESULTS AND DISCUSSION

The ligand L^2 was prepared by refluxing (quinolin-8-ylamino)-acetic acid ethyl ester (1.0 mmol) and hydrazine hydrate (10 mmol) in ethanol in a water bath for 6 h (Scheme 5.2). The final product and all the intermediates were characterized thoroughly by CHN analysis, $^1\text{H-NMR}$

CHAPTER 5

(Figure 5.1 and Figure 5.2) and ^{13}C -NMR (Figure 5.3), HRMS (Figure 5.4) and IR (Figure 5.5) studies.



Scheme 5.2. Synthetic route to the probe L².

5.3.1 Uv-Vis absorption studies

The Uv-Vis absorption spectrum of L² with Cu²⁺ was investigated by spectrophotometric titration in acetonitrile solution. L² exhibits strong bands around 350 nm and 256 nm. Upon the addition of Cu²⁺ (1 equivalent), the absorption intensity decreased at 350 nm and increased at 299 nm (Figure 5.7a) which further confirms the coordination between Cu²⁺ and L². The absorbance of L² at 299 nm increases with increase in the concentration of Cu²⁺ due to ligand to metal charge transfer (LMCT). All these data were fitted to the Benesi–Hildebrand equation to get the formation constant and stoichiometry of complexation, where A₀ and A_{max} are the absorbance of the pure ligand in absence and presence of excess metal ions, respectively. A linear least-squares fit of (A_{max} - A₀)/(A - A₀) against 1/[M] clearly demonstrates a 1 : 1 complexation (n = 0.99) giving an apparent formation constant K_f = (4.934 ± 0.05) × 10⁴ M⁻¹ (Figure 5.7b).

$$\frac{(A_{max} - A_0)}{(A - A_0)} = 1 + \frac{1}{K[M]^n} \quad \dots \dots (1)$$

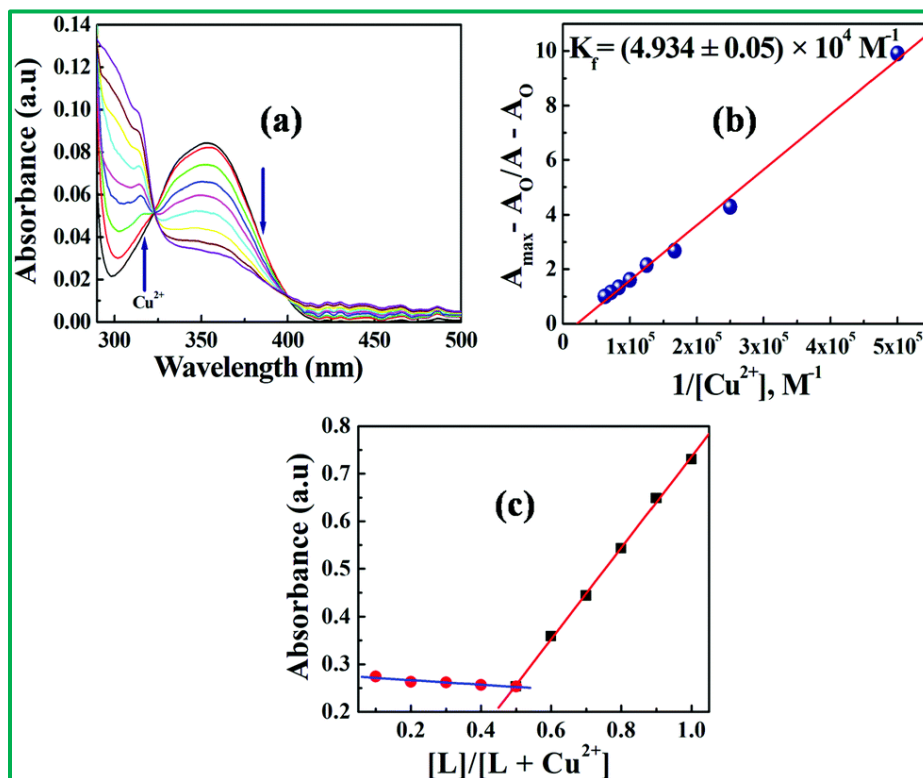


Figure 5.7. (a) Changes in UV-Vis absorption spectra of L² (20 µM) in MeCN solutions with various amounts of Cu²⁺ (0–0.8 equivalent); (b) Benesi–Hildebrand least-squares fit; and (c) Job's plot.

The composition of the complex was further determined by Job's method (**Figure 5.7(c)**) and also supported by mass analysis. ESI-MS⁺ (m/z): 320.3290 ([L²)Cu^{II}(Cl)] + Li⁺) (**Figure 5.6**).

5.3.2 Fluorescence quenching studies

Recording of the emission spectra of L² and its fluorescence titration with Cu²⁺ were performed in acetonitrile solution with a fixed concentration of L² (20 µM) (**Figure 5.8(a)**). The fluorescence quenching of the ligand (L²) is characterized by a linear Stern–Volmer (SV) plot and analyzed using the classical Stern–Volmer (SV) eqn (2)⁴⁷

$$\frac{F_0}{F} = 1 + K_{SV}[Q] \quad \dots \dots (2)$$

Where F₀ and F are the steady state fluorescence intensities at the maximum wavelength in the absence and presence of a quencher (Q), respectively, [Q] is the quencher concentration and K_{SV}

is the Stern–Volmer constant. The evaluated parameter is $K_{SV} = (5.32 \pm 0.03) \times 10^4 \text{ M}^{-1}$ (Figure 5.8(b)).

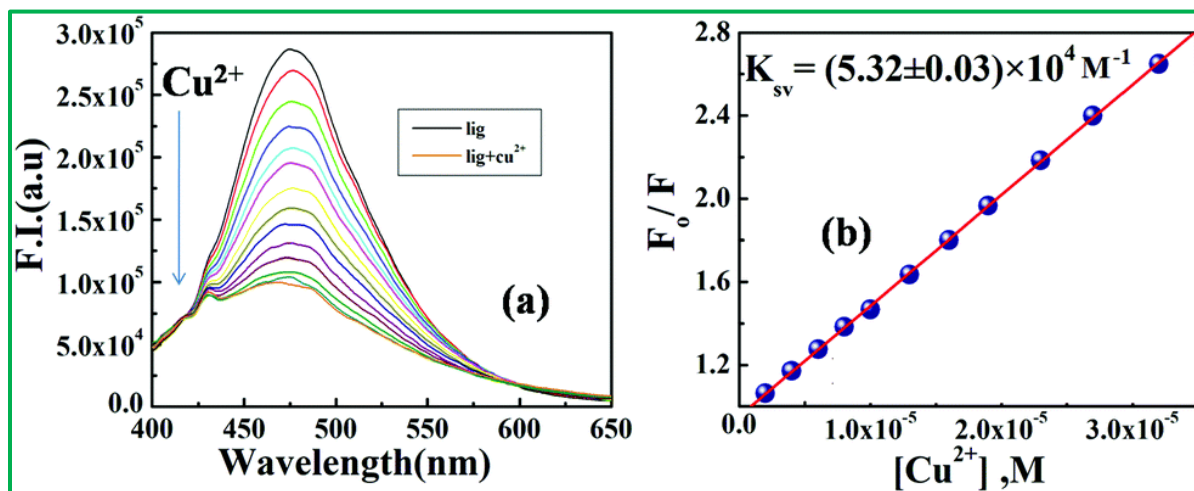


Figure 5.8. (a) Fluorescence emission changes of L^2 ($20 \mu\text{M}$) in MeCN solutions upon addition of Cu^{2+} (0–2.7 equivalent, $\lambda_{\text{ex}} = 380 \text{ nm}$, $\lambda_{\text{em}} = 475 \text{ nm}$); and (b) linear Stern–Volmer plot.

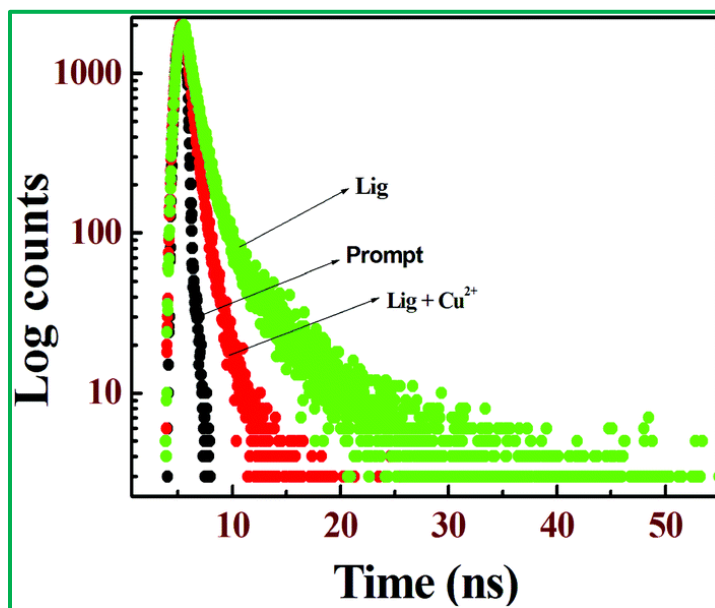


Figure 5.9. Lifetime plot of L^2 and $(L^2 + \text{Cu}^{2+})$ in MeCN solutions.

The addition of Cu^{2+} into the L^2 solution leads to a gradual decrease in the fluorescence intensity (FI) at 475 nm which gets saturated upon addition of ~ 2.7 equivalents of Cu^{2+} yielding a ~ 3.0 fold decrease in F.I. arising mainly due to an electron transfer (ET) from the quinoline

fluorophore to chelated Cu^{2+} and is evidenced from the substantial decrease in the lifetime of the Cu^{2+} complex ($\tau_{\text{complex}} = 0.579 \text{ ns}$) in comparison with the free ligand (L^2) ($\tau_{\text{ligand}} = 1.08 \text{ ns}$)⁴⁸ (Figure 5.9).

Selective quenching of fluorescence of L^2 by Cu^{2+} was checked for other metal ions (~5 equivalent) like Cr^{3+} , Co^{2+} , Hg^{2+} , Mg^{2+} , Mn^{2+} , Dy^{3+} , Pb^{2+} , Fe^{3+} , Zn^{2+} and Sm^{3+} and found to have negligible effects on fluorescence quenching (Figure 5.10).

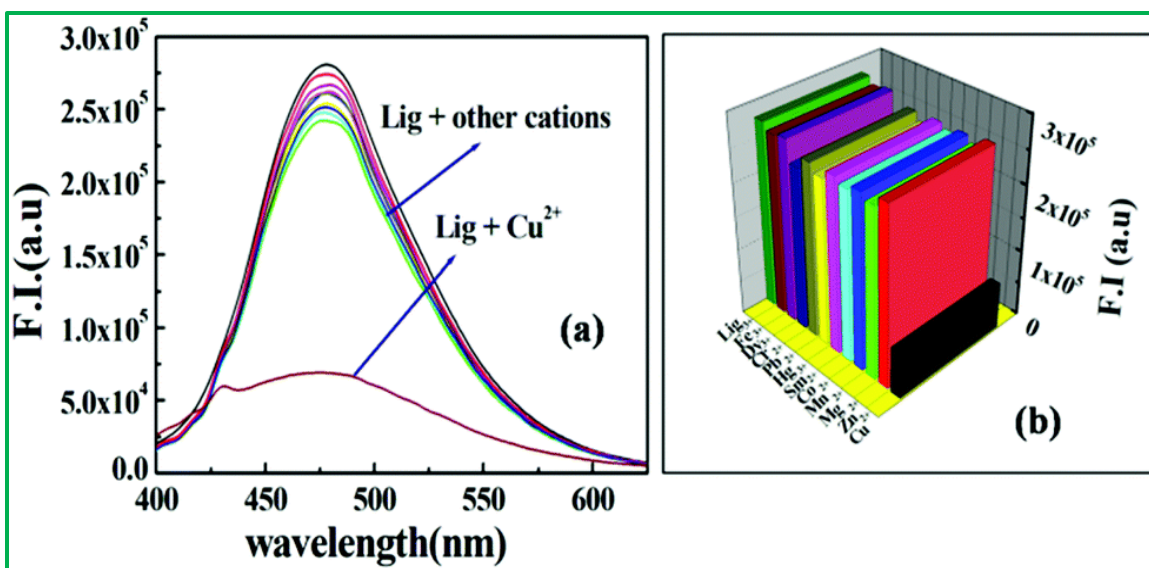
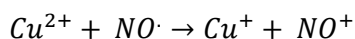


Figure 5.10. (a) Fluorescence emission spectra in the presence of different cations like Cr^{3+} , Co^{2+} , Hg^{2+} , Mg^{2+} , Mn^{2+} , Dy^{3+} , Fe^{3+} , Pb^{2+} , Zn^{2+} , Sm^{3+} and Cu^{2+} ; 5 equivalents of these cations were added to L^2 (20 μM) in MeCN solutions; and (b) the corresponding histogram plot.

5.3.3 HNO-induced reduction of Cu^{2+} and HNO-sensing

Treatment of a 20 μM solution of $[\text{Cu}^{\text{II}}\text{-L}^2]^+$ with ~0.5 equivalent of Angeli's salt restored the emission intensity by ~2.8 fold that of complexed L^2 , owing to the reduction of the paramagnetic Cu^{2+} ion. The consumption of 0.5 equivalent of HNO clearly indicates that HNO acts as a 2e⁻ reducing agent leading to the formation of NO^+ as follows:⁴⁹



The positive ion electrospray mass spectrum of this reduced species showed a peak with (m/z) 301.0127, which corresponds to $\{[\text{Cu}^{\text{I}}(\text{L}^2)] + \text{Na}^+\}$ complex (calculated m/z = 301.01)(Figure

CHAPTER 5

5.11). In aqueous solution, Angeli's salt generates NO_2^- and HNO^{50} which on subsequent treatment with $[\text{Cu}^{\text{II}}\text{-L}^2]^+$ reduces Cu(II) to Cu(I) without displacement of metal ions.

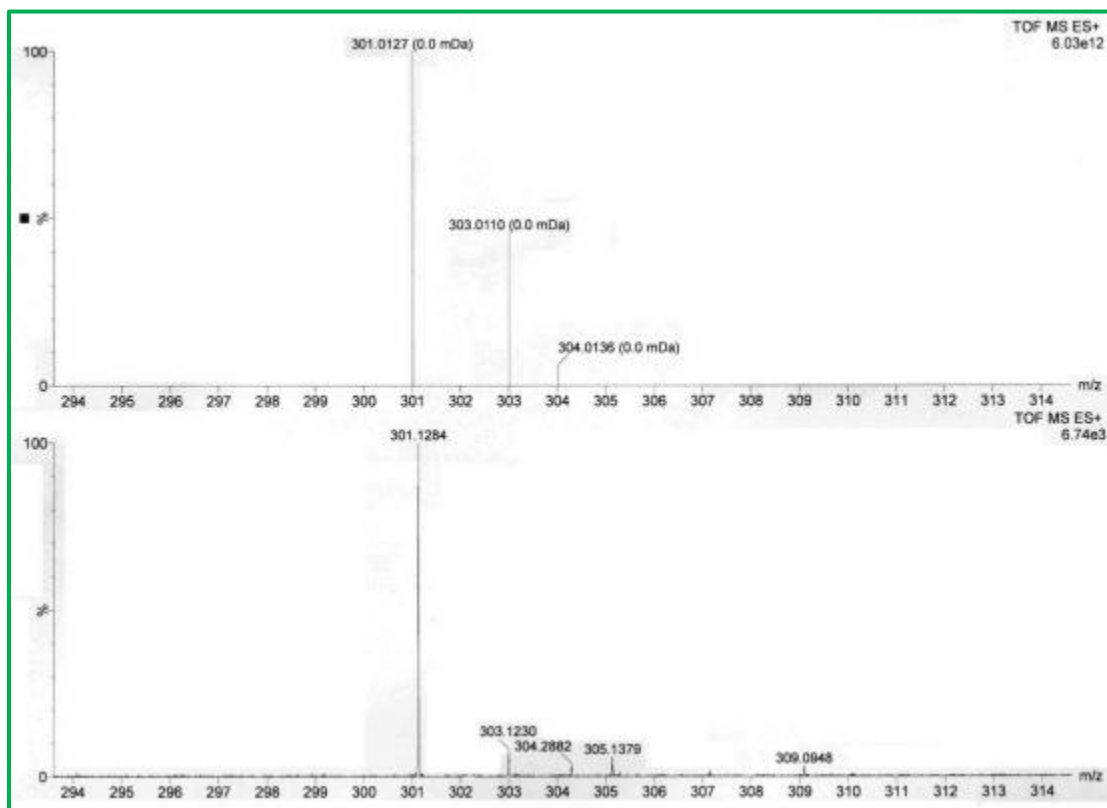


Figure 5.11. Mass spectrum of $[\text{Cu}(\text{L}^2)\text{Cl}]^+$ with $\text{Na}_2\text{N}_2\text{O}_3$ in MeCN and H_2O .

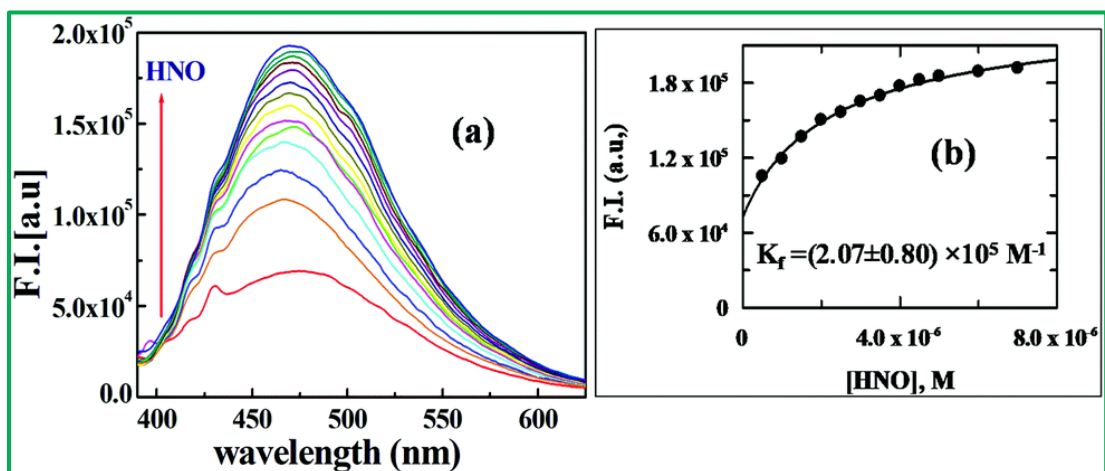


Figure 5.12. (a) Fluorescence emission changes of $[\text{Cu}^{\text{II}}\text{-L}^2]^+$ (20 μM) in MeCN solutions upon addition of HNO (0–0.5 equivalent), $\lambda_{\text{ex}} = 380 \text{ nm}$, $\lambda_{\text{em}} = 469 \text{ nm}$; (b) non-linear fitting plot.

CHAPTER 5

A 2.8-fold increase in the emission was observed, demonstrating fast HNO detection with significant turn-on (**Figure 5.12a**). The formation constant of the $[\text{Cu}^{\text{II}}\text{-L}^2]^+$ complex with HNO was determined by the nonlinear curve fitting method and found to be $(2.07 \pm 0.80) \times 10^5 \text{ M}^{-1}$ on the basis of the fluorescence titration experiments (**Figure 5.12b**). $[\text{Cu}^{\text{II}}\text{-L}^2]^+$ displayed a negligible change in emission when treated with 100 μM of NaNO_2 , indicating that the turn-on response induced by Angeli's salt is due to HNO production and not by the NO_2^- side product (**Figure 5.13**). The selectivity of the ligand towards HNO was further checked by performing the same experiment in the presence of NO, KO_2 , H_2O_2 , NO_2^- , TEMPO and $\cdot\text{OH}$ which failed to induce significant emission enhancement of the $[\text{Cu}^{\text{II}}\text{-L}^2]^+$ complex manifesting the selectivity of the $[\text{Cu}^{\text{II}}\text{-L}^2]^+$ complex (1) towards HNO. (**Figure 5.13**)

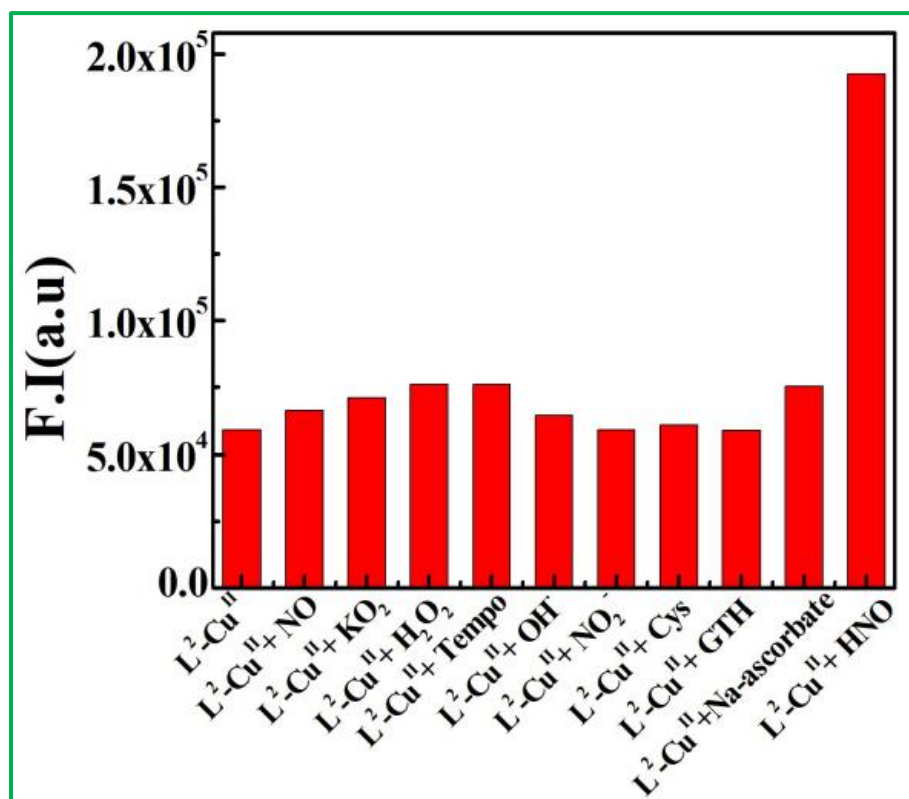
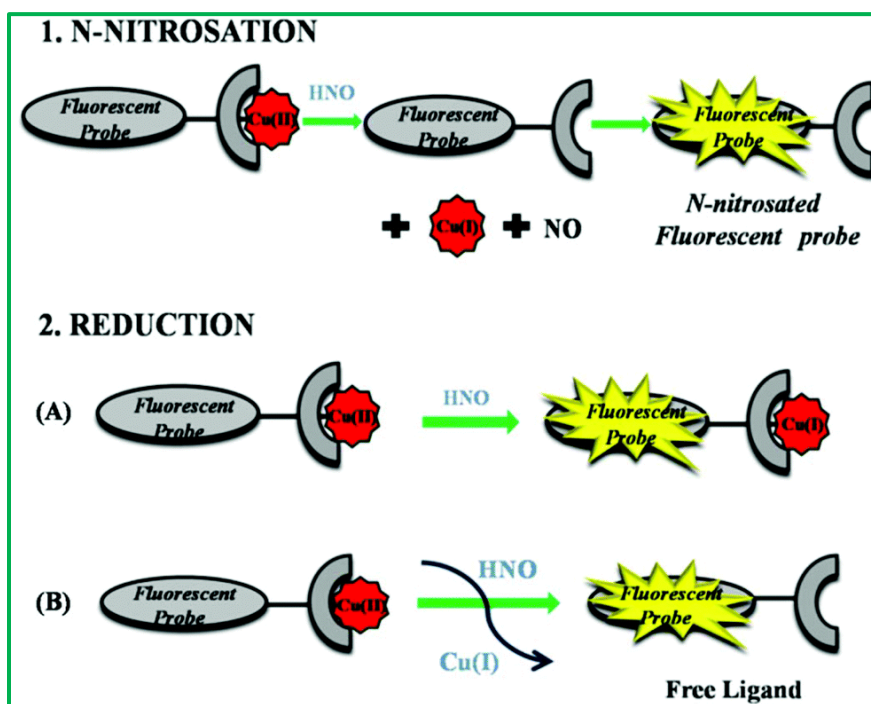


Figure 5.13. Bar chart illustrating fluorescence responses of $[\text{Cu}^{\text{II}}\text{-L}^2]^+$ complex at 469 nm ($\lambda_{\text{ex}} = 380 \text{ nm}$) towards different biological anions in CH_3CN . X^{n} = NO, KO_2 , H_2O_2 , TEMPO radical, OH, NO_2^- , cysteine, glutathione, sodium ascorbate and HNO.

HNO-induced fluorescence enhancement in the Cu^{2+} systems may occur in more than one way (please see **Scheme 5.3**). As revealed from **Scheme 5.3**, the enhancement of fluorescence

CHAPTER 5

intensity may occur by (1): turn on sensing with N-nitrosation with the removal of reduced Cu(I); 2(A): turn on sensing by the reduction of Cu(II) to Cu(I) with HNO without the removal of the metal, bound to the receptor; and 2(B): turn on sensing by the reduction of Cu(II) to Cu(I) with HNO and the removal of reduced metal ions. In our case, mechanism 2 (A) is operative and formation of $[\text{Cu}^{\text{I}}-\text{L}^2]$ species is determined by the EPR (Figure 5.14) studies.



Scheme 5.3. Typical mechanism for HNO detection.

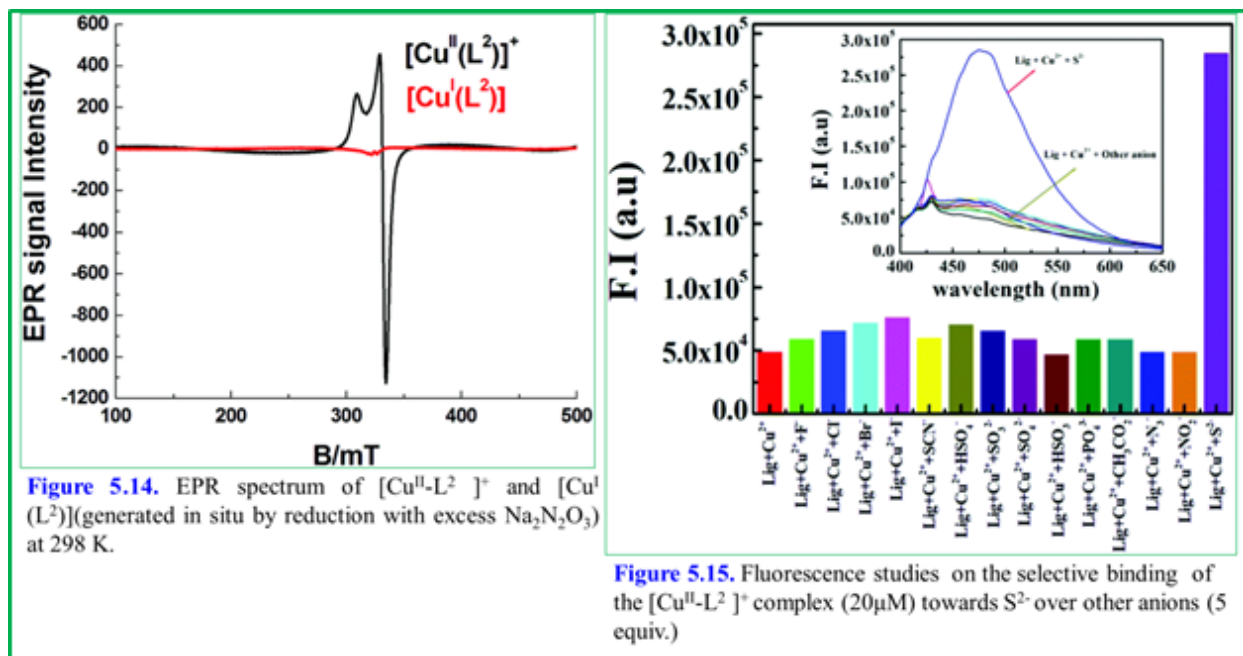
The EPR spectrum of $[\text{Cu}^{\text{II}}-\text{L}^2]^+$, prepared separately, is typically an axial type with $g_{\perp} = 2.04$, $g_{\parallel} = 2.18$ and $g_{\text{av}} = 2.11$ manifesting the presence of paramagnetic Cu^{II} ions. When this complex was treated with a 3-fold excess of HNO generated from $\text{Na}_2\text{N}_2\text{O}_3$ (a HNO donor) and the resultant solution was subjected to the EPR study in MeCN, the previous signal vanishes to the baseline indicating a complete reduction of $[\text{Cu}^{\text{II}}-\text{L}^2]^+$ to $[\text{Cu}^{\text{I}}(\text{L}^2)]$ and is responsible for the regeneration of the fluorescence properties of the complex.

5.3.4 S^{2-} Induced displacement of Cu^{2+} and S^{2-} sensing

From the earlier studies, we can conclude that L^2 selectively binds with Cu^{2+} to form the $[\text{Cu}^{\text{II}}-\text{L}^2]^+$ complex with a remarkable change in its spectral properties. As Cu^{2+} can coordinate with S^{2-} to form the stable species CuS, we conjectured that the $[\text{Cu}^{\text{II}}-\text{L}^2]^+$ ensemble can serve as a

CHAPTER 5

candidate for a turn-on fluorescent sensor for S^{2-} . To strengthen this idea, the fluorescence spectra of the $[Cu^{II}-L^2]^+$ ensemble were studied in the presence of ~ 5 equivalent of different anions such as F^- , Cl^- , Br^- , SO_3^{2-} , NO_2^- , SO_4^{2-} , SO_3^{2-} , PO_4^{3-} , N_3^- , HSO_4^- , HSO_3^- , SCN^- , CH_3COO^- and I^- which did not cause any remarkable fluorescence response (**Figure 5.15**).



However, the $[Cu^{II}-L^2]^+$ ensemble shows an obvious selective fluorescence ON behavior with S^{2-} . This fact strongly suggests that the ligand L^2 was freed from the $[Cu^{II}-L^2]^+$ complex in presence of S^{2-} . The formation constant of $[Cu^{II}-L^2]^+$ with S^{2-} was determined to be $(1.89 \pm 0.02) \times 10^4 M^{-1}$ on the basis of the fluorescence titration experiments (**Figure 5.16**). Also the absorbance behavior of the $[Cu^{II}-L^2]^+$ complex with S^{2-} was almost a reversible process compared to the Uv-Vis spectroscopic titration of L^2 with Cu^{2+} (**Figure 5.17**). The absorption peak and intensity changes were similar but in the reverse direction to the titration curve obtained with Cu^{2+} (**Figure 5.7a**). This phenomenon also suggests that L^2 is released from the $[Cu^{II}-L^2]^+$ complex and CuS is formed. From the above fact we can conclude that L^2 is recyclable efficiently. As illustrated in **Scheme 5.1**, the addition of copper ions into L^2 caused fluorescence quenching. Subsequently, the added sulfide ion captured copper(II) ions, resulting in fluorescence enhancement. Furthermore, the proposed mechanism was also well supported by the ESI- MS^+ (m/z) data (**Figure 5.18**).

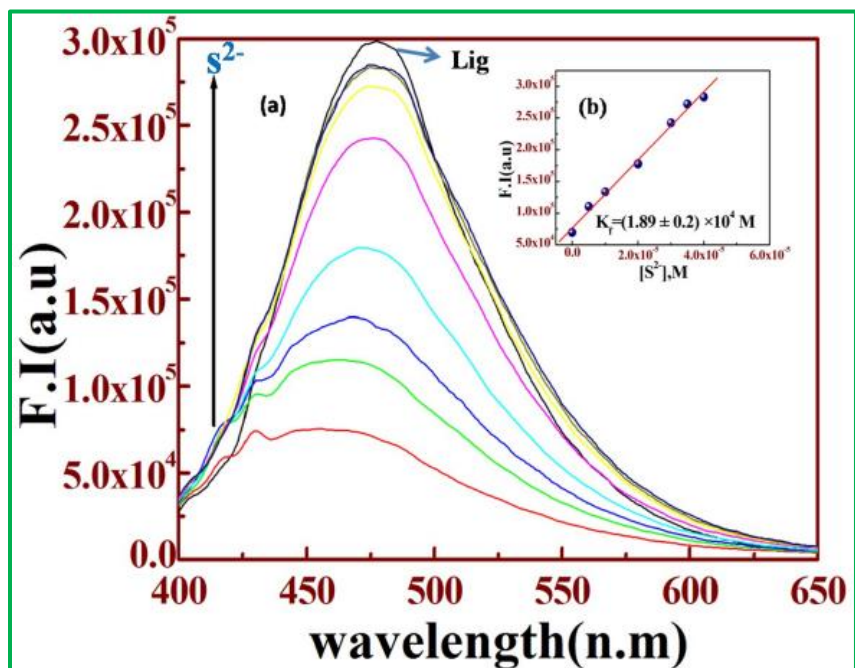


Figure 5.16. Fluorescence emission changes of $[\text{Cu}^{\text{II}}\text{-L}^2]^+$ ($20 \mu\text{M}$) in MeCN solutions upon addition of S^{2-} ($50\mu\text{M}$), $\lambda_{\text{ex}}=380\text{nm}$, $\lambda_{\text{em}}=478 \text{ nm}$);(b) Linear fitting plot.

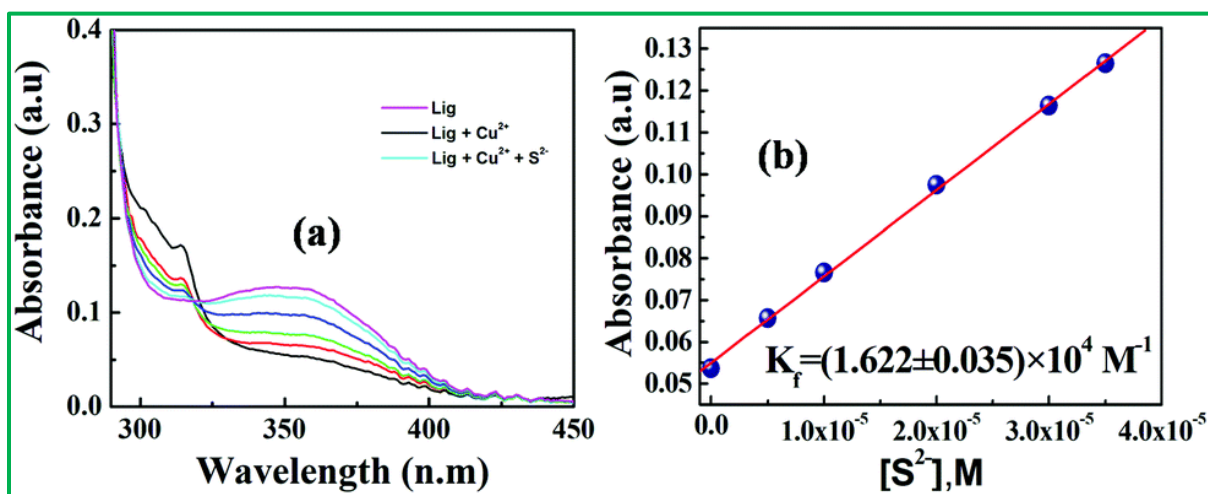


Figure 5.17. (a) Changes in UV-Vis absorption spectra of $[\text{Cu}^{\text{II}}\text{-L}^2]^+$ ($20 \mu\text{M}$) in MeCN solutions with gradual addition of S^{2-} ($0\text{--}1.8$ equivalent). (b) Linear fitting of absorbance vs. $[\text{S}^{2-}]$ plot.

From pH 7 to 10 no obvious change in the fluorescence intensity (FI) of the probe ($[\text{Cu}^{\text{II}}\text{-L}^2]^+$) was observed; however it is comparable with the F.I. obtained when L^2 is quenched by Cu^{2+} ions in the fluorescence titration, thereby justifying the usefulness of the probe for the detection of HNO and S^{2-} (**Figure 5.19**).

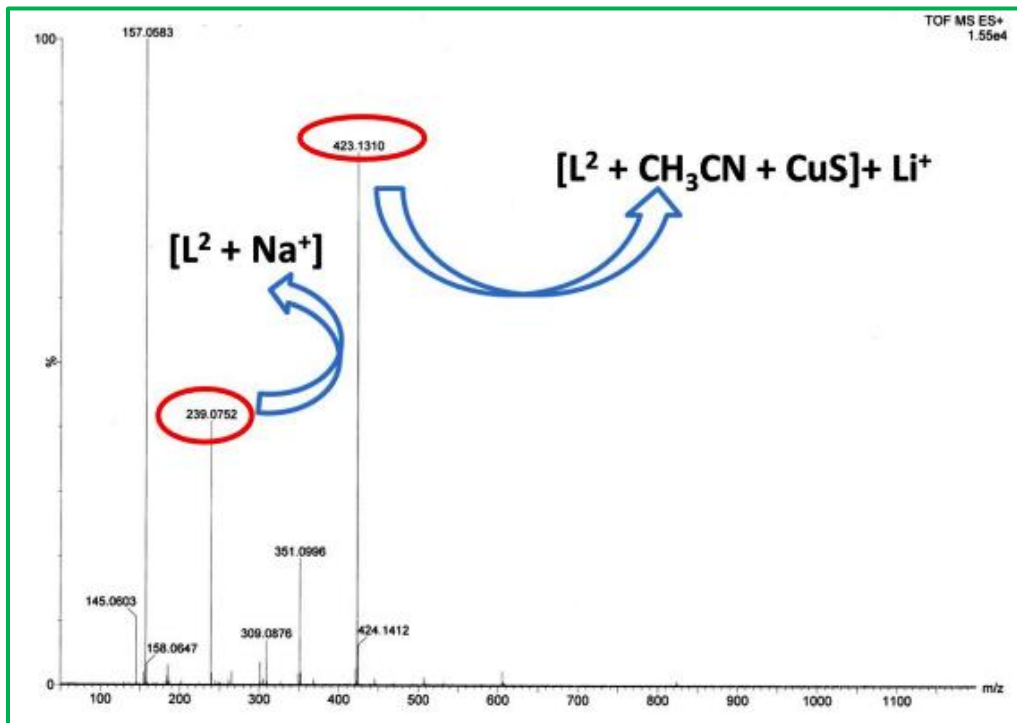


Figure 5.18. Mass spectrum of $\text{Cu-L}^2 + \text{Na}_2\text{S}$ in MeCN and H_2O .

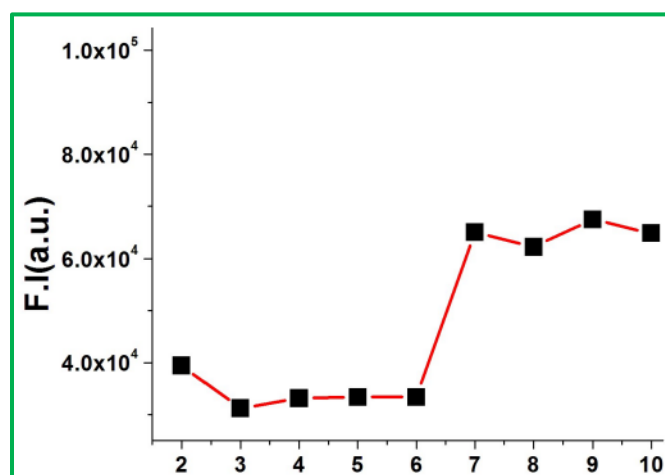


Figure 5.19. pH dependence of fluorescence responses of $[\text{Cu}^{\text{II}}\text{-L}^2]^+$ complex.

5.3.5 Geometry optimization and electronic structure

In order to get some idea of the coordination mode of the ligand with Cu^{2+} ions, we carried out DFT optimization on L^2 , $[(\text{L}^2)\text{Cu}^{\text{II}}\text{Cl}]$ and $[\text{Cu}^{\text{I}}\text{-L}^2]$ complexes. The optimized geometries of L^2 , $[(\text{L}^2)\text{CuCl}]$ and $[\text{Cu}^{\text{I}}\text{-L}^2]$ complexes are shown in **(Figure 5.20)**.

CHAPTER 5

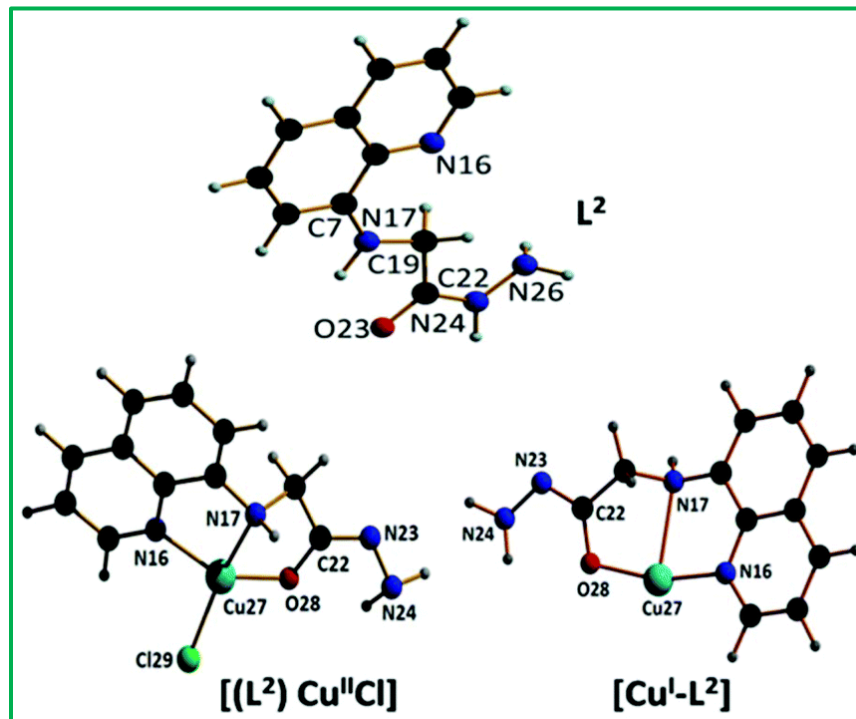


Figure 5.20. Optimized structures of L^2 , $[(L^2)Cu^{II}Cl]$ and $[Cu^I-L^2]$ complexes.

The compositions of these complexes (L^2 , $[(L^2)CuCl]$ and $[Cu^I-L^2]$) were adopted based on HRMS studies. L^2 , $[(L^2)CuCl]$ and $[Cu^I-L^2]$ complexes have a C_1 point group. The important optimized geometrical parameters of the ligand and complexes are listed in **Table 5.1**.

Table 5.1a. Selective bond distance and bond angles of L^2

Bond distance (\AA^0)		Bondangle ($^\circ$)	
N24-N26	1.39	C7 N17 C19	129.776
C22-O23	1.25	C19 C22 O23	122.608
C7-N17	1.37	C19 C22 N24	117.167
N17-C19	1.45	C22 N24 N26	122.772
C19-C22	1.52		
C22-N24	1.37		

CHAPTER 5

Table 5.1b. Selective bond distance and bond angles of $[\text{Cu}^{\text{II}}(\text{L}^2)\text{Cl}]$.

Bond distance (\AA)		Bondangle ($^\circ$)	
Cu27-Cl29	2.16	N17Cu27O28	84.356
O28-Cu27	1.90	N17Cu27N16	79.411
N16-Cu27	2.06	O28Cu27Cl29	101.149
N17-Cu27	2.24	N16Cu27Cl29	102.904

Table 5.1c. Selective bond distance and bond angles of $[\text{Cu}^{\text{I}}(\text{L}^2)]$.

Bond distance (\AA)		Bondangle ($^\circ$)	
N17-Cu27	2.42	N17Cu27O28	85.02
N16-Cu27	1.91	N17Cu27N16	81.35
O28-Cu27	1.87	N28C22N23	125.17
N23-N24	1.40		

In case of the $[\text{Cu}^{\text{II}}(\text{L}^2)(\text{Cl})]$ complex, the Cu^{2+} center was found to adopt a distorted tetrahedral geometry. The calculated Cu–N bond distances are found in the range of 2.06 \AA – 2.24 \AA and the Cu–O bond distances are 1.90 \AA which are comparable to the reported values.⁴⁸ On complexation there is a slight increase in C–N, N–N and N–O bond distances with respect to that in the free ligand. **Table 5.2** describes the changes in bond lengths in $[\text{Cu}^{\text{II}}(\text{L}^2)(\text{Cl})]$ compared to the free ligand. In the case of L^2 in the ground state, the electron density of the HOMO and HOMO–1 orbitals resides mainly on the quinolin-8-amine moiety, whereas for the LUMO and LUMO+1 orbitals, it remains on the quinoline moiety.

Table 5.2 Change in bond lengths (\AA) for $[\text{Cu}^{\text{II}}(\text{L}^2)(\text{Cl})]$ compared to free L^2 in the ground state calculated at B3LYP levels

	L^2	$[\text{Cu}^{\text{II}}(\text{L}^2)(\text{Cl})]$
N24–N26	1.39	1.38
C22–O23	1.25	1.32

CHAPTER 5

C7–N17	1.37	1.44
N17–C19	1.45	1.50
C22–N24	1.37	1.29

The energy gap between the HOMO and LUMO is 3.78 eV (Figure 5.21). In the case of the HOMO–1 and HOMO–2 orbitals in the $[\text{Cu}^{\text{II}}(\text{L}^2)(\text{Cl})]$ complex, the electronic contribution comes mainly from the (quinolin-8-ylamino)-acetic acid hydrazide moiety and in the case of the LUMO and LUMO+1 orbitals, it remains on the quinoline moiety. The HOMO–LUMO energy gap is 2.23 eV (Figure 5.21). In case of the HOMO–1 and HOMO–2 orbitals in $[\text{Cu}^{\text{I}}-\text{L}^2]$ complex, the electronic contribution comes mainly from the amino acetic acid hydrazide moiety and (quinolin-8-ylamino)-acetic acid hydrazide moiety, whereas in case of the LUMO, it comes from the quinolin-8-amine moiety. The HOMO–LUMO energy gap is 0.09 eV (Figure 5.21)

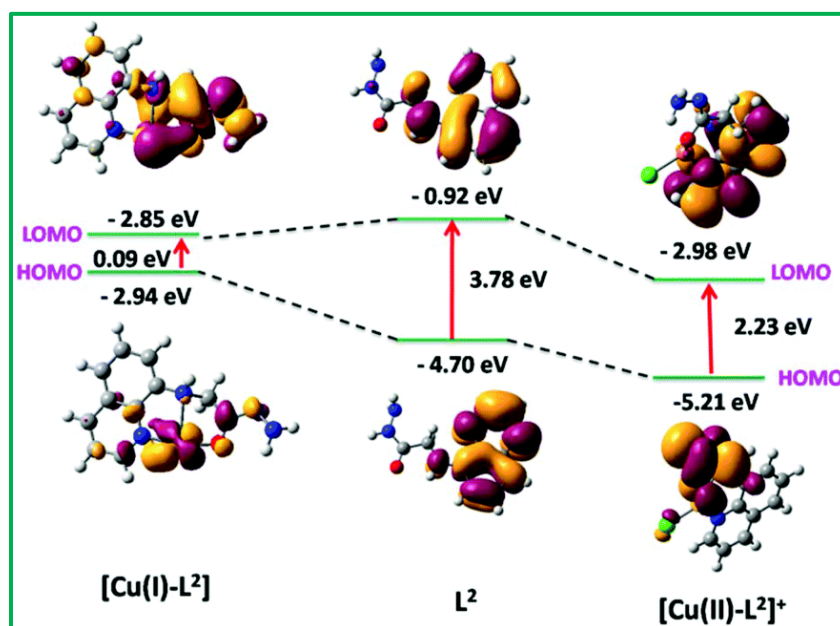


Figure 5.21. Frontier molecular orbitals of L^2 , $[\text{Cu}^{\text{II}}-\text{L}^2]^+$ and $[\text{Cu}^{\text{I}}-\text{L}^2]$ complexes.

The UV-Vis absorption spectrum of the ligand used in the present work was calculated at room temperature in CH_3CN by the TDDFT method. The ligands show three well resolved bands at 200, 256 and 350 nm and all have an ILCT character. These bands are assigned to the $\text{S}_0 \rightarrow \text{S}_{31}$,

CHAPTER 5

$S_0 \rightarrow S_{14}$ and $S_0 \rightarrow S_6$ electronic transitions, respectively (Figure 5.22a). The absorption energies and associated oscillator strengths are given in Table 5.3 and Table 5.4.

Table 5.3. The comparable calculated optical transitions with experimental UV/Vis values for the ligand (L^2), and $[Cu^{II}-L^2]^+$ and $[Cu^I-L^2]$ complexes

Ligand and Cu^{2+} - complex	Theoretical (nm)	Experimental (nm)	Electronic transition	f
Ligand	331.82	350	$S_0 \rightarrow S_6$	0.2682
Ligand	256.60	256	$S_0 \rightarrow S_{14}$	0.2029
Ligand	205.44	200	$S_0 \rightarrow S_{31}$	0.1193
$[Cu^{II}-L^2]^+$	331.66	352	$S_0 \rightarrow S_{15}$	0.0110
$[Cu^{II}-L^2]^+$	325.91	315	$S_0 \rightarrow S_{17}$	0.0222
$[Cu^{II}-L^2]^+$	249.88	256	$S_0 \rightarrow S_{38}$	0.0104
$[Cu^I-L^2]$	350.57	350	$S_0 \rightarrow S_4$	0.0304
$[Cu^I-L^2]$	291.72	287	$S_0 \rightarrow S_{12}$	0.0183

Table 5.4. Selected parameters for the vertical excitation (UV-Vis absorptions) of L^2 ; electronic excitation energies (eV) and oscillator strength (f), configurations of the low-lying excited states of L^2 ; calculation of the $S_0 \rightarrow S_n$ energy gaps on optimized ground-state geometries (UV-vis absorption).

Electronic transition	Composition	Excitation energy (eV)	Oscillator Strength(f)	CI	Assignment	λ_{exp} (nm)
$S_0 \rightarrow S_6$	HOMO \rightarrow LUMO+1	3.7365	0.2682	0.25046	ILCT	350
$S_0 \rightarrow S_{14}$	HOMO-1 \rightarrow LUMO+3	4.8318	0.2029	0.37123	ILCT	256
$S_0 \rightarrow S_{31}$	HOMO-6 \rightarrow LUMO+4	6.0349	0.1193	0.35030	ILCT	200

CHAPTER 5

The UV-Vis spectrum of the $[\text{Cu}^{\text{II}}(\text{L}^2)(\text{Cl})]$ complex shows three absorption bands at 256, 315 and 352 nm in CH_3CN at room temperature which correspond well to the TDDFT calculated absorption bands located at 250, 326 and 332 nm. These three absorption bands can be assigned to the $\text{S}_0 \rightarrow \text{S}_{38}$, $\text{S}_0 \rightarrow \text{S}_{17}$ and $\text{S}_0 \rightarrow \text{S}_{15}$ transitions, respectively (Figure 5.22b) originating from an admixture of LMCT and ILCT transitions (Table 5.5).

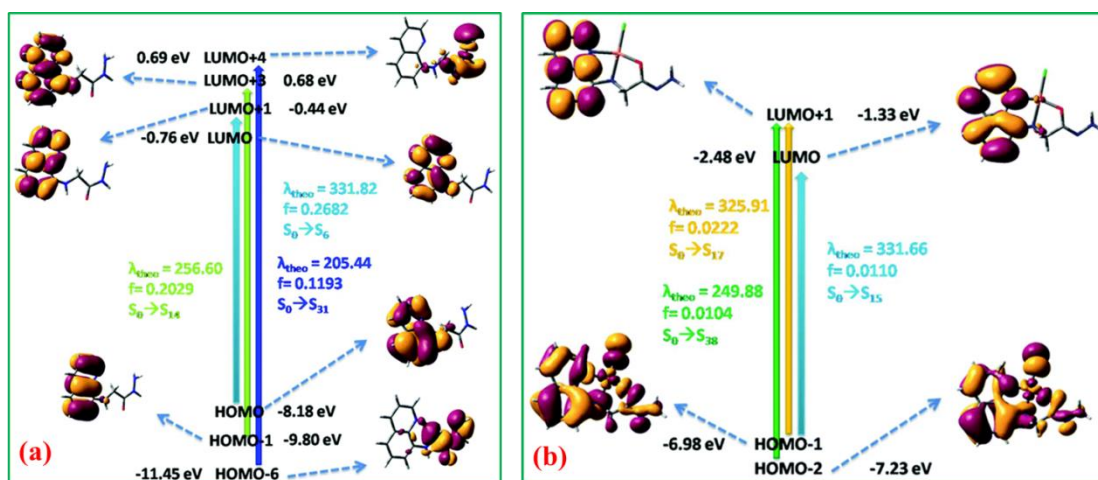


Figure 5.22. (a) Frontier molecular orbitals involved in the UV-Vis absorption of L^2 in CH_3CN . (b) Frontier molecular orbitals involved in the UV-Vis absorption of $[\text{Cu}^{\text{II}}(\text{L}^2)(\text{Cl})]$ in CH_3CN .

Table 5.5: Selected parameters for the vertical excitation (UV-Vis absorptions) of $[\text{Cu}^{\text{II}}(\text{L}^2)\text{Cl}]$; electronic excitation energies (eV) and oscillator strength (f), configurations of the low-lying excited states of $[\text{Cu}^{\text{II}}(\text{L}^2)\text{Cl}]$; calculation of the $\text{S}_0 \rightarrow \text{S}_n$ energy gaps on optimized ground-state geometries (UV-Vis absorption)

Electronic transition	Composition	Excitation energy (eV)	Oscillator Strength (f)	CI	Assignment	λ_{exp} (nm)
$\text{S}_0 \rightarrow \text{S}_{15}$	HOMO-1 \rightarrow LUMO	3.7383	0.110	0.74643	ILCT/MLCT	352
$\text{S}_0 \rightarrow \text{S}_{17}$	HOMO-1 \rightarrow LUMO+1	3.8042	0.0222	0.26103	ILCT/MLCT	315
$\text{S}_0 \rightarrow \text{S}_{38}$	HOMO-2 \rightarrow LUMO+1	4.9618	0.0104	0.16877	ILCT/MLCT	256

CHAPTER 5

The UV-Vis spectrum of the $[\text{Cu}^{\text{I}}-\text{L}^2]$ complex shows two absorption bands at 287 and 350 nm in CH_3CN at room temperature (Figure 5.23a) which correspond well to the TDDFT calculated absorption bands located at 292 and 351 nm. These two absorption bands can be assigned to the $\text{S}_0 \rightarrow \text{S}_{12}$ and $\text{S}_0 \rightarrow \text{S}_4$ transitions respectively (Figure 5.23b) originating from an admixture of LMCT and ILCT transitions (Table 5.6).

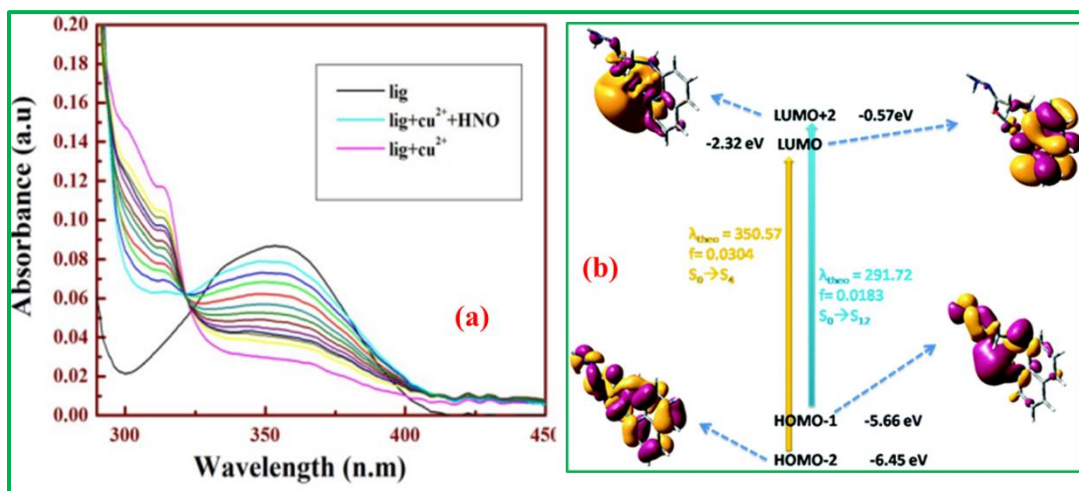


Figure 5.23. (a) Changes in UV-vis absorption spectra of $[\text{Cu}^{\text{II}}-\text{L}^2]^+$ (20 μM) in MeCN solutions with various amounts of HNO (0-2.5 equivalent). (b) Frontier molecular orbitals involved in the UV-Vis absorption of $[\text{Cu}^{\text{I}}-\text{L}^2]$ in CH_3CN .

Table 5.6. Selected parameters for the vertical excitation (UV-VIS absorptions) of $[\text{Cu}^{\text{I}}(\text{L}^2)]$; electronic excitation energies (eV) and oscillator strength (f), configurations of the low-lying excited states of $[\text{Cu}^{\text{I}}(\text{L}^2)]$; calculation of the $\text{S}_0 \rightarrow \text{S}_n$ energy gaps on optimized ground- state geometries (UV Vis absorption).

Electronic transition	Composition	Excitation energy(eV)	Oscillator Strength(f)	CI	Assignment	λ_{exp} (nm)
$\text{S}_0 \rightarrow \text{S}_4$	HOMO-2 \rightarrow LUMO	3.5366	0.0304	0.28325	ILCT/MLCT	350
$\text{S}_0 \rightarrow \text{S}_{12}$	HOMO-1 \rightarrow LUMO+ 2	4.2501	0.0183	0.56234	ILCT/MLCT	287

5.4 CONCLUSION

In summary, a new ligand, (quinolin-8-ylamino)-acetic acid hydrazide (L^2), has been synthesized and characterized. Taking this ligand a Cu(II) based sensor (1) has been developed by the complexation between (quinolin-8-ylamino)-acetic acid hydrazide (L^2) and Cu^{2+} ions. Complex (1) has also been characterized by ESI-MS⁺, X band EPR spectrum and CHN analysis. The EPR spectrum of $[Cu^{II}-L^2]^+$, prepared separately, is typically an axial type with $g_{\perp} = 2.04$, $g_{\parallel} = 2.18$ and $g_{av} = 2.11$ manifesting the presence of paramagnetic Cu^{II} ions; however on treatment with Angeli's salt, the EPR signal vanishes to the baseline indicating the complete reduction of paramagnetic Cu^{2+} to diamagnetic Cu^+ ions. The sensor (1) is highly selective for the recognition of HNO and S^{2-} over other biologically abundant anions with prominent enhancement in absorption and emission intensities. The sensor $[Cu^{II}-L^2]^+$ (1) shows weak fluorescence due to ET (electron transfer) but upon addition of HNO and S^{2-} , a large enhancement in the fluorescence intensity (F.I.) was observed over other possible competitive anions on the basis of the reduction of Cu(II) to Cu(I) and formation of CuS, respectively. The 1 : 1 complexation was characterized by Job's plot and the corresponding K_f values were evaluated to be $(4.93 \pm 0.05) \times 10^4 M^{-1}$ for Cu^{2+} obtained from Uv-Vis absorption titration. Quantum yields of L^2 and $[Cu-L^2 + S^{2-}]$ and $[Cu-L^2 + HNO]$ complexes in acetonitrile (CH_3CN) are found to be 0.107, 0.09, and 0.07, respectively, using acidic quinine sulphate as the standard.

References

1. Haugland, R. P. J. T. M. P.; Handbook, A guide to fluorescent probes and labeling technologies. **2005**.
2. Bertini, I.; Gray, H. B.; Lippard, S. J.; Valentine, J. S., *Bioinorganic chemistry*. University science books: 1994.
3. Bogdanova, A. Y.; Gassmann, M.; Nikinmaa, M., Copper ion redox state is critical for its effects on ion transport pathways and methaemoglobin formation in trout erythrocytes. *Chem.-Biol. Interact.* **2002**, *139* (1), 43-59.
4. Stouthart, X. J. H. X.; Haans, J. L. M.; Lock, R. A. C.; Bonga, S. E. W., Effects of water pH on copper toxicity to early life stages of the common carp (*Cyprinus carpio*). *Environ. Toxicol. Chem.* **1996**, *15* (3), 376-383.
5. Fahmy, M.A.; Potential genotoxicity in copper sulphate treated mice. *Cytologia*, **2000**, *65*(3), 235-242.
6. Gaggelli, E.; Kozlowski, H.; Valensin, D.; Valensin, G., Copper Homeostasis and Neurodegenerative Disorders (Alzheimer's, Prion, and Parkinson's Diseases and Amyotrophic Lateral Sclerosis). *Chem. Rev.* **2006**, *106* (6), 1995-2044.
7. Dujols, V.; Ford, F.; Czarnik, A. W., A Long-Wavelength Fluorescent Chemodosimeter Selective for Cu(II) Ion in Water. *J. Am. Chem. Soc.* **1997**, *119* (31), 7386-7387.
8. Kim, S.; Minier, M. A.; Loas, A.; Becker, S.; Wang, F.; Lippard, S. J., Achieving Reversible Sensing of Nitroxyl by Tuning the Ligand Environment of Azamacrocyclic Copper(II) Complexes. *J. Am. Chem. Soc.* **2016**, *138* (6), 1804-1807.
9. Wrobel, A. T.; Johnstone, T. C.; Deliz Liang, A.; Lippard, S. J.; Rivera-Fuentes, P., A Fast and Selective Near-Infrared Fluorescent Sensor for Multicolor Imaging of Biological Nitroxyl (HNO). *J. Am. Chem. Soc.* **2014**, *136* (12), 4697-4705.
10. Bogdan, C., Nitric oxide and the immune response. *Nat. Immunol.* **2001**, *2* (10), 907-916.
11. Brecht, D. S.; Hwang, P. M.; Snyder, S. H., Localization of nitric oxide synthase indicating a neural role for nitric oxide. *Nature* **1990**, *347* (6295), 768-770.
12. Bullen, M. L.; Miller, A. A.; Andrews, K. L.; Irvine, J. C.; Ritchie, R. H.; Sobey, C. G.; Kemp-Harper, B. K., Nitroxyl (HNO) as a Vasoprotective Signaling Molecule. *Antioxid. Redox Signal.* **2010**, *14* (9), 1675-1686.

CHAPTER 5

13. Liu, P.; Jing, X.; Yu, F.; Lv, C.; Chen, L., A near-infrared fluorescent probe for the selective detection of HNO in living cells and in vivo. *Analyst* **2015**, *140* (13), 4576-4583.
14. Rivera-Fuentes, P.; Lippard, S. J., Metal-Based Optical Probes for Live Cell Imaging of Nitroxyl (HNO). *Acc. Chem. Res.* **2015**, *48* (11), 2927-2934.
15. Feelisch, M., Nitroxyl gets to the heart of the matter. *Proc. Natl. Acad. Sci. U.S.A.* **2003**, *100* (9), 4978-4980.
16. Fukuto, J.M.; Chiang, K.; Hsieh, R.; Wong, P; Chaudhuri, G.; The pharmacological activity of nitroxyl: a potent vasodilator with activity similar to nitric oxide and/or endothelium-derived relaxing factor. *J. Pharmacol. Exp. Ther.*, **1992**, *263*(2), 546-551.
17. Stock, U. A., Tissue engineering of heart valves - hype or hope? *J. Thromb. Haemost.* **2005**, *94* (09), 469-470.
18. Choe, C.-u.; Lewerenz, J.; Fischer, G.; Uliasz, T. F.; Espey, M. G.; Hummel, F. C.; King, S. B.; Schwedhelm, E.; Böger, R. H.; Gerloff, C.; Hewett, S. J.; Magnus, T.; Donzelli, S., Nitroxyl exacerbates ischemic cerebral injury and oxidative neurotoxicity. *J. Neurochem.* **2009**, *110* (6), 1766-1773.
19. Choe, C.-U.; Lewerenz, J.; Gerloff, C.; Magnus, T.; Donzelli, S., Nitroxyl in the Central Nervous System. *Antioxid. Redox Signal.* **2011**, *14* (9), 1699-1711.
20. Fukuto, J. M.; Carrington, S. J., HNO Signaling Mechanisms. *Antioxid. Redox Signal.* **2011**, *14* (9), 1649-1657.
21. Jing, X.; Yu, F.; Chen, L., Visualization of nitroxyl (HNO) in vivo via a lysosome-targetable near-infrared fluorescent probe. *Chem. Commun.* **2014**, *50* (91), 14253-14256.
22. Doctorovich, F.; Bikiel, D.E.; Pellegrino, J.; Suárez, S.A.; Martí, M.A.; How to Find an HNO Needle in a (Bio)-Chemical Haystack. *Progress in Inorganic Chemistry* **2014**, *58*, 145-184.
23. Nelli, S.; Hillen, M.; Buyukafsar, K.; Martin, W., Oxidation of nitroxyl anion to nitric oxide by copper ions. *Br J Pharmacol* **2000**, *131* (2), 356-362.
24. Guidotti, T. L., Hydrogen Sulfide: Advances in Understanding Human Toxicity. *Int. J. Toxicol.* **2010**, *29* (6), 569-581.

CHAPTER 5

25. Evans, C.L.; The toxicity of hydrogen sulphide and other sulphides. *Quarterly Journal of Experimental Physiology and Cognate Medical Sciences: Translation and Integration*, **1967**, 52(3), pp.231-248.
26. Reiffenstein, R. J.; Hulbert, W. C.; Roth, S. H., Toxicology of Hydrogen Sulfide. *Annu. Rev. Pharmacol. Toxicol.* **1992**, 32 (1), 109-134.
27. Gao, M.; Yu, F.; Chen, H.; Chen, L., Near-Infrared Fluorescent Probe for Imaging Mitochondrial Hydrogen Polysulfides in Living Cells and in Vivo. *Anal. Chem.* **2015**, 87 (7), 3631-3638.
28. Gao, M.; Wang, R.; Yu, F.; You, J.; Chen, L., Imaging and evaluation of sulfane sulfur in acute brain ischemia using a mitochondria-targeted near-infrared fluorescent probe. *J. Mater. Chem. B* **2018**, 6 (17), 2608-2619.
29. Gao, M.; Wang, R.; Yu, F.; Chen, L., Evaluation of sulfane sulfur bioeffects via a mitochondria-targeting selenium-containing near-infrared fluorescent probe. *Biomaterials* **2018**, 160, 1-14.
30. Gao, M.; Yu, F.; Lv, C.; Choo, J.; Chen, L., Fluorescent chemical probes for accurate tumor diagnosis and targeting therapy. *Chem. Soc. Rev.* **2017**, 46 (8), 2237-2271.
31. Brown, D. I.; Griendling, K. K., Regulation of Signal Transduction by Reactive Oxygen Species in the Cardiovascular System. *Circ. Res.* **2015**, 116 (3), 531-549.
32. Wang, R.; Yu, F.; Chen, L.; Chen, H.; Wang, L.; Zhang, W., A highly selective turn-on near-infrared fluorescent probe for hydrogen sulfide detection and imaging in living cells. *Chem. Commun.* **2012**, 48 (96), 11757-11759.
33. Saluja, P.; Kaur, N.; Singh, N.; Jang, D. O., A benzimidazole-based fluorescent sensor for Cu²⁺ and its complex with a phosphate anion formed through a Cu²⁺ displacement approach. *Tetrahedron Lett.* **2012**, 53 (26), 3292-3295.
34. Cao, X.; Lin, W.; He, L., A Near-Infrared Fluorescence Turn-On Sensor for Sulfide Anions. *Org. Lett.* **2011**, 13 (17), 4716-4719.
35. Hou, F.; Huang, L.; Xi, P.; Cheng, J.; Zhao, X.; Xie, G.; Shi, Y.; Cheng, F.; Yao, X.; Bai, D.; Zeng, Z., A Retrievable and Highly Selective Fluorescent Probe for Monitoring Sulfide and Imaging in Living Cells. *Inorg. Chem.* **2012**, 51 (4), 2454-2460.

CHAPTER 5

36. Zhang, L.; Lou, X.; Yu, Y.; Qin, J.; Li, Z., A New Disubstituted Polyacetylene Bearing Pyridine Moieties: Convenient Synthesis and Sensitive Chemosensor toward Sulfide Anion with High Selectivity. *Macromolecules* **2011**, *44* (13), 5186-5193.
37. Choi, M. G.; Cha, S.; Lee, H.; Jeon, H. L.; Chang, S.-K., Sulfide-selective chemosignaling by a Cu²⁺ complex of dipicolylamine appended fluorescein. *Chem. Commun.* **2009**, (47), 7390-7392.
38. Lou, X.; Mu, H.; Gong, R.; Fu, E.; Qin, J.; Li, Z., Displacement method to develop highly sensitive and selective dual chemosensor towards sulfide anion. *Analyst* **2011**, *136* (4), 684-687.
39. Zhang, R.; Yu, X.; Yin, Y.; Ye, Z.; Wang, G.; Yuan, J., Development of a heterobimetallic Ru(II)–Cu(II) complex for highly selective and sensitive luminescence sensing of sulfide anions. *Anal. Chim. Acta* **2011**, *691* (1), 83-88.
40. Smith, P. A.; Hein, G. E. The alleged role of nitroxyl in certain reactions of aldehydes and alkyl halides. *J. Am. Chem. Soc.* **1960**, *82* (21), 5731-5740.
41. Frisch, M.J.; Trucks, G.W.; Schlegel, H.B.; Scuseria, G.E.; Robb, M.A.; Cheeseman, J.R.; Scalmani, G.; Barone, V.; Mennucci, B.; Petersson, G.A.; 2005. Gaussian 09, Revision D. 01, Gaussian, Inc.: Wallingford, CT (2009).(b) *S. J. Chem. Sci*, *117*, p.477.
42. Casida, M. E.; Jamorski, C.; Casida, K. C.; Salahub, D. R., Molecular excitation energies to high-lying bound states from time-dependent density-functional response theory: Characterization and correction of the time-dependent local density approximation ionization threshold. *J. Chem. Phys.* **1998**, *108* (11), 4439-4449.
43. Stratmann, R. E.; Scuseria, G. E.; Frisch, M. J., An efficient implementation of time-dependent density-functional theory for the calculation of excitation energies of large molecules. *J. Chem. Phys.* **1998**, *109* (19), 8218-8224.
44. Barone, V.; Cossi, M., Quantum Calculation of Molecular Energies and Energy Gradients in Solution by a Conductor Solvent Model. *J. Phys. Chem. A* **1998**, *102* (11), 1995-2001.
45. Cossi, M.; Barone, V., Time-dependent density functional theory for molecules in liquid solutions. *J. Chem. Phys.* **2001**, *115* (10), 4708-4717.

CHAPTER 5

46. Cossi, M.; Rega, N.; Scalmani, G.; Barone, V., Energies, structures, and electronic properties of molecules in solution with the C-PCM solvation model. *J. Comput. Chem.* **2003**, *24* (6), 669-681.
47. Liu, Y.; Ai, K.; Cheng, X.; Huo, L.; Lu, L., Gold-Nanocluster-Based Fluorescent Sensors for Highly Sensitive and Selective Detection of Cyanide in Water. *Adv. Funct. Mater.* **2010**, *20* (6), 951-956.
48. Alam, R.; Mistri, T.; Mondal, P.; Das, D.; Mandal, S. K.; Khuda-Bukhsh, A. R.; Ali, M., A novel copper(ii) complex as a nitric oxide turn-on fluorosensor: intracellular applications and DFT calculation. *Dalton Trans.* **2014**, *43* (6), 2566-2576.
49. Liochev, S. I.; Fridovich, I., The mode of decomposition of Angeli's salt ($\text{Na}_2\text{N}_2\text{O}_3$) and the effects thereon of oxygen, nitrite, superoxide dismutase, and glutathione. *Free Radic. Biol. Med.* **2003**, *34* (11), 1399-1404.
50. Murphy, M. E.; Sies, H., Reversible conversion of nitroxyl anion to nitric oxide by superoxide dismutase. *Proc. Natl. Acad. Sci. U.S.A.* **1991**, *88* (23), 10860-10864.

CHAPTER 6

Highlights of the Thesis

CHAPTER 6

After the elaborate description, the overall view of the thesis is summarized chapter wise to highlight the aims of our project that may indicate the extent to which we have achieved our dream for the entire titled project.

Chapter 1

This chapter deals with the short introduction about the reactive bio-molecule NO (Nitric Oxide) and its kin HNO (nitroxyl). The endogenous synthesis of NO and HNO and their key role in physiological and pathological processes has been elaborately explained along with the brief review of previously reported NO and HNO probes utilizing fluorescence method.

Chapter 2

In this chapter, we have described a new N-nitrosation based fluorescent sensor (**NDAQ**) utilizing 8-aminoquinoline and Nitrobenzoxadiazole as fluorophoric units. The probe exhibits ~27 fold fluorescence enhancement at $\lambda_{em} = 542$ nm with high sensitivity (LOD=7 nM) and shorter response time, eliminating the interference of reactive species (RCS/ ROS/RNS). Furthermore, all the photophysical studies of NDAQ have been performed in pure aqueous medium at physiological pH, indicating its good stability under physiological condition. The kinetic assay illustrates the second-order dependency w.r.to [NO] and first order with [NDAQ]. The biological studies reveal the successful application of the probe to track both endogenous and exogenous NO in living organisms.

Chapter 3

The chapter 3 represents a simple, least-cytotoxic as well as an efficient fluorescent sensor **HqEN₄₈₀** for nitric oxide (NO). The probe was synthesized utilizing (quinolin-8-yloxy)-acetic acid ethyl ester (L^1) and N,N-dimethyl ethylene diamine to recognize NO in 100% aqueous solution. Its marked selectivity and sensitivity towards NO, makes it a highly suitable probe for nitric oxide under in vitro conditions with the possibility of in vivo monitoring of NO. Upon addition of 3.5 equivalents of NO, there is ~7 fold enhancement in fluorescence intensity in aqueous solution with a corresponding K_f value of $(1.75 \pm 0.07) \times 10^4 \text{ M}^{-1}$. In terms of the $3\sigma/\text{slope}$ method, the LOD for nitric oxide was found to be 53 nM thus, making the probe highly suitable to track NO in biological systems.

Chapter 4

This chapter deals with a new dihydropyridine based nitric oxide sensitive probe (**CQME**) with benzochromene as the fluorophore unit. The probe exhibits ~30 fold enhancement in the emission intensity at 615 nm on excitation at 470 nm resulting a huge stoke-shifts of 145 nm assuring a minimum interference from the excitation light for in vivo applications. Investigation of the cause of this enhancement reveals that the cleavage of C-C bond between benzochromene and 1,4-dihydropyridine (DIPY) units occurs due to nitration on the 2H-pyran ring of benzochromene moiety leading to the formation of 2-nitro-3H-benzo[f]chromene (PYNO₂) and dimethyl 2,6-dimethylpyridine-3,5-dicarboxylate (PYMAA) as major products. While the simple chromene-DIPY based probe (**SALDPY**) gives dimethyl 4-(2H-chromen-3-yl)-2,6-dimethylpyridine-3,5-dicarboxylate (SALPY) as the major product with a very small amount of C-nitrosated product (SALNO₂). Now, the biocompatibility, high selectivity and sensitivity (~42 nM) along with pH independency of CQME makes it a premier candidate to be utilized to trace both endogenous and exogenous nitric oxide (NO) in biological systems.

Chapter 5

This chapter represents a Cu(II) based sensor (**1**) for highly sensitive and selective recognition of HNO and S²⁻ over other biologically abundant anions with prominent enhancement in absorption and emission intensities. This was synthesized by complexation between (quinolin-8-ylamino)-acetic acid hydrazide (L²) and Cu²⁺ ions. The sensor (1) exhibits weak fluorescence due to ET (electron transfer) but upon addition of HNO and S²⁻, a large enhancement in fluorescence intensity (F.I.) was observed over other possible competitive anions on the basis of reduction of Cu(II) to Cu(I) and formation of CuS, respectively. The 1:1 complexation was characterized by mass spectrometry (MS), elemental analysis and Job's plot. The corresponding K_f value for Cu²⁺ from Uv-Vis absorption titration was evaluated as $(4.934 \pm 0.05) \times 10^4 \text{ M}^{-1}$. DFT studies also supports the sensing mechanism of Cu(II) based sensor (1) towards HNO and S²⁻.

List of Publications

1. Dual response fluorescent sensor for HNO and S²⁻ ions using Cu (II) complex based probe assistant with detailed DFT studies
Dutta, A.; Alam, R.; Islam, A. S. M.; Dutta, A.; Ali, M. *Dalton Trans.*, 2018,**47**, 11563-11571.
2. A smart molecular probe for selective recognition of nitric oxide in 100% aqueous solution with cell imaging application and DFT studies
Dutta, A.; Islam, A.S.M.; Maiti, D.; Sasmal, M.; Prodhan, C.; Ali, M. *Org. Biomol. Chem.*, 2019,**17**, 2492-2501.
3. Dansyl appended CuII-complex based Nitroxyl (HNO) sensing with living cell application and DFT studies
Maiti, D.; Islam, A.S.M.; **Dutta, A.**; Sasmal, M.; Prodhan, C.; Ali, M. *Dalton Trans.*, 2019, **48**, 2760-27716.
4. A Coumarin Embedded Highly Sensitive Nitric Oxide Fluorescent Sensor: Kinetic Assay and Bio-imaging Applications
Maiti, D.; Islam, A.S.M.; Sasmal, M.; **Dutta, A.**; Katarkar, A.; Ali, M. *Org. Biomol. Chem.*, 2020, **18**, 8450
5. Design of a Pyrene Scaffold Multifunctional Material: Real-Time Turn-On Chemosensor for Nitric Oxide, AIEE Behavior, and Detection of TNP Explosive
Islam, A.S.M.; Sasmal, M.; Maiti, D.; **Dutta, A.**; Show, B.; Ali, M. *ACS Omega*, 2018, **3**, 10306–10316.
6. Phenazine Embedded Copper (II) Complex as a Fluorescent Probe for the Detection of NO and HNO with Bioimaging Application
Islam, A.S.M.; Sasmal, M.; Maiti, D.; **Dutta, A.**; Ganguly S.; Katarkar, A.; Gangopadhyay, S.; Ali, M., *ACS Appl. Bio Mater.*, 2019, **25**, 1944-1955
7. Site-Selective Interaction of Human Serum Albumin with 4-Chloro-7-nitro-1,2,3-benzoxadiazole Modified Olanzapine Derivative and Effect of β -Cyclodextrin on Binding: In the Light of Spectroscopy and Molecular Docking
Sasmal, M.; Islam, A.S.M.; Bhowmick, R.; Maiti, D.; **Dutta, A.**; Ali, M., *ACS Appl. Bio Mater.* 2019, **2**, 8, 3551–3561

Appendix

8. Serum Albumin Inspired Self-Assembly/Disassembly of a Fluorogenic Nanoprobe for Real-Time Monitoring and Quantification of Urinary Albumin with Live Cell Imaging Application
Sasmal, M.; Islam, A.S.M.; Moni, D.; Maiti, D.; **Dutta, A.**; Ali, M., ***ACS Appl. Bio Mater.*** 2022, 5, 12, 5854–5864.

Cite this: *Dalton Trans.*, 2018, **47**, 11563

A dual response fluorescent sensor for HNO and S²⁻ ions using a Cu(II) complex based probe assisted by detailed DFT studies†

Ananya Dutta,^a Rabiul Alam,^a Abu Saleh Musha Islam,^a Arpan Dutta^a and Mahammad Ali *^{a,b}

A Cu(II) based sensor (**1**) prepared by the complexation between (quinolin-8-ylamino)-acetic acid hydrazide (**L**²) and Cu²⁺ ions has been developed for a highly sensitive and selective recognition of HNO and S²⁻ over other biologically abundant anions with prominent enhancement in absorption and emission intensities. The sensor (**1**) shows weak fluorescence due to ET (electron transfer) but upon addition of HNO and S²⁻ a large enhancement in the fluorescence intensity (F.I.) was observed over other possible competitive anions on the basis of reduction of Cu(II) to Cu(I) and formation of CuS, respectively. The 1 : 1 complexation was characterized by mass spectrometry (MS), elemental analysis and Job's plot. The corresponding *K_f* value was evaluated to be $(4.934 \pm 0.05) \times 10^4 \text{ M}^{-1}$ for Cu²⁺ from UV-Vis absorption titration. Quantum yields of **L**² and [Cu-L² + S²⁻] and [Cu-L² + HNO] complexes in acetonitrile (CH₃CN) are found to be 0.107, 0.09 and 0.07, respectively, using quinine sulphate as the standard.

Received 7th July 2018,
Accepted 24th July 2018
DOI: 10.1039/c8dt02784f

rsc.li/dalton

Introduction

In many areas and disciplines, fluorescent sensors are in high demand because of their selective and efficient signaling properties for the detection of various chemical and biological analytes.¹ Copper, an essential trace metal ion, plays an important role in various biological and metabolic processes, the level of which can be regulated haemostatically.² Accumulation of a large excess of copper in the brain and the liver is highly toxic and causes Alzheimer's, Parkinson's, Prion, Menkes and Wilson's diseases.³⁻⁶ Fluorescence measurement is one of the great techniques to detect Cu²⁺ because of its sensitivity and specificity and real-time monitoring with a fast response time.⁷ Moreover, the Cu²⁺ complexes have the ability to sense other substances.⁸

Nitric oxide (NO) is an important signaling agent for various processes that involve the cardiovascular,⁹ immune¹⁰ and nervous systems.¹¹ HNO, the one-electron reduced and protonated derivative of NO, displays distinctive chemistry and biochemistry different from that of NO.¹²⁻¹⁴

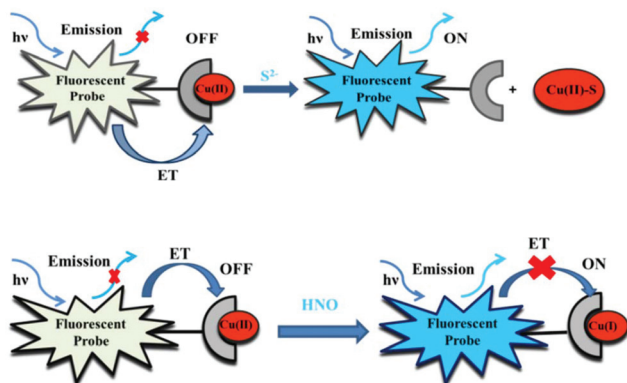
Recent studies reveal that exogenous administration of HNO increases the contractility of heart cells,¹⁵ leads to vasorelaxation in muscle cells¹⁶ and decreases platelet aggregation.¹⁷ HNO also exacerbates ischemia-related injury¹⁸ and induces neurotoxicity.¹⁹ These lead to the conclusion that HNO plays a crucial role in biology. Detecting HNO in biological systems is a challenge that has caught the attention of chemists. Difficulties associated with HNO sensing include differentiation from NO and other biologically relevant analytes, rapid detection in low concentrations and compatibility of the sensing mechanism with biological environments, particularly at neutral or slightly acidic pH, high ionic strength and a temperature of 37 °C.

The most effective strategy for detecting HNO is to take advantage of its redox activity.^{20,21} Probes that are able to be reduced selectively by HNO act as sensors if an appropriate output signal is linked to the reduction step. Although there are various chemical reactions that can be used to detect and trap HNO,²² usually, azanone (HNO, nitroxyl) reacts with copper(II) ions, resulting in the formation of nitric oxide and Cu⁺.²³ This strategy is utilized for the construction of copper-based pro-fluorescent HNO probes.

We discuss here on the systems that collocate a Cu(II) coordination complex with a fluorophoric moiety. The sensing mechanism of such probes depends on the unpaired electron of the Cu(II) center which quenches the fluorescence of a photoemissive ligand by either electron or energy transfer (Scheme 1). Reduction of Cu(II) to Cu(I) by HNO restores the fluorescence of the ligand.

^aDepartment of Chemistry Jadavpur University, Kolkata 700 032, India.
E-mail: m_ali2062@yahoo.com, mali@chemistry.jdvu.ac.in; Fax: +91-33-2414-6223
^bVice-Chancellor, Aliah University, II-A/27, Action Area II, Newtown, Action Area II, Kolkata, West Bengal 700160, India

† Electronic supplementary information (ESI) available. See DOI: 10.1039/c8dt02784f



Scheme 1 General mechanism of S^{2-} sensing and HNO sensing using the copper complex.

Hydrogen sulfide (H_2S), a deadly chemical species, is naturally produced by geological and microbial activities.²⁴ Exposure to H_2S can trigger eye and respiratory tract irritation.²⁵ Inhalation of excess H_2S can result in the loss of consciousness, cardiac arrest and in extreme cases, death.²⁶ H_2S exerts a regulative function of the intracellular redox status and functions as an endogenous signalling molecule.²⁷ It can regulate the activities of ion channels and act as a tumor suppressor and it may be the actual signalling molecule in cell signal transduction.^{28–31}

Once protonated, HS^- or H_2S is even more toxic than sulfide (S^{2-}) itself. Abnormal concentrations of H_2S can cause Alzheimer's disease, Down syndrome and liver cirrhosis.³² Therefore, it is essential to develop a rapid and sensitive method for the detection of sulfide anions.

By utilizing the displacement approach, the ligand metal ion “ensemble” that is non-fluorescent due to metal-ion-induced fluorescence quenching, however, becomes fluorescent on subsequent treatment of the ensemble with an anion which displaces the metal ion from the coordination sphere of the original organic receptor and releases the ligand into the solution with a revival of the fluorescence^{33–35} (Scheme 1).

As sulfide is known to react with copper ions to form very stable CuS ($K_{sp} = 6.3 \times 10^{-36}$),³⁵ among various approaches for sulfide sensing, this reversible sensing exploiting copper sulfide affinity attracted our special attention.^{36–39}

In this paper, we report a Cu-based sensor (**1**) prepared by the complexation between (quinolin-8-ylamino)-acetic acid hydrazide (**L**²) and Cu^{2+} ions which has been developed for a highly sensitive and selective recognition of HNO and S^{2-} over other possible competitive anions on the basis of the reduction of $Cu(II)$ to $Cu(I)$ and forming CuS . The 1 : 1 complexation between the probe and Cu^{2+} was characterized by mass spectrometry (MS), elemental analysis and Job's plot. The photophysical properties and recognition behaviours of the chemosensor have been investigated in detail through UV-Vis absorption spectra, fluorescence spectra, MS and theoretical calculations.

Experimental section

Materials and methods

8-Aminoquinoline, ethyl bromoacetate (Sigma Aldrich), hydrazine hydrate (Sigma Aldrich), absolute ethanol and salts of Cr^{3+} , Co^{2+} , Hg^{2+} , Mg^{2+} , Mn^{2+} , Dy^{3+} , Pb^{2+} , Zn^{2+} , Sm^{3+} , F^- , Br^- , Cl^- , I^- , SCN^- , HSO_4^- , SO_3^{2-} , SO_4^{2-} , HSO_3^- , PO_4^{3-} , CH_3COO^- , N_3^- , NO_2^- and S^{2-} were obtained from commercial suppliers and used without further purification. Angeli's salt was prepared by the reported method.⁴⁰ Solvents like MeOH (methanol), MeCN (acetonitrile) *etc.* (Merck, India) were of reagent grade. All other reagents were procured from commercial sources and used without further purification.

Physical measurements

Elemental analyses were carried out using a CHN analyzer (PerkinElmer 240). Infrared spectra were recorded in the solid state on a Nicolet Magna IR 750 series-II FTIR spectrometer in the range $400\text{--}4000\text{ cm}^{-1}$. 1H -NMR spectra were recorded in $DMSO-d_6$ on a Bruker 300 MHz NMR spectrometer with TMS ($\delta = 0$) acting as an internal standard. ESI-MS⁺ (m/z) of the ligand and complexes were recorded on a Waters XEVO G2QToF HRMS spectrometer. An Agilent diode-array spectrophotometer (Model, Agilent 8453) was used for UV-Vis studies. Steady-state fluorescence studies were carried out on a PTI QM-40 spectrofluorometer. Lifetimes were measured using a Horiba Jobin-Yvon Hamamatsu MCP photomultiplier (R3809) and data were analyzed by using the IBH DAS6 software. X-band EPR spectra were recorded on an EPR-Spectrometer (Model: JEOL, JES-FA 200).

Preparation of (quinolin-8-ylamino)-acetic acid ethyl ester (**L**¹)

A mixture of 8-aminoquinoline (5 mmol), ethyl bromoacetate (7.5 mmol) and anhydrous K_2CO_3 (12.5 mmol) in acetonitrile was refluxed in a water bath for 8 h. The mixture was then filtered and the solvent was removed under reduced pressure. The resulting oily product was purified by column chromatography on silica gel, using DCM : MeOH (9 : 1) as the eluent to afford **L**¹ (85% yield). **L**¹ was characterized by 1H NMR analysis. 1H NMR (in $DMSO-d_6$, 300 MHz, ppm): δ_{ppm} : 1.20 (m, 3H, $-CH_3$), 4.17 (m, 4H, $-CH_2$, $-CH_2$), 6.57 (d, 1H, $-ArH$), 6.86 (s, 1H, $-ArH$), 7.36 (m, 1H, $-ArH$), 7.50 (m, 1H, $-ArH$), 8.21 (d, 1H, $-ArH$), 8.75 (s, 1H, $-NH$) (Fig. S1†).

Preparation of (quinolin-8-ylamino)-acetic acid hydrazide (**L**²)

The resulting (quinolin-8-ylamino)-acetic acid ethyl ester (1.0 mmol) and hydrazine hydrate (10 mmol) in ethanol were refluxed in a water bath for 6 h. After cooling, the solid that separated out was filtered and washed with water, dried and recrystallized from ethanol. Needle shaped crystals were obtained. Yield ~70%. CHN analysis for $C_{11}H_{12}N_4O$ calculated (%): C, 61.10; H, 5.59; N, 25.91 found (%): C, 60.90; H, 5.58; N, 25.81. 1H NMR (300 MHz, $DMSO-d_6$) δ_{ppm} : 3.85 (s, 2H, $-CH_2$), 4.27 (s, 2H, $-NH_2$), 6.53 (d, 1H, $-ArH$), 6.82 (m, 1H, $-ArH$), 7.35 (m, 1H, $-ArH$), 7.50 (m, 1H, $-ArH$), 8.22 (d, 1H, $-ArH$), 8.75 (s, 1H, $-NH$) and 9.19 (s, 1H, $-NH$) (Fig. S1a†). ^{13}C -NMR:

(300 MHz, DMSO- d_6) δ_{ppm} : 45.18, 105.16, 114.43, 122.25, 128.13, 128.66, 136.40, 138.01, 144.51, 147.60, 169.34 (Fig. S2†). ESI-MS⁺ (m/z): 239.07 ($L^2 + Na^+$) (Fig. S3†). IR spectrum: $-NH_2$ (3430 cm^{-1}), $-NH$ (3302 cm^{-1}), $-C=O$ (1640 cm^{-1}) (Fig. S4†).

Solution preparation for UV-Vis and fluorescence studies

For both UV-Vis and fluorescence titrations, a stock solution of $1.0 \times 10^{-3}\text{ M}$ of the ligand (L^2) was prepared in degassed CH_3CN under a nitrogen atmosphere. $1.0 \times 10^{-2}\text{ M}$ stock solutions of $CuCl_2 \cdot 2H_2O$ and Na_2S in water were prepared separately under a N_2 atmosphere. Similarly, $1.0 \times 10^{-3}\text{ M}$ stock solution of Angeli's salt in water was prepared in degassed water under a nitrogen atmosphere. Stock solutions of tested metal ions as well as anions were prepared in CH_3CN-H_2O under anaerobic conditions by purging nitrogen gas in a gas tight vessel. 2.5 ml of degassed CH_3CN was pipetted out in a gas tight cuvette to which $20\text{ }\mu\text{M}$ of L^2 was added. Then metal ions were added incrementally starting from 0 to $24\text{ }\mu\text{M}$ in a regular interval of volume by injecting into the headspace of the gas tight cuvette before measuring fluorescence. Likewise titration of the resulting complex, $[Cu^II(L^2)]^+$, was carried out by the incremental addition of Angeli's salt (0– $10\text{ }\mu\text{M}$). The path lengths of the cells for absorption and emission studies were 1 cm. Fluorescence measurements were performed using a $5\text{ nm} \times 3\text{ nm}$ slit width.

Preparation of sensor (1)

Copper(II) chloride dihydrate, $CuCl_2 \cdot 2H_2O$ (65 mg, 0.5 mmol), was dissolved in 10 ml of freshly distilled acetonitrile and to this yellow solution, ligand L^2 (108 mg, 0.5 mmol) was added. The color of the solution changed to light green. The resulting mixture was stirred for 3 h. The volume of the solution was reduced to 5 ml under reduced pressure and diethyl ether (10 mL) was added and kept at $0\text{ }^\circ\text{C}$ for 12 h to afford complex (1) as microcrystals (M.W. 314.23). Yield: 138 mg (~80%). CHN analyses for $C_{11}H_{11}ClCuN_4O$, calculated (%): C, 42.04; H, 3.53; N, 17.83 found (%): C, 42.03; H, 3.54; N, 17.84. ESI-MS⁺ (m/z): 320.3290 ($[(L^2)Cu^II(Cl)] + Li^+$) (Fig. S3a†).

Job's plot

The composition of the complex was determined by Job's method. In this method, we carried out the absorption measurements of a series of solutions keeping the sum of two reactants constant in a fixed volume but varying molar concentrations of Cu^{2+} ions and plotted against the molar fraction of the fluorophore. A minimum absorbance appeared at the molar ratio of the reactants which was found to be 1:1 with respect to the ligand for the Cu^{2+} complex.

Computational details

L^2 was fully optimized using a Gaussian 09 W software package.⁴¹ The B3LYP functional was adopted with 6-31G as the basis set for all the atoms (C, H, N and O) and for the Cu complex we used the B3LYP/6-31+g(d,p) basis set. The global minima of all these species were confirmed by the positive

vibrational frequencies. Time dependent density functional theory (TDDFT)^{42,43} with the B3LYP density functional associated with the conductor-like polarizable continuum model (CPCM)^{44–46} was applied for the study of the low-lying excited states of the ligand and the complexes in CH_3CN using the optimized geometry of the ground state (S_0). The vertical excitation energies of the lowest 40 singlet states are also computed here.

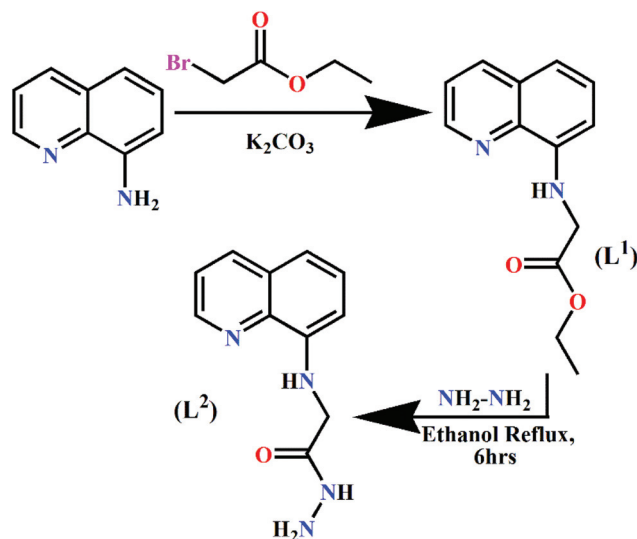
Results and discussion

The ligand L^2 was prepared by refluxing (quinolin-8-ylamino)-acetic acid ethyl ester (1.0 mmol) and hydrazine hydrate (10 mmol) in ethanol in a water bath for 6 h (Scheme 2). The final product and all the intermediates were characterized thoroughly by CHN analysis, 1H (Fig. S1†) and ^{13}C -NMR (Fig. S2†), HRMS (Fig. S3†) and IR (Fig. S4†) studies.

UV-Vis absorption studies

The UV-Vis absorption spectrum of L^2 with Cu^{2+} was investigated by spectrophotometric titration in acetonitrile solution. L^2 exhibits strong bands around 350 nm and 256 nm. Upon addition of Cu^{2+} (1 equivalent), the absorption intensity decreased at 350 nm and increased at 299 nm (Fig. 1a) which further confirms the coordination between Cu^{2+} and L^2 . The absorbance of L^2 at 299 nm increases with the increasing concentration of Cu^{2+} due to ligand to metal charge transfer (LMCT).

All these data were fitted to the Benesi–Hildebrand equation to get the formation constant and stoichiometry of complexation, where A_0 and A_{max} are the absorbances of the pure ligand in the absence and presence of excess metal ions, respectively. A linear least-squares fit of $(A_{\text{max}} - A_0)/(A - A_0)$ against $1/[M]$ clearly demonstrates a 1:1 complexation



Scheme 2 Synthetic route to the probe L^2 .

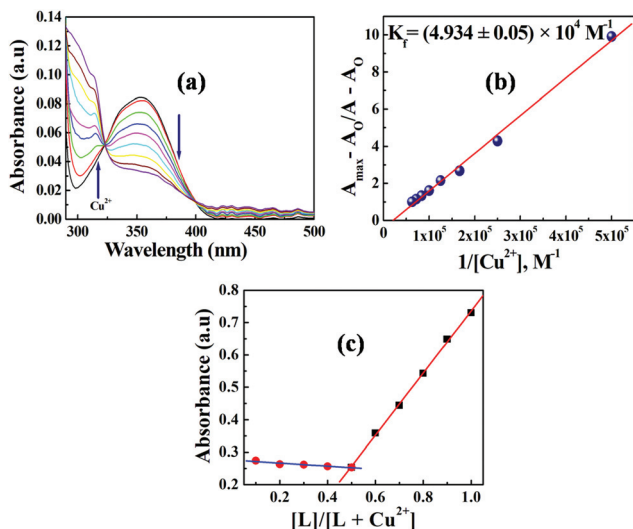


Fig. 1 (a) Changes in UV-Vis absorption spectra of L^2 ($20 \mu\text{M}$) in MeCN solutions with various amounts of Cu^{2+} (0–0.8 equivalent); (b) Benesi-Hildebrand least-squares fit; and (c) Job's plot.

($n = 0.99$) giving an apparent formation constant $K_f = (4.934 \pm 0.05) \times 10^4 \text{ M}^{-1}$ (Fig. 1b).

$$\frac{(A_{\max} - A_0)}{(A - A_0)} = 1 + \frac{1}{K[M]^n}$$

Fluorescence quenching studies

Recording of the emission spectra of L^2 and its fluorescence titration with Cu^{2+} were performed in acetonitrile solution with a fixed concentration of L^2 ($20 \mu\text{M}$) (Fig. 2(a)).

The fluorescence quenching of the ligand (L^2) is characterized by a linear Stern-Volmer (SV) plot and analyzed using the classical Stern-Volmer (SV) eqn (1)⁴⁷

$$\frac{F_0}{F} = 1 + K_{\text{SV}}[Q] \quad (1)$$

where F_0 and F are the steady state fluorescence intensities at the maximum wavelength in the absence and presence of a quencher (Q), respectively, $[Q]$ is the quencher concentration and K_{SV} is the Stern-Volmer constant. The evaluated parameter is $K_{\text{SV}} = (5.32 \pm 0.03) \times 10^4 \text{ M}^{-1}$.

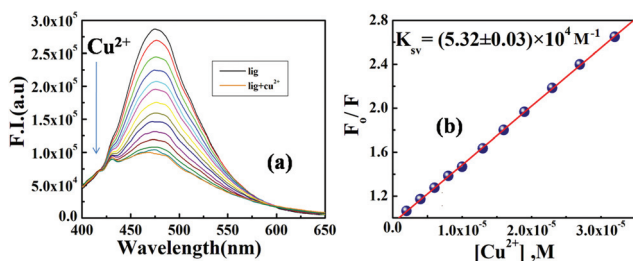


Fig. 2 (a) Fluorescence emission changes of L^2 ($20 \mu\text{M}$) in MeCN solutions upon addition of Cu^{2+} (0–2.7 equivalent, $\lambda_{\text{ex}} = 380 \text{ nm}$, $\lambda_{\text{em}} = 475 \text{ nm}$); and (b) linear Stern-Volmer plot.

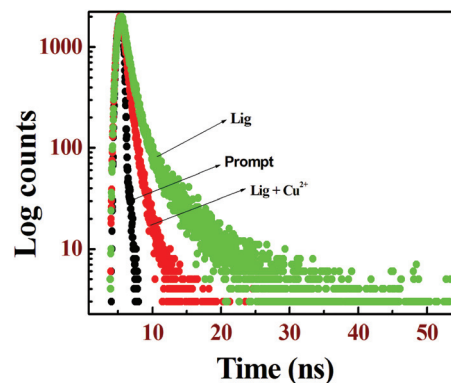


Fig. 3 Lifetime plot of L^2 and ($L^2 + \text{Cu}^{2+}$) in MeCN solutions.

The addition of Cu^{2+} into the L^2 solution leads to a gradual decrease in the fluorescence intensity (FI) at 475 nm which gets saturated upon addition of ~ 2.7 equivalents of Cu^{2+} yielding a ~ 3.0 fold decrease in FI arising mainly due to the electron transfer (ET) from the quinoline fluorophore to chelated Cu^{2+} and is evidenced from the substantial decrease in the lifetime of the Cu^{2+} complex ($\tau_{\text{complex}} = 0.579 \text{ ns}$) in comparison with the free ligand (L^2) ($\tau_{\text{ligand}} = 1.08 \text{ ns}$)⁴⁸ (Fig. 3).

The composition of the complex was further determined by Job's method [Fig. 1(c)] and supported by mass analysis. ESI-MS⁺ (m/z): 320.3290 ($[(L^2)\text{Cu}^{\text{II}}(\text{Cl})] + \text{Li}^+$) [Fig. S3a†]. Selective quenching of fluorescence of L^2 by Cu^{2+} was checked for other metal ions like Cr^{3+} , Co^{2+} , Hg^{2+} , Mg^{2+} , Mn^{2+} , Dy^{3+} , Pb^{2+} , Fe^{3+} , Zn^{2+} and Sm^{3+} and found to have negligible effects on fluorescence quenching (Fig. 4).

HNO-induced reduction of Cu^{2+} and HNO-sensing

Treatment of a $20 \mu\text{M}$ solution of $[\text{Cu}^{\text{II}}\text{-}L^2]^+$ with ~ 0.5 equivalent of Angeli's salt restored the emission intensity by ~ 2.8 fold that of complexed L^2 , owing to the reduction of the paramagnetic Cu^{2+} ion. The consumption of 0.5 equivalent of HNO clearly indicates that HNO acts as a $2e^-$ reducing agent leading to the formation of NO^+ as follows:⁴⁹

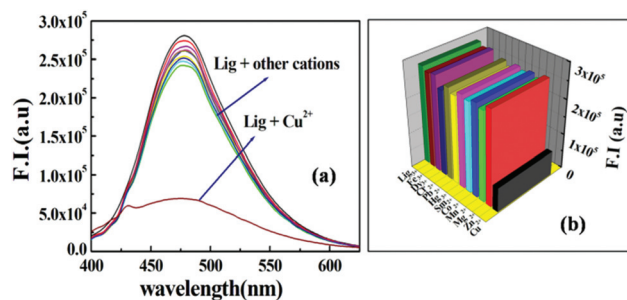
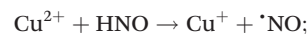
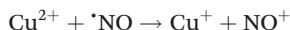


Fig. 4 (a) Fluorescence emission spectra in the presence of different cations like Cr^{3+} , Co^{2+} , Hg^{2+} , Mg^{2+} , Mn^{2+} , Dy^{3+} , Fe^{3+} , Pb^{2+} , Zn^{2+} , Sm^{3+} and Cu^{2+} ; 5 equivalents of these cations were added to L^2 ($20 \mu\text{M}$) in MeCN solutions; and (b) the corresponding histogram plot.



The positive ion electrospray mass spectrum of this reduced species showed a peak with (m/z) 301.0127, which corresponds to $\{[\text{Cu}^{\text{I}}(\text{L}^2)] + \text{Na}^+\}$ complex (calculated $m/z = 301.01$) (Fig. S3b[†]). In aqueous solution, Angeli's salt generates NO_2^- and HNO^{50} which on subsequent treatment with $[\text{Cu}^{\text{II}}-\text{L}^2]^+$ reduces Cu(II) to Cu(I) without displacement of metal ions. A 2.8-fold increase in the emission was observed, demonstrating fast HNO detection with significant turn-on (Fig. 5). $[\text{Cu}^{\text{II}}-\text{L}^2]^+$ displayed a negligible change in emission when treated with 100 μM of NaNO_2 , indicating that the turn-on response induced by Angeli's salt is due to HNO production and not by the NO_2^- side product (Fig. S5[†]).

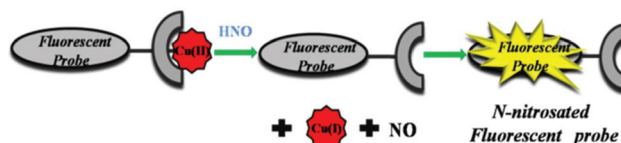
The selectivity of the ligand towards HNO was further checked by performing the same experiment in the presence of NO, KO_2 , H_2O_2 , NO_2^- , TEMPO and $\cdot\text{OH}$ which failed to induce significant emission enhancement of the $[\text{Cu}^{\text{II}}-\text{L}^2]^+$ complex manifesting the selectivity of the $[\text{Cu}^{\text{II}}-\text{L}^2]^+$ complex (1) towards HNO (Fig. S5[†]).

The formation constant of the $[\text{Cu}^{\text{II}}-\text{L}^2]^+$ complex with HNO was determined by the nonlinear curve fitting method and found to be $(2.07 \pm 0.80) \times 10^5 \text{ M}^{-1}$ on the basis of the fluorescence titration experiments (Fig. 5b).

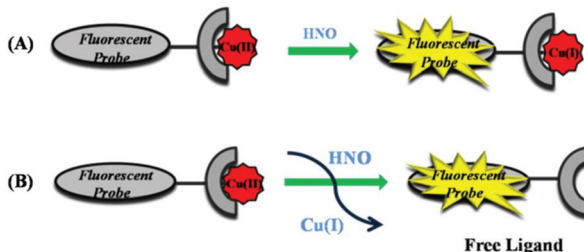
HNO-induced fluorescence enhancement in the Cu^{2+} systems may occur in more than one way (please see Scheme 3). As revealed from Scheme 3, the enhancement of fluorescence intensity may occur by (1): turn on sensing with *N*-nitrosation with the removal of reduced Cu(I); 2(A): turn on sensing by the reduction of Cu(II) to Cu(I) with HNO without the removal of the metal bound to the receptor; and 2(B): turn on sensing by the reduction of Cu(II) to Cu(I) with HNO and the removal of reduced metal ions. In our case, mechanism 2 (A) is operative and formation of $[\text{Cu}^{\text{I}}-\text{L}^2]$ species is determined by the EPR (Fig. 6) studies.

The EPR spectrum of $[\text{Cu}^{\text{II}}-\text{L}^2]^+$, prepared separately, is typically an axial type with $g_{\perp} = 2.04$, $g_{\parallel} = 2.18$ and $g_{\text{av}} = 2.11$ manifesting the presence of paramagnetic Cu^{II} ions. When this complex was treated with a 3-fold excess of HNO generated from $\text{Na}_2\text{N}_2\text{O}_3$ (a HNO donor) and the resultant solution was subjected to the EPR study in MeCN, the previous signal vanishes to the baseline indicating a complete reduction of

1. N-NITROSATION



2. REDUCTION



Scheme 3 Typical mechanism for HNO detection.

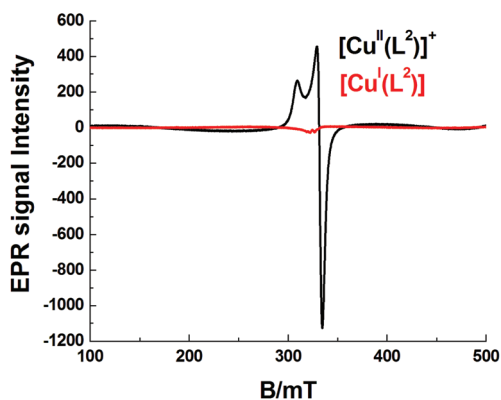


Fig. 6 EPR spectrum of $[\text{Cu}^{\text{II}}-\text{L}^2]^+$ (20 μM) and $[\text{Cu}^{\text{I}}(\text{L}^2)]$ (generated *in situ* by reduction with excess $\text{Na}_2\text{N}_2\text{O}_3$) at 298 K.

$[\text{Cu}^{\text{II}}-\text{L}^2]^+$ to $[\text{Cu}^{\text{I}}(\text{L}^2)]$ and is responsible for the regeneration of the fluorescence properties of the complex.

S^{2-} -Induced displacement of Cu^{2+} and S^{2-} sensing

From the earlier studies, we can conclude that L^2 selectively binds with Cu^{2+} to form the $[\text{Cu}^{\text{II}}-\text{L}^2]^+$ complex with a remarkable change in its spectral properties. As Cu^{2+} can coordinate with S^{2-} to form the stable species CuS , we conjectured that the $[\text{Cu}^{\text{II}}-\text{L}^2]^+$ ensemble can serve as a candidate for a turn-on fluorescent sensor for S^{2-} . To strengthen this idea, the fluorescence spectra of the $[\text{Cu}^{\text{II}}-\text{L}^2]^+$ ensemble were studied in the presence of 5 equivalents of different anions such as F^- , Cl^- , Br^- , SO_3^{2-} , NO_2^- , SO_4^{2-} , SO_3^{2-} , PO_4^{3-} , N_3^- , HSO_4^- , HSO_3^- , SCN^- , CH_3COO^- and I^- which did not cause any remarkable fluorescence response (Fig. 7). However, the $[\text{Cu}^{\text{II}}-\text{L}^2]^+$ ensemble shows an obvious selective fluorescence ON behavior with S^{2-} . This fact strongly suggests that the ligand L^2 was freed from the $[\text{Cu}^{\text{II}}-\text{L}^2]^+$ complex in the presence of S^{2-} . The formation constant of $[\text{Cu}^{\text{II}}-\text{L}^2]^+$ with S^{2-} was determined to be

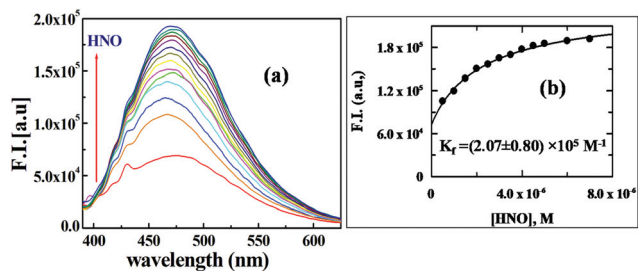


Fig. 5 (a) Fluorescence emission changes of $[\text{Cu}^{\text{II}}-\text{L}^2]^+$ (20 μM) in MeCN solutions upon addition of HNO (0–0.5 equivalent), $\lambda_{\text{ex}} = 380 \text{ nm}$, $\lambda_{\text{em}} = 469 \text{ nm}$; (b) non-linear fitting plot.

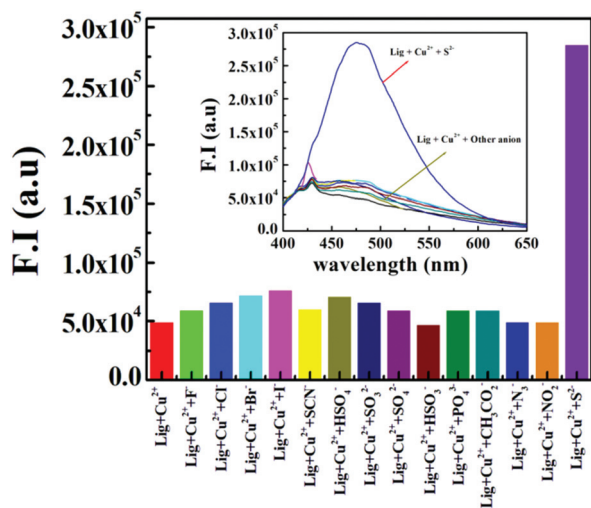


Fig. 7 Fluorescence studies on the selective binding of the $[\text{Cu}^{\text{II}}\text{-L}^2]^+$ complex ($20\ \mu\text{M}$) towards S^{2-} over other anions (5 equiv.).

(1.89 ± 0.02) $\times 10^4\ \text{M}^{-1}$ on the basis of the fluorescence titration experiments (Fig. S6†).

Also the absorbance behaviour of the $[\text{Cu}^{\text{II}}\text{-L}^2]^+$ complex with S^{2-} was almost a reversible process compared to the UV-Vis spectroscopic titration of L^2 with Cu^{2+} (Fig. 8). The absorption peak and intensity changes were similar but in the reverse direction to the titration curve obtained with Cu^{2+} (Fig. 1). This phenomenon also suggests that L^2 is released from the $[\text{Cu}^{\text{II}}\text{-L}^2]^+$ complex and CuS is formed. From the above fact we can conclude that L^2 is recyclable efficiently.

As illustrated in Scheme 1, the addition of copper ions into L^2 caused fluorescence quenching. Subsequently, the added sulfide ion captured copper(II) ions, resulting in fluorescence enhancement. Furthermore, the proposed mechanism was also well supported by the ESI-MS⁺ (m/z) data (Fig. S3c†).

From pH 7 to 10 no obvious change in the fluorescence intensity (FI) of the probe ($[\text{Cu}^{\text{II}}\text{-L}^2]^+$) was observed; however it is comparable to the FI when L^2 is quenched by Cu^{2+} ions in the fluorescence titration, thereby justifying the usefulness of the probe for the detection of HNO and S^{2-} (Fig. S7†).

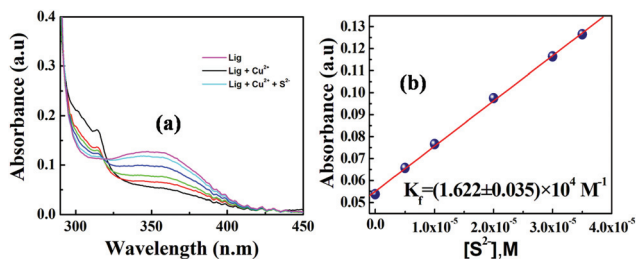


Fig. 8 (a) Changes in UV-Vis absorption spectra of $[\text{Cu}^{\text{II}}\text{-L}^2]^+$ ($20\ \mu\text{M}$) in MeCN solutions with gradual addition of S^{2-} (0–1.8 equivalent). (b) Linear fitting of absorbance vs. $[\text{S}^{2-}]$ plot.

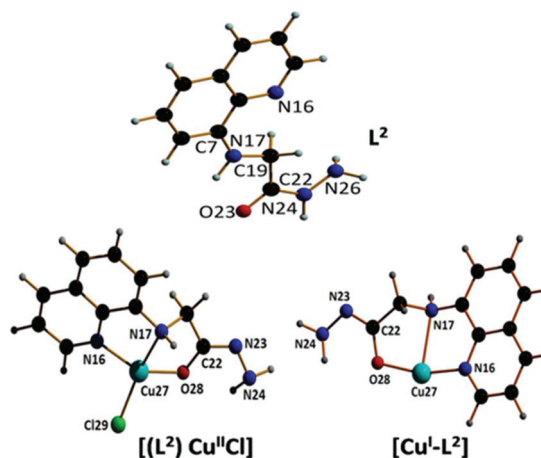


Fig. 9 Optimized structures of L^2 , $[(\text{L}^2)\text{Cu}^{\text{II}}\text{Cl}]$ and $[\text{Cu}^{\text{I}}\text{-L}^2]$ complexes.

Geometry optimization and electronic structure

In order to get some idea of the coordination mode of the ligand with Cu^{2+} ions, we carried out DFT optimization on L^2 , $[(\text{L}^2)\text{Cu}^{\text{II}}\text{Cl}]$ and $[\text{Cu}^{\text{I}}\text{-L}^2]$ complexes. The optimized geometries of L^2 , $[(\text{L}^2)\text{Cu}^{\text{II}}\text{Cl}]$ and $[\text{Cu}^{\text{I}}\text{-L}^2]$ complexes are shown in Fig. 9. These compositions of the complexes were adopted based on HRMS studies. L^2 , $[(\text{L}^2)\text{Cu}^{\text{II}}\text{Cl}]$ and $[\text{Cu}^{\text{I}}\text{-L}^2]$ complexes have a C1 point group. The important optimized geometrical parameters of the ligand and complexes are listed in Table S1.†

In the case of the $[\text{Cu}^{\text{II}}(\text{L}^2)(\text{Cl})]$ complex, the Cu^{2+} centre was found to adopt a distorted tetrahedral geometry. The calculated Cu–N bond distances are found in the range of $2.06\ \text{\AA}$ – $2.24\ \text{\AA}$ and the Cu–O bond distances are $1.90\ \text{\AA}$ which are comparable to the reported values.⁴⁸

On complexation there is a slight increase in C–N, N–N and N–O bond distances with respect to that in the free ligand. Table 1 describes the changes in bond lengths in $[\text{Cu}^{\text{II}}(\text{L}^2)(\text{Cl})]$ compared to the free ligand.

In the case of L^2 in the ground state, the electron density of the HOMO and HOMO–1 orbitals resides mainly on the quinolin-8-amine moiety, whereas for the LUMO and LUMO+1 orbitals it remains on the quinoline moiety. The energy gap between the HOMO and LUMO is $3.78\ \text{eV}$ (Fig. 10).

In the case of the HOMO–1 and HOMO–2 orbitals in the $[\text{Cu}^{\text{II}}(\text{L}^2)(\text{Cl})]$ complex the electronic contribution comes

Table 1 Change in bond lengths (\AA) for $[\text{Cu}^{\text{II}}(\text{L}^2)(\text{Cl})]$ compared to free L^2 in the ground state calculated at B3LYP levels

	L^2	$[\text{Cu}^{\text{II}}(\text{L}^2)(\text{Cl})]$
N24–N26	1.39	1.38
C22–O23	1.25	1.32
C7–N17	1.37	1.44
N17–C19	1.45	1.50
C22–N24	1.37	1.29

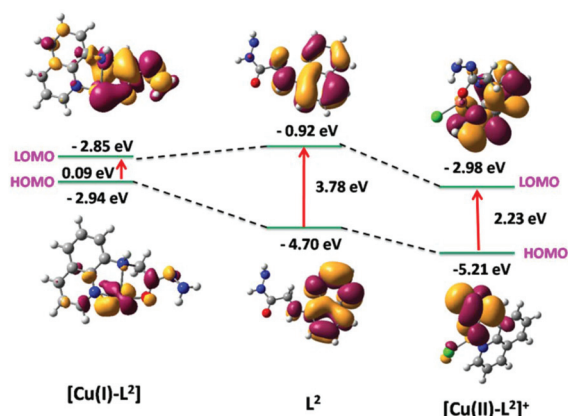


Fig. 10 Frontier molecular orbitals of L^2 , $[Cu^{II}-L^2]^+$ and $[Cu^I-L^2]$ complexes.

mainly from the (quinolin-8-ylamino)-acetic acid hydrazide moiety and in the case of the LUMO and LUMO+1 orbitals it remains on the quinoline moiety. The HOMO–LUMO energy gap is 2.23 eV (Fig. 10).

In the case of the HOMO–1 and HOMO–2 orbitals in the $[Cu^I-L^2]$ complex the electronic contribution comes mainly from the amino acetic acid hydrazide moiety and (quinolin-8-ylamino)-acetic acid hydrazide moiety and in the case of the LUMO it comes from the quinolin-8-amine moiety. The HOMO–LUMO energy gap is 0.09 eV (Fig. 10).

The UV-Vis absorption spectrum of the ligand used in the present work was calculated at room temperature in CH_3CN by the TDDFT method. The ligands show three well resolved bands at 200, 256 and 350 nm and all have an ILCT character. These bands are assigned to the $S_0 \rightarrow S_{31}$, $S_0 \rightarrow S_{14}$ and $S_0 \rightarrow S_6$

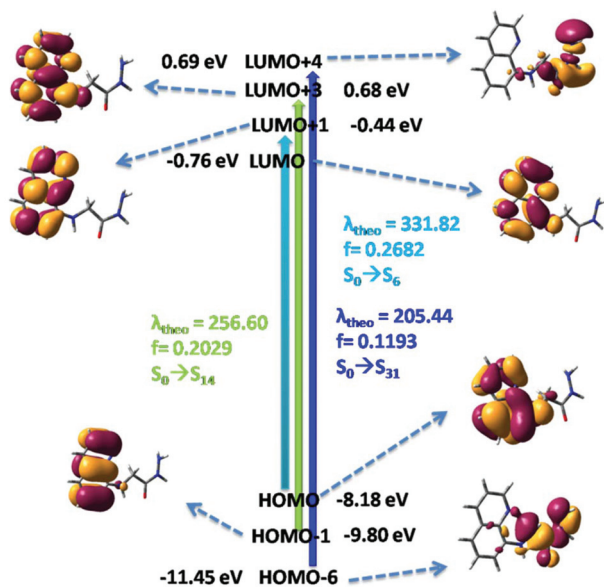


Fig. 11 Frontier molecular orbitals involved in the UV-Vis absorption of L^2 in CH_3CN .

Table 2 The comparable calculated optical transitions with experimental UV/Vis values for the ligand (L^2), and $[Cu^{II}-L^2]^+$ and $[Cu^I-L^2]$ complexes

Ligand and Cu^{2+} -complex	Theoretical (nm)	Experimental (nm)	Electronic transition	f
Ligand	331.82	350	$S_0 \rightarrow S_6$	0.2682
Ligand	256.60	256	$S_0 \rightarrow S_{14}$	0.2029
Ligand	205.44	200	$S_0 \rightarrow S_{31}$	0.1193
$[Cu^{II}-L^2]^+$	331.66	352	$S_0 \rightarrow S_{15}$	0.0110
$[Cu^{II}-L^2]^+$	325.91	315	$S_0 \rightarrow S_{17}$	0.0222
$[Cu^{II}-L^2]^+$	249.88	256	$S_0 \rightarrow S_{38}$	0.0104
$[Cu^I-L^2]$	350.57	350	$S_0 \rightarrow S_4$	0.0304
$[Cu^I-L^2]$	291.72	287	$S_0 \rightarrow S_{12}$	0.0183

electronic transitions, respectively (Fig. 11). The absorption energies and associated oscillator strengths are given in Table 2 and Table S2.†

The UV-Vis spectrum of the $[Cu^{II}(L^2)(Cl)]$ complex shows three absorption bands at 256, 315 and 352 nm in CH_3CN at room temperature which correspond well to the TDDFT calculated absorption bands located at 250, 326 and 332 nm. These three absorption bands can be assigned to the $S_0 \rightarrow S_{38}$, $S_0 \rightarrow S_{17}$ and $S_0 \rightarrow S_{15}$ transitions, respectively (Fig. 12) originating from an admixture of LMCT and ILCT transitions (Table S3†).

The UV-Vis spectrum of the $[Cu^I-L^2]$ complex shows two absorption bands at 287 and 350 nm in CH_3CN at room temperature (Fig. S8†) which correspond well to the TDDFT calculated absorption bands located at 292 and 351 nm. These two absorption bands can be assigned to the $S_0 \rightarrow S_{12}$ and $S_0 \rightarrow S_4$ transitions, respectively (Fig. 13) originating from an admixture of LMCT and ILCT transitions (Table S4†).

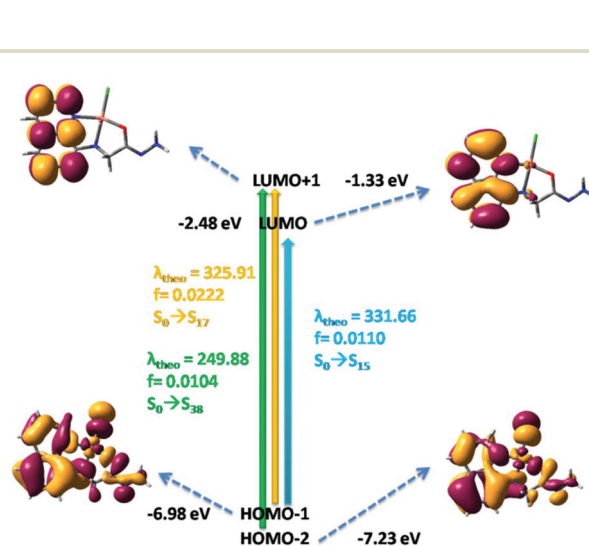


Fig. 12 Frontier molecular orbitals involved in the UV-Vis absorption of $[Cu^{II}(L^2)(Cl)]$ in CH_3CN .

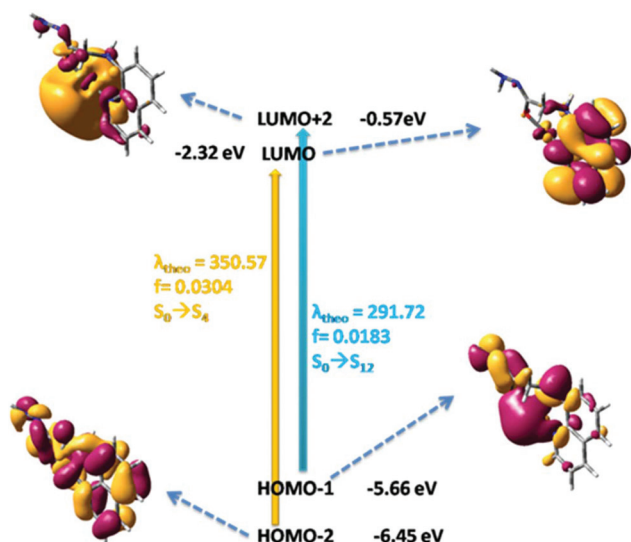


Fig. 13 Frontier molecular orbitals involved in the UV-Vis absorption of $[\text{Cu}^{\text{I}}\text{-L}^2]$ in CH_3CN .

Conclusion

In summary, a new ligand, (quinolin-8-ylamino)-acetic acid hydrazide (L^2), has been synthesized and characterized. Taking this ligand a Cu(II) based sensor (**1**) has been developed by the complexation between (quinolin-8-ylamino)-acetic acid hydrazide (L^2) and Cu^{2+} ions. Complex (**1**) has also been characterized by ESI-MS⁺, X band EPR spectrum and CHN analysis. The EPR spectrum of $[\text{Cu}^{\text{II}}\text{-L}^2]^+$, prepared separately, is typically an axial type with $g_{\perp} = 2.04$, $g_{\parallel} = 2.18$ and $g_{\text{av}} = 2.11$ manifesting the presence of paramagnetic Cu^{II} ions; however on treatment with Angeli's salt the EPR signal vanishes to the baseline indicating the complete reduction of paramagnetic Cu^{2+} to diamagnetic Cu^+ ions. The sensor (**1**) is highly selective for the recognition of HNO and S^{2-} over other biologically abundant anions with prominent enhancement in absorption and emission intensities. The sensor $[\text{Cu}^{\text{II}}\text{-L}^2]^+$ (**1**) shows weak fluorescence due to ET (electron transfer) but upon addition of HNO and S^{2-} a large enhancement in the fluorescence intensity (F.I.) was observed over other possible competitive anions on the basis of the reduction of Cu(II) to Cu(I) and formation of CuS, respectively. The 1:1 complexation was characterized by Job's plot and the corresponding K_f values were evaluated to be $(4.93 \pm 0.05) \times 10^4 \text{ M}^{-1}$ for Cu^{2+} obtained from UV-Vis absorption titration. Quantum yields of L^2 and $[\text{Cu}\text{-L}^2 + \text{S}^{2-}]$ and $[\text{Cu}\text{-L}^2 + \text{HNO}]$ complexes in acetonitrile (CH_3CN) are found to be 0.107, 0.09, and 0.07, respectively, using acidic quinine sulphate as the standard.

Conflicts of interest

There are no conflicts to declare.

Acknowledgements

Financial supports from the CSIR (Ref. 01(2896)/17/EMR-II), New Delhi and the DST (Ref. No. 809 (Sanc)/ST/P/S&T/4G-9/2104), West Bengal, India are gratefully acknowledged. A. Dutta gratefully acknowledges DST-INSPIRE for junior research fellowship (JRF).

References

- R. P. Haugland, *The Molecular Probes Handbook: A Guide to Fluorescent Probes and Labelling Technologies*, Invitrogen Carlsbad, CA, 10th edn, 2005.
- (a) S. J. Lippard and J. M. Berg, *Principles of Bioinorganic Chemistry*, University Science Books, Mill Valley, CA, 1994; (b) H. B. Gray, E. I. Stiefel, J. S. Valentine and I. Bertini, *Biological Inorganic Chemistry: Structure and Reactivity*, University Science Books, Herndon, VA, USA, 2007; (c) E. L. Que, D. W. Domaille and C. J. Chang, *Chem. Rev.*, 2008, **108**, 1517; (d) D. J. Thiele and J. D. Gitlin, *Nat. Chem. Biol.*, 2008, **4**, 145.
- A. Y. Bogdanova, M. Gassmann and M. Nikinmaa, *Chem.-Biol. Interact.*, 2002, **139**, 43.
- X. J. H. X. Stouthart, J. L. M. Hanns, R. A. C. Lock and S. E. W. Bonga, *Environ. Toxicol. Chem.*, 1996, **15**, 376.
- M. A. Fahmy, *Cytologia*, 2000, **65**, 235.
- E. Gaggelli, H. Kozłowski, D. Valensin and G. Valensin, *Chem. Rev.*, 2006, **106**, 1995.
- (a) V. Dujols, F. Ford and A. W. Czarnik, *J. Am. Chem. Soc.*, 1997, **119**, 7386; (b) Y. Xiang, A. J. Tong, P. Y. Jin and Y. Ju, *Org. Lett.*, 2006, **8**, 2863.
- S. Kim, M. A. Minier, A. Loas, S. Becker, F. Wang and S. J. Lippard, *J. Am. Chem. Soc.*, 2016, **138**, 1804.
- A. T. Wrobel, T. C. Johnstone, A. D. Liang, S. J. Lippard and P. R-Fuentes, *J. Am. Chem. Soc.*, 2014, **136**, 4697.
- C. Bogdan, *Nat. Immunol.*, 2001, **2**, 907.
- D. S. Bredt, P. M. Hwang and S. H. Snyder, *Nature*, 1990, **347**, 768.
- M. L. Bullen, A. A. Miller, K. L. Andrews, J. C. Irvine, R. H. Ritchie, C. G. Sobey and B. K. Kemp-Harper, *Antioxid. Redox Signaling*, 2011, **14**, 1675.
- P. Liu, X. Jing, F. Yu, C. Lv and L. Chen, *Analyst*, 2015, **140**, 4576.
- P. R. Fuentes and S. J. Lippard, *Acc. Chem. Res.*, 2015, **48**, 2927.
- M. Feelisch, *Proc. Natl. Acad. Sci. U. S. A.*, 2003, **100**, 4978.
- J. M. Fukuto, K. Chiang, R. Hsieh, P. Wong and G. J. Chaudhuri, *Pharmacol. Exp. Ther.*, 1992, **263**, 546.
- E. Bermejo, D. A. Saenz, F. Alberto, R. E. Rosenstein, S. E. Bari and M. A. Lazzari, *Thromb. Haemostasis*, 2005, **94**, 469.
- C.-U. Choe, J. Lewerenz, G. Fischer, T. F. Uliasz, M. G. Espey, F. C. Hummel, S. B. King, E. Schwedhelm, R. H. Böger, C. Gerloff, S. J. Hewett, T. Magnus and S. J. Donzelli, *Neurochem.*, 2009, **110**, 1766.

- 19 C.-U. Choe, J. Lewerenz, C. Gerloff, T. Magnus and S. Donzelli, *Antioxid. Redox Signaling*, 2011, **14**, 1699.
- 20 J. M. Fukuto and S. J. Carrington, *Antioxid. Redox Signaling*, 2011, **14**, 1649.
- 21 X. Jing, F. Yu and L. Chen, *Chem. Commun.*, 2014, **50**, 14253.
- 22 F. Doctorovich, D. E. Bikiel, J. Pellegrino, S. A. Suárez and M. A. Martí, in *Progress in Inorganic Chemistry*, ed. K. D. Karlin, John Wiley & Sons, Inc., Hoboken, NJ, 2014, vol. 58, p. 145.
- 23 S. Nelli, M. Hillen, K. Buyukafsar and W. Martin, *J. Pharmacol.*, 2000, **131**, 356.
- 24 T. L. Guidotti, *Int. J. Toxicol.*, 2010, **29**, 569.
- 25 C. L. Evans, *Q. J. Exp. Physiol. Cogn. Med. Sci.*, 1967, **52**, 231.
- 26 J. R. Reiffenstein, W. C. Hulbert and S. H. Roth, *Annu. Rev. Pharmacol. Toxicol.*, 1992, **32**, 109.
- 27 M. Gao, F. Yu, H. Chen and L. Chen, *Anal. Chem.*, 2015, **87**, 3631.
- 28 M. Gao, R. Wang, F. Yu, J. Youc and L. Chen, *J. Mater. Chem. B*, 2018, **6**, 2608.
- 29 M. Gao, R. Wang, F. Yu and L. Chen, *Biomaterials*, 2018, **160**, 1.
- 30 M. Gao, F. Yu, C. Lv, J. Choo and L. Chen, *Chem. Soc. Rev.*, 2017, **46**, 2237.
- 31 M. Gao, F. Yu, H. Chen and L. Chen, *Anal. Chem.*, 2015, **87**, 3631.
- 32 R. Wang, F. Yu, L. Chen, H. Chen, L. Wang and W. Zhang, *Chem. Commun.*, 2012, **48**, 11757.
- 33 P. Saluja, N. Kaur, N. Singh and D. O. Jang, *Tetrahedron Lett.*, 2012, **53**, 3292.
- 34 X. W. Cao, W. Y. Lin and L. W. He, *Org. Lett.*, 2011, **13**, 4716.
- 35 F. P. Hou, L. Huang, P. X. Xi, J. Cheng, X. F. Zhao, G. Q. Xie, Y. J. Shi, F. J. Cheng, X. J. Yao, D. C. Bai and Z. Z. Zeng, *Inorg. Chem.*, 2012, **51**, 2454.
- 36 L. Zhang, X. Lou, Y. Yu, J. Qin and Z. Li, *Macromolecules*, 2011, **44**, 5186.
- 37 M. G. Choi, S. Cha, H. Lee, H. L. Jeon and S.-K. Chang, *Chem. Commun.*, 2009, 7390.
- 38 X. D. Lou, H. L. Mu, R. Gong, E. Q. Fu, J. G. Qin and Z. Li, *Analyst*, 2011, **136**, 684.
- 39 R. Zhang, X. J. Yu, Y. J. Yin, Z. Q. Ye, G. L. Wang and J. L. Yuan, *Anal. Chim. Acta*, 2011, **691**, 83.
- 40 P. A. S. Smith and G. E. Hein, *J. Am. Chem. Soc.*, 1960, **82**, 5731.
- 41 M. J. Frisch, *et al.*, *GAUSSIAN 09 (Revision A.1)*, Gaussian, Inc., Wallingford, CT, 2009.
- 42 M. E. Casida, C. Jamoroski, K. C. Casida and D. R. Salahub, *J. Chem. Phys.*, 1998, **108**, 4439.
- 43 R. E. Stratmann, G. E. Scuseria and M. J. Frisch, *J. Chem. Phys.*, 1998, **109**, 8218.
- 44 V. Barone and M. Cossi, *J. Phys. Chem.*, 1998, **102**, 1995.
- 45 M. Cossi and V. Barone, *J. Chem. Phys.*, 2001, **115**, 4708.
- 46 M. Cossi, N. Rega, G. Scalmani and V. Barone, *J. Comput. Chem.*, 2003, **24**, 669.
- 47 Y. Liu, K. Ai, X. Cheng, L. Huo and L. Lu, *Adv. Funct. Mater.*, 2010, **20**, 951.
- 48 R. Alam, T. Mistri, P. Mondal, D. Das, S. K. Mandal, A. R. Khuda-Bukhsh and M. Ali, *Dalton Trans.*, 2014, **43**, 2566.
- 49 S. I. Liochev and I. Fridovich, *Free Radical Biol. Med.*, 2003, **34**, 1399.
- 50 M. E. Murphy and H. Sies, *Proc. Natl. Acad. Sci. U. S. A.*, 1991, **88**, 10860.



Cite this: *Org. Biomol. Chem.*, 2019, **17**, 2492

A smart molecular probe for selective recognition of nitric oxide in 100% aqueous solution with cell imaging application and DFT studies†

Ananya Dutta,^a Abu Saleh Musha Islam,^a Debjani Maiti,^a Mihir Sasmal,^a Chandraday Pradhan^b and Mahammad Ali^{*a,c}

Herein, a simple, least-cytotoxic as well as an efficient fluorescent sensor **HqEN₄₈₀** was prepared from (quinolin-8-yloxy)-acetic acid ethyl ester (**L¹**) and *N,N*-dimethylethylene diamine to recognize NO in 100% aqueous solution. Its marked selectivity and sensitivity towards NO, makes it a highly suitable probe for nitric oxide under *in vitro* conditions with the possibility of *in vivo* monitoring of NO. Upon addition of 3.5 equivalents of NO, there is an approximately 7 fold enhancement in fluorescence intensity in aqueous solution with a corresponding K_f value of $(1.75 \pm 0.07) \times 10^4 \text{ M}^{-1}$. Quantum yields of **HqEN₄₈₀** and [**HqEN₄₈₀-NO**] compounds are determined to be 0.04 and 0.22, respectively, using acidic quinine sulphate as a standard. In terms of the 3σ method, the LOD for nitric oxide was found to be 53 nM thus, making the probe suitable for tracking NO in biological systems.

Received 23rd January 2019,
Accepted 5th February 2019

DOI: 10.1039/c9ob00177h

rsc.li/obc

Introduction

Nitric oxide (NO), originating from L-arginine by the action of nitric oxide synthases¹ (NOS), has not only been identified as a highly reactive gaseous free radical but also as a signalling agent for its various functions in the cardiovascular, immune, and central nervous systems.² Nitric oxide modulates gene transcription^{3,4} and *m*-RNA translation through binding with iron-responsive elements.^{5,6} It also regulates the production of post-translational modifications of proteins by adenosine 5'-diphosphate ribosylation^{7,8} indicating its pivotal role in the human body. However, in high concentration NO exhibits a toxic effect on all cells, including the cells that are able to produce it. Misregulation of NO production may cause diseases like stroke, cancer, hypertension, neurodegeneration and endothelial dysfunction.⁹⁻¹²

Nitric oxide with a half-life less than 10 seconds makes its detection quite challenging in biological systems.¹³ To date, various techniques such as electrochemical, fluorescence, electron spin resonance *etc.* have emerged to monitor NO gene-

ration and its biological activities in living cells.¹⁴ Compared to all other approaches the fluorescence technique is the most favourable one due to its high sensitivity and experimental feasibility.

Most of the fluorescent probes are mainly of two types: one is based on the *o*-phenylenediamine (OPD) moiety¹⁵⁻²¹ and the other is based on metal ligand complexes.²²⁻²⁷ Between these two, the former one produces triazole derivatives upon treatment with nitric oxide under aerated conditions with concomitant generation of fluorescence intensity. Some limitations still exist with the OPD based probes. Firstly, they may undergo self-oxidation due to the existence of an electron rich diamino-benzene fragment. Secondly they may exhibit a false positive response towards dehydroascorbic acid (DHA) and ascorbic acid (AA) resulting in wrong interpretation of data. Another important drawback of this strategy is associated with pH dependency of fluorescence intensity of the product as the formed triazole contains a secondary amine which can be protonated. The metal-complex based nitric oxide sensors also possess various disadvantages like biological incompatibility,^{22,28} easy leakage from the cells²⁹ or side effects from the metal ions.³⁰

Considering these aforementioned limitations for the detection of NO, recently a few novel strategies have been developed which include (1) nitrosation reaction,^{31,32} (2) reaction with thiosemicarbazide³³ leading to the formation of oxadiazole, (3) reaction with acylhydrazide leading to the formation of 1,2,3,4-oxatriazole,³⁴ (4) generation of the Se-NO bond³⁵ and so on (Scheme 1). Usually, most of the organic

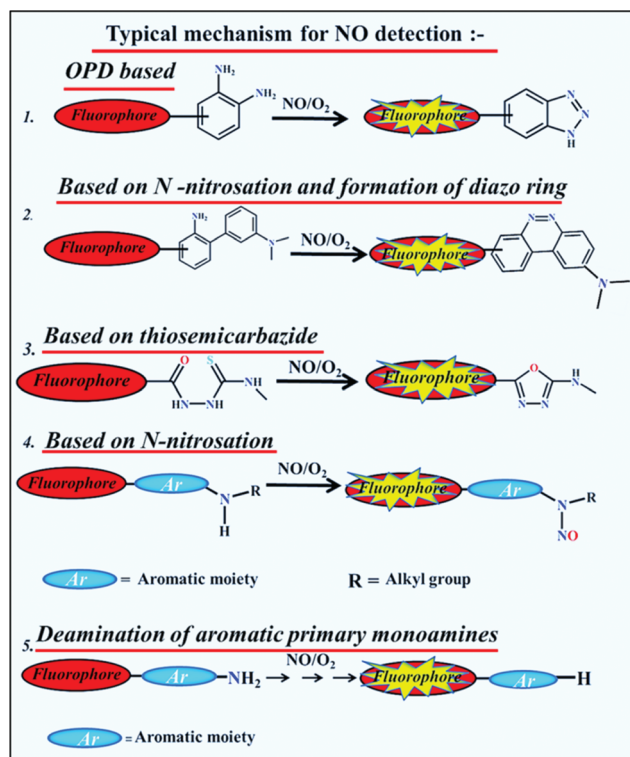
^aDepartment of Chemistry Jadavpur University, Kolkata 700 032, India.

E-mail: m_ali2062@yahoo.com, mali@chemistry.jdvu.ac.in; Fax: +91-33-2414-6223

^bMolecular & Human Genetics Division, CSIR-Indian Institute of Chemical Biology, 4 Raja S.C. Mallick Road, Kolkata-700032, India

^cVice-Chancellor, Aliah University, II-A/27, Action Area II, Newtown, Action Area II, Kolkata, West Bengal 700160, India. E-mail: vc_au@aliah.ac.in

†Electronic supplementary information (ESI) available. See DOI: 10.1039/c9ob00177h

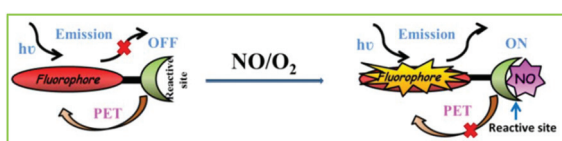


Scheme 1 Different strategies for the detection of NO.

fluorescent probes are associated with poor water solubility which is contrary to the real physiological conditions.

All the above discussions lead us to conclude that a fluorescent nitric oxide probe should satisfy some basic requirements like low cytotoxicity, and good water solubility along with high NO selectivity. Taking all these parameters in mind we have been interested to design an *N*-nitrosation based probe on the quinoline platform which could display a positive response towards nitric oxide selectively in purely aqueous medium (Scheme 2).

Quinoline has excellent photostability and the presence of the pyridine moiety magnifies its fluorescence properties by acting as an electron acceptor.³⁶ The present probe **HqEN**₄₈₀ shows good response to NO and is inert towards reactive oxygen, nitrogen and sulphur species in a biological milieu. Here, NO directly reacts with the secondary nitrogen atom of the amide group to generate the *N*-N=O moiety leading to the enhancement of fluorescence intensity through blocking of the PET process. The fluorescence based bio-imaging experi-



Scheme 2 General mechanism for NO sensing using a *N*-nitrosation based probe.

ment has also been executed in HepG2 cells by using **HqEN**₄₈₀.

Experimental section

Physical measurements

An IR 750 series-II FTIR (Nicolet Magna) spectrophotometer was used to record IR spectra in the solid state for both pure ligand (**HqEN**₄₈₀) and its NO product (**HqEN**₄₈₀-NO) in the range of 400–4000 cm⁻¹ on KBr pellets. Electronic spectra of the probe as well as the product of its reaction with NO were recorded on an Agilent 8453 Diode-array UV-Vis spectrophotometer using HPLC grade H₂O as a solvent with a 1 cm quartz cuvette in the range of 200–900 nm. Fluorescence studies were performed on a PTI (model QM-40) spectrofluorimeter. ¹H NMR spectra were recorded in DMSO-d₆ as well as in CDCl₃ on a Bruker 300 MHz instrument while ¹³C NMR spectra were recorded on a Bruker 75 MHz instrument using trimethylsilane ($\delta = 0$) as an internal standard. ESI-MS⁺ (*m/z*) spectra were recorded using a high resolution mass spectrometer (model: QTOF Micro YA263). Time correlated single photon counting (TCSPC) measurements using a picosecond diode laser (IBH nanoled-07) in an IBH fluorocube apparatus were performed to determine fluorescence lifetimes. A Hamamatsu MCP photomultiplier (R3809) was used to collect the fluorescence decay data which were further examined by using the IBH DAS6 software. To obtain cell images, a fluorescence microscope (Leica DM3000, Germany) was used. The pH values of the reaction solutions were measured with a digital pH meter (model: Systronics 335, India) in the pH range of 2–12 which was prior calibrated using buffers of pH 4, 7 and 10.

Materials and methods

8-Hydroxyquinoline, ethyl-bromoacetate, *N,N*-dimethylethylenediamine (Sigma-Aldrich) and propylamine (Sigma-Aldrich) were used to synthesize the ligands. Salts of Cd²⁺, Sm³⁺, Co²⁺, Mg²⁺, Mn²⁺, Na⁺, K⁺, Zn²⁺, Dy³⁺, Eu²⁺, Ni²⁺, Cu²⁺, Cr³⁺, Hg²⁺, Fe³⁺, Pb²⁺, Al³⁺, F⁻, PPI, N₃⁻, CO₃²⁻, Cl⁻, CH₃COO⁻, ClO₄⁻, SO₄²⁻, NO₃⁻, S₂O₄²⁻, H₂PO₄⁻, NO₂⁻, S²⁻, other biological anions like H₂O₂, O₂⁻, TEMPO radical, ClO⁻, ascorbic acid, ONOO⁻, DHA, NO⁺, HNO *etc.* as well as all the amino acids were purchased either from Sigma-Aldrich or from other commercial suppliers and used without further purification. Solvents like EtOH (ethanol), MeCN (acetonitrile), *etc.* (Merck, India) were of reagent grade and dried before use.

Preparation of (quinolin-8-yloxy)-acetic acid ethyl ester (L¹)

A mixture of 8-hydroxyquinoline (5 mmol, 0.73 g), ethyl bromoacetate (7.5 mmol, 1.25 g) and anhydrous K₂CO₃ (12.5 mmol, 1.73 g) in acetonitrile was refluxed on a water bath for 8 h. After cooling, the reaction mixture was filtered and then the solvent was removed under reduced pressure. The resulting oily product was further purified by column chrom-

atography on silica gel, using ethyl acetate : pet ether (3 : 2) as the eluent to afford **L¹** (85% yield).

Preparation of *N*-(2-dimethylamino-ethyl)-2-(quinolin-8-yloxy)-acetamide (**HqEN₄₈₀**)

The resulting (quinolin-8-yloxy)-acetic acid ethyl ester (**L¹**) (1.0 mmol) and *N,N*-dimethylethylenediamine (10 mmol) in ethanol were refluxed on a water bath for 6 h. After cooling, the reaction mixture was concentrated under vacuum and the resulting oily product was subjected to column chromatography on silica gel (60–120 mesh) by using DCM as the eluent to obtain **HqEN₄₈₀** in pure form. Yield: 85%. ¹H NMR (300 MHz, DMSO-*d*₆) δ_{ppm}: 2.14 (m, 6H, –CH₃, –CH₃), 2.33 (m, 2H, –CH₂), 3.28 (m, 2H, –CH₂), 4.72 (s, 2H, –CH₂), 7.28 (d, 1H, –ArH), 7.61–7.49 (m, 3H, –ArH), 8.34 (d, 1H, –ArH), 8.37 (d, 1H, –ArH) and 8.90 (m, 1H, –NH) (Fig. S1†). ¹³C-NMR: (75 MHz, DMSO-*d*₆) δ_{ppm}: 36.41, 45.10, 57.95, 69.15, 112.16, 121.15, 122.08, 126.85, 129.17, 136.17, 139.83, 149.40, 153.79, 167.80 (Fig. S1a†). ESI-MS⁺ (*m/z*): 296.22 (**HqEN₄₈₀** + Na⁺) (Fig. S2†). IR spectrum: –NH (3411 cm^{–1}), –C=O (1668 cm^{–1}) (Fig. S3†).

Preparation of *N*-propyl-2-(quinolin-8-yloxy)acetamide (**HqPA**)

L¹ (1 mmol) was dissolved in 25 mL of EtOH. To this ethanolic solution propylamine (10 mmol) was added dropwise and refluxed for 5 h. The reaction mixture was then cooled to room temperature and the formed precipitate was filtered, washed with cold ethanol, and dried in air affording a white solid. Now **HqPA** was further purified by recrystallization from ethanol. Yield: 80%. ESI-MS⁺ (*m/z*): 269.01 (**HqPA** + H₂O + Li) (Fig. S4†). ¹H NMR (300 MHz, CDCl₃) δ_{ppm}: 0.86 (d, 3H, –CH₃), 3.59 (m, 2H, –CH₂), 3.91 (m, 2H, –CH₂), 4.67 (s, 2H, –CH₂), 7.05 (m, 1H, –ArH), 7.43–7.49 (m, 3H, –ArH), 8.18 (d, 1H, –ArH), 8.85 (d, 1H, –ArH) and 9.11 (s, 1H, –NH) (Fig. S5†).

Solution preparation for UV-Vis absorption and fluorescence studies

To study the UV-Vis and fluorescence response of **HqEN₄₈₀** and **HqPA** towards NO, stock solutions of 1.0 × 10^{–3} M of the probes were prepared in Milli-Q Millipore water. The stock solution of nitric oxide (1.74 × 10^{–3} M in deoxygenated deionized water) was prepared by bubbling nitric oxide gas for 15 min in a sealed vial with the help of a syringe. The nitric oxide gas was purified by passing through a drying tube containing solid NaOH pellets.³⁷ The OH[•] and ONOO[–] solutions were prepared by a reported methods.³⁸ HNO was synthesized from Angeli's salt.³⁹ The solutions of other metal ions as well as anions were prepared either in H₂O or in alcohol. An aqueous solution of 10.0 mM 4-(2-hydroxyethyl)piperazine-1-ethanesulfonic acid (HEPES) buffer was prepared and the pH was adjusted to 7.20 by using HCl and NaOH. The ionic strength of the buffer solution was maintained at 0.10 M (NaCl) throughout the measurements. Then 2.5 mL of this buffer solution was pipetted out into a cuvette to which 20 μM of the probe **HqEN₄₈₀** or **HqPA** was added and then NO was added incrementally in a regular interval of volume and fluo-

rescence spectra were recorded for each solution using 5 nm × 3 nm slit width.

Calculation of LOD

The analytical detection limit was obtained by performing fluorescence titration of **HqEN₄₈₀** with NO by adding aliquots in a micromolar concentration of NO to 20 μM **HqEN₄₈₀** in 2.5 mL buffer and the LOD was calculated by the 3σ method.

$$\text{LOD} = 3 \times S_d/S \quad (1)$$

where *S_d* is the standard deviation of the intercept of the blank (**HqEN₄₈₀** only) obtained from a plot of fluorescence intensity (FI) versus [**HqEN₄₈₀**], and *S* is the slope obtained from the linear part of the plot of FI versus [NO].

Calculation of the quantum yield

Fluorescence quantum yields (Φ) were determined by using the equation:

$$\Phi_{\text{sample}} = (\text{OD}_{\text{std}} \times A_{\text{sample}}) / (\text{OD}_{\text{sample}} \times A_{\text{std}}) \times \Phi_{\text{std}} \quad (2)$$

here, *A_{sample}* and *A_{std}* represent the areas under the fluorescence spectral curves. The optical densities of the sample and standard are designated as OD_{sample} and OD_{std}, respectively, at the excitation wavelength. Here, acidic quinine sulphate was taken as the standard ($\Phi_{\text{std}} = 0.54$) for the quantum yield calculation of **HqEN₄₈₀** and **HqEN₄₈₀-NO**.

Computational details

The optimization of ground state electronic structures of both the ligand and NO adduct was performed by using the DFT method⁴⁰ associated with the conductor-like polarizable continuum model (CPCM).⁴¹ Becke's hybrid function⁴² with the Lee-Yang-Parr (LYP) correlation function⁴³ were applied throughout the study. The geometries of the ligand and the NO product were fully optimized without any symmetry constraints. On the basis of the optimized ground state geometry, the absorption spectral properties of **HqEN₄₈₀** and [**HqEN₄₈₀-NO**] in water were calculated by time-dependent density functional theory (TDDFT)⁴⁴ associated with the conductor-like polarizable continuum model (CPCM).⁴¹ We have computed the lowest 40 singlet-singlet transitions and the presence of electronic correlation in the TDDFT (B3LYP) method⁴⁵ enables to obtain accurate electronic excitation energies. For H, C, N and O atoms, we employed 6-31+G basis sets for the optimization of the ground state. The calculated electron density plots for frontier molecular orbitals were constructed by using Gauss View 5.1 software. All the calculations were done with the Gaussian 09 W software package.⁴⁶ The Gauss Sum 2.1 program⁴⁷ was utilized to calculate the molecular orbital contributions from groups or atoms.

Cell culture

Human hepatocellular liver carcinoma (HepG2) cell lines (NCCS, Pune, India) were grown in DMEM supplemented with 10% FBS and antibiotics (penicillin-100 μg ml^{–1}; streptomycin-

cin-50 $\mu\text{g ml}^{-1}$). The cells were cultured at 37 °C in 95% air, 5% CO_2 incubator.

Cell imaging study

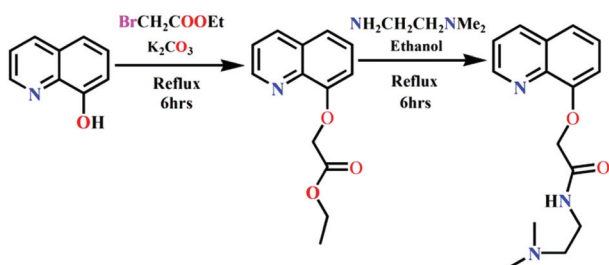
HepG2 cells were cultured in a 35 × 10 mm culture dish on a cover-slip for 24 h at 37 °C. The cells were treated with 10 μM solutions of **HqEN**₄₈₀, prepared by dissolving **HqEN**₄₈₀ in the mixed solvent DMSO:water = 1:9 (v/v) and incubated for 1 hour at 37 °C. To study the adduct formation of **HqEN**₄₈₀ with intracellular NO, HepG2 cells were preincubated separately with 10, 20 and 40 μM of sodium nitroprusside (SNP) for 60 min at 37 °C, followed by washing them thrice with 1× PBS and subsequent incubation with 10 μM **HqEN**₄₈₀ for 60 min at 37 °C. Fluorescence images of HepG2 cells were obtained by using a fluorescence microscope (Leica DM3000, Germany) with an objective lens of 40× magnification.

Cell cytotoxicity assay

In order to evaluate the cytotoxic effect of ligand **HqEN**₄₈₀, a cell viability assay was done by using 3-(4,5-dimethylthiazol-2-yl)-2,5-diphenyltetrazolium bromide (MTT).⁴⁸ HepG2 cells (1×10^5 cells per well) were cultured in 96-well plates and incubated at 37 °C with variable concentrations of **HqEN**₄₈₀ (starting from 5, 10, 20, 40, 60, 80 and 100 μM) for 24 hours. After incubation, 10 μl of MTT solution [5 mg ml^{-1} , dissolved in 1× phosphate-buffered saline (PBS)] were added to each well of a 96-well culture plate and incubated at 37 °C for 4 hours. Media were decanted from wells followed by incorporation of 100 μL of 0.04 N acidic isopropyl alcohol into each well so that intracellular formazan crystals (blue-violet) thereby formed become easily soluble. The absorbance of each solution was measured at 595 nm (EMax Precision MicroPlate Reader, Molecular Devices, USA). Values were calculated as mean \pm standard errors of three independent experiments. The cell viability was represented as the optical density ratio of treatment to control.

Results and discussion

As delineated in Scheme 3, the receptor **HqEN**₄₈₀ was designed in order to achieve the selective detection of NO over other commonly interfering species (such as ascorbic acid, ROS, RNS and so on) by the reaction between (quinolin-8-yloxy)-acetic acid ethyl ester (**L**¹) and *N,N*-dimethylethylene diamine



Scheme 3 Synthetic route for the probe **HqEN**₄₈₀.

in alcoholic medium. The receptor, designated as **HqEN**₄₈₀, was well-characterized by ¹H NMR (Fig. S1†), ¹³C NMR (Fig. S1a†), HRMS (Fig. S2†) and IR (Fig. S3†).

In aqueous buffer the receptor exhibits sensitive and selective fluorogenic response towards NO. The negligible or no reactivity of this probe to other ROS and RNS arises due to the controlled electron density by the introduction of a carbonyl group such as CONH.⁴⁹ Here hydroxyquinoline is suitable as a fluorophoric moiety because of its many biological activities such as fungicides, antibacterial properties, *etc.*

Spectral response of **HqEN**₄₈₀ to NO

UV-Vis absorption studies. **HqEN**₄₈₀ exhibits high selectivity as well as high sensitivity towards NO. By keeping the concentration fixed for the probe **HqEN**₄₈₀ (20 μM) in 10.0 mM HEPES buffer (pH = 7.20), the addition of NO generates a new absorption peak at 355 nm which increases gradually with the gradual addition of NO (Fig. 1a). The linear dependence of absorbance as a function of [NO] was analyzed with the help of eqn (3)³³ which under the conditions $1 \gg c x$ with $n = 1$ becomes eqn (4).

$$y = \frac{(a + b \times c \times x^n)}{(1 + c \times x^n)} \quad (3)$$

$$y = a + (b \times c)x \quad (4)$$

where a = absorbance of the free probe, b = absorbance of the probe in the presence of excess of NO, and c = formation constant, K_f . It is interesting to note that linear least-squares analysis of UV-Vis titration data gives $K_f = (3.35 \pm 0.06) \times 10^4 \text{ M}^{-1}$ (Fig. 1b).

Fluorescence studies. To analyse the emission spectral behaviour of the probe **HqEN**₄₈₀ we have performed fluorescence studies in purely aqueous medium (10.0 mM HEPES buffer, pH = 7.20) at $\lambda_{\text{ex}} = 390 \text{ nm}$. The probe **HqEN**₄₈₀ in aqueous solution is weakly fluorescent because of PET from

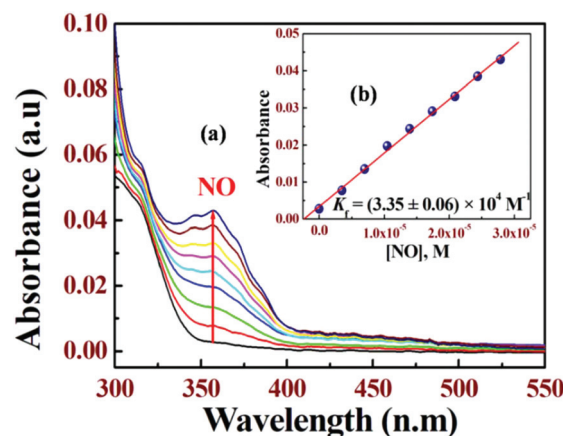
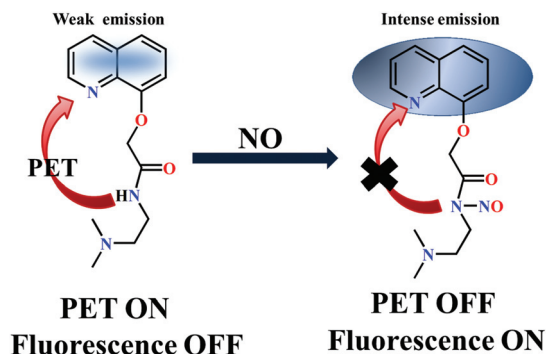


Fig. 1 (a) Changes in UV-Vis absorption spectra of **HqEN**₄₈₀ (20 μM) in aqueous HEPES buffer (10 mM) at pH 7.20 and $\mu = 0.10 \text{ M}$ NaCl with various amounts of NO (0–0.8 equivalents); (b) plot of absorbance vs. [NO].



Scheme 4 Schematic representation of *N*-nitrosation based fluorescent probe HqEN_{480} for NO.

the amide nitrogen atom to the quinoline fluorophoric moiety. However, on reaction with NO the PET is blocked, leading to the formation of an electron deficient N–N=O moiety (Scheme 4). The apparent formation constant (K_f) of $\text{HqEN}_{480}\text{-NO}$, formed by the reaction between HqEN_{480} and NO, was determined by performing the fluorescence titration of HqEN_{480} (20 μM) in aqueous solution (2.5 ml) with NO (0–70 μM) at 25 °C. The fluorescence spectra display a gradually increased emission band at 480 nm (Fig. 2a) resulting in an approximately 7-fold enhancement in fluorescence intensity which is adequate to detect nitric oxide intracellularly. By adopting eqn (3)³³ under the conditions $1 \gg c \times x$ with $n = 1$ (where a , b and c represent the same denotation as mentioned for UV-Vis studies previously but in terms of fluorescence intensity), the slope of the curve gives $b \times c$, which ultimately provides $c = K_f = \text{formation constant} = (1.75 \pm 0.07) \times 10^4 \text{ M}^{-1}$ (taking $b = 2.60 \times 10^5$) (Fig. 2b). The excellent agreement between two K_f values obtained from absorption and fluorescence titrations definitely proves the self-consistent nature of our results.

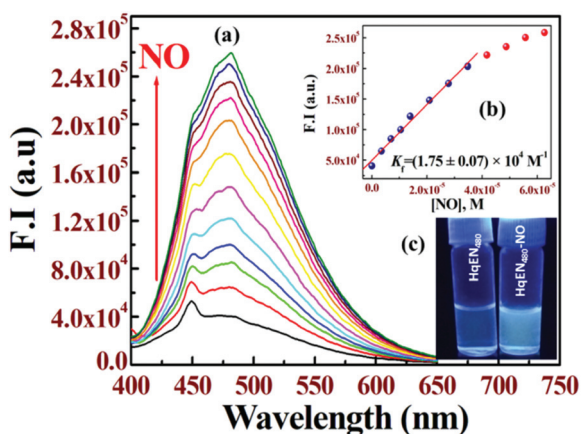


Fig. 2 (a) Fluorescence titration of HqEN_{480} (20 μM) with variable concentrations of NO (0–70 μM) at 25 °C in aqueous HEPES buffer (10 mM) at pH 7.20 and $\mu = 0.10 \text{ M NaCl}$. (b) Plot of FI vs. [NO]. (c) UV exposed emission image of HqEN_{480} and $\text{HqEN}_{480}\text{-NO}$.

Again, at $\lambda_{\text{ex}} = 350 \text{ nm}$, a plot of F.I. vs. [NO] also shows enhancement in fluorescence intensity approximately about ~ 8 fold but it is not suitable for biological applications (Fig. S6†). So, the entire fluorescence studies were performed at $\lambda_{\text{ex}} = 390 \text{ nm}$.

To compare the fluorescence behaviour of HqEN_{480} towards NO we have synthesized an *N*-nitrosation based fluorescent analogue, HqPA , following the same synthetic procedure. The fluorescence titration of HqPA with NO under identical reaction conditions displays a ~ 4 fold enhancement in fluorescence intensity at the same excitation and emission wavelengths ($\lambda_{\text{ex}} = 390 \text{ nm}$, $\lambda_{\text{em}} = 480 \text{ nm}$) while HqEN_{480} displays ~ 7 fold fluorescence enhancement (Fig. S7†). The slightly improved fluorescence response of HqEN_{480} towards NO compared to HqPA may arise due to the presence of a terminal $-\text{CH}_2\text{CH}_2\text{NMe}_2$ group whose electron donating capability is higher than the $-\text{CH}_2\text{CH}_2\text{CH}_3$ group making the probe HqEN_{480} more sensitive towards NO. For HqPA , we have also performed the selectivity studies by various ions (Fig. S8†).

Sensing mechanism

Usually, the *N*-nitrosation based probes display a “turn-on” fluorescence response specifically towards NO without interference from the other commonly known reactive species. Herein, we designed a probe HqEN_{480} based on quinoline as a fluorophoric moiety along with *N,N*-dimethylethylenediamine. The role of a side chain having terminal $-\text{NMe}_2$ is quite attractive. Here the $-\text{NMe}_2$ group functioning as an electron rich centre facilitates the amide ($-\text{CONHR}$) nitrogen atom to be more reactive towards NO. As expected, the newly designed HqEN_{480} probe is weakly fluorescent because of the considerable fluorescence quenching through a photoinduced electron transfer (PET) process from the amide nitrogen atom to the quinoline moiety but HqEN_{480} is capable of exhibiting large fluorescence magnification in response to NO through blocking of the PET process with concomitant formation of the electron deficient N–N=O moiety (Scheme 4).

Confirmation of the sensing mechanism

To investigate the mechanism responsible for the gradual increment of fluorescence intensity of the probe HqEN_{480} in response to NO, the water soluble probe was allowed to react with excess NO in aerated MeCN medium. After evaporating, the desired product $\text{HqEN}_{480}\text{-NO}$ was isolated and the detailed analyses were performed by using $^1\text{H NMR}$ (Fig. S9†), $^{13}\text{C NMR}$ (Fig. S9a†), ESI-MS⁺ (Fig. S10†) and FT-IR (Fig. S11†) spectrometers. The investigation reveals that the peak at 338.3941 ($\text{HqEN}_{480}\text{-NO} + 2\text{H}_2\text{O}$) arises due to the reaction of HqEN_{480} with NO resulting in the formation of the N–N=O moiety. The $^1\text{H-NMR}$ spectra also reveal that the single peak responsible for the amide $-\text{NH}$ proton of HqEN_{480} at 8.90 ppm vanishes on treatment with NO leading to a conclusion that the NO is attached to the amide $-\text{N}$ atom. There is also evidence in favour of this sensing mechanism through IR studies which clearly demonstrate that upon reaction with NO, the product $\text{HqEN}_{480}\text{-NO}$ shows a new peak at 1382 cm^{-1} corresponding to

$-N-N=O^{50}$ with concomitant suppression of N–H stretching frequency at 3411 cm^{-1} . So we easily conclude that nitric oxide is attached with the amide $-N$ atom. The N -nitrosation based fluorescent analogue, **HqPA**, also goes through a similar mechanism to that characterised by $^1\text{H NMR}$ (Fig. S12[†]). The magnitude of quantum yield for the compound **HqEN**₄₈₀-NO was $\Phi = 0.22$ and that for the ligand (**HqEN**₄₈₀) was 0.04 (using acidic quinine sulfate as the standard). In terms of the 3σ method the magnitude of limit of detection (LOD) for nitric oxide was found to be 53 nM (Fig. S13[†]) indicating that the probe **HqEN**₄₈₀ is highly suitable for tracking NO in biological systems. From the absorption data the detection limit (LOD) of NO was determined (using 3σ method) to obtain a value of 1 μM (Fig. S13a[†]). So, based on all the above experiments, results and discussions it is apparent that the probe **HqEN**₄₈₀ is an efficient nitric oxide sensor.

TCSPC studies

The average life-time of the probe **HqEN**₄₈₀ ($\tau_0 = 4.03\text{ ns}$) increases upon treatment with $\sim 70\text{ }\mu\text{M}$ nitric oxide ($\tau_0 = 8.89\text{ ns}$) and the nature of the decay curve changes from the bi-exponential to mono-exponential one on reaction with nitric oxide (Fig. 3). This study reveals that the addition of NO results in greater stability of the product **HqEN**₄₈₀-NO in the excited state.

Selectivity study

The specificity of the probe **HqEN**₄₈₀ was verified by recording the fluorescence spectra of **HqEN**₄₈₀ in the presence of various metal ions (Na^+ , Cu^{2+} , Mg^{2+} , K^+ , Dy^{3+} , Eu^{2+} , Zn^{2+} , Sm^{3+} , Co^{2+} , Ni^{2+} , Pb^{2+} , Cr^{3+} , Cd^{2+} , Mn^{2+} , Fe^{3+} , Al^{3+} , Hg^{2+}) (Fig. 4), anions (S^{2-} , SO_4^{2-} , NO_3^- , NO_2^- , H_2PO_4^- , $\text{S}_2\text{O}_4^{2-}$, ClO_4^- , OAc^- , HCO_3^- , Cl^- , CO_3^{2-} , PPI , N_3^- , F^-) (Fig. 5), amino acids (alanine, arginine, cysteine, homocysteine and so on) (Fig. S14[†]) including biological interfering species (OCl^- , ascorbic acid, OH^\cdot , O_2^- , tempo, ONOO^- , HNO , H_2O_2 , DHA , NO^+ , NO) (Fig. 6).

However, in aqueous solution for the above cases, there is no remarkable change in fluorescence intensity except for NO, where the probe **HqEN**₄₈₀ exhibits ~ 7 fold increment in fluo-

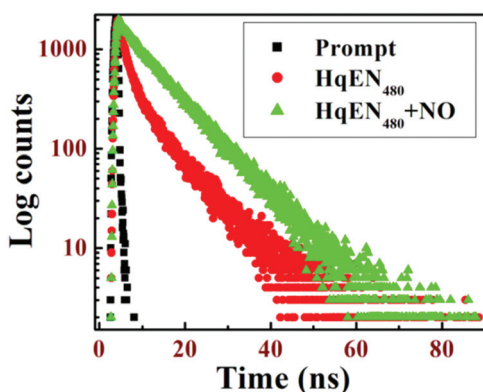


Fig. 3 Lifetime plot of **HqEN**₄₈₀ and (**HqEN**₄₈₀ + NO) at 25 °C in aqueous HEPES buffer (10 mM) at pH 7.20 and $\mu = 0.10\text{ M}$ NaCl.

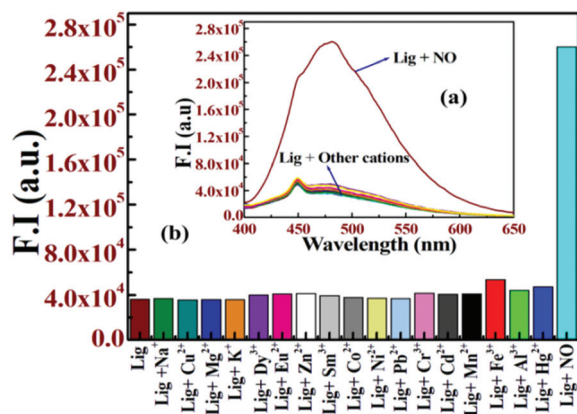


Fig. 4 (a) Fluorescence response of **HqEN**₄₈₀ in the presence of various cations (Na^+ , Cu^{2+} , Mg^{2+} , K^+ , Dy^{3+} , Eu^{2+} , Zn^{2+} , Sm^{3+} , Co^{2+} , Ni^{2+} , Pb^{2+} , Cr^{3+} , Cd^{2+} , Mn^{2+} , Fe^{3+} , Al^{3+} , Hg^{2+}) (100 μM) in the aqueous solution of **HqEN**₄₈₀ (20 μM) ($\lambda_{\text{ex}} = 390\text{ nm}$); (b) the corresponding bar plot.

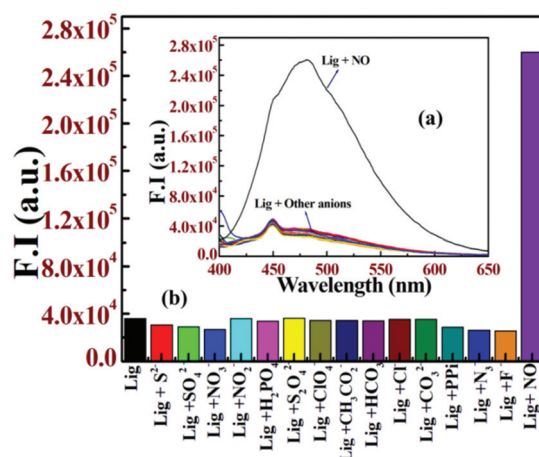


Fig. 5 (a) Fluorescence response of **HqEN**₄₈₀ towards NO over various anions; (b) the corresponding bar plot.

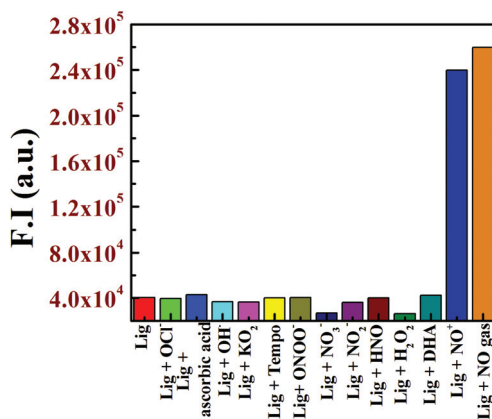


Fig. 6 Bar plot illustrating fluorescence responses of **HqEN**₄₈₀ towards NO over other reactive species. (OCl^- , ascorbic acid, OH^\cdot , O_2^- , tempo, ONOO^- , NO_3^- , NO_2^- , HNO , H_2O_2 , DHA , NO^+ and NO gas.)

rescence intensity. As a result the fluorescence emission spectra clearly shows that **HqEN**₄₈₀ is highly selective and specific towards nitric oxide in aqueous solution at pH = 7.2.

The selective behaviour of **HqEN**₄₈₀ towards NO over other ROS/RNS was further deliberated by using the UV-Vis absorption method as illustrated in Fig. S15.† Interestingly, both the fluorescence and absorbance spectra of the probe **HqEN**₄₈₀ reveal selectivity towards NO even in the presence of competing ions (Fig. S16†) (such as hydrogen peroxide, peroxyxynitrite, ascorbic acid, dehydroascorbic acid and so on) (Fig. S17†).

pH study

To analyse the pH effects on the ability of the probe **HqEN**₄₈₀ to sense nitric oxide, we recorded the fluorescence spectra by taking 20 μM **HqEN**₄₈₀ with 3.5 equivalents (70 μM) of NO at various pH values in HEPES buffer. As displayed in Fig. 7 the probe **HqEN**₄₈₀ is weakly fluorescent as well as stable and shows good detectable response towards NO over a wide range of pH = 4–10. However, the probe displays the best response towards NO in the pH range of 5–7 leading to the conclusion that the probe is suitable for monitoring NO in living systems.

Geometry optimization and electronic structure

Herein, the receptor, **HqEN**₄₈₀, is able to show selective positive response towards NO resulting in the formation of the *N*-nitrosated product, [**HqEN**₄₈₀-NO], which leads to electronic as well as structural changes in their geometries. In order to have a detailed idea about the photophysical properties of the probe **HqEN**₄₈₀ and its *N*-nitrosated product, we have carried out DFT and TDDFT calculations at the B3LYP/6-31G level of the Gaussian 09 program.

The optimized geometries of **HqEN**₄₈₀ and its NO bound form, [**HqEN**₄₈₀-NO], are shown in Fig. 8. **HqEN**₄₈₀ and [**HqEN**₄₈₀-NO] both belong to the C₁ point group. The nature of all stationary points for both free ligand and its NO product

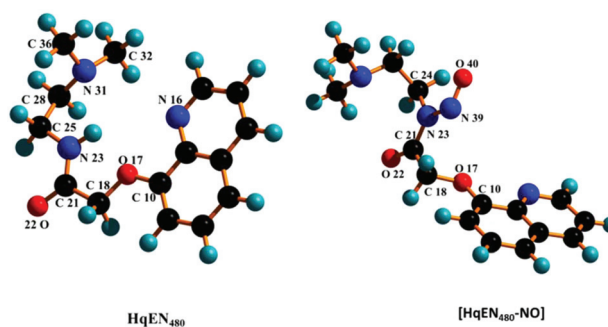


Fig. 8 Optimized geometry of ligand **HqEN**₄₈₀ and the NO product [**HqEN**₄₈₀-NO].

was identified by performing normal mode analysis and all the frequencies turned out to be positive indicating their global minima.

In the ground state for **HqEN**₄₈₀, the electron density distributed mainly over HOMO–1 molecular orbitals of the 8-methoxyquinoline ring moiety and LUMO molecular orbitals of the quinolin-8-ol portion of the ligand. On the other hand, for HOMO molecular orbitals, the electron density resides mainly on the ethyl-dimethyl-amine fragment of the ligand **HqEN**₄₈₀. For the free ligand, the energy gap between HOMO and LUMO is 4.17 eV (Fig. 9). In the case of [**HqEN**₄₈₀-NO], the HOMO and HOMO–1 molecular orbitals carry most of the electron density in the ethyl-dimethyl-amine fragment and 8-methoxyquinoline moiety of the *N*-nitrosated ligand, whereas for the LUMO orbital the electron clouds are mainly distributed over the *N*-nitrosoformamide fragment. For LUMO+1, the electron cloud localized on the quinolin-8-ol moiety and the contribution of electron density for LUMO+2 orbitals originate from the *N*-nitroso-2-hydroxyacetamide portion respectively. Fig. 9 shows that for the NO product, the HOMO–LUMO energy gap is 2.75 eV which is less than that of **HqEN**₄₈₀ (4.17 eV). Enhancement in fluorescence intensity for

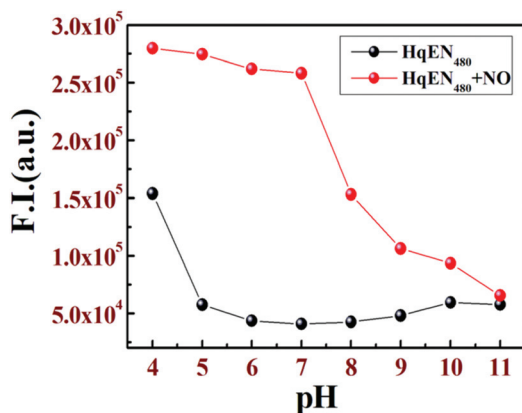


Fig. 7 pH dependent fluorescence responses of **HqEN**₄₈₀ and **HqEN**₄₈₀-NO at 25 °C in aqueous HEPES buffer (10 mM) at pH 7.20 and μ = 0.10 M NaCl.

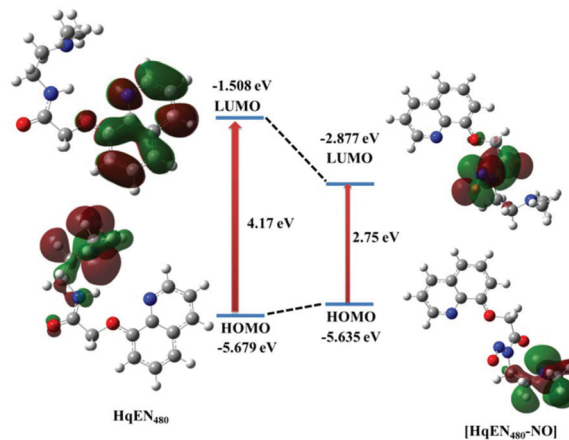


Fig. 9 Frontier molecular orbital of ligands **HqEN**₄₈₀ and [**HqEN**₄₈₀-NO].

the NO product arises mainly due to the electron withdrawing nature of the $-N=N=O$ moiety blocking the PET process.

The ligand **HqEN₄₈₀** shows absorption bands at 314.00 nm at room temperature and the corresponding calculated absorption band is found at 307.10 nm which indicates an excellent agreement with our experimental results. This band arises due to $S_0 \rightarrow S_2$ electronic transitions (Fig. S18[†]). The absorption energies as well as their oscillator strengths are described in Table S3.[†]

The complex [**HqEN₄₈₀-NO**] shows absorption bands at 304.47 nm at room temperature. These absorption bands can be assigned to the $S_0 \rightarrow S_8$ transitions (Fig. S19[†]). For [**HqEN₄₈₀-NO**], the absorption energies and their oscillator strengths are also given in Table S4.[†]

NO detection in living cells

As **HqEN₄₈₀** showed extensively selective reaction with nitric oxide (NO), it had been further checked for its NO sensing ability in living cells. A cell viability assay using MTT was performed to check the cytotoxic effects of **HqEN₄₈₀**, by calculating the % cell viability of HepG2 cells (Fig. 10). More than 80% cell viability is reflected by no significant decrease in formazan production up to 20 μ M concentration of **HqEN₄₈₀**. Hence, further cell imaging experiments were carried out with 10 μ M of **HqEN₄₈₀** at which cell viability is more than 85% and much more effective for *in vitro* monitoring of NO molecules. The incubation of 10 μ M **HqEN₄₈₀** for 1 hour exhibited no intracellular fluorescence on HepG2 cells (Fig. 11).

However, upon incubation of HepG2 cells with 10 μ M of SNP, which is provided as an exogenous source for NO, followed by incubation with 10 μ M **HqEN₄₈₀**, a distinct blue fluorescence was observed inside the cells due to the reaction between the exogenously produced NO molecules and the ligand. Fluorescence emission was mostly localized in the cytoplasmic region of the cell, indicating the formation of **HqEN₄₈₀-NO** outside the nucleus. Keeping the **HqEN₄₈₀** concentration constant (10 μ M) and increasing the concentration of SNP from 10 μ M, 20 μ M, to 40 μ M a concentration-dependent increase in the intracellular blue fluorescence is quite apparent. These results suggest that the ligand **HqEN₄₈₀** with

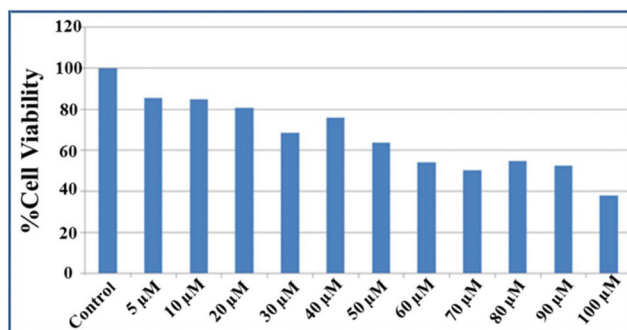


Fig. 10 Percent (%) cell viability of HepG2 cells treated with different concentrations (5–100 μ M) of **HqEN₄₈₀** for 24 hours determined by the MTT assay.

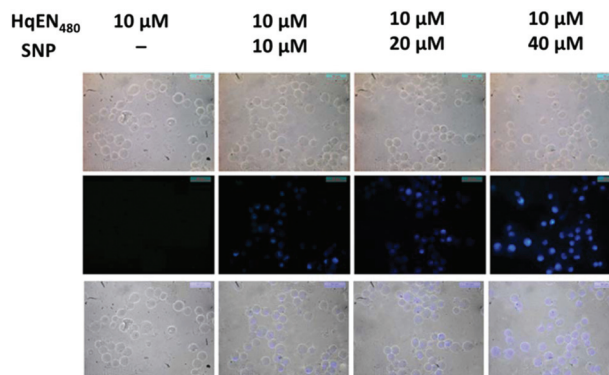


Fig. 11 The fluorescence images of HepG2 cells were captured (40 \times) after incubation with 10 μ M, 20 μ M and 40 μ M of sodium nitroprusside (SNP) for 60 min at 37 $^{\circ}$ C, followed by washing thrice with 1 \times PBS and incubation with 10 μ M of **HqEN₄₈₀** for 60 min at 37 $^{\circ}$ C. The fluorescence images show the absence of signal by the fluorophore **HqEN₄₈₀** (10 μ M) in the absence of NO molecule induced from SNP, while the fluorescence gradually increases, highly at 40 μ M of SNP concentration.

low cytotoxicity and biocompatibility has a high potential for *in vitro* application as a sensor of intracellular NO molecules, as well as for their detection in biological samples.

Conclusion

In summary, herein we present a new fluorescent probe **HqEN₄₈₀** which exhibits a dramatic turn on fluorescence response towards NO in 100% aqueous solution by utilizing the *N*-nitrosation based reaction, with cell imaging applications. Its pronounced selectivity towards NO over other interfering species makes it a suitable fluorescent probe for tracking NO in biological systems. Moreover, the *N*-nitrosated product was analysed and well characterised by ESI-MS⁺, NMR and IR studies. The presence of a highly electron withdrawing group $-N=N=O$ within the fluorophoric moiety pulls the electron density from the amide nitrogen atom leading to blocking of the PET process with concomitant enhancement in fluorescence intensity. The sensing reaction of **HqEN₄₈₀** towards NO shows high sensitivity as evidenced from the very low detection limit of 53 nM. Thus it clearly indicates the suitability of the probe for monitoring NO in macrophage cultures⁵¹ due to the presence of NO in micromolar concentrations in these types of cells. Fluorescence titration gives a high formation constant, $(1.75 \pm 0.07) \times 10^4 \text{ M}^{-1}$, for the reaction between **HqEN₄₈₀** and NO at pH 7.2. Thus, low cytotoxicity towards biological systems, water solubility, and cell-permeability along with very low LOD (53 nM) demonstrates that **HqEN₄₈₀** is a highly desirable probe for tracking NO in living cells.

Conflicts of interest

There are no conflicts of interest to declare.

Acknowledgements

Financial support from the CSIR (Ref.01(2896)/17/EMR-II), New Delhi and the DST, (Ref. No. 809 (Sanc)/ST/P/S&T/4G-9/2104) West Bengal, India is gratefully acknowledged. A. Dutta gratefully acknowledge DST-INSPIRE for their financial support as a junior research fellow (JRF).

References

- 1 L. Chen, D. Wu and J. Yoon, *Sens. Actuators, B*, 2018, **259**, 347–353.
- 2 (a) V. Calabrese, C. Mancuso, M. Calvani, E. Rizzarelli, D. A. Butterfield and A. M. Stella, *Nat. Rev. Neurosci.*, 2007, **8**, 766–775; (b) C. Szabo, *Nat. Rev. Drug Discovery*, 2016, **15**, 185–203.
- 3 B. V. Khan, D. G. Harrison, M. T. Olbrych, R. W. Alexander and R. M. Medford, *Proc. Natl. Acad. Sci. U. S. A.*, 1996, **93**, 9114–9119.
- 4 T. Gudi, G. K. Hong, A. B. Vaandrager, S. M. Lohmann and R. B. Pilz, *FASEB J.*, 1999, **13**, 2143–2152.
- 5 K. Pantopoulos and M. W. Hentze, *Proc. Natl. Acad. Sci. U. S. A.*, 1995, **92**, 1267–1271.
- 6 X. B. Liu, P. Hill and D. J. Haile, *Blood Cells, Mol., Dis.*, 2002, **29**, 315–326.
- 7 N. Pozdnyakov, A. Lloyd, V. N. Reddy and A. A. Sitaramayya, *Biochem. Biophys. Res. Commun.*, 1993, **192**, 610–615.
- 8 B. Brune, S. Dimmeler, L. M. Y. Vedia and E. G. Lapetina, *Life Sci.*, 1994, **54**, 61–70.
- 9 S. Taysi, C. Uslu, F. Akcay and M. Y. Sutbeyaz, *Surg. Today*, 2003, **33**, 651–654.
- 10 G. P. Biro, *Curr. Drug Discovery Technol.*, 2012, **9**, 194–203.
- 11 D. Y. Choi, Y. J. Lee, J. T. Hong and H. J. Lee, *Brain Res. Bull.*, 2012, **87**, 144–153.
- 12 S. Yuan, R. P. Patel and C. G. Kevil, *Am. J. Physiol.: Lung Cell. Mol. Physiol.*, 2015, **308**, L403–L415.
- 13 D. D. Thomas, L. A. Ridnour, J. S. Isenberg, W. Flores-Santana, C. H. Switzer, S. Donzelli, *et al.*, *Free Radical Biol. Med.*, 2008, **45**, 18–31.
- 14 W. Hu, D. Boateng, J. Kong and X. Zhang, *Austin J. Biosens. Bioelectron.*, 2015, **1**, 1–9.
- 15 H. Kojima, Y. Urano, K. Kikuchi, T. Higuchi, Y. Hirata and T. Nagano, *Angew. Chem., Int. Ed.*, 1999, **38**, 3209–3212.
- 16 E. Sasaki, H. Kojima, H. Nishimatsu, Y. Urano, K. Kikuchi, Y. Hirata and T. Nagano, *J. Am. Chem. Soc.*, 2005, **127**, 3684–3685.
- 17 H. Yu, X. Zhang, Y. Xiao, W. Zou, L. Wang and L. Jin, *Anal. Chem.*, 2013, **85**, 7076–7084.
- 18 H.-X. Zhang, J.-B. Chen, X.-F. Guo, H. Wang and H.-S. Zhang, *Anal. Chem.*, 2014, **86**, 3115–3123.
- 19 C.-B. Huang, J. Huang and L. Xu, *RSC Adv.*, 2015, **5**, 13307–13310.
- 20 X. Liu, S. Liu and G. Liang, *Analyst*, 2016, **141**, 2600–2605.
- 21 J. Zhou, C. Wang, Y. Zhao and Q. Song, *Anal. Methods*, 2017, **9**, 1611–1616.
- 22 M. H. Lim and S. J. Lippard, *J. Am. Chem. Soc.*, 2005, **127**, 12170–12171.
- 23 M. H. Lim, D. Xu and S. J. Lippard, *Nat. Chem. Biol.*, 2006, **2**, 375–380.
- 24 M. H. Lim, B. A. Wong, W. H. Pitcock, D. Mokshagundam, M.-H. Baik and S. J. Lippard, *J. Am. Chem. Soc.*, 2006, **128**, 14364–14373.
- 25 M. D. Pluth, L. E. McQuade and S. J. Lippard, *Org. Lett.*, 2010, **12**, 2318–2321.
- 26 L. E. McQuade, J. Ma, G. Lowe, A. Ghatpande, A. Gelperin and S. J. Lippard, *Proc. Natl. Acad. Sci. U. S. A.*, 2010, **107**, 8525–8530.
- 27 X. Chen, L. Sun, Y. Chen, X. Cheng, W. Wu, L. Ji and H. Chao, *Biomaterials*, 2015, **58**, 72–81.
- 28 K. J. Franz, N. Singh, B. Spingler and S. Lippard, *Inorg. Chem.*, 2000, **39**, 4081–4092.
- 29 L. McQuade and S. Lippard, *Curr. Opin. Chem. Biol.*, 2010, **14**, 43–49.
- 30 P. Wardman, *Free Radical Biol. Med.*, 2007, **43**, 995–1022.
- 31 (a) J. Miao, Y. Huo, X. Lv, Z. Li, H. Cao, H. Shi, Y. Shi and W. Guo, *Biomaterials*, 2016, **78**, 11–19; (b) A. S. M. Islam, M. Sasmal, D. Maiti, A. Dutta, B. Show and M. Ali, *ACS Omega*, 2018, **3**, 10306–10316.
- 32 D. Maiti, A. S. M. Islam, M. Sasmal, C. Prodhon and M. Ali, *Photochem. Photobiol. Sci.*, 2018, **17**, 1213–1221.
- 33 A. S. M. Islam, R. Bhowmick, K. Pal, A. Katarkar, K. Chaudhuri and M. Ali, *Inorg. Chem.*, 2017, **56**(8), 4324–4331.
- 34 A. S. M. Islam, R. Bhowmick, B. C. Garain, A. Katarkar and M. Ali, *J. Org. Chem.*, 2018, **83**(21), 13287–13295.
- 35 C. Sun, W. Shi, Y. Song, W. Chen and H. Ma, *Chem. Commun.*, 2011, **47**, 8638–8640.
- 36 C.-G. Dai, X.-L. Liu, X.-J. Du, Y. Zhang and Q.-H. Song, *ACS Sens.*, 2016, **1**, 888–895.
- 37 Š. Mesároš, S. Grunfeld, A. Mesárošová, D. Bustin and T. Malinski, *Anal. Chim. Acta*, 1997, **339**, 265–270.
- 38 S. Miyamoto, G. R. Martinez, A. P. B. Martins, M. H. G. Medeiros and P. Di Mascio, *J. Am. Chem. Soc.*, 2003, **125**, 4510–4517.
- 39 A. Dutta, R. Alam, A. S. M. Islam, A. Dutta and M. Ali, *Dalton Trans.*, 2018, **47**, 11563–11571.
- 40 R. G. Parr and W. Yang, *Density Functional Theory of Atoms and Molecules*, Oxford University Press, Oxford, 1989.
- 41 (a) V. Barone and M. Cossi, *J. Phys. Chem. A*, 1998, **102**, 1995–2001; (b) M. Cossi and V. Barone, *J. Chem. Phys.*, 2001, **115**, 4708; (c) M. Cossi, N. Rega, G. Scalmani and V. Barone, *J. Comput. Chem.*, 2003, **24**, 669–681.
- 42 A. D. Becke, *J. Chem. Phys.*, 1993, **98**, 5648.
- 43 C. Lee, W. Yang and R. G. Parr, *Phys. Rev.*, 1998, **37**, 785.
- 44 (a) M. E. Casida, C. Jamoroski, K. C. Casida and D. R. Salahub, *J. Chem. Phys.*, 1998, **108**, 4439; (b) R. E. Stratmann, G. E. Scuseria and M. J. Frisch, *J. Chem. Phys.*, 1998, **109**, 8218; (c) R. Bauernschmitt and R. Ahlrichs, *Chem. Phys. Lett.*, 1996, **256**, 454–464.
- 45 (a) T. Liu, H. X. Zhang and B. H. Xia, *J. Phys. Chem. A*, 2007, **111**, 8724–8730; (b) X. Zhou, H. X. Zhang, Q. J. Pan,

- B. H. Xia and A. C. Tang, *J. Phys. Chem. A*, 2005, **109**, 8809–8818; (c) X. Zhou, A. M. Ren and J. K. Feng, *J. Organomet. Chem.*, 2005, **690**, 338–347; (d) A. Albertino, C. Garino, S. Ghiani, R. Gobetto, C. Nervi, L. Salassa, E. Rosenverg, A. Sharmin, G. Viscardi, R. Buscaino, G. Cross and M. Milanese, *J. Organomet. Chem.*, 2007, **692**, 1377–1391.
- 46 M. J. Frisch, G. W. Trucks, H. B. Schlegel, G. E. Scuseria, M. A. Robb, J. R. Cheeseman, G. Scalmani, V. Barone, B. Mennucci, G. A. Petersson, H. Nakatsuji, M. Caricato, X. Li, H. P. Hratchian, A. F. Izmaylov, J. Bloino, G. Zheng, J. L. Sonnenberg, M. Hada, M. Ehara, K. Toyota, R. Fukuda, J. Hasegawa, M. Ishida, T. Nakajima, Y. Honda, O. Kitao, H. Nakai, T. Vreven, J. A. Montgomery Jr., J. E. Peralta, F. Ogliaro, M. Bearpark, J. J. Heyd, E. Brothers, K. N. Kudin, V. N. Staroverov, R. Kobayashi, J. Normand, K. Raghavachari, A. Rendell, J. C. Burant, S. S. Iyengar, J. Tomasi, M. Cossi, N. Rega, J. M. Millam, M. Klene, J. E. Knox, J. B. Cross, V. Bakken, C. Adamo, J. Jaramillo, R. Gomperts, R. E. Stratmann, O. Yazyev, A. J. Austin, R. Cammi, C. Pomelli, J. W. Ochterski, R. L. Martin, K. Morokuma, V. G. Zakrzewski, G. A. Voth, P. Salvador, J. J. Dannenberg, S. Dapprich, A. D. Daniels, Ö. Farkas, J. B. Foresman, J. V. Ortiz, J. Cioslowski and D. J. Fox, *Gaussian 09, (Revision A.1)*, Gaussian, Inc., Wallingford, CT, 2009.
- 47 N. M. O'Boyle, A. L. Tenderholt and K. M. Langner, *J. Comput. Chem.*, 2008, **29**, 839–845.
- 48 P. R. Twentyman and M. Luscombe, *Br. J. Cancer*, 1987, **56**, 279–285.
- 49 (a) T. Peng, X. Chen, L. Gao, T. Zhang, W. Wang, J. Shen and D. Yang, *Chem. Sci.*, 2016, **7**, 5407–5413; (b) X. Wu, L. Li, W. Shi, Q. Gong and H. Ma, *Angew. Chem., Int. Ed.*, 2016, **55**, 14728–14732; (c) K. Xu, M. Qiang, W. Gao, R. Su, N. Li, Y. Gao, Y. Xie, F. Kong and B. Tang, *Chem. Sci.*, 2013, **4**, 1079–1086.
- 50 X. Hu, J. Wang, X. Zhu, D. Dong, X. Zhang, S. Wu and C. Duan, *Chem. Commun.*, 2011, **47**, 11507–11509.
- 51 T. Chen, R. Zamora, B. Zuckerbraun and T. R. Billiar, *Curr. Mol. Med.*, 2003, **3**, 519–526.